Imperial College London

Department of Mechanical Engineering

Detailed Microkinetic Analysis of Reactions in the C/H/O/N system over Platinum

Aliki Marina Tsopelakou

Thesis submitted for the degree of Doctor of Philosophy

of Imperial College London

2020

Abstract

The present PhD thesis considers an alternative theoretical framework based on Variational Transition State Theory (VTST) for estimating Arrhenius parameters for adsorption reactions. The estimation of rate data suitable for microkinetic analysis of reaction pathways in heterogeneous catalytic systems typically requires sticking coefficients. The use of VTST enables the construction of chemical mechanisms without the dependency on experimental data for sticking coefficients, for the final determination of the rate parameters. The energetics of the surface reactions are derived using the Unity Bond Index-Quadratic Exponential Potential (UBI-QEP) method.

A comprehensive chemical mechanism is developed for the description of the surface reactions associated with the catalytic removal of the three principal oxides of nitrogen (NO, NO_2 and N_2O) from automotive exhaust gases through the use of supported platinum catalysts. The reference five-step Pt catalytic mechanism [1] for NO removal has been updated to 21 reversible reaction steps featuring all principal oxides of nitrogen. Gas phase reactions are considered, via a comprehensive C/H/O/N mechanism that includes ammonia. The NO_x reduction mechanism was applied under nearly stoichiometric conditions, various metal loadings and coat amounts. A rigorous comparison with experimental data [2], obtained by Toyota Motor Europe, for nine different Test Cases was performed along with the analysis of modifications to the energetics and rate parameters. The outcomes obtained for CO, NO and C_3H_6 conversion against temperature present a promising agreement with the experimental data [2].

The same framework, with the absence of the nitrogen and propene containing catalytic chemistry, is implemented to study the ethane auto-thermal catalytic cracking in a quartz lined tubular reactor. The validation of the mechanism was carried out via experimental measurements provided by BP Chemicals [3]. The absence and presence of CO in the feed stream were studied to further explore the catalytic activity of the chemical system.

The work provides a framework for the development of heterogeneous reaction mechanisms, without the reliance on experimental sticking coefficients, focusing on the reduction of NOx emissions from the automotive exhaust gases. The proposed method can be further augmented and used for the generation of novel heterogeneous reaction mechanisms.

Declaration of Originality

The present PhD thesis is an own original work of Aliki Marina Tsopelakou and all else is appropriately referenced and acknowledged.

Copyright Declaration

The copyright of this thesis rests with the author and is made available under a Creative Commons Attribution Non-Commercial No Derivatives license. Researchers are free to copy, distribute or transmit the thesis on the condition that they attribute it, that they do not use it for commercial purposes and that they do not alter, transform or build upon it. For any reuse or redistribution, researchers must make clear to others the license terms of this work.

Aliki Marina Tsopelakou

December 2020

The only real voyage of discovery

consists not in seeking new landscapes

but in having new eyes . . .

Marcel Proust

Acknowledgements

First of all, I would like to express my sincere thanks to my supervisor, Prof. Peter Lindstedt for offering me ample support, invaluable guidance and broad vision to shape this research thesis. I would like also to thank Toyota Motor Europe for making this project possible via its financial support and particularly express my gratitude to my industrial supervisor Dr. Konstantinos Gkagkas and Dr. Hai Nguyen for their guidance and continuous interest on my work. I am also thankful to the Engineering and Physical Sciences Research Counsil (EPSRC) and the Centre for Doctoral Training (CDT) in Theory and Simulation of Materials (TSM) for funding this PhD studentship.

Many thanks principally to Dr. Matthew Eaton that entrusted me with the teaching of Thermodynamics II laboratory, as well as, to Ms. Serena Dalrymple and Ms. Kate Lewis for their support on administrative issues. Following, I would like to thank my collegues Dr. Fabian Hampp, Dr. Marcus Schiener, Dr. Tao Li, Dr. Lu Tian, Dr. Panagiotis Simatos, Seyedhamed Shariatmadar, Daniel Greenblatt, Sam Hughes, Omer Rathore, Giovanni Tretola, Dr. Daniel Fredrich and Stephen Winn. My indebted heartful thank you to my friends Sokratia Georgaka, Angeliki Poulou, Antonis Sergis, Konstantinos Kouloulias, Efstathios Karlis, Stavros Bontitsopoulos and Nasos Giannenas for the pleasant and memorable moments we shared, during this amazing journey.

I feel also the need to express my gratitude to Prof. Fotis Diakonos, Prof. Efstathios Stiliaris and Prof. Ioannis Lelidis from the Department of Physics of the National and Kapodistrian University of Athens for their support and guidance. A big thank you to my friends in Greece, Efi Tzovara, Giorgos Fragkoulidis, Andreas Foteas and especially Giorgos Margazoglou who supported my decisions and encouraged me to pursue this research path.

Last but not least, I am more than grateful towards my family for their continuous motivation all these years. I would like to mention my parents, Panagiotis and Ioanna, for their unconditional love and support, as well as for raising me to never give up despite the difficulties. I am also thankful to my brother Aris for his love and support and my loving grandparents Aristomenis, Aliki Marina, Dimitra and Xenophon for the values they have provided me with and the useful advice that will accompany me throughout my professional and personal life. A special mention to my adorable grandmother Aliki Marina who significantly encouraged my scientific inclination since I was a kid and always surrounds me with her wonderful love, constant support and incredible patience, constituting my everlasting source of inspiration.

The current dissertation is dedicated to
my grandparents Aristomenis & Aliki Marina

Contents

Abstract 3

Declaration of Originality 5

Copyright Declaration 7

Acknowledgements 11

Contents 14

List of Figures 17

List of Tables 22

Nomenclature 25

1 Introduction 30
- 1.1 Background and motivation . . . 30
- 1.2 Literature review . . . 33
  - 1.2.1 NO_x removal from automotive exhaust gases . . . 33
  - 1.2.2 Reaction mechanisms for the heterogeneous catalytic removal of nitrogen oxides . . . 35
  - 1.2.3 Auto-thermal catalytic cracking for olefins production . . . 37
- 1.3 Current contribution . . . 38
- 1.4 Thesis outline . . . 40

2 Theoretical framework 42
- 2.1 Computational methods . . . 42
- 2.2 Thermodynamic properties . . . 46
- 2.3 Physical properties . . . 47
  - 2.3.1 Transport properties . . . 47
  - 2.3.2 Diffusion in porous media . . . 49
    - 2.3.2.1 Representation of diffusion coefficients . . . 53
- 2.4 Gas phase chemistry . . . 55
- 2.5 Catalytic chemistry . . . 55
  - 2.5.1 Determination of pre-exponential Arrhenius factors . . . 56
  - 2.5.2 Determination of partition functions . . . 57

2.5.3 Binding configurations and bond lengths of species for Pt catalysts 60
2.6 Determination of temperature dependencies, β . . . 61
2.7 Calculation of reaction activation energies . . . 62
2.7.1 Atomic heats of adsorption . . . 64
2.7.2 Dissociation and total bond energies . . . 65
2.7.3 Heats of adsorption . . . 65
2.7.4 Reaction barriers . . . 68
2.7.4.1 Surface diffusion barriers . . . 72
2.7.5 Comparison of activation energy data . . . 73
2.8 Observables . . . 73
2.8.1 Conversion . . . 74
2.8.2 Selectivity . . . 74
2.8.3 Oxygen to Carbon ratio . . . 75

3 Rate parameter determination 76
3.1 Determination of rate constants for adsorption reactions . . . 76
3.2 Determination of mobile and immobile transition state . . . 86
3.2.1 Determination of sticking coefficients for C/H/O containing species 86
3.2.2 Determination of sticking coefficients for nitrogen containing species 90
3.2.3 Determination of sticking coefficients for hydrocarbons . . . 93
3.2.4 Effect of variable T_{q^v} on sticking coefficients determination . . . 95
3.3 Reaction class based estimation of reaction rate parameter . . . 96
3.3.1 Comparison of selected rate constants . . . 100
3.3.1.1 Treatment of C_2H_4 catalytic chemistry . . . 105
3.4 Summary . . . 106

4 Multi-scale simulation of NOx removal using Pt/Al_2O_3 catalysts 109
4.1 Experimental Data . . . 109
4.1.1 Experimental Setup . . . 110
4.2 Computational Methods . . . 113
4.2.1 Gas phase chemistry . . . 115
4.2.2 Surface chemistry . . . 116
4.3 Results . . . 117
4.3.1 Methodology . . . 117
4.3.1.1 Global catalytic C_3H_6 step sub-mechanism . . . 117
4.3.1.2 Towards detailed C_3H_6 catalytic chemistry . . . 118
4.3.2 Mechanism evaluation for nine different test cases . . . 121
4.3.2.1 Effect of alternative heat of adsorption for $N_2O(s_2)$ . . . 122
4.3.2.2 Effect of different CO desorption energies . . . 123
4.3.2.3 Effect of vibrational partition function fixed at 800 K, for CO direct adsorption reaction . . . 125
4.3.2.4 Effect of vibrational partition function fixed at 800 K . . . 126
4.3.2.5 Effect of immobile TS for the H_2 direct adsorption reaction 128
4.3.2.6 Test Cases . . . 129

4.3.2.7 Effect of vibrational partition function fixed at 800 K, for CO direct adsorption reaction - Test Cases 1 - 9 147
4.3.3 Implementation of the detailed C_3H_6 catalytic chemistry 151
4.3.3.1 Effect of residence time 157
4.3.4 Consideration of metal dispersion 162
4.4 Summary 164

5 Ethane auto-thermal catalytic cracking over Pt/Al_2O_3 catalysts 167
5.1 Experimental Data 167
5.1.1 Experimental Setup 168
5.2 Computational Methods 169
5.2.1 Gas phase chemistry 169
5.2.2 Surface chemistry 170
5.3 Results 170
5.3.1 Methodology 170
5.3.1.1 Effect of diffusion barrier 171
5.3.1.2 Effect of efficiency factor 172
5.3.1.3 Effect of H_2 immobile TS 174
5.3.2 Mechanism evaluation in the absence and presence of CO co-feed 174
5.3.2.1 Ethane and oxygen conversion against the O/C feed ratio 175
5.3.2.2 Ethylene and methane selectivity against the O/C feed ratio 177
5.3.2.3 Mol fractions distribution 179
5.3.2.4 Temperature and velocity distribution 180
5.4 Summary 181

6 Conclusions and Future Perspectives 184
6.1 Conclusions 184
6.2 Future Perspectives 187

A Surface reaction mechanism 203

B Surface species data 232

C Gas phase reaction mechanisms 244

D Gas phase transport and thermochemical properties 267

E Knudsen efficiency factors 293

List of Figures

2.1 Schematic of a catalytic pore inside the reactor . . . 43
2.2 Comparison of diffusion coefficients for representative chemical species . . 54
2.3 Schematic of a potential energy surface . . . 60
2.4 Schematic of C_3H_6 adsorption on Pt(111). . . . 61
2.5 Adsorbate configurations on fcc(111) Pt surface . . . 68
2.6 Adsorption modes of O_2 and N_2O on Pt . . . 68
2.7 Adsorption mode of CH_3COO on Pt surface . . . 69
2.8 Multi-dimensional UBI potential diagram . . . 70

3.1 Schematic of CO adsorption on Pt (111) . . . 78
3.2 Schematic of a potential energy surface . . . 82
3.3 Comparison of mobile and immobile sticking coefficients for H_2, at T_{q^v} = 298 K . . . 87
3.4 Comparison of of mobile and immobile sticking coefficients for H_2, at T_{q^v} = 800 K . . . 88
3.5 Comparison of of mobile and immobile sticking coefficients for O_2, at T_{q^v} = 298 K . . . 88
3.6 Comparison of of mobile and immobile sticking coefficients for O_2, at T_{q^v} = 800 K . . . 89
3.7 Comparison of of mobile and immobile sticking coefficients for CO, at $T_{q^v} = 298$ K . . . 89
3.8 Comparison of of mobile and immobile sticking coefficients for CO, at $T_{q^v} = 800$ K . . . 90
3.9 Comparison of of mobile and immobile sticking coefficients for NO, at $T_{q^v} = 298$ K and $T_{q^v} = 800$ K . . . 91
3.10 Comparison of of mobile and immobile sticking coefficients for NO_2, at $T_{q^v} = 298$ K and $T_{q^v} = 800$ K . . . 92
3.11 Comparison of of mobile and immobile sticking coefficients for N_2O, at $T_{q^v} = 298$ K and $T_{q^v} = 800$ K . . . 92
3.12 Comparison of of mobile and immobile sticking coefficients for N_2, at T_{q^v} = 298 K and $T_{q^v} = 800$ K . . . 93
3.13 Comparison of of mobile and immobile sticking coefficients for C_3H_6, at $T_{q^v} = 298$ K and $T_{q^v} = 800$ K . . . 93
3.14 Comparison of of mobile and immobile sticking coefficients for C_3H_5, at $T_{q^v} = 298$ K and $T_{q^v} = 800$ K . . . 94

3.15 Comparison of of mobile and immobile sticking coefficients for C_2H_4, at $T_{q^v} = 298$ K and $T_{q^v} = 800$ K . . . 94
3.16 Comparison of of mobile and immobile sticking coefficients for O_2, with a variable T_{q^v} . . . 95
3.17 Comparison of of mobile and immobile sticking coefficients for CO, with a variable T_{q^v} . . . 95
3.18 Comparison of of mobile and immobile sticking coefficients for NO, with a variable T_{q^v} . . . 96
3.19 Representation of the Tolman cone . . . 98
3.20 Comparison of O_2 adsorption and desorption rate constants . . . 101
3.21 Comparison of CO adsorption and desorption rate constants . . . 102
3.22 Arrhenius plots of O_2 and CO adsorption and desorption reactions, at $T_{q^v} = 298$ K and $T_{q^v} = 800$ K . . . 102
3.23 Arrhenius plots of NO and NO_2 adsorption and desorption reactions, at $T_{q^v} = 298$ K and $T_{q^v} = 800$ K . . . 103
3.24 Arrhenius plots of N_2O and N_2 adsorption and desorption reactions, at $T_{q^v} = 298$ K and $T_{q^v} = 800$ K . . . 103
3.25 Arrhenius plots of C_3H_6 and C_3H_5 adsorption and desorption reactions, at $T_{q^v} = 298$ K and $T_{q^v} = 800$ K . . . 104
3.26 Comparison of C_2H_4 adsorption and desorption rate constants . . . 104
3.27 Arrhenius plots of O_2 and NO_2 adsorption and desorption reactions, with a variable T_{q^v} . . . 105

4.1 Schematic of the adsorbate geometry of C_3H_6, C_3H_5, C_2H_5CH, C_2H_5C . . 118
4.2 CO conversion compared to TME [2] - Test Case 5, for an alternative $N_2O(s_2)$ heat of adsorption . . . 122
4.3 NO and C_3H_6 conversion compared to TME [2] - Test Case 5, for an alternative $N_2O(s_2)$ heat of adsorption . . . 123
4.4 CO, NO and C_3H_6 conversion compared to TME [2] - Test Case 5, for different CO desorption energies . . . 124
4.5 CO, NO and C_3H_6 conversion compared to TME [2] - Test Case 5, at a fixed $T_{q^v} = 800$ K, for CO adsorption reaction . . . 125
4.6 CO, NO and C_3H_6 conversion compared to TME [2] - Test Case 5, for a fixed $T_{q^v} = 800$ K . . . 127
4.7 CO, NO and C_3H_6 conversion compared to TME [2] - Test Case 5, for an immobile TS of H_2 adsorption . . . 128
4.8 CO, NO and C_3H_6 conversion compared to TME [2] for the global catalytic C_3H_6 step sub-mechanism - Test Case 1 . . . 132
4.9 CO, NO and C_3H_6 conversion compared to TME [2] for the global catalytic C_3H_6 step sub-mechanism - Test Case 2 . . . 133
4.10 CO, NO and C_3H_6 conversion compared to TME [2] for the global catalytic C_3H_6 step sub-mechanism - Test Case 3 . . . 134
4.11 CO, NO and C_3H_6 conversion compared to TME [2] for the global catalytic C_3H_6 step sub-mechanism - Test Case 4 . . . 137
4.12 CO, NO and C_3H_6 conversion compared to TME [2] for the global catalytic C_3H_6 step sub-mechanism - Test Case 5 . . . 138

4.14.1 Flow fields of the CO mol fractions at 550 K, 650 K and 750 K, for Test Case 5 . . . 139
4.14.2 Flow fields of the NO mol fractions at 550 K, 650 K and 750 K, for Test Case 5 . . . 140
4.14.3 Flow fields of the C_3H_6 mol fractions at 550 K, 650 K and 750 K, for Test Case 5 . . . 141
4.15 CO, NO and C_3H_6 conversion compared to TME [2] for the global catalytic C_3H_6 step sub-mechanism - Test Case 6 . . . 142
4.16 CO, NO and C_3H_6 conversion compared to TME [2] for the global catalytic C_3H_6 step sub-mechanism - Test Case 7 . . . 144
4.17 CO, NO and C_3H_6 conversion compared to TME [2] for the global catalytic C_3H_6 step sub-mechanism - Test Case 8 . . . 145
4.18 CO, NO and C_3H_6 conversion compared to TME [2] for the global catalytic C_3H_6 step sub-mechanism - Test Case 9 . . . 146
4.19 CO, NO and C_3H_6 conversion compared to TME [2] for the global catalytic C_3H_6 step sub-mechanism - Test Case 1. Comparison of the $T_{q^v} = 298$ K with $T_{q^v} = 800$ K [14, 15], for the CO direct adsorption reaction. . . . 147
4.20 CO, NO and C_3H_6 conversion compared to TME [2] for the global C_3H_6 catalytic analysis step - Test Case 2. Comparison of the $T_{q^v} = 298$ K with $T_{q^v} = 800$ K [14, 15], for the CO direct adsorption reaction. . . . 148
4.21 CO, NO and C_3H_6 conversion compared to TME [2] for the global C_3H_6 catalytic analysis step - Test Case 3. Comparison of the $T_{q^v} = 298$ K with $T_{q^v} = 800$ K [14, 15], for the CO direct adsorption reaction. . . . 148
4.22 CO, NO and C_3H_6 conversion compared to TME [2] for the global C_3H_6 catalytic analysis step - Test Case 4. Comparison of the $T_{q^v} = 298$ K with $T_{q^v} = 800$ K [14, 15], for the CO direct adsorption reaction. . . . 149
4.23 CO, NO and C_3H_6 conversion compared to TME [2] for the global C_3H_6 catalytic analysis step - Test Case 6. Comparison of the $T_{q^v} = 298$ K with $T_{q^v} = 800$ K [14, 15], for the CO direct adsorption reaction. . . . 149
4.24 CO, NO and C_3H_6 conversion compared to TME [2] for the global C_3H_6 catalytic analysis step - Test Case 7. Comparison of the $T_{q^v} = 298$ K with $T_{q^v} = 800$ K [14, 15], for the CO direct adsorption reaction. . . . 150
4.25 CO, NO and C_3H_6 conversion compared to TME [2] for the global C_3H_6 catalytic analysis step - Test Case 8. Comparison of the $T_{q^v} = 298$ K with $T_{q^v} = 800$ K [14, 15], for the CO direct adsorption reaction. . . . 150
4.26 CO, NO and C_3H_6 conversion compared to TME [2] for the global C_3H_6 catalytic analysis step - Test Case 9. Comparison of the $T_{q^v} = 298$ K with $T_{q^v} = 800$ K [14, 15], for the CO direct adsorption reaction. . . . 151
4.27 Reaction pathway analysis of C_3H_6 on the surface . . . 152
4.28 CO, NO and C_3H_6 conversion for the detailed C_3H_6 catalytic chemistry compared to TME [2] - Test Case 1 . . . 152
4.29 CO, NO and C_3H_6 conversion for the detailed C_3H_6 catalytic chemistry compared to TME [2] - Test Case 2 . . . 153
4.30 CO, NO and C_3H_6 conversion for the detailed C_3H_6 catalytic chemistry compared to TME [2] - Test Case 3 . . . 153

4.31 CO, NO and C_3H_6 conversion for the detailed C_3H_6 catalytic chemistry compared to TME [2] - Test Case 4 154
4.32 CO, NO and C_3H_6 conversion for the detailed C_3H_6 catalytic chemistry compared to TME [2] - Test Case 5 154
4.33 CO, NO and C_3H_6 conversion for the detailed C_3H_6 catalytic chemistry compared to TME [2] - Test Case 6 155
4.34 CO, NO and C_3H_6 conversion for the detailed C_3H_6 catalytic chemistry compared to TME [2] - Test Case 7 155
4.35 CO, NO and C_3H_6 conversion for the detailed C_3H_6 catalytic chemistry compared to TME [2] - Test Case 8 156
4.36 CO, NO and C_3H_6 conversion for the detailed C_3H_6 catalytic chemistry compared to TME [2] - Test Case 9 156
4.37 Surface plots of NO_2 and HNO_2 concentrations obtained from the plug flow reactor model. 157
4.38 Surface plots of NO_2 and HNO_2 concentrations obtained from the plug flow reactor model. 158
4.39 Comparison of NO, NO_2, HNO_2, NO_3, HNO_3 concentrations against time. 160
4.40 Comparison of NO, NO_2, HNO_2, NO_3, HNO_3 mol fractions against temperature at the exit of the catalytic converter. 161
4.41 NO and NOx conversions compared to TME Test Case 5 161
4.42 CO, NO and C_3H_6 conversion compared to TME [2] - Test Case 1 - Consideration of metal dispersion. 162
4.43 CO, NO and C_3H_6 conversion compared to TME [2] - Test Case 5 - Consideration of metal dispersion. 163
4.44 CO, NO and C_3H_6 conversion compared to TME [2] - Test Case 9 - Consideration of metal dispersion. 164

5.1 Conversion of C_2H_6 and O_2 at the reactor outlet against the (O/C) feed ratio, at a low (θ = 12% [99]) and high (θ = 20% [100]) diffusion barrier, in the absence and presence of CO co-feed. Comparison with BP Chemicals [3] experimental data 171
5.2 Selectivity to C_2H_4 and CH_4 at the reactor outlet against the (O/C) feed ratio, at a low (θ = 12% [99]) and high (θ = 20% [100]) diffusion barrier, in the absence and presence of CO co-feed. Comparison with BP Chemicals [3] experimental data 172
5.3 Conversion of C_2H_6 and O_2 at the reactor outlet against the (O/C) feed ratio in the absence and presence of CO co-feed, for different efficiency factors. Comparison with BP Chemicals [3] experimental data 173
5.4 Selectivity to C_2H_4 and CH_4 at the reactor outlet against the (O/C) feed ratio in the absence and presence CO co-feed, for different efficiency factors. Comparison with BP Chemicals [3] experimental data 173
5.5 Conversion of C_2H_6 and O_2 at the reactor outlet against the (O/C) feed ratio, for H_2 mobile and immobile TS, in the absence and presence CO co-feed. Comparison with BP Chemicals [3] experimental data 174

5.6 Selectivity to C_2H_4 and CH_4 at the reactor outlet against the (O/C) feed ratio, for H_2 mobile and immobile TS, in the absence and presence CO co-feed. Comparison with BP Chemicals [3] experimental data 175
5.7 Reaction pathway analysis of CO on the surface, in presence of CO co-feed, at O/C = 0.525 176
5.8 Conversion of C_2H_6 and O_2 at the reactor outlet against the (O/C) feed ratio, for two different desorption energies of CO, in the absence and presence of CO co-feed. Comparison with BP Chemicals [3] experimental data . . 176
5.9 Reaction pathway analysis of C_2H_6 on the surface, in presence of CO co-feed, at O/C = 0.525 177
5.10 Selectivity to C_2H_4 and CH_4 at the reactor outlet against the (O/C) feed ratio, for two different desorption energies of CO, in the absence and presence co-feed. Comparison with BP Chemicals [3] experimental data . . . 178
5.11 Flow fields of C_2H_6, O_2, C_2H_4, CH_4 mol fractions at O/C = 0.525, in presence of CO co-feed. 179
5.12 Contour plots of temperature and velocity at O/C = 0.525, in presence of CO co-feed. 180
5.13 Wall and centerline reactor temperatures as a function of the (O/C) feed ratio in absence of CO co-feed. 181
5.14 Wall and centerline reactor temperatures as a function of the (O/C) feed ratio in presence of CO co-feed. 181

List of Tables

1.1 Five-step reaction mechanism for NO removal produced by Chatterjee et al. [1] . . . 35
1.2 Nitrogen containing reactions already proposed in previous studies [24, 25, 26, 27] . . . 36
1.3 Additional surface reaction that has to be considered . . . 36
1.4 Direct adsorption and desorption reactions studied and compared to experimental data, where available . . . 36

2.1 Diffusion coefficients applied in Chapter 4 . . . 54
2.2 Variation of the average Knudsen efficiency factor values with the temperature, for different Pt loadings. The values indicated in a bold font are applied in Chapter 4, apart from Section 4.3.4 which illustrates the effect of the different metal loadings. . . . 55
2.3 Binding configurations of NO, NO_2, N_2O, N_2, N, C_3H_6, C_3H_5, C_2H_5CH, C_2H_5C species . . . 62
2.4 UBI-QEP atomic binding energies of H, O, C, N . . . 64
2.5 Total bond energies of NO, NO_2, N_2O, N_2, N, C_3H_6, C_3H_5, C_2H_5CH, C_2H_5C species . . . 65
2.6 Heats of adsorption of NO, NO_2, N_2O, N_2, N, C_3H_6, C_3H_5, C_2H_5CH, C_2H_5C species on a platinum surface . . . 66
2.7 Heats of adsorptions for different molecular coordinations on the metal surface . . . 67
2.8 Comparison of UBI-QEP and VTST based activation energies . . . 73

3.1 List of reaction classes for determination of pre-exponential factors and activation energies . . . 97
3.2 Geometrical parameters of NO, NO_2, N_2O, N_2, N, C_3H_6, C_3H_5, C_2H_5CH, C_2H_5C attached on the metal surface . . . 99
3.3 Partition function dependency of exponent β . . . 99
3.4 Comparison of the equations of rate constants for different reaction classes and approaches . . . 101
3.5 Updated C_2H_4 direct adsorption reactions . . . 106

4.1 Initial mixture composition provided by TME [2] . . . 110
4.2 Experimental Conditions TME [2] . . . 110
4.3 Experimental TME measurements of pore distribution [2] . . . 111

4.4 Calculated porosities, tortuosities and site densities based on TME measurements [2] . . . 111
4.5 Calculated volumes, projected areas and number of Pt atoms for PGM particles based on TME measurements [2] . . . 112
4.6 Calculated loss of area and dispersion efficiency factor, at different Pt loadings. . . . 113
4.7 Calculated area ratios, considering the dispersion efficiency and 1.43 factors, at different Pt loadings and coat amounts. . . . 114
4.8 Calculated Knudsen efficiency factors, at different Pt loadings, via the geometrical [11] and Giani et al. [55] approach, at 600 K. . . . 115
4.9 Global catalytic C_3H_6 step sub-mechanism . . . 119
4.10 Detailed C_3H_6 surface reaction sub-mechanism . . . 120
4.11 Experimental Conditions TME [2] - Test Case 5 . . . 122
4.12 Experimental Conditions TME [2] - Test Case 1 . . . 132
4.13 Experimental Conditions TME [2] - Test Case 2 . . . 133
4.14 Experimental Conditions TME [2] - Test Case 3 . . . 134
4.15 Experimental Conditions TME [2] - Test Case 4 . . . 137
4.16 Experimental Conditions TME [2] - Test Case 5 . . . 138
4.17 Experimental Conditions TME [2] - Test Case 6 . . . 142
4.18 Experimental Conditions TME [2] - Test Case 7 . . . 144
4.19 Experimental Conditions TME [2] - Test Case 8 . . . 145
4.20 Experimental Conditions TME [2] - Test Case 9 . . . 146
4.21 Gas phase reactions describing the NO conversion to NO_2 and HNO_2. . . . 159
4.22 Application of a constant area ratio, at different Pt loadings and coat amounts, considering the dispersion efficiency factor. . . . 164

5.1 Experimental Conditions BP Chemicals [3] . . . 168
5.2 Initial mixture composition provided by BP Chemicals [3] . . . 168

A.1 Surface reaction mechanism corresponding to $\theta = 12\%$ [99] of the magnitude of $Q_{C,H,O,N}$. The global catalytic C_3H_6 step sub-mechanism is considered. . . . 203
A.2 Surface reaction mechanism corresponding to $\theta = 20\%$ [100] of the magnitude of $Q_{C,H,O,N}$. The global catalytic C_3H_6 step sub-mechanism is considered. . . . 216
A.3 Detailed C_3H_6 reaction sub-mechanism corresponding to $\theta = 12\%$ [99] of the magnitude of $Q_{C,H,O,N}$. . . . 229
A.4 Detailed C_3H_6 reaction sub-mechanism corresponding to $\theta = 20\%$ [100] of the magnitude of $Q_{C,H,O,N}$. . . . 230

C.1 Gas phase mechanism (C_1 - C_2 - C_3) implemented in Chapters 4 and 5. . . . 244
C.2 Modified collision dependencies . . . 255
C.3 Fall-off parameters . . . 255
C.4 Additional gas phase mechanism (-N) implemented in Chapter 4. . . . 256
C.5 Modified collision dependencies . . . 260
C.6 Fall-off parameters . . . 260

C.7 Additional gas phase mechanism (-C_4) implemented in Chapter 5 260
C.8 Modified collision dependencies 266
C.9 Fall-off parameters 266

D.1 Gas phase (C_1 - C_2 - C_3) transport properties implemented in Chapters 4 and 5 267
D.2 Additional gas phase (-N) transport properties implemented in Chapter 4 270
D.3 Additional gas phase (-C_4) transport properties implemented in Chapter 5 271
D.4 Gas phase thermochemical properties implemented in Chapters 4 and 5 . 272
D.5 Additional gas phase thermochemical properties implemented in Chapter 4 283
D.6 Additional gas phase thermochemical properties implemented in Chapter 5 287

E.1 Variation of the average Knudsen efficiency factor values with the temperature, for different Pt loadings. 293

Nomenclature

A	Arrhenius pre-exponential factor	[kmol, m, s]
$A_{B(s)_x}$	Projected surface area of species $B(s)_x$	[m^2]
A_{Mt}	Surface area of the catalytic site	[m^2 or $Å^2$]
$B_0[z]$	Zero-order Bessel function of the first kind	[-]
b	Nearest neighbour distance between surface atoms	[m]
C_p	Heat capacity at constant pressure	[kJ]
C_V	Heat capacity at constant volume	[kJ]
C_{int}	Heat capacity distribution from the internal energy	[-]
C_{trans}	Heat capacity distribution from translational modes	[-]
C_{rot}	Normalised heat capacity contribution from rotational modes	[-]
C_{vib}	Normalised heat capacity contribution from vibrational modes	[-]
C_i	Species conversion	[%]
D_{ij}	Diffusion coefficient for a mixture of two gases	[m^2/s]
D_i^{eff}	Average effective diffusivity	[m^2/s]
D_i^K	Knudsen diffusion in a cylindrical pore	[m^2/s]
$D^{K,eff}$	Average Knudsen effective diffusion coefficient	[m^2/s]
$\bar{D}_i^{eff}$	Diffusion coefficient - Bosanquet formula	[m^2/s]
E	Total bond energy	[kJ/mol]
E_{AA}	Bond energy of homonuclear diatomic molecule AA	[kJ/mol]
E_{AB}	Bond energy of diatomic molecule AB	[kJ/mol]
E_R	Bond energy of reactants	[kJ/mol]
E_P	Bond energy of products	[kJ/mol]
E_A	Activation energy (reaction barrier)	[kJ/mol]
$E_{A,diff}$	Activation energy corrected for surface diffusion	[kJ/mol]
$E_{A,g}$	Gas phase isomerisation barrier	[kJ/mol]
$E_{A,s}$	Surface activation barrier	[kJ/mol]
$E_{A,s}^f$	Forward surface activation barrier	[kJ/mol]
$E_{A,s}^r$	Reverse surface activation barrier	[kJ/mol]
E_{diff}	Diffusion reaction barrier	[kJ/mol]
$E_{R,diff}$	Diffusion barrier for each reactant species	[kJ/mol]
$E_{A_x}^t$	Translational energy barrier at x direction	[kJ/mol]
$E_{A_y}^t$	Translational energy barrier at y direction	[kJ/mol]
E_A^r	Rotational energy barrier	[kJ/mol]

F	Ratio of the catalytic active area over the geometrical area	[-]
H^0	Standard enthalpy	[kJ]
h	Plank constant	[J s]
h_i	Specific enthalpy of species i	[J/kg]
h_m	Mixture enthalpy	[J/kg]
I_a	Moment of inertia around axis a	[kg m^2]
J_i	Diffusive flux	[kmol m^{-2} s^{-1}]
K_{eq}	Equilibrium constant	[-]
k	Rate constant	[kmol,m,s]
k_B	Boltzmann constant	[J/K]
M_p	Maximum molar uptake of the catalyst	[kmol/kg]
$M_{w,i}$	Molecular weight of species i	[kg/kmol]
M_w	Mean molecular weight	[kg/kmol]
M_{red}	Reduced molecular weight of a reacting pair	[kg/kmol]
m^*	Effective mass of a reacting pair	[kg]
m	Number of equivalent minima in a full rotation	[-]
N_{sc}	Number of species on the surface	[-]
N_A	Avogadro's number	[mol^{-1}]
n^*	Inverse of the mean molecular weight	[kmol/kg]
n	Number of catalytic surface sites	[-]
$n'_{a,m}$	Number of atoms included in species m	[-]
n_{pf}	Number of atoms including maximum packing density	[-]
P	Pressure	[Pa]
Q_A	Heat of adsorption of species A	[kJ/mol]
Q_0	Atomic heat of adsorption	[kJ/mol]
Q_{A_2}	Heat of adsorption of a homonuclear diatomic molecule	[kJ/mol]
Q_{AB}	Heat of adsorption of a diatomic molecule AB	[kJ/mol]
Q_R	Heat of adsorption of reactants	[kJ/mol]
Q_P	Heat of adsorption of products	[kJ/mol]
Q_{red}	Reduced heat of adsorption of products	[kJ/mol]
Q_{TST}	Interpolated heat of adsorption	[kJ/mol]
Q	Overall molecular partition function	[m^{-2} or m^{-3}]
q^t	Translational partition function (1D, 2D, 3D)	[m^{-1} or m^{-2} or m^{-3}]
q^r	Rotational partition function	[-]
q^v	Vibrational partition function	[-]
q^e	Electronic partition function	[-]
q_{HO}	Harmonic oscillator partition function	[-]
R	Universal gas constant	[J K^{-1} mol^{-1}]
R_i	Net rate of formation of species i	[reaction dependent]
R_j^f	Rate of reaction j	[reaction dependent]
r_R	Molecular radius of species R	[m]
r_p	Pore radius	[m]

r_{Pt}	Radius of Pt atom	[m or Å]
S^0	Standard entropy	[kJ]
$S^a_{i,k}$	Selectivity of atoms a of species i towards species (products) k	[%]
S_v	Specific surface area per total volume	[1/m]
S_m	Specific surface area per total mass	[m^2/g]
s_0	Mobile sticking coefficient for adsorption reactions	[-]
$s_{0,I}$	Immobile sticking coefficient for adsorption reactions	[-]
T	Temperature	[K]
T_{adiab}	Adiabatic flame temperature of the inlet mixture	[K]
T_{q^v}	Temperature of the vibrational partition function	[K]
u	Velocity at axial direction	[m/s]
u_s	Stephan velocity	[m/s]
ν_{corr}	Hindered rotor correction to the vibrational partition function	[-]
v	Velocity at radial direction	[m/s]
v_c	Correction velocity (zero sum of fluxes at the cell interface)	[m/s]
ν_i	Vibrational frequencies	[s^{-1}]
x	Number of required reactant metal sites	[-]
$x(r)$	Bond index	[-]
$x_{AB,TS}$	Bond index of A-B adsorbate at the transition state	[-]
$[X_i^f]$	Gas phase concentration of species of species X_i	[kmol/m^3]
Y_i	Mass fraction of species i	[-]
$Y'_{a,m}$	Scaled mass fraction of atoms a included in species m	[-]
$[Z_i^f]$	Surface coverage of species i	[-]
Z_{rot}	Rotational collision number	[-]
Z_{vib}	Collision number for internal energy transfer	[-]
†	Transition state	

Greek symbols

β	Temperature dependency	[-]
Γ	Catalytic site density	[kmol/m^2]
Γ^*	Catalytic site density	[sites/m^2]
ΔE^{zp}	Zero-pont energy	[kJ/mol]
ΔG	Change in Gibbs free energy	[kJ/mol]
ΔH_s	Change in surface enthalpy of a reaction	[kJ/mol]
ΔH_s^r	Change in surface enthalpy of a reverse reaction	[kJ/mol]
$\Delta H^{\ddagger}$	Enthalpy of activation	[kJ/mol]
$\Delta S^{\ddagger}$	Entropy of activation	[kJ/mol]
ΔS_{vap}	Entropy of vaporization	[J K^{-1} mol^{-1}]
ΔT_g	Temperature difference between wall and gas	[K]
ΔT_w	Temperature difference between wall and bath	[K]

δ	Thermal de Broglie wavelength	[m]
ε_{LJ}	Depth of the Lennard-Jones potential well	[-]
η_D	Dispersion efficiency factor	[-]
η_e	Efficiency factor of surface reactions	[-]
θ	Percentage of the heat of adsorption magnitude of chemisorbed species	[-]
κ_1	Conductive heat transfer factor	[-]
κ_2	Radiative heat loss	[-]
λ_g	Thermal conductivity of gas mixture	[K m W^{-}1]
λ_w	Thermal conductivity of the wall	[K m W^{-}1]
μ_i	Viscosity of species i	[Pa s]
ξ_i	Mass flow of species i	[kg/s]
ρ	Fluid density	[kg/m^3]
ρ_s	Average density of the catalyst	[kg/m^3]
σ^*	Collision diameter of gases i and j	[m]
σ	Rotational symmetry number	[-]
σ_{LJ}	Finite distance at which the inter-particle potential is zero	[-]
τ_g	Tortuosity	[-]
ϕ_g	Porosity	[-]
ψ	Scaling parameter of diffusion correction	[-]

Abbreviations

ATC	Auto-Thermal Cracking
BOC-MP	Bond Order Conversion - Morse Potential
CFD	Computational Fluid Dynamics
DFT	Density Functional Theory
HC	Hydrocarbons
LANL2DZ	Los Alamos National Laboratory 2-Double-Z
NO_x	Oxides of nitrogen
O/C	Oxygen to Carbon feed ratio
PES	Potential Energy Surface
PGM	Platinum Group Metal
SCR	Selective Catalytic Reduction
SCTR	Short Contact Time Reactors
SNCR	Selective non Catalytic Reduction
SDD	Struttgart-Dresden
TME	Toyota Motor Europe
TST	Transition State Theory
TWC	Three Way Catalysts
UBI-QEP	Unity Bond Index-Quadratic Exponential Potential
VTST	Variational Transition State Theory

Chapter 1

Introduction

In this Chapter, the background and motivation of the research presented in this dissertation are given. The fundamentals on the exhaust gas pollutants and the reaction mechanisms for the heterogeneous catalytic removal of oxides of nitrogen along with the auto-thermal cracking (ATC) catalytic process for olefins production are reported in the literature review. Then, the contribution of the current investigation and the structure of the thesis, are outlined.

1.1 Background and motivation

The continuous quest for improvements in vehicle efficiency leads to a requirement of careful control of combustion processes for reliable and stable operation - be it in a conventional or hybrid configuration. Therefore, a proper understanding of the effects of heterogeneous chemistry interactions can be expected to support the development of better technologies. The field of surface chemistry constitutes an area of significant scientific interest to the design of internal combustion engines, and is of particular importance to the fields of catalysis, electrochemistry and geochemistry.

A catalyst is a compound that affects the rate of reaction without itself being consumed in the progress [4]. The key concept of catalysis is thus that the reactants associate with the catalytic material, undergo a chemical transformation and finally dissociate from the catalyst. Although, there are different kinds of catalysts, the main focus of the current work is based on heterogeneous catalysts and the corresponding gas-surface kinetics. A heterogeneous catalyst can be envisioned as a relatively large extended surface composed

of active sites, that are local positions on which a molecule can adsorb, react and finally desorb. Well-defined single crystal surfaces of catalytically active materials (e.g. Pt, Rh, Pd) find wide-spread application in a number of industrial processes (e.g. development of battery technologies), as well as in exhaust emission control devices (e.g. catalytic converters) for the purification of exhaust gases from the internal combustion engines.

It is well known that combustion engines are a significant source of harmful pollutants. Gasoline represents an indicative paradigm as it consists of hydrocarbons containing approximately 45% alkenes and alkynes, 35% aromatic compounds and 20% butanes and pentanes [5]. Consequently, the understanding of chemical kinetic mechanisms that take place on metal surfaces and the development of computational models are of vital importance for improving the efficiency of industrial catalytic processes and reducing harmful gaseous emissions from exhaust pipes. Accurate and predictive models can prevent from the high experimental cost, the material placement and the catalyst aging.

A microscopic picture of kinetics in terms of molecular level properties can be illustrated by two important theories, collision theory and Variational Transition State Theory (VTST). According to collision theory, the reacting species are assumed to be hard spheres that collide with each other in order to allow a reaction to occur. This can be realized if the chemical species that collide, possess a certain minimum value of internal energy, equal to the activation energy of the reaction. The number of collisions occuring for the products' formation per second per unit volume can be expressed through the collision frequency. In adsorption processes, the rate constants are calculated using sticking coefficients, s_0, that describe the ratio of the number of adsorbate atoms on the metal surface to the total number of atoms that collide with the metal sites. Their value varies between 1 (all impinging atoms stick) and 0 (no atoms stick). The coefficient can be a function of surface temperature, surface coverage (θ) and structural details. When arriving at a site on a surface, an adatom has three options. There is a probability that it will adsorb to the surface (P_a), a probability that it will migrate to another site on the surface (P_m), and a probability that it will desorb and return to the bulk gas (P_d). For an empty site ($\theta = 0$) the sum of these three options is unity: $P_a + P_m + P_d = 1$.

As the accurate determination of sticking coefficients is a time consuming process that requires an experimental investigation, the introduction of a theoretical method able to predict chemical reaction rates and mechanisms is of a significant importance. Variational

Transition State Theory (VTST) is here used for this purpose, as a more accurate form of the Transition State Theory (TST). The TST applies statistical thermodynamics to derive expressions for rate coefficients, through the Eyring equation [6],

$$k = \frac{k_B T}{h} e^{\frac{\Delta S^{\ddagger}}{R}} e^{-\frac{\Delta H^{\ddagger}}{RT}} \tag{1.1}$$

where k is the reaction rate constant, T is the absolute temperature, k_B is Boltzmann's constant, h is Planck's constant, $\Delta H^{\ddagger}$ is the enthalpy of activation, R is the gas constant, and $\Delta S^{\ddagger}$ is the entropy of activation. As the change of the Gibbs free energy, $\Delta G = \Delta H - T\,\Delta S$, is related to the molecular partition function, Q, the Eyring equation can be replaced by the Arrhenius equation, leading to Eq. (1.2),

$$k = \frac{k_B T}{h} \frac{Q_{\ddagger}}{Q_{reac}} e^{-\frac{E_A}{RT}} \tag{1.2}$$

with $Q_{\ddagger}$ and Q_{reac} being the partition functions of the transition state and the reactant phase, respectively and E_A the activation energy. Therefore, molecular partition functions, that describe the sum of all possible energy states in the various degrees of freedom of a molecule, are directly applied for the evaluation of reaction rate constants, instead of experimental based sticking coefficients.

Detailed microkinetic modelling enables a description of the chemical kinetics dominating a studied system and becomes the method of choice for heterogeneous systems due to its potential to complement and generalize experimental findings. The coupling of a computational fluid dynamics (CFD) framework with detailed microkinetic analysis explores the interactions of the fluid flow with the chemistry of the system. Microkinetic models for heterogeneous reactions in the low coverage limit typically use the extended Arrhenius form ($k = AT^{\beta}e^{-E_A/RT}$) to express reaction rates, where A is the pre-exponential factor, β the temperature dependency, E_A the activation energy and R the gas constant. Accordingly, the three terms A, β and E_A must be determined. The latter can, for example, be obtained using Density Functional Theory (DFT) [7, 8, 9] or via semi-empirical methods such as the Unity Bond Index-Quadratic Exponential Potential (UBI-QEP) method [10].

Vincent et al. [11] established a consistent class based method to investigate the production of ethylene through the selective dehydrogenation of ethane in short contact time

reactors (SCTR) featuring a supported platinum catalyst. The study also suggested that altering gas phase conditions can result in ethylene consumption, leading to methane and carbon deposition. The gas phase chemistry used was developed by Lindstedt and co-workers [12, 13]. The estimation of chemisorption energetics and surface reactivity was based on the UBI-QEP formalism, integrated with DFT and experimental values for a limited number of species [11]. The rate constants were determined using collision theory with experimentally derived or estimated sticking coefficients. Kraus and Lindstedt [14, 15] introduced a theoretical framework for the determination of direct adsorption and desorption rate constants, without any dependency on experimental values, through an innovative application of Variational Transition State theory (VTST). It has been shown [11, 14, 15] that both systematic approaches can reproduce complex partial oxidation data over transition metals such as Pt and Rh.

The aim of the current investigation is to (i) develop a comprehensive C/H/O/N reaction mechanism, by further extending the pre-existing reaction schemes [11, 14, 15] for the removal of all major oxides of nitrogen via the contribution of Pt calalysts supported by Al_2O_3 foams (Pt/Al_2O_3), at nearly stoichiometric conditions and low temperatures (400 K - 800 K) and (ii) implement the C/H/O reaction mechanism on Pt/Al_2O_3 catalysts for the investigation of the effect of CO co-feed on the performance of an auto-thermal catalytic cracking reactor, under fuel rich conditions and a higher temperature window (844 K - 1300 K). The applied mechanism developed using VTST, follows the Kraus and Lindstedt [14, 15] framework, in conjuction with some assumptions [16] and modifications for particularly sensitive reactions in order to better reproduce the chemical system. Platinum can be used both as a reduction and oxidation catalyst and its choice was made based on the comparatively comprehensive studies and experimental data available for validation.

1.2 Literature review

1.2.1 NO_x removal from automotive exhaust gases

Environmental studies related to air pollution have indicated that certain constituents (e.g. hydrocarbons (HC) and oxides of nitrogen (NO_x)) in automotive exhaust gases play

an important role in the formation of photochemical smog, acid rain and ground-level ozone precursors [17]. As the oxides of nitrogen originate from the combustion processes taking place in vehicles, their minimization is of paramount significance from biological and ecological point of view.

Catalytic converters, containing noble metals (platinum, palladium, rhodium, gold, silver) or base metals (nickel, zinc, iron etc) and coated on to a porous medium in order to broaden the chemically active surface, are used to control harmful emissions. Three way catalysts (TWC) were firstly installed in 1979 [5] and their latest generation seems to perform quite well under stoichiometric conditions. For example, the conversion of NO_x to N_2 is very effective by using a TWC for a stoichiometric gasoline engine, while for lean-burn engines and diesel engines is not so effective due to the exhaust gas composition and/or temperature. For example, unburned hydrocarbons (HCs) prefer to unfavourably oxidise with a large oxygen content in the exhaust rather than reduce NO_x to N_2 [18].

Several experimental studies have investigated the effect of platinum catalysts on the reduction of NO_x emissions along with the existance of a reductant (e.g. ammonia, oxygenated hydrocarbon, hydrocarbon), through the method of Selective Catalytic Reduction (SCR). The SCR system can use an external hydrocarbon (HC) as reductant by injection, or a HC emitted by the combustion engine. Kumar et al. [19] studied the suitability of cordierite/Pt catalyst for light and medium duty vehicles, as well as, the effect of selective catalytic reduction on bio-diesel blends in order to reduce the oxides of nitrogen in a single cylinder diesel engine. A maximum NO_x and NH_3 conversion of 60% and 34%, respectively, was found.

Selective catalytic reduction of NO_x emissions from diesel engines in the presence of hydrocarbons over Ag-Pt/Al_2O_3 catalysts, have been explored by Resitoglu et al. [20], at different engine loads and exhaust gas temperatures, under actual operating conditions. It was concluded that a HC reductant consisting of 15% biodiesel and 85% ethanol had the highest conversion performance. A study of catalytic removal of nitric oxide with hydrogen and carbon monoxide in the presence of excess oxygen was conducted by Yokota et al. [21]. The Pt/zeolite catalyst used, presented a high NO_x conversion efficiency, but the strong poisoning by CO and C_3H_6, as well as the formation of N_2O by NO_x were reported as significant disadvantages. Thus, an improved type of catalyst, Pt-Mo-$NaSiO_2$, was introduced, with a higher temperature range for NO_x conversion and a

lower N_2O formation obtained. As illustrated above, numerous research developments have been made to achieve desirable conversion rates in NO_x emissions through the use of HC reductants along with different types of platinum catalysts in order to eliminate the critical pollutants.

1.2.2 Reaction mechanisms for the heterogeneous catalytic removal of nitrogen oxides

Despite the relative wealth of studies of nitrogen containing species interacting with catalytic Pt sites, detailed microkinetic models for the removal of oxides of nitrogen from exhaust gases over Pt remain incomplete. Chatterjee et al. [1] produced a reaction mechanism for NO removal in a three-way catalyst based on five reaction steps using a collision theory based approach [22]. The s appearing in the reactions below denotes the catalyst site.

Table 1.1: Five-step reaction mechanism for NO removal produced by Chatterjee et al. [1].

No.	Reactions
1	$NO(g) + s \rightarrow NO(s)$
2	$NO(s) \rightarrow NO(g) + s$
3	$N(s) + N(s) \rightarrow N_2(g) + 2s$
4	$NO(s) + s \rightarrow N(s) + O(s)$
5	$N(s) + O(s) \rightarrow NO(s) + s$

A similar reaction mechanism was proposed for NO reduction over Rh. Despite the simplicity, encouraging agreement with experimental data was obtained. More recent studies, including the review by Sun et al. [23] covering a wider range of materials for the catalytic decomposition of NO to N_2 and O_2 outlines the need to consider additional NO_2 and N_2O reaction pathways. However, the proposed reactions were schematic in nature (reaction rate parameters were not determined) and hence not developed with microkinetic modelling in mind. The issue is, however, important as competitive oxidative pathways for NO may lead to NO_2 and N_2O formation. Furthermore, additional surface reactions were proposed leading to the need to consider associated reactions.

The inclusion of such reaction steps describing the catalytic oxidation of NO to NO_2 and N_2O is arguably essential as combinations such as Pt/Al_2O_3 can be used for nitric acid production [24]. There are also studies that outline the reaction of NO and O_2 to NO_2 over Pt in the context of reaction pathways as well as catalyst deactivation [25]. Studies of NO over Pt(111) are more plentiful and include data on adsorption and desorption [26]. At temperatures above 400 K, the dissociative adsorption of NO_2 (9) is more likely to occur [27]. In addition, the reverse reactions of reaction steps (7) and (8) need to be considered along with the direct adsorption of N_2O on the surface. Further surface reactions, such as reaction (10) below, are required. Data on the adsorption of N_2O on Pt(111) are also available [28].

Table 1.2: Nitrogen containing reactions already proposed in previous studies [24, 25, 26, 27].

No.	Reactions
6	$NO(s) + NO(s) \rightleftharpoons O(s) + N_2O(s)$
7	$N_2O(s) \rightleftharpoons N_2(g) + O(s)$
8	$NO_2(g) + s \rightleftharpoons NO_2(s)$
9	$NO_2(g) + 2s \rightleftharpoons NO(s) + O(s)$

Table 1.3: Additional surface reaction that has to be considered.

No.	Reaction
10	$NO(s) + O(s) \rightleftharpoons N_2O(s) + s$

Table 1.4: Direct adsorption and desorption reactions studied and compared to experimental data, where available.

Reactions
$NO(g) + 3s \rightleftharpoons NO(s_3)$
$NO_2(g) + s \rightleftharpoons NO_2(s)$
$N_2(g) + 2s \rightleftharpoons N_2(s_2)$
$N_2O(g) + 2s \rightleftharpoons N_2O(s_2)$
$N(g) + s \rightleftharpoons N(s)$

In the current Thesis, the above direct adsorption and desorption reactions are studied with results compared to experimental data, where available, as presented in Chapter 3. The additional nitrogen containing surface reactions, outlined above, are included along with the additional chemical pathways that need to be considered due to the inclusion of all major oxides of nitrogen in the mechanism. The applied surface configurations of adsorbed nitrogen based species have been informed by the VTST computations outlined below and the related literature data.

1.2.3 Auto-thermal catalytic cracking for olefins production

Steam cracking is a process of decomposition of higher molecular weight organic compounds into smaller molecular fragments by imposing high temperature and, industrially, high pressure. This process is a non-catalytic, thermal cracking process for the production of light olefins (e.g. ethylene, propylene), performed in the presence of steam at high temperatures (700°C - 950°C) and short residence times, ranging from a few seconds to a fraction of a second. More than 150 million metric tons of ethylene and propylene are annually worldwide produced via the steam thermal cracking process [29]. Ethylene is typically produced by steam cracking of ethane leading to 60% ethane conversion and 85% ethylene selectivity at high temperatures of approximately 800°C, to provoke the following homogeneous pyrolysis reaction [30].

$$C_2H_6 \rightarrow C_2H_4 + H_2$$

The major disadvantages of the steam cracking process is the formation of coke deposits on the tube walls and the high energy consumption. Although the presence of steam reduces the carbon formation, the periodic shutting down of the reactor results in a loss of productivity [30].

The presence of a catalyst allows the dehydrogenation process to be carried out at lower pressures and temperatures (550°C), as well as provides a higher selectivity towards a single olefin [30]. The use of short contact time reactors (SCTRs) enables the production of comparable results to the steam cracking, with a high resistance to coking [22]. Schmidt and co-workers [31, 32, 33] produced competitive selectivity and conversion rates through the use of Pt/Sn for SCTRs, compared with the conventional steam crackers. They also

outlined that the oxidative dehydrogenation processes of alkanes occured in SCTRs have residence times between 10^{-1} s and 10^{-4} s.

A theoretical framework for investigations of SCTRs was established by Deutschmann and co-workers [34, 35], by applying a 2D elliptic model with laminar flow and heterogeneous chemistry featuring a noble metal coated monolith. Vincent et al. [11] developed and applied a semi-automatic class-based framework for generating reaction mechanisms to the study of the ethane dehydrogenation over alumina supported platinum catalyst in SCTRs. Different inlet velocities, reactor lengths and catalytic loadings were studied [11, 36].

Bodke et al. [30] emphasized that the addition of hydrogen to the feed stream, in a 2:1 H_2:O_2 (v/v) ratio, favored the ethylene selectivity by diverting the oxygen to water vapour formation and consequently, reduce the alkanes oxidation. The same amount of hydrogen co-feed was used in the BP Chemicals [3] experimental study on auto-thermal catalytic cracking of ethane over a 3% Pt/Al_2O_3 catalyst in a quartz lined tubular reactor, presented in Chapter 5.

1.3 Current contribution

The current study addresses a detailed microkinetic analysis of reactions in the C/H/O/N chemical system over platinum. In particular, it proposes a model for multi-scale simulations of nitrogen oxides removal from automotive exhaust gases through the use of supported platinum catalysts. A large number of existing studies in the broader literature have examined the interactions of nitrogen containing species with catalytic platinum sites. However, detailed microkinetic models for the removal of oxides of nitrogen from exhaust gases over platinum remain incomplete. Additionally, the C/H/O reaction mechanism on Pt/Al_2O_3 is also examined and validated via experimental data at different stoichiometric conditions and temperature ranges aiming to further establish the performance and functionality of the mechanism.

The basis of the work is the model produced by Kraus and Lindstedt [14, 15] who developed a systematic and theoretical framework through the use of VTST for the determination of rate constants for adsorption reactions. In particular, use of VTST for rate constant evaluation was applied for the $C_2H_6/H_2/O_2/Pt$ system to investigate of the

partial oxidation of ethane over platinum and methane over platinum and rhodium. This work extends the model proposed by Kraus and Lindstedt [14, 15] by augmenting the reaction mechanism and altering the evaluating method applied to adsorption reactions. At the same time, it focuses on the heterogeneous catalytic removal of oxides of nitrogen. A further analysis of related sticking coefficient data is also presented. The reference five-step state-of-the-art platinum catalytic mechanism, developed by Chatterjee et al. [1], for NO removal via three-way catalysts has been updated to 21 reversible reaction steps featuring all principle oxides of nitrogen. A detailed investigation on the significant impact of the diffusion transport limitations in porous media was also conducted.

Data regarding the CO, NO and C_3H_6 conversion against temperature was provided by Toyota Motor Europe [2] for nine different test cases, for this purpose. The datasets contain experimental results at different platinum loading configurations and Al_2O_3 dispersions. Furthermore, experimental data for auto-thermal cracking of ethane were offered by BP Chemicals [3] to explore the impact of CO co-feed on the ATC reactor efficiency. This data was used in the development and validation of the updated model for the examination of ethane/oxygen conversion and methane/ethylene selectivity against oxygen to carbon (O/C) feed ratio. The current investigation further extends the temperature window applied, compared to that corresponding to the NOx removal from automotive exhaust gases. The outcome also ensures the consistency of the proposed reaction mechanism and its capability to be successfully reproduced under different (more extreme) conditions.

Thus, this study refines the pre-existing VTST based framework [14, 15] by including some modifications/assumptions that better determine the adsorption rate constants and consequently, better describe the behaviour of the studied chemical system. Hence, the Thesis presents a step towards developing a robust methodology for catalytic systems. The production of a validated reaction mechanism, capable of predicting the chemical evolution of catalytic heterogeneous systems and removing harmful exhaust gases, can offer a better insight of the catalytic reduction mechanisms and set the basis for the continued extension of the model to other supported catalysts, such as rhodium and palladium.

1.4 Thesis outline

In Chapter 1, the background and motivation of this PhD Thesis are presented. A representative literature review on nitrous oxide removal from automotive exhaust gases, along with the heterogeneous catalytic reaction mechanisms developed for this purpose, is presented. The auto-thermal catalytic cracking process for olefin production was also reviewed. Subsequently, the current contribution and the thesis outline are presented.

In Chapter 2, the theoretical framework and, in particular, the computational and mathematical modelling are introduced along with the gas phase and the catalytic chemical mechanisms. The impact of diffusion transport limitations on the metal surface is also discussed. Finally, the methods for the determination of the pre-exponential Arrhenius factors and activation energies are outlined.

Chapter 3 is concerned with the rate parameter determination of direct, dissociative and Eley-Rideal adsorption reactions. The investigation of mobile or immobile transition state of the adsorbing species on the platinum surface, through the evaluation of the corresponding sticking coefficients, constitutes a core contribution of this study. At the end of this chapter, a comparison of the proposed mechanism with previously developed reaction frameworks [11, 14, 15] is presented.

Chapter 4 is devoted to a rigorous comparison of the developed mechanism with experimental data provided by Toyota Motor Europe (TME) [2] for CO, NO and C_3H_6 conversion against temperature, for nine different test cases. A multi-scale simulation was performed for the removal of harmful constituents from the automotive exhaust gases, through the use of Pt/Al_2O_3 catalyst, at different metal loadings and coat amounts. The impact of diffusion limitations is also discussed.

In Chapter 5, the heterogeneous platinum mechanism outlined in Chapter 4, without the inclusion of nitrogen and propene catalytic reactions, is applied to simulate the auto-thermal catalytic cracking of ethane over a 3% Pt/Al_2O_3 catalyst in a quartz lined tubular reactor at different stoichiometric conditions and temperature ranges compared to the corresponding ones used in Chapter 4. According to the experimental data provided by BP Chemicals [3], carbon monoxide was added to the auto-thermal cracking reactor aiming to explore the degree of catalytic contamination. The case of the absence of CO co-feed was also compared to the corresponding experimental data [3].

Finally, in Chapter 6 the thesis concludes with a summary of the critical findings of the present work and suggestions regarding future research directions.

Chapter 2

Theoretical framework

This Chapter outlines the computational and mathematical modelling which constitutes a further extension of the pre-existing contributions [11, 14, 15]. Firstly, the physical framework is presented, along with the corresponding properties, equations and assumptions. A detailed description on the diffusion mechanisms applied in the current work is also included. Subsequently, the gas-phase and catalytic chemistries are analysed, as the two foundations of this investigation. Finally, the methods for the determination of the pre-exponential Arrhenius factors, derived from partition functions, and the energetics used for the chemical kinetic model, are illustrated.

2.1 Computational methods

A 2D parabolic FORTRAN code [12] was used to simulate a single, virtual, representative axisymmetric or planar pore [11] corresponding to the experimental device. This reduction of the simulation domain to a representative pore, allows for simpler modelling and faster computations. As shown in Fig. 2.1, the pore is typically simulated as a cylindrical channel divided into three different sections. The first corresponds to the inert section that is typically not included in the simulations, if appropriate initial conditions are available. The second refers to the catalytic section and its support of Al_2O_3, which is the main focus of the current thesis. In this section, the gas-phase chemistry is coupled with the surface chemistry, while the third section of the pore belongs to the outflow, where only gas-phase reactions occur.

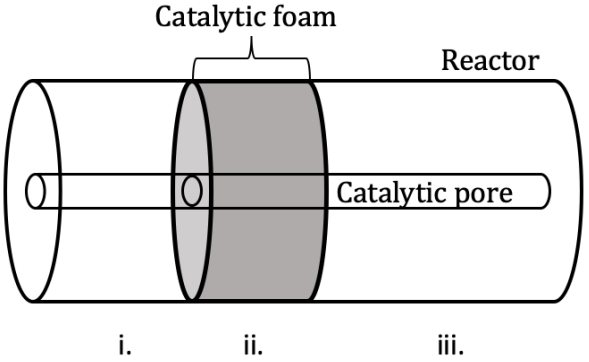


Fig. 2.1: Schematic of a catalytic pore inside the reactor: i. Inert section, ii. Catalytic section, iii. Gas-phase section

As the pores were approximated by a cylindrical or planar (r=1) geometry, the flow field has been processed by the two-dimensional boundary layer equations, as implemented by Vincent et al. [11]. The following differential equations concern the conservation of mass, momentum, species and enthalpy with Eq. (2.5) expressing the mass fluxes for the axi-symmetric geometry.

$$\frac{\partial(\rho u)}{\partial x} + \frac{1}{r}\frac{\partial(r\rho v)}{\partial r} = 0 \tag{2.1}$$

$$\rho u\frac{\partial Y_i}{\partial x} + \rho v\frac{\partial Y_i}{\partial r} = -\frac{1}{r}\frac{\partial(rJ_i)}{\partial r} + M_{w,i}R_i \tag{2.2}$$

$$\rho u\frac{\partial u}{\partial x} + \rho v\frac{\partial u}{\partial r} = -\frac{\partial P}{\partial x} + \frac{1}{r}\frac{\partial}{\partial r}\left(r\mu\frac{\partial u}{\partial r}\right) \tag{2.3}$$

$$\rho u\frac{\partial h_m}{\partial x} + \rho v\frac{\partial h_m}{\partial r} = \frac{1}{r}\frac{\partial}{\partial r}\left(\frac{\lambda_g}{C_p}r\frac{\partial h_m}{\partial r}\right) + \frac{1}{r}\frac{\partial}{\partial r}\left[\sum_{i=1}^{N_g} h_i r\left(-J_i - \frac{\lambda_g}{C_p}\frac{\partial Y_i}{\partial r}\right)\right] \tag{2.4}$$

$$-J_i = \rho D_i\left(\frac{\partial Y_i}{\partial r} - Y_i\frac{1}{n^*}\frac{\partial n^*}{\partial r}\right) - \rho v_c Y_i \tag{2.5}$$

In the above equations, x and r are, the axial and radial coordinates, respectively. Similarly, u, v are the components of velocity for axial and radial direction, while ρ is the density of the fluid, h_m is the enthalpy of the mixture, C_p is the specific heat capacity at constant pressure, μ is the viscosity, λ_g is the thermal conductivity, n^* is the inverse of the mean molecular weight and P is the pressure. The gas phase mass fractions are denoted by Y_i. The species are characterized by their respective enthalpy h_i, molar mass $M_{w,i}$, diffusion coefficients D_i, diffusive flux J_i and net rate of formation R_i. Finally, the

term v_c is a correction velocity chosen so that the sum of all fluxes is zero at the cell interfaces.

The system of boundary layer equations described above depends on the assumption that the axial dimension of the flow field is substantially larger than the radial. Thus, the viscous forces of the boundary layer are dominant within the narrow radial direction of the flow. Additionally, the axial velocity within the flow is of the order of the free stream velocity, while a non-slip condition (zero fluid velocity relative to the boundary) is applied at the wall.

The axial diffusive fluxes diminish compared to the radial diffusive flux and convective transport, while the radial momentum equation neglects pressure variations along the (narrow) pore radius. These approximations determine a transition from an elliptic to a parabolic set of equations which entails a much simpler algorithm.

Raja et al. [37] discuss the case of applying this method by comparing it, in a catalytic monolith channel simulation, to a full set of Navier-Stokes equations and a plug-flow approximation in which axial diffusive terms are omitted. It was concluded that the boundary layer approximation provides a much reduced computational cost compared to the Navier-Stokes simulations and greater applicability, in terms of Reynolds number range, than the plug flow model. The boundary layer equations are thus considered appropriate for work in the porous foam.

Summarizing, the main disadvantage with the parabolic approach is that it does not account for heat transfer flow back upstream inside the support material as it is a down-stream marching computation. On the other hand, an advantage with the approach is that the detailed gas and catalytic surface chemistry can be applied with reasonable computational expense along with good grid resolution along the wall.

The surface chemistry is balanced with the gas phase chemistry through the Eq. (2.6),

$$J_i + \rho Y_i u_s = \eta_e \bar{R}_i M_{w,i} \tag{2.6}$$

where the $J_i + \rho Y_i u_s$ term represents the flow of each gas phase species i at the gas-wall interface, while the $\eta_e \bar{R}_i M_{w,i}$ term is the mass-weighted production rate of i at the

catalytic wall. The Stefan velocity u_s is defined as,

$$u_s = \frac{1}{\rho} \sum^{i \to N_s} \bar{R}_i M_{w,i} \quad \left[\frac{\mathrm{m}}{\mathrm{s}}\right] \tag{2.7}$$

The efficiency factor η_e accounts for diffusion limitations, as shown in Section 2.3.2, and can be determined according to the size of the pores given by available experimental data, or based on values already used in the literature. The sensitivity was previously studied for values in the range $0.1 \leq \eta_e \leq 0.4$ (e.g. [11, 14, 15]). In general, on metal monolayer surfaces without a microporous structure $\eta_e = 1$. Concerning the modeling of the relevant computational domains, 40 geometrically radial cells, refined in the proximity of the wall, are used in the simulations. Every NMESH* timesteps the code performs an advanced adaptive remeshing of the grid structure. This is based on the local value of the fluid flux and allows for improved numerical stability. The typical size of the grid mesh width varies typically from about 2 μm to 20 μm. In cases where the wall and exit temperatures are not known, the energy balance at the wall, for both gas phase species, N_g and surface species, N_s, can be calculated from Eq. (2.8),

$$\lambda_g \Delta T_g - \sum^{i \to N_s} \left(J_i + \rho Y_i u_s\right) h_i = \lambda_w \kappa_1 \Delta T_w - \sum^{i \to N_s + N_g} \bar{R}_i M_{w,i} h_i, \tag{2.8}$$

where the $\lambda_g \Delta T_g$ and the $\lambda_w \kappa_1 \Delta T_w$ correspond to the heat transfer from the wall to the gas phase and from the bath (environment) to the wall, respectively. The thermal conductivities λ_g and λ_w, as well as, the κ_1 were treated as by Vincent et al. [11]. More specifically, κ_1 depends on the direction of heat transfer at the bath-wall interface, with $\kappa_1 = 1$ if $\Delta T_w \leq 0$, otherwise $\kappa_1 = 0$ [11].

Finally, the catalytic site density Γ and the radiative heat loss factor κ_2 were adjusted according to the case examined. The radiative heat loss κ_2 typically ranges from 0 to 0.15 and can be introduced in the system, for each cell, via Eq. (2.9),

$$T = T_{adiab} \left(1 - \kappa_2 \left(\frac{T_{adiab}}{T'_{adiab}}\right)^4\right), \tag{2.9}$$

*typically NMESH=50

where T'_{adiab} is the maximum value of the adiabatic temperature for the reactant mixture concerned assuming chemical equilibrium [38].

2.2 Thermodynamic properties

The required thermodynamic properties describing the elementary chemical reactions and species are the specific heat capacities C_p, the enthalpies H and the entropies S. Their evaluation is based on the use of the standard seven coefficient JANAF polynomials [39] using the following temperature dependent formulas:

$$\frac{C_p}{R} = a_1 + a_2 T + a_3 T^2 + a_4 T^3 + a_5 T^4 \tag{2.10}$$

$$\frac{H^0}{RT} = a_1 + \frac{a_2}{2} T + \frac{a_3}{3} T^2 + \frac{a_4}{4} T^3 + \frac{a_5}{5} T^4 + \frac{a_6}{T} \tag{2.11}$$

$$\frac{S^0}{R} = a_1 \ln T + a_2 T + \frac{a_3}{2} T^2 + \frac{a_4}{3} T^3 + \frac{a_5}{4} T^4 + a_7 \tag{2.12}$$

The fits of the seven coefficients a_1 - a_7 cover two temperature ranges, $T \leq 1000\,K$ and $T > 1000\,K$. The first five polynomial coefficients, as well as the seventh are the same for both gas and surface phase. However, the sixth term a_6 for surface species was adjusted as in Eq. (2.13),

$$a_{6A_s} = a_{6A_g} - \frac{Q_{A_s}}{R} \tag{2.13}$$

where the a_{6A_g} is the sixth coefficient of the gas phase molecule A_g and Q_{A_s} is the heat of adsorption of the corresponding surface species.

In general terms, the equilibrium constant K_{eq} of a reaction, which is only a function of temperature, can be obtained from the Gibbs free energy $\Delta G = R\,T\,\ln K_{eq}$. An ideal process would be to calculate the Gibbs free energy of a reaction on both surface and gas phase, and then calculate the equilibrium constant K_{eq}. Given the fact that the equilibrium constant, as well as the forward constant k_f calculated from the Arrhenius equation, are known, the reverse rate constant k_r can be found from the Eq. (2.14).

$$K_{eq} = \frac{k_f}{k_r} \rightarrow k_r = k_f \cdot K_{eq}^{-1} \tag{2.14}$$

Consequently, the reverse rate constant is also a function of the temperature for a given reaction. The change in the Gibbs free energy is calculated using thermodynamic properties of species via $\Delta G = \Delta H - T\,\Delta S$. Therefore, ΔG is linked with ΔS and ΔH. Concerning reactions that occur on the surface, Eq. (2.13) provides a correction for the value of enthalpy with the contribution of the coefficient a_6. The estimation of the entropy is more difficult. Nevertheless, Sellers et al. [40, 41] found a strong correlation between the standard entropy of adsorption of small molecules and Trouton's rule [42] for small gas phase molecules on metal surfaces. Trouton's rule states that the entropy of vaporization is almost the same value, about 85-88 $\mathrm{J\,K^{-1}\,mol^{-1}}$, for various kinds of liquids at their boiling points. The entropy of vaporization is defined as the ratio between the enthalpy of vaporization and the boiling temperature. It is named after Frederick Thomas Trouton and it can be mathematically expressed as,

$$\Delta S_{vap} = 10.5 \cdot R \tag{2.15}$$

where R is the gas constant. In addition, Zhao et al. [43] considered the entropy of vaporization for 477 different organic compounds and predicted a comparatively narrow range of 73–102 $\mathrm{J\,K^{-1}\,mol^{-1}}$. There are, however, several exceptions. For example, the entropies of vaporization of hydrogen (45 $\mathrm{J\,K^{-1}\,mol^{-1}}$), water (118 $\mathrm{J\,K^{-1}\,mol^{-1}}$) and methanol (113 $\mathrm{J\,K^{-1}\,mol^{-1}}$) are far from the predicted values [44, 45].

2.3 Physical properties

This section is concerned with the description of the transport properties applied in the current chemical system with a significant mention of diffusion phenomena associated with catalytic porous materials.

2.3.1 Transport properties

The following transport properties, used as input values in order to describe the transport of chemical species, are based on the approach of Jones and Lindstedt [46].

1. The Lennard-Jones potential $V_{L,J} = 4\varepsilon_{LJ}[(\frac{\sigma_{LJ}}{r})^{12} - (\frac{\sigma_{LJ}}{r})^{6}]$, where ε_{LJ} is the depth of the potential well, which is the region surrounding a local minimum of potential

energy, σ_{LJ} is the finite distance at which the inter-particle potential is zero and r is the distance between the particles. These are parameters for a particular species.

2. The rotational collision number, Z_{rot}.

3. A normalized heat capacity contribution from rotational modes, C_{rot}. The $C_{rot} = 1$ is used when more accurate data is unavailable.

4. The viscosity of each species, μ_i. The Lennard-Jones parameters, σ_{LJ}, ε_{LJ} and Z_{rot}, can be obtained from databases, for each species. The viscosity is calculated using the Chapman-Enskog equation [47],

$$\mu_i = 2.6693 \frac{(M_{w,i}T)^{1/2}}{\sigma_{LJ}^2 f(T)} \tag{2.16}$$

where $f(T) = \frac{k_B T}{\varepsilon_{LJ}}$ and k_B is Boltzmann's constant.

5. Molecular weight of each species $M_{w,i}$. The mean molecular weight, M_w, is calculated as the sum of the molecular weight of each mixture constituent multiplied by the corresponding fractional amount.

6. The thermal conductivity, λ_g, which is related to the viscosity, μ_i, the molecular weight, $M_{w,i}$, the diffusion coefficient, D_i, the rotational collision number, Z_{rot} and the rotational heat capacity, C_{rot}, is expressed according to the Eq. (2.17),

$$\frac{\lambda_g M_{w,i}}{\mu_i} = f_{trans} C_{trans} + f_{int} C_{int}, \tag{2.17}$$

where f_{trans} is the translational factor, f_{int} is the factor of internal energy, C_{trans} is the heat capacity distribution from translational modes and C_{int} is the heat capacity distribution from the internal energy. Equation (2.17) fits reasonably well for non-polar molecules and may be expressed in terms of an Eucken factor, f_E, derived from Eq. (2.18), with $f_{trans} = 5/2$ and $C_{trans} = (3/2)R$. Furthermore, the transport of internal energy will be a simple diffusion process, and $f_{int} = \rho D_i/\mu$, where ρ is the density and D_i the diffusion coefficient. Therefore, the Eucken factor can be expressed as,

$$f_E = \frac{\lambda_g M_{w,i}}{\mu_i C_V} = \frac{\rho D_i}{\mu_i} + \frac{3}{2}\left(\frac{5}{2} - \frac{\rho D_i}{\mu_i}\right)\frac{R}{C_V} \tag{2.18}$$

Many polyatomic molecules and all polar molecules give experimental values of $\lambda_g M_{w,i}/\mu C_V$ that are consistently lower than predicted by Eq. (2.18). Mason and Monchick [48] tried to explain this quantitatively on the assumption that, in these cases, comparatively rapid energy transfer between translational and internal modes renders the Eucken assumption invalid. Starting from semi-classical kinetic theory, making simplifying assumptions and taking into account collision numbers Z_{rot} and Z_{vib} for internal energy transfer, an alternative function Eq. (2.19) was derived by Chang and Uhlenbeck [49]:

$$f_{MM} = \frac{\lambda_g M_{w,i}}{\mu_i C_V} = f_E - \frac{2}{\pi C_V}\left(\frac{5}{2} - \frac{\rho D_i}{\mu_i}\right)^2 \left[\frac{C_{rot}}{Z_{rot}} + \frac{C_{vib}}{Z_{vib}}\right] \tag{2.19}$$

Due to the fact that, $\rho D_i/\mu_i \sim 1/N_{sc}$, where N_{sc} is the number of species on the surface and the heat capacity, at a constant volume, can be expressed as $C_V = C_p - R$, the result can be written as in Eq. (2.20):

$$\frac{\lambda_g M_{w,i}}{\mu_i R} = \frac{1}{N_{sc}}\left[\frac{C_p}{R} - 1\right] + \frac{3}{2}\left(\frac{5}{2} - \frac{1}{N_{sc}}\right) - \frac{2}{\pi R}\left(\frac{5}{2} - \frac{1}{N_{sc}}\right)^2 \left[\frac{C_{rot}}{Z_{rot}} + \frac{C_{vib}}{Z_{vib}}\right] \tag{2.20}$$

It is at once clear that only very rapid relaxation, leading to small values of Z_{rot} and Z_{vib}, would be expected to produce a significant effect, which means that, for most molecules, only rotational modes come into consideration. Therefore, the final equation, Eq. (2.21), represents the relation used for the calculation of the thermal conductivity.

$$\frac{\lambda_g M_{w,i}}{\mu_i R} = \frac{1}{N_{sc}}\left[\frac{C_p}{R} - \frac{5}{2}\right] + \frac{15}{4} - \frac{2}{\pi}\left(\frac{5}{2} - \frac{1}{N_{sc}}\right)^2 \left[\frac{C_{rot}/R}{Z_{rot}}\right] \tag{2.21}$$

2.3.2 Diffusion in porous media

In heterogeneous processes, the reactants of a system are in different phases and the reaction proceeds in the boundary layer, at the phase interface. As the heterogeneous systems consist a combination of a solid with gaseous or liquid phases, the transportation of a substance from the bulk of a gas or liquid to the solid surface is especially important.

Diffusion describes the transport of mass in gases, liquids and solids under the influence of the concentration gradient and proceeds spontaneously due to microscopic movement

of mass. The diffusion mechanisms differ for gases or liquids and solids. More specifically, for gases or liquids a statistical movement according to the temperature can be observed, while for solids direct exchange of lattice places, movement via lattice sites, vacancies, defects or movement on the grain surface are apparent.

The characteristic diffusion coefficient (D_i) can be described as a molecular transport quantity. The simplest way to model diffusion in the gas phase is via Fick's model, which describes the transport as a product of the diffusion coefficient and the concentration (mass fraction) gradient of a particular component. The form below is valid for dilute mixtures, (e.g. gas phase) with no change in the mean molecular weight.

$$J_i = \rho D_i \frac{\partial Y_i}{\partial r} \tag{2.22}$$

Diffusion in porous catalysts is of a major importance to the understanding of catalytic systems. There is a wide variety of porous materials both in nature and industry, such as sand stone, porous rock, filter paper, nanotubes etc. Their main characteristic is the cavities observed in a solid matrix, that can be partially or fully connected. A porous surface can include cavities, channels, cells or pores. Porous catalysts are used in order to provide a very large catalytic surface in a small volume, at low cost. More specifically, the pore size (pore width) is defined as the distance between two opposite walls of the pore and can be classified according to the standards adopted by the International Union of Pure and Applied Chemistry (IUPAC). Pores with a diameter <2 nm are named micropores, with 2–50 nm are mesopores and with >50 nm macropores. Following this terminology, the micro- and mesopores are at the nanoscale while macropores at the micro-scale.

The diffusive-reactive balance in a catalyst pore inside a porous material, where the convective fluxes can be ignored, may be written as,

$$J_i = \rho D_i^{eff} \frac{\partial Y_i}{\partial r} = M_{w,i} \bar{R}_i \tag{2.23}$$

In Eq. (2.23), the average reaction rate has been introduced along with the simplified version of Fickian diffusion. The above equation includes the assumption that the diffusion coefficient inside a micro porous structure is the same as in the gas phase. This is well known to be incorrect as most studies suggest that the (average) effective diffusivity

is around one order of magnitude less [11, 50, 51]. This can be solved by introducing an efficiency factor η_e so that $\bar{D}_i^{eff} = \eta_e D_i^{eff}$. Therefore,

$$\rho \bar{D}_i^{eff} \frac{\partial Y_i}{\partial r} = \eta_e M_{w,i} \bar{R}_i \tag{2.24}$$

The diffusion process is restricted by two asymptotic regimes, the molecular/bulk/-continuum diffusion, where molecule – molecule interactions play the most significant role and the Knudsen diffusion, where molecule – wall interactions determine the process. A typical diffusion coefficient for a molecule in the gas phase is in the range of 10^{-6} to 10^{-5} m^2/s. Depending on the pores size measured experimentally, the appropriate porous media diffusion mechanism must be selected.

Micro-scale simulations can be performed in order to evaluate the diffusion coefficients and a combination of reaction-diffusion processes inside the washcoat layer can accordingly be simulated. The system consists of a gas phase and a solid phase composed by individual catalyst support microparticles. The binary diffusion coefficient, D_{ij}, for a mixture of two gases [52] can be written as,

$$D_{ij} = \frac{T^{3/2}}{P} \frac{1.86 \cdot 10^{-2}}{\Omega^{(1,1)} \left(\frac{\sigma_i^* + \sigma_j^*}{2} \right)^2} \sqrt{\frac{M_{w,i} + M_{w,j}}{M_{w,i}\, M_{w,j}}} \quad \left[\frac{m^2}{s} \right] \tag{2.25}$$

where T is the temperature in K, P is the pressure in Pa, M_i and M_j are the molecular weights of molecules i and j in kg/kmol, σ^* the collision diameter of gases i and j in m, and $\Omega^{(1,1)}$ is the collision integral which is a function of temperature.

The mixture average diffusion coefficient, implemented in the 2D parabolic FORTRAN code [12, 14, 15], can be expressed via Eq. (2.26),

$$D_i^{eff} = \frac{1 - Y_i}{\sum_{i \neq j} \frac{X_j}{D_{ij}} \frac{1}{n_j}} \quad \left[\frac{m^2}{s} \right] \tag{2.26}$$

where Y_i is the mass fraction of molecule i, X_j is the mole number Y_j/M_w in units kmol/kg, D_{ij} is the binary diffusion coefficient in m^2/s and n_j is the mole number of j in kmol/kg.

The above effective gas phase diffusivity has to be compared with Knudsen diffusion, which prevails in micro- and meso-scale pores. For a characteristic cylindrical pore the

Knudsen diffusion can be defined as,

$$D_i^K = \frac{2}{3} r_p \sqrt{\frac{8RT}{\pi M_{w,i}}} \approx \frac{2}{3} r_p \sqrt{\frac{8RT}{\pi M_w}} \quad \left[\frac{m^2}{s}\right] \tag{2.27}$$

where r_p is the pore radius, while the approximation of using the mean molecular weight, M_w, is only valid for species with similar molecular weights. For porous solids, such as in the present work, the media porosity (ϕ_g) and the tortuosity factor (τ_g) have to be considered. Hence, the "average" Knudsen effective diffusion coefficient is defined as,

$$D^{K,eff} = \frac{2}{3} \frac{\phi_g}{\tau_g} r_p \sqrt{\frac{8RT}{\pi M_w}} \quad \left[\frac{m^2}{s}\right] \tag{2.28}$$

If the molecular weight is accounted for each species separately, without using the mean molecular weight approximation, the expression is written as,

$$D_i^{K,eff} = \frac{2}{3} \frac{\phi_g}{\tau_g} r_p \sqrt{\frac{8RT}{\pi M_{w,i}}} \quad \left[\frac{m^2}{s}\right] \tag{2.29}$$

The porous media porosity ϕ_g can be geometrically calculated from Eq. (2.30) [11], assuming that the idealized pore is treated as a cylindrical channel,

$$S_v = \frac{2\phi_g}{r_p(1-\phi_g)} \tag{2.30}$$

where S_v is the specific surface area (SSA) per total volume. The (micro-) tortuosity is in the absence of further data, considered as the reverse of the porous media porosity (unimodal pores), $\tau_g = 1/\phi_g$ [53, 54]. An alternative way of computing the porous media porosity via the cubic cell model, was proposed by Giani et al. [55] based on Eq. (2.31), providing lower values of porosities, as shown in Table 4.4.

$$S_v = \frac{\sqrt{3\pi\phi_g}}{r_p\sqrt{1-\phi_g}} \tag{2.31}$$

Finally, for heterogeneous reactions in a porous solid, the conditions may be such that the system is located between the Knudsen and molecular diffusion limits. For conditions where the mean free path length is roughly equal to the pore diameter, an additional formula for the evaluation of the diffusion coefficient is required. Typically, the diffusion

coefficient in the transition region is evaluated through the Bosanquet formula [56] given in Eq. (2.32). It may be noted that $D_i^{eff} \propto T^{3/2}$, while $D_i^{K,eff} \propto T^{1/2}$ and, accordingly, the balance of the contributions will change in the transition regime.

$$\bar{D}_i^{eff} = \left(\frac{1}{D_i^{eff}} + \frac{1}{D_i^{K,eff}} \right)^{-1} \quad \left[\frac{m^2}{s} \right] \tag{2.32}$$

2.3.2.1 Representation of diffusion coefficients

The Knudsen diffusion prevails micro- and meso-scale porous structures, as mentioned before, and its application on the current study depends on the size of pores measured experimentally. For example, Knudsen diffusion is not a limiting factor for the ethane auto-thermal catalytic cracking data [3] explored in Chapter 5, while the TME data [2], validated in Chapter 4, demonstrate that Knudsen diffusion limitations dominate species transport inside catalytic material due to the small size of pores measured experimentally. In particular, the maximum pore size of the porous surface was 21.3 nm (mesopores) for all Test Cases, examined in Chapter 4. The average of pore diameter is 17.8 nm, 18.1 nm and 18.8 nm for 0.5 wt% Pt, 1 wt% Pt and 3 wt% Pt, respectively. Consequently, the Knudsen porous media diffusion mechanism must be selected, as analyzed in Section 2.3.2. As shown in Table 2.1, for the system studied in Chapter 4, the diffusion coefficient can be expected to be limited by Knudsen diffusion which ranges from around 10^{-6} to 10^{-7}, depending on each chemical species. Table 2.1 presents an indicative relationship at a specific temperature of 600 K, where the specific surface area (SSA) per total mass, S_m, is 110 m^2/g, the total specific pore volume per grams of catalyst is 0.52 cm^3/g and the pore radius, r_p, is 9.05 nm [2]. Thus, the porosity and tortuosity are equal to 0.49 and 2.04, respectively, as calculated from Eq. (2.30). A comparison of the D_i^{eff}, $D_i^{K,eff}$ and $\bar{D}_i^{eff}$ diffusion coefficients for NO, CO_2, C_3H_6, H_2 and N_2 against temperature is illustrated in Fig. 2.2.

The Knudsen diffusion efficiency factor, η_e, is defined by the ratio $\bar{D}_i^{eff}/D_i^{eff}$, while the respective mean value $\bar{\eta}_e$ of selected chemical species, for each temperature and Pt loading is shown in Table 2.2. The temperature dependence of $\bar{\eta}_e$ is accounted in the simulations presented in Chapter 4. The selection of the species aims to present the different ranges of D_i^{eff}, $D_i^{K,eff}$, $\bar{D}_i^{eff}$ and $\bar{D}_i^{eff}/D_i^{eff}$ to which the chemical species belong. Molecular

Table 2.1: Mixture average diffusion coefficients D_i^{eff} (m^2/s), Knudsen effective diffusion coefficients $D_i^{K,eff}$ (m^2/s), Bosanquet formula [56] $\bar{D}_i^{eff}$ (m^2/s) and Knudsen diffusion efficiency factor $\bar{D}_i^{eff}/D_i^{eff}$ for selected species, for all the Test Cases presented in Chapter 4, at 600 K. The values of porosities were obtained from Eq. (2.30).

Species	D_i^{eff} (m^2/s)	$D_i^{K,eff}$ (m^2/s)	$\bar{D}_i^{eff}$ (m^2/s)	$\bar{D}_i^{eff}/D_i^{eff}$
N_2	$3.17 \cdot 10^{-5}$	$9.76 \cdot 10^{-7}$	$9.47 \cdot 10^{-7}$	$2.99 \cdot 10^{-2}$
O_2	$2.92 \cdot 10^{-5}$	$9.13 \cdot 10^{-7}$	$8.85 \cdot 10^{-7}$	$3.03 \cdot 10^{-2}$
CO	$2.90 \cdot 10^{-5}$	$9.76 \cdot 10^{-7}$	$9.44 \cdot 10^{-7}$	$3.26 \cdot 10^{-2}$
NO	$2.87 \cdot 10^{-5}$	$9.43 \cdot 10^{-7}$	$9.13 \cdot 10^{-7}$	$3.18 \cdot 10^{-2}$
CO_2	$2.18 \cdot 10^{-5}$	$7.79 \cdot 10^{-7}$	$7.52 \cdot 10^{-7}$	$3.45 \cdot 10^{-2}$
H_2O	$3.39 \cdot 10^{-5}$	$1.22 \cdot 10^{-6}$	$1.18 \cdot 10^{-6}$	$3.47 \cdot 10^{-2}$
C_3H_6	$1.63 \cdot 10^{-5}$	$7.96 \cdot 10^{-7}$	$7.59 \cdot 10^{-7}$	$4.66 \cdot 10^{-2}$
C_2H_4	$2.28 \cdot 10^{-5}$	$9.75 \cdot 10^{-7}$	$9.35 \cdot 10^{-7}$	$4.10 \cdot 10^{-2}$
NO_2	$2.45 \cdot 10^{-5}$	$7.61 \cdot 10^{-7}$	$7.38 \cdot 10^{-7}$	$3.01 \cdot 10^{-2}$
H_2	$1.07 \cdot 10^{-4}$	$3.64 \cdot 10^{-6}$	$3.52 \cdot 10^{-6}$	$3.29 \cdot 10^{-2}$

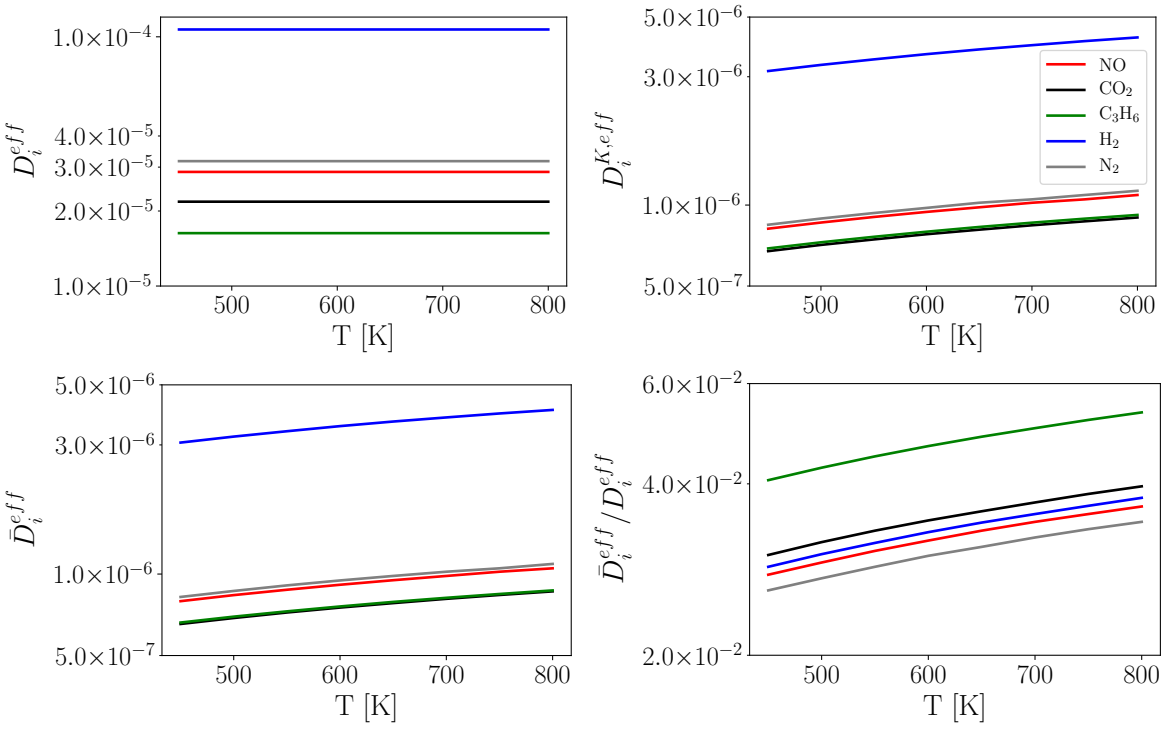


Fig. 2.2: Comparison of D_i^{eff}, $D_i^{K,eff}$, $\bar{D}_i^{eff}$ diffusion coefficients for representative chemical species as a function of temperature. The Knudsen diffusion efficiency factor $\bar{D}_i^{eff}/D_i^{eff}$ is also illustrated against temperature.

Table 2.2: Variation of the average Knudsen efficiency factor values with the temperature, for different Pt loadings. The values indicated in a bold font are applied in Chapter 4, apart from Section 4.3.4 which illustrates the effect of the different metal loadings. The values of porosities were obtained from Eq. (2.30).

T [K]	$\bar{\eta}_e$ [–] (0.5 wt%)	$\bar{\eta}_e$ [–] (1 wt%)	$\bar{\eta}_e$ [–] (3 wt%)
450	$3.19 \cdot 10^{-2}$	$\mathbf{3.00 \cdot 10^{-2}}$	$3.36 \cdot 10^{-2}$
500	$3.36 \cdot 10^{-2}$	$\mathbf{3.15 \cdot 10^{-2}}$	$3.53 \cdot 10^{-2}$
550	$3.51 \cdot 10^{-2}$	$\mathbf{3.30 \cdot 10^{-2}}$	$3.70 \cdot 10^{-2}$
600	$3.66 \cdot 10^{-2}$	$\mathbf{3.44 \cdot 10^{-2}}$	$3.86 \cdot 10^{-2}$
650	$3.81 \cdot 10^{-2}$	$\mathbf{3.58 \cdot 10^{-2}}$	$4.01 \cdot 10^{-2}$
700	$3.95 \cdot 10^{-2}$	$\mathbf{3.71 \cdot 10^{-2}}$	$4.15 \cdot 10^{-2}$
750	$4.08 \cdot 10^{-2}$	$\mathbf{3.84 \cdot 10^{-2}}$	$4.29 \cdot 10^{-2}$
800	$4.21 \cdot 10^{-2}$	$\mathbf{3.96 \cdot 10^{-2}}$	$4.43 \cdot 10^{-2}$

hydrogen is a light element, with a low M_w, presenting higher D_i^{eff}, $D_i^{K,eff}$ and $\bar{D}_i^{eff}$ diffusion coefficients compared to the other chemical species, as expected.

2.4 Gas phase chemistry

Two gas phase mechanisms, consisting of C_1-C_2-C_3-N and C_1-C_2-C_3-C_4 , have been used in the simulations presented in Chapters 4 and 5, respectively. The C_1-C_2 [57, 58, 59], which constitutes the basic mechanism for all the cases studied, is applied without any modifications to maintain consistency with previous work [14, 15]. The C_3-N [57, 58, 59, 60, 61, 62, 63, 64] and C_3-C_4 [57, 58, 59] containing gas phase mechanisms are introduced in Chapters 4 and 5, respectively, along with the corresponding thermochemical and transport data used for the study of the chemical systems.

2.5 Catalytic chemistry

The framework of the catalytic chemistry is based on the determination of pre-exponential Arrhenius factors and the calculation of the activation energies. The determination of the pre-exponential Arrhenius factors includes a thorough derivation of mobile and immobile sticking coefficients based on Variational Transition State Theory (VTST) calculations.

The work builds on the approach outlined by Tsopelakou et al. [65] who derived reaction rates for C/H/O/N adsorption reactions covering a temperature range of 298 – 2000 K. The implementation of all the other reactions, surface bimolecular, surface unimolecular with and without additional sites, isomerisations with and without additional sites, direct desorption and recombination, is based on previous work [14, 15]. Concerning the -N, $-C_3H_6$ and C_3H_5 containing part of the current mechanism, all the geometrical characteristics, (e.g. radii, projected areas), of the above reaction classes, have been calculated using Steric [66]. The temperature of the vibrational partition function is typically fixed at 298 K based on agreement with available experimental data for sticking coefficients. However, the choice is not a limitation of the method and alternative choices are discussed in Chapter 3. The considered adsorption reactions feature one, two or three Pt sites and provide an insight into the expected value range associated with mobile and immobile transition states. From a general point of view, the adsorption of atoms and molecules need to distinguish the cases of direct or indirect adsorption. The direct (immobile) adsorption describes a process where a particle collides with the surface and stays at the point of impact as an adsorbed species, while during the indirect (mobile) adsorption a particle firstly adsorbs in a weakly bound precursor state, in which it moves freely until the formation of a bond with an adsorption site. All the reaction data derived in the current work use the extended Arrhenius form for pre-exponential factors, temperature dependencies and activation energies.

2.5.1 Determination of pre-exponential Arrhenius factors

The evaluation of the pre-exponential factors, A, constitutes a significant step for the determination of the rate constants through the extended Arrhenius equation. The 2D collision theory based method used by Vincent et al. [11] requires estimates and/or experimental data on sticking coefficients. By contrast, in the VTST approach applied by Kraus and Lindstedt [14, 15] all the adsorption and desorption reactions parameters were obtained using the position of a transition state which is variationally determined by minimizing the desorption rate using the canonical variational criterion method [67]. The pre-exponential factors were then calculated from the ratio of partition functions of the transition state and reactant phase. The VTST approach is also applied in the current

work for the Pt system to evaluate the pre-exponential factors via partition functions as outlined below.

2.5.2 Determination of partition functions

Partition functions are here used to estimate rate and equilibrium constants for adsorption reactions. The considered moieties typically have some translational degree of freedom. However, molecules also possess internal degrees of freedom (e.g. via vibration and rotation) in the gas phase, in the transition state, as well as, in the adsorbed state. Partition functions for gas phase and adsorbed species are accordingly required to determine the pre-exponential factors for adsorption processes. The overall molecular partition function $Q = q^t q^r q^v q^e$ is given by the product of the translational, q^t, rotational, q^r, vibrational, q^v and electronic, q^e partition functions which are calculated using well established classical formulas [8]. The following are examples of partition functions for reactants (X) and transition states ($\ddagger$),

$$Q_\ddagger/S = q_\ddagger^{t''}\, q_\ddagger^r\, q_\ddagger^v\, q_\ddagger^e \qquad \left[\frac{1}{\mathrm{m}^2}\right] \tag{2.33}$$

$$Q_X/V = q_x^{t'''}\, q_x^r\, q_x^v\, q_x^e \qquad \left[\frac{1}{\mathrm{m}^3}\right] \tag{2.34}$$

where t indicates the translational, r the rotational, v the vibrational and e the electronic partition functions. The corresponding expressions for the surface are given below.

$$Q_{(s)}/S = q_{(s)}^r\, q_{(s)}^v\, q_{(s)}^e \qquad [-] \tag{2.35}$$

$$Q_{(x(s(n))}/S = q_{x(s_n)}^r\, q_{x(s_n)}^v\, q_{x(s_n)}^e \qquad [-] \tag{2.36}$$

The electronic partition functions are assumed unity and the above expressions suggest that atoms in the catalyst are fixed (do not translate), but may have vibrational and rotational partition functions. The same applies to surface bonded species, where the transition state may be considered fixed or mobile. The translational 1D, 2D and 3D partition functions are:

$$q^t/L = q^{'t} = \frac{\sqrt{2\pi m^* k_B T}}{h} \qquad \left[\frac{1}{\mathrm{m}}\right] \tag{2.37}$$

$$q^t_{\ddagger}/S = q^{''t} = \frac{2\pi m^* k_B T}{h^2} \qquad \left[\frac{1}{\mathrm{m}^2}\right] \tag{2.38}$$

$$q^t_x/V = q^{'''t} = \left[\frac{2\pi m^* k_B T}{h^2}\right]^{3/2} \qquad \left[\frac{1}{\mathrm{m}^3}\right] \tag{2.39}$$

The effective mass of a reacting pair is evaluated as,

$$m^* = \frac{m_X m_{(s)}}{m_X + m_{(s)}} \text{ [kg]} \quad \text{or} \quad M^*_w = \frac{M_{w,X} M_{w,(s)}}{M_{w,X} + M_{w,(s)}} \qquad \left[\frac{\mathrm{kg}}{\mathrm{kmol}}\right] \tag{2.40}$$

where the molecular weight, M_w, has been introduced. The general expression for the reduced mass of k reactants can be written as,

$$\frac{1}{m^*} = \sum_{i=1}^{k} \frac{1}{m_i} \quad \text{or} \quad \frac{1}{M^*_w} = \sum_{i=1}^{k} \frac{1}{M_{w,i}} \quad \text{and} \quad m_i = \frac{M_{w,i}}{N_A} \tag{2.41}$$

The rotational partition function for linear species is written in term of the moment of inertia, I, and the symmetry factor, σ.

$$q^r = \frac{8\pi^2 I k_B T}{\sigma h^2} \qquad [-] \tag{2.42}$$

For non-linear molecules, the moments of inertia around the three principal axis (x,y,z) are used.

$$q^r = \frac{8\pi^2 \sqrt{8\pi^3 I_x I_y I_z} (k_B T)^{3/2}}{\sigma h^3} \qquad [-] \tag{2.43}$$

For atoms $q^r = 1$. The vibrational partition function, with the imaginary leading frequency omitted for the transition state, is given below. The Pitzer-Gwinn correction factor (ν_{corr}) has been also introduced.

$$q^v = \nu_{corr} \Pi_i (1 - e^{-\frac{h\nu_i}{k_B T}})^{-1} \qquad [-] \tag{2.44}$$

The moments of inertia, I, and the vibrational frequencies, ν_i, were obtained using Gaussian09 [67] and based on the configuration of each chemical species participating in the reaction. Three sets of vibrational frequencies are required. One for the gas phase, one for the adsorbed state and one for the transition state forming part of the adsorption process. The gas phase vibrational frequencies are determined using the M06-2X density functional [68] with the 6-31G(2df,p) basis set following an initial structure optimization at the same level of theory. Adsorbed species are modelled as attached to x metal atoms and as required by their surface coordination, using the M06 functional, as the additional exchange in M06-2X made convergence difficult. More advanced metal cluster approaches have not been applied in the current work. The choice of a simplified instead of an idealised "bulk" surface treatment was retained form previous work [14, 15] as it leads to a reduction in computational cost and enables a semi-automatic calculation of electronic structures. The 6-311G(d,p) basis set was implemented for C, O, H and N. The Stuttgart-Dresden (SDD) and Los Alamos National Laboratory 2-double-z (LANL2DZ) effective core potential methods were used for the surface [69]. In general terms, the effective core potentials reduce the computational cost for systems with multiple centres and describe relativistic effects in deep core electrons. Therefore, they are suitable for heavy transition metals such as Pt, Rh and Pd.

Figure 2.3 illustrates a potential energy surface (PES) which desribes the energy of a system consisting of atoms/molecules in terms of their relative position in the phase space. In particular, the local minima correspond to the bond lengths of the stable molecule at a fixed bond angle and the transition state (saddle point) demonstrates the passage from one minimum to a neighbouring one, by crossing the intermediate barrier. It is assumed that, the potential energy surface of molecular systems is sufficiently smooth, i.e. without discontinuities. However, such surfaces can be complex due to the interplay of the available molecular degrees of freedom, posing multiple local minima and maxima.

In the current approach, the transition state was found by a relaxed potential energy surface scan starting from the adsorbed species, moving along the predicted direction of desorption. The above combination of the M06 functional with 6-311G(d, p) and SDD or LANL2DZ basis sets was used for this search. The position of the transition state was based on the shape of the PES, ensuring it has a single imaginary frequency acting along the direction of the breaking bond. In adsorbed and transition state phases, hindered

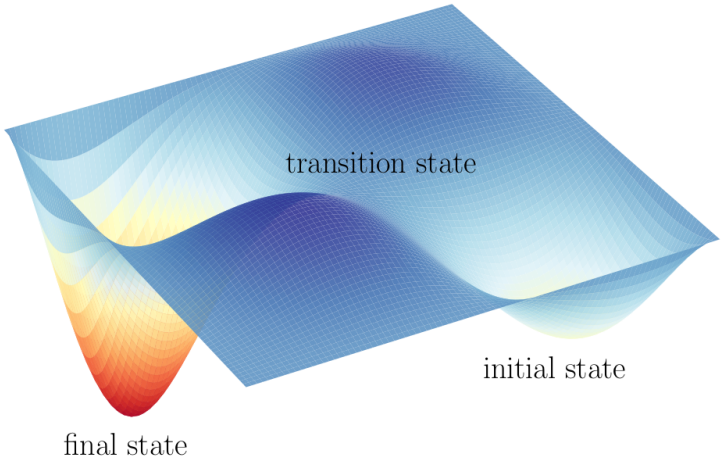


Fig. 2.3: Schematic of a potential energy surface (PES) in the vicinity of two minima, divided by a barrier. The initial and final states correspond to the reactant-gas phase and product-adsorbed phase of a molecule, respectively. The passage from the one phase to the other occurs through a dividing surface located at the saddle point.

rotors, were treated automatically using Pitzer and Gwinn method [70], as implemented in Gaussian09 [67]. The hindered rotors represent the internal rotational effects that are inherent in most molecules, when one part of a molecule can rotate with respect to the others and, at high excitation energies, begins to rotate freely. The internal rotation in the transition state is here treated using a "frozen transition state" approximation, by implementing a fixed value for the bond distance between the gas phase atom and the metal atom, for the determination of the transition state in the optimisation.

2.5.3 Binding configurations and bond lengths of species for Pt catalysts

The first step in producing a reaction mechanism for heterogeneous catalysis involves the determination of the bonding configuration for all chemical species on the catalyst. The configurations examined in the current work include adsorption of different species on top, bridge or on hollow sites. Smaller species with free valence electrons tend to be chemisorbed on the surface, with the most stable state preferring the highest order of coordination. Larger molecules with full valence shells will weakly bond to the surface on an on-top site. All species behave within the spectrum between these two extremes, with surface coverage, pressure and temperature also influencing the chemistry. Species may have multiple binding modes which must be considered depending on the model

parameters. The choice of the configuration and the number of metal sites used for each nitrogen containing and C_3H_6, C_3H_5, C_2H_5CH, C_2H_5C molecules depend on the accurate location of transition state and the required convergence obtained by Gaussian09 [67].

Figure 2.4 illustrates the adsorption of a C_3H_6 molecule on Pt(111). The pi-bond of C_3H_6 splits, while the resulting molecules, C_2H_3 and CH_3, attach on the metal surface. The bond length information is useful both in the context of VTST calculations, as well as, for estimating the geometric characteristics of the adsorbed molecules on a metal surface. The five nitrogen containing species along with the C_3H_6, C_3H_5, C_2H_5CH and C_2H_5C are shown in Table 2.3, where the configuration on the Pt surface and the bond lengths are presented. The study of C_3H_5 on the surface and its alternative adsorbate mode C_2H_5C, result as an outcome from the C_3H_6 and C_2H_5CH dissociation adsorption reactions and have to be included in the current mechanism for reasons of completeness.

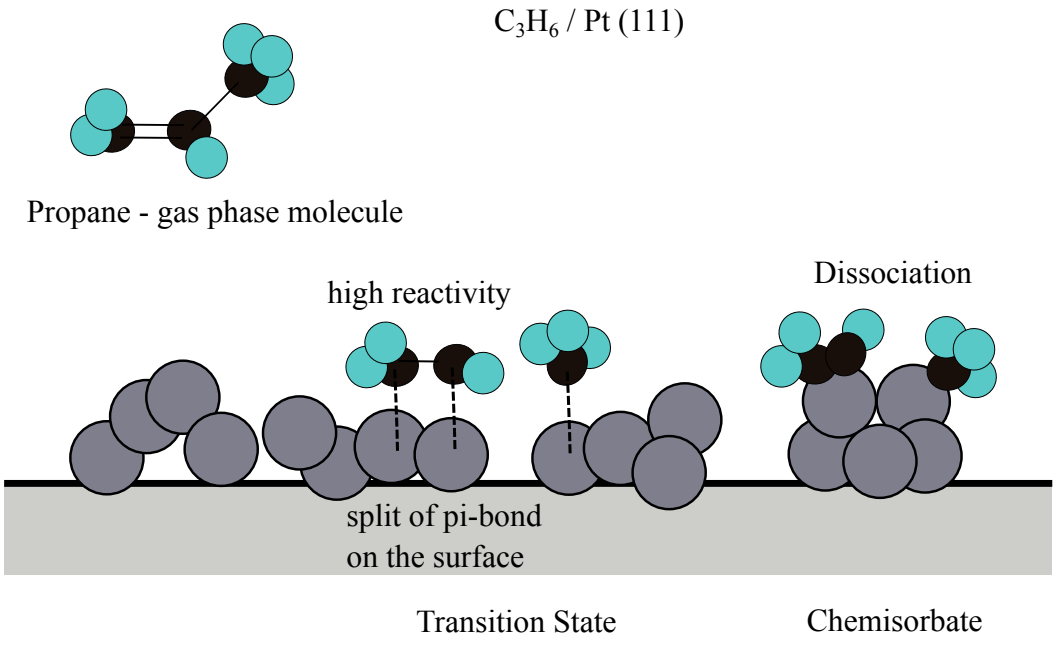


Fig. 2.4: Schematic of C_3H_6 adsorption on Pt(111).

2.6 Determination of temperature dependencies, β

In general, the temperature dependency of the vibrational partition function consists of an exponential function which would require a curve fitting in order to be estimated for the overall temperature dependency. Such a determination can be made quite readily and

Table 2.3: Molecular weight, bond type, bond sites, configuration and bond lenghts [71] of NO, NO_2, N_2O, N_2, N, C_3H_6, C_3H_5, C_2H_5CH and C_2H_5C on gas phase and Pt surface. When an atom within a molecule is bonded directly to the surface, is indicated in a bold font.

Species	Mw	Bond type	Bond sites	Configuration	Bond length (Å) Gas	Bond length (Å) Surface
NO	30.01	**N** - **O**	$N(s_2)$	in bridge	1.40	2.12
			O(s)	on-top		1.55
NO_2	28.01	N - **O**	O(s)	on-top	1.40	1.55
		N=O			1.21	
N_2O	44.01	**N** - N	$N(s_2)$	in bridge	1.45	2.12
		N=O			1.21	
N_2	46.05	**N=N**	N(s)	in bridge	1.25	2.12
			N(s)			2.12
N	14.01	**N**	N(s)	on-top		2.12
C_3H_6	42.08	**C** - **C**	C(s)	in bridge	1.54	1.97
			C(s)			1.97
		C−H			1.09	
C_3H_5	41.07	C - **C**	C(s)	on-top	1.54	1.97
		C−H			1.09	
		C=C			1.34	
C_2H_5CH	42.08	**C** - C	$C(s_2)$	in bridge	1.54	1.97
		C−C			1.54	
		C−H			1.09	
C_2H_5C	41.07	**C** - C	$C(s_3)$	in hollow	1.54	1.97
		C−C			1.54	
		C−H			1.09	

different approaches are presented in Chapter 3. The temperature dependencies of the translational and rotational partition functions can be evaluated directly for both mobile and immobile transition states. The temperature dependency, β, can be 0, 1/2, 1 or 3/2 depending on the geometry and state of the species.

2.7 Calculation of reaction activation energies

The determination of activation barriers for the generation of reaction mechanisms, is based on the Unity Bond Index-Quadratic Exponential Potential (UBI-QEP) method

which is the most general two-body interaction potential. The latter [10] provides heats of adsorption of molecules in different coordination modes as well as the corresponding activation energies. First-principles *ab initio* and Density Functional Theory (DFT) methods can be used for the calculation of reaction barriers. However, they do not offer a systematic way to obtain a sufficient level of accuracy for the current purposes. Both quantum mechanical methods describe the structural characteristics of molecules (e.g. bond lengths and angles, vibrational frequencies, charge moments etc.), though their application in the current formulations remains challenging due to the computational cost.

The model parameters used for the evaluation of surface energetics should be of thermodynamic origin and treat both energy minima (molecular chemisorption energies) and maxima/saddle points (reaction activation barriers). The analytic phenomenological approach initially developed by Shustorovich [72], and used for this purpose was the Bond Order Conversion-Morse Potential (BOC-MP) method. After some changes, implemented by Shustorovich and Sellers [10], the formalism evolved to the UBI-QEP method which introduces a bond index of a two-center bond, $x(r)$, constituting an exponential function of the two center bond distance, r, and postulate its conservation at unity, as shown in Eq. (2.45), for all active bonds involved [10]. Subsequently, direct algebraic operations of minimizing the total energy of the chemisorbed system are performed and described by Eq. (2.46), in terms of the maximum atomic binding energies Q_A, Q_B and gas-phase molecular bond dissociation energies, D_{AB}. By optimizing the energy with respect to x_A and x_B, the minimum-energy path in terms of x_{AB} is described by the Eq. (2.47).

$$x_A + x_B + x_{AB} = 1 \tag{2.45}$$

$$E_{AB}^{UBI-QEP} = Q_A(x_A^2 - 2x_A) + Q_B(x_B^2 - 2x_B) + D_{AB}(x_{AB}^2 - 2x_{AB}) \tag{2.46}$$

$$\begin{aligned} E_{AB}^{UBI-QEP} = {} & [Q_AQ_B/(Q_A+Q_B) + D_{AB}]x_{AB}^2 + [2Q_AQ_B/(Q_A+Q_B) - 2D_{AB}]x_{AB} \\ & + Q_AQ_B/(Q_A+Q_B) - Q_A - Q_B \end{aligned} \tag{2.47}$$

The UBI-QEP method is unique among the current theoretical approaches and has been successfully applied in various complex systems, where mechanisms might comprise tens or hundreds of intermediates and elementary steps. These include processes of real chemical interest, such as industrial heterogeneous catalytic reactions. Finally, it should be stressed that the UBI-QEP method is complementary to the use of (more accurate) quantum mechanical and hybrid approaches that combine data obtained with both methods [11]. This approach to barrier calculations was also applied by Kraus and Lindstedt [14, 15] for the formulation of comprehensive C/H/O mechanisms over Pt and Rh.

Finally, the input values required by the UBI-QEP method are the heats of adsorption for monoatomic, diatomic and polyatomic molecules on different configuration modes and the total gas phase bond energies, E. Subsequently, the activation energies, E_A, in a thermodynamically consistent way can be determined.

2.7.1 Atomic heats of adsorption

The atomic heats of adsorption correspond to the heat of adsorption of a single atom on top of a single metal surface. The atomic heats of adsorption for H, O, C and N on Pt, used in the current work, are obtained from Shustorovich and Sellers [10] and are presented in Table 2.4.

Table 2.4: UBI-QEP atomic binding energy Q_{0A} (kJ/mol). All values presented are for a fcc(111) Pt surface and are taken at the zero-coverage limit. The values used in the current work are indicated in a bold font. The following values were also obtained via an estimation from other studies [73, 74, 75].

Atoms	Q_{0A} (kJ/mol)
H	**153.1** [10, 72, 76, 77]
O	**213.4** [10, 72, 76, 77]
C	**376.6** [10, 72, 76, 77]
N	**291.2** [10, 72, 76, 77]

2.7.2 Dissociation and total bond energies

The bond dissociation energy, D, is one measure of the strength of a bond. Except for diatomic molecules, the bond dissociation energy differs from the total bond energy, E. While the bond dissociation energy, is the energy of a single chemical bond, the total bond energy, is the bond dissociation energies of all bonds in a molecule. The total bond energies can be calculated through the enthalpies of formation [78].

Table 2.5: Total bond energies (kJ/mol) calculated from tabulated enthalpies of formation [78].

Species	Total bond energies E_{AB} (kJ/mol)
NO	585.56
NO_2	892.71
N_2O	1022.94
N_2	945.33
N	0
C_3H_6	3435.04
C_3H_5	3038
C_2H_5CH	3208
C_2H_5C	2792

2.7.3 Heats of adsorption

The heat of adsorption is an indicator of the strength of the interaction between an adsorbate and a solid adsorbent. The corresponding values are evaluated by direct application of the UBI-QEP method [10], while additional values from literature sources are also provided in Table 2.6, along with the number of metal sites (s) involved in the process of adsorption. However, the adsorption mode used for the different chemical species may differ from the corresponding one used in bibliography, leading to possible discrepancies on the heat of adsorptions presented in Table 2.6. For example, N_2O is attached in a bridge configuration in this study, while Avery [28] proposed an on top configuration on the platinum surface, through the N atom. The heats of adsorption of H, O, C (C_1-C_2) containing species are retained from previous work [11], while the NO, NO_2, N_2O, N_2, C_3H_6, C_3H_5, C_2H_5CH and C_2H_5C adsorbates are estimated in the current work.

Table 2.6: Heats of adsorption of chemical species on a platinum surface. The values used in the current work are indicated in a bold font.

Adsorbates	Heats of adsorption (kJ/mol)
H(s)	**255** [10, 11, 79, 80], 267 [81], 281 [82]
O(s)	**356** [10, 11, 79, 80], 311 [82], 316 [83]
$C(s_3)$	**628** [11], 627 [10, 79, 80], 659 [84], 636 [85]
N(s)	**485**, 496 [86]
$NO(s_3)$	**71.8**, 80.7 [87]
$NO_2(s)$	**41.2**, 46 [88], 61 [87]
$N_2O(s_2)$	**72.6**, 23.4-25.3 [89], 21.9 [28]
$N_2(s_2)$	**45.2**, 46 [10], 50.2 [90], 40 [91], 38 [92]
$C_3H_6(s_2)$	**39.1**, 32.8 [93], 48.9 [94], 72.4 [1]
$C_3H_5(s)$	**41.52**
$C_2H_2CH(s_2)$	**84.33**
$C_2H_2C(s_3)$	**115**
$C_2H_4(s_2)$	**99** [11], 48.9 [79], 46 [80], 99 [95], 151 [85], 171 [96, 97]

For the calculation of the heats of adsorption, the atomic heat of adsorption Q_0 of a single atom on top of a single site, is required. The corresponding values for H, O, C and N on Pt, are presented in Table 2.4. In Table 2.7, the Q_{0A} corresponds to the atomic heat of adsorption of A, the Q_A is the maximum atomic binding energy, which is the observable atomic heat of adsorption for atom A in the zero coverage limit, Q_{AB} is the heat of adsorption of a molecule AB and Q_{A_2} is the heat of adsorption of a homonuclear diatomic molecule. The total bond energy E_{AB} symbolises the bond energy of atoms A and B, while the value of n depends on the nature of the configuration assumed and it can be equal to 1, 2 or 3 for on-top, in bridge or hollow configurations. A relevant schematic of the latter configurations is illustrated in Fig. 2.5.

The diatomic adsorption can be expressed through three different formulations based on the binding strength (weak, strong, medium bonding) of the chemical species attached to the metal (e.g. Pt) surface. The moderate binding strength is calculated by an interpolation of the two extremes, as shown in Table 2.7. The UBI-QEP method can treat more complex adsorption cases. An indicative paradigm is the bridging geometry of diatomic molecules, where the chemical species can adsorb with more than one contact atom, as

Table 2.7: Expressions of heats of adsorption according to the metal surface coordination of the adsorbate. [72]

Molecular coordination type	**Heats of adsorption**
Monoatomic	$Q_A = \left(2 - \frac{1}{n}\right) Q_{0A}$
Diatomic - weakly bonded	$Q_{AB} = \frac{Q_{0A}^2}{Q_{0A}/n + E_{AB}}$
Diatomic - strongly bonded	$Q_{AB} = \frac{Q_A^2}{Q_A + E_{AB}}$
Diatomic - medium bonded	$Q_{AB} = \frac{1}{2}\left(\frac{Q_{0A}^2}{Q_{0A}/n + E_{AB}} + \frac{Q_A^2}{Q_A + E_{AB}}\right)$
Bridged geometry	$Q_{AB} = \frac{ab(a+b) + E_{AB}(a-b)^2}{ab + E_{AB}(a+b)}$ $a = Q_A^2 \frac{Q_A + 2Q_B}{(Q_A + Q_B)^2}$, $b = Q_B^2 \frac{Q_B + 2Q_A}{(Q_B + Q_A)^2}$
Diatomic - homonuclear	$Q_{A_2} = \frac{ab(a+b) + E_{AA}(a-b)^2}{ab + E_{AA}(a+b)}$ $a = b = \frac{3}{4} Q_A$, leading to $Q_{A_2} = \frac{9Q_{0A}^2}{(6Q_{0A} + 16E_{AA})}$
Quasi-diatomic	$Q_{AB} = \frac{ab(a+b) + E_{AB}(a-b)^2}{ab + E_{AB}(a+b)}$ $a = Q_{0A}\left(1 - \frac{mQ_{0X}}{mQ_{0A} + Q_{0X}}\right)$ $b = Q_{0B}\left(1 - \frac{m'Q_{0Y}}{m'Q_{0B} + Q_{0Y}}\right)$
Chelation	$Q_{AXB} = Q_{AX} + Q_{BX} - \frac{Q_{AX}Q_{BX}}{Q_{AX} + Q_{BX}}$

the O_2 adsorption on Pt surface. The adsorption of N_2O on the metal surface via the in bridge -N attachment on Pt is also presented in Fig. 2.6.

The polyatomic adsorbates with a structure $X_m - A - B - Y_{m'}$ can be treated as quasi-diatomic, assuming that the molecule is attached to the surface via A and B featuring also X and Y secondary groups with m, m' showing the number of the different types of atoms

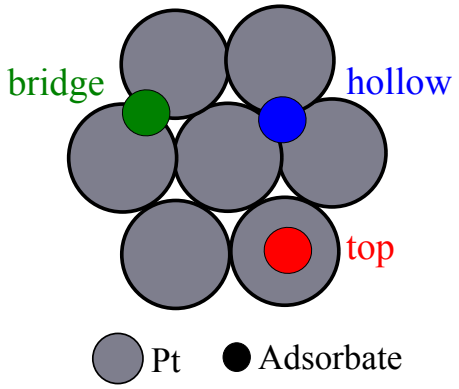


Fig. 2.5: Adsorbate configurations (on-top (n=1), in bridge (n=2), hollow (n=3)) on fcc(111) Pt surface.

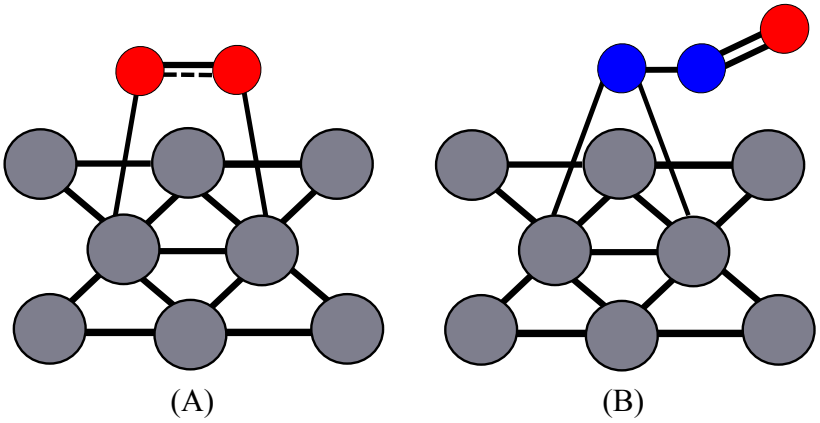


Fig. 2.6: Adsorption modes: (A) Bridging geometry of O_2 on Pt, (B) in bridge -N adsorption on Pt for N_2O.

bonded to A and B. Finally, the binding of chelates, $M-A-X-B-M$, is treated as a special case of quasi-diatomic binding, where the two contact atoms (e.g. oxygen atoms) are not bonded to one another, but with the X group (e.g. CH_3-C) which is far from the surface, as shown in Fig. 2.7. The chelating coordination is not used in the current work, as chelating compounds are not included in the studied reaction mechanism. Acetate (CH_3COO) exhibits this form of bonding with oxygens as the contact atoms and carbon as the non-interacting atom.

2.7.4 Reaction barriers

Following the calculation of the heats of adsorption of reactants, Q_R, the activation barriers, E_A, can be determined based on the type of reaction examined. For direct adsorption reactions, the UBI-QEP method assumes $E_A = 0$ and for desorption reactions

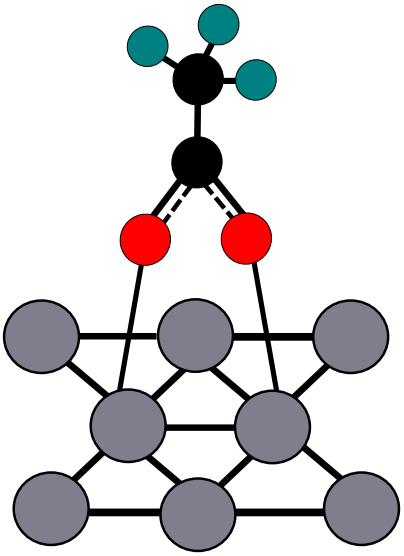


Fig. 2.7: Chelating mode of CH_3COO on Pt surface.

the activation energies are assumed to be equal to the heat of adsorption of the desorbing species, $E_A = Q_R$. For all other processes, the activation energy equals to the surface enthalpy, $E_A = \Delta H_s$, or is assumed as 0 when $E_A < 0$ for exothermic reactions on the surface. Concerning endothermic reactions, the surface enthalpy, the reduced heat of adsorption and the surface barrier have to be evaluated. For heterogeneous surface phase reactions the correction for gas phase reactants, has also to be taken into account. More specifically, the surface enthalpy is given by Eq. (2.48), where R and P indicate the reactants and products, respectively.

$$\Delta H_s = \sum_{\forall r}(E_R + Q_R) - \sum_{\forall p}(E_P + Q_P) \tag{2.48}$$

The reduced heat of adsorption can be calculated from Eq. (2.49).

$$Q_{red} = \frac{\prod_{\forall p} Q_P}{\sum_{\forall p} Q_P} \tag{2.49}$$

And finally, the surface barrier $E_{A,s}$ is determined by Eq. (2.50).

$$E_{A,s} = \frac{1}{2}(\Delta H_s + Q_{red}) \tag{2.50}$$

The energy barriers provided by the UBI-QEP method tend to overestimate the true

activation energies, as the value of the bond index at the transition state can not be accurately determined and a zero $x_{AB,TS}$ is initially applied for the derivations as the dissociated fragments are independent of each other and not linked via the UBI condition. Thus, the energy difference between the transition state and the chemisorbed state can not give the correct value of the barrier height. Since the AB dissociation energy profile is described by a quadratic expression, presented in Eq. (2.47), two solutions can be obtained. However, only one extremum corresponds to the AB chemisorption minimum. The second solution is usually an illegitimate value of x_A or x_B (e.g. outside the legitimate range of $0 \leq x \leq 1$).

On the dissociation side of energy minimum, the energy increases, while the x_{AB} decreases until the end of the range is encountered, as illustrated in Fig. 2.8. Given the fact that the bond distance is finite, in the true transition state and therefore, the bond index must be greater than zero, a value of $x_{AB,TS} = 0.5$ is applied. Hence, the simplest possible interpolation is made between the enthalpy change of the reaction and the reduced heat of adsorption of the products. In principle, the location of the transition state can be determined more accurately through the use of VTST, which can also determine the nature of the transition state (e.g. loose or strong).

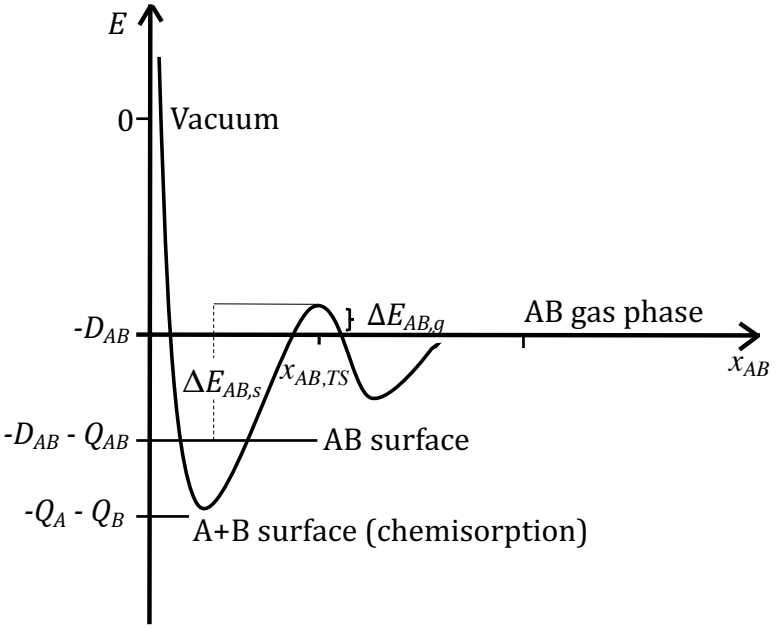


Fig. 2.8: Multi-dimensional UBI potential diagram, where the reaction coordinate $x_{AB,TS}$ is the A-B bond index at the transition state.

The surface barrier calculated with the correction for gas phase reactants given by Eq.(2.51), provides the final result, where the sum is over all gas phase reactants, r_g.

$$E_A = E_{A,s} - \sum_{\forall r_g} Q_R \tag{2.51}$$

For exothermic reactions, the forward barrier $E^f_{A,s}$ can be calculated from the reverse (endothermic barrier) $E^r_{A,s}$ and the enthalpy, using the energy conservation with the correction for gas phase reactants included.

$$E^f_{A,s} = E^r_{A,s} + \Delta H^r_s \tag{2.52}$$

$$E_A = E^f_{A,s} - \sum_{\forall r_g} Q_R \tag{2.53}$$

For isomerisation reactions with and without a catalyst site, the UBI-QEP method can not explain definitely the estimation of surface activation energies. The current estimation method is based on the gas phase isomerisation barriers as used by Vincent et al. [11]. The method is applied for a reaction where $Q_R < Q_P$ and features the following steps.

- Interpolation of the heats of adsorption.

$$Q_{TST} = Q_R + \frac{Q_P(Q_P - Q_R)}{Q_P + Q_R} \tag{2.54}$$

- Calculation of the surface barrier for the forward direction where $E^f_{A,g}$ refers to the gas phase g.

$$E^f_A = E^f_{A,g} - Q_{TST} + Q_R \tag{2.55}$$

- Calculation of the surface barrier for the reverse direction.

$$E^r_A = E^r_{A,g} - Q_{TST} + Q_P \tag{2.56}$$

2.7.4.1 Surface diffusion barriers

Shustorovich and Sellers [10] proposed a further diffusion correction to the reaction barrier which is particularly significant when the apparent activation barrier is competitive or smaller than the diffusion barrier of the most strongly bound species. The implementation of the diffusion correction remains from Vincent et al. [11]. The diffusion barrier is applied to the surface bimolecular, surface unimolecular with and without site and recombination reactions for which the UBI-QEP method predicts a non-zero barrier.

Experimental studies [98] of the diffusion barrier E_{diff} demonstrate values between $\theta = 10\%$ and $\theta = 20\%$ of the Q_R, where R corresponds to C, H, O, N reactants. Based on DFT calculations for different transition metals, Nilekar et al. [99] suggested a diffusion barrier at $\theta = 12\%$ of the heat of adsorption, which is also used in the current work, given the fact that it has provided on an adequate estimation in past work [11]. However, the higher value of $\theta = 20\%$ [100] of the heat of adsorption, was also examined for the investigation of stronger transport limitations associated with the movement of chemical species between catalyst sites. Such limitations directly impact the reactions on the surface. Both cases are analytically presented in Chapter 4. More specifically, the diffusion barrier for each reactant species is estimated from expression of the kind shown in Eq. (2.57).

$$E_{R,diff} = \theta \times Q_R \tag{2.57}$$

Therefore, the mutual diffusion barrier for the reaction has the form of an interpolation between the diffusion energies of the two reactants and is given by Eq. (2.58).

$$E_{diff} = \frac{\prod E_{R,diff}}{\frac{1}{2}\sum E_{R,diff}} \tag{2.58}$$

The value of the mutual diffusion barrier is bounded by the values of its component barriers and in contrast to the apparent activation barrier, it takes the value of the lesser of the two component barriers when one is much larger than the other. The scaling parameter ψ is estimated as,

$$\psi = \frac{E_A}{E_A + E_{diff}} \tag{2.59}$$

while the correction of E_A for diffusion is evaluated from Eq. (2.60).

$$E_{A,diff} = \psi E_A + (1 - \psi) E_{diff} \tag{2.60}$$

2.7.5 Comparison of activation energy data

A comparison of activation energy data obtained with the UBI-QEP method [10] and the current VTST approach, as presented in Chapter 3, has been made for a set of nitrogen containing reactions. The reaction barriers that correspond to the VTST approach, are determined from the total thermal energies at the three different phases (gas phase, transition state and adsorbed state) calculated from the respective partition functions (translational, vibrational, rotational, electronic). The M06-2X density functional with 6-31G(2df,p) and M06 functional with 6-311G(d,p) basis set, were applied for the gas and adsorbed phase, respectively, via Gaussian09 software [67]. As shown in Table 2.8, the two different activation energy data can be termed very satisfactory.

Table 2.8: Comparison of the activation energies ΔE_A (kJ/mol) obtained from the UBI-QEP method [10] and VTST based approach, through the application of M06 functional and 6-311G(d, p) basis set via Gaussian09 software [67] for direct desorption reactions.

No.	Reaction		ΔE_A	$\Delta E_A(Gaussian09)$
R1	$NO(g) + 3s \rightleftharpoons NO(s_3)$	f.	0	
		r.	71.8	63.8
R2	$NO_2(g) + s \rightleftharpoons NO_2(s)$	f.	0	
		r.	41.2	44.6
R3	$N_2O(g) + 2s \rightleftharpoons N_2O(s_2)$	f.	0	
		r.	72.6	65.4
R4	$N_2(g) + 2s \rightleftharpoons N_2(s_2)$	f.	0	
		r.	45.2	46.9

2.8 Observables

In this Section, the two major observables, namely the species conversion and selectivity, used in the data analysis and interpretation, are described. Validation using available

experimental data is performed in Chapters 4 and 5. The oxygen to carbon ratio (O/C) as used in Chapter 5, is also presented.

2.8.1 Conversion

The species conversion C_i characterizes the progress of the reaction. The downstream conversion of a species i is given by the mass flow difference of the inlet $\xi_{i,0}$ and the selected position $\xi_{i,\ell}$. In particular, the mass flow requires a radial integration per unit area, and the formula performed here is the following,

$$C_i = \frac{\xi_{i,0} - \xi_{i,\ell}}{\xi_{i,0}} = 1 - \frac{\xi_{i,\ell}}{\xi_{i,0}} \tag{2.61}$$

$$\xi_{i,\ell} = \sum_{j=1}^{N_{cells}} \pi(r_j^2 - r_{j-1}^2)\frac{1}{2}\left((\rho Y_i U)_{j,\ell} + (\rho Y_i U)_{j-1,\ell}\right), \tag{2.62}$$

where r_j is the transverse (or radial) position of node j. Furthermore, Y_i is the mass fraction of species i, while ρ and U are the density and the velocity of the fluid respectively [14, 15].

2.8.2 Selectivity

The species selectivity $S_{i,k}^a$ provides a measure of the products distribution. In principle, a high selectivity towards k, means that k is produced more exclusively from species i. In the current work, the following definition is applied,

$$S_{i,k}^a = \frac{\xi_{a,k,\ell}}{\left(\sum_{m\neq i}^{m\to N_k} \xi_{a,m,\ell}\right) - \xi_{a,i,\ell}} \tag{2.63}$$

$$\xi_{a,m,\ell} = \sum_{j=0}^{N_{cells}} \pi(r_j^2 - r_{j-1}^2)\frac{1}{2}\left((\rho Y'_{a,m} U)_{j,\ell} + (\rho Y'_{a,m} U)_{j-1,\ell}\right), \quad Y'_{a,m} = Y_m \frac{n'_{a,m} M_{w,a}}{M_{w,m}} \tag{2.64}$$

where S_k^i includes the ratio of the radially integrated mass flux of the selected product k over the fluxes of all products m minus the flux of species i. A further scaling of the mass fractions by $n'_{a,m}M_{w,a}$ is required, corresponding to the total weight of atoms a in species m. Finally, summing all the selectivities for all atoms will give unity [14, 15].

2.8.3 Oxygen to Carbon ratio

The O/C ratio, given by Eq. (2.65), is the ratio of the mass of atomic oxygen to the mass of carbon in the feed. The nO_i and nC_i correspond to the number of oxygen and carbon atoms in species i, while the $M_{w,O}$ and $M_{w,C}$ are the molecular weights of oxygen and carbon, respectively. The X_i is the molar fraction. The O/C mass ratio is used as an input parameter in the 2D parabolic FORTRAN code [12], when related experimental data are available for comparison. However, the O/C ratio, presented in Chapter 5, corresponds to the oxygen to carbon mole ratio.

$$O/C = \frac{m_O}{m_C} = \frac{\sum_{i=1}^{N_g}(nO_i \cdot M_{w,O} \cdot X_i)}{\sum_{i=1}^{N_g}(nC_i \cdot M_{w,C} \cdot X_i)} \tag{2.65}$$

The above nomenclature has been introduced for consistency with previous studies and common practice in the field of ATC.

Chapter 3

Rate parameter determination

The determination of rate constants for direct, dissociative and Eley-Rideal adsorption reactions, as well as, the final estimation of the reaction rate parameters of the corresponding reaction classes, constitute the main objectives of the current Chapter. A range of chemical adsorption reactions have been selected in order to investigate the mobile or immobile transition state of the adsorbing species on the platinum surface. The validation was obtained through the use of related experimental values from literature. The sticking coefficients that are here expressed through a theoretical framework emerging from VTST, represent the means of this verification. Finally, selected rate constants for adsorption and desorption reactions, calculated by both the previous developed reaction mechanisms [11, 14, 15] and the current approach, have been compared and discussed.

3.1 Determination of rate constants for adsorption reactions

The pre-exponential temperature-dependent factor for adsorption reactions is typically determined using collision theory combined with experimentally derived or estimated sticking coefficients, s_0, that describe the probability of a molecule attaching to the surface [7, 8, 9, 10, 11]. However, published values, even for well-studied reactions and adsorbates, often differ by one order of magnitude or more. More specifically, investigations for the adsorption of H_2 on Pt (111) present differences by orders of magnitude between studies. Vincent et al. [11], following a review, preferred $s_0 = 0.046$, with Kasemo

et al. [101] suggesting $s_0 = 0.62$. However, values of s_0 in the range $3.8 \cdot 10^{-5}$ to $6.5 \cdot 10^{-4}$ have been reported at very low pressure for a range of temperatures (313 – 473 K) [102]. Similarly, Carrington et al. [103] and Kasemo et al. [101] reported values of $s_0 = 5.6 \cdot 10^{-4}$ and $s_0 = 0.38$ for O_2 on Pt (111), respectively. Subsequently, a difference of one order of magnitude can be noticed in the values of sticking coefficients applied for some hydrocarbons on Pt surfaces between the studies conducted by Mhadeshwar and Vlachos [104] and Vincent et al. [11]. By contrast, the reported values for CO on Pt (111) vary from 0.5 [105] to 1 [103] with $s_0 = 0.84$ [1, 11] the most recent value – a comparatively modest range. Regarding the nitrogen containing species, the sticking coefficient data, suitable for validation of the current approach, are scarce. Chatterjee et al. [1] and Brown [106] provided the experimental sticking coefficients of 0.85 and 0.20 for the NO adsorption reaction, respectively. Additionally, Segner et al. [27] and Koop and Deutschmann [87] proposed sticking coefficient values at 0.97 and 0.90 for the corresponding NO_2 adsorption reactions.

Consequently, the use of experimental data for sticking coefficients can be subject to conjecture even for well-studied reactions, as shown in the latter case of NO adsorption reaction. The formulation of self-consistent reaction mechanisms that can demonstrate an efficient alternative that avoids/reduces the dependency on conjectural data is accordingly beneficial. The systematic framework of Kraus and Lindstedt [14, 15] does in principle overcome the need for experimental parameters through the application of Variational Transition State Theory (VTST) for the determination of adsorption and desorption reactions. The approach can be combined with increasingly accurate energy data for surface reactions.

The current work is applying the approach, defined in terms of classical transition state theory, to develop a comprehensive C/H/O/N mechanism for various applications, but with a ultimate purpose, the removal of all major oxides of nitrogen using Pt catalytic support on Al_2O_3. In comparison with the previous VTST based mechanism [14, 15] the outlined approach offers the advantage of overcoming the difficulty on the estimation of the rotational partition function, included in the rate constant expression, through the use of an approximation introducing by Sprowl et al. [16], as outlined below. The approach can be combined with classical TST to derive limiting sticking coefficients for mobile and immobile transition states [107].

In adsorption processes, the sticking coefficient describes the ratio of the number of atoms that adsorb on a surface to the total number of atoms that impinge upon that surface during the same period of time. Free molecules in the gas phase "hit" metal sites and either return back to their initial state or are accommodated. In the latter case, the precursor-molecule leads to either mobility or immobility of the transition state. Figure 3.1 illustrates the adsorption of CO molecule on Pt (111). The CO precursor-molecule is mobile and presents both loose (1st) and strong (2nd) transition states as obtained with Gaussian09 [67]. Finally, the CO molecule dissociates and chemisorbs.

Different theoretical structures of the base planes of platinum (e.g. Pt(100), Pt(110), Pt(111)) imply different electrochemical surface behaviours e.g. for microcrystalline electrodes. The Pt(111) structure constitutes the prevailing choice in the current work, as a non-reconstructed close packed surface that enables species adsorption in its fcc hollow sites. The latter base plane better represents the surface kinetics of the technical Pt particles due to its geometrical consideration (e.g. very dense structure) and morphology.

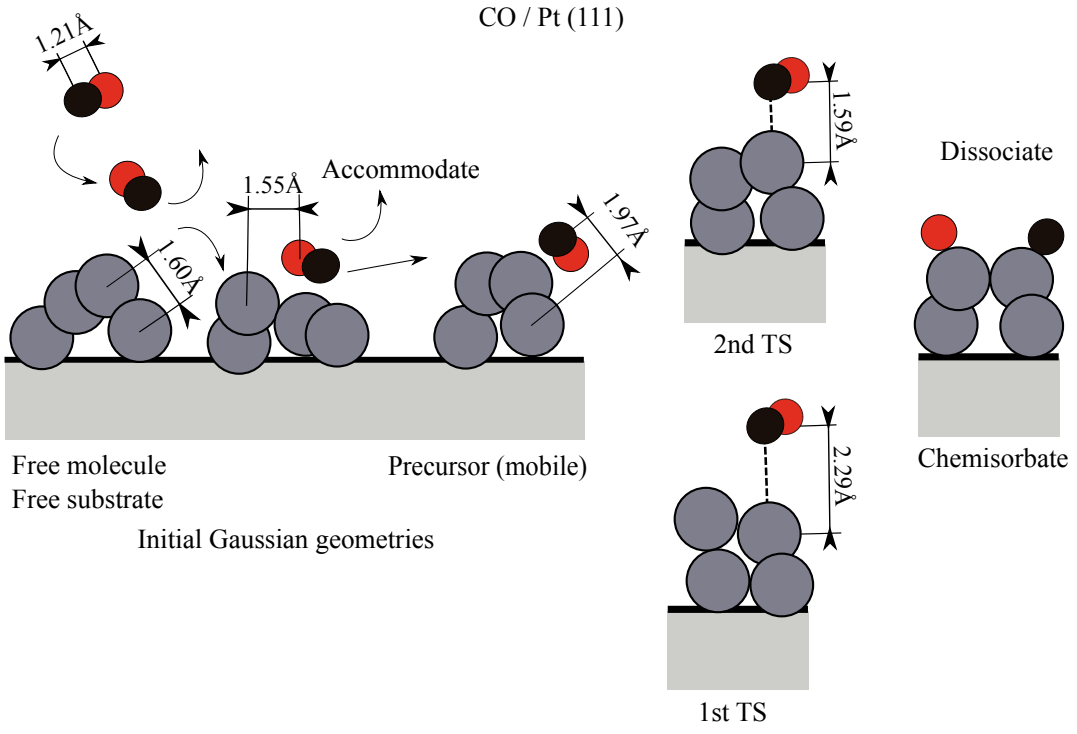


Fig. 3.1: Schematic of CO adsorption on Pt (111) with the related bond lengths in Å [71, 108].

The current mechanism evaluates the VTST framework for estimating sticking coefficients and rate constants via the mobile and immobile transition states. Concerning the

adsorption of CO, the mobile sticking coefficient is estimated at $5.3 \cdot 10^{-2}$ with an immobile equivalent of $8.2 \cdot 10^{-6}$ at 800 K. The corresponding value used by Vincent et al. [11] was 0.84 which is broadly consistent with a mobile transition state. The pre-exponential factor that arises from VTST [14, 15] is given by the following expression:

$$A(T) = \sqrt{\frac{k_B\,T}{2\pi\,m^*}}\,\frac{1}{\delta}\,\frac{(Q_\ddagger/S)}{(Q_X/V)} \qquad \left[\frac{m}{s}\right] \tag{3.1}$$

From the classical theory of reaction rates, it follows that the crossing frequency to products may be written as,

$$k(T) = \sqrt{\frac{k_B\,T}{2\pi\,m^*}}\,\frac{1}{\delta} \qquad \left[\frac{1}{s}\right] \tag{3.2}$$

where m^* is the effective mass of the complex in the direction of the reaction coordinate and δ is length of the top of the barrier. Equation (3.1) includes the assumption that the vibrational partition function for the catalyst (not the adsorbate) is unity. If the characteristic distance used in the evaluation of the partition function is assumed to be δ in the direction perpendicular to the catalyst surface, along the reaction coordinate, and the surface area is S, then the volume is $V = \delta \cdot S$. It is common to remove one degree of freedom from the translational partition function in order to eliminate δ. The following results if the translational motion in the one degree of freedom, along the reaction coordinate, is extracted from $Q_\ddagger$.

The imposition of $Q_\ddagger = Q_\ddagger^*$ demands that δ ($= \Lambda$, the thermal de Broglie wavelength) follows as,

$$\delta = \frac{1}{q'^t} = \frac{h}{\sqrt{2\,\pi\,m^*\,k_B\,T}} \qquad [\mathrm{m}] \tag{3.3}$$

From Eq. (3.2) is noted that δ^{-1} is the one-dimensional component of the translational partition function q'^t [m^{-1}]. It follows from Eq. (3.1) - Eq. (3.3) that the pre-exponential factor can be expressed as,

$$A(T) = \frac{k_B\,T}{h}\,\frac{(Q_\ddagger/S)}{(Q_X/V)} \qquad \left[\frac{\mathrm{m}}{\mathrm{s}}\right] \tag{3.4}$$

The expression in Eq. (3.4) assumes, and is restricted to, an irreversible reaction on the surface and partial equilibrium between reactants and the transition state. In collision theory-based approaches [27, 28] the pre-exponential factor can be expressed as,

$$A(T)_c = s_0 \sqrt{\frac{k_B\, T}{2\pi\, m^*}} \quad \left[\frac{\mathrm{m}}{\mathrm{s}}\right] \tag{3.5}$$

From Eqns. (3.4), (3.5) and the extracted degree of freedom, δ, it follows that:

$$s_0 = \frac{1}{\delta}\frac{(Q_\ddagger/S)}{(Q_X/V)} = \frac{q_\ddagger^{'t}\, q_\ddagger^{''t}\, q_\ddagger^r\, q_\ddagger^v}{q_x^{'''t}\, q_x^r\, q_x^v} = \frac{q_\ddagger^r q_\ddagger^v}{q_x^r q_x^v} \quad [-] \tag{3.6}$$

The resulting values for the sticking coefficient are consistent with the movement of the adsorbed molecules along the catalyst surface, which are free to rotate and vibrate. The translational partition functions cancel in this case. Naturally, if no changes occur in the internal coordinates $q_\ddagger^r = q_x^r$ and $q_\ddagger^v = q_x^v$ the sticking coefficient will become unity. Hence, according to the transition state theory, adsorption becomes more likely if the molecule in the mobile physisorbed precursor state retains its freedom to rotate and vibrate as it did in the gas phase. This situation corresponds to minimal entropy loss in the adsorption process. In general, the transition from the gas phase into a confinement in two dimensions will always be associated with a loss in entropy and the sticking coefficient is normally smaller than unity. If the transition state complex is assumed fixed, $q_\ddagger^{''t}$, then Eq. (3.7) follows from the translational partition functions,

$$s_{0,I} = \frac{q_\ddagger^v}{(q^{''t}\cdot S)\, q_x^r\, q_x^v} = \frac{s_0}{(q^{''t}\cdot S)\, q_\ddagger^r} \simeq \frac{\Gamma^*}{q^{''t}}\frac{q_\ddagger^v}{q_x^r\, q_x^v} = \Gamma^* q^{'t}\frac{q_\ddagger^v}{q_x^{'''}\, q_x^r\, q_x^v} \tag{3.7}$$

where S is the projected area, which depends on the catalyst structure (e.g. type of metal), and Γ^* the site density [sites/m^2]. The immobile sticking coefficient, $s_{0,I}$, for the direct adsorption process describes a molecule that lands immediately at its final adsorption site without the possibility of moving over the surface. In this case, only the vibrational degrees of freedom of the molecule remain in the transition state. Given the fact that a considerable amount of entropy is lost when the molecule is "frozen in" on an adsorption site, the values of immobile sticking coefficients are small compared to the

mobile equivalent. In cases where the rotational partition function is difficult to determine (e.g. through consideration of hindered rotors and translations), the relationship of Sprowl et al. [16] shown in Eq. (3.8) and described in detail below, is particularly useful.

$$(q^r)^2 = \frac{q^{''t}}{\Gamma^*} \rightarrow q^r = \frac{q^{'t}}{\sqrt{\Gamma^*}} \tag{3.8}$$

Sprowl et al. [16] proposed a new theoretical method to estimate partition functions and entropies of adsorbed species based on the evaluation of the hindered translator and rotor models associated with motions parallel to the surface. The potential energies surfaces were estimated through Density Functional Theory (DFT), for the evaluation of the entropies. The harmonic transition state theory assumes that an adsorbate is a localized oscillator with only vibrational modes [109, 110, 111, 112, 113, 114], underestimating the experimental entropies due to the existence of translations and rotations parallel to the surface.

Consequently, a hindered translator and rotor method was applied for the calculation of the respective partition functions without taking into account any adsorbate-adsorbate interactions [16]. The partition function for a 2D hindered translator was calculated based on Hill's [115] implementation for the potential energy function describing the two-dimensional (xy) motion, as shown in Eq.(3.9),

$$V(x,y) = V_0 + \frac{E^t_{A_x}}{2}\left(1 - \cos\frac{2\pi x}{b}\right) + \frac{E^t_{A_y}}{2}\left(1 - \cos\frac{2\pi y}{b}\right) \tag{3.9}$$

where $E^t_{A_x}$, $E^t_{A_y}$ are the translational energy barrier at x and y direction, respectively, associated with the linear decomposition of the 2D potential energy function, while b is the nearest neighbour distance between surface atoms, assumed to be the same for both directions. The $E^t_{A_x}$ and $E^t_{A_y}$ are assumed the same at Sprowl et al. [16] approach, for simplicity reasons, as shown in Fig. 3.2.

At high temperatures, the adsorbate freely translates on the surface, while at low temperatures it vibrates about the local minima. However, at intermediate temperatures, where the transition occurs from one kind of adsorption to the other, the respective translational partition function, q^t_{xy}, is described by the classical partition function $q_{\text{classical}}$, the

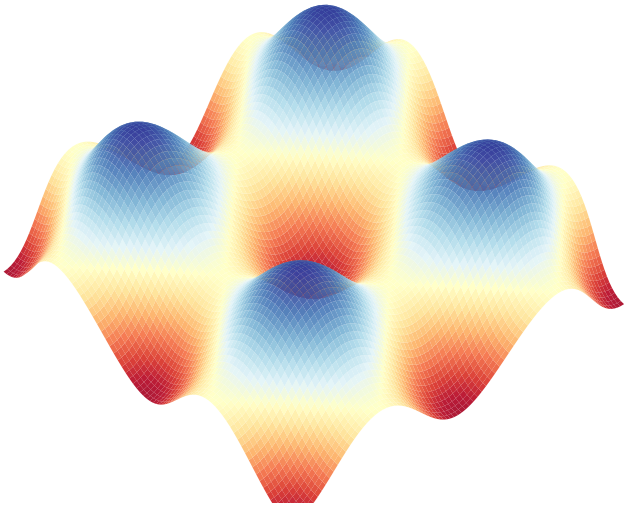


Fig. 3.2: Schematic of the potential energy surface of Eq.(3.9) with $E^t_{A_x} = E^t_{A_y}$.

quantum harmonic oscillator partition function q_{HO}, as presented below, and the classical harmonic oscillator partition function $q_{\text{HO-classical}}$, shown in Eq.(3.10).

$$q^t_{xy} = q_{\text{classical}} \frac{q_{\text{HO}}}{q_{\text{HO-classical}}} \tag{3.10}$$

The $q_{\text{classical}}$ corresponds to the partition function coming from the ideal gas model [115] expressed through the following equation,

$$q_{\text{classical}} = \Gamma^* \left(\pi r_x T_x\right) e^{-\frac{r_x}{T_x}} B_0^2 \left[\frac{r_x}{2T_x}\right], \tag{3.11}$$

where Γ^* indicates the number of surface (Pt) sites per area $[m^2]$, r_x is the ratio of the energy barrier height to the vibrational frequency times Plank's constant $r_x = E^t_{A_x}/h\nu_x$, T_x is the dimensionless temperature defined as $T_x = kT/h\nu_x$, while $B_0[z] = \frac{1}{2\pi i} \oint dt \, \exp(\frac{z}{2}\,(t - \frac{1}{t}))t^{-1}$ is the zero-order Bessel function of the first kind.

The single harmonic oscillator oscillating in two directions, x and y, which are assumed identical, is expressed by Eq. (3.12).

$$q^t_{\text{HO}} = \left(\frac{e^{-\frac{1}{2T_x}}}{1 - e^{-\frac{1}{T_x}}}\right)^2 \tag{3.12}$$

In the classical limit ($T_x \to \infty$), the terms in the numerator and denominator of Eq. (3.12) are expanded via Taylor series to a first order approximation concluding in Eq. (3.13).

$$q^t_{\text{HO}-\text{classical}} = \lim_{T_x \to \infty} q^t_{\text{HO}} \approx \lim_{T_x \to \infty} \left(\frac{1 - \frac{1}{2T_x}}{1 - (1 - \frac{1}{T_x})} \right)^2 \approx T_x^2 \tag{3.13}$$

Combining Eqns. (3.11)-(3.13) the final equation obtained is described by Eq. (3.14).

$$q^t_{\text{xy}} = \frac{\Gamma^* \left(\pi r_x / T_x\right) e^{-\frac{r_x}{T_x}} e^{-\frac{1}{T_x}} B_0^2 \left[\frac{r_x}{2T_x}\right]}{\left(1 - e^{-\frac{1}{T_x}}\right)^2} \tag{3.14}$$

The use of Padé approximant for the zero-point energy, ΔE^{zp}, presented by Eq. (3.15), is particularly useful as it accounts for the overestimation of the zero-point energy in the harmonic oscillator function. McClurg et al. [116] implemented this approximant in the related expression for hindered rotors, described below in order to accurately calculate the zero-energy point contribution at low temperatures. However, the partition function q^t_{xy} is accurate at higher temperatures.

$$\Delta E^{\text{zp}} = \frac{h\nu_x}{2 + 16 r_x} \tag{3.15}$$

Therefore, the partition function for the translator, according to Sprowl et al. [16], is the following, where the factor 2 indicates the two degrees of freedom x and y, which have the same potential energy function.

$$q^t = q^t_{\text{xy}} e^{2\frac{\Delta E^{\text{zp}}}{kT}} \tag{3.16}$$

By substituting the corresponding Eqns. (3.14) and (3.15) for T_x into Eq. (3.16), the following equation can be obtained.

$$q^t = q^t_{\text{xy}} e^{\frac{2}{(2+16r_x)T_x}} = \frac{\Gamma^* \frac{\pi r_x}{T_x} e^{-\frac{r_x}{T_x}} e^{-\frac{1}{T_x}} B_0^2 \left[\frac{r_x}{2T_x}\right]}{\left(1 - e^{-\frac{1}{T_x}}\right)^2} e^{\frac{2}{(2+16r_x)T_x}} \tag{3.17}$$

The interpolation function f^t is defined by Eq. (3.18), which is analogous to the hindered rotor interpolation function of McClurg et al. [116], described by Eq. (3.23). However,

the q^t is divided by Γ^*, as it refers to the whole surface consisted of Γ^* sites, whereas q^t_{HO} is defined here for a single harmonic oscillator site.

$$f^t = \frac{q^t/\Gamma^*}{q^t_{\mathrm{HO}}} \tag{3.18}$$

Dividing Eq. (3.17) by Eq. (3.12), the interpolation function can be calculated,

$$f^t = P^t e^{\frac{2}{(2+16r_x)T_x}} \tag{3.19}$$

where

$$P^t = \frac{q^t_{\mathrm{xy}}}{\Gamma^* q^t_{\mathrm{HO}}} = \frac{\pi r_x}{T_x} e^{-\frac{r_x}{T_x}} B_0^2 \left[\frac{r_x}{2T_x}\right] \tag{3.20}$$

Analogously the above implementation for the hindered translator partition function can be applied for the evaluation of the respective hindered rotor partition function [16]. The potential energy function for hindered rotation, based on McClurg et al. [116], is expressed by Eq. (3.21), where the E^r_A is the rotation energy barrier and m is the number of equivalent minima in a full rotation. Only the hindered rotation of the whole adsorbate about an axis perpendicular to the surface is considered in the following analysis.

$$V(\phi) = \frac{E^r_A}{2}(1 - \cos(m\phi)) \tag{3.21}$$

The ratio of the energy barrier height to the harmonic oscillator frequency times Plank's constant is given by $r_r = E^r_A/h\nu_x$, while T_r, is defined as $T_r = kT/h\nu_r$. Subsequently, the quantum harmonic oscillator partition function is expressed by the Eq. (3.22), which is identical to Eq. (3.12) for the hindered translator case. However, the square observed in Eq. (3.12) for the accounting of two modes, is not applied here due to the existence of one rotational mode.

$$q^r_{\mathrm{HO}} = \frac{e^{-\frac{1}{2T_r}}}{1 - e^{-\frac{1}{T_r}}} \tag{3.22}$$

The respective interpolation function for hindered rotations [116] is given below, where McClurg et al. [116] concluded to Eq. (3.24) through the use of Padé approximant for the zero-point energy, ΔE^{zp}, as described for the hindered translators.

$$f^r = \frac{q^r}{q^r_{\mathrm{HO}}} \tag{3.23}$$

$$f^r = P^r e^{\frac{\Delta E^{\mathrm{zp}}}{kT}} = P^r e^{\frac{1}{(2+16r_r)T_r}} \tag{3.24}$$

The P^r corresponds to the approximation of q^r/q^r_{HO} introduced by Pitzer and Gwinn [70] and is given by Eq. (3.25).

$$P^r = \sqrt{\frac{\pi r_r}{T_r}} e^{-\frac{r_r}{2T_r}} B_0 \left[\frac{r_r}{2T_r}\right] \tag{3.25}$$

Combining the Eq. (3.22) – (3.25), the partition function for hindered rotors can be obtained from Eq. (3.26).

$$q^r = f^r \times q^r_{\mathrm{HO}} = \frac{\sqrt{\frac{\pi r_r}{T_r}} e^{-\frac{r_r}{2T_r}} e^{-\frac{1}{2T_r}} B_0 \left[\frac{r_r}{2T_r}\right]}{1 - e^{-\frac{1}{T_r}}} e^{\frac{1}{(2+16r_r)T_r}} \tag{3.26}$$

Equations (3.26) and (3.17) look very similar, however a difference based on the number of modes used in the partition functions of hindered translators and rotors indicate that they are not the same. In particular, the interpolation function f^t equals to $(f^r)^2$, which is squared as there are two translational modes and one rotational mode. Therefore, Eq. (3.8) can be extracted from the respective partition functions. The latter equation was determined by Sprowl et. al [16] and used in the current work for the consideration of hindered rotors and translators.

Consequently, by calculating the ratio of Eqns. (3.6) and (3.7) and applying Eq. (3.8) a simple relationship between the limiting sticking coefficients can be evaluated,

$$s_0 = s_{0,I} \frac{q'''^t}{(\Gamma^*)^{3/2}} \tag{3.27}$$

The mobile and immobile rate constants are here evaluated through the use of the corresponding sticking coefficients in order to obtain the pre-exponential factor that will be used for the calculation of the reaction rates. The computational implementation of surface reactions typically features a division of the rate constant by $\Gamma^{(n-1)}$, where n is the reaction order in surface sites/species. However, in adsorption reactions the order will be Γ^n. Therefore, the rate constant for a mobile transition state can be calculated by Eq. (3.28), where, for example, $\Gamma = 2.72 \cdot 10^{-8}$ kmol/m^2 [124], for platinum, n is the

$$k(T) = \frac{1}{\Gamma^{(n-1)}} \left[\frac{1}{\Gamma} \frac{s_0}{x^x} \sqrt{\frac{k_B T}{2\pi m^*}} \right] \quad \left[\frac{\mathrm{m}^3}{\mathrm{kmol\,s}} \right] \left[\frac{\mathrm{m}^2}{\mathrm{kmol}} \right]^{n-1} \tag{3.28}$$

number of metal sites and x is the surface coordination of the adsorbing species. The latter factor, x^x, was also included in the expressions of mobile and immobile sticking coefficients for consistency reasons with published mechanisms [11, 14, 15]. However, the inclusion of the factor depends on the nature of the transition state. The rate constant for the immobile transition state follows by simply replacing s_0 with the immobile sticking coefficient $s_{0,I}$.

3.2 Determination of mobile and immobile transition state

In an attempt to identify whether the examined chemical species feature mobile or immobile transition states, experimental data from bibliographic sources are utilized for validation. The choice of mobile or immobile sticking coefficients for the calculation of rate constants is inextricably connected with the nature of the transition state assumed. Given the fact that experimental data concerning some chemical species are scarce, the validation was achieved for some of the cases presented below. More specifically, data for sticking coefficients of -N and -HC containing species on transition metals are comparatively rare. Hence, the more comprehensive data sets available for C/H/O species are considered in order to validate the approach.

3.2.1 Determination of sticking coefficients for C/H/O containing species

Sticking coefficients for mobile and immobile transition states, for H_2, O_2 and CO adsorption on a Pt (111) surface against temperature are shown in Figs. 3.3–3.8. The s, 2s, 3s denote a single, two and three Pt sites, respectively. The species have been selected due to the availability of several data sets for comparisons. The immobile sticking coefficient was evaluated using Eq. (3.7), while the mobile sticking coefficient for the two effective core

potentials [69], follows from Eq. (3.27), based on the approximation of Sprowl et al. [16]. The comparison of SDD and LANL2DZ effective core potentials for metal surfaces did not show significant difference. However, the LANL2DZ was additionally examined for reasons of completeness. Both s_0 and $s_{0,I}$ were evaluated over a wide temperature range with the temperature for the vibrational partition function, T_{q^v}, fixed at 298 K, as shown in Eq. (2.44). The latter consideration is applied in Chapters 4 and 5, as a base case. However, an additional evaluation of mobile and immobile sticking coefficients is conducted in this Chapter, at $T_{q^v} = 800$ K, as suggested by Kraus and Lindstedt [14, 15]. The impact of $T_{q^v} = 800$ K was also examined in Chapters 4 and 5.

In the current Section, a comparison with published experimental data on sticking coefficients of H_2, O_2, CO, NO, NO_2, C_3H_6 and C_2H_4 has been included for T_{q^v}, set at both 298 K and 800 K. The mobile and immobile transition state of O_2, CO and NO was also examined with a variable T_{q^v} from 298 K to 800 K, as presented in Section 3.2.4.

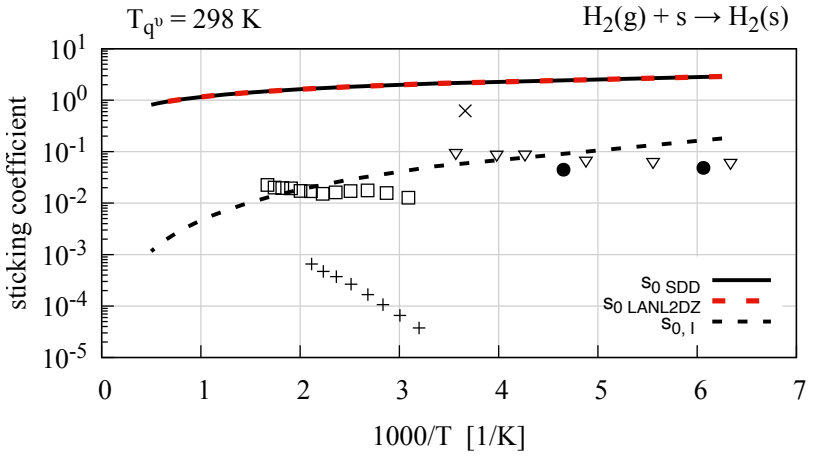


Fig. 3.3: Comparison of mobile s_0 and immobile $s_{0,I}$ sticking coefficients for SDD and LANL2DZ effective core potentials [69] with experimental data (Johansson et al. [102] (+), Kasemo et al. [101] (×), Seebauer et al. [117] (▽),Verheij et al. [118] (□), Poelsema et al. [119] (•)), for H_2 adsorption on one Pt site, at $T_{q^v} = 298$ K. The data aligns with an immobile transition state.

Figures 3.3 and 3.4 strongly suggest that the sticking coefficient of H_2 on Pt (111) corresponds to an immobile transition state. A possible explanation is that H_2 is a light element with a significant probability to stick on the catalyst (c.f. inside the metal structure) and remain immobile. The respective mobile transition state demonstrates values of $s_0 > 1$ for both $T_{q^v} = 298$ K and $T_{q^v} = 800$ K, constituting an unphysical outcome. The latter results from the application of the Sprowl et al. [16] approximation

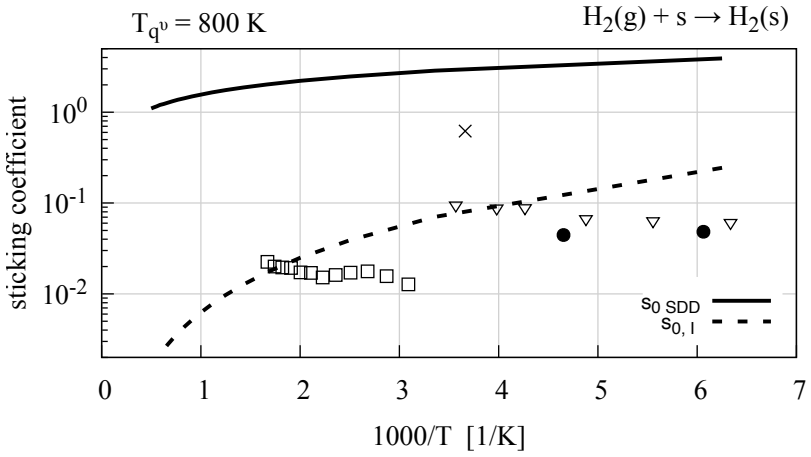


Fig. 3.4: Comparison of mobile s_0 and immobile $s_{0,I}$ sticking coefficients for SDD effective core potential [69] with experimental data (Johansson et al. [102] (+), Kasemo et al. [101] (×), Seebauer et al. [117] (▽),Verheij et al. [118] (□), Poelsema et al. [119] (•)) for H_2 adsorption on one Pt site, at $T_{q^v} = 800$ K. The data aligns with an immobile transition state.

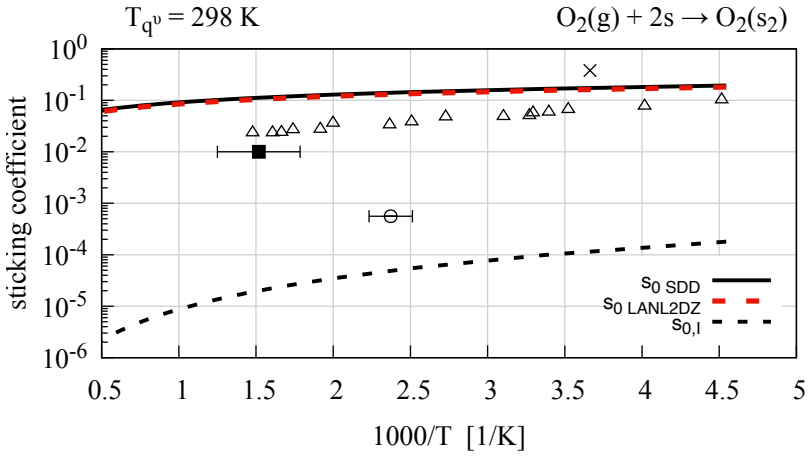


Fig. 3.5: Comparison of mobile s_0 and immobile $s_{0,I}$ sticking coefficients for SDD and LANL2DZ effective core potentials [69] with experimental data (Kasemo et al. [101] (×), Carrington et al. [103] (○), Zafiris et al. [105] (■), Elg et al. [120] (△)) for O_2 adsorption on two Pt sites, at $T_{q^v} = 298$ K.

for the determination of the rotational partition function, through the consideration of hindered rotors and translators and appears exclusively in the case of H_2 adsorption on the surface. All the other species adsorption on Pt surface, present sticking coefficient values lower than one, for the base case of $T_{q^v} = 298$ K. Both mobile and immobile transition states of H_2 have been examined in Chapters 4 and 5 in order to investigate the impact on the chemical system. Subsequently, as observed in Fig. 3.5, O_2 shows that there is a good agreement between experimental data and a mobile transition state,

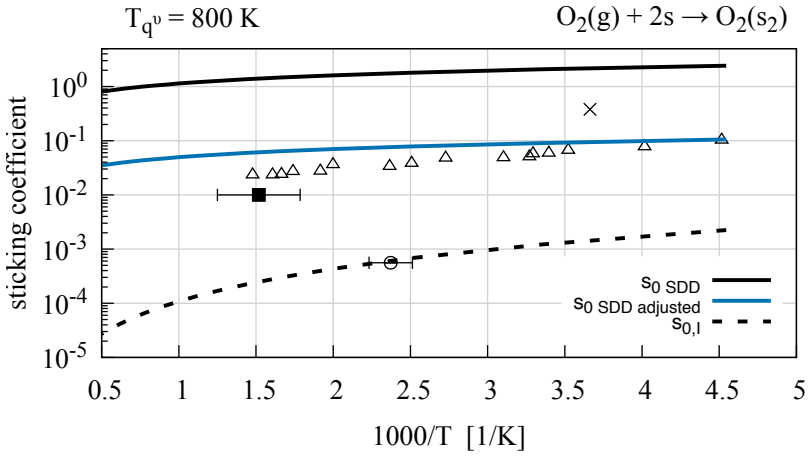


Fig. 3.6: Comparison of mobile s_0 and immobile $s_{0,I}$ sticking coefficients for SDD effective core potential [69] with experimental data (Kasemo et al. [101] (×), Carrington et al. [103] (○), Zafiris et al. [105] (■), Elg et al. [120] (△)) for O_2 adsorption on two Pt sites, at $T_{q^v} = 800$ K. The blue line is scaled by a constant factor 0.04 derived from the measurements at 220 K.

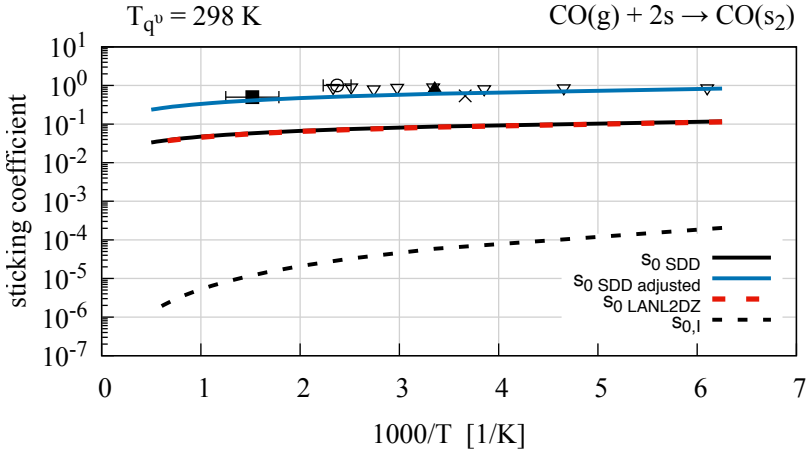


Fig. 3.7: Comparison of mobile s_0 and immobile $s_{0,I}$ sticking coefficients for SDD and LANL2DZ effective core potentials [69] with experimental data (Kasemo et al. [101] (×), Carrington et al. [103] (○), Zafiris et al. [105] (■), Seebauer et al. [117] (▽), Chatterjee et al. [1] (▲)) for CO adsorption on two Pt sites, at $T_{q^v} = 298$ K. The blue line is scaled by a constant factor 7.06 derived from the measurements at 160 K.

at $T_{q^v} = 298$ K. However, the choice of $T_{q^v} = 800$ K for the evaluation of mobile and immobile sticking coefficients for the O_2 adsorption reaction, does not favour neither the mobile nor the immobile transition state, based on the available experimental data.

Regarding the case of CO adsorption on two Pt sites, the experimental data seem to successfully reproduce the calculated mobile sticking coefficients at $T_{q^v} = 800$ K, while the respective values, at $T_{q^v} = 298$ K under-predict the experimental data. In the latter

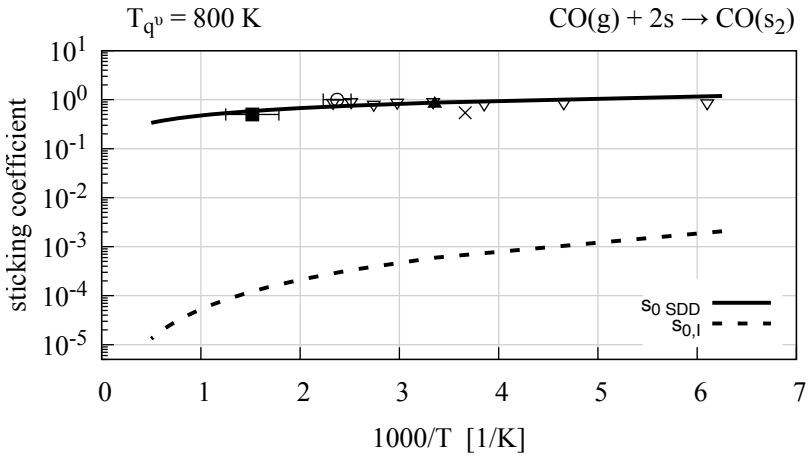


Fig. 3.8: Comparison of mobile s_0 and immobile $s_{0,I}$ sticking coefficients for SDD and LANL2DZ effective core potentials [69] with experimental data (Kasemo et al. [101] (×), Carrington et al. [103] (○), Zafiris et al. [105] (■), Seebauer et al. [117] (▽), Chatterjee et al. [1] (▲)) for CO adsorption on two Pt sites, at $T_{q^v} = 800$ K.

case, the predicted values follow the trend of a mobile transition state, as shown by the blue line. This suggests that a single, accurate, data point at 160 K would be sufficient to reproduce the experimental data. The discrepancy between CO and the other chemical species is not clear at present. Finally, the use of different effective core potentials in the internal configuration of H_2, O_2 and CO does not significantly affect the obtained results, as shown in Figs. 3.3, 3.5 and 3.7.

3.2.2 Determination of sticking coefficients for nitrogen containing species

Limited sticking coefficient data are available for the nitrogen containing species (NO, NO_2, N_2O and N_2) considered here. For NO, Chatterjee et al. [1] used a constant value of 0.85 consistent with the value of around 0.90 cited by Haug et al. [26]. However, it is also notable that more recent work featuring alternative measurement techniques (e.g. molecular beam scattering) at 300 K suggests a value of 0.20 [106]. The current prediction, obtained using VTST, based on the approximation by Sprowl et al. [16] and adsorption via the N atom on two Pt sites and via the O atom on one Pt site, is 0.14 at 298 K with the temperature dependency shown in Fig. 3.9. The value of 0.14 at 298 K is more in line with more recent data [106], while the case of $T_{q^v} = 298$ K represents better

the experimental data compared to $T_{q^v} = 800$ K, where the unphysical result of $s_0 > 1$ is obtained.

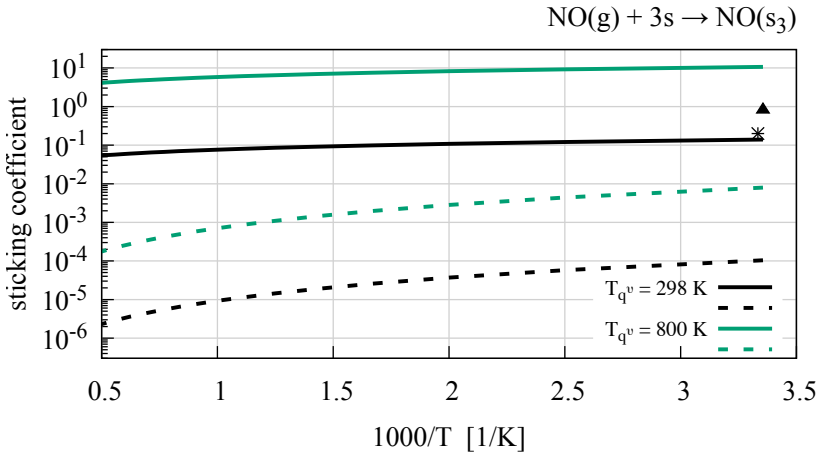


Fig. 3.9: Comparison of mobile s_0 (−) (−) and immobile $s_{0,I}$ (−−) (−−) sticking coefficients for SDD effective core potential [69] with experimental data (Chatterjee et al. [1] (▲), Brown [106] (∗)) for NO adsorption on three Pt sites, at $T_{q^v} = 298$ K (black line) and $T_{q^v} = 800$ K (green line).

The computed sticking coefficients for NO_2 are $1.0 \cdot 10^{-2}$ and $3.1 \cdot 10^{-6}$ for s_0 and $s_{0,I}$ at 298 K, respectively, for the single Pt site configuration. Segner et al. [27] suggest a sticking coefficient of 0.97 at 298 K, while Koop and Deutschmann [87] proposed a value of 0.90. The reasons for the discrepancy, mainly for $T_{q^v} = 298$ K, can not be established with certainty in the absence of further data. However, it is clear that a mobile transition state applies.

There are no corresponding measurements of the sticking coefficient for N_2O attached on two platinum sites. However, Koop and Deutschmann [87] suggested a sticking coefficient of 0.025 for N_2O attachment on one Pt site. This value is in a good agreement with the s_0 equal to 0.015 at 298 K obtained through the application of $T_{q^v} = 298$ K. An adsorption through the terminal N atom has been also suggested by Avery [28], without providing a sticking coefficient value. The latter study also suggests that the adsorption is weak with an initial heat of adsorption around 6 kcal/mol. Accordingly, the predicted sticking probability associated with a mobile transition state as shown in Fig. 3.11, is used in the current investigation.

Sticking coefficients for N_2 on Pt are scarce. There are two major configurations: (i) a chemisorbed σ-bonded arrangement with N_2 vertical to the surface and (ii) a chemisorbed

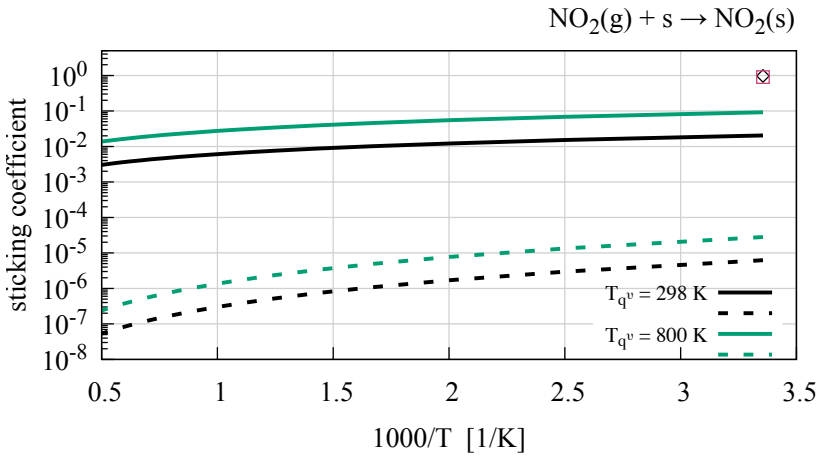


Fig. 3.10: Comparison of mobile s_0 (−) (−) and immobile $s_{0,I}$ (−−) (−−) sticking coefficients for SDD effective core potential [69] with experimental data (Segner et al. [27] (◇), Koop and Deutschmann [87] (□)) for NO_2 adsorption on one Pt site, at $T_{q^v} = 298$ K and $T_{q^v} = 800$ K.

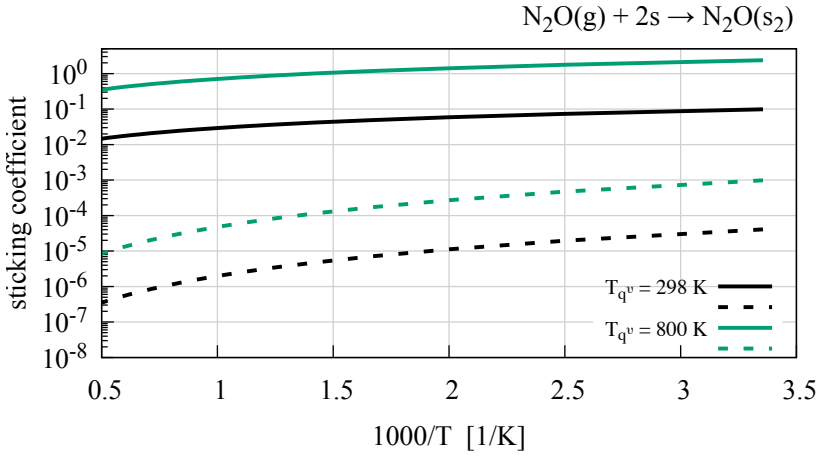


Fig. 3.11: Mobile s_0 (−) (−) and immobile $s_{0,I}$ (−−) (−−) sticking coefficients through the use of the SDD effective core potential [69] for N_2O adsorption on two Pt sites, at $T_{q^v} = 298$ K and $T_{q^v} = 800$ K.

π-bonded state that is nearly parallel to the surface [121]. Alternative measurement techniques (e.g. thermal desorption spectroscopy) suggest a sticking coefficient equal to 0.15 [91] which better agrees with the s_0 values calculated at $T_{q^v} = 298$ K. Hence, significant uncertainties prevail for Pt and the current values for immobile and mobile sticking coefficients are shown in Fig. 3.12.

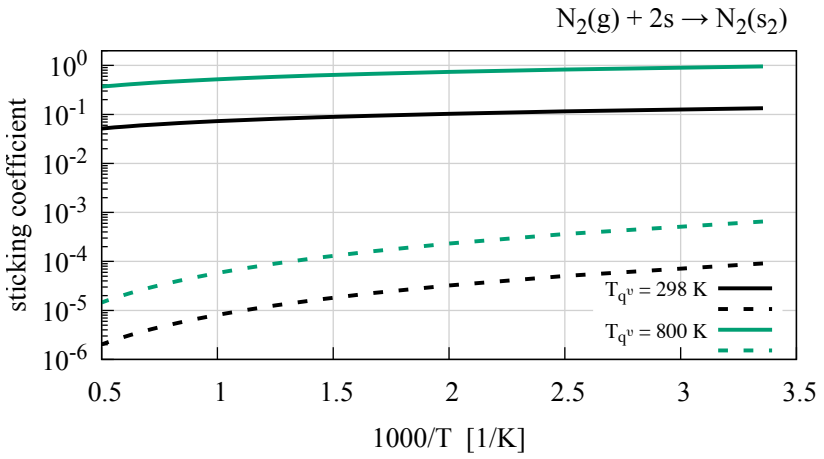


Fig. 3.12: Mobile s_0 (−) (−) and immobile $s_{0,I}$ (−−) (−−) sticking coefficients through the use of the SDD effective core potential [69] for N_2 adsorption on two Pt sites, at $T_{q^v} = 298$ K and $T_{q^v} = 800$ K.

3.2.3 Determination of sticking coefficients for hydrocarbons

Sticking coefficients for mobile and immobile transition states, for the most representative hydrocarbons of the current work, C_3H_6, C_3H_5 and C_2H_4 attached on a Pt (111) surface against temperature, are shown in Figs. 3.13–3.15, at $T_{q^v} = 298$ K and $T_{q^v} = 800$ K. Limited experimental data are available for comparison. However, Chatterjee et al. [1]

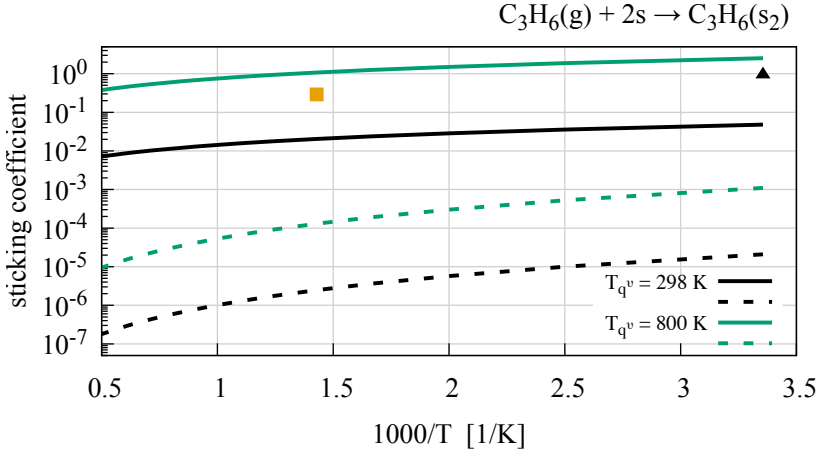


Fig. 3.13: Comparison of mobile s_0 (−) (−) and immobile $s_{0,I}$ (−−) (−−) sticking coefficients for SDD effective core potential [69] with experimental data (Chatterjee et al. [1] (▲), Perger et al. [122] (■)) for C_3H_6 adsorption on two Pt sites, at $T_{q^v} = 298$ K (black line) and $T_{q^v} = 800$ K (green line).

suggested a sticking coefficient equal to 0.98 for C_3H_6 adsorption on two platinum sites, and Perger et al. [122] proposed a value of 0.29, determined under heterogeneous ignition

temperatures. Both sources are located between the calculations of the mobile transition state at $T_{q^v} = 298$ K and $T_{q^v} = 800$ K. Related experimental data for the C_3H_5 adsorption on one Pt site are not available but a mobile transition state can be assumed, as results from other similar hydrocarbons. The C_2H_4 adsorption on two Pt sites suggests a mobile transition state determined at $T_{q^v} = 298$ K validated by the experimental data [22], as shown in Fig. 3.15. Hence, for reasons of consistency the corresponding values for C_3H_6 and C_3H_5 are used.

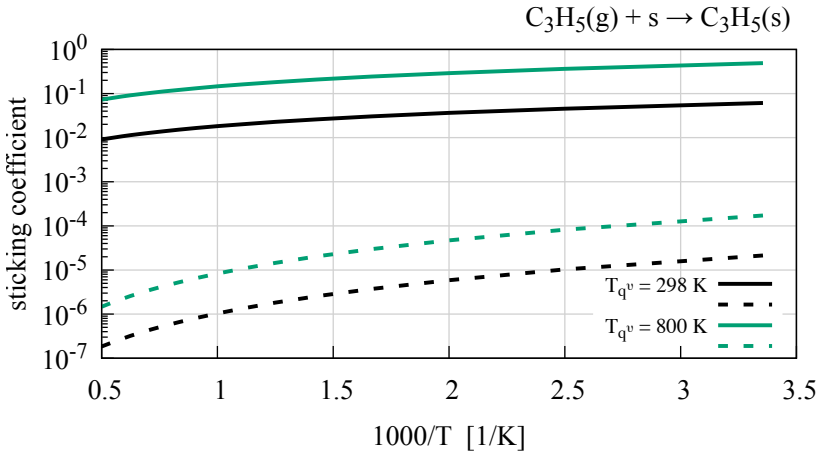


Fig. 3.14: Mobile s_0 (−) (−) and immobile $s_{0,I}$ (−−) (−−) sticking coefficients through the use of the SDD effective core potential [69] for C_3H_5 adsorption on one Pt site, at $T_{q^v} = 298$ K and $T_{q^v} = 800$ K.

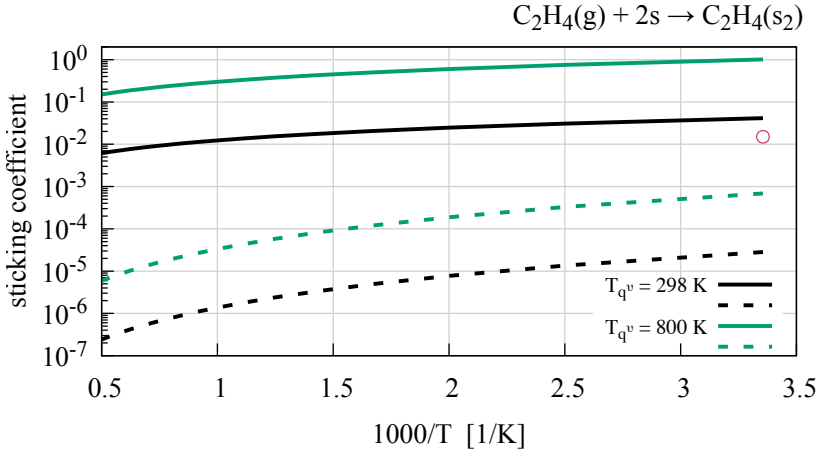


Fig. 3.15: Comparison of mobile s_0 (−) (−) and immobile $s_{0,I}$ (−−) (−−) sticking coefficients for SDD effective core potential [69] with experimental data (Zerkle et al. [22] (○)) for C_2H_4 adsorption on two Pt sites, at $T_{q^v} = 298$ K and $T_{q^v} = 800$ K.

3.2.4 Effect of variable T_{q^v} on sticking coefficients determination

The mobile and immobile transition state of O_2, CO and NO are examined below, when the temperature of the vibrational partition function, T_{q^v}, is not fixed, but varies from 298 K to 800 K together with temperature.

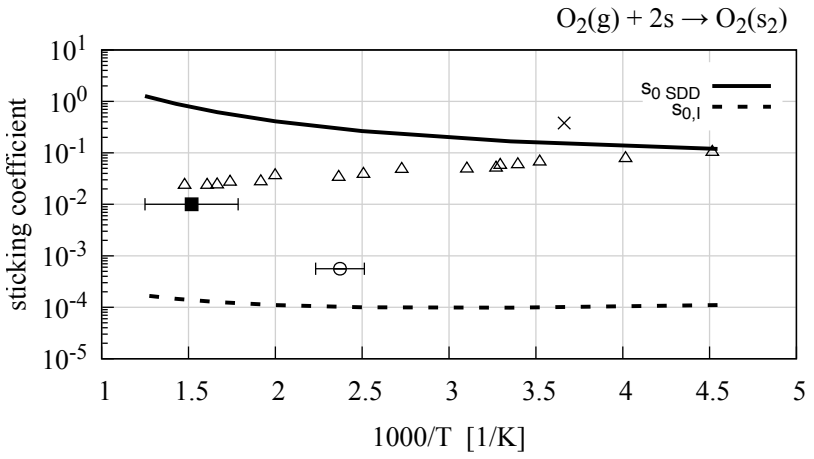


Fig. 3.16: Comparison of mobile s_0 and immobile $s_{0,I}$ sticking coefficients for SDD effective core potential [69] with experimental data (Kasemo et al. [101] (×), Carrington et al. [103] (○), Zafiris et al. [105] (■), Elg et al. [120] (△)) for O_2 adsorption on two Pt sites, with a variable $T_{q^v} = T$ [K].

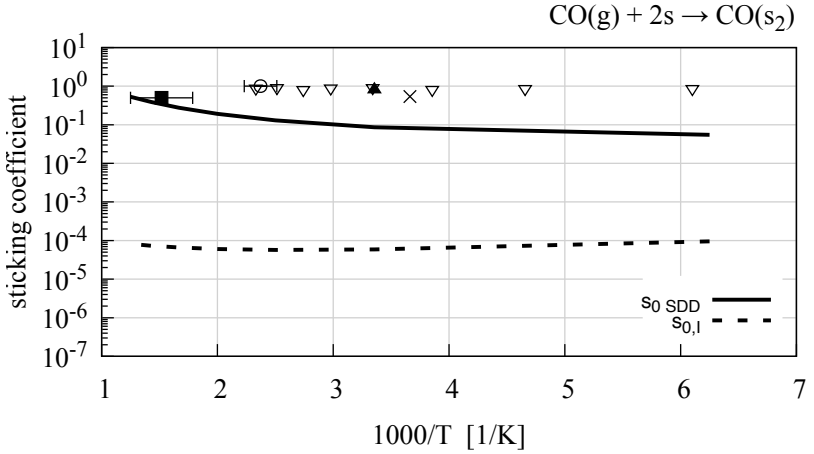


Fig. 3.17: Comparison of mobile s_0 and immobile $s_{0,I}$ sticking coefficients for SDD effective core potential [69] with experimental data (Kasemo et al. [101] (×), Carrington et al. [103] (○), Zafiris et al. [105] (■), Seebauer et al. [117] (▽), Chatterjee et al. [1] (▲)) for CO adsorption on two Pt sites, with a variable $T_{q^v} = T$ [K].

The behaviour of a mobile transition state for O_2, CO and NO, shown in Figs. 3.16 – 3.18, is not supported by the corresponding experimental data. Therefore, a fixed temperature for the vibrational partition function appears a reasonable choice. The similar trend observed in Figs. 3.16 – 3.18, is attributed to the temperature dependency of mobile (β = -1/2) and immobile (β = -2) transition state, which is the same for all the adsorption reactions studied with a variable T_{q^v}.

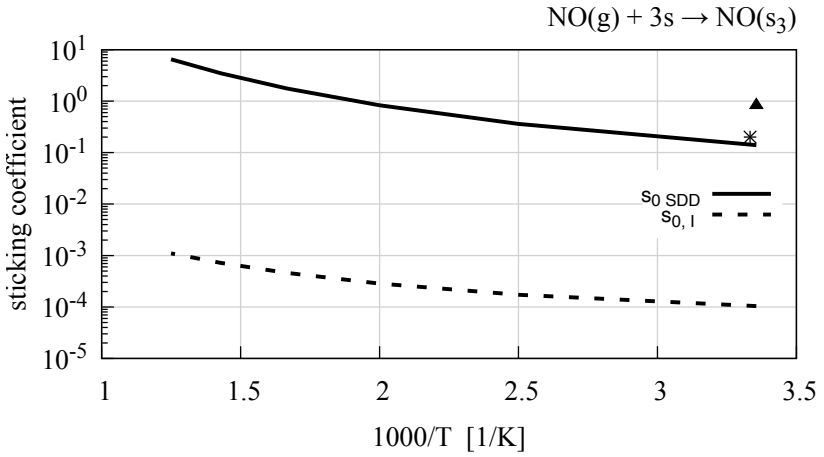


Fig. 3.18: Comparison of mobile s_0 and immobile $s_{0,I}$ sticking coefficients for SDD effective core potential [69] with experimental data (Chatterjee et al. [1] (▲), Brown [106] (∗)) for NO adsorption on three Pt sites, with a variable $T_{q^v} = T$ [K].

3.3 Reaction class based estimation of reaction rate parameter

The reaction classes (direct adsorption, dissociative adsorption, Eley-Rideal adsorption, surface bimolecular, surface unimolecular with or without additional surface sites, isomerisations with or without additional surface sites, direct desorption and recombination) are presented in Table 3.1, along with the way of calculation the energy barriers via the UBI-QEP formalism [10], which remain unchanged from Kraus and Lindstedt [14, 15]. However, the different treatment of rate constants for the adsorption reactions, based on the approximation for the rotational partition function derived by Sprowl et al. [16] as outlined above, is used due to difficulties in estimating hindered rotors impacted by the surface.

Table 3.1: Reaction classes and equations for the determination of rate constants and activation energies. The evaluation of the reaction-dependent sticking coefficient s_0 follows the Eq. (3.27).

Reaction classes	AT^{β}	E_A
Direct adsorption $A + x(s) \rightarrow A(s)_x$	$\frac{s_0}{x^x}\frac{1}{\Gamma_{Pt}}\sqrt{\frac{k_BT}{2\pi m^*}}$	0
Dissociative adsorption $AB + x(s) \rightarrow C(s)_y + D(s)_z$	$\frac{s_0}{x^x}\frac{1}{\Gamma_{Pt}}\sqrt{\frac{k_BT}{2\pi m^*}}$	E_A or ΔH_s or 0
Eley-Rideal adsorption $A + B(s)_x \rightarrow C(s)_y + D(s)_z$	$\frac{s_0}{x^x}\frac{1}{\Gamma_{Pt}}\sqrt{\frac{k_BT}{2\pi m^*}}\frac{A_{B(s)_x}}{A_{Mt}}$	E_A or ΔH_s or 0
Direct desorption $A(s)_x \rightarrow A + (s)_x$	$\frac{k_BT}{h}\frac{Q_{A\ddagger}}{Q_{A(s)_x}}$	Q_A
Isomerisations with site $A(s)_x + (s)_y \rightarrow C(s)_z$	$\frac{2(r_{A(s)_x}+r_{Mt})}{3x^xA_{Mt}}\sqrt{\frac{\pi RT}{2M_{A(s)}}}$	$E_{A,iso}$ or 0
Isomerisations without site $A(s)_x \rightarrow C(s)_y$	$\frac{1}{x^x}\frac{k_BT}{h}$	$E_{A,iso}$ or 0
Surface bimolecular $A(s)_x + B(s)_y \rightarrow C(s)_y + D(s)_z$	$\frac{2(r_{A(s)_x}+r_{B(s)_y})}{3x^xA_{Mt}}\sqrt{\frac{\pi RT}{2M_{red}}}$	$E_{A,dif}$ or ΔH_s or 0
Surface unimolecular with site $A(s)_x + (s)_y \rightarrow C(s)_y + D(s)_z$	$\frac{2(r_{A(s)_x}+r_{Mt})}{3x^xA_{Mt}}\sqrt{\frac{\pi RT}{2M_{A(s)}}}$	$E_{A,dif}$ or ΔH_s or 0
Surface unimolecular without site $A(s)_x \rightarrow C(s)_y + D(s)_z$	$\frac{1}{x^x}\frac{k_BT}{h}$	E_A or ΔH_s or 0
Recombination $A(s)_x + B(s)_y \rightarrow AB + z(s)$	$\frac{2(r_{A(s)_x}+r_{B(s)_y})}{3x^xA_{Mt}}\sqrt{\frac{\pi RT}{2M_{red}}}$	$E_{A,dif}$ or ΔH_s or 0

The rate constants $A \cdot T^{\beta}$ for direct adsorption and dissociative adsorption reactions, as shown in Table 3.1, are calculated through the same expression. However, the partition functions used for the evaluation of s_0 and $s_{0,I}$ correspond to different products, depending on the type of adsorption reaction, even if the reactants are the same. Furthermore, for the calculation of the rotational and vibrational partition functions for the transition state, the product with the biggest molecular weight, M_w is preferred in the determination of the sticking coefficients. The pre-exponential factor in Eley-Rideal adsorption reactions contains an extra term consisting of the ratio of the projected areas of the adsorbate and the catalytic site, $\frac{A_{B(s)x}}{A_{Mt}}$ [14, 15]. For surface bimolecular, recombination, surface unimolecular and isomerisation reactions involving a surface site, the molecular radii of the reactants, $r_{A(s)_x}$ and $r_{B(s)_x}$ and the projected areas of the adsorbate, $A_{B(s)_x}$, are calculated using Steric [66]. Using the molecular configuration and connectivity as the main inputs, the radial profile and the projected areas for the nitrogen containing and C_3H_6, C_3H_5, C_2H_5CH, C_2H_5C species, can be obtained. The molecular radius of a reactant is considered as the radius of the smallest sphere fully covering the whole molecule. Figure 3.19 represents the Tolman cone including the molecular nitrogen attached on two platinum sites, where a is the Tolman cone angle and r_N, r_{Pt} the atomic nitrogen and platinum radii. Table 3.2 presents the corresponding geometrical parameters.

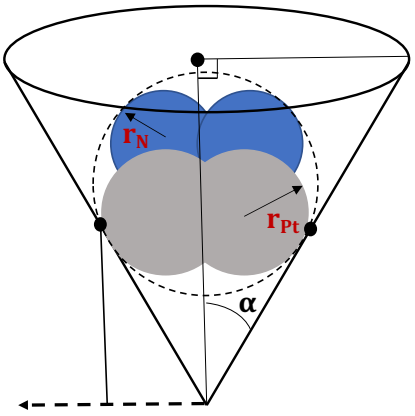


Fig. 3.19: Representation of the Tolman cone including the N_2 attached on two Pt sites.

Furthermore, for the above reaction classes, the reduced molecular weight of the reacting pair can be calculated as $M_{red} = \prod M_{w,R} / \sum M_{w,R}$. A factor $\frac{1}{3}$ is used as a scaling factor of the rate constant in order to maintain the consistency with Vincent et al. [11]

Table 3.2: Geometrical parameters calculated from Steric [66]. The projected area and radius of Pt are $A_{Pt} = 6.07$ Å^2 and $r_{Pt} = 1.75$ Å.

Species	Projected area (Å^2)	Radius (Å)
$NO(s_3)$	10.82	2.12
$NO_2(s)$	14.44	2.41
$N_2O(s_2)$	15.03	2.53
$N_2(s_2)$	11.31	2.18
N(s)	7.55	1.55
$C_3H_6(s_2)$	26.18	4.67
$C_3H_5(s)$	23.91	3.73
$C_2H_5CH(s_2)$	25.12	3.63
$C_2H_5C(s_3)$	29.59	3.98

Table 3.3: Possible combinations of partition functions for the evaluation of the exponent β based on Eq. (3.7) and Eq. (3.27). The vibrational partition functions do not present any temperature dependency if the temperature is fixed.

Possible combinations of partition functions	β
q''^t (2.38), q'''^t (2.39), q^r (2.43) (non linear species)	-1
q''^t (2.38), q'''^t (2.39), q^r (2.42) (linear species)	-0.5
q''^t (2.38), q'''^t (2.39), q^r (atom)	0.5
q''^t (2.38), q''^t (2.38), q^r (2.43) (non linear species)	-1.5
q''^t (2.38), q''^t (2.38), q^r (2.42) (linear species)	-1
q''^t (2.38), q''^t (2.38), q^r (atom)	0

and, consequently, Nilekar et al. [99]. More specifically, the pre-exponential factors calculated from Vincent et al. [11] at 1050 K vary from 3×10^{12} to 3×10^{13} while those proposed by Nilekar et al. [99] are estimated at the range 3.9×10^{12} to 5.2×10^{12}. The $\frac{1}{x^x}$ factor constitutes an additional scaling, where x corresponds to the number of metal atoms required for a reaction. The two scaling factors were retained from previous work [14, 15] and are not included in direct desorption reactions. The $\frac{1}{x^x}$ scaling can be questioned for

adsorption reactions, in particular for mobile transition states, when the impact becomes significant for $n \geq 3$, as discussed below. The reaction rate data for a reaction j featuring n_g gas phase and n_s surface species is presented in the following form,

$$R_j^f = \frac{k_j^f}{\Gamma^{n-1}} \prod_{i=1}^{n_g} [X_i^f] \prod_{k=1}^{n_s} Z_i^f \tag{3.29}$$

where n_g indicates the sum of all the reactants involved in a reaction, $[X_i^f]$ corresponds to the gas phase concentration of species i and Z_i^f to the surface coverage, which takes into account the number of Pt sites occupied by species i. The units of the resulting reaction rate are (kmol m^{-2} s^{-1}). The impact of the sticking coefficients resulting from different partition function forms, on the β factor, are shown in Table 3.3.

3.3.1 Comparison of selected rate constants

Comparison of selected direct adsorption and desorption rate constants, are shown in Figs. 3.20 – 3.27. The current rate constants were calculated using the Sprowl et al. [16] approximation, for the rotational partition functions, as described in Section 3.1. The determinations of Kraus and Lindstedt [14, 15] and Vincent et al. [11] rely on a direct application of the VTST and collision theory, respectively, for both adsorption and desorption reactions.

Table 3.4 presents the different treatment of direct, dissociative and Eley-Rideal adsorption reactions in the VTST approach of Kraus and Lindstedt [14, 15] and the current mechanism. The desorption reactions shown were determined similarly to the previous work [14, 15]. A fixed temperature of 298 K instead of 800 K used by Kraus and Lindstedt [14, 15], is applied in the current mechanism for the evaluation of the vibrational partition function. However, an investigation on the effect of $T_{q^v} = 800$ K in the rate constants determination, presented in Figs. 3.22 – 3.26 and considered in Chapter 4, is conducted. The rate constants, of all the other reaction classes (isomerisations with and without site, surface bimolecular, surface unimolecular with and without site and recombination) are calculated as in the previous VTST approach [14, 15].

The value of the mobile sticking coefficient s_0 for the different reaction classes is expressed through the immobile sticking coefficient, $s_{0,I}$, and the corresponding partition

Table 3.4: Comparison of the rate constants of different reaction classes for Kraus and Lindstedt [14, 15] mechanism and the present work.

Reaction classes	Kraus and Lindstedt [14, 15]	Present Work
Direct adsorption	$k(T) = \frac{1}{x^x}\frac{k_B T}{h}\frac{Q_\ddagger}{Q_g}$	$k(T) = \frac{s_0}{x^x}\frac{1}{\Gamma_{Pt}}\sqrt{\frac{k_B T}{2\pi m^*}}$
Dissociative adsorption	$k(T) = \frac{1}{x^x}\frac{k_B T}{h}\frac{Q_\ddagger}{Q_g}$	$k(T) = \frac{s_0}{x^x}\frac{1}{\Gamma_{Pt}}\sqrt{\frac{k_B T}{2\pi m^*}}$
Eley-Rideal adsorption	$k(T) = \frac{1}{x^x}\frac{k_B T}{h}\frac{Q_\ddagger}{Q_g}\frac{A_{B(s)_x}}{A_{Mt}}$	$k(T) = \frac{s_0}{x^x}\frac{1}{\Gamma_{Pt}}\sqrt{\frac{k_B T}{2\pi m^*}}\frac{A_{B(s)_x}}{A_{Mt}}$
Direct desorption	$k(T) = \frac{k_B T}{h}\frac{Q_{A\ddagger}}{Q_{A(s)_x}}$	$k(T) = \frac{k_B T}{h}\frac{Q_{A\ddagger}}{Q_{A(s)_x}}$

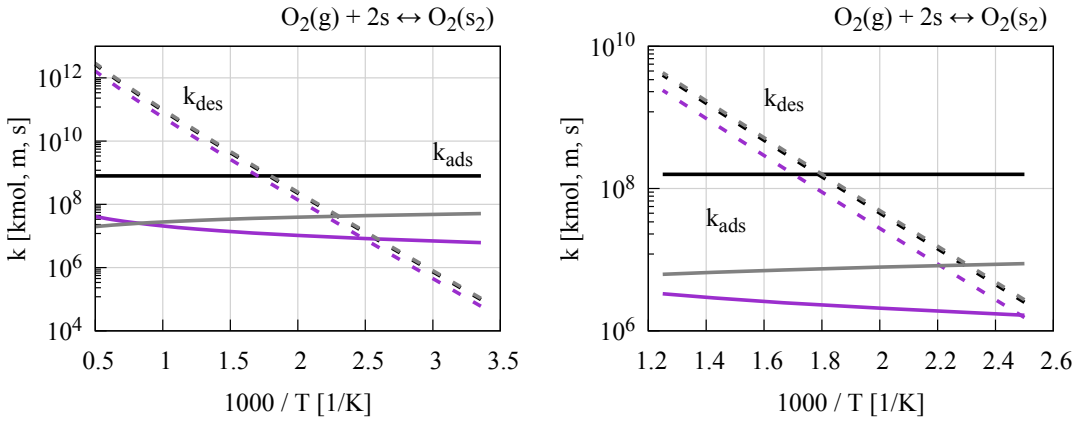


Fig. 3.20: Direct adsorption (−) (−) (−) and desorption (−−) (−−) (−−) O_2 rate constants. The temperature ranges are 298 K – 2000 K (left) and 400 K – 800 K (right). Rate parameters from the current mechanism (−), Kraus and Lindstedt [14, 15] (−) and Vincent et al. [11] mechanism (−) are presented. The T_{q^v} is fixed at 298 K for the current mechanism. The units of rate constants are in $[\frac{\mathrm{m}^3}{\mathrm{kmol\,s}}]$ and $[\frac{1}{s}]$ for direct adsorption and desorption reactions, respectively.

functions, as shown in Eq. (3.27). Regarding the collision theory based approach [11], experimentally derived or estimated sticking coefficients have been used for the determination of rate constants in adsorption reactions. The applied temperature range for the related Arrhenius plots varies from 298 K to 2000 K. However, a narrower temperature range, from 400 K to 800 K, is also presented in Figs. 3.20, 3.21 and 3.26, constituting the selected temperature window studied in Chapter 4, due to the availability of related experimental data [2].

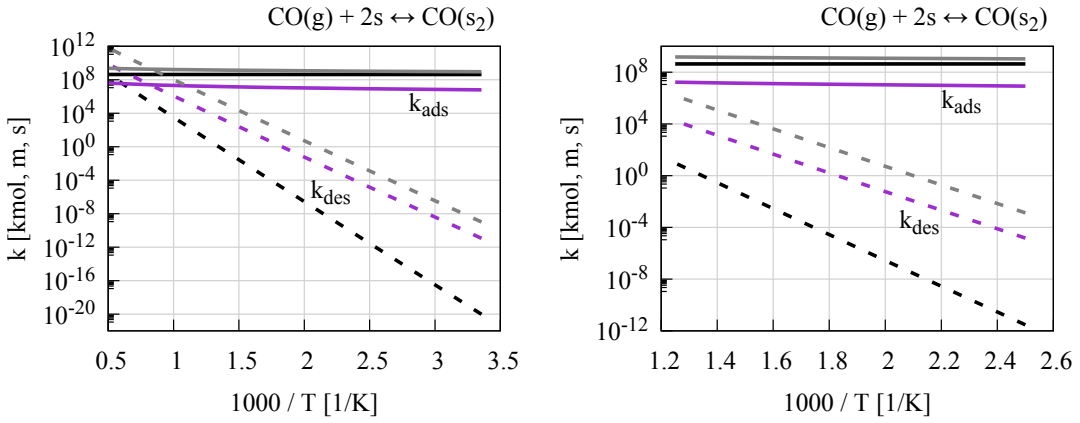


Fig. 3.21: Direct adsorption (−) (−) (−) and desorption (−−) (−−) (−−) CO rate constants. The temperature ranges are 298 K – 2000 K (left) and 400 K – 800 K (right). Rate parameters from the current mechanism (−), Kraus and Lindstedt [14, 15] (−) and Vincent et al. [11] mechanism (−) are presented. The T_{q^v} is fixed at 298 K for the current mechanism. The units of rate constants are in $[\frac{\mathrm{m}^3}{\mathrm{kmol\,s}}]$ and $[\frac{1}{s}]$ for direct adsorption and desorption reactions, respectively.

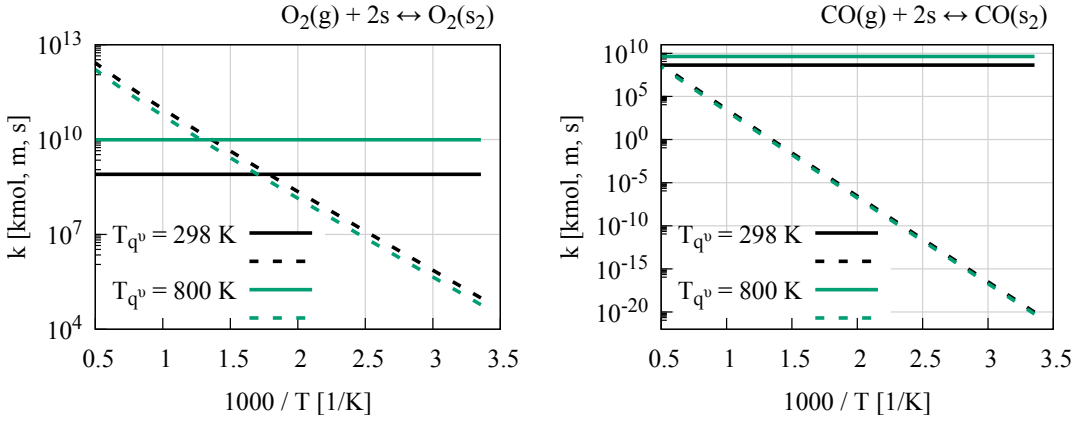


Fig. 3.22: Direct adsorption (−) (−) and desorption (−−) (−−) O_2 and CO rate constants, at $T_{q^v} = 298$ K and $T_{q^v} = 800$ K, for the current mechanism. The units of rate constants are in $[\frac{\mathrm{m}^3}{\mathrm{kmol\,s}}]$ and $[\frac{1}{s}]$ for direct adsorption and desorption reactions, respectively.

Regarding the direct adsorption and desorption of oxygen and carbon monoxide, presented in Figs. 3.20 and 3.21, the current mechanism demonstrates a two orders of magnitude higher adsorption rate constant, compared to the corresponding rate obtained from Kraus and Lindstedt [14, 15], where the VTST formalism along with a T_{q^v} fixed at 800 K was applied for the determination of rate constants, without the use of Sprowl et al. [16] approximation for the treatment of rotational partition functions. Vincent et al. [11], following the collision theory based approach, illustrates almost the same behaviour with

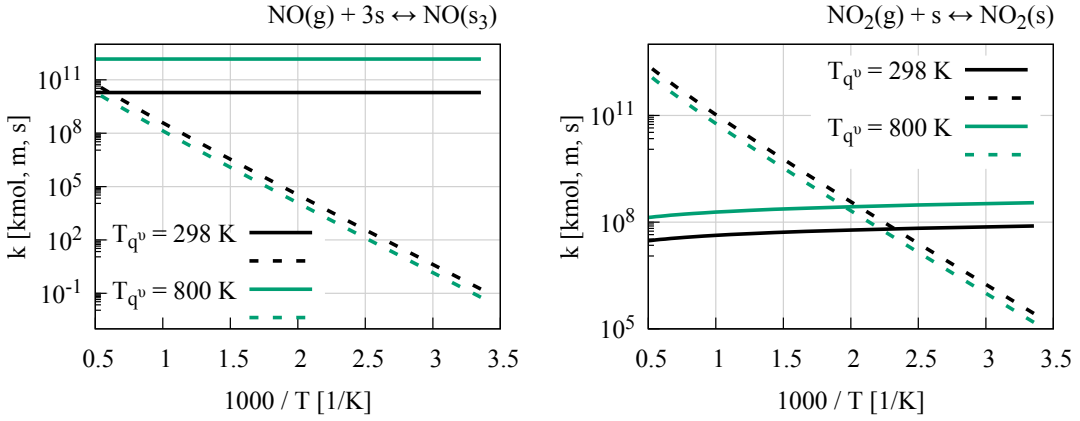


Fig. 3.23: Direct adsorption (−) (−) and desorption (−−) (−−) NO and NO_2 rate constants, at $T_{q^v} = 298$ K and $T_{q^v} = 800$ K, for the current mechanism. The units of rate constants are in $[\frac{\mathrm{m}^3}{\mathrm{kmol\,s}}]$ and $[\frac{1}{s}]$ for direct adsorption and desorption reactions, respectively.

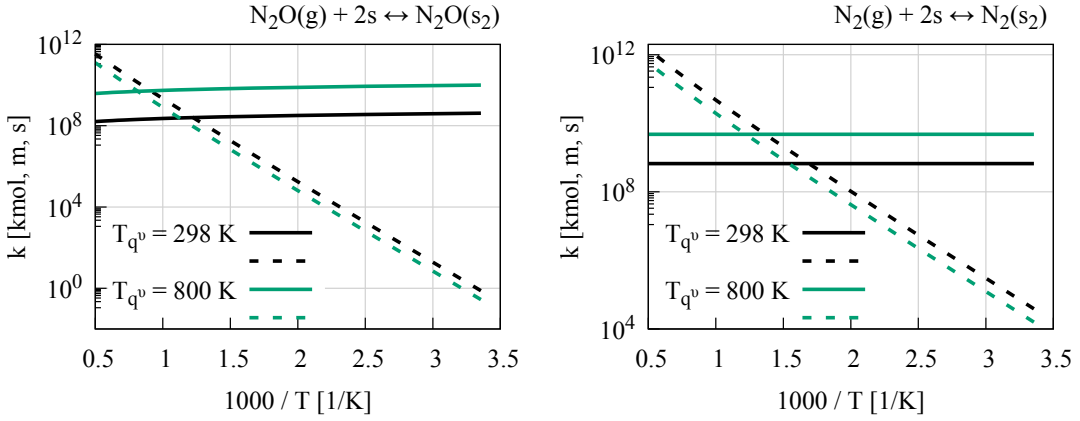


Fig. 3.24: Direct adsorption (−) (−) and desorption (−−) (−−) N_2O and N_2 rate constants, at $T_{q^v} = 298$ K and $T_{q^v} = 800$ K, for the current mechanism. The units of rate constants are in $[\frac{\mathrm{m}^3}{\mathrm{kmol\,s}}]$ and $[\frac{1}{s}]$ for direct adsorption and desorption reactions, respectively.

the other approaches, for the CO adsorption rate and seems to favour the adsorption of O_2 at lower temperatures. Additionally, the desorption rates are in a broad agreement over all the temperature range for all mechanisms. A comparison of direct adsorption and desorption O_2 and CO rate constants at $T_{q^v} = 298$ K and $T_{q^v} = 800$ K, is presented in Fig. 3.22. Although the direct desorption rate constants do not obviously differ between the two cases, the effect of T_{q^v} is significant for the O_2 adsorption rate constant, with a difference of one order of magnitude. For both O_2 and CO desorption reactions, a higher rate constant can be noticed at higher temperatures for the respective range.

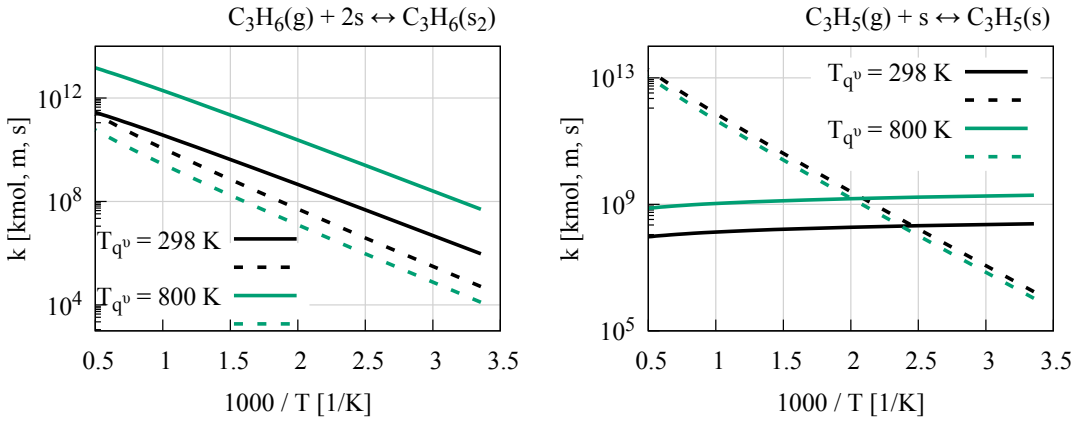


Fig. 3.25: Direct adsorption (−) (−) and desorption (−−) (−−) C_3H_6 and C_3H_5 rate constants, at $T_{q^v} = 298$ K and $T_{q^v} = 800$ K, for the current mechanism. The units of rate constants are in $[\frac{\mathrm{m}^3}{\mathrm{kmol\,s}}]$ and $[\frac{1}{s}]$ for direct adsorption and desorption reactions, respectively.

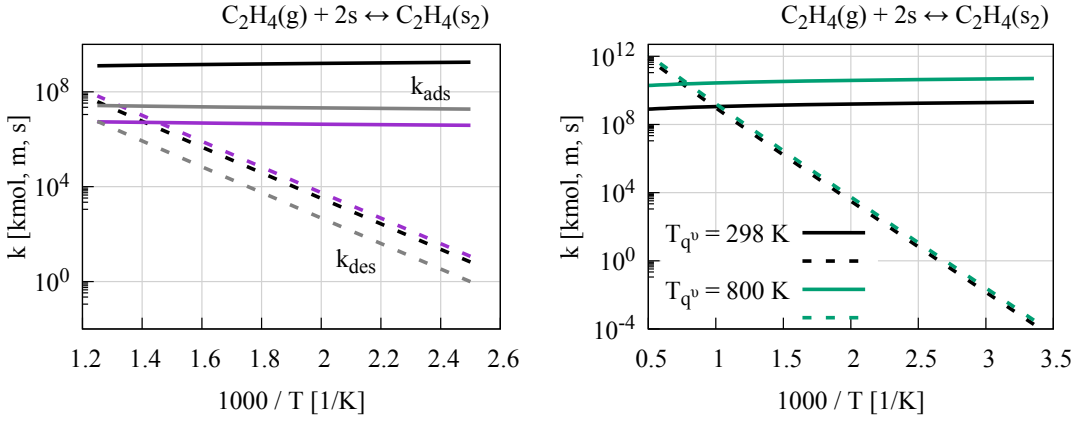


Fig. 3.26: Direct adsorption (−) (−) (−) and desorption (−−) (−−) (−−) C_2H_4 rate constants. Rate parameters from the current mechanism (−), Kraus and Lindstedt [14, 15] (−) and Vincent et al. [11] mechanism (−) are presented. The T_{q^v} is fixed at 298 K for the current mechanism while the temperature range is 400 K – 800 K (left). Direct adsorption (−) (−) and desorption (−−) (−−) C_2H_4 rate constants, at $T_{q^v} = 298$ K and $T_{q^v} = 800$ K, for the current mechanism (right).

As nitrogen containing reaction pathways were not included in the previous VTST [14, 15] and collision theory based approach [11], the related rate constants were only evaluated through the current work. All the nitrogen containing reactions outline that the determination of the current mechanism favours desorption with the gradual increase of temperature, while the NO_2 and N_2O adsorption reactions are favoured at temperatures below 1000 K, as shown in Figs. 3.23 and 3.24, for both $T_{q^v} = 298$ K and $T_{q^v} = 800$ K. The rate constants of the NO and N_2 direct adsorption reactions are constant in the

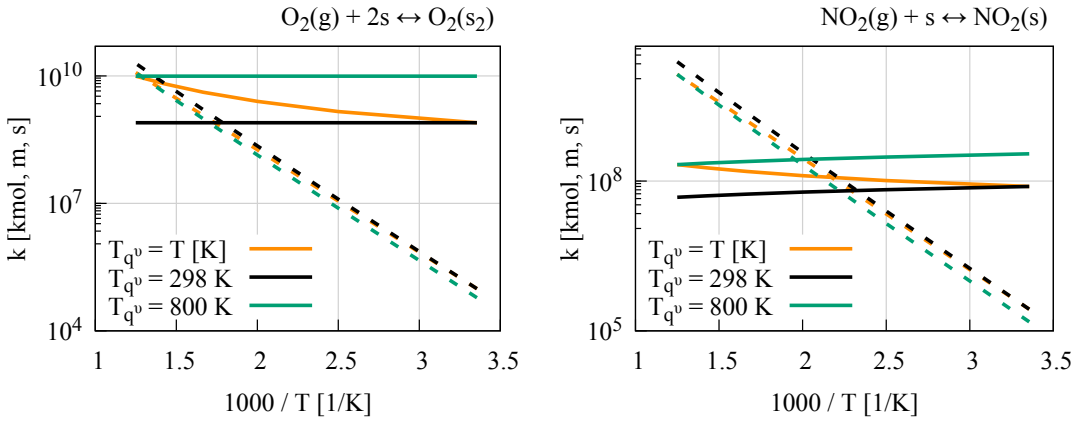


Fig. 3.27: Direct adsorption (−) (−) (−) and desorption (−−) (−−) (−−) O_2 and NO_2 rate constants, at $T_{q^v} = 298$ K, $T_{q^v} = 800$ K and a variable $T_{q^v} = T$ [K], for the current mechanism. The units of rate constants are in $[\frac{\text{m}^3}{\text{kmol s}}]$ and $[\frac{1}{s}]$, for direct adsorption and desorption reactions, respectively.

whole temperature range, due to the zero temperature dependency, β.

Representative hydrocarbon containing reaction pathways are shown in Figs. 3.25 and 3.26 for the two different T_{q^v} examined. A sharp decline of the C_3H_6 adsorption rate constants can be noticed for lower temperatures for both T_{q^v}, due to the application of a global irreversible C_3H_6 direct adsorption reaction, described in Chapter 4. Both C_3H_5 and C_2H_4 adsorption reactions are favoured at lower temperatures. Finally, the adsorption and desorption reactions of O_2 and NO_2 are illustrated in Fig. 3.27 when $T_{q^v} = 298$ K, $T_{q^v} = 800$ K and T_{q^v}, is not fixed, but varies from 298 K to 800 K together with temperature T [K]. The latter case is located between the two extreme fixed temperatures for both direct adsorption and desorption reactions, indicating that while the T_{q^v} increases a higher O_2 and NO rate constant is obtained. However, as a curve fitting is required for the estimation of overall temperature dependency, the choice of a fixed temperature for the evaluation of the vibrational partition function facilitates the calculations with arguably acceptable accuracy, while maintaining agreement with measured sticking coefficients.

3.3.1.1 Treatment of C_2H_4 catalytic chemistry

The operating conditions of the catalytic converter, described in Chapter 4, features a different temperature window, from 400 K to 800 K, compared to the cases studied in the past, which feature temperatures higher than 800 K [14, 15]. As a result the C_2H_4

catalytic chemistry was reviewed in order to deal with the C_2H_4 conversion, which can affect the whole chemical system and especially the C_3H_6 conversion.

The C_2H_4 and C_3H_6 molecules convert in a similar way when they interact with the metal surface, by breaking the pi-bond and permitting the unsaturated bond to dominate the conversion. Following a rate analysis based on C_2H_4 surface chemistry, a hindered conversion was noticed due to the complete desorption of C_2H_4 at higher temperatures. This suggests a mobile transition state which permits the omission of the $\frac{1}{x^x}$ scaling factor from the C_2H_4 direct adsorption reactions presented in Table 3.5.

Table 3.5: Updated C_2H_4 direct adsorption reactions

Reactions
$C_2H_4(g) + 2\,s \rightarrow C_2H_4(s_2)$
$C_2H_4(g) + 2\,s \rightarrow CHCH_3(s_2)$

Furthermore, as discussed in Chapter 5, the approximated isomerisation reactions on the surface, introduced by analogy to the gas phase [11], are not sufficiently accurate and have hence been omitted.

3.4 Summary

The evaluation of rate constants for adsorption reactions through the determination of the mobile and immobile transition state of the adsorbing species on the platinum surface, are analytically presented in the current Chapter. Section 3.1 establishes the methodology used for the calculation of rate constants via the Sprowl et al. [16] approximation, which accounts for hindered rotors and translators. This approach was validated with various experimental studies used for representative chemical species, in order to study the respective mobility on the metal surface.

Apart from the H_2 adsorbing species which sticks on the surface and remains immobile, as resulting from the comparison of the proposed methodology with experimental studies [101, 102, 117, 118, 119], the remaining species correspond to a mobile transition state. However, both cases of mobility and immobility of H_2 on the Pt surface are examined in Chapters 4 and 5, as a means of comparison. Subsequently, a complete evaluation of both

sticking coefficients and rate constants for the selected species, considered in the current Chapter, is undertaken for three different cases related to the respective temperature of the vibrational partition function. In particular, a comparison of a fixed T_{q^v} at 298 K and 800 K, and a variable T_{q^v}, with available experimental data [1, 101, 103, 105, 106, 117, 120] enhances the use of $T_{q^v} = 298$ K as the prevailing choice. Given the fact that $T_{q^v} = 800$ K seems to be a consistent choice for the CO adsorption reaction, both $T_{q^v} = 298$ K and $T_{q^v} = 800$ K have been considered for the calculation of rate constants. The impact of the $T_{q^v} = 800$ K application, exclusively on the CO direct adsorption reaction, as well as, on the whole surface chemical network is studied in Chapter 4.

Figures 3.20, 3.21 and 3.26 illustrate the O_2, CO and C_2H_4 direct adsorption and desorption rate constants of the proposed reaction mechanism along with the respective rate constants obtained from the previous VTST [14, 15] and collision theory based mechanisms [11] at two different temperature ranges 298 K – 2000 K and 400 K – 800 K for the O_2 and CO reactions. The temperature range presented for the C_2H_4 adsorption and desorption reactions for all the mechanisms is 400 K – 800 K. The use of a narrower range contributes in a better identification of the compared mechanisms. The difference of the corresponding rate constants evaluated for each mechanism ranges from one to three orders of magnitude, depending on the reaction examined. The rate constants calculated by the VTST based approach [14, 15] differ by around two to three orders of magnitude from the respective rates of the proposed mechanism, while a smaller difference of around one order of magnitude can be observed with the rate constants of the collision theory based mechanism [11]. The former difference can be attributed to difficulties in determining the rotational partition function on the surface. Therefore, based on these calculations, higher reaction rates are expected, while the slower ones correspond to the VTST based approach [14, 15]. The latter imposes inevitable changes on the treatment of representative rate constants (e.g. C_2H_4 catalytic reactions) calculated in previous works [11, 14, 15], as shown in Section 3.3.1.1.

Finally, an important addition outlined in the current Chapter is the evaluation of the $-$N containing and C_3H_6, C_3H_5 rate constants, through the determination of their mobile or immobile transition state. As described in Sections 3.2.2 and 3.2.3 all the -N containing and C_3H_6, C_3H_5 chemical species present a mobile transition state, when compared with

available experimental studies. This sub-mechanism included in the current reaction mechanism is extensively validated in Chapter 4, via a series of Test Cases.

Chapter 4

Multi-scale simulation of NOx removal using Pt/Al_2O_3 catalysts

The removal of the three principal oxides of nitrogen (NO, NO_2 and N_2O) from automotive exhaust gases through the use of supported Pt catalysts is a topic of significant practical interest and amenable to studies using heterogeneous microkinetic catalysis. This Chapter is devoted to a rigorous comparison of the proposed reaction mechanism, introduced in Chapters 2 and 3, with experimental data obtained by Toyota Motor Europe (TME) [2] for nine different Test Cases. The results obtained for CO, NO and C_3H_6 conversion against temperature were first used in a fully predictive mode followed by related adjustments described in Section 4.3.1. The choice of a Pt/Al_2O_3 catalyst was made due to the availability of related experimental data [2].

4.1 Experimental Data

An experimental investigation of the conversion rates of the pollutants CO, NO and C_3H_6 as a function of temperature, using a Pt/Al_2O_3 catalytic packed reactor, at different metal loadings and coat amounts, was provided by TME [2]. Errors related to the experimental measurements [2] were not available and some uncertainties remain regarding the impact of the catalyst preparation (e.g. calcination, sintering and dispersion) on the final activity.

4.1.1 Experimental Setup

The experimental conditions used in the current work comprise nine different Test Cases [2]. The Pt loading corresponds to 0.5, 1 or 3 wt% depending on the case examined. The reactor bed consists of a 50 mm long catalytic section with a diameter of 30 mm. The washcoat is supported by a substrate with a cell density of 400 cpsi (number of cells per square inch) and the channel diameter was estimated as 1.246 mm with a wall thickness of 0.4826 mm. The flow velocity was determined as 0.47 m/s, while the noble metal loading, the coat amount and the ratio of the active metal surface per geometrical area, vary according to the Test Case applied. The species inlet mol fractions used for the simulations follows the mixture provided by TME [2] as shown in Table 4.1, while the experimental conditions are presented in Table 4.2. Experiments [2] were conducted at atmospheric pressure.

Table 4.1: Initial mixture composition provided by TME [2].

Species	Mol fractions
CO	0.0065
CO_2	0.1
C_3H_6	0.001
NO	0.0015
O_2	0.0068
H_2O	0.03
N_2	0.8542

Table 4.2: Experimental conditions provided by TME [2].

Experimental Conditions	
Cell density	400 cells/inch^2
Channel diameter	1.246 mm
Channel length	50 mm
Velocity	0.47 m/s
Temperature at the entrance of the catalytic converter	371.5 K
Temperature range	$450 - 800$ K

The Knudsen porous media diffusion mechanism was selected for the respective implementations, due to the small size of pores measured experimentally, as described in Section 2.3.2.1. The specific surface area (SSA) of supported material along with the values related to the pore distribution, at different Pt loadings, are presented in Table 4.3. As the latter physical quantities measured experimentally [2] show a slight discrepancy for the different Pt loadings, the mid-point case corresponding to 1 wt% Pt was used for the evaluation of the porosity and tortuosity implemented in the current simulations, for the calculation of the Knudsen effective diffusion coefficients, $D_i^{K,eff}$. However, the porosities and tortuosities obtained at 0.5 wt% Pt and 3 wt% Pt, are also evaluated and included in Table 4.4 for the purpose of completeness.

Table 4.3: Experimental measurements [2] of pore distribution at different Pt loadings and coat amounts.

Pt loading	SSA (m^2/gr)	Coat amount (g/L)	Total pore volume (cm^3/gr)	Average of pore diameter (nm)	Maximum pore size (nm)
0.5 wt %	118.2	60	0.4975	17.818	21.3
1 wt %	110.1	92	0.5192	18.099	21.3
3 wt %	114.3	171	0.5131	18.791	21.3

Table 4.4: Calculated porosities, tortuosities and site densities based on TME measurements [2], at different Pt loadings. The values applied in the current simulations are indicated in a bold font.

Pt loading	Porosity [11]	Tortuosity [11]	Porosity [55]	CO adsorption amount (cm^3/gr)	Site density (kmol/m^2)
0.5 wt %	0.51	1.96	0.32	0.1691	$1.01 \cdot 10^{-10}$
1 wt %	**0.49**	**2.04**	0.28	0.3130	$2.11 \cdot 10^{-10}$
3 wt %	0.51	1.96	0.32	1.1415	$7.33 \cdot 10^{-10}$

Additionally, two different approaches of porosities calculation are shown in Table 4.4 based on the geometrical [11] and Giani et al. [55] expressions presented in Section 2.3.2. The latter approach substantially reduces the Knudsen diffusion efficiency factor, resulting from the lower values of porosities obtained. The site density Γ is a measure of the amount of available catalyst sites per unit area and constitutes a fundamental parameter in the estimation of the heterogeneous reaction rates. The actual value of Γ can be evaluated

via Eq. (4.1) [11], where ρ_s is the average density of the catalyst ($3.2 \cdot 10^3$ kg/m^3), S_v is the specific surface area per unit volume of solid and the M_p corresponds to the maximum molar uptake of the catalyst, calculated by the CO adsorption amount (cm^3/gr), shown in Table 4.4 for each Pt loading.

$$\Gamma = \frac{\rho_s M_p}{S_v} \tag{4.1}$$

Given the fact that the Pt content is not perfectly dispersed as individual atoms, the site densities listed in Table 4.4 for each Pt loading are further reduced by a factor related to the loss in calculated areas due to the agglomeration. The volumes of the Platinum Group Metal (PGM) particle are shown in Table 4.5, for each Pt loading, while the volume of a single Pt atom is equal to $1.11 \cdot 10^{-29}$ m^3, for $r_a = 1.38 \cdot 10^{-10}$ m. The number, n, of Pt atoms packed into the larger volume results from the volume ratio. However, atoms are approximated as hard spheres, and the maximum packing density is selected at 0.74 [123] for a face-centered cubic surface, concluding to the n_{pf} values presented in Table 4.5.

Table 4.5: Calculated volumes (V_{Pt}) , projected areas (A_{Pt}) and number of Pt atoms for PGM particles (n_{pf}), based on TME measurements [2], at different Pt loadings. The calculation of n_{pf} considers a packing density of 0.74.

Pt loading	PGM particle diameter (m) [2]	V_{Pt} (m^3)	A_{Pt} (m^2)	n_{pf}	$n_{pf}/2$
0.5 wt %	$3.85 \cdot 10^{-9}$	$2.99 \cdot 10^{-26}$	$2.33 \cdot 10^{-17}$	1987	993
1 wt %	$4.16 \cdot 10^{-9}$	$3.77 \cdot 10^{-26}$	$2.72 \cdot 10^{-17}$	2506	1253
3 wt %	$3.42 \cdot 10^{-9}$	$2.09 \cdot 10^{-26}$	$1.84 \cdot 10^{-17}$	1393	696

Assuming that the Pt loading is distributed as half spheres on the surface, the $n_{pf}/2$ is taken into account for the final calculation of the area loss. The latter is evaluated as the ratio of the atomic projected area, A_a, over the PGM particle projected area of the surface perimeter, A_{Pt}, divided by the $n_{pf}/2$. The dispersion efficiency factors, η_D, shown in Table 4.6 for each Pt loading, are considered as the inverse of the area loss and are used in order to be consistent with the experimental data [2] for CO adsorption adsorption amount. The values of η_D, especially for 0.5 wt% and 1 wt% Pt loading, agree comparatively with the respective value presented by Chatterjee et al. [1] at 0.33.

Table 4.6: Calculated loss of area and dispersion efficiency factor (η_D), at different Pt loadings.

Pt loading	$\frac{A_a}{A_{\mathrm{Pt}}/(n_{pf}/2)}$	η_D
0.5 wt %	2.57	0.39
1 wt %	2.78	0.36
3 wt %	2.28	0.44

Finally, the average Knudsen efficiency factor, $\bar{\eta}_e$, originates from the corresponding average value of $\bar{D}_i^{eff}/D_i^{eff}$ ratio of the selected species, listed in Table 2.1. The values of the average Knudsen efficiency factor are indicative and slightly differ based on the temperature and Pt loading applied, as shown in Table 2.2.

4.2 Computational Methods

A 2D parabolic FORTRAN code [12] adapted for heterogeneous applications [11, 14, 15], was used to simulate a single, virtual, representative axisymmetric pore corresponding to the experimental device. The simulation contained 40 geometrically refined cells in the radial direction, corresponding to 1 μm resolution close to the catalytic surface. The gas temperature at the entrance of the reactor was set to 371.5 K with wall and exit temperatures set according to the experimental data [2] ranging from 450 K to 800 K.

The area ratios, F, presented in Table 4.7, correspond to the ratio of the catalytic active surface area over the geometrical area as calculated based on the experimental data [2] for each Test Case. Particularly, the catalytic active surface area is evaluated from the product of the Pt metal projected surface, for the radius of a Pt atom, $r_a = 1.38 \cdot 10^{-10}$ m and the CO adsorption amount, while the geometrical area results from the product of the channel perimeter, cell density (e.g. number of cells) and channel length. An experimental factor of 1.43 [2], resulting from the assumption of an average of more than one Pt site per CO molecule adsorbed, is further taken into account. The inclusion of the dispersion efficiency factor η_D, results in the area ratio denoted F' in Table 4.7. The alternative value, F'', contains only the factor of 1.43, omitting the consideration of dispersion and, as such, indicates an upper limit. Each Test Case corresponds to a

different value of the area ratio due to the different coat amounts applied, even for the same Pt loading. The upper limit area ratio, F'', is applied in Sections 4.3.2 and 4.3.3.

Table 4.7: Calculated area ratios (F) and (F'). The values of F' include the dispersion efficiency and the 1.43 experimental factor, associated with the average number of Pt sites, related to CO adsorption amount. Different experimental Pt loadings and coat amounts, are shown. Finally, F'' only contains the factor of 1.43 scaling, and thus constitutes an upper limit.

Test Cases	Pt loading	Coat amount (g/L)	η_D	F	F'	F''
1	0.5 wt %	60	0.39	6.94	3.87	9.92
2	0.5 wt %	92	0.39	10.50	5.85	15.01
3	0.5 wt %	171	0.39	19.52	10.87	27.91
4	1 wt %	60	0.36	12.84	6.61	18.36
5	1 wt %	92	0.36	19.43	10.00	27.79
6	1 wt %	171	0.36	36.13	18.60	51.67
7	3 wt %	60	0.44	46.82	29.46	66.96
8	3 wt %	92	0.44	70.87	44.59	101.34
9	3 wt %	171	0.44	131.77	82.91	188.43

As shown by Chatterjee et al. [1] (e.g. Eq. (4.2)), the mass-weighted production rate at the catalytic wall includes the average diffusion efficiency factors listed in Table 2.2. The product of the area ratio, e.g. F, for each Test Case and the net rate of formation R_i provides the effective applied reaction rate.

$$J_i + \rho Y_i u_s = \eta_e F R_i M_{w,i} \Leftrightarrow J_i + \rho Y_i u_s = \eta_e \bar{R}_i M_{w,i} \tag{4.2}$$

The catalytic site density for Pt, ($\Gamma = 2.72 \cdot 10^{-8}$ kmol/m^2 [124]), was directly implemented in the expression of the rate constant, shown in Eq. (3.28), and corresponds to a pure Pt surface with 100% metal dispersion. The upper limit area ratios, F'', without the consideration of the dispersion efficiency factor, are applied in Sections 4.3.2 and 4.3.3 following an adjustment for the site density ratio ($= 7.75 \cdot 10^{-3}$) resulting from the mid-point case at 1% Pt loading shown in Table 4.4. The current maximum Knudsen efficiency factor, obtained from the geometrical approach [11], is presented in Section 2.3.2.1. A comparison of the Knudsen efficiency factors including the expression proposed by Giani et al. [55], is shown in Table 4.8. The above parameter choices hence correspond to the

maximum expected catalytic activity and it was found necessary, based on Test Case 5, to reduce the effective reaction rate by a constant factor of 4.44. The latter is similar as to the impact of dispersion and the reduced Knudsen diffusion efficiency and was applied to computations in Sections 4.3.2 and 4.3.3. Furthermore, some uncertainties prevail in relation to the catalyst preparation (e.g. the impact of calcination, sintering and loss of activity over time). The impact of dispersion is further considered in Section 4.3.4. Finally, radiative heat loss was not imposed in the computations.

Table 4.8: Calculated Knudsen efficiency factors, at different Pt loadings, via the geometrical [11] and Giani et al. [55] approach, at 600 K.

Pt loading	η_e [11]	η_e [55]
0.5 wt %	$3.66 \cdot 10^{-2}$	$1.43 \cdot 10^{-2}$
1 wt %	$3.44 \cdot 10^{-2}$	$1.24 \cdot 10^{-2}$
3 wt %	$3.86 \cdot 10^{-2}$	$1.70 \cdot 10^{-2}$

4.2.1 Gas phase chemistry

A detailed mechanism which stems from the work of Leung and Lindstedt [12], Lindstedt and Skevis [59], Lindstedt and Meyer [13], Sun et al. [125], Vincent et al. [11] and Kraus and Lindstedt [14, 15] was adopted as the basis of the gas phase chemistry along with the corresponding thermochemical and transport data. The aim of the current investigation is not the gas phase kinetics, but the surface chemistry, so no attempt was made to develop the C_1-C_2 mechanism further.

The C_1-C_2 basis gas-phase mechanism comprises 271 reactions and 44 gas phase species: H_2, O_2, H, OH, O, H_2O, HO_2, H_2O_2, C_2H_6, C_2H_5, C_2H_4, C_2H_2, CH_4, CH_3, CH_2s, CH_2t, CH, C_1, CO, CO_2, CH_2O, CHO, CH_3OH, CH_3O, CH_2OH, C_2O, C_2H, C_2HO, C_2H_2O, C_2H_3, CH_3CHO, CH_3CO, C_2, CH_2CHO, H_2C_2, CH_3OO, CH_3OOH, $CHCH_2O$, C_2H_4O, C_2H_4OOH, C_2H_5O, C_2H_5OO, C_2H_5OOH, N_2. However, it is further augmented by a comprehensive -C_3 [12] and -N [60, 61, 62, 63, 64] containing mechanism which is composed of 431 additional reactions and 62 additional species : C_3H, C_3H_2, C_3H_2l, C_3H_3, C_3H_4a, C_3H_4p, C_3H_4b, C_3H_5a, C_3H_5s, C_3H_5t, C_3H_5b, C_3H_6b, C_3H_6, C_3H_7n, C_3H_7i, C_3H_8, C_3H_2O, C_3H_3O, C_3H_4O, C_3H_5O, C_3H_5Op, C_3H_5Ot, C_3H_5Oa, C_3H_6O, C_3H_6Oa, C_3H_6Op, C_3H_7Oi, C_3H_7On, C_3H_6OH, C_3H_7OOHi, C_3H_7OOHn, C_3H_7OOi, C_3H_7OOn, C_3H_6OOH,

NH_3, NH_2, NH, N, N_2H_2, NNH, HNO, NO, NO_2, N_2O, HCN, CN, NCO, HNCO, HOCN, HNO_2, H_2CN, HCNO, HNC, CH_3NO_2, CH_2NO_2, N_2, N_3, NO_3, N_2O_5, N_2O_3, HNO_3, N_2O_4, HN_3. The mechanism has been comprehensively validated [60, 61, 62, 63, 64] with particular emphasis on the performance under SNCR (selective non-catalytic reduction) conditions for NO removal in the presence of ammonia [60, 61, 62]. Hence, it provides a link between two alternative technologies and, more importantly in the current context, also permits the computation of interconversion of oxides of nitrogen in the exhaust pipe after to the catalytic converter. The mechanism has also been found to perform well under more extended conditions [126].

4.2.2 Surface chemistry

The surface chemistry applied in this chapter, constitutes an extension of Kraus and Lindstedt [14, 15] catalytic chemistry based on VTST calculations, as mentioned in Chapter 2. The basis surface mechanism comprises 320 reversible catalytic reactions and 34 surface species: $C_2H_6(s_2)$, $CH_2CH_3(s)$, $C_2H_4(s)$, $C_2H_4(s_2)$, $CHCH_3(s_2)$, $CHCH_2(s)$, $CHCH_2(s_3)$, $CCH_3(s_3)$, $CCH_2(s_2)$, $CCH_2(s_3)$, $C_2H_2(s_3)$, $CH_3(s)$, $CH_2(s_2)$, $CH(s_3)$, $CO(s_2)$, $CO_2(s_2)$, $CH_3OH(s)$, $CH_3O(s)$, $CH_2OH(s)$, $CH_2O(s)$, $CHOH(s_2)$, CHO(s), CCH(s), $C(s_3)$, $COH(s_3)$, COOH(s), $H_2(s)$, $O_2(s_2)$, O(s), OH(s), H(s), $H_2O(s)$, OOH(s), $H_2O_2(s_2)$. However, it is further augmented by a comprehensive -C_3 and -N element based mechanism which is composed of 32 additional reversible catalytic reactions and 7 additional surface species: $C_3H_6(s_2)$, $C_3H_5(s)$, N(s), $NO(s_3)$, $NO_2(s)$, $N_2O(s_2)$, $N_2(s_2)$. The latter -C_3 surface mechanism was further updated by 11 reversible catalytic reactions and 2 additional surface species: $C_2H_5CH(s_2)$ and $C_2H_5C(s_3)$.

The applied surface configurations of the 9 additional surface species along with the corresponding bond type and bond lengths are included in Table 2.3. Additionally, the respective total bond energies are presented in Table 2.5. The geometrical parameters, used as input data, for the determination of recombination, surface bimolecular, surface unimolecular and isomerisations with site reaction classes, are calculated by the Steric program [66], as illustrated in Table 3.2.

4.3 Results

4.3.1 Methodology

The methodology applied to model the TME data [2] is based on the determination of mobile and immobile sticking coefficients via VTST and the application of Sprowl at al. [16] approximation for the treatment of rotational partition functions, as discussed in Chapter 3. Apart from the molecular adsorption reactions of NO and C_2H_4, which were treated using a mobile transition state prior to surface attachment, resulting in the omission of the $\frac{1}{x^x}$ scaling factor from the rate constant expression, shown in Eq. (3.28), the C_3H_6 and C_2H_5CH direct adsorption reactions, are also subject to the same consideration along with the adjustments presented in Sections 4.3.1.1 and 4.3.1.2.

4.3.1.1 Global catalytic C_3H_6 step sub-mechanism

The overall surface chemistry for C_3H_6 adsorption and decomposition is not well established at present. The analysis performed below and applied in the simulations of Section 4.3.2.6, suggests a global activation energy of 39.4 kJ/mol. This is broadly consistent with the value of 41 kJ/mol estimated by TME [2]. Therefore, an energy correction ε to the activation energy E_A of the C_3H_6 adsorption reaction was introduced to better describe the C_3H_6 behaviour on the Pt surface, in the whole temperature range (450 K < T < 800 K). The value of 39.4 kJ/mol is evaluated based on the following expression, where $T_0 = 450$ K and $T_1 = 800$ K.

$$\varepsilon = R\,\frac{T_1\,T_0}{T_1 - T_0}\,\ln 100 \approx 39.4\,\mathrm{kJ/mol}. \tag{4.3}$$

Consequently, from Eq. (4.4), the constant term $\exp\left(\frac{\varepsilon}{R\,T_0}\right)$ can be absorbed into the pre-exponential factor A, as shown in Eq. (4.5).

$$k_{\text{eff}} = A\,T^{\beta}\,\exp\left(-\frac{E_A + \varepsilon}{R\,T}\right)\exp\left(\frac{\varepsilon}{R\,T_0}\right) \tag{4.4}$$

$$k_{\text{eff}} = A'\,T^{\beta}\,\exp\left(-\frac{E_A + \varepsilon}{R\,T}\right) \tag{4.5}$$

Therefore, the pre-exponential factor used for the C_3H_6 direct adsorption reaction is given by Eq. (4.6),

$$A' = A \exp\left(\frac{\varepsilon}{R\,T_0}\right), \tag{4.6}$$

where ε is the constant value of energy, given by the Eq. (4.3) for the temperature interval between T_0 and T_1. Subsequently, for the intermediate temperatures T in the $T_0 < T < T_1$ interval, Eq. (4.5) allows for a smooth monotonic interpolation of k_{eff}. Hence, an irreversible C_3H_6 adsorption reaction was used.

The surface reversible reactions, with the exception of the initial adsorption, involved in the C_3H_6 sub-mechanism are presented in Table 4.9, where the global C_3H_6 direct adsorption reaction has been included. The surface bimolecular reaction (4), shown in Table 4.9 was also disabled following a sensitivity analysis for the identification of the rate-limiting steps [127]. The values of the rate constants were evaluated based on the implementation of a T_{q^v} fixed at 298 K.

4.3.1.2 Towards detailed C_3H_6 catalytic chemistry

Given the fact that a use of a global irreversible adsorption reaction of C_3H_6 does not allow for a detailed and completely accurate description of the proposed chemical mechanism,

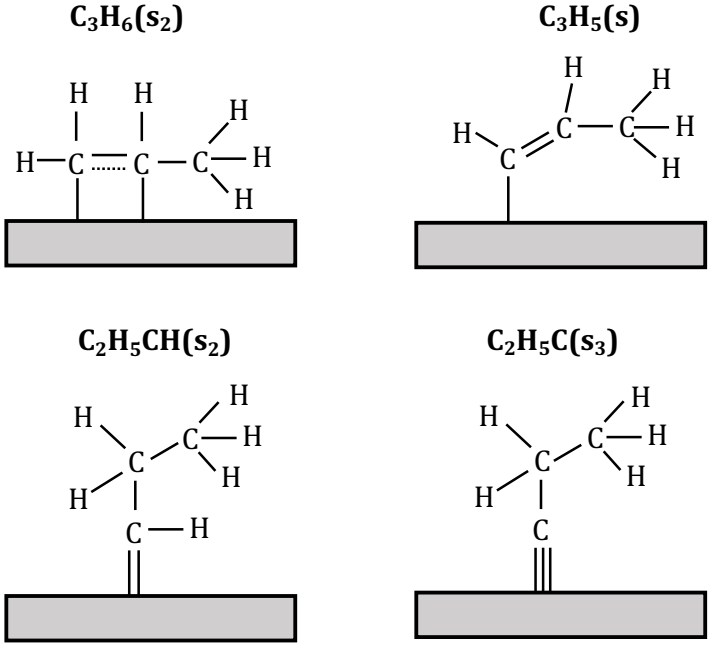


Fig. 4.1: Schematic of the adsorbate geometry of C_3H_6, C_3H_5, C_2H_5CH, C_2H_5C. These diagrams do not accurately represent the molecular interaction.

Table 4.9: Global catalytic C_3H_6 step sub-mechanism at $\theta = 20\%$ [100] of the magnitude of $Q_{C,H,O,N}$. The units of the pre-exponential factors, A, are [kmol, m^2, s], depending on the reaction class and the activation energies, E_A, are evaluated in kJ/mol.

#	Reactions	A	β	E_A
1	$C_3H_6 + 2\,s \rightarrow C_3H_6(s_2)$	1.33006E+14	-0.50	39.40
2	$C_3H_6(s_2) \rightarrow C_3H_6 + 2\,s$	0.00000E+00	1.00	39.13
3	$C_3H_6(s_2) \rightarrow CH_3(s) + CHCH_2(s)$	2.08366E+10	1.00	100.47
4	$CH_3(s) + CHCH_2(s) \rightarrow C_3H_6(s_2)$	0.00000E+00	0.50	0.00
5	$s + C_3H_5a \rightarrow C_3H_5(s)$	4.21289E+09	-0.50	0.00
6	$C_3H_5(s) \rightarrow C_3H_5a + s$	1.10134E+11	1.00	41.52
7	$C_3H_5(s) + 4\,s \rightarrow CCH_3(s_3) + CH_2(s_2)$	1.32573E+07	0.50	113.74
8	$CH_2(s_2) + CCH_3(s_3) \rightarrow C_3H_5(s) + 4\,s$	6.02307E+09	0.50	60.54
9	$C_3H_5(s) + 2\,s \rightarrow CH_2(s_2) + CHCH_2(s)$	8.48464E+08	0.50	85.98
10	$CH_2(s_2) + CHCH_2(s) \rightarrow C_3H_5(s) + 2\,s$	6.28757E+09	0.50	37.66
11	$C_3H_5(s) + 3\,s \rightarrow C_2H_2(s_3) + CH_3(s)$	1.25698E+08	0.50	0.00
12	$CH_3(s) + C_2H_2(s_3) \rightarrow C_3H_5(s) + 2\,s$	6.35120E+09	0.50	63.07
13	$C_3H_5(s) + 3\,s \rightarrow C(s_3) + CH_2CH_3(s)$	1.25698E+08	0.50	6.70
14	$C(s_3) + CH_2CH_3(s) \rightarrow C_3H_5(s) + 3\,s$	6.03919E+09	0.50	101.66
15	$O(s) + C_3H_5a + 3\,s \rightarrow C_2H_4(s) + COH(s_3)$	4.69320E+08	-0.50	0.00
16	$C_2H_4(s) + COH(s_3) \rightarrow C_3H_5a + O(s) + 3\,s$	5.37732E+09	0.50	97.43
17	$OH(s) + C_3H_5a + 3\,s \rightarrow CHCH_3(s_2) + CHOH(s_2)$	3.89821E+07	-0.50	34.44
18	$CHCH_3(s_2) + CHOH(s_2) \rightarrow C_3H_5a + OH(s) + 3\,s$	5.38703E+09	0.50	45.46
19	$OH(s) + C_3H_5(s) \rightarrow C_3H_6 + O(s) + s$	6.38270E+09	0.50	0.00
20	$s + O(s) + C_3H_6 \rightarrow C_3H_5(s) + OH(s)$	1.70040E+10	-0.50	15.39
21	$C_3H_6(s_2) \rightarrow C_3H_5(s) + H(s)$	2.08366E+10	1.00	87.68
22	$H(s) + C_3H_5(s) \rightarrow C_3H_6(s_2)$	1.97271E+10	0.50	0.00

further investigation has to be conducted towards this direction. Alternative propene and propenyl adsorption modes on the Pt surface have been determined based on the configurations suggested by Chatterjee et al. [1]. More specifically, based on the previous approach, described in Section 4.3.1.1, the C_3H_6 attaches on two Pt sites through a bridged configuration by breaking of the *pi*-bond. On the other hand, the C_2H_5CH isomer requires a hydrogen transfer as the carbon atom attaches directly on two Pt sites, as illustrated in Fig. 4.1.

Both configurations are included in the more detailed C_3H_6 reaction network. An alternative surface configuration of C_2H_5C on the metal surface was also explored via a

dissociative adsorption on three Pt sites and also incorporated in the mechanism. The new reactions added in the previous reaction scheme correspond to the (23) - (42) presented in Table 4.10. In order to decouple the rates of the desorption steps related to the thermodynamics applied for $C_3H_6(s_2)$ and $C_2H_5CH(s_2)$, the isomerisation reactions (25) and (26) were removed due to potential inaccuracies as highlighted for the -C_2 mechanism in Section 3.3.1.1. The oxidation pathways (35) - (42) are included as they enable a more sophisticated order of magnitude estimates, while the dissociative adsorption sequence (33) - (34) is also considered for the mitigation of the H bond split via the respective heat of adsorption.

Table 4.10: Detailed C_3H_6 surface reaction sub-mechanism at $\theta = 20\%$ [100] of the magnitude of $Q_{C,H,O,N}$. The units of the pre-exponential factors, A, are [kmol, m^2, s], depending on the reaction class and the activation energies, E_A, are evaluated in kJ/mol.

#	**Reaction**	A	β	E_A
1	$C_3H_6 + 2\,s \rightarrow C_3H_6(s_2)$	3.55043E+10	-0.50	0.00
2	$C_3H_6(s_2) \rightarrow C_3H_6 + 2\,s$	1.25250E+09	1.00	39.13
3	$C_3H_6(s_2) \rightarrow CH_3(s) + CHCH_2(s)$	2.08366E+10	1.00	100.47
4	$CH_3(s) + CHCH_2(s) \rightarrow C_3H_6(s_2)$	6.13949E+09	0.50	0.00
5	$s + C_3H_5a \rightarrow C_3H_5(s)$	4.21289E+09	-0.50	0.00
6	$C_3H_5(s) \rightarrow C_3H_5a + s$	1.10134E+11	1.00	41.52
7	$C_3H_5(s) + 4\,s \rightarrow CCH_3(s_3) + CH_2(s_2)$	1.32573E+07	0.50	113.74
8	$CH_2(s_2) + CCH_3(s_3) \rightarrow C_3H_5(s) + 4\,s$	6.02307E+09	0.50	60.54
9	$C_3H_5(s) + 2\,s \rightarrow CH_2(s_2) + CHCH_2(s)$	8.48464E+08	0.50	85.98
10	$CH_2(s_2) + CHCH_2(s) \rightarrow C_3H_5(s) + 2\,s$	6.28757E+09	0.50	37.66
11	$C_3H_5(s) + 3\,s \rightarrow C_2H_2(s_3) + CH_3(s)$	1.25698E+08	0.50	0.00
12	$CH_3(s) + C_2H_2(s_3) \rightarrow C_3H_5(s) + 2\,s$	6.35120E+09	0.50	63.07
13	$C_3H_5(s) + 3\,s \rightarrow C(s_3) + CH_2CH_3(s)$	1.25698E+08	0.50	6.70
14	$C(s_3) + CH_2CH_3(s) \rightarrow C_3H_5(s) + 3\,s$	6.03919E+09	0.50	101.66
15	$O(s) + C_3H_5a + 3\,s \rightarrow C_2H_4(s) + COH(s_3)$	4.69320E+08	-0.50	0.00
16	$C_2H_4(s) + COH(s_3) \rightarrow C_3H_5a + O(s) + 3\,s$	5.37732E+09	0.50	97.43
17	$OH(s) + C_3H_5a + 3\,s \rightarrow CHCH_3(s_2) + CHOH(s_2)$	3.89821E+07	-0.50	34.44
18	$CHCH_3(s_2) + CHOH(s_2) \rightarrow C_3H_5a + OH(s) + 3\,s$	5.38703E+09	0.50	45.46
19	$OH(s) + C_3H_5(s) \rightarrow C_3H_6 + O(s) + s$	6.38270E+09	0.50	0.00
20	$s + O(s) + C_3H_6 \rightarrow C_3H_5(s) + OH(s)$	1.70040E+10	-0.50	15.39
21	$C_3H_6(s_2) \rightarrow C_3H_5(s) + H(s)$	2.08366E+10	1.00	87.68
22	$H(s) + C_3H_5(s) \rightarrow C_3H_6(s_2)$	1.97271E+10	0.50	0.00

#	Reaction	A	β	E_A
23	$C_3H_6 + 2\,s \rightarrow C_2H_5CH(s_2)$	9.82480E+10	-0.50	0.00
24	$C_2H_5CH(s_2) \rightarrow C_3H_6 + 2\,s$	1.35849E+10	1.00	84.33
25	$C_3H_6(s_2) \rightarrow C_2H_5CH(s_2)$	0.00000E+00	1.00	0.00
26	$C_2H_5CH(s_2) \rightarrow C_3H_6(s_2)$	0.00000E+00	1.00	0.00
27	$C_2H_5CH(s_2) + 2\,s \rightarrow CH_2CH_3(s) + CH(s_3)$	8.22495E+08	0.50	47.67
28	$CH(s_3) + CH_2CH_3(s) \rightarrow C_2H_5CH(s_2) + 2\,s$	6.26159E+09	0.50	59.76
29	$C_2H_5CH(s_2) + 2\,s \rightarrow C_2H_5C(s_3) + H(s)$	8.22495E+08	0.50	104.79
30	$H(s) + C_2H_5C(s_3) \rightarrow C_2H_5CH(s_2) + 2\,s$	2.07501E+10	0.50	0.00
31	$s + C_2H_5C(s_3) \rightarrow C(s_3) + CH_2CH_3(s)$	3.55218E+09	0.50	0.00
32	$C(s_3) + CH_2CH_3(s) \rightarrow C_2H_5C(s_3) + s$	6.03919E+09	0.50	177.76
33	$C_3H_6 + 4\,s \rightarrow C_2H_5C(s_3) + H(s)$	5.41354E+09	-0.50	156.58
34	$H(s) + C_2H_5C(s_3) \rightarrow C_3H_6 + 4\,s$	2.07501E+10	0.50	0.00
35	$O(s) + C_2H_5CH(s_2) \rightarrow CH_2CH_3(s) + CHO(s) + s$	6.00026E+09	0.50	0.00
36	$s + CHO(s) + CH_2CH_3(s) \rightarrow C_2H_5CH(s_2) + O(s)$	5.29470E+09	0.50	126.98
37	$OH(s) + C_2H_5CH(s_2) \rightarrow CH_2CH_3(s) + CH_2O(s) + s$	6.24300E+09	0.50	0.00
38	$s + CH_2O(s) + CH_2CH_3(s) \rightarrow C_2H_5CH(s_2) + OH(s)$	5.27471E+09	0.50	98.01
39	$O(s) + C_2H_5C(s_3) \rightarrow CH_2CH_3(s) + CO(s_2) + s$	6.43992E+09	0.50	0.00
40	$s + CO(s_2) + CH_2CH_3(s) \rightarrow C_2H_5C(s_3) + O(s)$	5.20069E+09	0.50	276.71
41	$OH(s) + C_2H_5C(s_3) \rightarrow CH_2CH_3(s) + CHO(s) + 2\,s$	6.67484E+09	0.50	0.00
42	$CHO(s) + CH_2CH_3(s) + 2\,s \rightarrow C_2H_5C(s_3) + OH(s)$	1.32368E+09	0.50	162.29

4.3.2 Mechanism evaluation for nine different test cases

The results presented below show computations featuring the use of the developed reaction mechanism. The key point is a one-to-one comparison of CO, NO and C_3H_6 conversion against temperature, with the experimental data [2]. The square symbols correspond to experimental data [2], while the lines to the calculations, for the temperature range of 450 K - 800 K. The diffusion limitations of $\theta = 12\%$ [99] and $\theta = 20\%$ [100] of the bond energy holding the chemisorbed species to the surface are explored. Given the fact that, the species migration from one lattice site to a neighbouring, depends on the diffusion barrier, an investigation of a low and upper limit θ of the $Q_{C,H,O,N}$ allows the study of the species mobility on the catalytic surface.

The experimental conditions [2] used below, are presented in Table 4.2. The composition of the inlet gas mixture is nearly stoichiometric, while in each of the following Test Cases, three experimental parameters (noble metal loading, coat amount and the ratio of active catalyst to geometrical surface area) are varied, as shown in Tables 4.12–4.20. In a link to the Chapters 2, 3 and 5 the effect of different parameters on the current experimental conditions [2] are presented in Sections 4.3.2.1–4.3.2.5, for the mid-Test Case 5 [2], at the low and upper limit of $\theta = 12\%$ [99] and $\theta = 20\%$ [100] of the $Q_{C,H,O,N}$, respectively. The C_3H_6 catalytic chemistry considering a global irreversible C_3H_6 direct adsorption reaction is applied below.

4.3.2.1 Effect of alternative heat of adsorption for $N_2O(s_2)$

Test Case 5

An alternative value for the heat of adsorption of $N_2O(s_2)$, suggested by Avery [28], is implemented in the following computations for the study of its impact on the current

Table 4.11: Experimental conditions provided by TME [2] for Test Case 5.

Pt loading	1 wt%
Al_2O_3 coat amount	92 g/L
Ratio of active catalytic surface to geometrical area	27.79

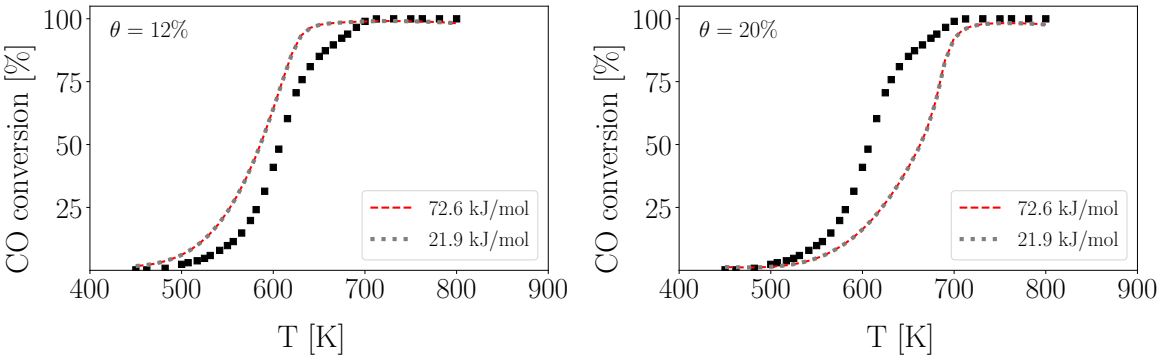


Fig. 4.2: Conversion of CO at the reactor outlet against the wall temperature. Implementation of $E_{C,H,O,N,diff}$ at $\theta = 12\%$ [99] and $\theta = 20\%$ [100] of the magnitude of $Q_{C,H,O,N}$. Comparison of the heat of adsorption ($Q_{N_2O(s_2)} = 72.6$kJ/mol) applied in the current computations with an alternative value ($Q_{N_2O(s_2)} = 21.9$kJ/mol) [28], along with the related experimental data provided by TME [2] for Test Case 5.

chemical system. The $Q_{N_2O(s_2)}$ used in the following Test Cases is equal to 72.6 kJ/mol and constitutes the input value applied in the proposed reaction mechanism. However, a large discrepancy with the respective value at 21.9 kJ/mol [28], presented in Table 2.6, leads to a further investigation. Figures 4.2 and 4.3 show a complete identification of the two cases examined. Therefore, the use of a lower heat of adsorption for $N_2O(s_2)$ does not influence the CO, NO and C_3H_6 conversion.

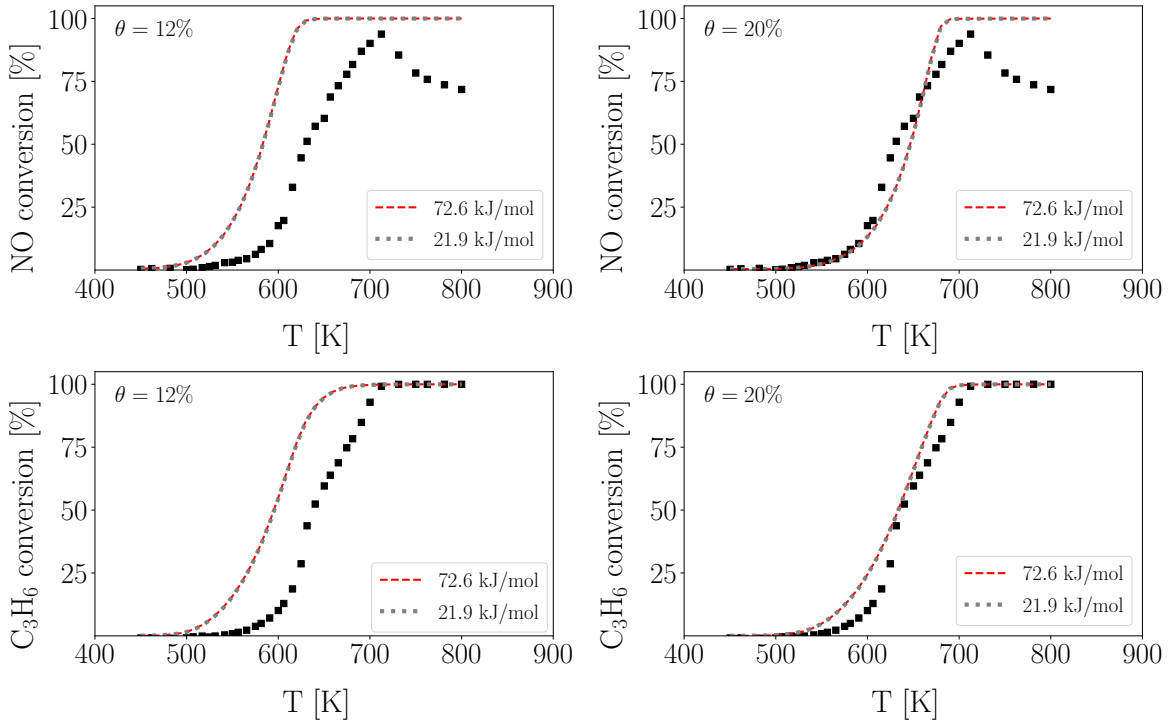


Fig. 4.3: Conversion of NO and C_3H_6 at the reactor outlet against the wall temperature. Implementation of $E_{C,H,O,N,diff}$ at $\theta = 12\%$ [99] and $\theta = 20\%$ [100] of the magnitude of $Q_{C,H,O,N}$. Comparison of the heat of adsorption ($Q_{N_2O(s_2)} = 72.6$kJ/mol) applied in the current computations with an alternative value ($Q_{N_2O(s_2)} = 21.9$kJ/mol) [28], along with the related experimental data provided by TME [2] for Test Case 5.

4.3.2.2 Effect of different CO desorption energies

Test Case 5

The effect of different CO desorption energies is examined in this Section. In particular, the previous applied CO desorption activation energy, evaluated at 134 kJ/mol [11, 14, 15] was compared to an updated value of 187 kJ/mol [128]. As illustrated in Fig. 4.4, no difference between the two cases is observed, however a slight impact of the 187 kJ/mol

in the chemical system is outlined in Chapter 5, resulting in this examination. The same experimental conditions shown in Table 4.11 are applied.

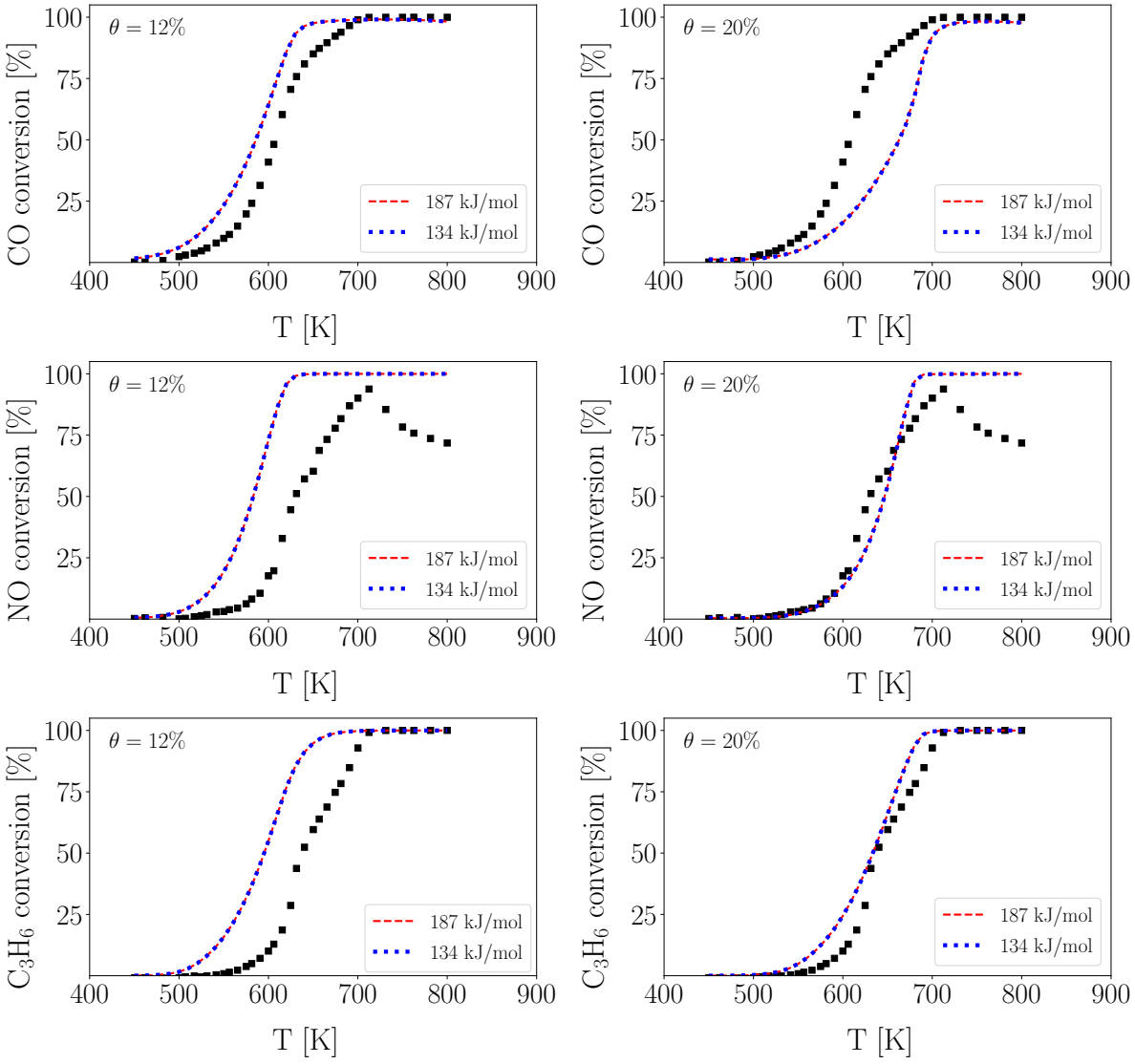


Fig. 4.4: Conversion of CO, NO and C_3H_6 at the reactor outlet against the wall temperature for different desorption energies set at 134 [11, 14, 15] and 187 kJ/mol [128]. Implementation of $E_{C,H,O,N,diff}$ at $\theta = 12\%$ [99] and $\theta = 20\%$ [100] of the magnitude of $Q_{C,H,O,N}$. Comparison with the experimental data provided by TME [2] for Test Case 5.

4.3.2.3 Effect of vibrational partition function fixed at 800 K, for CO direct adsorption reaction

Test Case 5

The effect of a vibrational partition function fixed at 800 K [14, 15] exclusively for CO direct adsorption reaction is examined below. For the rest of catalytic reactions a fixed T_{q^v} at 298 K is applied.

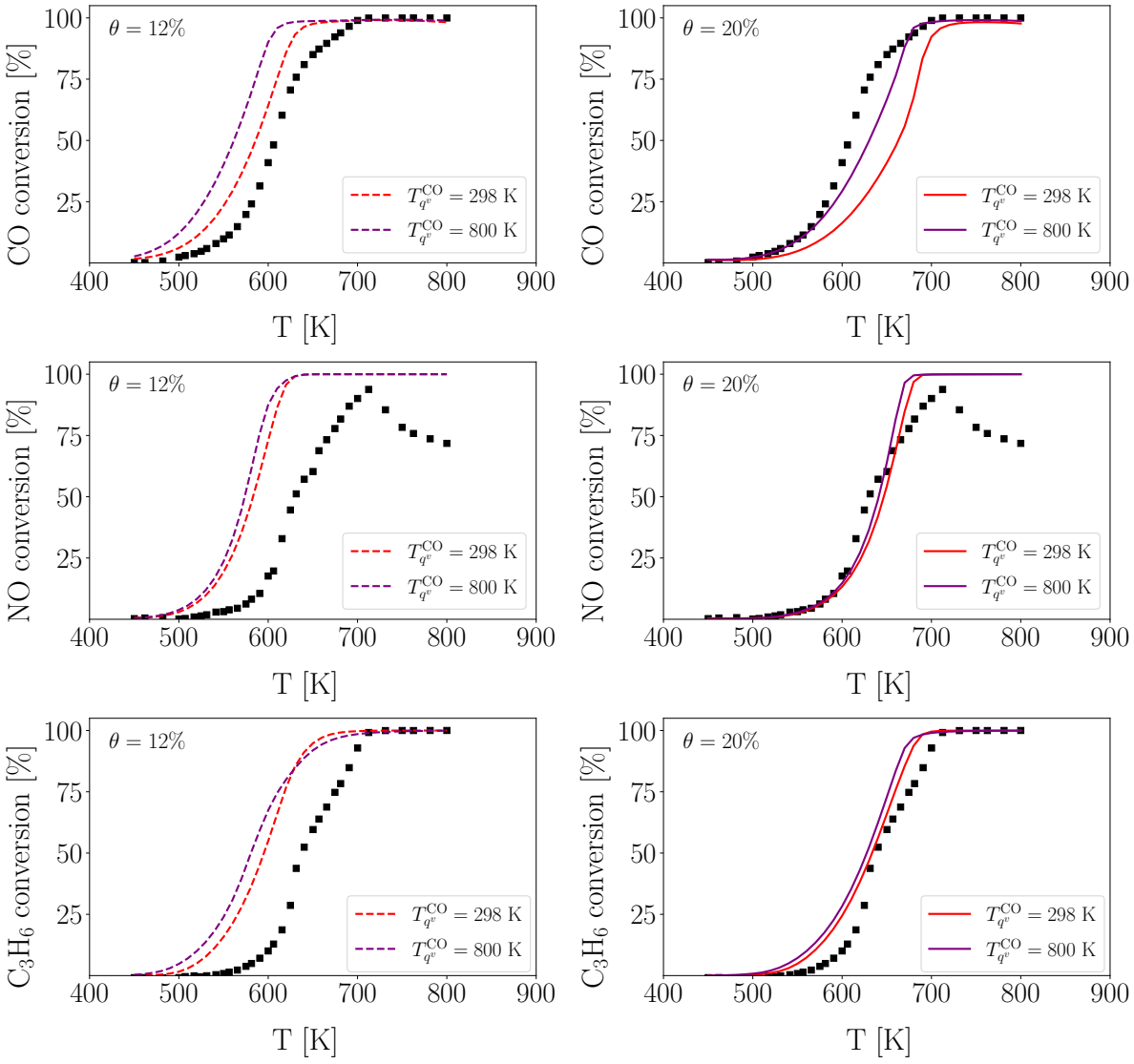


Fig. 4.5: Conversion of CO, NO and C_3H_6 at the reactor outlet against the wall temperature. Implementation of $E_{C,H,O,N,diff}$ at $\theta = 12\%$ [99] and $\theta = 20\%$ [100] of the magnitude of $Q_{C,H,O,N}$. Comparison of the $T_{q^v} = 298$ K applied in the main computations with $T_{q^v} = 800$ K [14, 15], exclusively for the CO adsorption reaction. Comparison with the experimental data provided by TME [2] for Test Case 5.

As shown in Fig. 3.8 for $T_{q^v} = 800$ K, the CO adsorption on two Pt sites presents a mobile transition state, as in the case of $T_{q^v} = 298$ K, however a better reproduction of the experimental data was obtained. Therefore, a related comparison over the experimental data provided by TME [2] can underline the performance of CO adsorption reaction at both T_{q^v} on the current system. Figure 4.5 demonstrates a slight difference between the two T_{q^v} for CO adsorption reaction, mainly for the NO and C_3H_6 conversion. The case of $T_{q^v}^{CO} = 800$ K agrees better with the experimental data [2] at the upper limit diffusion barrier ($\theta = 20\%$ [100]) indicating a faster conversion compared to the low limit diffusion barrier.

In general terms, despite the larger discrepancy with the related experimental sticking coefficients shown in Fig. 3.7, the present results do not impose an alteration of the general methodology used at $T_{q^v} = 298$ K, for all the species. However, the $T_{q^v}^{CO} = 800$ K can be adopted for CO direct adsorption reaction, for more accurate and consistent results. The same experimental conditions shown in Table 4.11 are applied.

4.3.2.4 Effect of vibrational partition function fixed at 800 K

Test Case 5

The effect of vibrational partition function fixed at 800 K, as proposed by Kraus and Lindstedt [14, 15] is examined below. A comparison between a fixed T_{q^v} at 298 K and 800 K, concerning the whole catalytic reaction mechanism, is presented in Fig. 4.6. The two different cases of T_{q^v} seem to completely agree at lower temperatures for both $\theta = 12\%$ [99] and $\theta = 20\%$ [100], especially for the CO adsorption. However, the $T_{q^v} = 298$ K, seems to better predict the experimental data [2]. This could be a reasonable outcome based on the results shown in Chapter 3, where the evaluated sticking coefficients of the most representative chemical species reproduce better the experimental data obtained from literature sources, at $T_{q^v} = 298$ K. The same experimental conditions shown in Table 4.11 are applied.

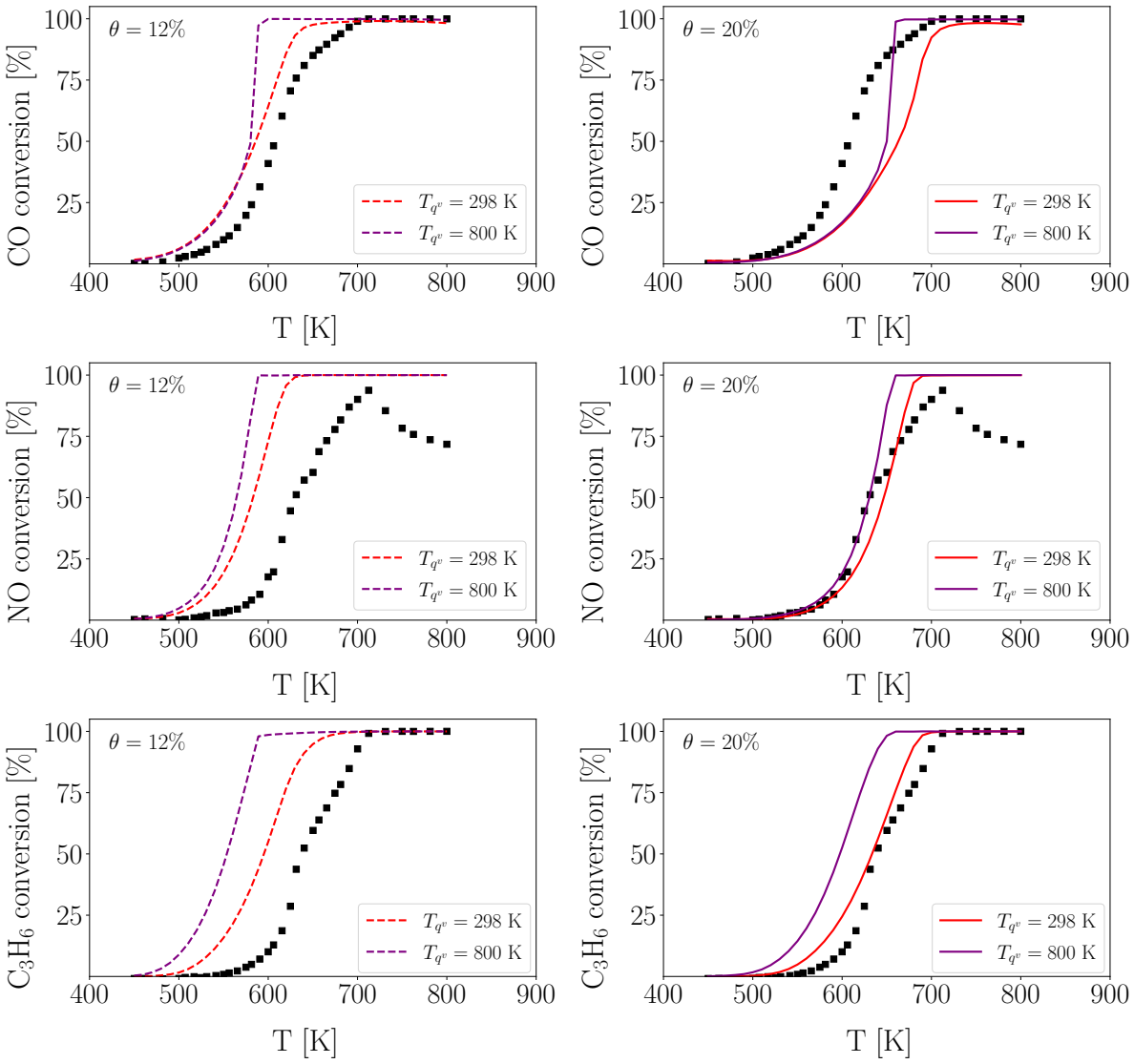


Fig. 4.6: Conversion of CO, NO and C_3H_6 at the reactor outlet against the wall temperature. Implementation of $E_{C,H,O,N,diff}$ at $\theta = 12\%$ [99] and $\theta = 20\%$ [100] of the magnitude of $Q_{C,H,O,N}$. Comparison of the $T_{q^v} = 298$ K applied in the current computations with $T_{q^v} = 800$ K [14, 15]. Comparison with the experimental data provided by TME [2] for Test Case 5.

4.3.2.5 Effect of immobile TS for the H_2 direct adsorption reaction

Test Case 5

In the context of the determination of mobile or immobile TS of chemical species, H_2 was found to present an immobile TS when it adsorbs on the Pt surface, based on an extensive comparison with experimental data from literature sources, shown in Fig. 3.3.

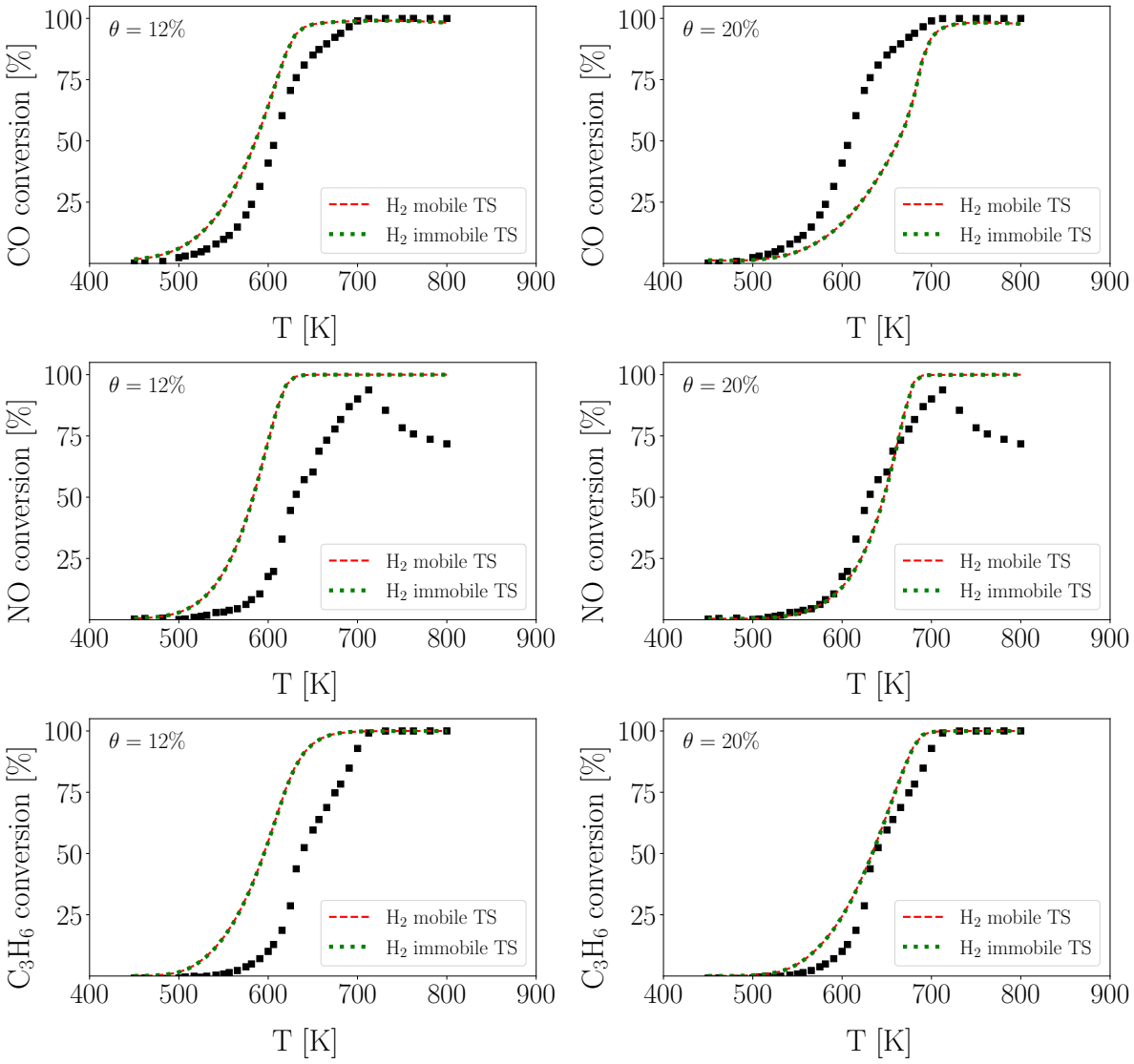


Fig. 4.7: Conversion of CO, NO and C_3H_6 at the reactor outlet against the wall temperature. Implementation of $E_{C,H,O,N,diff}$ at $\theta = 12\%$ [99] and $\theta = 20\%$ [100] of the magnitude of $Q_{C,H,O,N}$. Comparison of the mobile and immobile TS of H_2 adsorption reaction, along with the related experimental data provided by TME [2] for Test Case 5.

Practically, the rate constant of the H_2 immobile TS of adsorption reaction is not evaluated based on the Sprowl et al. [16] approximation and the respective expression of sticking coefficient, described by Eq. (3.27). Equation (3.7) for the immobile sticking coefficient is directly applied in the expression of the rate constant, via Eq. (3.28). The comparison of the two transition states of H_2 does not lead to any alteration in the final outcome. Therefore, the nature of the H_2 adsorption on the metal surface does not influence the conversion of CO, NO and C_3H_6. The rest of the H_2 adsorption reaction classes (e.g. dissociative adsorption, Eley-Rideal adsorption) included in the proposed reaction mechanism are determined via the assumption of a mobile TS retained from previous works [14, 15]. The same experimental conditions shown in Table 4.11 are applied.

4.3.2.6 Test Cases

In the context of the previous investigations of Test Case 5, shown in Sections 4.3.2.1-4.3.2.5, the alternative values $Q_{N_2O(s_2)}$ = 72.6 kJ/mol and $Q_{CO(s_2)}$ = 187 kJ/mol are preferred in the surface reaction mechanism. However, no appreciable differences were noticed when compared with alternative values. Additionally, the case of a fixed T_{q^v} at 298 K is implemented in the following Test Cases. However, following the examination of the effect of the T_{q^v} fixed at 800 K, exclusively for the CO direct adsorption reaction and for the whole catalytic mechanism, presented in Sections 4.3.2.3 and 4.3.2.4, respectively, the need to identify the corresponding impact for all the Test Cases arose. Section 4.3.2.7 demonstrates the effect of a T_{q^v} = 800 K on CO direct adsorption reaction based on the related behaviour shown in Fig. 3.8. It should be noted that the revised value for CO adsorption also provides agreement with experimental data for sticking coefficients as discussed in Section 3.2.1. Finally, as shown in Section 4.3.2.5 the use of an immobile TS for the H_2 direct adsorption reaction instead of a mobile does not affect the obtained results. Therefore, the respective mobile TS is retained from Kraus and Lindstedt [14, 15]. The C_3H_6 catalytic chemistry considering a global irreversible C_3H_6 direct adsorption reaction is applied below.

Test Cases 1 - 3

The conversion rates of CO, NO and C_3H_6 as a function of temperature are shown in Figs. 4.8–4.10, for the Test Cases 1, 2 and 3, corresponding to the lower Pt loading at 0.5 wt%. Diffusion barriers set at $\theta = 12\%$ [99] and $\theta = 20\%$ [100] of the magnitude of bond energy holding the chemisorbed species to the surface, are examined.

Concerning the Test Case 1, shown in Fig. 4.8, the conversion of NO and C_3H_6 starts at 450 K and increases up to 100%. The CO conversion begins in the same temperature as the two other chemical species, but it can not reach the maximum of 100%. The NO and C_3H_6 are completely converted at 700 K. Although, CO conversion shows a good agreement with experimental data [2] at low temperatures, its conversion evolves at a low rate, especially when a higher diffusion barrier, $E_{C,H,O,N,diff}$, is imposed. The NO and C_3H_6 profiles agree with the experimental data [2] for the same case. As noted in Section 4.3.2.7, the use of a higher sticking coefficient resulting from a fixed $T_{q^v} = 800$ K for the CO adsorption reaction improves the agreement significantly.

Figure 4.9 presents the CO, NO and C_3H_6 conversion against temperature, for Test Case 2. The CO conversion reproduces the experimental data [2] to a satisfactory degree, mainly for the intermediate temperatures, for the case of $\theta = 12\%$ [99]. The NO and C_3H_6 conversions qualitatively seem to follow the trend of the experimental points [2] and the case of $\theta = 20\%$ [100] contributes to better agreement.

As shown in Fig. 4.10 corresponding to Test Case 3, the CO conversion reproduces the experimental data [2] to an adequate level, when a lower diffusion barrier is applied, while the computational lines of NO and C_3H_6 conversions indicate the case of $\theta = 20\%$ [100], as a method of choice.

Summarizing, a consistent behaviour of the species conversion against temperature for the corresponding diffusion barriers can be noticed, for the Test Cases 1 - 3. The low Pt loading impacts to a more significant degree the CO conversion compared to NO and C_3H_6. More specifically, as shown in Fig. 4.8, the low Pt loading leads to a poor conversion level of CO for the lowest coat amount between the three cases, and subsequently ratio of active catalytic surface to geometrical area. A gradual increase of the two latter parameters can be observed for Test Cases 2 and 3, leading to a better performance of CO against temperature. The higher coat amount enables the expansion

of the Pt surface leading to a more efficient metal dispersion. This favours the completion of CO conversion in Test Case 3 for both $\theta = 12\%$ [99] and $\theta = 20\%$ [100], and in Test Case 2 for the lower diffusion barrier.

Figures 4.8–4.10 show that the NO and C_3H_6 are converted slower, under a higher diffusion barrier, following the trend of experimental data [2]. Given the fact that, the diffusion barrier equals the value of the potential barrier that has to be overcome by the molecule in order to occupy a new balanced position on a neighbouring atom of the catalytic surface, it is possible that CO may need a lower diffusion barrier for a better reproduction of the experimental data [2]. The diffusion energy barrier of an atom or molecule is correlated with the respective binding energy on the metal surface. The higher binding energy of CO at 187 kJ/mol leads to a lower diffusion rate on the surface, compared to the respective values at 71.8 kJ/mol and 39.1 kJ/mol of NO and C_3H_6. However, the impact of the CO sticking coefficient is also significant, as outlined above.

Test Case 1

Table 4.12: Experimental conditions provided by TME [2] for Test Case 1.

Pt loading	0.5 wt%
Al_2O_3 coat amount	60 g/L
Ratio of active catalytic surface to geometrical area	9.92

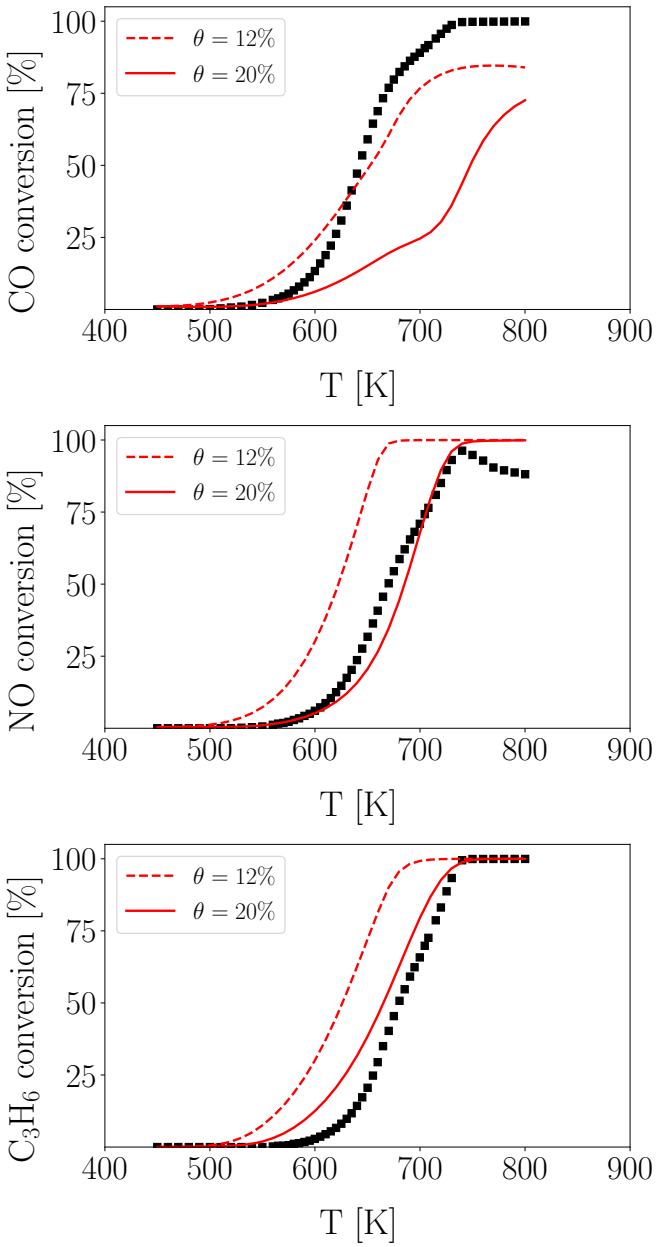


Fig. 4.8: Conversion of CO, NO and C_3H_6 at the reactor outlet against the wall temperature, for the global catalytic C_3H_6 step sub-mechanism. Implementation of $E_{C,H,O,N,diff}$ at $\theta = 12\%$ [99] (−) and $\theta = 20\%$ [100] (−−) of the magnitude of $Q_{C,H,O,N}$. Comparison with the experimental data provided by TME [2] for Test Case 1.

Test Case 2

Table 4.13: Experimental conditions provided by TME [2] for Test Case 2.

Pt loading	0.5 wt%
Al_2O_3 coat amount	92 g/L
Ratio of active catalytic surface to geometrical area	15.01

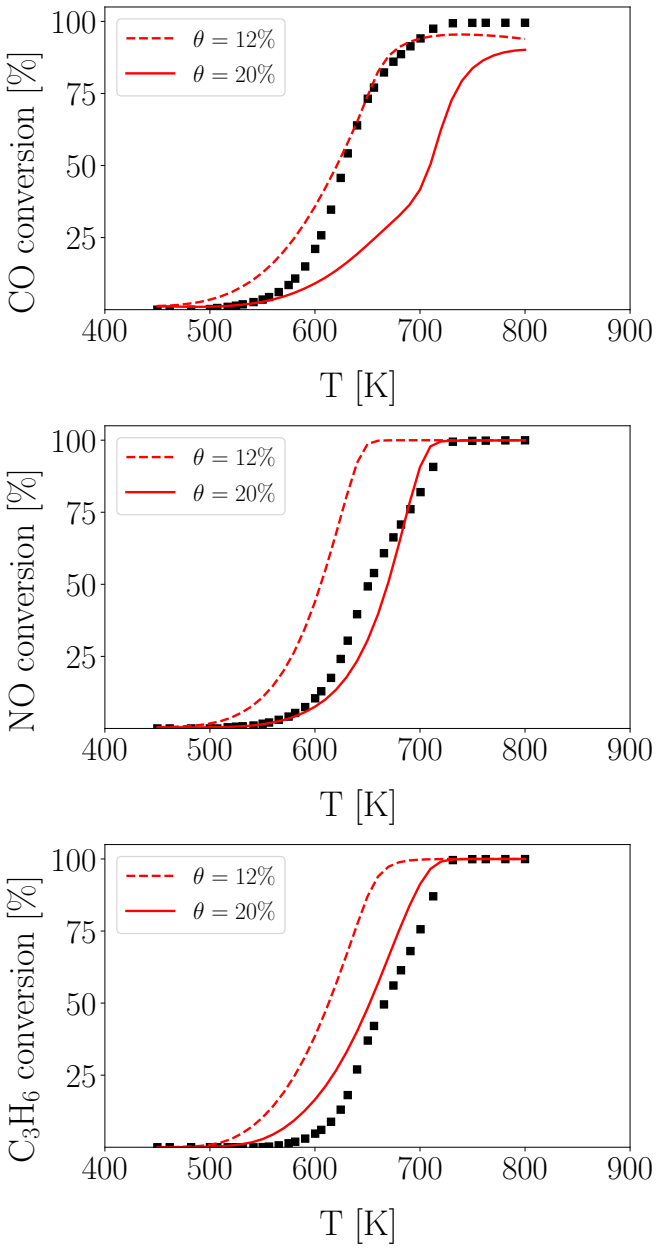


Fig. 4.9: Conversion of CO, NO and C_3H_6 at the reactor outlet against the wall temperature, for the global catalytic C_3H_6 step sub-mechanism. Implementation of $E_{C,H,O,N,diff}$ at $\theta = 12\%$ [99] (−) and $\theta = 20\%$ [100] (−−) of the magnitude of $Q_{C,H,O,N}$. Comparison with the experimental data provided by TME [2] for Test Case 2.

Test Case 3

Table 4.14: Experimental conditions provided by TME [2] for Test Case 3.

Pt loading	0.5 wt%
Al_2O_3 coat amount	171 g/L
Ratio of active catalytic surface to geometrical area	27.91

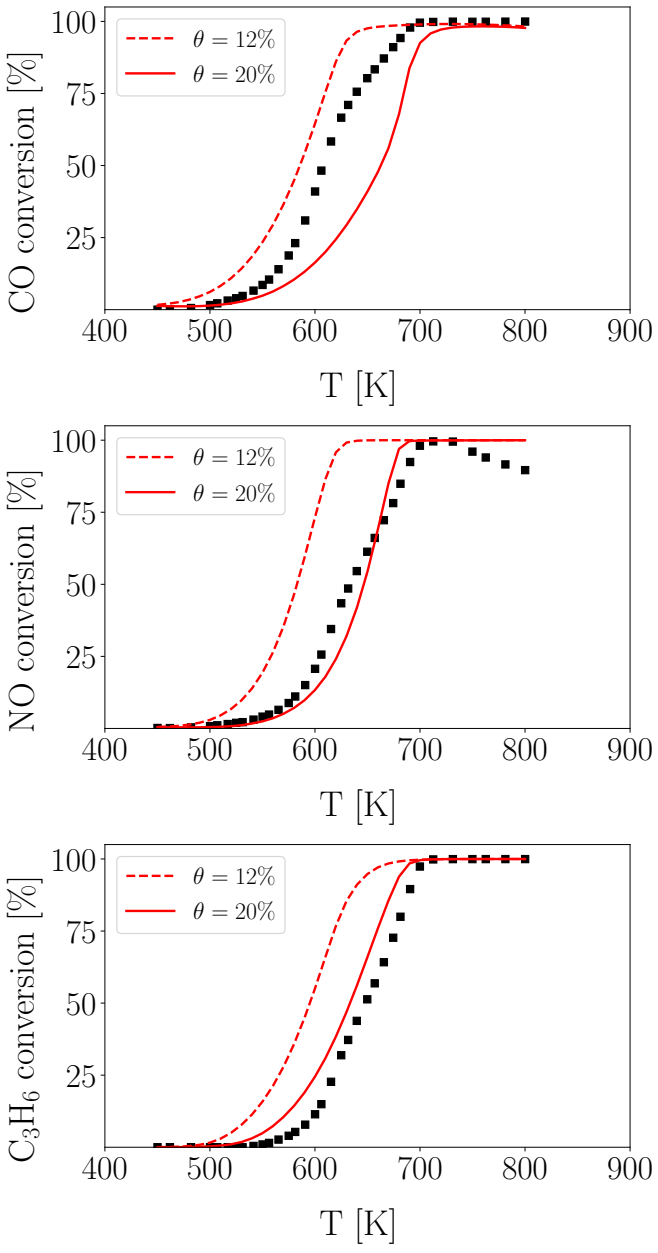


Fig. 4.10: Conversion of CO, NO and C_3H_6 at the reactor outlet against the wall temperature, for the global catalytic C_3H_6 step sub-mechanism. Implementation of $E_{C,H,O,N,diff}$ at $\theta = 12\%$ [99] (−) and $\theta = 20\%$ [100] (−−) of the magnitude of $Q_{C,H,O,N}$. Comparison with the experimental data provided by TME [2] for Test Case 3.

Test Cases 4 - 6

The following Test Cases 4 - 6, correspond to an intermediate Pt loading at 1 wt%, while the coat amount changes gradually from 60 g/L to 171 g/L, as also shown for Test Cases 1 - 3. However, the values corresponding to the ratio of active catalytic surface to geometrical surface present higher values compared to the ones illustrated in Tables 4.12-4.14, due to the higher metal loading applied.

Figure 4.11 illustrates the conversion rates of the studied species, for Test Case 4. As the metal loading increases from 0.5 wt% to 1 wt%, the CO and NO conversion better follow the trend of the experimental points [2], especially for the lower diffusion barrier corresponding to $\theta = 12\%$ [99]. The case of $\theta = 20\%$ [100] for C_3H_6 presents a better agreement with the experimental data [2], mainly at lower temperatures, up to 600 K. Additionally, a decrease of NO conversion rate can be noticed after 660 K, in the experimental data [2] of the following Test Cases, as well as in Test Cases 1 and 3. The latter behaviour is not reflected in the current computations as complete conversion of NO was obtained. The incorporation of HC–NH_3 processes into the reaction mechanism, occuring on the catalytic surface, may explain this behaviour noticed in some of the examined Test Cases. Such an inclusion opens a window towards the study of HC–N catalytic reactions based on the recent observations outlined by TME [2]. Furthermore, interactions between some of the oxygenated compounds from the catalytic converter and nitrogen in the gas phase, may also lead to this outcome.

The CO, NO and C_3H_6 conversions as a function of temperature are also shown in Fig. 4.12, for Test Case 5. In this Test Case, an additional calculation was added as a means of comparison. In particular, a different diffusion consideration was imposed based on the element-based reactant. For C, H, O - element based reactants a lower diffusion barrier, $E_{C,H,O,diff}$, was applied through $\theta = 12\%$ [99] of the magnitude of the corresponding heat of adsorption $Q_{C,H,O}$, while for the N - element based reactants a higher diffusion barrier, $E_{N,diff}$ was used via a $\theta = 20\%$ [100] of Q_N. As also observed in the Test Case 4, the lower diffusion barrier favours the CO conversion towards the respective experimental data [2], while the NO and C_3H_6 represent better the experiments when the higher diffusion barrier is applied. The implementation of a "mixed" diffusion

barrier depending on the type of reactant, illustates that an extensive analysis of diffusion barriers and their coupling to activation energies could further improve agreement.

Almost the same behaviour for Test Case 5, can be observed in Fig. 4.15 for Test Case 6, for all the species conversions examined at $\theta = 12\%$ [99] and $\theta = 20\%$ [100]. As the Al_2O_3 coat amount increases gradually from Test Case 4 to Test Case 6, allowing a better dispersion of Pt sites, the catalytic activity is automatically impacted leading to a better representation of species conversion towards the experimental data [2]. The C_3H_6 successfully reproduces the experimental data [2] at $\theta = 20\%$ [100].

Test Case 4

Table 4.15: Experimental conditions provided by TME [2] for Test Case 4.

Pt loading	1 wt%
Al_2O_3 coat amount	60 g/L
Ratio of active catalytic surface to geometrical area	18.36

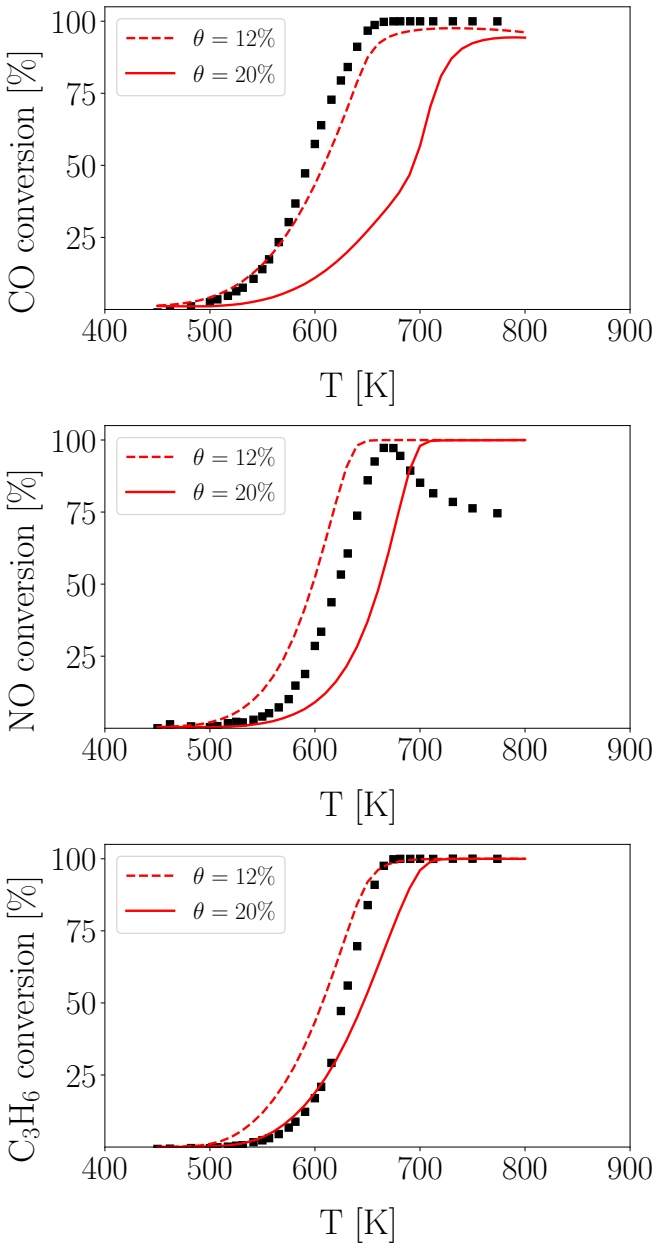


Fig. 4.11: Conversion of CO, NO and C_3H_6 at the reactor outlet against the wall temperature, for the global catalytic C_3H_6 step sub-mechanism. Implementation of $E_{C,H,O,N,diff}$ at $\theta = 12\%$ [99] (−) and $\theta = 20\%$ [100] (−−) of the magnitude of $Q_{C,H,O,N}$. Comparison with the experimental data provided by TME [2] for Test Case 4.

Test Case 5

Table 4.16: Experimental conditions provided by TME [2] for Test Case 5.

Pt loading	1 wt%
Al_2O_3 coat amount	92 g/L
Ratio of active catalytic surface to geometrical area	27.79

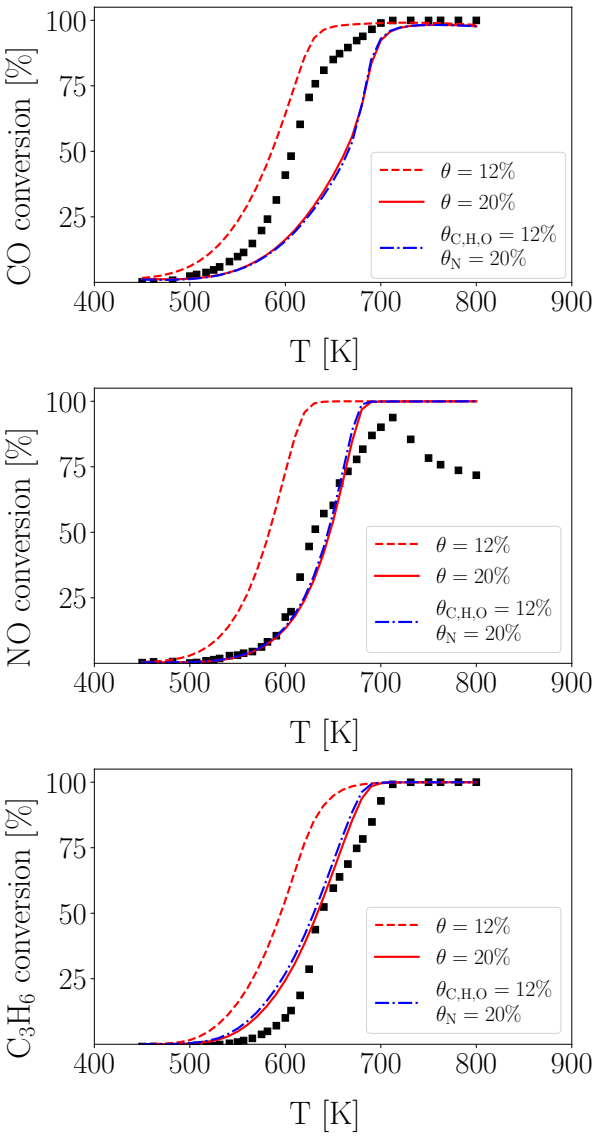


Fig. 4.12: Conversion of CO, NO and C_3H_6 at the reactor outlet against the wall temperature, for the global catalytic C_3H_6 step sub-mechanism. Implementation of $E_{C,H,O,N,diff}$ at $\theta = 12\%$ [99] (−) and $\theta = 20\%$ [100] (−−) of the magnitude of $Q_{C,H,O,N}$. An additional case of $E_{C,H,O,diff}$ and $E_{N,diff}$ evaluation at $\theta_{C,H,O} = 12\%$ [99] and $\theta_N = 20\%$ [100] (−·−) of the magnitude of $Q_{C,H,O}$ and Q_N, respectively, is included. Comparison with the experimental data provided by TME [2] for Test Case 5.

In Figs. 4.14.1–4.14.3, the mol fractions of CO, NO and C_3H_6 at 550 K, 650 K and 750 K are shown, for the different implementation of the diffusion barrier, $E_{C,H,O,N,diff}$, at $\theta = 12\%$ [99] (left column) and $\theta = 20\%$ [100] (right column) of the magnitude of $Q_{C,H,O,N}$. The input and experimental data [2] correspond to the Test Case 5. The y range demonstrates the radial position, while the downstream distance corresponds to the length of the simulated catalytic bed. The computational domain simulates the upper half, i.e from 0.0 to 0.623 mm, while the lower half, which is the symmetric counterpart, is simply the mirrored data from the upper half, and was included for aesthetic reasons.

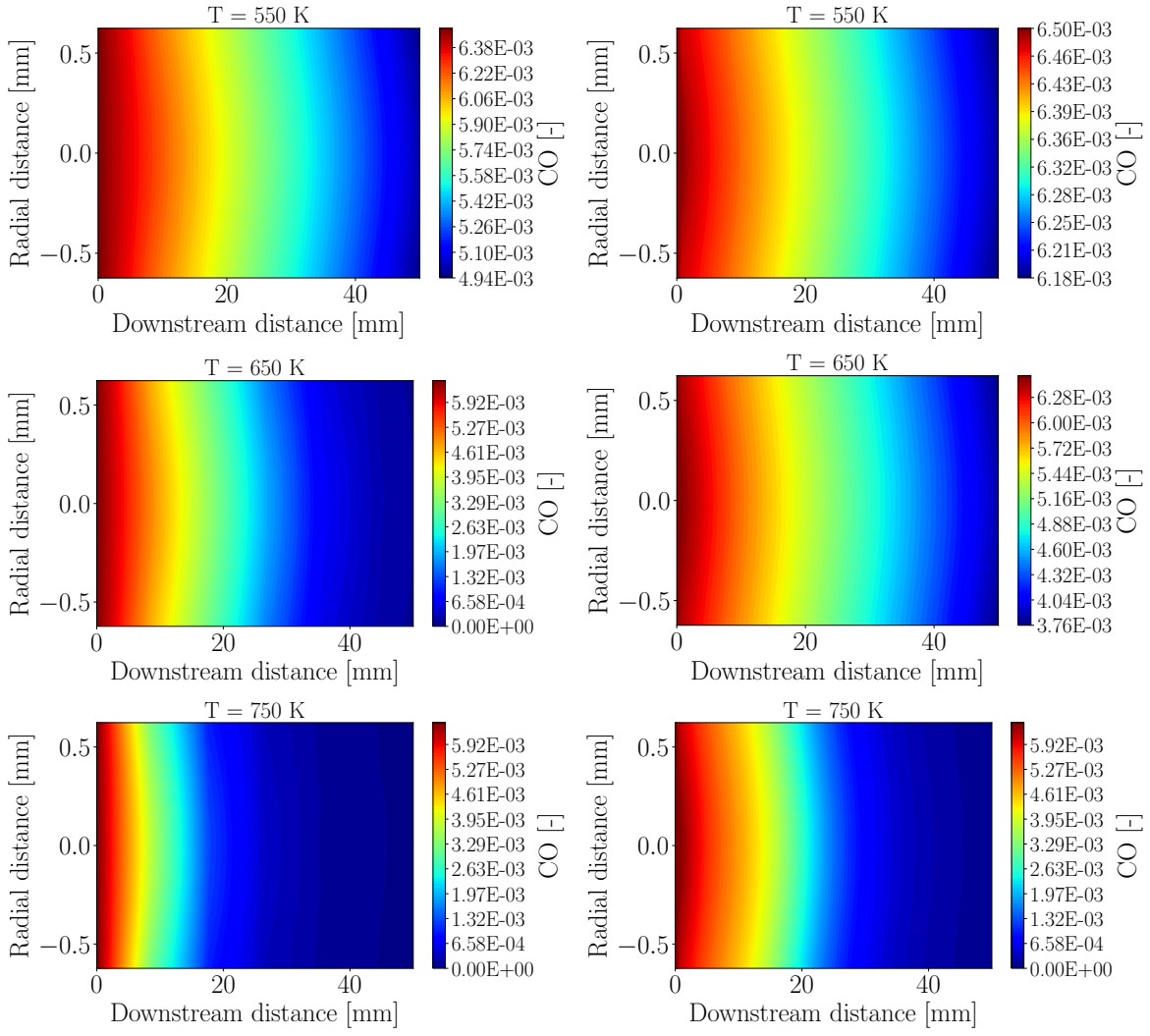


Fig. 4.14.1: Flow fields of the CO mol fractions at 550 K, 650 K and 750 K, for Test Case 5. The two columns correspond to the implementation of the diffusion barrier, $E_{C,H,O,N,diff}$, at $\theta = 12\%$ [99] (left) and $\theta = 20\%$ [100] (right) of the magnitude of $Q_{C,H,O,N}$.

The mol fraction profiles show that with the gradual increase of the temperature, the species conversion occurs at a greater rate. In particular, the NO and C_3H_6 are converted within the first millimeters at 750 K, and then vanish, for both $\theta = 12\%$ [99] (left column) and $\theta = 20\%$ [100] (right column) cases. The higher value of $E_{C,H,O,N,diff}$ applied through the $\theta = 20\%$ [100] (right column) of the magnitude of $Q_{C,H,O,N}$, consists a higher diffusion limitation compared to the respective $\theta = 12\%$ [99] case, leading to a slower conversion, for all temperatures and especially for 550 K and 650 K. The CO conversion is much slower and smoother, with a complete consumption at around 20 mm and 30 mm, for $\theta = 12\%$ [99] (left) and $\theta = 20\%$ [100] (right), respectively, at 750 K.

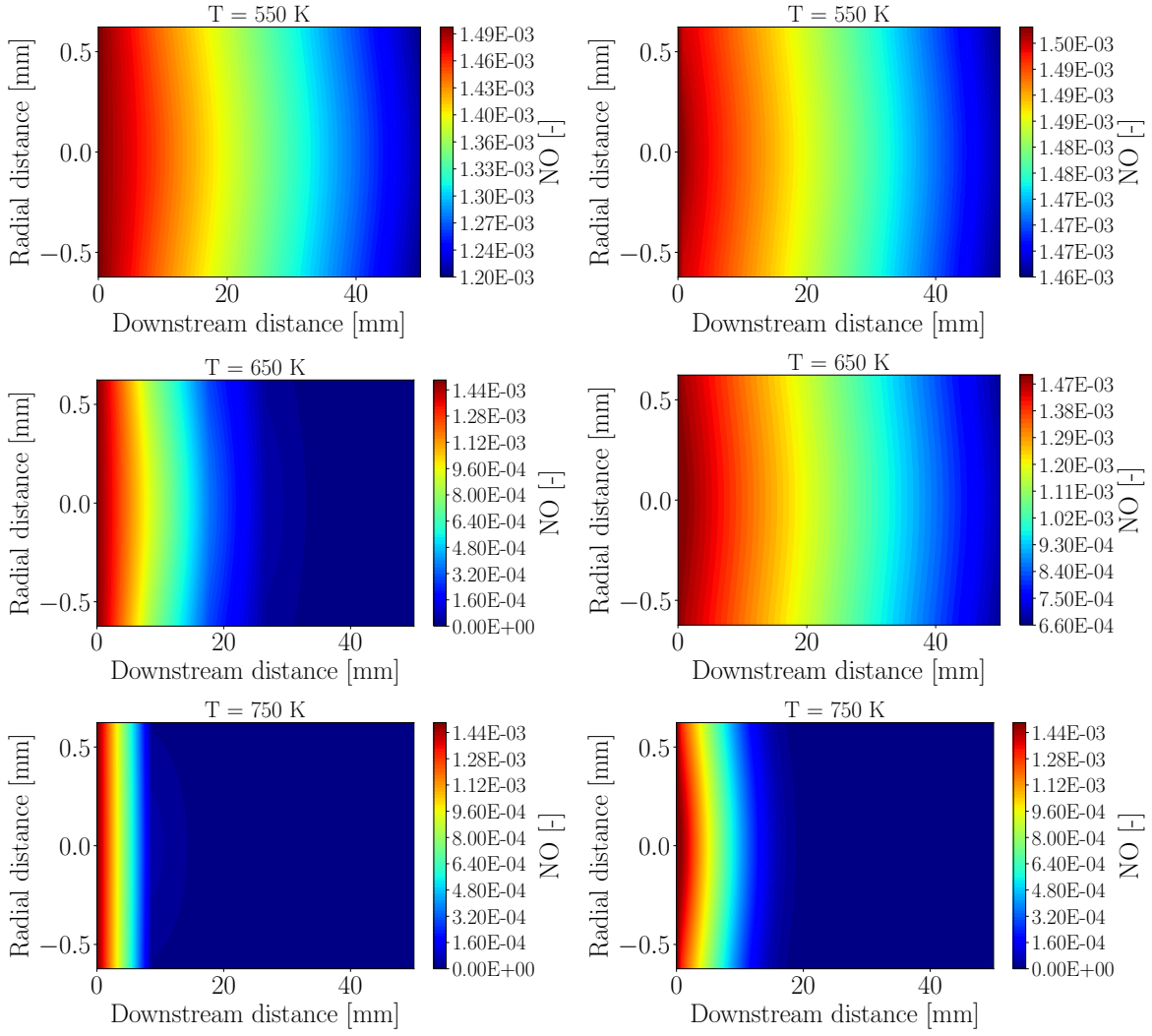


Fig. 4.14.2: Flow fields of the NO mol fractions at 550 K, 650 K and 750 K, for Test Case 5. The two columns correspond to the implementation of the diffusion barrier, $E_{C,H,O,N,diff}$, at $\theta = 12\%$ [99] (left) and $\theta = 20\%$ [100] (right) of the magnitude of $Q_{C,H,O,N}$.

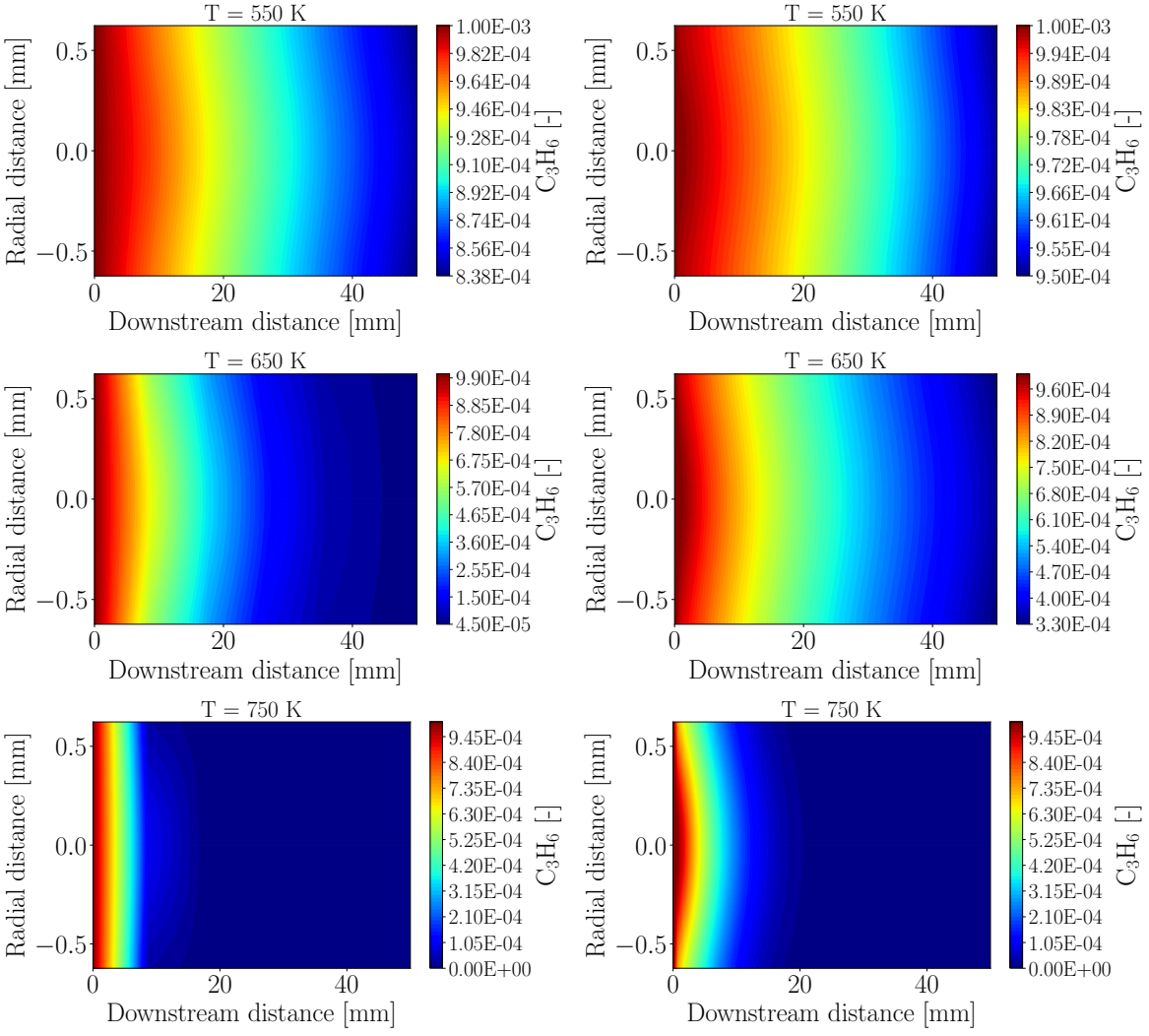


Fig. 4.14.3: Flow fields of the C_3H_6 mol fractions at 550 K, 650 K and 750 K, for Test Case 5. The two columns correspond to the implementation of the diffusion barrier, $E_{C,H,O,N,diff}$, at $\theta = 12\%$ [99] (left) and $\theta = 20\%$ [100] (right) of the magnitude of $Q_{C,H,O,N}$.

Test Case 6

Table 4.17: Experimental conditions provided by TME [2] for Test Case 6.

Pt loading	1 wt%
Al_2O_3 coat amount	171 g/L
Ratio of active catalytic surface to geometrical area	51.67

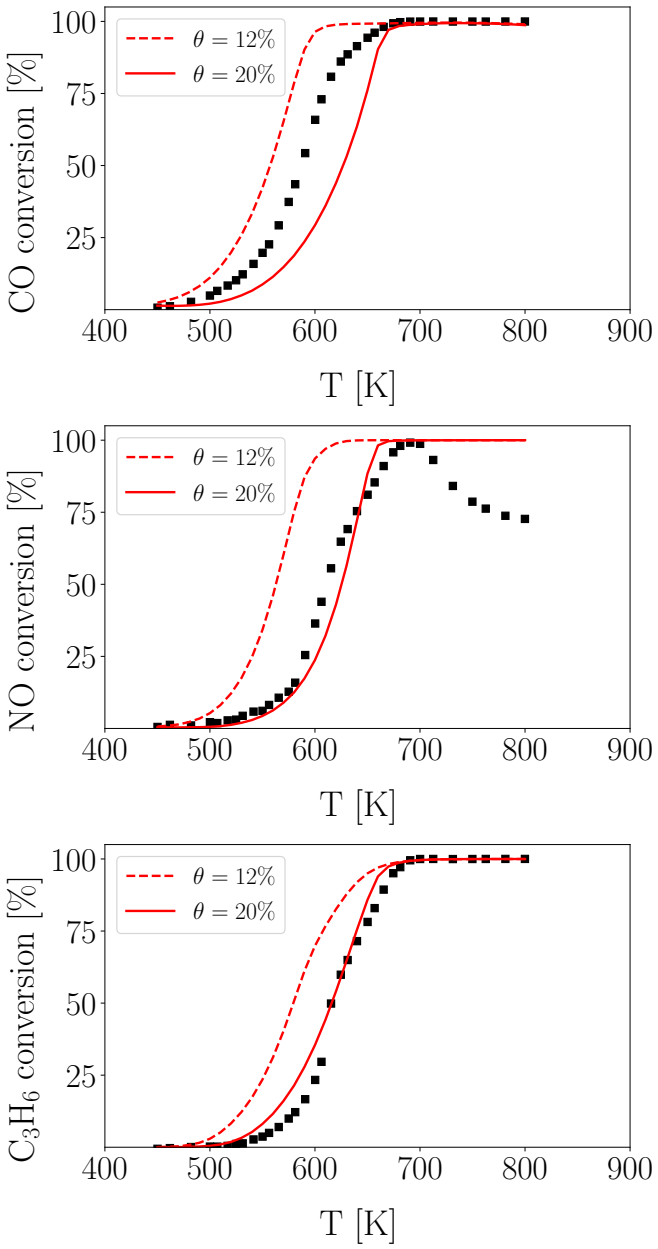


Fig. 4.15: Conversion of CO, NO and C_3H_6 at the reactor outlet against the wall temperature, for the global catalytic C_3H_6 step sub-mechanism. Implementation of $E_{C,H,O,N,diff}$ at $\theta = 12\%$ [99] (−) and $\theta = 20\%$ [100] (−−) of the magnitude of $Q_{C,H,O,N}$. Comparison with the experimental data provided by TME [2] for Test Case 6.

Test Cases 7 - 9

The last three Test Cases 7 - 9 corresponding to the highest Pt loading at 3 wt%, indicate that the use of the diffusion barrier at the upper limit of $\theta = 20\%$ [100] better describes the experimental measurements [2] for all the species conversion. A larger deviation can be observed when a lower diffusion barrier is applied. The higher metal loading shows that less species diffusion is required under the given experimental conditions [2]. The NO and C_3H_6 conversions present a sharper slope after the light-off temperatures, for the low diffusion barrier applied. As the active catalytic surface increases, the chemical system is activated more rapidly, resulting to complete conversion earlier, compared to the experimental data [2]. Therefore, by accounting for a higher diffusion limitation a better agreement with the experimental data [2], can be obtained.

To sum up, the majority of the Test Cases investigated, follow qualitatively the trend of the experimental points [2] with discrepancies mainly observed because of the diffusion barriers applied, in conjuction with the inclusion of the scaling factor $1/x^x$ in the adsorption reactions. The latter, may affect, in some cases, the calculation of rate constants, as the impact for mobile transition states may be significant. The implementation of a higher diffusion barrier favours the NO and C_3H_6 conversion in all the Test Cases, while at lower Pt loadings, the CO conversion presents a better agreement with the experimental data [2], under the use of lower diffusion barriers. This allows the freely movement of the adsorbed species over the surface. However, at higher temperatures and lower Pt loadings the experimental data [2] are under-predicted, as the diffusion barrier prevents the complete CO conversion. Finally, all the Test Cases presented are based on computations under a fixed temperature at 298 K for the vibrational partition function and an assumption of a mobile TS for H_2 retained from previous studies [11, 14, 15].

Test Case 7

Table 4.18: Experimental conditions provided by TME [2] for Test Case 7.

Pt loading	3 wt%
Al_2O_3 coat amount	60 g/L
Ratio of active catalytic surface to geometrical area	66.96

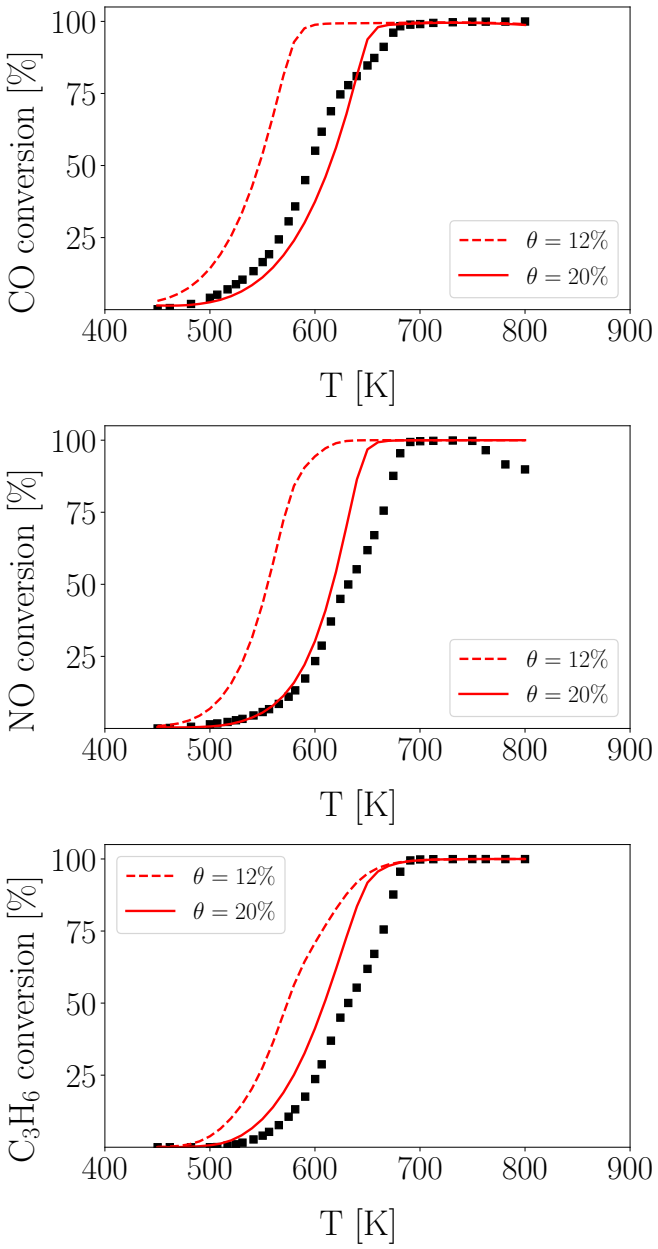


Fig. 4.16: Conversion of CO, NO and C_3H_6 at the reactor outlet against the wall temperature, for the global catalytic C_3H_6 step sub-mechanism. Implementation of $E_{C,H,O,N,diff}$ at $\theta = 12\%$ [99] (−) and $\theta = 20\%$ [100] (−−) of the magnitude of $Q_{C,H,O,N}$. Comparison with the experimental data provided by TME [2] for Test Case 7.

Test Case 8

Table 4.19: Experimental conditions provided by TME [2] for Test Case 8.

Pt loading	3 wt%
Al_2O_3 coat amount	92 g/L
Ratio of active catalytic surface to geometrical area	101.34

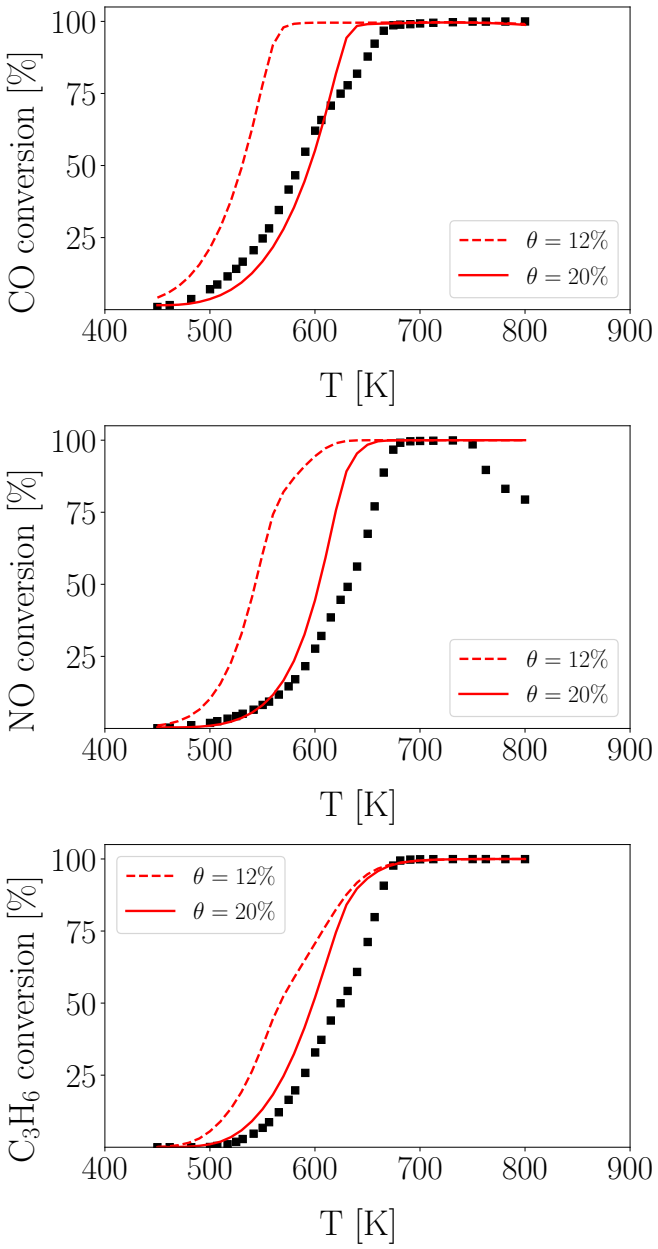


Fig. 4.17: Conversion of CO, NO and C_3H_6 at the reactor outlet against the wall temperature, for the global catalytic C_3H_6 step sub-mechanism. Implementation of $E_{C,H,O,N,diff}$ at $\theta = 12\%$ [99] (−) and $\theta = 20\%$ [100] (−−) of the magnitude of $Q_{C,H,O,N}$. Comparison with the experimental data provided by TME [2] for Test Case 8.

Test Case 9

Table 4.20: Experimental conditions provided by TME [2] for Test Case 9.

Pt loading	3 wt%
Al_2O_3 coat amount	171 g/L
Ratio of active catalytic surface to geometrical area	188.43

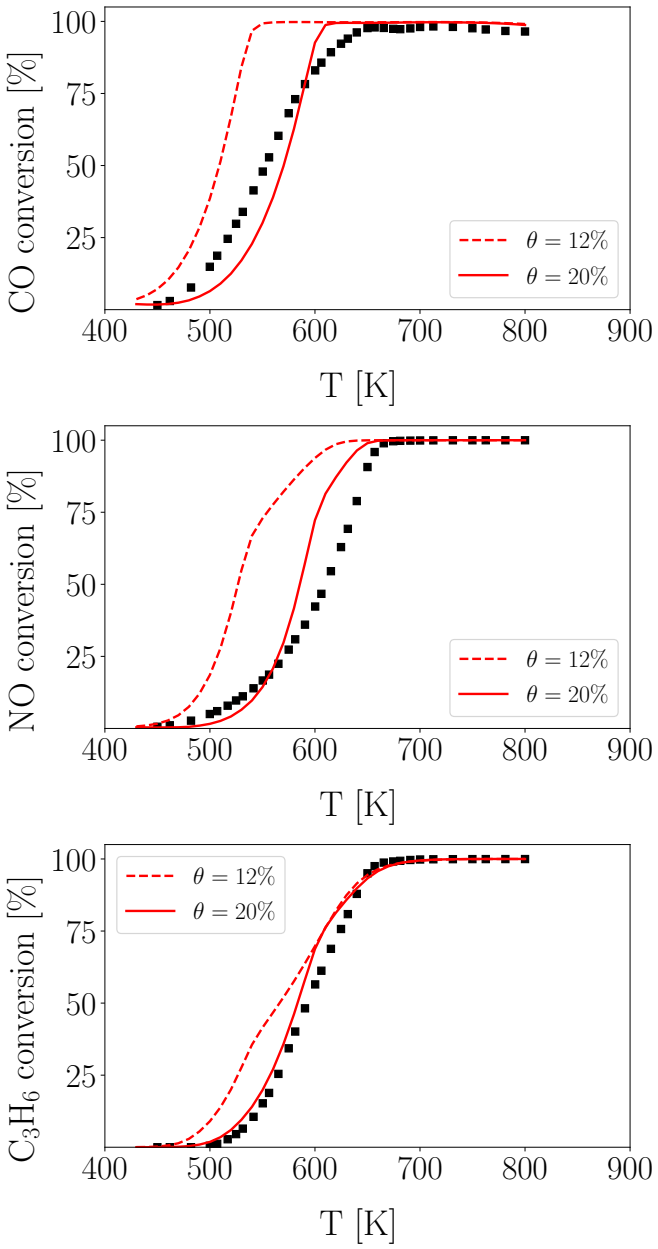


Fig. 4.18: Conversion of CO, NO and C_3H_6 at the reactor outlet against the wall temperature, for the global catalytic C_3H_6 step sub-mechanism. Implementation of $E_{C,H,O,N,diff}$ at $\theta = 12\%$ [99] (−) and $\theta = 20\%$ [100] (−−) of the magnitude of $Q_{C,H,O,N}$. Comparison with the experimental data provided by TME [2] for Test Case 9.

4.3.2.7 Effect of vibrational partition function fixed at 800 K, for CO direct adsorption reaction - Test Cases 1 - 9

The following Test Cases illustrate the effect of $T_{q^v} = 800$ K exclusively applied on the CO direct adsorption reaction, while a $T_{q^v} = 298$ K was used, in the remaining catalytic mechanism. The discussion developed in Section 4.3.2.6 applies also here, with the advantage of a better prediction of the CO conversion through the implementation of an alternative T_{q^v} value. Test Case 5 is omitted as it is already presented in Section 4.3.2.3, while $\theta = 20\%$ [100], is used in the current investigation, due to the better performance demonstrated in Section 4.3.2.6. The global irreversible C_3H_6 direct adsorption reaction is applied. The application of $T_{q^v} = 800$ K for the CO direct adsorption reaction favours the agreement for CO conversion for the whole range of Pt loadings, while the respective NO and C_3H_6 conversions show a slight discrepancy between the two approaches at $T_{q^v} = 298$ K and $T_{q^v} = 800$ K. Finally, the current investigation sets the scene for defining the optimum conditions for the application of the detailed C_3H_6 catalytic chemistry.

Test Case 1

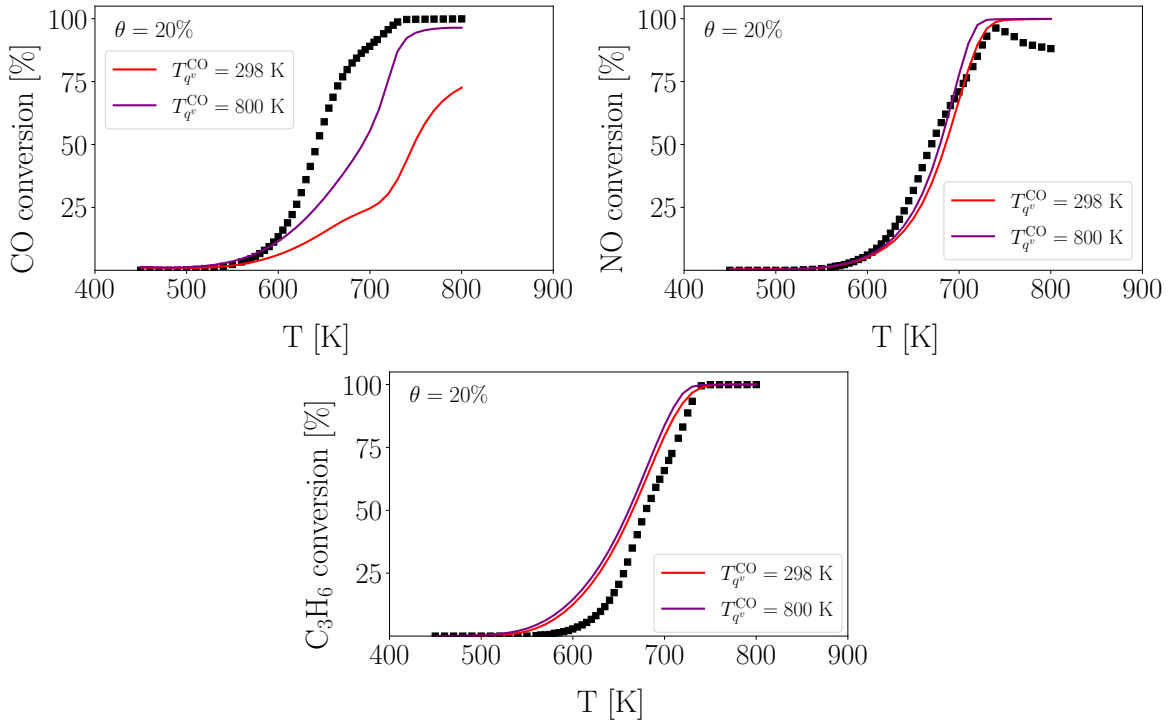


Fig. 4.19: Conversion of CO, NO and C_3H_6 at the reactor outlet against the wall temperature, for the global catalytic C_3H_6 step sub-mechanism, at $\theta = 20\%$ [100]. Comparison of the $T_{q^v} = 298$ K with $T_{q^v} = 800$ K [14, 15], for the CO direct adsorption reaction. Comparison with the experimental data provided by TME [2] for Test Case 1.

Test Case 2

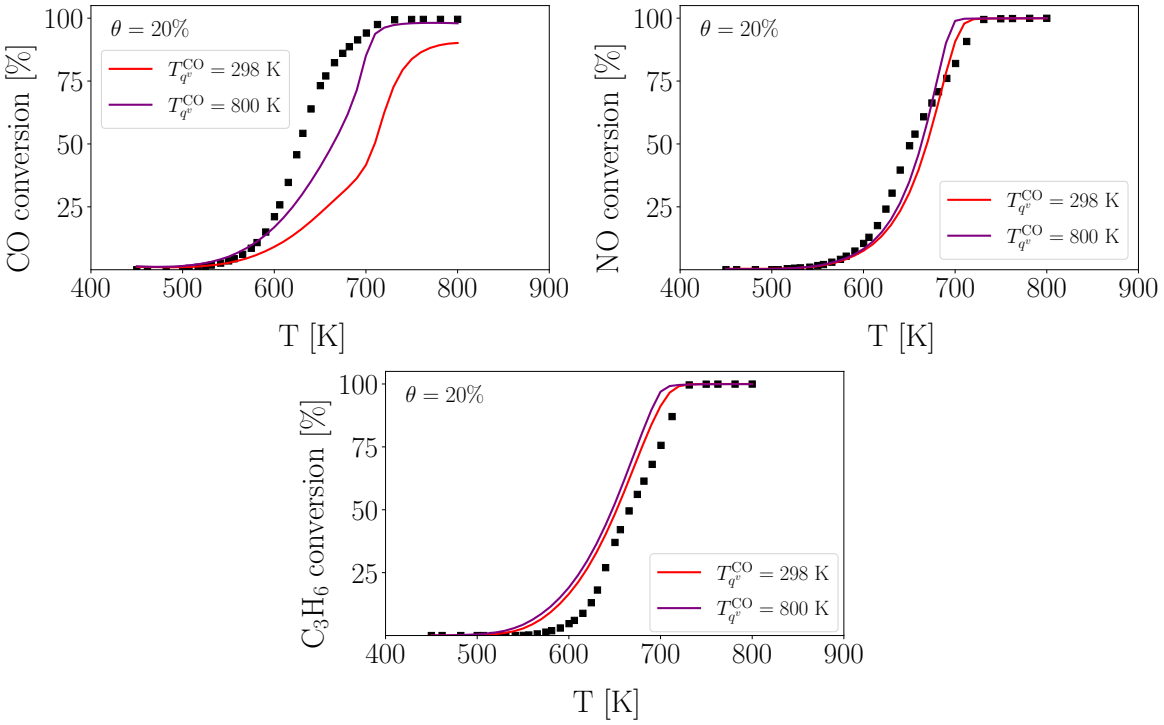


Fig. 4.20: Same as in Fig. 4.19 for Test Case 2.

Test Case 3

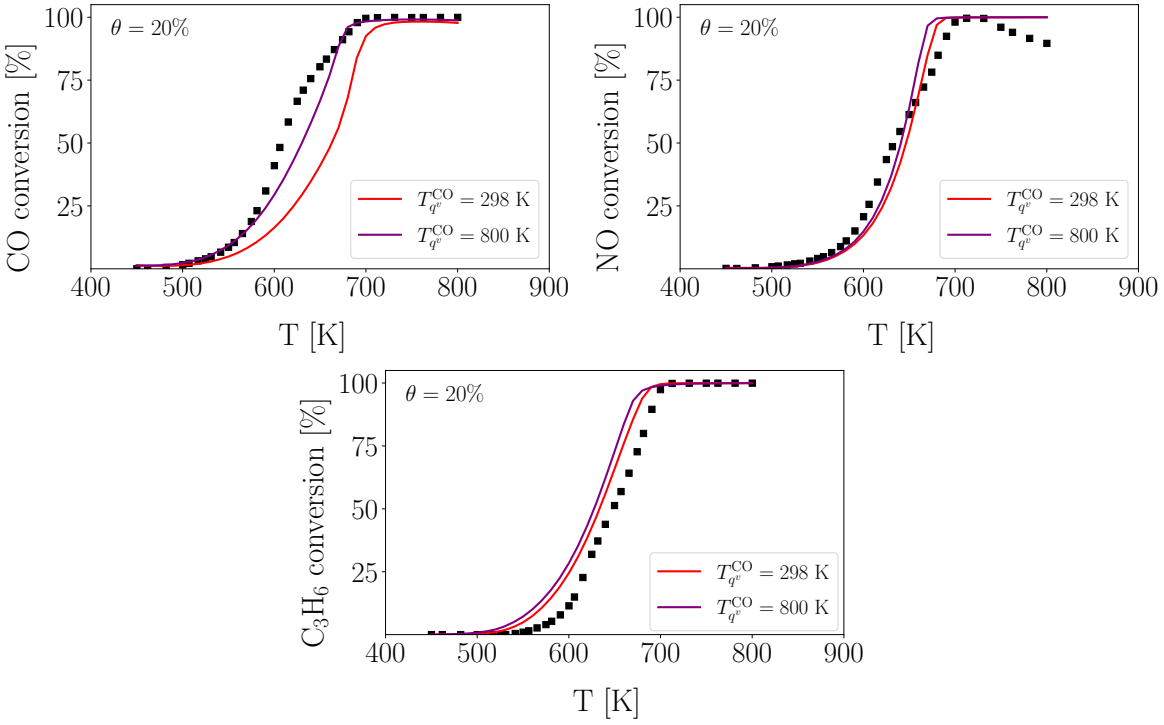


Fig. 4.21: Same as in Fig. 4.19 for Test Case 3.

Test Case 4

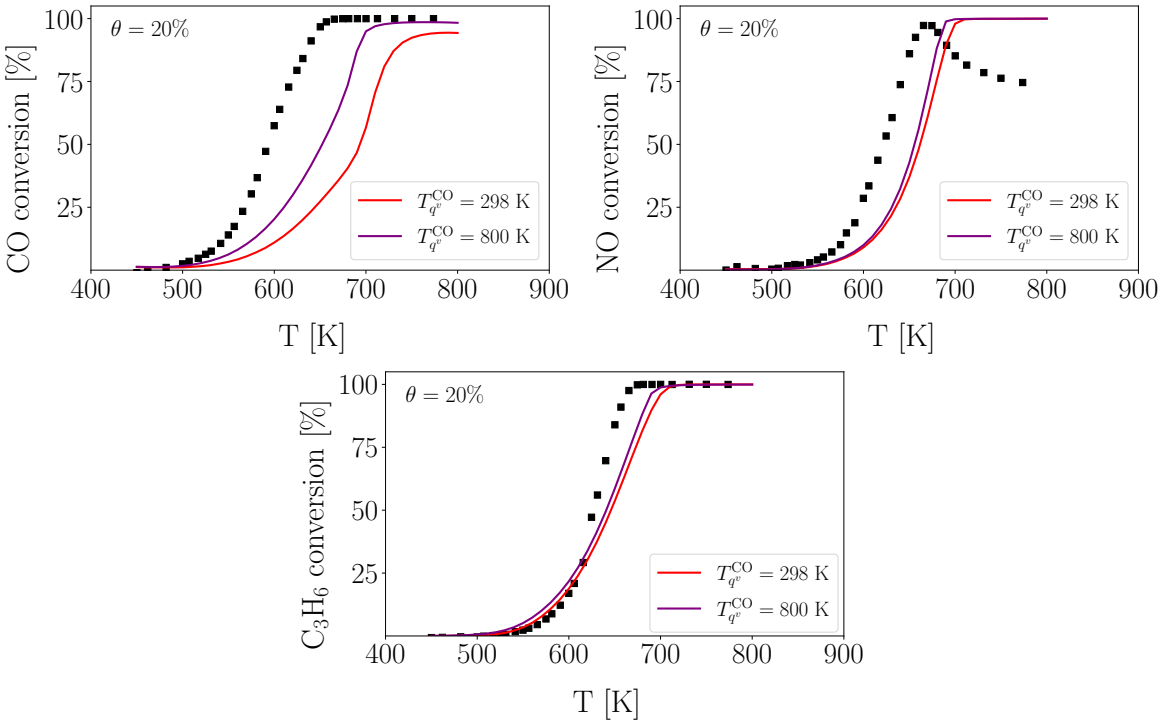


Fig. 4.22: Same as in Fig. 4.19 for Test Case 4.

Test Case 6

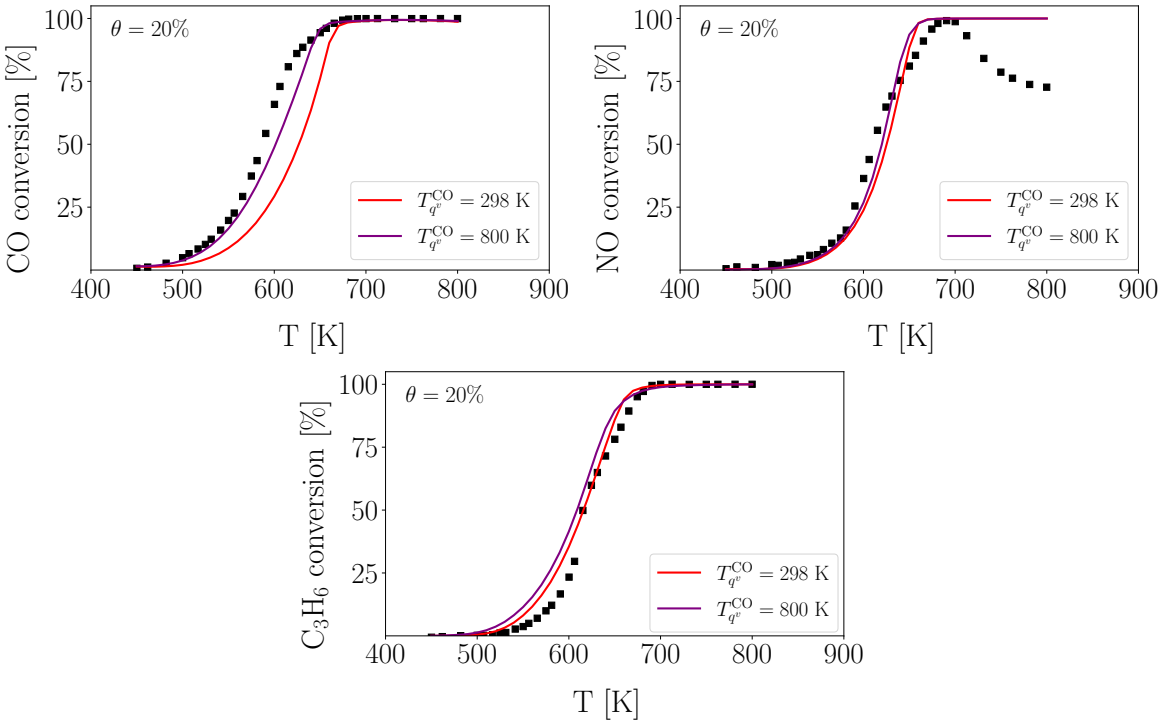


Fig. 4.23: Same as in Fig. 4.19 for Test Case 6.

Test Case 7

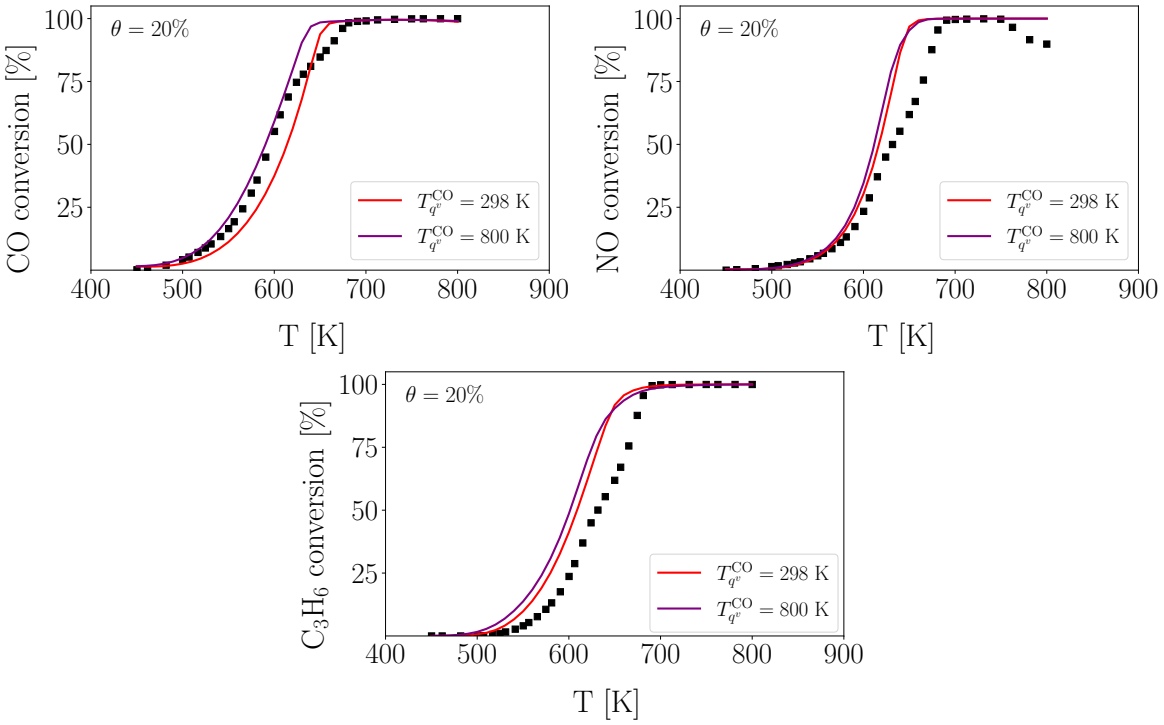


Fig. 4.24: Same as in Fig. 4.19 for Test Case 7.

Test Case 8

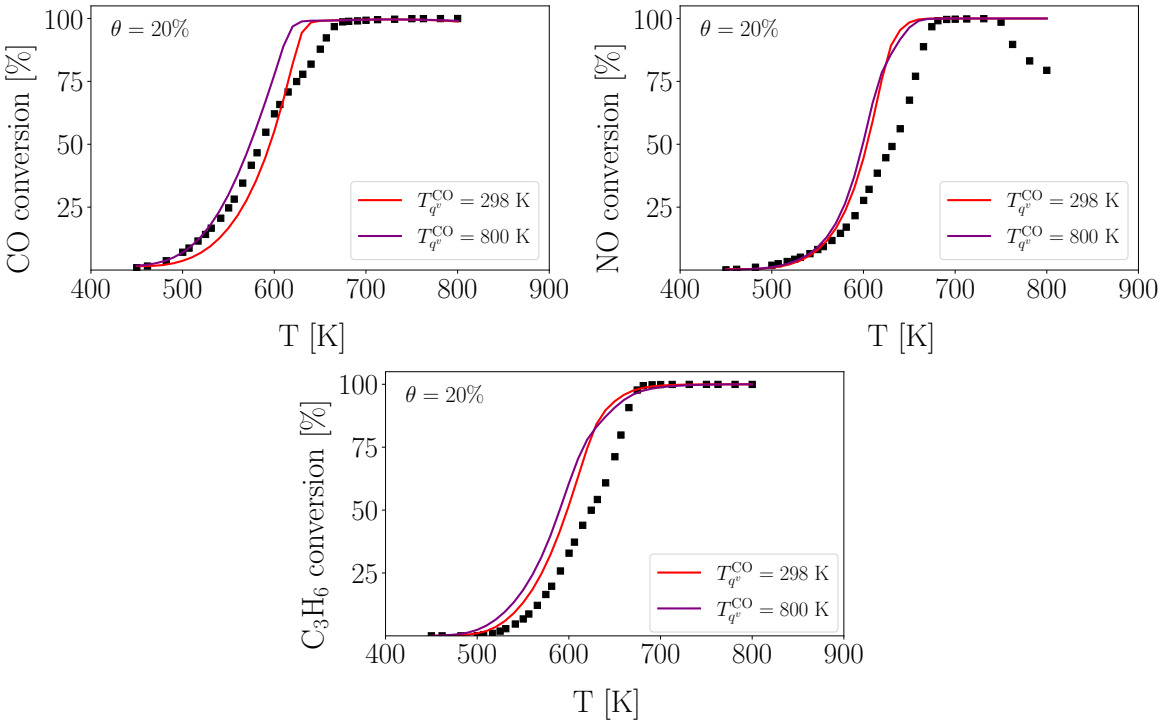


Fig. 4.25: Same as in Fig. 4.19 for Test Case 8.

Test Case 9

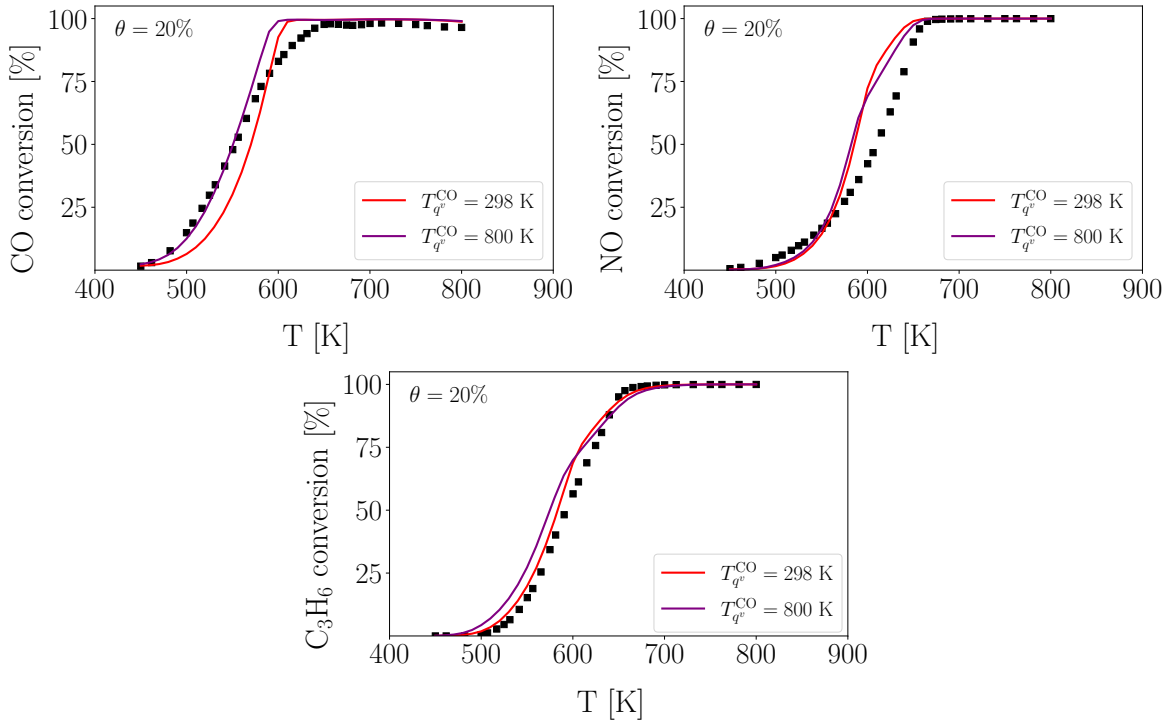


Fig. 4.26: Same as in Fig. 4.19 for Test Case 9.

4.3.3 Implementation of the detailed C_3H_6 catalytic chemistry

The current Section is devoted to a comparison of experimental data [2] with the proposed reaction mechanism featuring detailed C_3H_6 catalytic chemistry, as described in Section 4.3.1.2. The optimal conditions of the higher diffusion barrier along with the T_{q^v} = 800 K for the CO adsorption reaction, are selected based on their desirable performance in the previous results. The systematic deviation of CO conversion from the experimental data [2], especially at the low Pt loadings remains, but is particularly improved through the use of the T_{q^v} = 800 K. The removal of the $1/x^x$ factor from the CO adsorption reaction, resulting in an increase of the rate by a factor of 4, constitutes a future step towards the elimination of the discrepancy observed. The factor $1/x^x$, is not included in the sticking coefficient definition applied in Section 3.1. The present investigation also shows a systematic early onset of the C_3H_6 conversion at the higher Pt loading. Figure 4.27 illustrates the major reaction pathways of C_3H_6 on the surface, for Test Case 8 at 500 K. The C_3H_6 is adsorbed on the surface by 26.5% and 73.5% leading

to $C_3H_6(s_2)$ and $C_2H_5CH(s_2)$, respectively. Additionally, the $C_3H_6(s_2)$ adsorbate almost exclusively desorbs to produce C_3H_6, while the $C_2H_5CH(s_2)$ forms $CH_2CH_3(s)$ by 50% and $CHO(s)$, $CH_2O(s)$ totally by 50%. Therefore, C_3H_6 adsorbs on the surface at high rate despite the low temperature. This may be attributed to the high Pt loading that facilitates this behaviour. However, C_3H_6 is likely to have a lower value for Knudsen diffusion due to its larger size. The latter should be considered in future work.

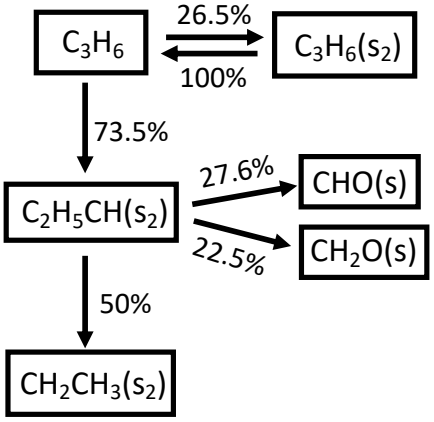


Fig. 4.27: Reaction pathway analysis of C_3H_6 on the surface.

Test Case 1

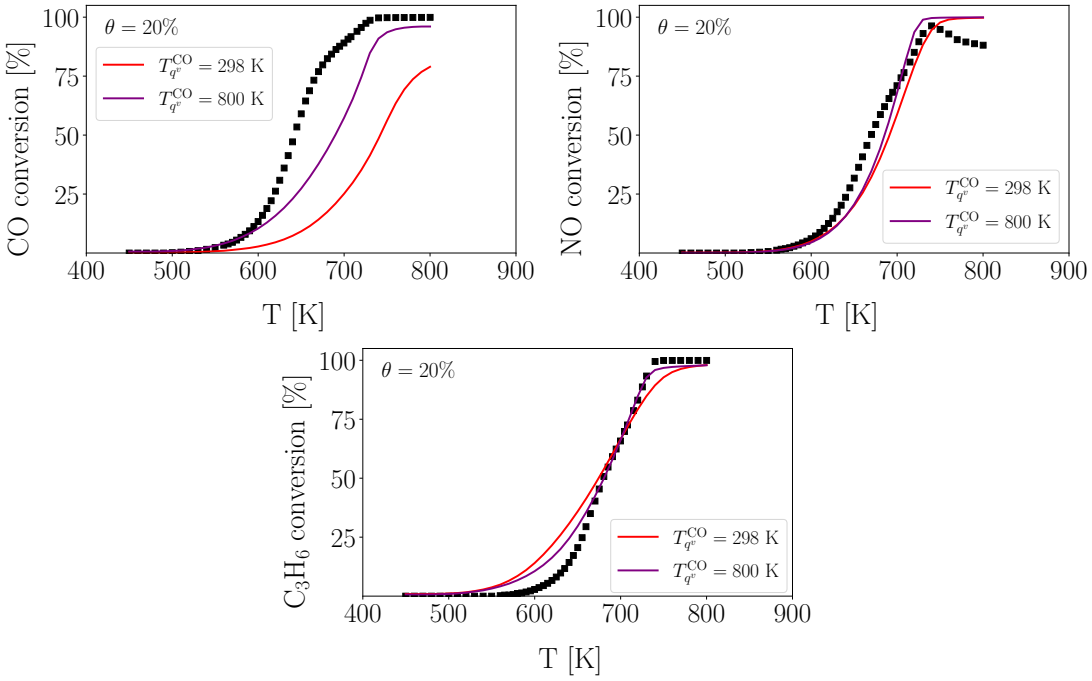


Fig. 4.28: Comparison of the $T_{q^v} = 298$ K with $T_{q^v} = 800$ K [14, 15], for the CO adsorption reaction, at $\theta = 20\%$ [100]. Comparison with the experimental data provided by TME [2] for Test Case 1.

Test Case 2

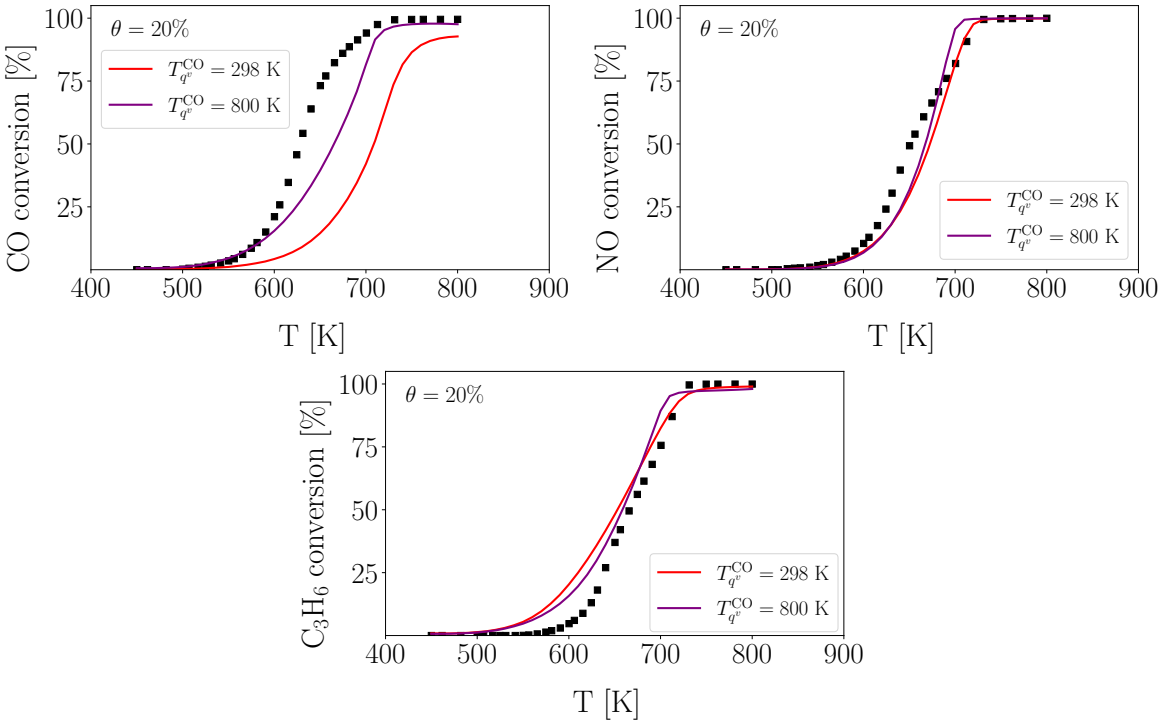


Fig. 4.29: Same as in Fig. 4.28 for Test Case 2.

Test Case 3

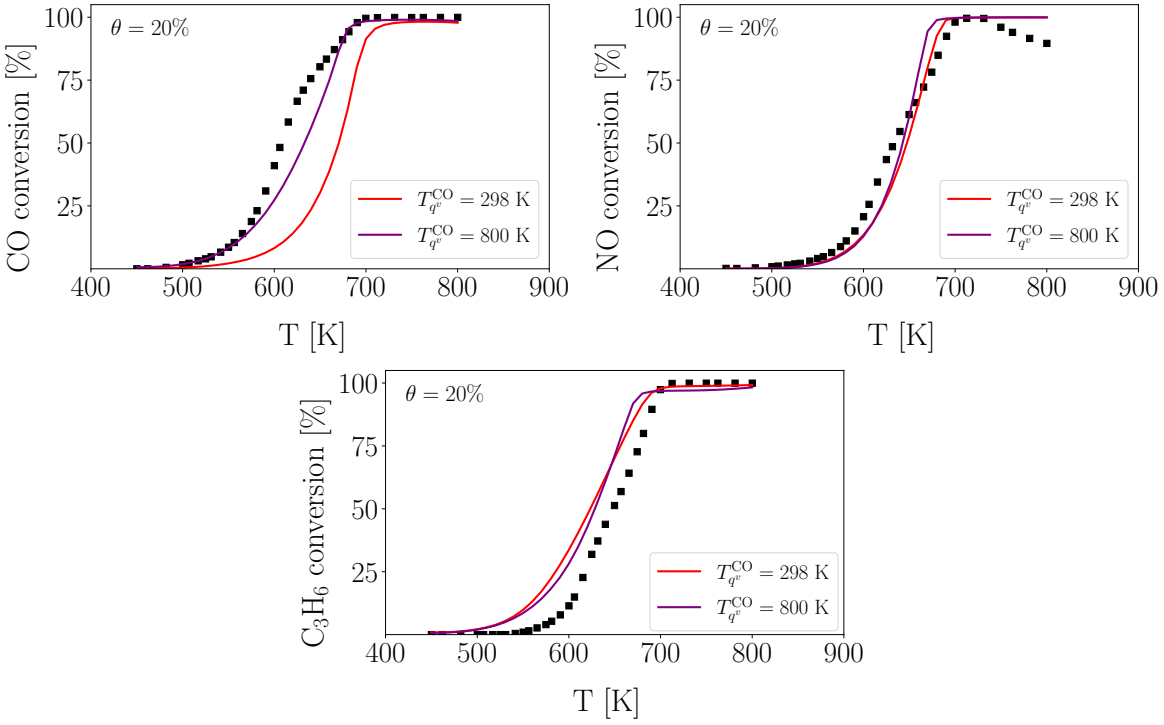


Fig. 4.30: Same as in Fig. 4.28 for Test Case 3.

Test Case 4

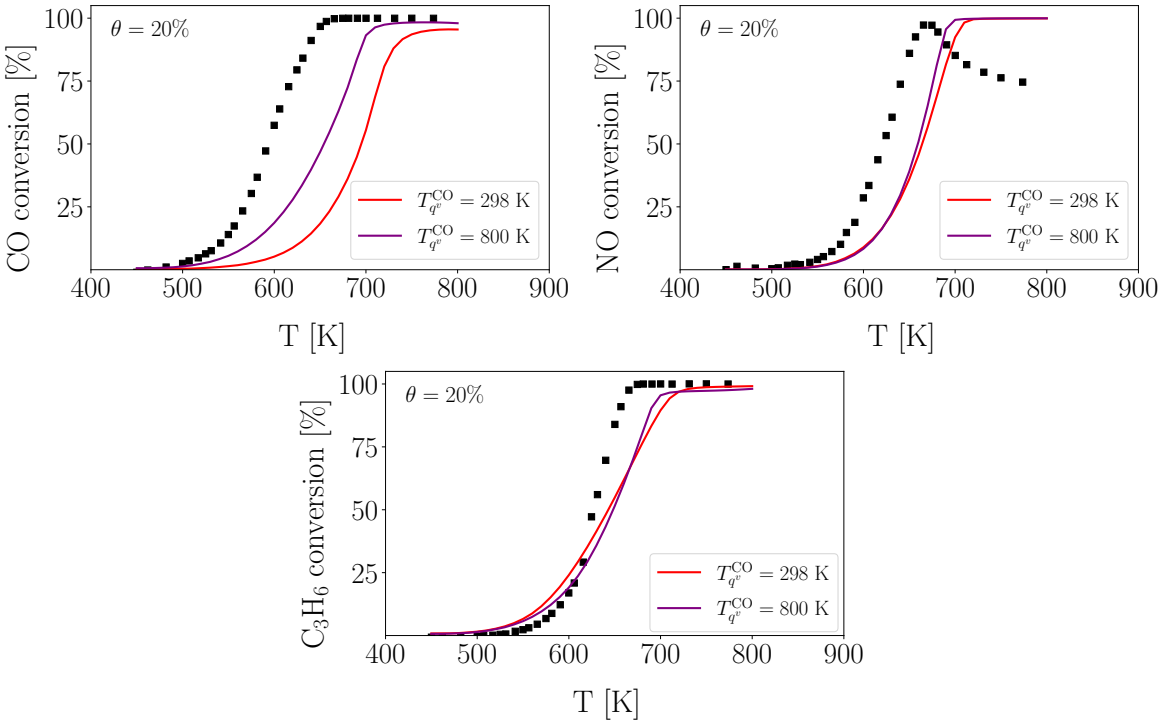


Fig. 4.31: Same as in Fig. 4.28 for Test Case 4.

Test Case 5

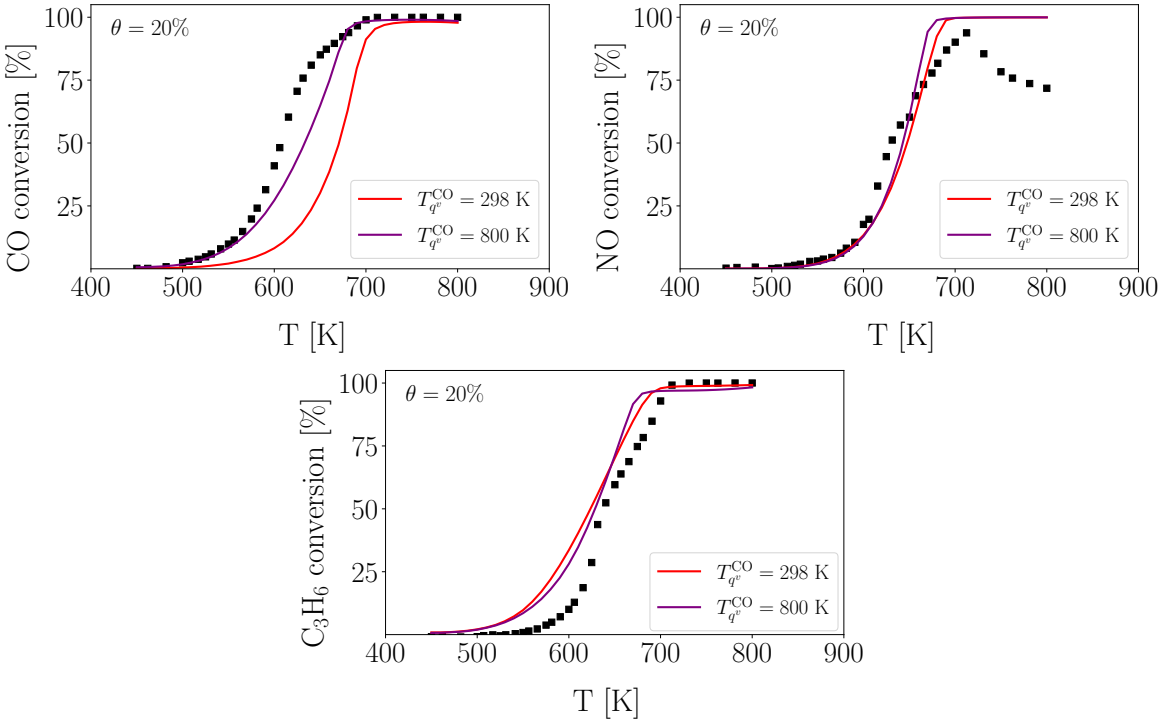


Fig. 4.32: Same as in Fig. 4.28 for Test Case 5.

Test Case 6

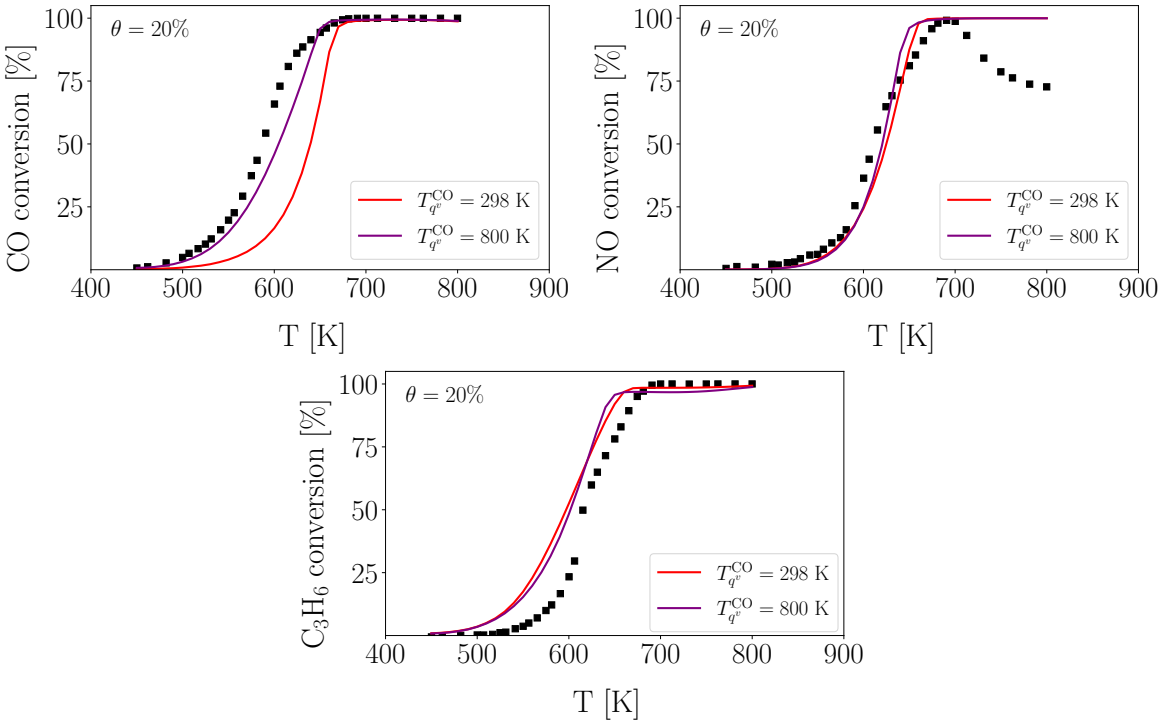


Fig. 4.33: Same as in Fig. 4.28 for Test Case 6.

Test Case 7

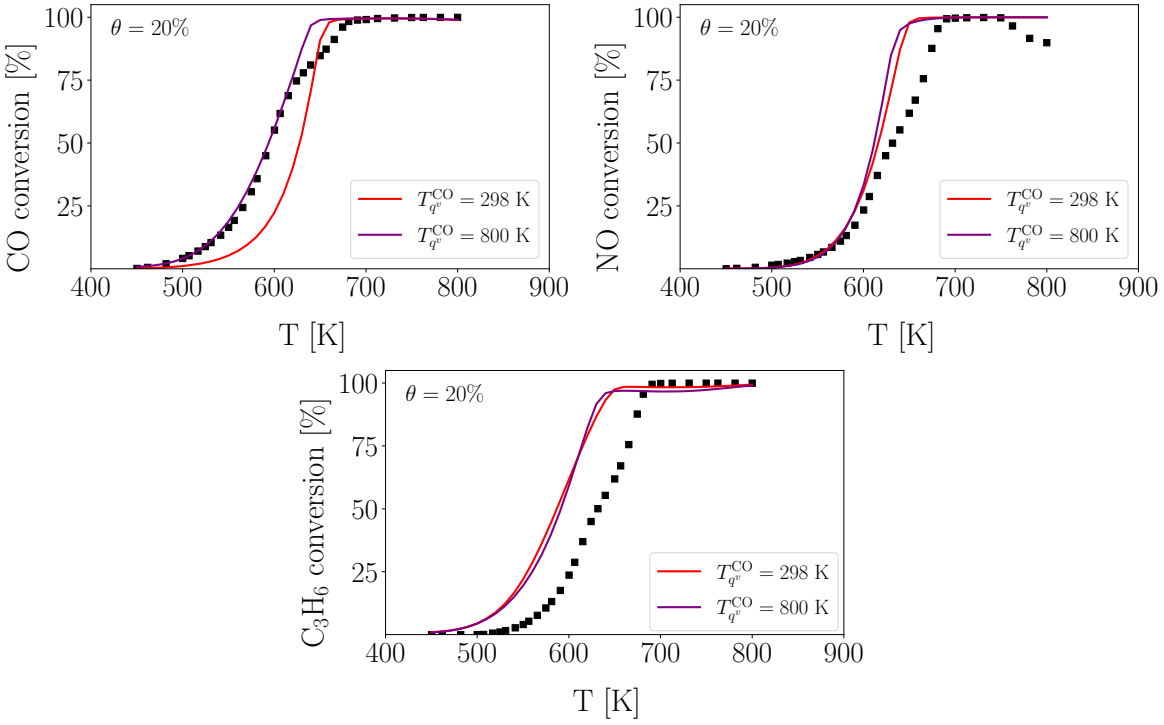


Fig. 4.34: Same as in Fig. 4.28 for Test Case 7.

Test Case 8

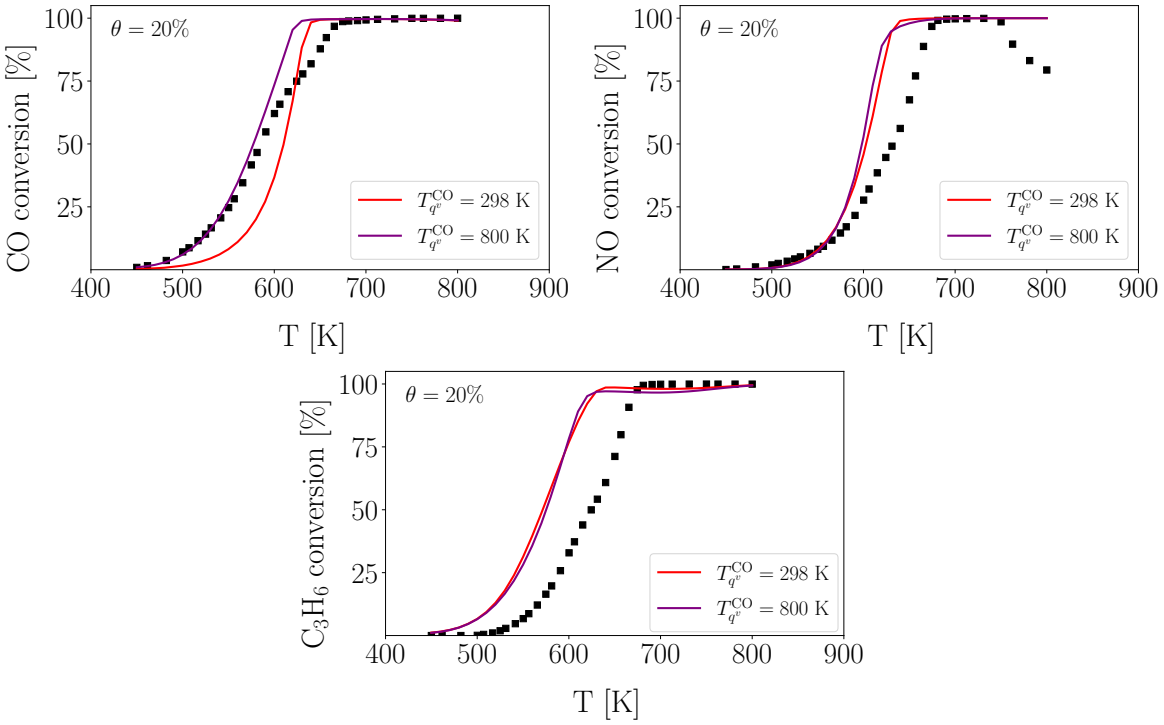


Fig. 4.35: Same as in Fig. 4.28 for Test Case 8.

Test Case 9

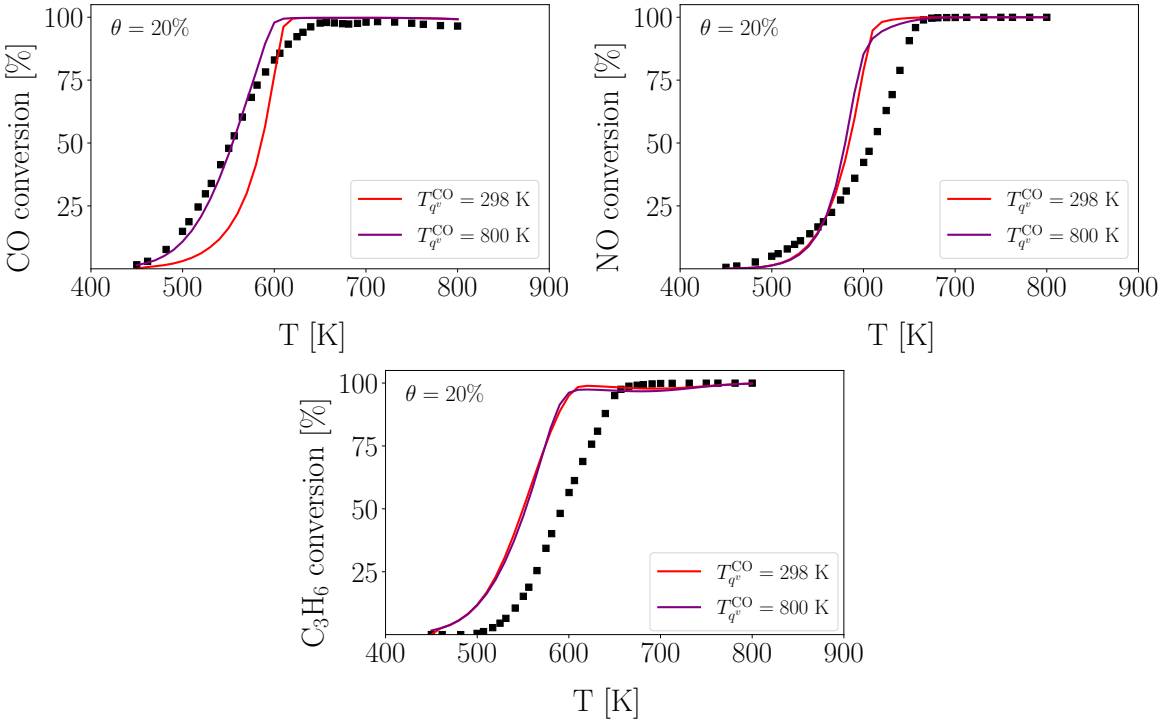


Fig. 4.36: Same as in Fig. 4.28 for Test Case 9.

4.3.3.1 Effect of residence time

A potentially significant factor that may influence the accuracy of the results for the NOx removal, particularly at higher temperatures, is the residence time between the end of the catalytic converter of the packed bed reactor and the probe sampling location, where the exhaust gases samples are obtained for analysis.

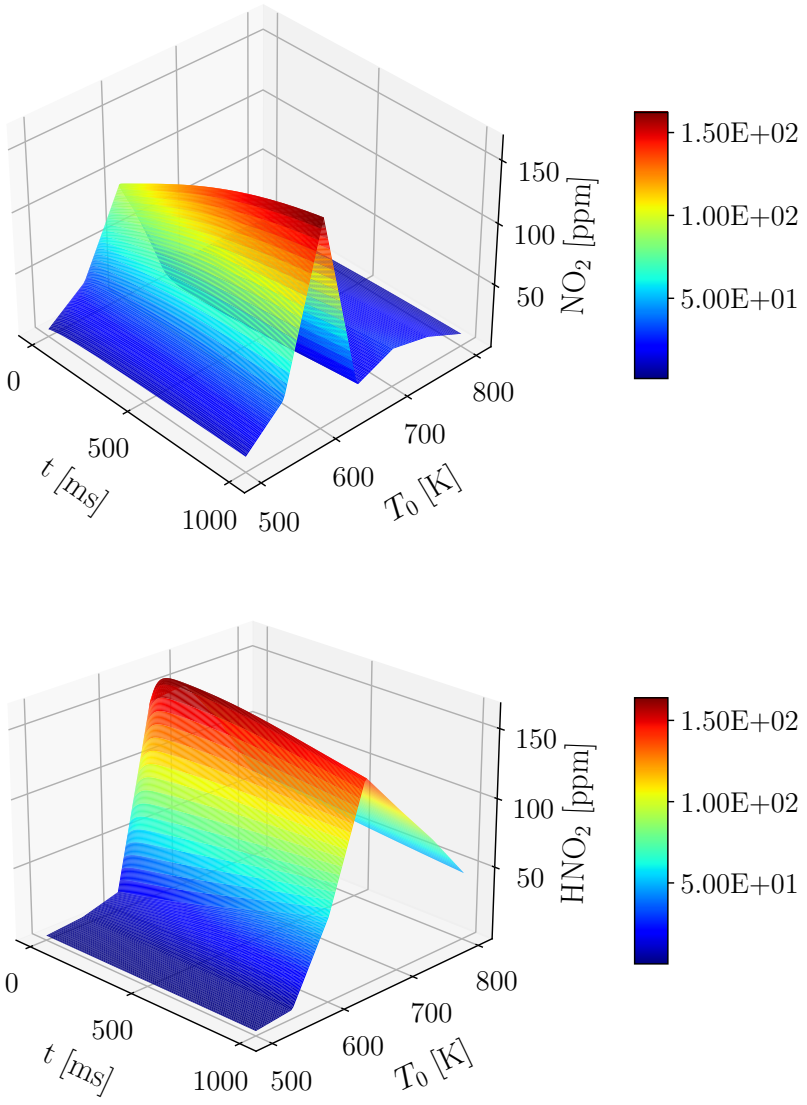


Fig. 4.37: Surface plots of NO_2 and HNO_2 concentrations [ppm] obtained from the plug flow reactor model for $E_{C,H,O,N,diff}$ equal to $\theta = 12\%$ [99] of the magnitude of $Q_{C,H,O,N}$, for Test Case 5.

As the distance between the two locations may be substantial, a greater amount of NO will be converted to NO_2. A plug flow reactor model was used to investigate the impact of increased residence time in the gas phase for reactants and products. By using the

final mixture composition at the exit of the catalytic converter, for Test Case 5, as the initial composition for the plug flow reactor model, the impact of the residence time in the sampling line can be assessed. The sampling assumed is adiabatic, therefore, no heat losses are assumed.

As shown in Figs. 4.37 and 4.38, catalytic converter temperatures, from 500 to 800 K, have been considered to derive the behaviour of NO_2 and HNO_2 concentrations as a function of time, based on the implementation of the diffusion barrier of each reactant species, $E_{C,H,O,N,diff}$. The latter range from 0 to 1 sec.

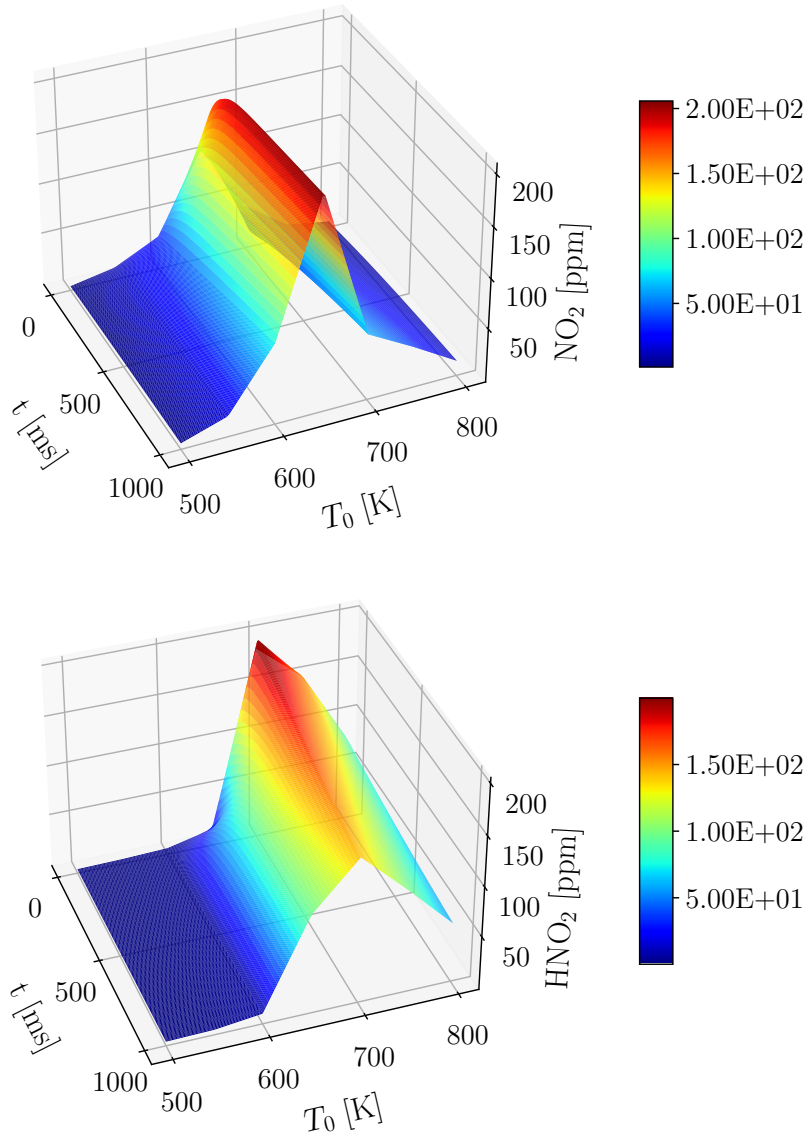


Fig. 4.38: Surface plots of NO_2 and HNO_2 concentrations [ppm] obtained from the plug flow reactor model for $E_{C,H,O,N,diff}$ equal to $\theta = 20\%$ [100] of the magnitude of $Q_{C,H,O,N}$, for Test Case 5.

The NO_2 concentration increases up to 600 K and after a decrease in the range of 650 K to 700 K, a slight increase can be observed until the 750 K, for the case of θ = 12% [99]. As observed in Fig. 4.38, the NO_2 concentration increases up to 700 K and then decreases sharply until the 800 K, for the θ = 20% [100] case. The HNO_2 concentration rises up to around 700 K for both θ = 12% [99] and θ = 20% [100], respectively and then declines until 800 K, as shown in Figs. 4.37 and 4.38. The difference in the peak temperatures of HNO_2 formation for θ = 12% [99] and θ = 20% [100] is attributed to the different implementation of diffusion barriers $E_{C,H,O,N,diff}$, in the computations. The amount of HNO_2 presents a peak at around 150 ppm and 190 ppm for θ = 12% [99] and θ = 20% [100], respectively, that can not be neglected. This reflects a potential route to NO_3 and HNO_3 formation. The inclusion of HNO_3 is also useful due to the H_2O complexes formation.

Table 4.21: Gas phase reactions describing the NO conversion to NO_2 and HNO_2.

Reactions			A	β	E_A
NNH + NO	→	HNO + N_2	9.10000E+08	0.00	0.00
HNO + M	→	H + M + NO	1.26000E+13	-0.43	207.03
HNO + H	→	H_2 + NO	4.50000E+08	0.72	2.75
OH + HNO	→	H_2O + NO	1.30000E+04	1.88	-4.01
HNO + O	→	NO + OH	3.60000E+10	0.00	0.00
HNO + NH_2	→	NH_3 + NO	2.00000E+10	0.00	4.20
NO + HNO	→	N_2O + OH	2.00000E+09	0.00	109.20
HNO + O_2	→	HO_2 + NO	3.16000E+09	0.00	12.60
HNO + NO_2	→	HNO_2 + NO	6.02200E+08	0.00	8.35
NO + HO_2	→	NO_2 + OH	2.17000E+09	0.00	-2.25
NO + O + M	→	M + NO_2	3.26000E+09	0.30	0.00
NO_2 + H	→	NO + OH	2.41000E+11	0.00	2.84
O + NO_2	→	NO + O_2	3.90000E+09	0.00	-1.00
2 NO_2	→	2 NO + O_2	1.62600E+09	0.00	109.72
NO_2 + HO_2	→	HNO_2 + O_2	4.64000E+08	0.00	-2.02
NO + M + OH	→	HNO_2 + M	1.99000E+11	-0.05	3.03
HNO_2 + H	→	H_2 + NO_2	1.20000E+10	0.00	25.04
OH + HNO_2	→	H_2O + NO_2	1.51000E+09	0.00	-2.17
O + HNO_2	→	NO_2 + OH	1.20000E+10	0.00	30.88

Therefore, the related gas phase chemistry was applied in the current reaction mechanism for completeness, as described in Section 4.2.1. Table 4.21 presents the gas phase reactions that take place in the NO to NO_2 and HNO_2 conversion.

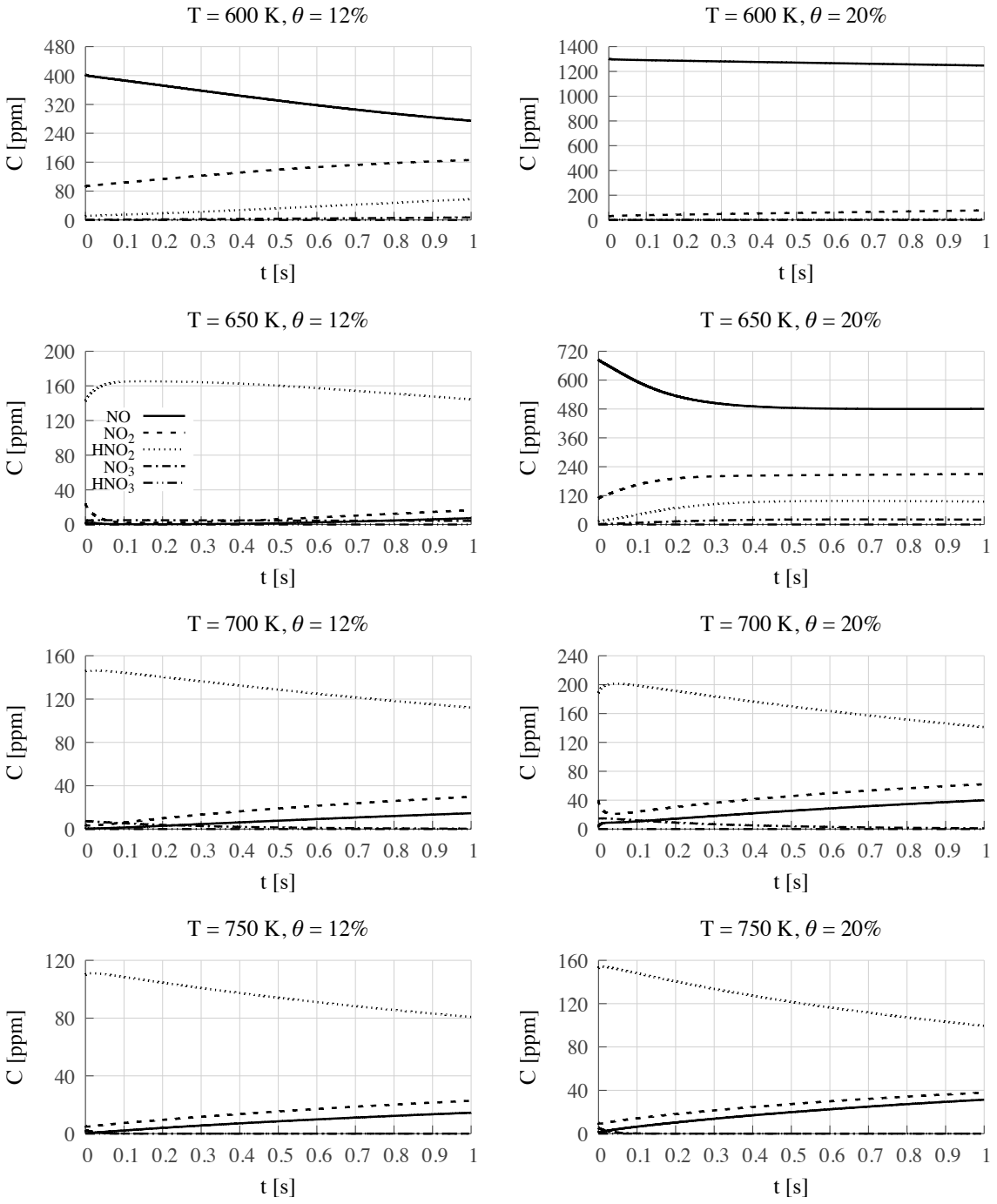


Fig. 4.39: Comparison of NO (−), NO_2 (−−), HNO_2 (· · ·), NO_3 (− · −), HNO_3 (− · ·−) concentrations [ppm] against time [s] for $\theta = 12\%$ [99] and $\theta = 20\%$ [100].

A third body M is used in some of the gas phase reactions of the current mechanism to stabilize the excited product by collision. It can be any inert molecule in the atmosphere (e.g. N_2, O_2) that can remove the energy of the excited product and dissipate it as heat.

A comparison of NO, NO_2, HNO_2, NO_3 and HNO_3 concentrations as a function of temperature, after a residence time of 1 sec, are presented in Fig. 4.39, for $\theta = 12\%$ [99] and $\theta = 20\%$ [100]. The computations outline a temperature window of 650 K - 700 K, where NO_3 can be formed, for both cases. Figure 4.40 illustrates the mol fractions of the studied nitrogen containing species as a function of temperature, for both $\theta = 12\%$ [99] and $\theta = 20\%$ [100]. The results confirm that there is an interconversion of NO, NO_2, HNO_2 and NO_3, mainly at temperatures above 550 K and 600 K, for $\theta = 12\%$ [99] and $\theta = 20\%$ [100], respectively.

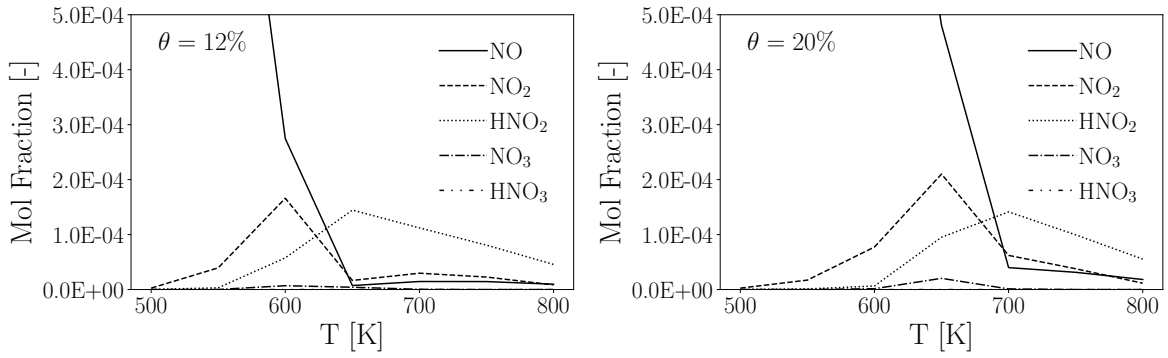


Fig. 4.40: Comparison of NO $(-)$, NO_2 $(--)$, HNO_2 $(\cdots)$, NO_3 $(-\cdot-)$, HNO_3 $(-\cdots-)$ mol fractions [-] against temperature [-] at the exit of the catalytic converter, for $\theta = 12\%$ and $\theta = 20\%$ [100].

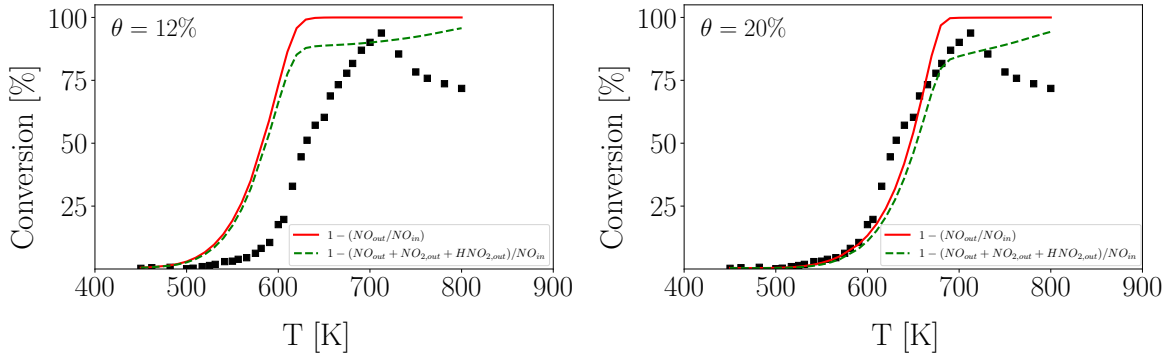


Fig. 4.41: Comparison of NO and NOx conversions with the experimental data provided by TME [2], for Test Case 5, for $\theta = 12\%$ [99] and $\theta = 20\%$ [100].

Consequently, the impact of NO_2 and HNO_2 were considered on the NOx conversion, additionally to NO, for the Test Case 5, as an indicative paradigm. Figure 4.41

demonstrates the evaluation of conversion based on the different implementation of the $E_{C,H,O,N,diff}$, by taking into account the NO, NO_2 and HNO_2 concentrations at the outlet of the catalytic converter. The inclusion of NO_2 and HNO_2 outputs in the calculation of the conversion, reduces its efficiency and concludes to a potentially significant production of NO_2.

4.3.4 Consideration of metal dispersion

The impact of dispersion is investigated below using the area ratio, F', which includes the platinum dispersion efficiency and the 1.43 [2] site density factors. The mid-point value of F', corresponding to Test Case 5, was applied along with the estimated site densities, shown in Table 4.4, for each Pt loading.

Test Case 1

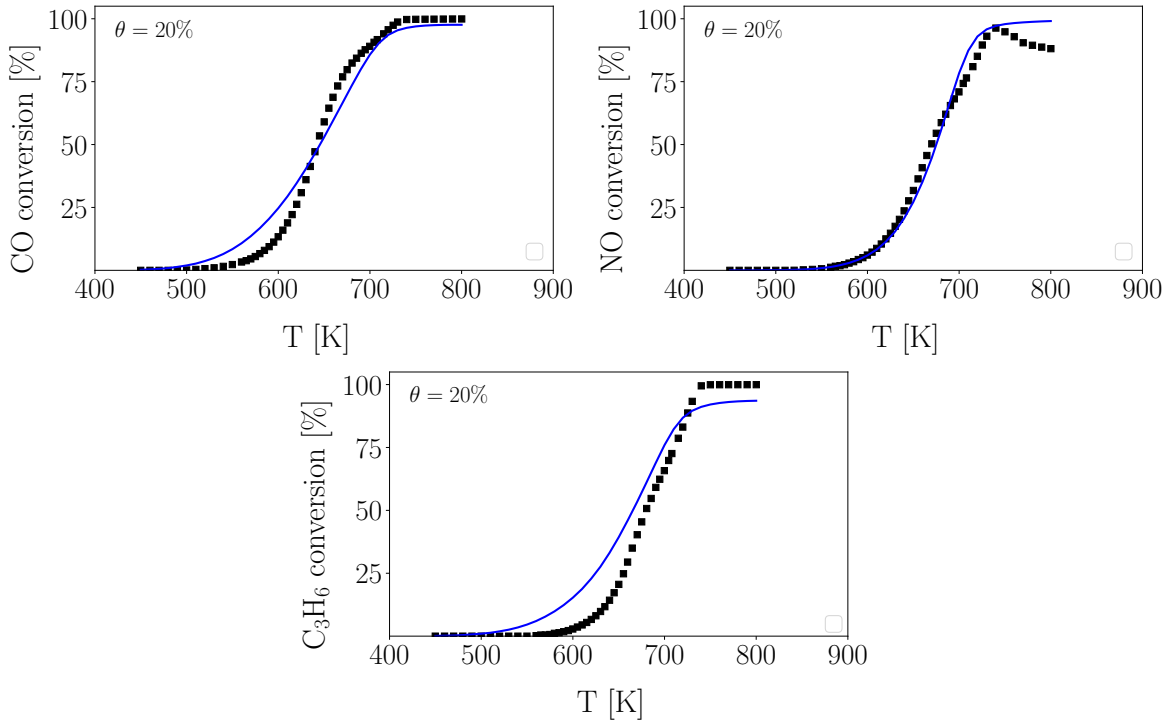


Fig. 4.42: Conversion of CO, NO and C_3H_6 at the reactor outlet against the wall temperature, for the detailed catalytic C_3H_6 sub-mechanism, at $\theta = 20\%$ [100]. Comparison with the experimental data provided by TME [2] for Test Case 1.

Test Case 5

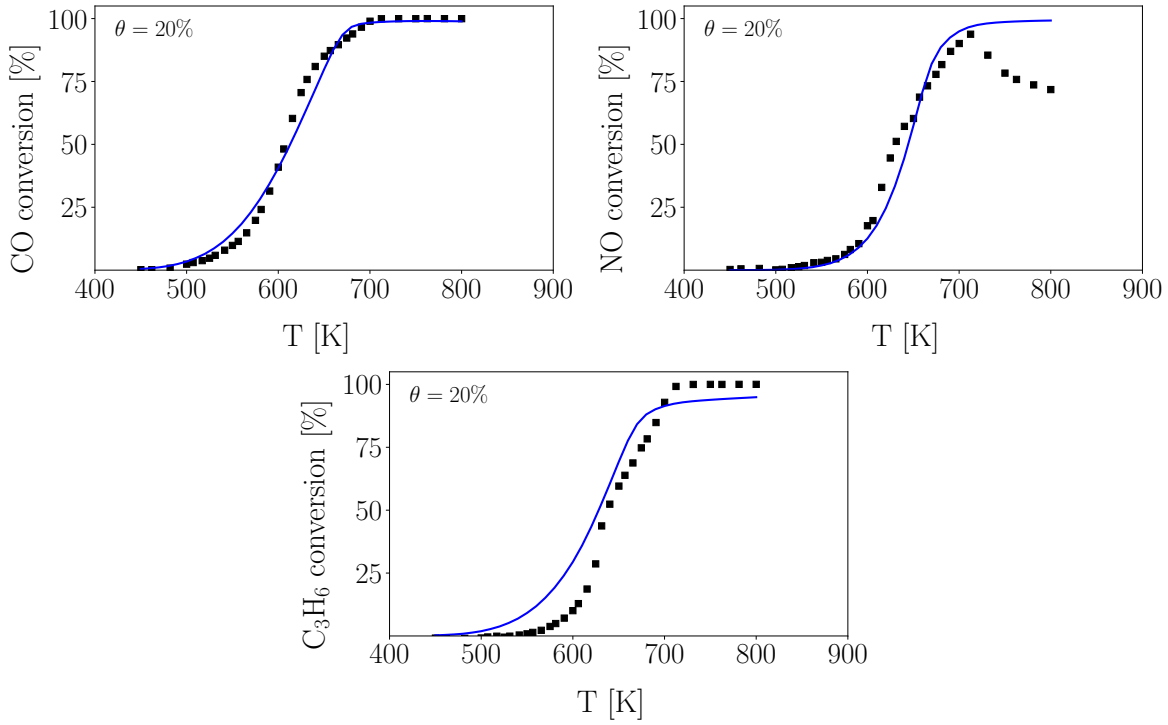


Fig. 4.43: Conversion of CO, NO and C_3H_6 at the reactor outlet against the wall temperature, for the detailed catalytic C_3H_6 sub-mechanism, at $\theta = 20\%$ [100]. Comparison with the experimental data provided by TME [2] for Test Case 5.

The applied reaction mechanism features the detailed C_3H_6 catalytic chemistry, along with the optimal conditions of the $T_{q^v} = 800$ K for the CO adsorption reaction and the higher diffusion barrier corresponding to $\theta = 20\%$ [100]. Results for Test Cases 1, 5 and 9, corresponding to the lower, median and higher Pt loading are shown in Figs. 4.42–4.44. The overall efficiency factor hence corresponds to the product of the constant F', a temperature-dependent Knudsen efficiency factor and the case dependent estimated Pt loading. The computations are further based on the porosities obtained from the geometrical expression, i.e. Eq. (2.30), and the same process can be applied using data obtained with the approach of Giani et al. [55]. The corresponding Knudsen efficiency factors are listed in Table 4.22. The inclusion of the dispersion efficiency reduces the uncertainty factor applied to provide optimal agreement for Test Case 5 to 1.58. The latter value is well within the uncertainties associated with the Knudsen diffusion efficiency. The results obtained suggest encouraging agreement with the experimental data [2].

Table 4.22: Application of a constant area ratio (F'), at different Pt loadings and coat amounts, considering the dispersion efficiency factor (η_D). The values (F = 27.79, η_D = 0.36, F' = 10.00 for Test Case 5) indicated in a bold font are applied for all the Test Cases. The Knudsen efficiency factors (η_e) for the geometrical [11] and Giani et al. [55] approach correspond to 600 K.

Test Cases	Pt loading	Coat amount	F	η_D	F'	Γ	η_e [11]	η_e [55]
1	0.5 wt %	60				$1.01 \cdot 10^{-10}$	$3.66 \cdot 10^{-2}$	$1.43 \cdot 10^{-2}$
5	1 wt %	92	**27.79**	**0.36**	**10.00**	$2.11 \cdot 10^{-10}$	$3.44 \cdot 10^{-2}$	$1.24 \cdot 10^{-2}$
9	3 wt %	171				$7.33 \cdot 10^{-10}$	$3.86 \cdot 10^{-2}$	$1.70 \cdot 10^{-2}$

Test Case 9

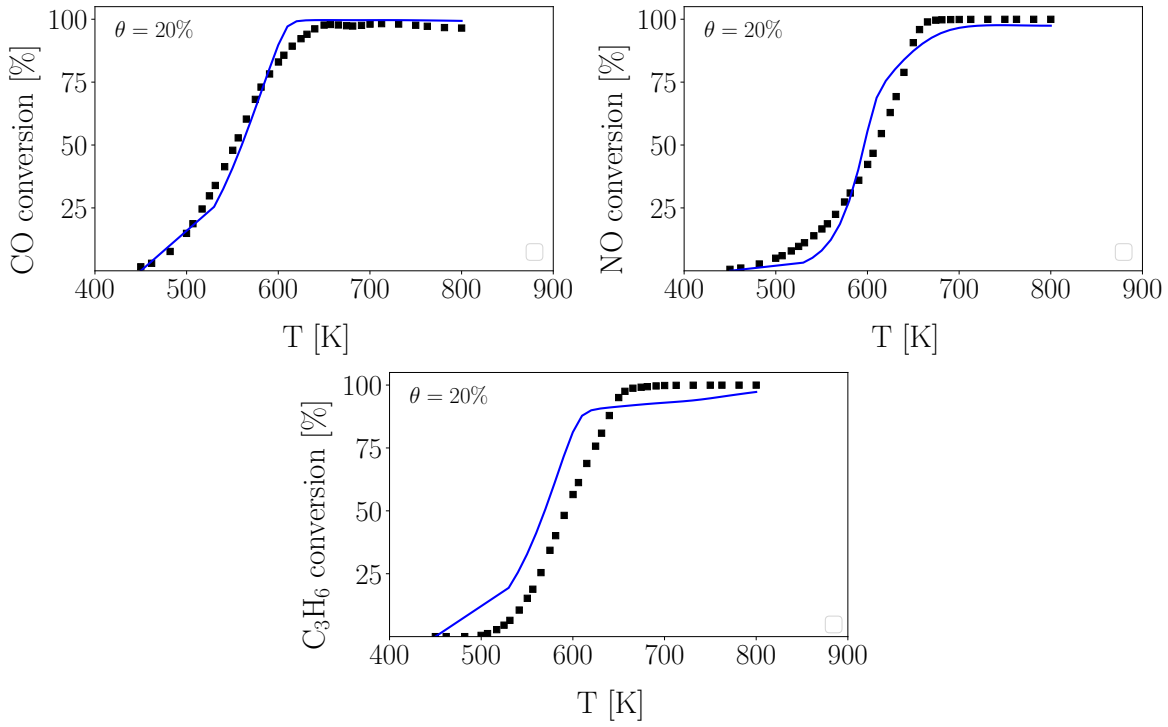


Fig. 4.44: Conversion of CO, NO and C_3H_6 at the reactor outlet against the wall temperature, for the detailed catalytic C_3H_6 sub-mechanism, at $\theta = 20\%$ [100]. Comparison with the experimental data provided by TME [2] for Test Case 9.

4.4 Summary

The developed class-based framework for heterogeneous reaction mechanisms described in Chapters 2 and 3 has been successfully applied and validated for the removal of the

principal oxides of nitrogen through the use of supported Pt catalysts. Two comprehensive -N and -C_3H_6 - C_3H_5 containing catalytic sub-mechanisms were constructed for the investigation of CO, NO and C_3H_6 conversions against temperature. The latter were validated with experimental data obtained by TME [2] for nine Test Cases varying in the noble metal loading (0.5 wt%, 1 wt%, 3 wt%), Al_2O_3 coat amount and the ratio of active catalytic surface to geometrical area. The Knudsen porous media diffusion mechanism, described in Section 2.3.2, was selected for the current computations due to its potential to describe the molecule-surface interactions for the size of catalytic pores measured experimentally.

Apart from the surface chemistry, the gas phase mechanism was also updated from the previous used by Kraus and Lindstedt [14, 15] considering -N and -C_3 containing gas phase species and reactions. Concerning the validation of the -N containing sub-mechanism an adjustment related to the treatment of NO molecular direct adsorption reaction using a mobile transition state prior to surface attachment was adopted, by removing the $\frac{1}{x^x}$ scaling factor from the rate constant expression, shown in Eq. (3.28).

On the other hand, the C_3H_6 catalytic chemistry required an extended investigation for an accurate establishment. A first step was realized through the use of a global irreversible C_3H_6 adsorption reaction with an activation energy calculated at 39.4 kJ/mol. The latter value is broadly consistent with the respective value of 41 kJ/mol estimated by TME [2]. Consequently, several computations based on the latter C_3H_6 implementation were conducted for validation, along with a comparison of two diffusion limitations at θ = 12% and θ = 20% of the magnitude of the heat of adsorption, $Q_{C,H,O,N}$.

Subsequently, the effect of different parameters analysed or listed in previous Chapters, was initially explored for a representative Test Case. In particular, Test Case 5 was selected as the mid-point case. Two different $N_2O(s_2)$ heats of adsorption were examined along with alternative CO desorption energies for diffusion barriers, of θ = 12% [99] and θ = 20% [100]. No difference was noticed from the comparison of the H_2 mobile and immobile transition state. However, the effect of a fixed T_{q^v} at 800 K either exclusively on CO direct adsorption reaction, or on the whole catalytic reaction network, was distinct. Following a comparison shown in Figs. 4.5 and 4.6, the application of a fixed T_{q^v} = 800 K proved to improve the agreement with the experimental measurements [2] for the CO conversion at θ = 20% [100]. Thus, it was adopted in the remaining Test Cases presented

in Section 4.3.2.7, showing the superiority of this approach compared to the case of a fixed $T_{q^v} = 298$ K for CO adsorption. The latter is also linked with the improved agreement of the calculated sticking coefficients with the experimental values, for the CO direct adsorption reaction, at $T_{q^v} = 800$ K, illustrated in Fig. 3.8.

The nine Test Cases provided by TME [2] are categorized based on the measured Pt loading. The low Pt loading cases (Test Cases 1 - 3) reproduce the experiments [2] less well compared to the higher Pt loadings. The higher Pt loading and thicker layers result in a better performance of the computed species conversions, while the case of the higher diffusion barrier corresponding to $\theta = 20\%$ [100] improves the agreement between the computational and experimental data [2]. An extended analysis of the fractional diffusion barrier θ (%) of the binding energy, $Q_{C,H,O,N}$, may further improve predictions. However, the comparisons already performed highlight that a θ close to 20 % better describes the stronger transport limitations associated with the movement of chemical species between catalyst sites. Nevertheless, it must be noted that the quantitative agreement is subject to uncertainties associated with the catalyst preparation.

Finally, a significant step towards the resolution of the initial C_3H_6 catalytic sub-mechanism accounting for a global irreversible C_3H_6 direct adsorption reaction has been done via the creation of a detailed C_3H_6 surface mechanism. An updated version was suggested through the consideration of alternative configurations of propene and propenyl on the metal sites (e.g. $C_2H_5CH(s_2)$ and $C_2H_5C(s_3)$), as illustrated in Fig. 4.1. The corresponding surface reactions, presented in Table 4.10, were taken into account. Adjustments related to the omission of $\frac{1}{x^x}$ scaling factor from the C_3H_6 and C_2H_5CH rate constants of direct adsorption reactions were made.

The detailed C_3H_6 surface reaction sub-mechanism was validated for the optimal conditions corresponding to the higher diffusion barrier and high CO sticking coefficient as shown in Section 4.3.3. A better agreement of CO conversion with the experimental data [2] can be highlighted, especially at low Pt loadings, where the deviation is more significant. This discrepancy can be also attributed to the inclusion of $1/x^x$ scaling factor in the expression of the CO rate constant in earlier work [11, 14, 15]. The removal of $1/x^x$ factor constitutes a future development towards the elimination of discrepancies of CO conversion with experimental data [2] and refinement of the detailed C_3H_6 catalytic chemistry.

Chapter 5

Ethane auto-thermal catalytic cracking over Pt/Al_2O_3 catalysts

This Chapter describes the evaluation of an extended heterogeneous chemical kinetic mechanism for the modeling of C_1-C_2-C_3-C_4 reacting flows over a platinum catalyst. The mechanism has been validated with the aid of experimental investigations of the auto-thermal catalytic cracking of ethane over a 3% Pt/Al_2O_3 catalyst in a quartz lined tubular reactor. According to the provided experimental data [3], CO co-feed was added to the auto-thermal cracking (ATC) reactor aiming to investigate the degree of catalytic poisoning, leading to reduced efficiencies. The addition of hydrogen to the feed stream, in a 2:1 H_2:O_2 (v/v) ratio, was also included in the experiments [3] conducted and was considered in the outlined computations.

5.1 Experimental Data

Experimental investigation of auto-thermal cracking of ethane was conducted by BP Chemicals [3] in order to study the catalytic activity in addition of CO to the feed stream. Out of the extensive collection of data sets, a case representing a Pt loading of 3% on Al_2O_3 was selected to investigate the impact of the current revised chemical mechanisms. Errors related to the experimental measurements [3] were not available.

5.1.1 Experimental Setup

The catalytic auto-thermal cracking of ethane was studied in a quartz lined tubular reactor with a metal loading of 3% Pt on Al_2O_3 foam. The experimental implemented conditions are presented in Table 5.1.

Table 5.1: Experimental conditions provided by BP Chemicals [3].

Experimental Conditions	
Foam porosity	45 pores/inch
Catalytic bed diameter	15 mm
Catalytic bed length	60 mm
GHSV	500000/h
Pressure	1.8 bar
Hydrogen co-feed	H_2:O_2 @ 2:1 (v/v)
Carbon monoxide co-feed	9 vol% in H_2
Oxygen to carbon mol ratio (O/C)	0.45 - 0.65

A number of trials were carried out with the reaction stability limits investigated by co-feeding carbon monoxide to the ATC reactor [3] with ethane and hydrogen. The diameter and depth of the examined catalytic bed are 15 and 60 mm, respectively. The Pt catalyst formulation features a catalytic foam with 45 pores per linear inch (ppi). The individual single – pore channels therefore featured an average diameter around 0.55 mm including a wall thickness of about 80 μm.

Table 5.2: Initial mixture composition provided by BP Chemicals [3].

Species	Mol fractions
CO	0.03
C_2H_6	0.363
O_2	0.169
H_2	0.338
N_2	0.1

A subset of the experimental data set is considered here with the hydrogen to oxygen volume ratio (H_2/O_2) set to 2 and the oxygen to carbon mol ratio (O/C) of the feed

varying from 0.45 to 0.65. The reactor pressure was set to 1.8 bar, while the volumetric flow rate of the gas phase species entering the reactor was set to 88 standard liters per minute. Experiments were also performed by using a CO co-feed at 9% by volume added to the hydrogen stream. The species inlet mol fractions used for the simulations follow the mixture provided by BP Chemicals [3], as shown in Table 5.2.

5.2 Computational Methods

A purpose-written, 2D parabolic FORTRAN code [12], introduced in Section 4.2, was used to model the relevant computational domain, corresponding to the top half of the duct reactor bounded by a catalytic wall. The simulation contained 40 geometrically refined cells in the radial direction, with 1 μm resolution close to the catalytic surface. The gas phase temperature at the entrance of the catalytic reactor was set to 298 K, while the wall and exit temperatures were both equal to 844 K. The catalytic site density (Γ) and the radiative heat loss factor (κ_2) were retained at their median values of $7.5 \cdot 10^{-8}$ kmol/m^2 and 7% [11], respectively.

5.2.1 Gas phase chemistry

A previously applied [11, 14, 15] C_1-C_2 gas phase mechanism [12, 13, 59, 125] described in Section 4.2.1 was further augmented for the implementation of the current simulations. Following a reaction rate analysis, the CH, CH_2, CH_3 and C_2H_5 radicals suggest that a further product outlet is required in the gas phase. Therefore, a C_3-C_4 mechanism [12, 59], comprised of 497 additional gas phase reactions and 71 gas phase species, such as, C_3H, C_3H_2, C_3H_2l, C_3H_3, C_3H_4a, C_3H_4p, C_3H_4b, C_3H_5a, C_3H_5s, C_3H_5t, C_3H_5b, C_3H_6b, C_3H_6, C_3H_7n, C_3H_7i, C_3H_8, C_3H_2O, C_3H_3O, C_3H_4O, C_3H_5O, C_3H_5Op, C_3H_5Ot, C_3H_5Oa, C_3H_6O, C_3H_6Oa, C_3H_6Op, C_3H_7Oi, C_3H_7On, C_3H_6OH, C_3H_7OOHi, C_3H_7OOHn, C_3H_7OOi, C_3H_7OOn, C_3H_6OOH, C_4H, C_4H_2, C_4H_3n, C_4H_3i, C_4H_4, C_4H_5s, C_4H_5t, C_4H_5i, C_4H_6s, C_4H_6t, C_4H_6f, C_4H_6b, C_4H_6m, C_4H_7i, C_4H_7n, C_4H_7s, C_4H_8i, C_4H_8n, C_4H_8s, C_4H_9i, C_4H_9t, C_4H_9n, C_4H_9s, C_4H_{10}n, C_4H_{10}i, C_4H_2O, C_4H_4O, C_4H_5Ox, C_4H_5Oy, C_4H_6Ob, C_4H_6Oa, C_4H_7Ox, C_4H_7Om, C_4H_8Ox, C_4H_8Om, C_4H_8OHi, $O_2C_4H_9O$ was applied along with the corresponding transport and thermochemical properties. Therefore,

the respective formation pathways can feature the CH, CH_2, CH_3, C_2H_5 radicals and reduce the methane selectivity which is tested in the current simulations. The -C_3 gas phase mechanism has been also applied in Chapter 4, while the nitrogen containing gas phase chemistry was not used in the present investigation.

5.2.2 Surface chemistry

The surface catalytic reactions applied in this Chapter retained from the previous published mechanism [14, 15], as the NOx removal mechanism was not applied due to the absence of related experimental data. However, the determination of the adsorption reactions was based on the mechanism outlined in Chapter 3, for $T_{q^v} = 298$ K. Following a sensitivity analysis, the efficiency factor, accounting for diffusion limitations within the microporous structure of the catalytic wall, was set to 0.05 and hence comparatively close to the $\eta_e = 0.1$ value used by Vincent et al. [11]. Wanker et al. [129] suggested also the value of $\eta_e = 0.1$ for catalytic temperatures above 800 K, while Kraus and Lindstedt [14, 15] set the respective value at 0.4. A current sensitivity analysis was performed in the range of 0.05 [65] $\leq \eta_e \leq$ 0.4 [14, 15], presented in Section 5.3.1.2.

5.3 Results

5.3.1 Methodology

The methodology applied to model the experimental data from BP Chemicals [3] is based on the determination of mobile and immobile sticking coefficients via VTST and the application of Sprowl at al. [16] approximation for the treatment of rotational partition functions, as discussed in Chapter 3. The update of the C_2H_4 catalytic chemistry, described in Section 3.3.1.1, was also applied in the current investigation as it provided a significant improvement in the validation of ethylene and methane selectivities against (O/C) ratio, with the related data [3], as shown in Section 5.3.2. Additionally, the presence of CO in the feed stream, resulting from the experimental data [3], poisons the catalyst more than the current model suggests. A sensitivity analysis on the efficiency factor (0.05 [65], 0.08, 0.1 [11], 0.2, 0.4 [14, 15]) and activation energy used for CO desorption reaction, were implemented. The initial value of 134 kJ/mol, suggested by Vincent

et al. [11] provides a starting point. However, a higher value of E_A may be required. A range of values (145 kJ/mol, 171 kJ/mol, 174 kJ/mol), cited by Vincent et al. [11] were examined along with the value of E_A = 187 kJ/mol proposed by Brown et al. [128]. The latter energy barrier was also applied in Chapter 4, for consistency reasons. Finally, the implementation of the higher limit diffusion barrier at θ = 20% [100] of the magnitude of the bond energy holding the chemisorbed species to the surface is considered in the following computations, as a slight difference is observed when θ = 12% [99] is applied.

5.3.1.1 Effect of diffusion barrier

A comparison between the two diffusion barriers corresponding to θ = 12% [99] and θ = 20% [100] of the magnitude of $Q_{C,H,O,N}$ is provided below. A slight difference can be observed between the two cases mainly for C_2H_4 and CH_4 selectivities in presence and absence of CO co-feed. Therefore, both diffusion barriers can be applied under the current experimental conditions [3]. However, the θ = 20% [100] was used for consistency reasons with Chapter 4, where a strong impact was noted due to the low temperatures.

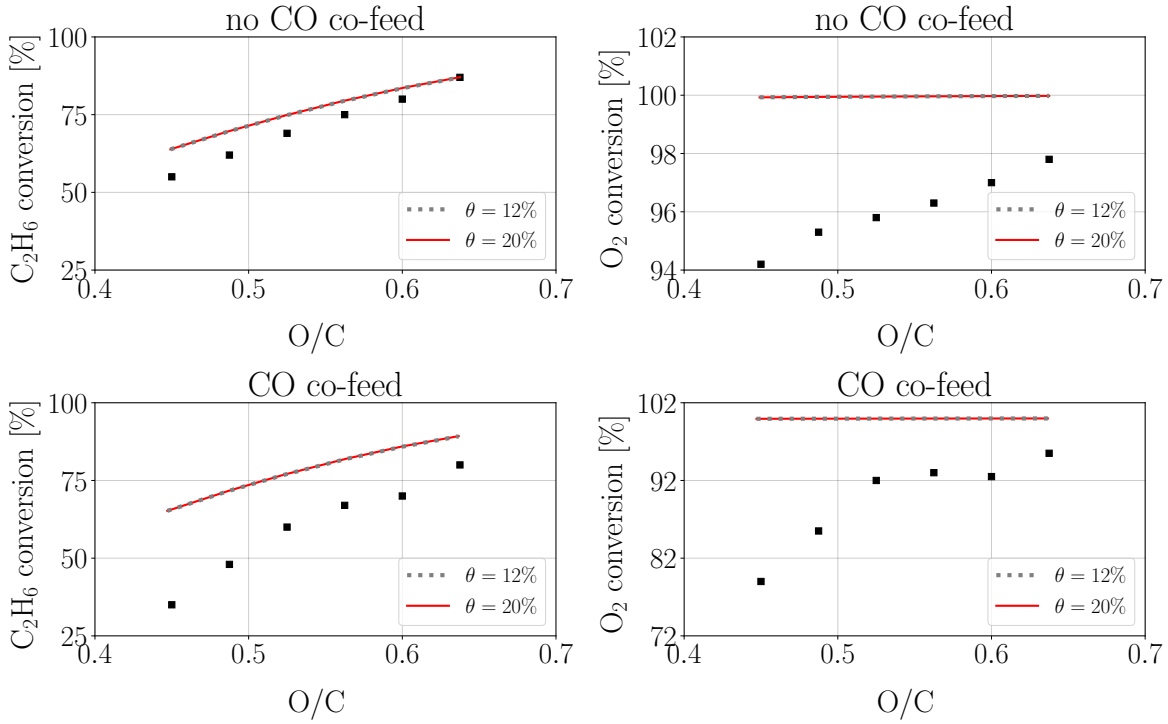


Fig. 5.1: Conversion of C_2H_6 and O_2 at the reactor outlet against the (O/C) feed ratio, at a low (θ = 12% [99]) and high (θ = 20% [100]) diffusion barrier, in the absence and presence of CO co-feed. Comparison with the experimental data provided by BP Chemicals [3].

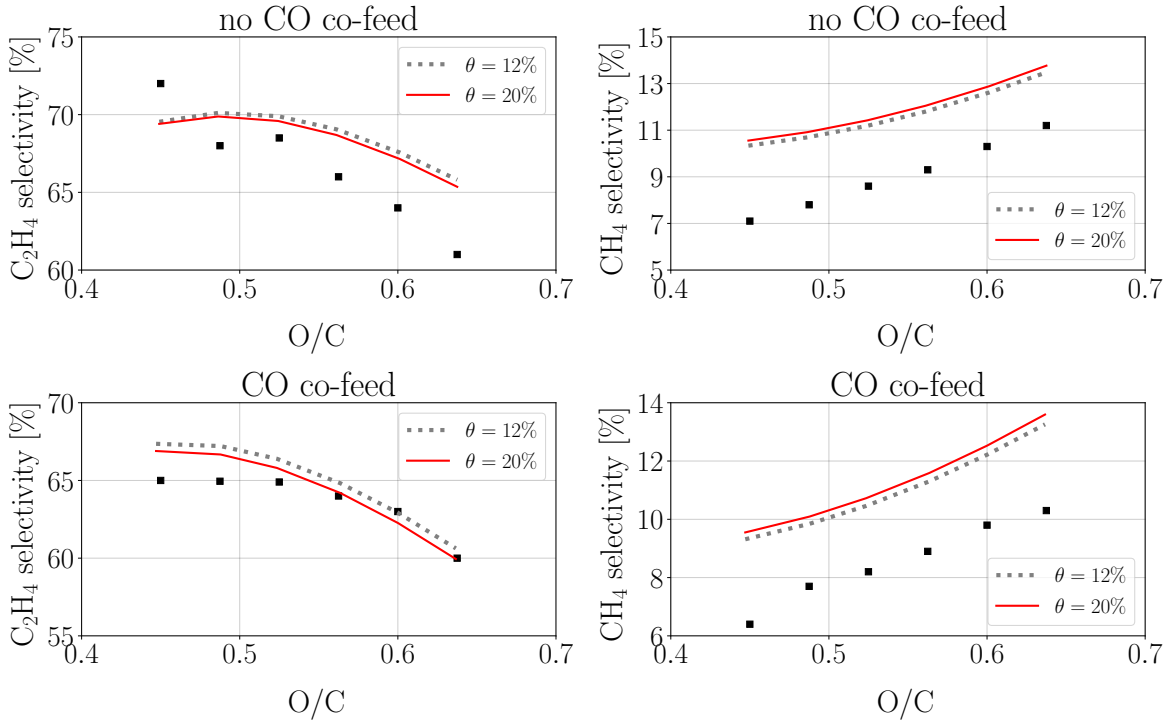


Fig. 5.2: Selectivity to C_2H_4 and CH_4 at the reactor outlet against the (O/C) feed ratio, at a low ($\theta = 12\%$ [99]) and high ($\theta = 20\%$ [100]) diffusion barrier, in the absence and presence of CO co-feed. Comparison with the experimental data provided by BP Chemicals [3].

5.3.1.2 Effect of efficiency factor

A various range of efficiency factors has been examined in the context of a sensitivity analysis aiming to improve the mechanism performance and confirm its validity through the use of the available experimental data [3]. As described in Section 5.2.2, the $\eta_e = 0.1$ and $\eta_e = 0.4$ applied by Vincent et al. [11] and Kraus and Lindstedt [14, 15], respectively, were considered along with lower and intermediate values, as presented in Figs. 5.3 and 5.4. The $\eta_e = 0.4$ [14, 15] shows a disagreement over the experimental data [3] compared with the other lower efficiency factor values. The discrepancy can be attributed to the difficulties in determining the rotational partition functions described in Section 3.1. The latter behaviour is more significant in the cases of C_2H_4 and CH_4 selectivities, where lower values close to 0.1 [11] successfully reproduce the experimental data [3]. Following the analysis below, a value of $\eta_e = 0.05$ was selected as the base case.

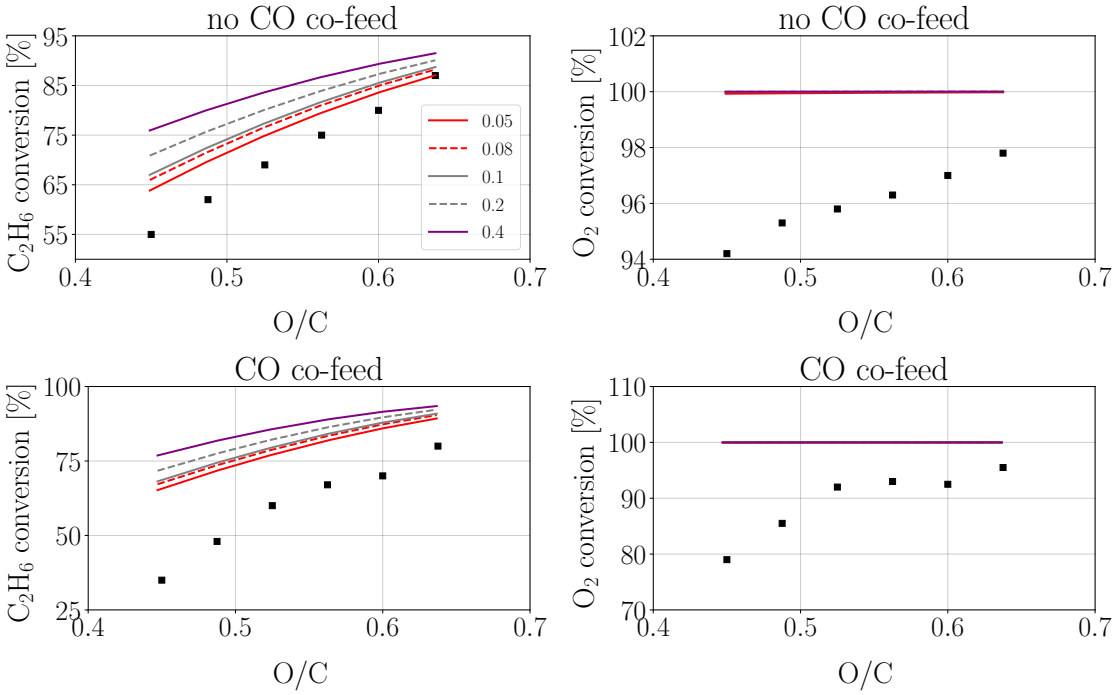


Fig. 5.3: Conversion of C_2H_6 and O_2 at the reactor outlet against the (O/C) feed ratio, for different efficiency factors (0.05 [65](−), 0.08(−−), 0.1 [11](−), 0.2(−−), 0.4 [14, 15](−)), in the absence and presence of CO co-feed. Comparison with the experimental data provided by BP Chemicals [3].

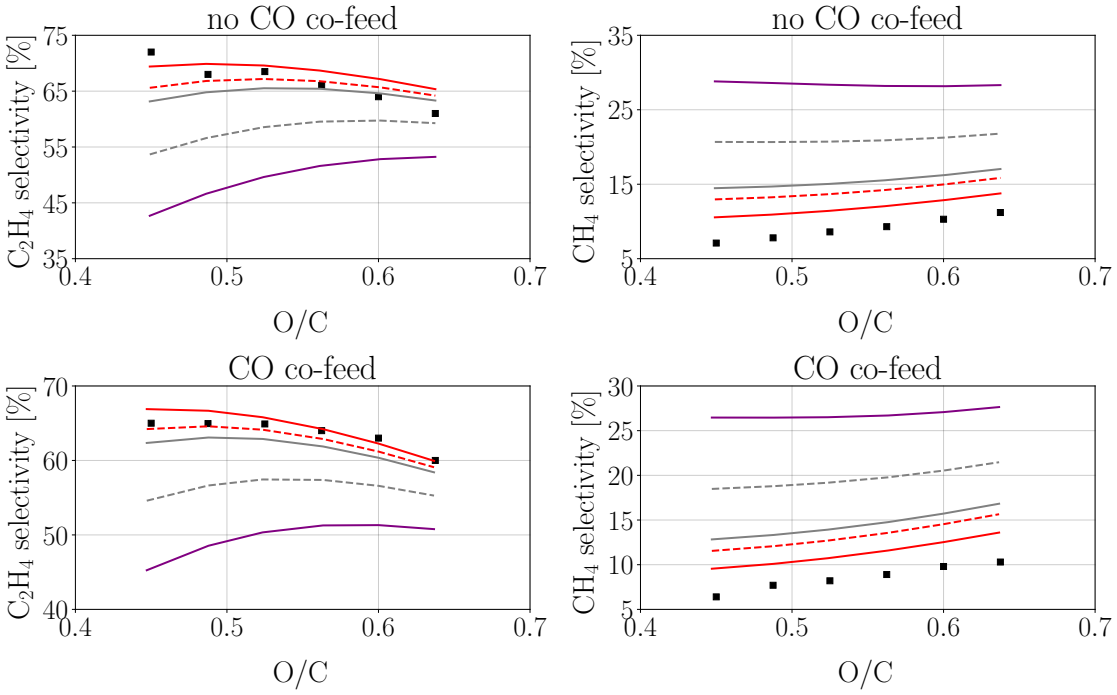


Fig. 5.4: Selectivity to C_2H_4 and CH_4 at the reactor outlet against the (O/C) feed ratio, for different efficiency factors (0.05 [65](−), 0.08(−−), 0.1 [11](−), 0.2(−−), 0.4 [14, 15](−)), in the absence and presence of CO co-feed. Comparison with the experimental data provided by BP Chemicals [3].

5.3.1.3 Effect of H_2 immobile TS

The effect of the H_2 immobile transition state was also examined through the use of the current experimental data provided by BP Chemicals [3] in the absence and presence of CO in the feed stream. This investigation is useful due to the existence of hydrogen co-feed in the experimental conditions [3]. However, following a comparison between the two transition states for the H_2 direct adsorption reaction, no difference has been observed for C_2H_6, O_2 conversion and C_2H_4 selectivity, while a very slight discrepancy is noticed for CH_4 selectivity, with and without CO co-feed. The same outcome was also illustrated in Section 4.3.2.5.

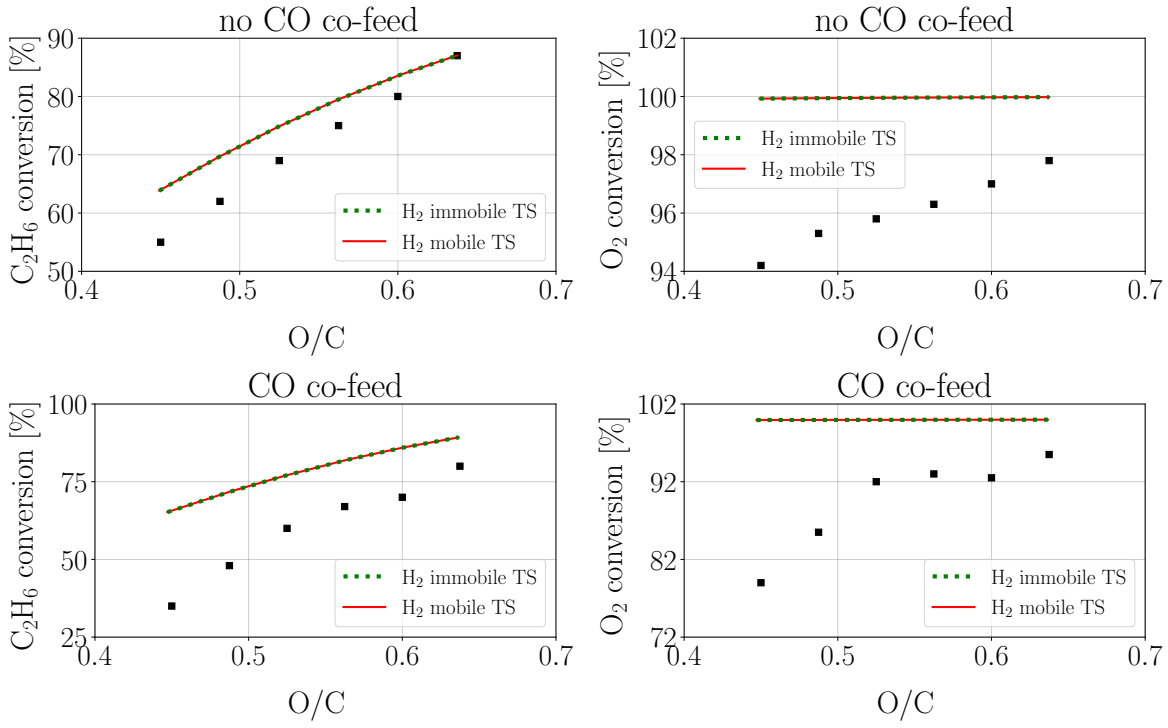


Fig. 5.5: Conversion of C_2H_6 and O_2 at the reactor outlet against the (O/C) feed ratio, for H_2 mobile and immobile TS, in the absence and presence CO co-feed. Comparison with the experimental data provided by BP Chemicals [3].

5.3.2 Mechanism evaluation in the absence and presence of CO co-feed

The results presented in Figs. 5.8 and 5.10 follow an extensive data production through the use of the developed reaction mechanism along with the updates outlined in Section 5.3.1. The key point is a one-to-one comparison of ethane, oxygen conversion and ethylene,

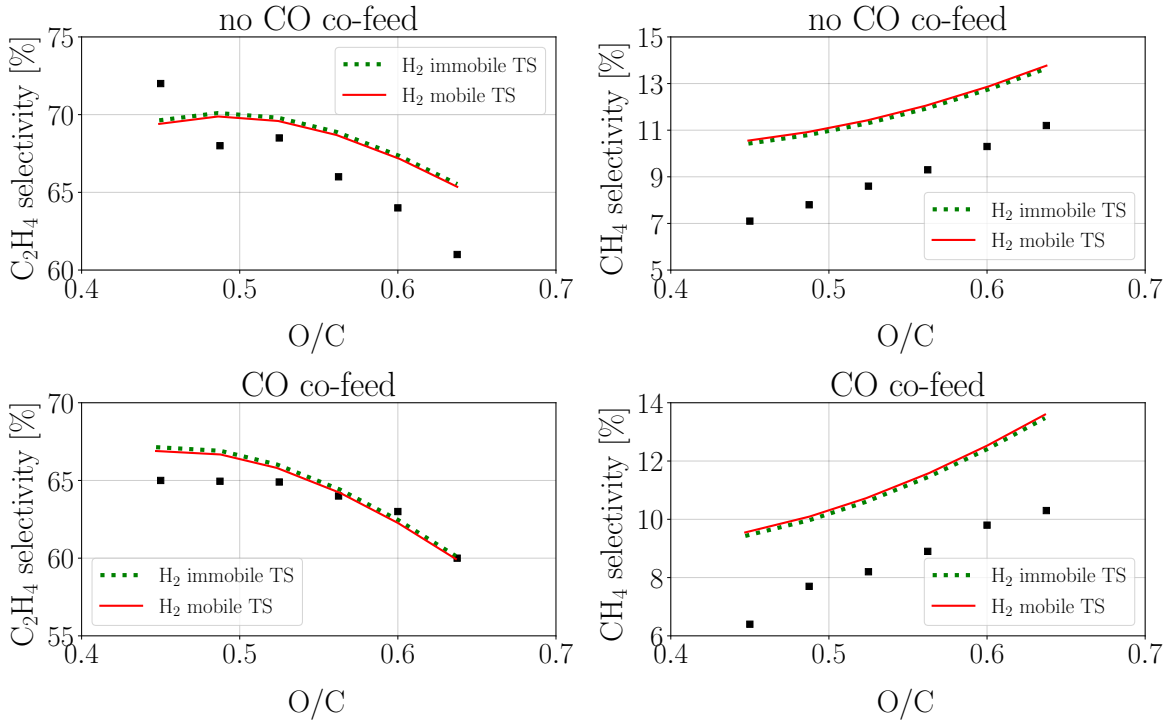


Fig. 5.6: Selectivity to C_2H_4 and CH_4 at the reactor outlet against the (O/C) feed ratio, for H_2 mobile and immobile TS, in the absence and presence CO co-feed. Comparison with the experimental data provided by BP Chemicals [3].

methane selectivity with experimental data provided by BP Chemicals [3], for the cases of absence and presence of CO co-feed. The conditions to initiate the setup are based on the experimental conditions [3] shown in Table 5.1. In Figs. 5.8– 5.10, the square symbols correspond to experimental data [3], while the solid red and blue lines to the calculations, for the (O/C) ratio range examined. The $\eta_e = 0.05$ was applied in all the cases. The temperature distribution at the wall and the middle of the duct reactor (channel) is described in Section 5.3.2.4.

5.3.2.1 Ethane and oxygen conversion against the O/C feed ratio

The ethane and oxygen conversion against the O/C feed ratio, ranging from 0.45 to 0.65, with and without CO in the feed stream, are shown in Fig. 5.8, for the two different desorption energies of CO, at 134 kJ/mol [11] and 187 kJ/mol [128]. For the case without CO co-feed, the computations successfully reproduce the experimental data [3], mainly at higher O/C ratios. Concerning the case where CO co-feed is added, the ethane conversion follows the same trend but over-predict by 45% and 24% the experimental data [3], at the lowest and highest O/C ratio, respectively. The significant over-prediction of C_2H_6

conversion by 45%, at low O/C ratios may be attributed to the absence of available Pt sites, and subsequently to a potential "poisoning" of the metal surface. The latter leads to a reduced catalytic efficiency and can result, for example, from carbon deposition.

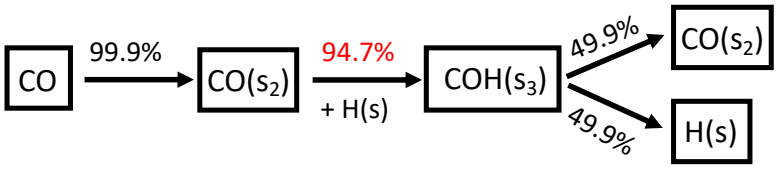


Fig. 5.7: Reaction pathway analysis of CO on the surface, in presence of CO co-feed, at O/C = 0.525.

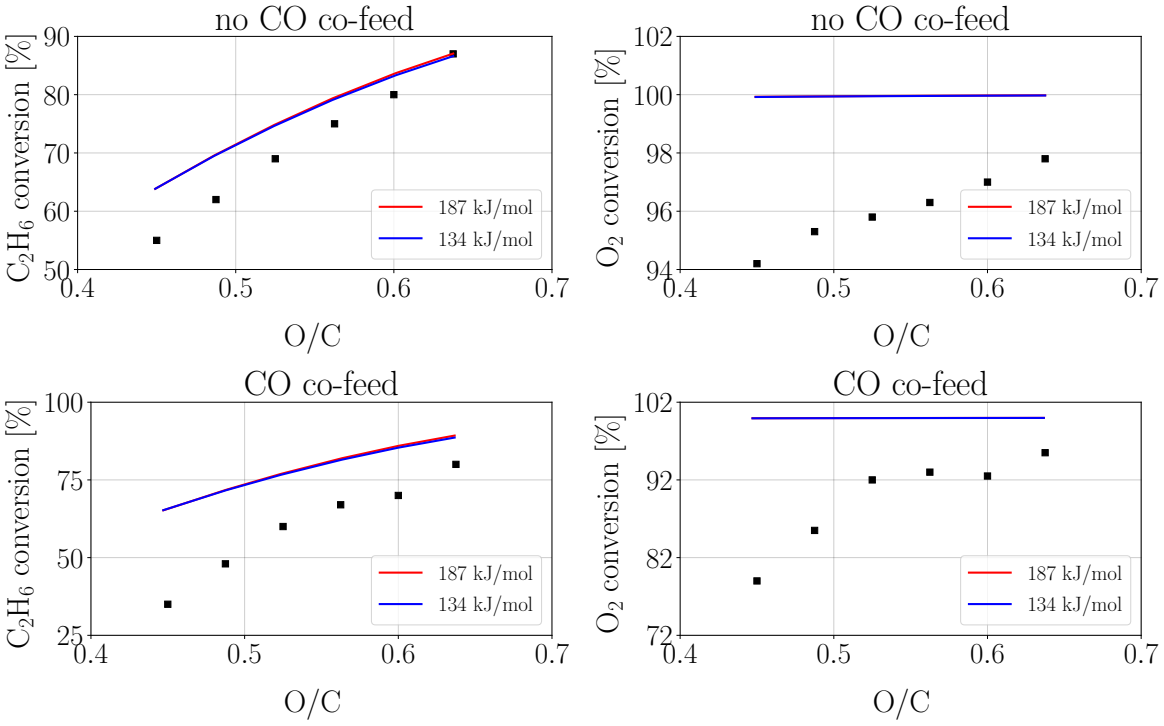


Fig. 5.8: Conversion of C_2H_6 and O_2 at the reactor outlet against the (O/C) feed ratio, for two different desorption energies of CO, at 134 kJ/mol [11] and 187 kJ/mol [128], in the absence and presence of CO co-feed. Comparison with the experimental data provided by BP Chemicals [3].

A surface reaction pathway analysis of CO, shown in Fig. 5.7, verifies the previous assumption and demonstrates the existence of another reaction pathway that removes the CO from the surface, resulting in $COH(s_3)$. The measured conversion of oxygen increases from 79% to 96% in presence of CO co-feed, and from 94% to 98% in absence of CO co-feed. The oxygen is fully consumed, based on the computations, for the whole O/C range, while larger deviations with the experimental data [3] can be observed as the

O/C ratio decreases. The over-prediction of the oxygen conversion may also be influenced by overall heat losses. The release of heat is the key driver in the activation of gas phase reactions, which start in the vicinity of the catalytic wall and then propagate towards the centre of the pore. No impact can be observed based on the different energy values of CO desorption, presented in Fig. 5.8.

5.3.2.2 Ethylene and methane selectivity against the O/C feed ratio

The ethylene and methane selectivity against the O/C feed ratio with and without CO in the feed stream are shown in Fig. 5.10, for the different desorption energies of CO, at 134 kJ/mol [11] and 187 kJ/mol [128]. The high conversion of ethane, results principally in the formation of ethylene. The more oxygen is present in the feed, the higher the conversion of fuel and the lower the selectivity to ethylene. In particular, the experimental selectivity to ethylene is found to decrease slightly, from 65% to 60% for the case of CO co-feed and from 72% to 61%, for the no CO co-feed case over the O/C range, in favour of a rise in methane from 6.4% to 10.3% for CO co-feed and from 7.1% to 11.2%, in absence of CO co-feed. The ethylene selectivity presents remarkable agreement with the BP Chemicals data [3], for both values of CO desorption energy, in presence and in absence of CO co-feed. The ratio of $C_2H_6(s_2)$ conversion on the surface to $CH_3(s)$ and $CH_2CH_3(s)$ substantially determines the CH_4/C_2H_4 ratio.

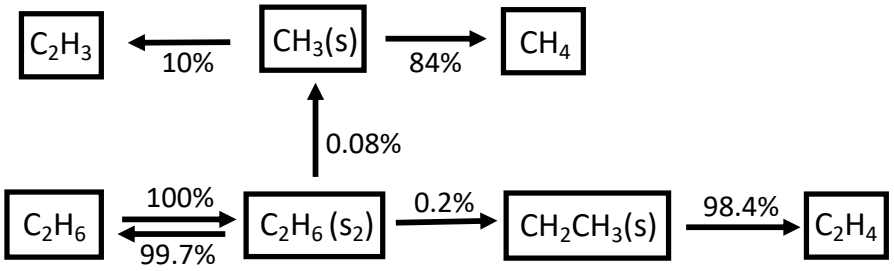


Fig. 5.9: Reaction pathway analysis of C_2H_6 on the surface, in presence of CO co-feed, at O/C = 0.525.

The updates considered for the ethylene catalytic chemistry, described in Section 3.3.1.1, were also included in the current simulations and favoured the behaviour observed. In absence of CO co-feed, the methane selectivity presents an over-prediction of around 3%, particularly at low O/C ratios, but in general terms follows the trend of the experimental data [3]. On the other hand, a slight improvement can be noticed on the addition of CO

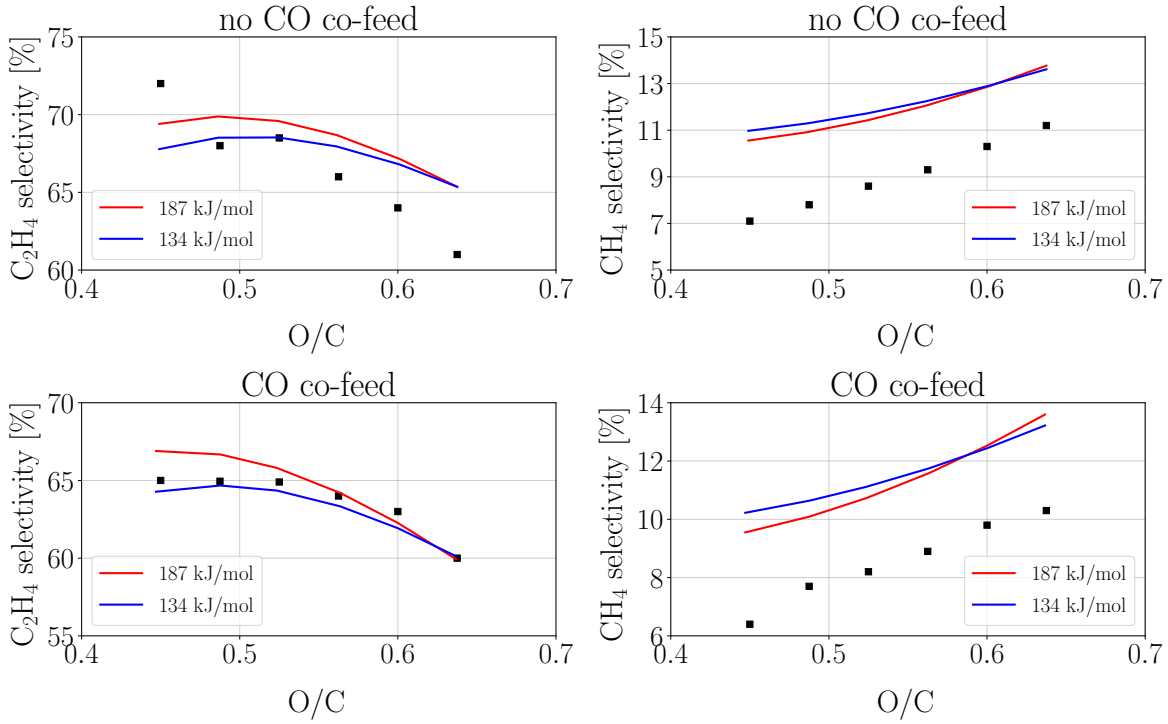


Fig. 5.10: Selectivity to C_2H_4 and CH_4 at the reactor outlet against the (O/C) feed ratio, for two different desorption energies of CO, at 134 kJ/mol [11] and 187 kJ/mol [128], in the absence and presence of CO co-feed. Comparison with the experimental data provided by BP Chemicals [3].

in the feed stream, as it directly affects the methane production. This is also apparent through the use of the higher CO desorption energy at 187 kJ/mol [128]. Overall, the formation of both ethylene and methane is exclusively due to the surface chemistry and their relative proportion is a key parameter in determining the viability of a practical industrial process.

More specifically, the simulation and study of ethane conversion play a significant role as it constitutes the primary input (fuel) to the chemical mechanism. Ethane is adsorbed on the surface, mostly molecularly. The ethane adsorbate, $C_2H_6(s_2)$ almost exclusively desorbs to produce C_2H_6 and in a quite lower percentage methyl ($CH_3(s)$) and ethyl radicals ($CH_2CH_3(s)$). Subsequently, the methyl radical desorbs from the surface to mainly produce methane, while the production of ethylene, is throughout the catalyst, due to the desorption of $CH_2CH_3(s)$. These pathways are displayed in Fig. 5.9.

5.3.2.3 Mol fractions distribution

Figure 5.11 indicates the mol fraction distribution of ethane, oxygen, ethylene and methane at O/C = 0.525, in addition of CO co-feed. The CO desorption energy applied, was 187 kJ/mol [128], as the impact of different CO desorption energies on the current chemical system is low. The computations are based on the proposed mechanism and the gas phase chemistry, described in Section 5.2.1. All the cases illustrate the evolution of the studied species along the catalytic bed length. The vertical axis expresses the radial distance. The computational domain features the upper half, i.e from 0.0 to 0.275 mm, while the lower half, which is the symmetric counterpart, is simply the mirrored data from the upper half, and was included for aesthetic reasons. Evidently, the ethane and oxygen are consumed by the end of the catalytic duct reactor, while the ethylene and methane are produced. The consumption of ethane and oxygen are predominantly through catalytic reactions almost at the entrance of the pore. The ethylene is produced more rapidly close to the catalytic wall, compared to methane.

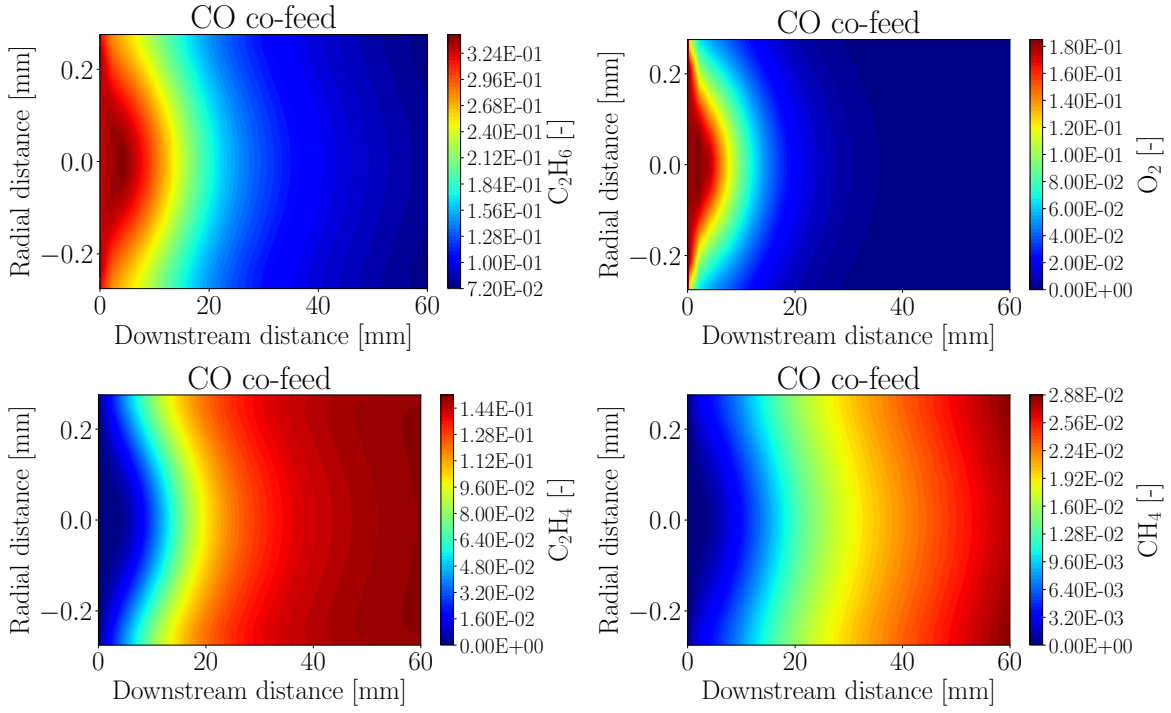


Fig. 5.11: Flow fields of C_2H_6, O_2, C_2H_4, CH_4 mol fractions at O/C = 0.525, in presence of CO co-feed.

5.3.2.4 Temperature and velocity distribution

The temperature and velocity contour plots, shown in Fig. 5.12, constitute a demonstration of temperature and velocity distribution along the catalytic reactor. Both correspond at O/C = 0.525 in presence of CO co-feed. The CO desorption energy applied, was 187 kJ/mol [128]. The temperature profile emphasizes the key role of the catalyst in releasing heat from the surface into the gas phase. The velocity field is an example of a pipe flow that features a laminar profile. The velocity is zero on the wall and maximum at the centerline, where it gradually increases.

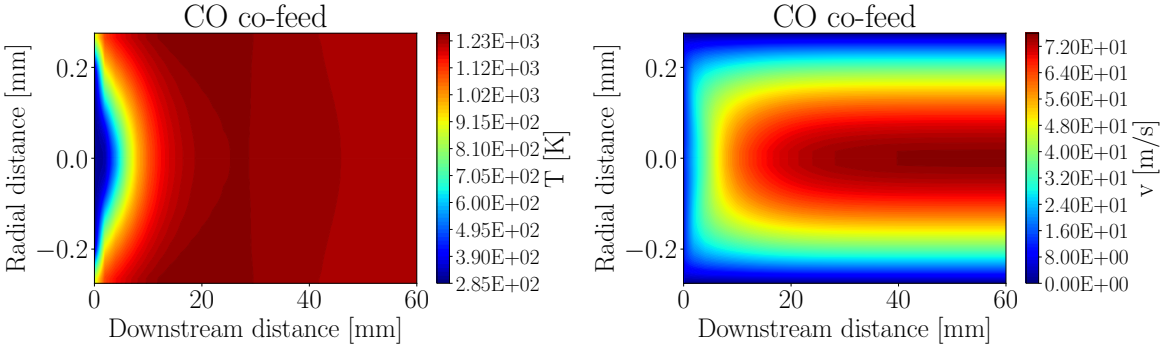


Fig. 5.12: Contour plots of temperature and velocity at O/C = 0.525, in presence of CO co-feed.

The wall temperature and the temperature at the middle of the duct reactor (channel) as a function of the downstream distance and O/C ratios are shown in Figs. 5.13 and 5.14, in the absence and presence of CO co-feed, respectively. The lines correspond to the six different O/C ratio cases. The temperature profiles are computed using a heat loss set at 0.07, retained from previous work [11]. The temperature comes to equilibrium and becomes constant before the reactor exit at 60 mm. A gradual drop in the temperature by about 20 K for both the wall temperature and temperature at the middle of the duct reactor, is recorded as the flow exits the catalytic section of the pore. The temperature distributions for both cases are almost identical. This is partly due to the fact that the temperature on the outside of the wall and the temperature in the entrance of the duct reactor are the same for both cases. However, it is also clear that the temperature reduces significantly as the mixtures get progressively more fuel rich.

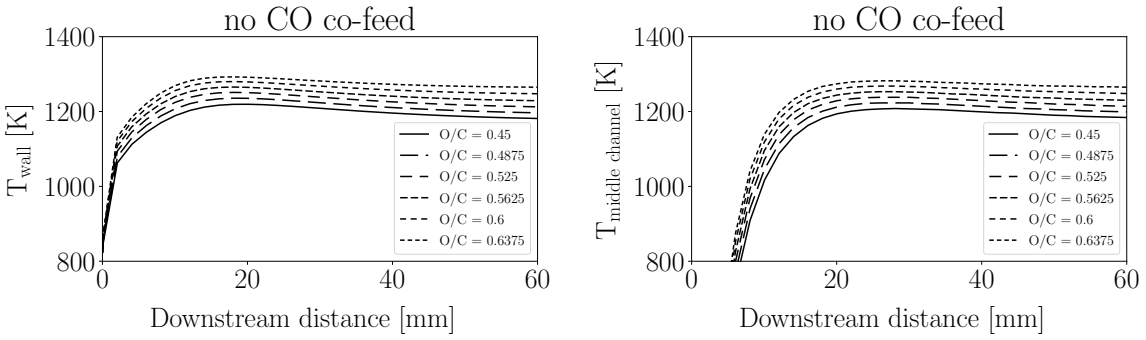


Fig. 5.13: Wall and centerline reactor temperatures as a function of the (O/C) feed ratio in absence of CO co-feed.

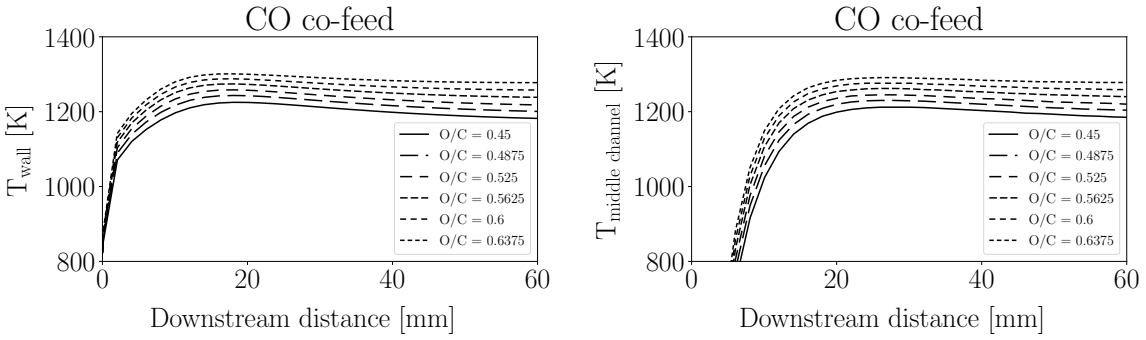


Fig. 5.14: Wall and centerline reactor temperatures as a function of the (O/C) feed ratio in presence of CO co-feed.

5.4 Summary

The catalytic auto-thermal cracking of ethane in a quartz lined tubular reactor with a metal loading of 3% Pt on Al_2O_3 foam was explored. The addition and absence of CO to the feed stream were studied, aiming to explore the degree of catalytic poisoning leading to reduced efficiencies. For this purpose, a comparison of the developed C/H/O heterogeneous chemical kinetic mechanism with related experimental data [3] provided by BP Chemicals was conducted, focusing on the study of ethane, oxygen conversion and ethylene, methane selectivity.

The sensitivities to different diffusion barriers and physical parameters (e.g. the efficiency factor) related to the diffusion limitations established within the microporous structure of the catalytic wall, as well as, chemical parameters (e.g. desorption energies of CO, application of H_2 immobile TS) were investigated for a better understanding of the model behaviour and for a more effective analysis. In particular, the choice of either a low ($\theta = 12\%$ [99]) or higher ($\theta = 20\%$ [100]) diffusion barrier slightly impacts the species

conversions and selectivities under the current experimental conditions [3]. However, Section 5.3.1.2 demonstrates that the effect of the efficiency factor plays a significant role on the interpretation of the experimental measurements [3]. As illustrated in Figs. 5.3 and 5.4, values close to $\eta_e = 0.1$ [11] better reproduce the experimental data [3] in the presence and absence of CO co-feed, while the $\eta_e = 0.4$ [14, 15] presents a major disagreement for all the cases. Therefore, the $\eta_e = 0.05$ was selected as a base case for the further investigation on the impact of different CO desorption energies, on the chemical system.

Concerning the CO heat of adsorption and activation energy sensitivity analysis, a thorough comparison of ethane, oxygen conversion and ethylene, methane selectivity against the O/C ratio, with experimental data [3], for a CO desorption energy equal to 134 kJ/mol [11] and 187 kJ/mol [128], was conducted. The alteration of the activation energy of CO desorption reaction, directly impacts the ethylene and methane selectivities, examined. More specifically, the use of $E_A = 187$ kJ/mol proposed by Brown et al. [128], seems to favor the methane selectivity with and without CO co-feed, while the application of $E_A = 134$ kJ/mol retained from Vincent et al. [11] work, contributes to a successful agreement of the ethylene selectivity computations with the data [3], mainly in presence of CO in the feed stream. However, the final outcome of the species conversions and selectivities against the O/C ratio, is not greatly influenced by the current variation on E_A values of CO desorption reaction. Therefore, both activation energies are compatible with the current reaction mechanism.

The model correctly reproduces the ethane conversion in absence of CO co-feed, especially at high O/C ratios. However, a significant discrepancy can be observed in the presence of CO co-feed, mainly at low O/C ratios, due to the absence of available Pt sites that enable the desorption in the gas phase. The latter case, indicates a reduced catalytic efficiency as $CO(s_2)$ results in $COH(s_3)$ by 94.7% and not in gas phase. On the other hand, the oxygen conversion does not seem to be affected by the increase of oxygen content, as it is totally consumed in the whole O/C range examined, due to heat losses. The O_2 consumption leads mainly to molecular, $O_2(s_2)$, and atomic oxygen adsorbates, O(s), by 37% and 30%, respectively, while the conclusion to $CO(s_2)$, $CO_2(s_2)$ and OOH(s) constitute less significant reaction pathways.

The updated catalytic C_2H_4 chemistry, presented in Section 3.3.1.1, and basically the omission of $\frac{1}{x^x}$ scaling factor from the C_2H_4 direct adsorption reactions as well as the decoupling of C_2H_4 isomerisation reactions on the surface, proved to improve the ethylene and methane selectivity. The latter reactions were based on an analogy with the gas phase and are not sufficiently accurate. As shown in Fig. 5.10, the ethylene selectivity successfully reproduces the experimental data [3] in presence of CO co-feed. The ethane conversion increases and leads to the formation of C_2H_4 with the aid of additional CO in the feed stream, while the major production of CH_4 comes from the dissociative desorption of CH_3(s) + H(s) by 84%. Sensitivity analyses indicate that under the current conditions the methane selectivity is relatively insensitive to the adsorption of methane.

Summarizing, the result of this study can be described as a working reaction mechanism for the heterogeneous chemical modelling of ethane, oxygen conversion and ethylene, methane selectivity over alumina supported platinum catalysts in ATC reactors. Additionally, this study investigates the sensitivities of the system to both physical and chemical parameters and presents the impact of CO addition or absence from the feed stream. Finally, the over-prediction of ethane conversion at low oxygen content, in presence of CO co-feed demonstrates a potential poisoning of the catalytic surface.

Chapter 6

Conclusions and Future Perspectives

In this Chapter, an overview of this thesis is presented along with a synopsis of the methods and findings described in the previous Chapters. Recommendations for further research are also discussed.

6.1 Conclusions

The present thesis focuses on the development of comprehensive heterogeneous reaction mechanisms considering an alternative theoretical framework based on the VTST for estimating Arrhenius parameters for adsorption reactions. Detailed microkinetic modelling describes the chemical kinetics dominating the studied system and uses the extended Arrhenius form to express reaction rates, while the VTST enables the construction of chemical mechanisms without, or with reduced, dependence on experimental data for the determination of rate parameters. Given the fact that the VTST used by Kraus and Lindstedt [14, 15], was found to be more systematic and quantitatively superior, compared to collision theory [11], was maintained in the current research. The energetics were calculated based on the UBI-QEP method [10, 72] as applied in previous works [11, 14, 15]. A computational fluid dynamics (CFD) framework was coupled with detailed microkinetic analysis through the use of an in-house 2D parabolic FORTRAN code [12] aiming to explore the interactions of the fluid flow with the chemistry of the system.

Diffusion limitations in porous media were also considered in the developed model, depending on the nature of the experimental data provided. Thus, the efficiency factor bridging the difference between the diffusion coefficients applied in the gas phase and

microporous catalytic surface, results from different diffusion mechanisms. Particularly, Knudsen diffusion limitations, applied in Chapter 4, can dominate species transport inside catalytic material due to the small size of pores. Averaged values of $\bar{\eta}_e$ of selected chemical species for each temperature, were presented in Section 2.3.2.1 and applied in Chapter 4. On the other hand, Knudsen diffusion does not constitute a limiting factor for the ethane auto-thermal catalytic cracking data [3], where a sensitivity analysis of efficiency factors already used [11, 14, 15] resulted in the efficiency factor value implemented in the respective simulations.

The core of the current work is the establishment of a comprehensive chemical mechanism methodology for the creation of catalytic reactions associated with the removal of the oxides of nitrogen from automotive exhaust gases through the use of supported Pt catalysts. At the beginning of the computational process, the pre-exponential factors of the extended Arrhenius equation, for C/H/O/N adsorption reactions were determined through the evaluation of the partition functions. The initial step of binding configurations and bond lengths of the chemical species, was required for the most accurate description of molecular interactions with the catalytic surface. The moments of inertia and the vibrational frequencies were obtained using Gaussian09 [67] software and based on the configuration of each chemical species participating in the reaction. The gas and adsorbed phase vibrational frequencies are determined using the M06-2X [68] and M06 [68] density functionals, respectively, along with the corresponding basis sets 6-31G(2df,p) and 6-311G(d,p). Subsequently, the mobile and immobile sticking coefficients were determined. The approximation of the Sprowl et al. [16] for the treatment of the rotational partition functions, was considered. More specifically, a detailed investigation of the mobile and immobile transition state of selected chemical species (H_2, O_2, CO, NO, NO_2, N_2O, N_2, C_3H_6, C_3H_5, C_2H_4) at different T_{q^v}, was conducted for two different effective core potential methods (SDD and LANL2DZ). However, no discrepancy was observed between the two alternatives. The comparison of a fixed T_{q^v} at 298 K and 800 K, and a variable T_{q^v}, with available experimental data obtained from literature sources, enhances the use of a fixed $T_{q^v} = 298$ K, as the prevailing choice for all the species adsorption examined, apart from CO. Following the study of the respective species mobility on the surface, except for H_2 which shows immobility when attached on the surface, the rest of

the chemical species investigated, present a mobile transition state.

This investigation constitutes an extension of the model developed by Kraus and Lindstedt [14, 15], that suggests a valid methodology for the modelling of heterogeneous chemistry over noble metals in industrial reactors. However, apart from the alteration of the evaluating method of adsorption reactions, a further revision of the catalytic chemistry, particularly for C_2H_4 surface reactions, was necessary for an efficient representation of the chemical system.

A rigorous comparison of results obtained with the developed C/H/O/N reaction mechanism, featuring two newly developed sub-mechanisms for the -N and C_3H_6 - C_3H_5 systems, and experimental data [2], was performed, at nearly stoichiometric inlet mixture conditions and specific temperature window (400 - 800 K). The impact of different Pt loadings and coat amounts on the CO, NO and C_3H_6 conversion was examined, while errors resulting from experimental measurements were not provided. Different scenarios based on the previous analysis for sticking coefficients and rate constants determinations, were considered. In particular, the use of $T_{q^v} = 800$ K instead of $T_{q^v} = 298$ K for the whole catalytic chemistry, or exclusively for the CO direct adsorption reaction, the implementation of an immobile transition state for H_2 adsorption, as well as the application of alternative values of heat of adsorption, constitute additional investigations.

A positive impact on the agreement between experimental [2] and computational data followed from the implementation of a higher sticking coefficient for the CO direct adsorption reaction arising from a fixed temperature of the vibrational partition function at 800 K. For this species alone, the use of the higher temperature of the vibrational partition function brings the computed sticking coefficient in better agreement with experimental data. This case was further explored for several Test Cases provided by TME [2]. Additionally, a critical investigation towards a detailed C_3H_6 catalytic chemistry, without the reliance on a global irreversible C_3H_6 direct adsorption reaction was conducted. The latter was validated via the experimental data [2], for all the Test Cases, under the optimal conditions of the high diffusion barrier and high CO sticking coefficient resulting from the application of $T_{q^v} = 800$ K. A promising step towards the complete and detailed description of the C_3H_6 surface chemistry was realized.

In the final case study, the C/H/O proposed mechanism, without the inclusion of the two additional -N and C_3H_6 - C_3H_5 sub-mechanisms, was validated with the aid of

experimental investigations on the auto-thermal catalytic cracking of ethane over a 3% Pt/Al_2O_3 catalyst in a quartz lined tubular reactor, conducted by BP Chemicals [3]. A higher temperature window was examined (844 - 1200 K) in a fuel rich environment instead of a nearly stoichiometric one, emphasizing the flexibility and functionality of the proposed surface mechanism in a different experimental environment. An extended analysis of different parameters (e.g. diffusion barriers, efficiency factors, CO desorption energies, assumption of an immobile TS for the H_2 adsorption reaction) was illustrated in Chapter 5, for a better understanding of the chemical system through the use of the developed reaction mechanism methodology under alternative experimental conditions [3]. The addition of CO on the feed stream was studied for the investigation of the reduced catalytic efficiency, due to the surface contamination.

6.2 Future Perspectives

Due to scope of the research carried out, many recommendations for future work can be proposed. An obvious starting point would be the refinement and extension of the developed catalytic reaction mechanism in order to be used for the generation of novel heterogeneous reduction chemical networks.

Concerning the refinement of the proposed chemical mechanism, sensitive reaction pathways, identified as part of the current work, could be further studied along with higher accuracy computational methods. An indicative paradigm constitutes the detailed investigation of the reaction pathways leading to catalytic poisoning.

Improvement of the current mechanism can be also achieved via the validation with a wider range of conditions and datasets, where available. For example, the high surface occupation of CO on Pt has been already studied, however a larger variation of carbon monoxide in the feed stream would provide a better picture of the effect of this co-feed. It will also shed more light on whether and by which mechanisms catalyst deactivation occurs. It would be also conceivable to incorporate some measure of coverage dependency in the model as suggested by Shustorovich and Sellers [10], and also presented by Chatterjee et al. [1]. Therefore, the zero coverage limit assumption that this model makes, necessites a further research.

Another interesting proposition would be the consideration of HC - NH_3 catalytic processes, that have not been studied yet. This will enable a spherical interpretation of the outcome already obtained and will possibly explain some of the discrepancies observed. Another critical aspect is the implementation of an improved and more complete mass transport model of chemical species in the porous support structure, accounting for Knudsen diffusion limitations. The latter will offer a better reproduction of the related experimental data [2], with higher accuracy.

The effectiveness of platinum metal on the emissions reduction mechanism has been already examined for a wide range of experimental cases provided by TME [2]. However, the validation of the proposed mechanism on other noble metals (e.g. Rh, Pd), or bimetallic catalysts including Pd/Pt [130] or Rh/Pt [131] would complement the current work and further validate the developed framework. Additionally, the usage of alternative metals as catalysts (e.g. Ir, Au, Ag, Ru) evaluated separately or in combination with Pt/Rh constitutes a further recommendation. The latter application can be extremely useful for industrial needs, due to the potential of cost reduction, after gaining a deeper understanding of the detailed reaction mechanisms associated with precious metal catalysts, enabling for their minimization. The use of alternative support materials to Al_2O_3 may also be pursued. Finally, coupling the heterogeneous chemistry interaction with CFD modelling of turbulent flows, will enable a more detailed and accurate description of combustion systems.

Bibliography

[1] D. Chatterjee, O. Deutschmann, and J. Warnatz, "Detailed surface reaction mechanism in a three-way catalyst," *Faraday Discuss.*, vol. 119, pp. 371–384, 2002.

[2] H. P. Nguyen and K. Gkagkas, "Experimental data (currently for Imperial College use only) provided by Toyota Motor Europe (TME)," *Private Communication*, 2019.

[3] B. Messenger, "Autothermal Cracking of Ethane with CO co-feed tests over Pt-only catalysts, BP Chemicals CONFIDENTIAL," 2001.

[4] H. S. Fogler, *Elements of Chemical Reaction Engineering (4th Edition)*. Prentice Hall, 4 ed., Sept. 2005.

[5] C. K. Narula, J. E. Allison, D. R. Bauer, and H. S. Gandhi, "Materials chemistry issues related to advanced materials applications in the automotive industry," *Chemistry of Materials*, vol. 8, no. 5, pp. 984–1003, 1996.

[6] H. Eyring, "The Activated Complex in Chemical Reactions," *The Journal of Chemical Physics*, vol. 3, no. 2, pp. 107–115, 1935.

[7] Y. Chen and D. G. Vlachos, "Hydrogenation of ethylene and dehydrogenation and hydrogenolysis of ethane on Pt(111) and Pt(211): A density functional theory study," *Journal of Physical Chemistry C*, vol. 114, no. 11, pp. 4973–4982, 2010.

[8] J. A. Dumesic, "The Microkinetics of heterogeneous catalysis," *American Chemical Society*, 1993.

[9] C. Mager-Maury, C. Chizallet, P. Sautet, and P. Raybaud, "Platinum nanoclusters stabilized on γ-alumina by chlorine used as a capping surface ligand: A density functional theory study," *ACS Catalysis*, vol. 2, p. 1346–1357, 05 2012.

[10] E. Shustorovich and H. Sellers, "The UBI-QEP method: A practical theoretical approach to understanding chemistry on transition metal surfaces," *Surface Science Reports*, vol. 31, no. 1, pp. 1–119, 1998.

[11] R. S. Vincent, R. P. Lindstedt, N. A. Malik, I. A. Reid, and B. E. Messenger, "The chemistry of ethane dehydrogenation over a supported platinum catalyst," *Journal of Catalysis*, vol. 260, no. 1, pp. 37–64, 2008.

[12] K. M. Leung and R. P. Lindstedt, "Detailed kinetic modeling of C1 – C3 alkane diffusion flames," *Combustion and Flame*, vol. 102, no. 1, pp. 129–160, 1995.

[13] R. Lindstedt and M. Meyer, "A dimensionally reduced reaction mechanism for methanol oxidation," *Proceedings of the Combustion Institute*, vol. 29, no. 1, pp. 1395 – 1402, 2002.

[14] P. Kraus and R. P. Lindstedt, "Variational transition state theory-based surface chemistry for the $C_2H_6/H_2/O_2/Pt$ system," *Energy & Fuels*, vol. 31, no. 3, pp. 2217–2227, 2017.

[15] P. Kraus and R. P. Lindstedt, "Microkinetic Mechanisms for Partial Oxidation of Methane over Platinum and Rhodium," *The Journal of Physical Chemistry C*, vol. 121, no. 17, pp. 9442–9453, 2017.

[16] L. H. Sprowl, C. T. Campbell, and L. Árnadóttir, "Hindered translator and hindered rotor models for adsorbates: Partition functions and entropies," *Journal of Physical Chemistry C*, vol. 120, pp. 9719–9731, 2016.

[17] M. A. Elliott, G. J. Nebel, and F. G. Rounds, "The composition of exhaust gases from diesel, gasoline and propane powered motor coaches," *Journal of the Air Pollution Control Association*, vol. 5, no. 2, pp. 103–108, 1955.

[18] B. Sawatmongkhon, *Modelling of Catalytic Aftertreatment of NOx Emissions Using Hydrocarbon as a Reductant, PhD Thesis*. PhD thesis, 2011.

[19] A. M. Kumar, J. Sreekumar, and P. Mohanan, "The effect of cordierite/pt catalyst on the nox reduction in a diesel and jatropha bio-diesel operated single cylinder engine," *Journal of Environmental Chemical Engineering*, vol. 3, no. 2, pp. 1125 – 1136, 2015.

[20] I. Resitoglu, A. Keskin, H. Ozarslan, and H. Bulut, "Selective catalytic reduction of nox emissions by hydrocarbons over Ag–Pt/Al_2O_3 catalyst in diesel engine," *International Journal of Environmental Science and Technology*, 2019.

[21] K. Yokota, M. Fukui, and T. Tanaka, "Catalytic removal of nitric oxide with hydrogen and carbon monoxide in the presence of excess oxygen," *Applied Surface Science*, vol. 121-122, pp. 273 – 277, 1997.

[22] D. K. Zerkle, M. D. Allendorf, M. Wolf, and O. Deutschmann, "Understanding Homogeneous and Heterogeneous Contributions to the Platinum-Catalyzed Partial Oxidation of Ethane in a Short-Contact-Time Reactor," *Journal of Catalysis*, vol. 196, no. 1, pp. 18–39, 2000.

[23] Q. Sun, Z. Wang, D. Wang, Z. Hong, M. Zhou, and X. Li, "A review on the catalytic decomposition of NO to N_2 and O_2: catalysts and processes," *Catalysis Science & Technology*, vol. 8, pp. 4563–4575, 2018.

[24] A. ul Rauf Salman, B. C. Enger, X. Auvray, R. Lødeng, M. Menon, D. Waller, and M. Rønning, "Catalytic oxidation of NO to NO_2 for nitric acid production over a Pt/Al_2O_3 catalyst," *Applied Catalysis A: General*, vol. 564, pp. 142 – 146, 2018.

[25] L. Cumaranatunge, S. Mulla, A. Yezerets, N. Currier, W. Delgass, and F. Ribeiro, "Ammonia is a hydrogen carrier in the regeneration of Pt/BaO/Al_2O_3 NOx traps with H_2," *Journal of Catalysis*, vol. 246, no. 1, pp. 29 – 34, 2007.

[26] C. Haug, W. Brenig, and T. Brunner, "NO on Pt(111): direct inelastic scattering and sticking/desorption," *Surface Science*, vol. 265, no. 1, pp. 56 – 66, 1992.

[27] J. Segner, W. Vielhaber, and G. Ertl, "Interaction of NO_2 with a Pt(111) surface," *Israel Journal of Chemistry*, vol. 22, no. 4, pp. 375–379, 1982.

[28] N. R. Avery, "An EELS study of N_2O adsorption on Pt(111)," *Surface Science*, vol. 131, no. 2, pp. 501 – 510, 1983.

[29] R. Le Van Mao, H. Yan, A. Muntasar, and N. Al-Yassir, "Blending of non-petroleum compounds with current hydrocarbon feeds to use in the thermo-catalytic steam-cracking process for the selective production of light olefins," in *New and Future Developments in Catalysis*, pp. 143 – 173, Elsevier, 2013.

[30] A. S. Bodke, D. A. Olschki, L. D. Schmidt, and E. Ranzi, "High Selectivities to Ethylene by Partial Oxidation of Ethane," *Science*, vol. 285, no. 5428, pp. 712–715, 1999.

[31] A. S. Bodke, D. Henning, L. D. Schmidt, S. S. Bharadwaj, J. J. Maj, and J. Siddall, "Oxidative Dehydrogenation of Ethane at Millisecond Contact Times: Effect of H_2 Addition," *Journal of Catalysis*, vol. 191, no. 1, pp. 62–74, 2000.

[32] L. Schmidt, M. Huff, and S. Bharadwaj, "Catalytic partial oxidation reactions and reactors," *Chemical Engineering Science*, vol. 49, no. 24, Part A, pp. 3981 – 3994, 1994.

[33] M. Huff and L. D. Schmidt, "Ethylene formation by oxidative dehydrogenation of ethane over monoliths at very short contact times," *The Journal of Physical Chemistry*, vol. 97, no. 45, pp. 11815–11822, 1993.

[34] O. Deutschmann, R. Schmidt, F. Behrendt, and J. Warnatz, "Numerical modeling of catalytic ignition," *Symposium (International) on Combustion*, vol. 26, no. 1, pp. 1747 – 1754, 1996.

[35] O. Deutschmann and L. D. Schmidt, "Modeling the partial oxidation of methane in a short-contact-time reactor," *AIChE Journal*, vol. 44, no. 11, pp. 2465–2477, 1998.

[36] R. S. Vincent, R. P. Lindstedt, N. A. Malik, I. A. Reid, and B. E. Messenger, "The dynamics of partial oxidation of ethane over platinum," *Proceedings of the Combustion Institute*, vol. 33, no. 2, pp. 1809–1817, 2011.

[37] L. L. Raja, R. J. Kee, O. Deutschmann, J. Warnatz, and L. D. Schmidt, "A critical evaluation of Navier–Stokes, boundary-layer, and plug-flow models of the flow and chemistry in a catalytic-combustion monolith," *Catalysis Today*, vol. 59, no. 1-2, pp. 47–60, 2000.

[38] C. Morley, "Gaseq: A chemical equilibrium programme for windows," 2009.

[39] A. Burcat and R. Branko, "Third millennium ideal gas and condensed phase thermodynamical database for combustion with updates from active thermochemical tables," *Technical Report*, 2013.

[40] H. Sellers and J. Gislason, "Adsorption and desorption rate constants for small molecules on metal surfaces: an example of Trouton's rule," *Surface Science*, vol. 426, no. 2, pp. 147–153, 1999.

[41] H. Sellers, "The generalized UBI-QEP method for modeling the energetics of reactions on transition metal surfaces," *Surface Science*, vol. 524, no. 1, pp. 29–39, 2003.

[42] F. Trouton, "Iv. on molecular latent heat," *The London, Edinburgh, and Dublin Philosophical Magazine and Journal of Science*, vol. 18, no. 110, pp. 54–57, 1884.

[43] L. Zhao, N. Ni, and S. H. Yalkowsky, "A Modification of Trouton's Rule by Simple Molecular Parameters for Hydrocarbon Compounds," *Industrial & Engineering Chemistry Research*, vol. 38, no. 1, pp. 324–327, 1999.

[44] R. S. Vincent, *Detailed modelling of catalytic chemistry in short contact time reactors*. PhD thesis, Imperial College London, 2008.

[45] P. J. Dauenhauer and O. A. Abdelrahman, "A universal descriptor for the entropy of adsorbed molecules in confined spaces," *ACS central science*, vol. 4, no. 9, pp. 1235–1243, 2018.

[46] W. P. Jones and R. P. Lindstedt, "Global reaction schemes for hydrocarbon combustion," *Combustion and Flame*, vol. 73, no. 3, pp. 233–249, 1988.

[47] J. Hirschfelder, C. Curtiss, and R. B. Bird., "Molecular theory of gases and liquids.," *Journal of Polymer Science*, vol. 17, no. 83, p. 116, 1955.

[48] E. A. Mason and L. Monchick, "Transport Properties of Polar-Gas Mixtures," *The Journal of Chemical Physics*, vol. 36, no. 10, pp. 2746–2757, 1962.

[49] C. Chang and E. Uhlenbeck, *Transport phenomena in polyatomic gases*. Engineering Research Institute, University of Michigan, 1951.

[50] R. Wanker, H. Raupenstrauch, and G. Staudinger, "A fully distributed model for the simulation of a catalytic combustor," *Chemical Engineering Science*, vol. 55, no. 20, pp. 4709–4718, 2000.

[51] Z. Bensetiti, D. Schweich, and C. Abreu, "The sensitivity of the catalyst effectiveness factor to pore size distribution," *Brazilian Journal of Chemical Engineering*, vol. 14, 1997.

[52] J. O. Hirschfelder, C. F. Curtiss, R. B. Bird, and E. Solomon, "Molecular theory of gases and liquids," *AIChE Journal*, vol. 1, no. 2, p. 272, 1955.

[53] S. Kolitcheff, E. Jolimaitre, A. Hugon, J. Verstraete, P.-L. Carrette, and M. Tayakout-Fayolle, "Tortuosity of mesoporous alumina catalyst supports: Influence of the pore network organization," *Microporous and Mesoporous Materials*, vol. 248, pp. 91–98, 2017.

[54] N. Wakao and J. M. Smith, "Diffusion and reaction in porous catalysts," *Industrial & Engineering Chemistry Fundamentals*, vol. 3, no. 2, pp. 123–127, 1964.

[55] L. Giani, G. Groppi, and E. Tronconi, "Mass-transfer characterization of metallic foams as supports for structured catalysts," *Industrial & Engineering Chemistry Research*, vol. 44, no. 14, pp. 4993–5002, 2005.

[56] J. Veldsink, R. van Damme, G. Versteeg, and W. van Swaaij, "The use of the dusty-gas model for the description of mass transport with chemical reaction in porous media," *The Chemical Engineering Journal and the Biochemical Engineering Journal*, vol. 57, no. 2, pp. 115 – 125, 1995.

[57] V. Sick, F. Hildenbrand, and P. Lindstedt, "Quantitative laser-based measurements and detailed chemical kinetic modeling of nitric oxide concentrations in methane-air

counterflow diffusion flames," *Symposium (International) on Combustion*, vol. 27, pp. 1401–1409, 1998.

[58] W. Juchmann, H. Latzel, D. Shin, G. Peiter, T. Dreier, H.-R. Volpp, J. Wolfrum, R. Lindstedt, and K. Leung, "Absolute radical concentration measurements and modeling of low-pressure $CH_4/O_2/NO$ flames," vol. 27, no. 1, pp. 469–476, 1998.

[59] R. P. Lindstedt and G. Skevis, "Chemistry of acetylene flames," *Combustion Science and Technology*, vol. 125, pp. 72–137, 1997.

[60] R. P. Lindstedt, F. C. Lockwood, and M. A. Selim, "Detailed kinetic modelling of chemistry and temperature effects on ammonia oxidation," *Combustion Science and Technology*, vol. 99, no. 4-6, pp. 253–276, 1994.

[61] R. P. Lindstedt and M. A. Selim, "Reduced reaction mechanisms for ammonia oxidation in premixed laminar flames," *Combustion Science and Technology*, vol. 99, no. 4-6, pp. 277–298, 1994.

[62] R. P. Lindstedt, F. C. Lockwood, and M. A. Selim, "A detailed kinetic study of ammonia oxidation," *Combustion Science and Technology*, vol. 108, no. 4-6, pp. 231–254, 1995.

[63] J. J. Driscoll, V. Sick, R. L. Farrow, P. E. Schrader, K.-A. Rizos, and R. P. Lindstedt, "No reburn and formation chemistry in methane diffusion flames," *Zeitschrift für Physikalische Chemie*, vol. 219, no. 5, pp. 679 – 698, 2005.

[64] K. Gkagkas, P. Lindstedt, and T. Kuan, "Transported pdf modelling of a high velocity bluff-body stabilised flame (HM_2) using detailed chemistry," *Flow, Turbulence and Combustion*, vol. 82, pp. 493–509, 2009.

[65] A.-M. Tsopelakou, R. P. Lindstedt, and K. Gkagkas, "Estimation of sticking coefficients using mobile and immobile transition states for catalytic platinum systems," *Proceedings of European Combustion Meeting, Lisboa, Portugal*, 2019.

[66] B. C. Taverner, "Improved algorithm for accurate computation of molecular solid angles," *Journal of Computational Chemistry*, vol. 17, no. 14, pp. 1612–1623, 1996.

[67] M. J. Frisch *et al.*, "Gaussian 09 Revision A.02," 2009. Gaussian Inc. Wallingford CT.

[68] Y. Zhao and D. Truhlar, "The M06 suite of density functionals for main group thermochemistry, thermochemical kinetics, noncovalent interactions, excited states, and transition elements: Two new functionals and systematic testing of four M06-class functionals and 12 other functionals," *Theoretical Chemistry Accounts*, vol. 120, no. 1-3, pp. 215–241, 2008.

[69] D. Andrae, U. Haeussermann, M. Dolg, H. Stoll, and H. Preuss, "Energy-adjusted ab initio pseudopotentials for the second and third row transition elements: molecular test for M2 (M=Ag, Au) and MH (M=Ru, Os)," *Theoretica Chimica Acta*, vol. 78, no. 4, pp. 247–266, 1991.

[70] K. S. Pitzer and W. D. Gwinn, "Energy Levels and Thermodynamic Functions for Molecules with Internal Rotation I. Rigid Frame with Attached Tops," *The Journal of Chemical Physics*, vol. 10, no. 7, pp. 428–440, 1942.

[71] T. Cottrell, *The strenghts of chemical bonds*. London, Butterworths, 1954.

[72] E. Shustorovich, "The bond-order conservation approach to chemisorption and heterogeneous catalysis: Applications and implications," vol. 37 of *Advances in Catalysis*, pp. 101 – 163, Academic Press, 1990.

[73] T. N. Rhodin and G. Ertl, *The nature of the surface chemical bond*. North-Holland Publishing Company, 1979.

[74] J. Vajo, W. Tsai, and W. Weinberg, "Mechanistic details of the heterogeneous decomposition of ammonia on platinum," *The Journal of Physical Chemistry*, vol. 89, no. 15, pp. 3243–3251, 1985.

[75] C. Bartholomew, P. Agrawal, and J. Katzer, "Sulfur poisoning of metals," in *Advances in catalysis*, vol. 31, pp. 135–242, Elsevier, 1982.

[76] E. Shustorovich, "Chemisorption phenomena: Analytic modeling based on perturbation theory and bond-order conservation," *Surface Science Reports*, vol. 6, no. 1, pp. 1–63, 1986.

[77] H. L. Sellers and J. T. Golab, *Theoretical and computational approaches to interface phenomena*. Springer, 1994.

[78] D. W. Rankin, "CRC handbook of chemistry and physics, 89th edition, edited by D. R. Lide," *Crystallography Reviews*, vol. 15, no. 3, pp. 223–224, 2009.

[79] P. P. Olivera, E. Patrito, and H. Sellers, "Direct synthesis of methanol over metallic catalysts," *Surface Science*, vol. 327, no. 3, pp. 330 – 357, 1995.

[80] I. Kuz'min and A. Zeigarnik, "Microkinetic modeling of ethane hydrogenolysis on metals," *Kinetics and catalysis*, vol. 45, no. 4, pp. 561–569, 2004.

[81] S. K. Desai, M. Neurock, and K. Kourtakis, "A periodic density functional theory study of the dehydrogenation of methanol over Pt (111)," *The Journal of Physical Chemistry B*, vol. 106, no. 10, pp. 2559–2568, 2002.

[82] J. Kua and W. A. Goddard, "Oxidation of methanol on 2nd and 3rd row group VIII transition metals (Pt, Ir, Os, Pd, Rh, and Ru): application to direct methanol fuel cells," *Journal of the American Chemical Society*, vol. 121, no. 47, pp. 10928–10941, 1999.

[83] T. Jacob, R. P. Muller, and W. A. Goddard, "Chemisorption of atomic oxygen on Pt (111) from DFT studies of Pt-clusters," *The Journal of Physical Chemistry B*, vol. 107, no. 35, pp. 9465–9476, 2003.

[84] A. Michaelides and P. Hu, "A density functional theory study of the reaction of C+ O, C+ N, and C+ H on close packed metal surfaces," *The Journal of Chemical Physics*, vol. 114, no. 13, pp. 5792–5795, 2001.

[85] J. Kua and W. A. Goddard, "Chemisorption of organics on platinum. 2. chemisorption of C_2Hx and CHx on Pt(111)," *The Journal of Physical Chemistry B*, vol. 102, no. 47, pp. 9492–9500, 1998.

[86] J. D. Gonzalez, K. Shojaee, B. S. Haynes, and A. Montoya, "The effect of surface coverage on N_2, NO and N_2O formation over Pt(111)," *Physical Chemistry Chemical Physics*, vol. 20, no. 39, pp. 25314–25323, 2018.

[87] J. Koop and O. Deutschmann, "Detailed surface reaction mechanism for Pt-catalyzed abatement of automotive exhaust gases," *Applied Catalysis B: Environmental*, vol. 91, no. 1-2, pp. 47–58, 2009.

[88] M. E. Bartram, R. Windham, and B. Koel, "Coadsorption of nitrogen dioxide and oxygen on platinum (111)," *Langmuir*, vol. 4, no. 2, pp. 240–246, 1988.

[89] K. Sawabe and Y. Matsumoto, "Structure of adsorbed N_2O on a Pt(111) surface and photodissociation at 193 nm: effective formation of oxygen adatoms," *Chemical physics letters*, vol. 194, no. 1-2, pp. 45–50, 1992.

[90] R. Van Hardeveld and A. Van Montfoort, "The influence of crystallite size on the adsorption of molecular nitrogen on nickel, palladium and platinum: An infrared and electron-microscopic study," *Surface Science*, vol. 4, no. 4, pp. 396–430, 1966.

[91] R. Shigeishi and D. A. King, "Chemisorption of nitrogen on platinum 111: Reflection-absorption infrared spectroscopy," *Surface Science*, vol. 62, no. 2, pp. 379–385, 1977.

[92] B. Nieuwenhuys and W. Sachtler, "Crystal face specificity of nitrogen adsorption on a platium field emission tip," *Surface Science*, vol. 34, no. 2, pp. 317–336, 1973.

[93] L. Nykanen and K. Honkala, "Density functional theory study on propane and propene adsorption on Pt(111) and PtSn alloy surfaces," *The Journal of Physical Chemistry C*, vol. 115, no. 19, pp. 9578–9586, 2011.

[94] Y.-L. Tsai, C. Xu, and B. E. Koel, "Chemisorption of ethylene, propylene and isobutylene on ordered Sn/Pt(111) surface alloys," *Surface science*, vol. 385, no. 1, pp. 37–59, 1997.

[95] S. G. Podkolzin, R. Alcalá, and J. A. Dumesic, "Density functional theory studies of acetylene hydrogenation on clean, vinylidene-and ethylidyne-covered Pt(111) surfaces," *Journal of Molecular Catalysis A: Chemical*, vol. 218, no. 2, pp. 217–227, 2004.

[96] J. Kubota, S. Ichihara, J. N. Kondo, K. Domen, and C. Hirose, "π-bonded ethene on Pt(111) surface studied by IRAS," *Surface science*, vol. 357, pp. 634–638, 1996.

[97] X.-L. Zhou, X.-Y. Zhu, and J. White, "A TPD, SIMS and $\Delta\varphi$ study of the influence of coadsorbed potassium on the adsorption and decomposition of ethylene on Pt(111)," *Surface science*, vol. 193, no. 3, pp. 387–416, 1988.

[98] J. Barth, "Transport of adsorbates at metal surfaces: from thermal migration to hot precursors," *Surface Science Reports*, vol. 40, no. 3, pp. 75 – 149, 2000.

[99] A. Nilekar, J. Greeley, and M. Mavrikakis, "A simple rule of thumb for diffusion on transition-metal surfaces," *Angewandte Chemie (International ed. in English)*, vol. 45, pp. 7046–9, 10 2006.

[100] J. Thomas and W. Thomas, *Principles and Practice of Heterogenous Catalysis.* Second Completely Revised Edition, Wiley – VCH Verlag GmBH & Co, ISBN 978-3-527-31458-4, Chapter 2, pp. 126, 2015.

[101] B. Kasemo and E. Törnqvist, "Weighing fractions of monolayers: Application to the adsorption and catalytic reactions of H_2, CO, and O_2 on Pt," *Physical Review Letters*, vol. 44, pp. 1555–1558, 1980.

[102] M. Johansson, O. Lytken, and I. Chorkendorff, "The sticking probability for H_2 on some transition metals at a hydrogen pressure of 1bar," *The Journal of Chemical Physics*, vol. 128, no. 3, p. 034706, 2008.

[103] L. C. Nett-Carrington and R. K. Herz, "Spatiotemporal patterns within a porous catalyst: dynamic carbon monoxide oxidation in a single-pellet reactor," *Chemical Engineering Science*, vol. 57, no. 8, pp. 1459 – 1474, 2002.

[104] A. Mhadeshwar and D. Vlachos, "A catalytic reaction mechanism for methane partial oxidation at short contact times, reforming, and combustion, and for oxygenate decomposition and oxidation on platinum," *Industrial & Engineering Chemistry Research - IND ENG CHEM RES*, vol. 46, 07 2007.

[105] G. Zafiris and R. Gorte, "CO oxidation on Pt/α-Al_2O_3(0001): Evidence for structure sensitivity," *Journal of Catalysis*, vol. 140, no. 2, pp. 418 – 423, 1993.

[106] W. A. Brown, "3.7.2 NO, CN and O_2 on metal surfaces: Datasheet from Landolt-Bornstein - Group III Condensed Matter Volume 42A3: "Adsorbed Layers on Surfaces" in Springer Materials," 2005.

[107] R. P. Lindstedt, "Private communication," January 2018.

[108] S. J. Jo, D. H. Park, and D. S. Heo, "Adsorption and dissociation reaction of carbon dioxide on Pt (111) and Fe (111) surface: MO-study," *Bulletin of the Korean Chemical Society*, vol. 21, no. 8, pp. 779–784, 2000.

[109] J. Dumesic, *Handbook of Heterogeneous catalysis*. Wiley-VCH, 2008.

[110] K. Reuter, D. Frenkel, and M. Scheffler, "The steady state of heterogeneous catalysis, studied by first-principles statistical mechanics," *Physical review letters*, vol. 93, no. 11, p. 116105, 2004.

[111] A. A. Gokhale, S. Kandoi, J. P. Greeley, M. Mavrikakis, and J. A. Dumesic, "Molecular-level descriptions of surface chemistry in kinetic models using density functional theory," *Chemical Engineering Science*, vol. 59, no. 22-23, pp. 4679–4691, 2004.

[112] K. Honkala, A. Hellman, I. Remediakis, A. Logadottir, A. Carlsson, S. Dahl, C. H. Christensen, and J. K. Nørskov, "Ammonia synthesis from first-principles calculations," *Science*, vol. 307, no. 5709, pp. 555–558, 2005.

[113] A. A. Gokhale, J. A. Dumesic, and M. Mavrikakis, "On the mechanism of low-temperature water gas shift reaction on copper," *Journal of the American Chemical Society*, vol. 130, no. 4, pp. 1402–1414, 2008.

[114] K. Reuter, "First-principles kinetic monte carlo simulations for heterogeneous catalysis: Concepts, status, and frontiers," *ChemInform*, vol. 43, no. 36, 2012.

[115] T. L. Hill, *An introduction to statistical thermodynamics*. Courier Corporation, 1986.

[116] R. B. McClurg, R. C. Flagan, and W. A. Goddard III, "The hindered rotor density-of-states interpolation function," *The Journal of Chemical Physics*, vol. 106, no. 16, pp. 6675–6680, 1997.

[117] E. Seebauer, A. Kong, and L. Schmidt, "Adsorption and desorption of NO, CO and H_2 on Pt(111): Laser-induced thermal desorption studies," *Surface Science*, vol. 176, no. 1-2, pp. 134–156, 1986.

[118] L. K. Verheij and M. B. Hugenschmidt, "Hydrogen adsorption on oxygen covered Pt(111)," *Surface Science*, vol. 324, no. 2-3, pp. 185–201, 1995.

[119] B. Poelsema, L. K. Verheij, and G. Comsa, "Temperature dependency of the initial sticking probability of H_2 and CO on Pt(111)," *Surface Science*, vol. 152-153, pp. 496–504, 1985.

[120] A.-P. Elg, F. Eisert, and A. Rosen, "The temperature dependence of the initial sticking probability of oxygen on Pt(111) probed with second harmonic generation," *Surface Science*, vol. 382, no. 1, pp. 57–66, 1997.

[121] A. Fohlisch and H. P. Bonzel, "3.7.1 CO and N_2 adsorption on metal surfaces - N_2 adsorption: Datasheet from Landolt-Bornstein - group III Condensed Matter Volume 42A4: "Adsorbed Layers on Surfaces" in Springer Materials," 2005.

[122] T. Perger, T. Kovács, T. Turányi, and C. Treviño, "Determination of the adsorption and desorption parameters for ethene and propene from measurements of the heterogeneous ignition temperature," *Combustion and Flame*, vol. 142, no. 1-2, pp. 107–116, 2005.

[123] W. D. Callister and D. G. Rethwisch, *Materials Science and Engineering*, vol. 5. John Wiley & sons NY, 2011.

[124] J. Mantzaras, R. Bombach, and R. Schaeren, "Hetero-/homogeneous combustion of hydrogen/air mixtures over platinum at pressures up to 10 bar," *Proceedings of the Combustion Institute*, vol. 32, no. 2, pp. 1937–1945, 2009.

[125] H. Sun, S. Yang, G. Jomaas, and C. Law, "High-pressure laminar flame speeds and kinetic modeling of carbon monoxide/hydrogen combustion," *Proceedings of the Combustion Institute*, vol. 31, no. 1, pp. 439 – 446, 2007.

[126] H. Kobayashi, A. Hayakawa, K. K. A. Somarathne, and E. C. Okafor, "Science and technology of ammonia combustion," *Proceedings of the Combustion Institute*, vol. 37, no. 1, pp. 109 – 133, 2019.

[127] J. Warnatz, "Resolution of gas phase and surface combustion chemistry into elementary reactions," *Proceedings of the Combustion Institute*, vol. 24, no. 1, pp. 553–579, 1992.

[128] W. Brown, R. Kose, and D. King, "Femtomole adsorption calorimetry on single-crystal surfaces," *Chemical reviews*, vol. 98, no. 2, pp. 797–832, 1998.

[129] R. Wanker, H. Raupenstrauch, and G. Staudinger, "A fully distributed model for the simulation of a catalytic combustor," *Chemical Engineering Science*, vol. 55, no. 20, pp. 4709–4718, 2000.

[130] M. Bonanni, *Detailed modelling of heterogeneous chemistry on palladium and platinum*. PhD thesis, Imperial College London, 2011.

[131] D. Hickman and L. Schmidt, "Synthesis gas formation by direct oxidation of methane over pt monoliths," *Journal of Catalysis*, vol. 138, no. 1, pp. 267 – 282, 1992.

Appendix A

Surface reaction mechanism

This Appendix contains the rate parameters of the surface mechanism developed for the current work. The mechanism listed is comprised of 320 reversible catalytic reactions, as implemented in Chapter 4 and shown in Tables A.1 and A.2, for θ = 12% [99] and θ = 20% [100] of the magnitude of $Q_{C,H,O,N}$, respectively. The global catalytic C_3H_6 step sub-mechanism is included in Tables A.1 and A.2, while Tables A.3 and A.4 correspond to the detailed C_3H_6 reaction sub-mechanism for θ = 12% [99] and θ = 20% [100] of the magnitude of $Q_{C,H,O,N}$, respectively. The reaction mechanism used in Chapter 5 is just composed by the first 288 reversible catalytic reactions of Tables A.1 and A.2 for the two different θ examined.

The catalytic sites (s) correspond to platinum sites. The activation barriers, E_A, and the pre-exponential factors, A, were calculated, as described in Chapters 2 and 3, respectively. The units of A are [kmol, m^2, s], depending on the reaction class and the E_A are evaluated in kJ/mol. The number (#) of the reactions accompanied by an asterisk (∗), corresponds to the reactions that have been removed from the current surface reaction mechanism.

Table A.1: Surface reaction mechanism corresponding to θ = 12% [99] of the magnitude of $Q_{C,H,O,N}$. The global catalytic C_3H_6 step sub-mechanism is considered.

#	**Reaction**	A	β	E_A
1	$C_2H_6 + 2\,s \rightarrow C_2H_6(s_2)$	4.76569E+10	-0.50	0.00
2	$C_2H_6(s_2) \rightarrow C_2H_6 + 2\,s$	4.06295E+11	1.00	36.10
3	$s + O(s) + C_2H_6 \rightarrow CH_2CH_3(s) + OH(s)$	2.39624E+09	-0.50	0.00
4	$CH_2CH_3(s) + OH(s) \rightarrow C_2H_6 + O(s) + s$	5.55266E+09	0.50	27.19
5	$s + OH(s) + C_2H_6 \rightarrow CH_2CH_3(s) + H_2O(s)$	2.86372E+09	-0.50	3.29
6	$CH_2CH_3(s) + H_2O(s) \rightarrow C_2H_6 + OH(s) + s$	5.59873E+09	0.50	11.85
7	$C_2H_6 + 2\,s \rightarrow 2\,CH_3(s)$	2.29579E+08	-0.50	50.31
8	$2\,CH_3(s) \rightarrow C_2H_6 + 2\,s$	6.05457E+09	0.50	0.00
9	$C_2H_6 + 2\,s \rightarrow CH_2CH_3(s) + H(s)$	5.00971E+08	-0.50	32.91
10	$CH_2CH_3(s) + H(s) \rightarrow C_2H_6 + 2\,s$	1.58541E+10	0.50	27.54
11	$s + C_2H_5 \rightarrow CH_2CH_3(s)$	2.34877E+08	-0.50	0.00
12	$CH_2CH_3(s) \rightarrow C_2H_5 + s$	2.60107E+10	1.00	163.00
13	$C_2H_5 + 2\,s \rightarrow C_2H_4(s) + H(s)$	3.23465E+07	-0.50	0.00
14	$C_2H_4(s) + H(s) \rightarrow C_2H_5 + 2\,s$	1.58188E+10	0.50	25.62

#	**Reaction**	A	β	E_A
15	$C_2H_5 + 3\ s \rightarrow C_2H_4(s_2) + H(s)$	3.51341E+07	-0.50	0.00
16	$C_2H_4(s_2) + H(s) \rightarrow C_2H_5 + 3\ s$	1.50167E+10	0.50	46.22
17	$C_2H_5 + 3\ s \rightarrow CH_2(s_2) + CH_3(s)$	3.98655E+06	-0.50	139.22
18	$CH_3(s) + CH_2(s_2) \rightarrow C_2H_5 + 3\ s$	6.16870E+09	0.50	0.00
19	$H(s) + C_2H_5 + 2\ s \rightarrow CHCH_3(s_2) + H_2(s)$	1.55736E+08	-0.50	131.54
20	$CHCH_3(s_2) + H_2(s) \rightarrow C_2H_5 + H(s) + 2\ s$	1.20373E+10	0.50	0.00
21	$C_2H_4 + 2\ s \rightarrow CHCH_3(s_2)$	3.13138E+10	-0.50	0.00
22	$CHCH_3(s_2) \rightarrow C_2H_4 + 2\ s$	2.05882E+10	1.00	294.00
23	$C_2H_3 + 3\ s \rightarrow CCH_3(s_3)$	1.94448E+09	-0.50	0.00
24	$CCH_3(s_3) \rightarrow C_2H_3 + 3\ s$	1.92432E+09	1.00	405.00
25	$s + C_2H_3 \rightarrow CHCH_2(s)$	8.26077E+08	-0.50	0.00
26	$CHCH_2(s) \rightarrow C_2H_3 + s$	2.93508E+10	1.00	184.00
27	$C_2H_3 + 3\ s \rightarrow CHCH_2(s_3)$	9.44764E+08	-0.50	0.00
28	$CHCH_2(s_3) \rightarrow C_2H_3 + 3\ s$	1.07488E+10	1.00	129.00
29	$C_2H_3 + 3\ s \rightarrow CCH_2(s_2) + H(s)$	1.00172E+08	-0.50	78.09
30	$CCH_2(s_2) + H(s) \rightarrow C_2H_3 + 3\ s$	1.48937E+10	0.50	31.48
31	$C_2H_3 + 4\ s \rightarrow C_2H_2(s_3) + H(s)$	1.26275E+08	-0.50	59.61
32	$C_2H_2(s_3) + H(s) \rightarrow C_2H_3 + 4\ s$	1.63611E+10	0.50	18.29
33	$C_2H_3 + 4\ s \rightarrow C(s_3) + CH_3(s)$	2.16839E+06	-0.50	77.76
34	$CH_3(s) + C(s_3) \rightarrow C_2H_3 + 4\ s$	5.82816E+09	0.50	27.82
35	$C_2H_3 + 5\ s \rightarrow CH_2(s_2) + CH(s_3)$	3.34229E+05	-0.50	299.38
36	$CH_2(s_2) + CH(s_3) \rightarrow C_2H_3 + 5\ s$	6.25503E+09	0.50	0.00
37	$C_2H_2 + 2\ s \rightarrow CCH_2(s_2)$	7.84804E+08	0.00	0.00
38	$CCH_2(s_2) \rightarrow C_2H_2 + 2\ s$	2.22914E+10	1.00	299.00
39	$C_2H_2 + 3\ s \rightarrow CCH_2(s_3)$	1.00146E+09	0.00	0.00
40	$CCH_2(s_3) \rightarrow C_2H_2 + 3\ s$	1.97263E+09	1.00	149.00
41	$s + CH_3 \rightarrow CH_3(s)$	2.07540E+10	-0.50	0.00
42	$CH_3(s) \rightarrow CH_3 + s$	3.21604E+10	1.00	159.00
43	$CH_3 + 3\ s \rightarrow CH_2(s_2) + H(s)$	1.44628E+09	-0.50	84.47
44	$CH_2(s_2) + H(s) \rightarrow CH_3 + 3\ s$	1.35262E+10	0.50	28.99
45	$CH_2t + 2\ s \rightarrow CH_2(s_2)$	1.12362E+10	-0.50	0.00
46	$CH_2(s_2) \rightarrow CH_2t + 2\ s$	2.24567E+10	1.00	283.00
47	$CH_2t + 4\ s \rightarrow CH(s_3) + H(s)$	1.63237E+09	-0.50	43.57
48	$CH(s_3) + H(s) \rightarrow CH_2t + 4\ s$	1.31483E+10	0.50	49.02
49	$CH + 3\ s \rightarrow CH(s_3)$	2.83595E+09	0.00	0.00
50	$CH(s_3) \rightarrow CH + 3\ s$	6.42738E+09	1.00	407.00
51	$CH + 4\ s \rightarrow C(s_3) + H(s)$	1.77138E+08	0.00	0.00
52	$C(s_3) + H(s) \rightarrow CH + 4\ s$	1.19364E+10	0.50	134.42
53	$C1 + 3\ s \rightarrow C(s_3)$	8.12015E+07	1.00	0.00
54	$C(s_3) \rightarrow C1 + 3\ s$	9.19010E+09	1.00	628.00
55	$s + O(s) + CO \rightarrow CO_2(s_2)$	4.87946E+09	0.00	0.00
56	$CO_2(s_2) \rightarrow CO + O(s) + s$	2.08366E+10	1.00	77.30
57	$OH(s) + CO + 2\ s \rightarrow CO_2(s_2) + H(s)$	1.45784E+09	0.00	8.62
58	$CO_2(s_2) + H(s) \rightarrow CO + OH(s) + 2\ s$	1.53187E+10	0.50	36.25
59	$s + CH_2O(s) + CO \rightarrow 2\ CHO(s)$	1.61064E+09	0.00	150.39
60	$2\ CHO(s) \rightarrow CH_2O(s) + CO + s$	4.90873E+09	0.50	0.00
61	$CH_2O(s) + CO + 3\ s \rightarrow CH_2(s_2) + CO_2(s_2)$	3.60274E+08	0.00	99.39
62	$CO_2(s_2) + CH_2(s_2) \rightarrow CH_2O(s) + CO + 3\ s$	5.74322E+09	0.50	0.00
63	$C_2H_6(s_2) + CO \rightarrow CH_2CH_3(s) + CHO(s)$	3.76156E+09	0.00	4.95
64	$CHO(s) + CH_2CH_3(s) \rightarrow C_2H_6(s_2) + CO$	5.29470E+09	0.50	0.00
65	$s + H_2O(s) + CO \rightarrow CHO(s) + OH(s)$	1.01333E+09	0.00	11.88

#	**Reaction**			A	β	E_A
66	CHO(s) + OH(s)	→	CO + H_2O(s) + s	5.09820E+09	0.50	0.00
67	CH_2CH_3(s) + CO + 2 s	→	C_2H_4(s_2) + CHO(s)	5.00147E+08	0.00	117.67
68	CHO(s) + C_2H_4(s_2)	→	CH_2CH_3(s) + CO + 2 s	5.12390E+09	0.50	0.00
69	$CHCH_3$(s_2) + CO + 2 s	→	CCH_3(s_3) + CHO(s)	4.33680E+08	0.00	3.04
70	CHO(s) + CCH_3(s_3)	→	$CHCH_3$(s_2) + CO + 2 s	5.16949E+09	0.50	0.00
71	s + CH_3OH(s) + CO	→	CH_2OH(s) + CHO(s)	4.44638E+09	0.00	0.81
72	CH_2OH(s) + CHO(s)	→	CH_3OH(s) + CO + s	4.86242E+09	0.50	0.00
73	s + CH_2CH_3(s) + CO	→	C_2H_4(s) + CHO(s)	2.00059E+09	0.00	148.67
74	CHO(s) + C_2H_4(s)	→	CH_2CH_3(s) + CO + s	5.33279E+09	0.50	0.00
75	s + OH(s) + CO	→	CHO(s) + O(s)	9.65546E+08	0.00	34.19
76	O(s) + CHO(s)	→	CO + OH(s) + s	4.79132E+09	0.50	0.00
77	s + C(s_3) + CO_2	→	2 CO(s_2)	9.77443E+08	0.00	0.00
78	2 CO(s_2)	→	C(s_3) + CO_2 + s	4.70876E+09	0.50	80.62
79	s + O(s) + CH_2O	→	CHO(s) + OH(s)	2.12670E+09	-0.50	0.00
80	CHO(s) + OH(s)	→	CH_2O + O(s) + s	5.09820E+09	0.50	47.06
81	s + OH(s) + CH_2O	→	CHO(s) + H_2O(s)	2.54159E+09	-0.50	0.00
82	CHO(s) + H_2O(s)	→	CH_2O + OH(s) + s	5.15363E+09	0.50	35.24
83	CH_2O + 2 s	→	CHO(s) + H(s)	4.44619E+08	-0.50	0.53
84	CHO(s) + H(s)	→	CH_2O + 2 s	1.43087E+10	0.50	44.52
85	s + CHO	→	CHO(s)	1.66541E+09	-0.50	0.00
86	CHO(s)	→	CHO + s	2.52417E+10	1.00	167.00
87	CHO + 3 s	→	CO(s_2) + H(s)	1.57308E+08	-0.50	0.00
88	CO(s_2) + H(s)	→	CHO + 3 s	1.37609E+10	0.50	107.45
89	H(s) + CHO + 2 s	→	CO(s_2) + H_2(s)	7.91383E+08	-0.50	0.00
90	CO(s_2) + H_2(s)	→	CHO + H(s) + 2 s	1.05821E+10	0.50	100.42
91	s + CH_3OH	→	CH_3OH(s)	1.12314E+09	-0.50	0.00
92	CH_3OH(s)	→	CH_3OH + s	3.29727E+10	1.00	44.10
93	s + O(s) + CH_3OH	→	CH_2OH(s) + OH(s)	9.34579E+08	-0.50	0.00
94	CH_2OH(s) + OH(s)	→	CH_3OH + O(s) + s	5.07843E+09	0.50	31.72
95	s + O(s) + CH_3OH	→	CH_3O(s) + OH(s)	9.22896E+08	-0.50	1.87
96	CH_3O(s) + OH(s)	→	CH_3OH + O(s) + s	5.06500E+09	0.50	46.22
97	s + CH_3O	→	CH_3O(s)	3.94297E+09	-0.50	0.00
98	CH_3O(s)	→	CH_3O + s	2.64242E+10	1.00	173.00
99	CH_3O + 2 s	→	CH_3(s) + O(s)	2.89297E+08	-0.50	31.88
100	CH_3(s) + O(s)	→	CH_3O + 2 s	5.15078E+09	0.50	33.92
101	CH_3O + 2 s	→	CH_2O(s) + H(s)	4.24720E+08	-0.50	0.00
102	CH_2O(s) + H(s)	→	CH_3O + 2 s	1.44089E+10	0.50	34.04
103	CO(s_2) + CH_3O	→	CH_2O(s) + CHO(s)	2.54115E+09	-0.50	116.55
104	CH_2O(s) + CHO(s)	→	CH_3O + CO(s_2)	4.89255E+09	0.50	0.00
105	H(s) + CH_3O	→	CH_3OH(s)	4.27655E+09	-0.50	0.00
106	CH_3OH(s)	→	CH_3O + H(s)	2.08366E+10	1.00	79.57
107	s + C_2H	→	CCH(s)	9.06087E+08	0.00	0.00
108	CCH(s)	→	C_2H + s	2.85007E+10	1.00	287.00
109	C_2 + 6 s	→	2 C(s_3)	2.22964E+05	0.00	0.00
110	2 C(s_3)	→	C_2 + 6 s	5.50717E+09	0.50	377.85
111	C_2H_6(s_2)	→	2 CH_3(s)	2.08366E+10	1.00	86.42
112	2 CH_3(s)	→	C_2H_6(s_2)	6.05457E+09	0.50	0.00
113	H(s) + C_2H_6(s_2)	→	CH_2CH_3(s) + H_2(s) + s	1.54829E+10	0.50	52.87
114	s + CH_2CH_3(s) + H_2(s)	→	C_2H_6(s_2) + H(s)	1.20294E+10	0.50	0.00
115	H(s) + C_2H_6(s_2)	→	CH_3(s) + CH_4 + 2 s	1.54829E+10	0.50	32.74
116	CH_3(s) + CH_4 + 2 s	→	C_2H_6(s_2) + H(s)	3.13089E+12	-0.50	0.00

#	Reaction			A	β	E_A
117	$C_2H_6(s_2) + O(s)$	$\rightarrow$	$C_2H_5 + OH(s) + 2\ s$	5.11340E+09	0.50	6.54
118	$OH(s) + C_2H_5 + 2\ s$	$\rightarrow$	$C_2H_6(s_2) + O(s)$	7.98272E+09	-0.50	27.29
119	$O(s) + C_2H_6(s_2)$	$\rightarrow$	$CH_2CH_3(s) + OH(s) + s$	5.11340E+09	0.50	6.54
120	$s + CH_2CH_3(s) + OH(s)$	$\rightarrow$	$C_2H_6(s_2) + O(s)$	5.55266E+09	0.50	27.19
121	$OH(s) + C_2H_6(s_2)$	$\rightarrow$	$CH_2CH_3(s) + H_2O(s) + s$	5.40841E+09	0.50	14.41
122	$s + CH_2CH_3(s) + H_2O(s)$	$\rightarrow$	$C_2H_6(s_2) + OH(s)$	5.59873E+09	0.50	11.85
123	$CH_3(s) + C_2H_6(s_2)$	$\rightarrow$	$CH_2CH_3(s) + CH_4 + 2\ s$	5.92480E+09	0.50	8.34
124	$CH_2CH_3(s) + CH_4 + 2\ s$	$\rightarrow$	$C_2H_6(s_2) + CH_3(s)$	4.58655E+12	-0.50	10.79
125	$C_2H_6(s_2)$	$\rightarrow$	$CH_2CH_3(s) + H(s)$	2.08366E+10	1.00	69.01
126	$CH_2CH_3(s) + H(s)$	$\rightarrow$	$C_2H_6(s_2)$	1.58541E+10	0.50	27.54
127	$O(s) + C_2H_6(s_2)$	$\rightarrow$	$CH_3(s) + CH_3O(s) + s$	5.11340E+09	0.50	65.83
128	$s + CH_3O(s) + CH_3(s)$	$\rightarrow$	$C_2H_6(s_2) + O(s)$	5.56880E+09	0.50	16.67
129	$OH(s) + C_2H_6(s_2)$	$\rightarrow$	$CH_2CH_3(s) + H_2O + 2\ s$	5.40841E+09	0.50	14.41
130	$CH_2CH_3(s) + H_2O + 2\ s$	$\rightarrow$	$C_2H_6(s_2) + OH(s)$	3.88003E+12	-0.50	0.00
131	$CH_2CH_3(s)$	$\rightarrow$	$C_2H_4 + H(s)$	2.08366E+10	1.00	22.76
132	$H(s) + C_2H_4$	$\rightarrow$	$CH_2CH_3(s)$	2.62333E+09	-0.50	8.17
133	$H(s) + CH_2CH_3(s)$	$\rightarrow$	$2\ CH_3(s)$	1.58541E+10	0.50	64.51
134	$2\ CH_3(s)$	$\rightarrow$	$CH_2CH_3(s) + H(s)$	6.05457E+09	0.50	20.84
135	$O(s) + CH_2CH_3(s)$	$\rightarrow$	$C_2H_4 + OH(s) + s$	5.25663E+09	0.50	23.55
136	$s + OH(s) + C_2H_4$	$\rightarrow$	$CH_2CH_3(s) + O(s)$	5.03010E+09	-0.50	24.92
137	$O(s) + CH_2CH_3(s)$	$\rightarrow$	$C_2H_4(s) + OH(s)$	5.25663E+09	0.50	23.55
138	$C_2H_4(s) + OH(s)$	$\rightarrow$	$CH_2CH_3(s) + O(s)$	5.57766E+09	0.50	83.23
139	$s + O(s) + CH_2CH_3(s)$	$\rightarrow$	$C_2H_4(s_2) + OH(s)$	5.25663E+09	0.50	24.21
140	$C_2H_4(s_2) + OH(s)$	$\rightarrow$	$CH_2CH_3(s) + O(s) + s$	5.33523E+09	0.50	96.05
141	$O(s) + CH_2CH_3(s)$	$\rightarrow$	$CH_2O(s) + CH_3(s)$	5.25663E+09	0.50	39.81
142	$CH_2O(s) + CH_3(s)$	$\rightarrow$	$CH_2CH_3(s) + O(s)$	5.60134E+09	0.50	58.00
143	$s + OH(s) + CH_2CH_3(s)$	$\rightarrow$	$C_2H_4(s_2) + H_2O(s)$	5.55266E+09	0.50	19.65
144	$C_2H_4(s_2) + H_2O(s)$	$\rightarrow$	$CH_2CH_3(s) + OH(s) + s$	5.38793E+09	0.50	80.48
145	$CH_2CH_3(s) + 2\ s$	$\rightarrow$	$C_2H_4(s_2) + H(s)$	8.22089E+08	0.50	16.07
146	$C_2H_4(s_2) + H(s)$	$\rightarrow$	$CH_2CH_3(s) + 2\ s$	1.50167E+10	0.50	46.22
147	$s + H(s) + CH_2CH_3(s)$	$\rightarrow$	$C_2H_4(s_2) + H_2(s)$	1.58541E+10	0.50	44.56
148	$C_2H_4(s_2) + H_2(s)$	$\rightarrow$	$CH_2CH_3(s) + H(s) + s$	1.14546E+10	0.50	41.64
149	$C_2H_4(s) + H(s)$	$\rightarrow$	$CH_2CH_3(s) + s$	1.58188E+10	0.50	25.62
150	$s + CH_2CH_3(s)$	$\rightarrow$	$C_2H_4(s) + H(s)$	3.28836E+09	0.50	22.76
151	$C_2H_4(s)$	$\rightarrow$	$C_2H_4 + s$	5.00567E+10	1.00	68.00
152	$s + C_2H_4$	$\rightarrow$	$C_2H_4(s)$	1.93895E+09	-0.50	0.00
153	$s + O(s) + C_2H_4(s)$	$\rightarrow$	$CH_2(s_2) + CH_2O(s)$	5.27779E+09	0.50	57.16
154	$CH_2O(s) + CH_2(s_2)$	$\rightarrow$	$C_2H_4(s) + O(s) + s$	5.74122E+09	0.50	0.00
155	$OH(s) + C_2H_4(s)$	$\rightarrow$	$CH_2O(s) + CH_3(s)$	5.57766E+09	0.50	47.01
156	$CH_2O(s) + CH_3(s)$	$\rightarrow$	$C_2H_4(s) + OH(s)$	5.60134E+09	0.50	0.00
157	$s + C_2H_4(s)$	$\rightarrow$	$CHCH_2(s) + H(s)$	3.34198E+09	0.50	98.96
158	$CHCH_2(s) + H(s)$	$\rightarrow$	$C_2H_4(s) + s$	1.58249E+10	0.50	21.47
159	$C_2H_4(s) + 3\ s$	$\rightarrow$	$CHCH_2(s_3) + H(s)$	1.23777E+08	0.50	115.86
160	$H(s) + CHCH_2(s_3)$	$\rightarrow$	$C_2H_4(s) + 3\ s$	1.50255E+10	0.50	0.00
161	$OH(s) + C_2H_4(s)$	$\rightarrow$	$CHCH_2(s) + H_2O(s)$	5.57766E+09	0.50	46.61
162	$CHCH_2(s) + H_2O(s)$	$\rightarrow$	$C_2H_4(s) + OH(s)$	5.66776E+09	0.50	0.00
163	$C_2H_4(s_2) + H_2O$	$\rightarrow$	$CH_2CH_3(s) + OH(s)$	1.53139E+11	-0.50	46.13
164	$OH(s) + CH_2CH_3(s)$	$\rightarrow$	$C_2H_4(s_2) + H_2O$	5.55266E+09	0.50	19.65
165	$C_2H_4(s_2)$	$\rightarrow$	$C_2H_4 + 2\ s$	1.40786E+11	1.00	99.00
166	$C_2H_4 + 2\ s$	$\rightarrow$	$C_2H_4(s_2)$	3.55395E+10	-0.50	0.00
167	$C_2H_4(s_2)$	$\rightarrow$	$CHCH_2(s) + H(s)$	2.08366E+10	1.00	114.46

#	Reaction	A	β	E_A
168	$CHCH_2(s) + H(s) \rightarrow C_2H_4(s_2)$	1.58249E+10	0.50	0.00
169	$O(s) + C_2H_4(s_2) \rightarrow CH_2(s_2) + CH_2O(s)$	5.03030E+09	0.50	79.51
170	$CH_2O(s) + CH_2(s_2) \rightarrow C_2H_4(s_2) + O(s)$	5.74122E+09	0.50	0.00
171	$OH(s) + C_2H_4(s_2) \rightarrow CH_2O(s) + CH_3(s) + s$	5.33523E+09	0.50	68.17
172	$s + CH_2O(s) + CH_3(s) \rightarrow C_2H_4(s_2) + OH(s)$	5.60134E+09	0.50	0.00
173	$C_2H_4(s_2) + 2\,s \rightarrow CHCH_2(s_3) + H(s)$	7.98328E+08	0.50	131.36
174	$H(s) + CHCH_2(s_3) \rightarrow C_2H_4(s_2) + 2\,s$	1.50255E+10	0.50	0.00
175	$CHCH_3(s_2) + H(s) \rightarrow C_2H_5 + 3\,s$	1.58531E+10	0.50	29.82
176	$C_2H_5 + 3\,s \rightarrow CHCH_3(s_2) + H(s)$	3.09566E+07	-0.50	84.31
177	$CHCH_3(s_2) + H(s) \rightarrow CH_2CH_3(s) + 2\,s$	1.58531E+10	0.50	29.82
178	$CH_2CH_3(s) + 2\,s \rightarrow CHCH_3(s_2) + H(s)$	8.22089E+08	0.50	110.43
179	$CHCH_3(s_2) \rightarrow C_2H_4(s_2)$	2.08366E+10	1.00	0.00
180	$C_2H_4(s_2) \rightarrow CHCH_3(s_2)$	2.08366E+10	1.00	176.52
181	$CHCH_3(s_2) + 2\,s \rightarrow CHCH_2(s_3) + H(s)$	8.37085E+08	0.50	69.62
182	$H(s) + CHCH_2(s_3) \rightarrow CHCH_3(s_2) + 2\,s$	1.50255E+10	0.50	18.58
183	$s + H(s) + CHCH_3(s_2) \rightarrow CCH_3(s_3) + H_2(s)$	1.58531E+10	0.50	75.93
184	$CCH_3(s_3) + H_2(s) \rightarrow CHCH_3(s_2) + H(s) + s$	1.14559E+10	0.50	40.55
185	$CHCH_3(s_2) + 2\,s \rightarrow CCH_3(s_3) + H(s)$	8.37085E+08	0.50	77.74
186	$CCH_3(s_3) + H(s) \rightarrow CHCH_3(s_2) + 2\,s$	1.50058E+10	0.50	65.43
187	$CHCH_3(s_2) \rightarrow CHCH_2(s) + H(s)$	2.08366E+10	1.00	52.73
188	$H(s) + CHCH_2(s) \rightarrow CHCH_3(s_2)$	1.58249E+10	0.50	44.99
189	$CCH_3(s_3) \rightarrow CHCH_2(s) + 2\,s$	2.08366E+10	1.00	0.00
190	$CHCH_2(s) + 2\,s \rightarrow CCH_3(s_3)$	8.51652E+08	0.50	77.94
191	$CHCH_2(s) + H(s) \rightarrow C_2H_4 + 2\,s$	1.58249E+10	0.50	21.47
192	$C_2H_4 + 2\,s \rightarrow CHCH_2(s) + H(s)$	6.00099E+08	-0.50	30.96
193	$CHCH_2(s) + 3\,s \rightarrow C(s_3) + CH_3(s)$	1.26171E+08	0.50	44.81
194	$CH_3(s) + C(s_3) \rightarrow CHCH_2(s) + 3\,s$	5.82816E+09	0.50	68.09
195	$s + H(s) + CHCH_2(s) \rightarrow CCH_2(s_2) + H_2(s)$	1.58249E+10	0.50	48.57
196	$CCH_2(s_2) + H_2(s) \rightarrow CHCH_2(s) + H(s) + s$	1.13873E+10	0.50	43.66
197	$O(s) + CHCH_2(s) \rightarrow C_2H_2 + OH(s) + s$	5.31391E+09	0.50	29.09
198	$s + OH(s) + C_2H_2 \rightarrow CHCH_2(s) + O(s)$	1.37021E+09	0.00	121.26
199	$OH(s) + CHCH_2(s) \rightarrow C_2H_2 + H_2O(s) + s$	5.61761E+09	0.50	21.26
200	$s + H_2O(s) + C_2H_2 \rightarrow CHCH_2(s) + OH(s)$	1.43802E+09	0.00	90.69
201	$CHCH_2(s) + 2\,s \rightarrow CCH_2(s_2) + H(s)$	8.51652E+08	0.50	50.35
202	$H(s) + CCH_2(s_2) \rightarrow CHCH_2(s) + 2\,s$	1.48937E+10	0.50	72.38
203	$CHCH_2(s) + 3\,s \rightarrow C_2H_2(s_3) + H(s)$	1.26171E+08	0.50	16.22
204	$H(s) + C_2H_2(s_3) \rightarrow CHCH_2(s) + 3\,s$	1.63611E+10	0.50	60.12
205	$H(s) + CHCH_2(s) \rightarrow C_2H_2 + H_2(s) + s$	1.58249E+10	0.50	41.25
206	$s + H_2(s) + C_2H_2 \rightarrow CHCH_2(s) + H(s)$	9.78993E+08	0.00	8.16
207	$O(s) + C_2H_2(s_3) \rightarrow CH(s_3) + CHO(s)$	5.51825E+09	0.50	83.22
208	$CH(s_3) + CHO(s) \rightarrow C_2H_2(s_3) + O(s)$	5.76374E+09	0.50	25.22
209	$s + O(s) + C_2H_2(s_3) \rightarrow C(s_3) + CHOH(s_2)$	5.51825E+09	0.50	66.94
210	$C(s_3) + CHOH(s_2) \rightarrow C_2H_2(s_3) + O(s) + s$	5.61672E+09	0.50	60.03
211	$O(s) + C_2H_2(s_3) \rightarrow CH_2(s_2) + CO(s_2)$	5.51825E+09	0.50	0.00
212	$CH_2(s_2) + CO(s_2) \rightarrow C_2H_2(s_3) + O(s)$	5.59733E+09	0.50	95.91
213	$O(s) + C_2H_2(s_3) \rightarrow C(s_3) + CH_2O(s)$	5.51825E+09	0.50	0.00
214	$C(s_3) + CH_2O(s) \rightarrow C_2H_2(s_3) + O(s)$	5.53252E+09	0.50	41.99
215	$O(s) + C_2H_2(s_3) + 2\,s \rightarrow CH(s_3) + COH(s_3)$	1.37956E+09	0.50	117.07
216	$CH(s_3) + COH(s_3) \rightarrow C_2H_2(s_3) + O(s) + 2\,s$	5.81989E+09	0.50	47.79
217	$O(s) + C_2H_2(s_3) \rightarrow CCH(s) + OH(s) + 2\,s$	5.51825E+09	0.50	93.78
218	$OH(s) + CCH(s) + 2\,s \rightarrow C_2H_2(s_3) + O(s)$	1.38112E+09	0.50	28.44

#	Reaction	A	β	E_A
219	$CHCH_2(s) + 3\ s \rightarrow CCH_2(s_3) + H(s)$	1.26171E+08	0.50	103.57
220	$H(s) + CCH_2(s_3) \rightarrow CHCH_2(s) + 3\ s$	1.50168E+10	0.50	0.00
221	$H(s) + CHCH_2(s_3) \rightarrow C_2H_4 + 4\ s$	1.50255E+10	0.50	0.00
222	$C_2H_4 + 4\ s \rightarrow CHCH_2(s_3) + H(s)$	2.89540E+08	-0.50	47.86
223	$CHCH_2(s_3) \rightarrow CHCH_2(s) + 2\ s$	2.08366E+10	1.00	0.00
224	$CHCH_2(s) + 2\ s \rightarrow CHCH_2(s_3)$	8.51652E+08	0.50	0.00
225	$CHCH_2(s_3) \rightarrow CCH_3(s_3)$	2.08366E+10	1.00	20.57
226	$CCH_3(s_3) \rightarrow CHCH_2(s_3)$	2.08366E+10	1.00	0.00
227	$CHCH_2(s_3) \rightarrow CCH_2(s_2) + H(s)$	2.08366E+10	1.00	22.86
228	$CCH_2(s_2) + H(s) \rightarrow CHCH_2(s_3)$	1.48937E+10	0.50	96.50
229	$s + CHCH_2(s_3) \rightarrow C(s_3) + CH_3(s)$	3.25564E+09	0.50	17.31
230	$CH_3(s) + C(s_3) \rightarrow CHCH_2(s_3) + s$	5.82816E+09	0.50	92.36
231	$H(s) + CHCH_2(s_3) \rightarrow C_2H_2 + H_2(s) + 3\ s$	1.50255E+10	0.50	17.27
232	$H_2(s) + C_2H_2 + 3\ s \rightarrow CHCH_2(s_3) + H(s)$	1.11965E+09	0.00	63.16
233	$H(s) + CHCH_2(s_3) \rightarrow C_2H_2(s_3) + H_2(s)$	1.50255E+10	0.50	17.27
234	$C_2H_2(s_3) + H_2(s) \rightarrow CHCH_2(s_3) + H(s)$	1.24112E+10	0.50	69.77
235	$H(s) + CHCH_2(s_3) \rightarrow CCH_2(s_2) + H_2(s) + s$	1.50255E+10	0.50	20.53
236	$s + H_2(s) + CCH_2(s_2) \rightarrow CHCH_2(s_3) + H(s)$	1.13873E+10	0.50	60.25
237	$H(s) + CHCH_2(s_3) \rightarrow CCH_2(s_2) + H_2 + 2\ s$	1.50255E+10	0.50	20.53
238	$CCH_2(s_2) + H_2 + 2\ s \rightarrow CHCH_2(s_3) + H(s)$	7.07027E+11	0.00	38.37
239	$H(s) + CHCH_2(s_3) \rightarrow C_2H_2(s_3) + H_2 + s$	1.50255E+10	0.50	17.27
240	$s + C_2H_2(s_3) + H_2 \rightarrow CHCH_2(s_3) + H(s)$	4.34190E+12	0.00	47.61
241	$s + CCH_3(s_3) \rightarrow C(s_3) + CH_3(s)$	3.25193E+09	0.50	44.60
242	$CH_3(s) + C(s_3) \rightarrow CCH_3(s_3) + s$	5.82816E+09	0.50	68.28
243	$H(s) + CCH_3(s_3) \rightarrow C(s_3) + CH_4 + s$	1.50058E+10	0.50	36.19
244	$s + C(s_3) + CH_4 \rightarrow CCH_3(s_3) + H(s)$	4.22250E+12	-0.50	96.67
245	$CCH_3(s_3) + H(s) \rightarrow CCH_2(s_2) + H_2(s) + s$	1.50058E+10	0.50	68.99
246	$s + H_2(s) + CCH_2(s_2) \rightarrow CCH_3(s_3) + H(s)$	1.13873E+10	0.50	68.28
247	$H(s) + CCH_2(s_2) \rightarrow CCH_3(s_3)$	1.48937E+10	0.50	72.56
248	$CCH_3(s_3) \rightarrow CCH_2(s_2) + H(s)$	2.08366E+10	1.00	50.14
249	$CCH_2(s_2) \rightarrow CCH(s) + H(s)$	2.08366E+10	1.00	133.72
250	$CCH(s) + H(s) \rightarrow CCH_2(s_2)$	1.52488E+10	0.50	31.20
251	$s + H(s) + CCH_2(s_2) \rightarrow C(s_3) + CH_3(s)$	1.48937E+10	0.50	52.90
252	$CH_3(s) + C(s_3) \rightarrow CCH_2(s_2) + H(s) + s$	5.82816E+09	0.50	52.87
253	$s + O(s) + CCH_2(s_2) \rightarrow CH_2(s_2) + CO(s_2)$	5.05950E+09	0.50	33.04
254	$CO(s_2) + CH_2(s_2) \rightarrow CCH_2(s_2) + O(s) + s$	5.59733E+09	0.50	136.00
255	$O(s) + CCH_2(s_2) \rightarrow CCH(s) + OH(s) + s$	5.05950E+09	0.50	95.34
256	$s + OH(s) + CCH(s) \rightarrow CCH_2(s_2) + O(s)$	5.52448E+09	0.50	41.55
257	$s + O(s) + CCH_2(s_2) \rightarrow C(s_3) + CH_2O(s)$	5.05950E+09	0.50	42.22
258	$CH_2O(s) + C(s_3) \rightarrow CCH_2(s_2) + O(s) + s$	5.53252E+09	0.50	108.77
259	$O(s) + CCH_2(s_2) \rightarrow CH_2(s_2) + CO + s$	5.05950E+09	0.50	33.04
260	$s + CH_2(s_2) + CO \rightarrow CCH_2(s_2) + O(s)$	5.00710E+09	0.00	18.35
261	$O(s) + CCH_2(s_2) \rightarrow C(s_3) + CH_2O$	5.05950E+09	0.50	42.22
262	$C(s_3) + CH_2O \rightarrow CCH_2(s_2) + O(s)$	1.13438E+10	-0.50	70.80
263	$s + OH(s) + CCH_2(s_2) \rightarrow C(s_3) + CH_2OH(s)$	5.37310E+09	0.50	56.59
264	$CH_2OH(s) + C(s_3) \rightarrow CCH_2(s_2) + OH(s) + s$	5.52043E+09	0.50	49.63
265	$CCH_2(s_2) + 3\ s \rightarrow C(s_3) + CH_2(s_2)$	1.22021E+08	0.50	139.61
266	$CH_2(s_2) + C(s_3) \rightarrow CCH_2(s_2) + 3\ s$	5.92507E+09	0.50	51.51
267	$CCH_2(s_3) + H(s) \rightarrow C_2H_3 + 4\ s$	1.50168E+10	0.50	0.00
268	$C_2H_3 + 4\ s \rightarrow CCH_2(s_3) + H(s)$	9.10007E+07	-0.50	228.09
269	$CCH_2(s_3) \rightarrow CCH_2(s_2) + s$	2.08366E+10	1.00	0.00

#	**Reaction**			A	β	E_A
270	s + $CCH_2(s_2)$	→	$CCH_2(s_3)$	3.29456E+09	0.50	0.00
271	H(s) + $CCH_2(s_3)$	→	$CHCH_2(s_3)$ + s	1.50168E+10	0.50	20.54
272	s + $CHCH_2(s_3)$	→	$CCH_2(s_3)$ + H(s)	3.25564E+09	0.50	76.07
273	H(s) + $CCH_2(s_3)$	→	$CCH_3(s_3)$ + s	1.50168E+10	0.50	0.00
274	s + $CCH_3(s_3)$	→	$CCH_2(s_3)$ + H(s)	3.25193E+09	0.50	103.35
275	H(s) + $CCH_2(s_3)$	→	CCH(s) + H_2 + 3 s	1.50168E+10	0.50	51.35
276	CCH(s) + H_2 + 3 s	→	$CCH_2(s_3)$ + H(s)	8.95897E+10	0.00	5.40
277	H(s) + $CCH_2(s_3)$	→	$C(s_3)$ + CH_3(s)	1.50168E+10	0.50	0.00
278	CH_3(s) + $C(s_3)$	→	$CCH_2(s_3)$ + H(s)	5.82816E+09	0.50	119.12
279	$C_2H_2(s_3)$ + H(s)	→	$CHCH_2(s_3)$ + s	1.63611E+10	0.50	85.43
280	s + $CHCH_2(s_3)$	→	$C_2H_2(s_3)$ + H(s)	3.25564E+09	0.50	0.00
281	$C_2H_2(s_3)$	→	$CCH_2(s_2)$ + s	2.08366E+10	1.00	73.96
282	s + $CCH_2(s_2)$	→	$C_2H_2(s_3)$	3.29456E+09	0.50	0.00
283	$C_2H_2(s_3)$	→	C_2H_2 + 3 s	3.91827E+10	1.00	134.00
284	C_2H_2 + 3 s	→	$C_2H_2(s_3)$	1.38965E+09	0.00	0.00
285	s + CCH(s) + H(s)	→	$CCH_2(s_3)$	1.52488E+10	0.50	63.22
286	$CCH_2(s_3)$	→	CCH(s) + H(s) + s	2.08366E+10	1.00	58.72
287	H_2O(s) + CCH(s) + 2 s	→	$C_2H_2(s_3)$ + OH(s)	1.39557E+09	0.50	0.00
288	OH(s) + $C_2H_2(s_3)$	→	CCH(s) + H_2O(s) + 2 s	5.82278E+09	0.50	63.61
289	H_2O(s) + CCH(s)	→	C_2H_2 + OH(s) + s	5.58227E+09	0.50	0.00
290	s + OH(s) + C_2H_2	→	CCH(s) + H_2O(s)	2.11772E+09	0.00	115.60
291	H(s) + CCH(s)	→	C_2H_2 + 2 s	1.52488E+10	0.50	0.00
292	C_2H_2 + 2 s	→	CCH(s) + H(s)	3.70468E+08	0.00	8.96
293	s + H(s) + CCH(s)	→	$C_2H_2(s_3)$	1.52488E+10	0.50	0.00
294	$C_2H_2(s_3)$	→	CCH(s) + H(s) + s	2.08366E+10	1.00	142.96
295	s + O(s) + CCH(s)	→	$CH(s_3)$ + CO	5.20866E+09	0.50	0.00
296	$CH(s_3)$ + CO	→	CCH(s) + O(s) + s	2.03430E+09	0.00	60.97
297	s + O(s) + CCH(s)	→	$C(s_3)$ + CHO	5.20866E+09	0.50	0.00
298	$C(s_3)$ + CHO	→	CCH(s) + O(s) + s	5.01442E+09	-0.50	18.13
299	O(s) + CCH(s) + 2 s	→	$C(s_3)$ + CHO(s)	1.30216E+09	0.50	0.00
300	CHO(s) + $C(s_3)$	→	CCH(s) + O(s) + 2 s	5.52482E+09	0.50	162.72
301	s + H_2O(s) + CCH(s)	→	$CCH_2(s_2)$ + OH(s)	5.58227E+09	0.50	15.81
302	$CCH_2(s_2)$ + OH(s)	→	CCH(s) + H_2O(s) + s	5.37310E+09	0.50	97.91
303	s + H_2(s) + CCH(s)	→	$CCH_2(s_2)$ + H(s)	1.16456E+10	0.50	0.00
304	$CCH_2(s_2)$ + H(s)	→	CCH(s) + H_2(s) + s	1.48937E+10	0.50	136.99
305	CCH(s) + 5 s	→	$C(s_3)$ + $CH(s_3)$	1.09826E+06	0.50	121.12
306	$CH(s_3)$ + $C(s_3)$	→	CCH(s) + 5 s	5.87571E+09	0.50	104.52
307	CH_3(s) + OH(s)	→	CH_3OH + 2 s	5.53948E+09	0.50	31.92
308	CH_3OH + 2 s	→	CH_3(s) + OH(s)	5.87013E+07	-0.50	15.30
309	CH_3(s) + H_2O(s)	→	CH_3OH + H(s) + s	5.63757E+09	0.50	21.29
310	s + H(s) + CH_3OH	→	CH_3(s) + H_2O(s)	2.57065E+08	-0.50	0.00
311	H(s) + CH_3(s)	→	CH_4 + 2 s	1.34946E+10	0.50	23.90
312	CH_4 + 2 s	→	CH_3(s) + H(s)	7.46193E+09	-0.50	48.55
313	s + H(s) + CH_3(s)	→	$CH_2(s_2)$ + H_2(s)	1.34946E+10	0.50	65.46
314	H_2(s) + $CH_2(s_2)$	→	CH_3(s) + H(s) + s	1.06151E+10	0.50	0.00
315	O(s) + CH_3(s)	→	CH_2O + H(s) + s	5.15078E+09	0.50	23.25
316	s + H(s) + CH_2O	→	CH_3(s) + O(s)	1.04152E+09	-0.50	44.34
317	O(s) + CH_3(s)	→	CH_2OH(s) + s	5.15078E+09	0.50	26.45
318	s + CH_2OH(s)	→	CH_3(s) + O(s)	2.94435E+09	0.50	83.39
319	O(s) + CH_3(s)	→	CH_3O(s) + s	5.15078E+09	0.50	33.92
320	s + CH_3O(s)	→	CH_3(s) + O(s)	2.93637E+09	0.50	70.89

#	Reaction	A	β	E_A
321	$O(s) + CH_3(s) \rightarrow CH_2O(s) + H(s)$	5.15078E+09	0.50	23.25
322	$CH_2O(s) + H(s) \rightarrow CH_3(s) + O(s)$	1.44089E+10	0.50	83.35
323	$OH(s) + CH_3(s) \rightarrow CH_4 + O(s) + s$	5.53948E+09	0.50	46.90
324	$s + O(s) + CH_4 \rightarrow CH_3(s) + OH(s)$	3.32184E+10	-0.50	15.02
325	$H_2O(s) + CH_3(s) \rightarrow CH_4 + OH(s) + s$	5.63757E+09	0.50	6.49
326	$s + OH(s) + CH_4 \rightarrow CH_3(s) + H_2O(s)$	5.83150E+10	-0.50	14.08
327	$OH(s) + CH_3(s) \rightarrow CH_3OH(s) + s$	5.53948E+09	0.50	31.92
328	$s + CH_3OH(s) \rightarrow CH_3(s) + OH(s)$	3.05521E+09	0.50	59.40
329	$s + CH_3(s) + H_2O \rightarrow CH_3OH(s) + H(s)$	2.27206E+11	-0.50	13.22
330	$H(s) + CH_3OH(s) \rightarrow CH_3(s) + H_2O + s$	1.53610E+10	0.50	10.84
331	$H_2O(s) + CH_3(s) \rightarrow CH_3OH(s) + H(s)$	5.63757E+09	0.50	21.29
332	$H(s) + CH_3OH(s) \rightarrow CH_3(s) + H_2O(s)$	1.53610E+10	0.50	10.84
333	$CH_2(s_2) + H_2O(s) \rightarrow CH_3(s) + OH(s) + s$	5.75301E+09	0.50	19.76
334	$s + OH(s) + CH_3(s) \rightarrow CH_2(s_2) + H_2O(s)$	5.53948E+09	0.50	60.95
335	$CH_2(s_2) + OH(s) \rightarrow CH_2OH + 3\ s$	5.64976E+09	0.50	30.03
336	$CH_2OH + 3\ s \rightarrow CH_2(s_2) + OH(s)$	1.26734E+07	-0.50	75.47
337	$H(s) + CH_2(s_2) \rightarrow CH_3(s) + 2\ s$	1.35262E+10	0.50	28.99
338	$CH_3(s) + 2\ s \rightarrow CH_2(s_2) + H(s)$	9.79879E+08	0.50	109.30
339	$O(s) + CH_2(s_2) \rightarrow CHO + H(s) + 2\ s$	5.25018E+09	0.50	0.00
340	$H(s) + CHO + 2\ s \rightarrow CH_2(s_2) + O(s)$	2.43827E+08	-0.50	163.08
341	$OH(s) + CH_2(s_2) \rightarrow CH_2O + H(s) + 2\ s$	5.64976E+09	0.50	27.29
342	$H(s) + CH_2O + 2\ s \rightarrow CH_2(s_2) + OH(s)$	2.69922E+08	-0.50	64.63
343	$CH_2(s_2) + H_2O(s) \rightarrow CH_3OH(s) + 2\ s$	5.75301E+09	0.50	0.00
344	$CH_3OH(s) + 2\ s \rightarrow CH_2(s_2) + H_2O(s)$	7.63801E+08	0.50	53.23
345	$OH(s) + CH_2(s_2) \rightarrow CH_2O(s) + H(s) + s$	5.64976E+09	0.50	27.29
346	$s + H(s) + CH_2O(s) \rightarrow CH_2(s_2) + OH(s)$	1.44089E+10	0.50	103.34
347	$s + CH_2(s_2) + H(s) \rightarrow CH(s_3) + H_2(s)$	1.35262E+10	0.50	94.60
348	$H_2(s) + CH(s_3) \rightarrow CH_2(s_2) + H(s) + s$	1.03779E+10	0.50	18.26
349	$OH(s) + CH_2(s_2) \rightarrow CH_2OH(s) + 2\ s$	5.64976E+09	0.50	30.03
350	$CH_2OH(s) + 2\ s \rightarrow CH_2(s_2) + OH(s)$	7.36089E+08	0.50	103.68
351	$CH_2(s_2) + H_2O(s) \rightarrow CH_2OH(s) + H(s) + s$	5.75301E+09	0.50	24.42
352	$s + H(s) + CH_2OH(s) \rightarrow CH_2(s_2) + H_2O(s)$	1.44461E+10	0.50	57.65
353	$CH(s_3) + H(s) \rightarrow CH_2(s_2) + 2\ s$	1.31483E+10	0.50	49.02
354	$CH_2(s_2) + 2\ s \rightarrow CH(s_3) + H(s)$	1.01650E+09	0.50	100.17
355	$H(s) + CH(s_3) \rightarrow C(s_3) + H_2(s)$	1.31483E+10	0.50	35.65
356	$C(s_3) + H_2(s) \rightarrow CH(s_3) + H(s)$	9.54955E+09	0.50	117.77
357	$H(s) + CH(s_3) \rightarrow C(s_3) + H_2 + s$	1.31483E+10	0.50	35.65
358	$s + C(s_3) + H_2 \rightarrow CH(s_3) + H(s)$	9.82745E+11	0.00	96.55
359	$O(s) + CH(s_3) \rightarrow CHO + 4\ s$	5.21415E+09	0.50	0.00
360	$CHO + 4\ s \rightarrow CH(s_3) + O(s)$	5.11175E+06	-0.50	31.28
361	$OH(s) + CH(s_3) \rightarrow CHO + H(s) + 3\ s$	5.62821E+09	0.50	32.35
362	$H(s) + CHO + 3\ s \rightarrow CH(s_3) + OH(s)$	3.74463E+07	-0.50	140.78
363	$OH(s) + CH(s_3) \rightarrow CHO(s) + H(s) + 2\ s$	5.62821E+09	0.50	32.35
364	$CHO(s) + H(s) + 2\ s \rightarrow CH(s_3) + OH(s)$	3.57717E+09	0.50	129.87
365	$OH(s) + C(s_3) \rightarrow CHO + 4\ s$	5.31413E+09	0.50	72.26
366	$CHO + 4\ s \rightarrow C(s_3) + OH(s)$	5.29908E+06	-0.50	3.63
367	$C(s_3) + H(s) \rightarrow CH(s_3) + s$	1.19364E+10	0.50	134.42
368	$s + CH(s_3) \rightarrow C(s_3) + H(s)$	4.11933E+09	0.50	22.10
369	$O(s) + C(s_3) \rightarrow CO + 4\ s$	4.87970E+09	0.50	54.10
370	$CO + 4\ s \rightarrow C(s_3) + O(s)$	2.07378E+06	0.00	92.77
371	$O(s) + C(s_3) \rightarrow CO(s_2) + 2\ s$	4.87970E+09	0.50	54.10

#	**Reaction**			A	β	E_A
372	$CO(s_2) + 2\ s$	$\rightarrow$	$C(s_3) + O(s)$	7.44321E+08	0.50	226.77
373	$OH(s) + C(s_3)$	$\rightarrow$	$CHO(s) + 3\ s$	5.31413E+09	0.50	72.26
374	$CHO(s) + 3\ s$	$\rightarrow$	$C(s_3) + OH(s)$	1.11978E+08	0.50	90.45
375	$OH(s) + C(s_3)$	$\rightarrow$	$CO + H(s) + 3\ s$	5.31413E+09	0.50	36.91
376	$H(s) + CO + 3\ s$	$\rightarrow$	$C(s_3) + OH(s)$	1.51916E+07	0.00	34.87
377	$OH(s) + C(s_3)$	$\rightarrow$	$CO(s_2) + H(s) + s$	5.31413E+09	0.50	36.91
378	$s + CO(s_2) + H(s)$	$\rightarrow$	$C(s_3) + OH(s)$	1.37609E+10	0.50	152.47
379	$C(s_3) + O_2$	$\rightarrow$	$CO(s_2) + O(s)$	3.95122E+09	0.00	0.00
380	$CO(s_2) + O(s)$	$\rightarrow$	$C(s_3) + O_2$	4.65178E+09	0.50	199.67
381	$H_2O(s) + C(s_3)$	$\rightarrow$	$CH(s_3) + OH(s)$	5.43728E+09	0.50	154.97
382	$OH(s) + CH(s_3)$	$\rightarrow$	$C(s_3) + H_2O(s)$	5.62821E+09	0.50	0.00
383	$CH_2O(s) + C(s_3)$	$\rightarrow$	$CH_2(s_2) + CO(s_2)$	5.53252E+09	0.50	0.00
384	$CO(s_2) + CH_2(s_2)$	$\rightarrow$	$C(s_3) + CH_2O(s)$	5.59733E+09	0.50	46.91
385	$CO(s_2)$	$\rightarrow$	$CO + 2\ s$	1.89929E+10	1.00	187.00
386	$CO + 2\ s$	$\rightarrow$	$CO(s_2)$	4.30773E+08	0.00	0.00
387	$O(s) + CO(s_2)$	$\rightarrow$	$CO_2(s_2) + s$	4.65178E+09	0.50	21.84
388	$s + CO_2(s_2)$	$\rightarrow$	$CO(s_2) + O(s)$	2.62137E+09	0.50	77.30
389	$O(s) + CO(s_2)$	$\rightarrow$	$CO_2 + 3\ s$	4.65178E+09	0.50	21.84
390	$CO_2 + 3\ s$	$\rightarrow$	$CO(s_2) + O(s)$	2.42025E+07	0.00	62.20
391	$OH(s) + CO(s_2)$	$\rightarrow$	$CO_2(s_2) + H(s)$	4.96572E+09	0.50	39.57
392	$CO_2(s_2) + H(s)$	$\rightarrow$	$CO(s_2) + OH(s)$	1.53187E+10	0.50	36.25
393	$s + CO(s_2) + O_2$	$\rightarrow$	$CO_2(s_2) + O(s)$	9.35703E+09	0.00	0.00
394	$CO_2(s_2) + O(s)$	$\rightarrow$	$CO(s_2) + O_2 + s$	4.81019E+09	0.50	126.64
395	$CH_3O(s) + CO(s_2)$	$\rightarrow$	$CH_3(s) + CO_2(s_2)$	4.75611E+09	0.50	22.16
396	$CO_2(s_2) + CH_3(s)$	$\rightarrow$	$CH_3O(s) + CO(s_2)$	5.58743E+09	0.50	47.54
397	$OH(s) + CO(s_2)$	$\rightarrow$	$COOH(s) + 2\ s$	4.96572E+09	0.50	47.79
398	$COOH(s) + 2\ s$	$\rightarrow$	$CO(s_2) + OH(s)$	6.48603E+08	0.50	29.32
399	$s + H_2(s) + CO(s_2)$	$\rightarrow$	$COH(s_3) + H(s)$	1.05821E+10	0.50	125.40
400	$H(s) + COH(s_3)$	$\rightarrow$	$CO(s_2) + H_2(s) + s$	1.44796E+10	0.50	28.86
401	$CO_2(s_2)$	$\rightarrow$	$CO_2 + 2\ s$	4.99858E+07	1.00	15.10
402	$CO_2 + 2\ s$	$\rightarrow$	$CO_2(s_2)$	3.86874E+08	0.00	0.00
403	$H(s) + CH_3OH(s)$	$\rightarrow$	$CH_4 + OH(s) + s$	1.53610E+10	0.50	7.62
404	$s + OH(s) + CH_4$	$\rightarrow$	$CH_3OH(s) + H(s)$	1.89891E+11	-0.50	7.35
405	$H(s) + CH_3OH(s)$	$\rightarrow$	$CH_2OH(s) + H_2(s)$	1.53610E+10	0.50	51.36
406	$CH_2OH(s) + H_2(s)$	$\rightarrow$	$CH_3OH(s) + H(s)$	1.10366E+10	0.50	0.00
407	$O(s) + CH_3OH(s)$	$\rightarrow$	$CH_2OH(s) + OH(s)$	5.03071E+09	0.50	8.04
408	$CH_2OH(s) + OH(s)$	$\rightarrow$	$CH_3OH(s) + O(s)$	5.07843E+09	0.50	31.72
409	$H(s) + CH_3O(s)$	$\rightarrow$	$CH_3OH + 2\ s$	1.44009E+10	0.50	24.13
410	$CH_3OH + 2\ s$	$\rightarrow$	$CH_3O(s) + H(s)$	1.92946E+08	-0.50	35.47
411	$H(s) + CH_3O(s)$	$\rightarrow$	$CH_3(s) + OH(s)$	1.44009E+10	0.50	30.45
412	$CH_3(s) + OH(s)$	$\rightarrow$	$CH_3O(s) + H(s)$	5.53948E+09	0.50	57.07
413	$CH_3O(s) + H_2O(s)$	$\rightarrow$	$CH_3OH(s) + OH(s)$	5.11649E+09	0.50	8.08
414	$OH(s) + CH_3OH(s)$	$\rightarrow$	$CH_3O(s) + H_2O(s)$	5.32122E+09	0.50	24.35
415	$H(s) + CH_3O(s)$	$\rightarrow$	$CH_4 + O(s) + s$	1.44009E+10	0.50	36.18
416	$s + O(s) + CH_4$	$\rightarrow$	$CH_3O(s) + H(s)$	1.09186E+11	-0.50	35.18
417	$H(s) + CH_3O(s)$	$\rightarrow$	$CH_3OH(s) + s$	1.44009E+10	0.50	24.13
418	$s + CH_3OH(s)$	$\rightarrow$	$CH_3O(s) + H(s)$	3.05521E+09	0.50	79.57
419	$CH_3O(s)$	$\rightarrow$	$CH_2O + H(s)$	2.08366E+10	1.00	0.00
420	$H(s) + CH_2O$	$\rightarrow$	$CH_3O(s)$	3.54884E+09	-0.50	40.29
421	$H(s) + CH_3O(s)$	$\rightarrow$	$CH_2O(s) + H_2(s)$	1.44009E+10	0.50	45.62
422	$CH_2O(s) + H_2(s)$	$\rightarrow$	$CH_3O(s) + H(s)$	1.10178E+10	0.50	44.62

#	Reaction	A	β	E_A
423	s + CH_3O(s) → CH_2O(s) + H(s)	2.93637E+09	0.50	0.00
424	CH_2O(s) + H(s) → CH_3O(s) + s	1.44089E+10	0.50	34.04
425	H(s) + CH_2OH(s) → CH_3OH + 2 s	1.44461E+10	0.50	29.49
426	CH_3OH + 2 s → CH_2OH(s) + H(s)	1.95388E+08	-0.50	20.59
427	CH_2OH(s) → CH_2OH + s	2.36220E+10	1.00	160.00
428	s + CH_2OH → CH_2OH(s)	1.13896E+09	-0.50	0.00
429	H(s) + CH_2OH(s) → CH_3(s) + OH(s)	1.44461E+10	0.50	37.38
430	OH(s) + CH_3(s) → CH_2OH(s) + H(s)	5.53948E+09	0.50	44.46
431	CH_2OH(s) + H_2O(s) → CH_3OH(s) + OH(s)	5.12966E+09	0.50	17.28
432	OH(s) + CH_3OH(s) → CH_2OH(s) + H_2O(s)	5.32122E+09	0.50	13.92
433	H(s) + CH_2OH(s) → CH_3OH(s) + s	1.44461E+10	0.50	29.49
434	s + CH_3OH(s) → CH_2OH(s) + H(s)	3.05521E+09	0.50	64.69
435	CH_2OH(s) → CH_2O + H(s)	2.08366E+10	1.00	12.09
436	H(s) + CH_2O → CH_2OH(s)	3.59376E+09	-0.50	15.29
437	H(s) + CH_2OH(s) → CH_2O(s) + H_2(s)	1.44461E+10	0.50	54.08
438	CH_2O(s) + H_2(s) → CH_2OH(s) + H(s)	1.10178E+10	0.50	30.00
439	O(s) + CH_2OH(s) → CH_2O + OH(s) + s	4.77901E+09	0.50	22.27
440	s + OH(s) + CH_2O → CH_2OH(s) + O(s)	6.89087E+09	-0.50	49.07
441	CH_2OH(s) + 2 s → $CHOH(s_2)$ + H(s)	7.36089E+08	0.50	79.28
442	H(s) + $CHOH(s_2)$ → CH_2OH(s) + 2 s	1.46587E+10	0.50	30.15
443	s + H(s) + CH_2OH(s) → $CHOH(s_2)$ + H_2(s)	1.44461E+10	0.50	81.72
444	H_2(s) + $CHOH(s_2)$ → CH_2OH(s) + H(s) + s	1.11917E+10	0.50	4.70
445	s + CH_2OH(s) → CH_2O(s) + H(s)	2.94435E+09	0.50	12.09
446	CH_2O(s) + H(s) → CH_2OH(s) + s	1.44089E+10	0.50	22.78
447	CH_2O(s) + H(s) → CH_2OH + 2 s	1.44089E+10	0.50	22.78
448	CH_2OH + 2 s → CH_2O(s) + H(s)	1.21150E+08	-0.50	0.00
449	CH_2O(s) → CH_2O + s	2.52101E+10	1.00	46.70
450	s + CH_2O → CH_2O(s)	2.05161E+09	-0.50	0.00
451	s + CH_2O(s) → CHO(s) + H(s)	2.98841E+09	0.50	47.23
452	CHO(s) + H(s) → CH_2O(s) + s	1.43087E+10	0.50	44.52
453	H(s) + CH_2O(s) → CHO(s) + H_2(s)	1.44089E+10	0.50	34.27
454	CHO(s) + H_2(s) → CH_2O(s) + H(s)	1.09557E+10	0.50	0.00
455	O(s) + CH_2O(s) → CHO(s) + OH(s)	4.79404E+09	0.50	0.00
456	CHO(s) + OH(s) → CH_2O(s) + O(s)	5.09820E+09	0.50	47.06
457	OH(s) + CH_2O(s) → CHO(s) + H_2O(s)	5.09689E+09	0.50	0.00
458	CHO(s) + H_2O(s) → CH_2O(s) + OH(s)	5.15363E+09	0.50	35.24
459	OH(s) + CH_2O(s) → CHO(s) + H_2O + s	5.09689E+09	0.50	0.00
460	s + CHO(s) + H_2O → CH_2O(s) + OH(s)	6.80071E+10	-0.50	0.31
461	$CHOH(s_2)$ + 2 s → $COH(s_3)$ + H(s)	7.58334E+08	0.50	41.43
462	H(s) + $COH(s_3)$ → $CHOH(s_2)$ + 2 s	1.44796E+10	0.50	86.41
463	$CHOH(s_2)$ → CHO(s) + H(s)	2.08366E+10	1.00	16.35
464	H(s) + CHO(s) → $CHOH(s_2)$	1.43087E+10	0.50	71.13
465	s + H(s) + $CHOH(s_2)$ → $COH(s_3)$ + H_2(s)	1.46587E+10	0.50	40.80
466	H_2(s) + $COH(s_3)$ → $CHOH(s_2)$ + H(s) + s	1.10747E+10	0.50	58.64
467	H(s) + $CHOH(s_2)$ → CHO(s) + H_2(s) + s	1.46587E+10	0.50	38.63
468	s + H_2(s) + CHO(s) → $CHOH(s_2)$ + H(s)	1.09557E+10	0.50	61.84
469	CHO(s) + 2 s → $CO(s_2)$ + H(s)	7.55853E+08	0.50	0.00
470	$CO(s_2)$ + H(s) → CHO(s) + 2 s	1.37609E+10	0.50	107.45
471	H(s) + CHO(s) → CO + H_2(s) + s	1.43087E+10	0.50	0.00
472	s + H_2(s) + CO → CHO(s) + H(s)	6.89865E+08	0.00	109.61
473	s + H(s) + CHO(s) → $CO(s_2)$ + H_2(s)	1.43087E+10	0.50	0.00

#	Reaction			A	β	E_A
474	$CO(s_2) + H_2(s)$	$\rightarrow$	$CHO(s) + H(s) + s$	1.05821E+10	0.50	100.42
475	$H(s) + CHO(s)$	$\rightarrow$	$CO(s_2) + H_2$	1.43087E+10	0.50	0.00
476	$CO(s_2) + H_2$	$\rightarrow$	$CHO(s) + H(s)$	6.41855E+10	0.00	78.46
477	$s + O(s) + CHO(s)$	$\rightarrow$	$CO(s_2) + OH(s)$	4.79132E+09	0.50	0.00
478	$CO(s_2) + OH(s)$	$\rightarrow$	$CHO(s) + O(s) + s$	4.96572E+09	0.50	151.94
479	$s + OH(s) + CHO(s)$	$\rightarrow$	$CO(s_2) + H_2O(s)$	5.09820E+09	0.50	0.00
480	$CO(s_2) + H_2O(s)$	$\rightarrow$	$CHO(s) + OH(s) + s$	5.02610E+09	0.50	139.18
481	$COH(s_3)$	$\rightarrow$	$CO(s_2) + H(s)$	2.08366E+10	1.00	0.00
482	$H(s) + CO(s_2)$	$\rightarrow$	$COH(s_3)$	1.37609E+10	0.50	68.96
483	$COOH(s) + 2\ s$	$\rightarrow$	$CO_2(s_2) + H(s)$	6.48603E+08	0.50	0.00
484	$H(s) + CO_2(s_2)$	$\rightarrow$	$COOH(s) + 2\ s$	1.53187E+10	0.50	14.66
485	$s + H(s) + COOH(s)$	$\rightarrow$	$CO(s_2) + H_2O(s)$	1.53322E+10	0.50	27.08
486	$H_2O(s) + CO(s_2)$	$\rightarrow$	$COOH(s) + H(s) + s$	5.02610E+09	0.50	83.50
487	$s + O(s) + COOH(s)$	$\rightarrow$	$CO_2(s_2) + OH(s)$	4.80082E+09	0.50	28.53
488	$OH(s) + CO_2(s_2)$	$\rightarrow$	$COOH(s) + O(s) + s$	5.07670E+09	0.50	106.16
489	$s + OH(s) + COOH(s)$	$\rightarrow$	$CO_2(s_2) + H_2O(s)$	5.06567E+09	0.50	28.64
490	$H_2O(s) + CO_2(s_2)$	$\rightarrow$	$COOH(s) + OH(s) + s$	5.10838E+09	0.50	82.16
491	$s + H_2$	$\rightarrow$	$H_2(s)$	3.48078E+10	0.00	0.00
492	$H_2(s)$	$\rightarrow$	$H_2 + s$	3.16156E+10	1.00	26.80
493	$s + O(s) + H_2$	$\rightarrow$	$H(s) + OH(s)$	4.17970E+10	0.00	0.00
494	$OH(s) + H(s)$	$\rightarrow$	$H_2 + O(s) + s$	1.24298E+10	0.50	101.31
495	$O_2(s_2) + H_2$	$\rightarrow$	$H(s) + OOH(s)$	1.32798E+11	0.00	0.00
496	$OOH(s) + H(s)$	$\rightarrow$	$H_2 + O_2(s_2)$	1.39551E+10	0.50	117.25
497	$O_2 + 2\ s$	$\rightarrow$	$O_2(s_2)$	7.92136E+08	0.00	0.00
498	$O_2(s_2)$	$\rightarrow$	$O_2 + 2\ s$	1.91839E+10	1.00	44.30
499	$s + H(s) + O_2$	$\rightarrow$	$O(s) + OH(s)$	6.28814E+08	0.00	0.00
500	$OH(s) + O(s)$	$\rightarrow$	$H(s) + O_2 + s$	4.66121E+09	0.50	166.38
501	$O_2 + 2\ s$	$\rightarrow$	$2\ O(s)$	2.03469E+08	0.00	0.00
502	$2\ O(s)$	$\rightarrow$	$O_2 + 2\ s$	4.26627E+09	0.50	147.81
503	$H(s) + O_2$	$\rightarrow$	$OOH(s)$	1.30300E+09	0.00	0.00
504	$OOH(s)$	$\rightarrow$	$H(s) + O_2$	2.08366E+10	1.00	73.94
505	$s + OH$	$\rightarrow$	$OH(s)$	5.32909E+09	0.00	0.00
506	$OH(s)$	$\rightarrow$	$OH + s$	3.25484E+10	1.00	247.00
507	$s + O$	$\rightarrow$	$O(s)$	1.89986E+08	1.00	0.00
508	$O(s)$	$\rightarrow$	$O + s$	3.12808E+10	1.00	356.00
509	$s + O(s) + H_2O$	$\rightarrow$	$2\ OH(s)$	2.81013E+10	-0.50	6.26
510	$2\ OH(s)$	$\rightarrow$	$H_2O + O(s) + s$	5.03981E+09	0.50	63.87
511	$s + H(s) + H_2O$	$\rightarrow$	$H_2(s) + OH(s)$	1.75147E+10	-0.50	13.15
512	$OH(s) + H_2(s)$	$\rightarrow$	$H_2O + H(s) + s$	9.77616E+09	0.50	0.00
513	$s + HO_2$	$\rightarrow$	$OOH(s)$	2.05387E+09	-0.50	0.00
514	$OOH(s)$	$\rightarrow$	$HO_2 + s$	2.60085E+10	1.00	204.00
515	$HO_2 + 2\ s$	$\rightarrow$	$O(s) + OH(s)$	2.47795E+08	-0.50	0.00
516	$OH(s) + O(s)$	$\rightarrow$	$HO_2 + 2\ s$	4.66121E+09	0.50	114.82
517	$HO_2 + 3\ s$	$\rightarrow$	$H(s) + O_2(s_2)$	1.37866E+08	-0.50	110.13
518	$H(s) + O_2(s_2)$	$\rightarrow$	$HO_2 + 3\ s$	1.35635E+10	0.50	0.00
519	$H_2O_2 + 2\ s$	$\rightarrow$	$H_2O_2(s_2)$	2.70654E+09	-0.50	0.00
520	$H_2O_2(s_2)$	$\rightarrow$	$H_2O_2 + 2\ s$	7.12037E+09	1.00	27.10
521	$s + H(s) + H_2O_2$	$\rightarrow$	$H_2O(s) + OH(s)$	4.59391E+08	-0.50	0.00
522	$H_2O(s) + OH(s)$	$\rightarrow$	$H_2O_2 + H(s) + s$	5.13543E+09	0.50	150.64
523	$H_2O_2 + 2\ s$	$\rightarrow$	$2\ OH(s)$	1.04903E+08	-0.50	0.00
524	$2\ OH(s)$	$\rightarrow$	$H_2O_2 + 2\ s$	5.03981E+09	0.50	168.33

#	Reaction	A	β	E_A
525	$H_2O_2 + 2\,s \rightarrow H_2O(s) + O(s)$	1.54095E+08	-0.50	0.00
526	$H_2O(s) + O(s) \rightarrow H_2O_2 + 2\,s$	4.76774E+09	0.50	123.39
527	$s + H(s) + H_2O_2 \rightarrow H_2(s) + OOH(s)$	6.48039E+08	-0.50	0.00
528	$OOH(s) + H_2(s) \rightarrow H_2O_2 + H(s) + s$	1.06844E+10	0.50	18.08
529	$O(s) + H_2(s) \rightarrow H(s) + OH(s)$	8.84834E+09	0.50	6.08
530	$OH(s) + H(s) \rightarrow H_2(s) + O(s)$	1.24298E+10	0.50	101.31
531	$s + H_2(s) \rightarrow 2\,H(s)$	8.92735E+09	0.50	40.13
532	$2\,H(s) \rightarrow H_2(s) + s$	1.34184E+10	0.50	72.64
533	$H(s) + O_2(s_2) \rightarrow O(s) + OH(s) + s$	1.35635E+10	0.50	0.00
534	$s + OH(s) + O(s) \rightarrow H(s) + O_2(s_2)$	4.66121E+09	0.50	166.38
535	$O_2(s_2) \rightarrow 2\,O(s)$	2.08366E+10	1.00	4.33
536	$2\,O(s) \rightarrow O_2(s_2)$	4.26627E+09	0.50	147.81
537	$H(s) + O_2(s_2) \rightarrow OOH(s) + 2\,s$	1.35635E+10	0.50	0.00
538	$OOH(s) + 2\,s \rightarrow H(s) + O_2(s_2)$	6.94856E+08	0.50	73.94
539	$O(s) + H(s) \rightarrow OH + 2\,s$	1.10870E+10	0.50	38.72
540	$OH + 2\,s \rightarrow H(s) + O(s)$	1.28517E+09	0.00	65.87
541	$H_2O(s) + O(s) \rightarrow 2\,OH(s)$	4.76774E+09	0.50	40.52
542	$2\,OH(s) \rightarrow H_2O(s) + O(s)$	5.03981E+09	0.50	63.87
543	$O(s) + H(s) \rightarrow OH(s) + s$	1.10870E+10	0.50	38.72
544	$s + OH(s) \rightarrow H(s) + O(s)$	3.46268E+09	0.50	107.22
545	$OH(s) + H(s) \rightarrow H_2O(s) + s$	1.24298E+10	0.50	39.09
546	$s + H_2O(s) \rightarrow H(s) + OH(s)$	3.47731E+09	0.50	80.38
547	$OH(s) + H(s) \rightarrow H_2O + 2\,s$	1.24298E+10	0.50	39.09
548	$H_2O + 2\,s \rightarrow H(s) + OH(s)$	5.87502E+09	-0.50	40.18
549	$2\,H(s) \rightarrow H_2 + 2\,s$	1.34184E+10	0.50	72.64
550	$H_2 + 2\,s \rightarrow 2\,H(s)$	8.42938E+09	0.00	13.34
551	$H(s) \rightarrow H + s$	3.51899E+10	1.00	255.00
552	$s + H \rightarrow H(s)$	1.89986E+08	1.00	0.00
553	$H_2O_2(s_2) + H(s) \rightarrow H_2O + OH(s) + 2\,s$	1.43342E+10	0.50	0.00
554	$OH(s) + H_2O + 2\,s \rightarrow H_2O_2(s_2) + H(s)$	2.16617E+11	-0.50	117.91
555	$OOH(s) + H(s) \rightarrow H_2O + O(s) + s$	1.39551E+10	0.50	0.00
556	$s + O(s) + H_2O \rightarrow H(s) + OOH(s)$	5.82302E+10	-0.50	96.65
557	$OOH(s) + H(s) \rightarrow H_2O_2 + 2\,s$	1.39551E+10	0.50	74.90
558	$H_2O_2 + 2\,s \rightarrow H(s) + OOH(s)$	2.17374E+08	-0.50	0.00
559	$H_2O(s) + H(s) \rightarrow H_2(s) + OH(s)$	1.29285E+10	0.50	47.27
560	$OH(s) + H_2(s) \rightarrow H_2O(s) + H(s)$	9.77616E+09	0.50	0.00
561	$OOH(s) + H(s) \rightarrow H_2O(s) + O(s)$	1.39551E+10	0.50	0.00
562	$H_2O(s) + O(s) \rightarrow H(s) + OOH(s)$	4.76774E+09	0.50	129.21
563	$H_2O_2(s_2) + H(s) \rightarrow H_2O(s) + OH(s) + s$	1.43342E+10	0.50	0.00
564	$s + H_2O(s) + OH(s) \rightarrow H_2O_2(s_2) + H(s)$	5.13543E+09	0.50	150.64
565	$OOH(s) + H(s) \rightarrow 2\,OH(s)$	1.39551E+10	0.50	0.00
566	$2\,OH(s) \rightarrow H(s) + OOH(s)$	5.03981E+09	0.50	132.16
567	$OOH(s) + H(s) \rightarrow H_2O_2(s_2)$	1.39551E+10	0.50	74.90
568	$H_2O_2(s_2) \rightarrow H(s) + OOH(s)$	2.08366E+10	1.00	23.92
569	$H_2O(s) \rightarrow H_2O + s$	3.23181E+10	1.00	40.20
570	$s + H_2O \rightarrow H_2O(s)$	3.45201E+10	-0.50	0.00
571	$s + OOH(s) \rightarrow O(s) + OH(s)$	2.77942E+09	0.50	10.38
572	$OH(s) + O(s) \rightarrow OOH(s) + s$	4.66121E+09	0.50	114.82
573	$H_2O_2(s_2) \rightarrow 2\,OH(s)$	2.08366E+10	1.00	0.00
574	$2\,OH(s) \rightarrow H_2O_2(s_2)$	5.03981E+09	0.50	168.33
575	$H_2O_2(s_2) \rightarrow H_2O(s) + O(s)$	2.08366E+10	1.00	0.00

#	Reaction	A	β	E_A
576	$H_2O(s) + O(s) \rightarrow H_2O_2(s_2)$	4.76774E+09	0.50	123.39
577	$N_2O + 2\,s \rightarrow N_2O(s_2)$	7.16064E+09	-0.50	0.00
578	$N_2O(s_2) \rightarrow N_2O + 2\,s$	1.34252E+10	1.00	72.57
579	$N_2O(s_2) + 2\,s \rightarrow N(s) + NO(s_3)$	6.40833E+08	0.50	7.69
580	$NO(s_3) + N(s) \rightarrow N_2O(s_2) + 2\,s$	4.70745E+09	0.50	46.27
581	$N_2O + 3\,s \rightarrow N_2(s_2) + O(s)$	2.86198E+07	-0.50	0.00
582	$O(s) + N_2(s_2) \rightarrow N_2O + 3\,s$	4.59599E+09	0.50	137.15
583	$NO + 3\,s \rightarrow NO(s_3)$	1.94052E+10	0.00	0.00
584	$NO(s_3) \rightarrow NO + 3\,s$	2.17814E+09	1.00	71.76
585	$NO + 2\,s \rightarrow N(s) + O(s)$	1.18545E+08	0.00	0.00
586	$O(s) + N(s) \rightarrow NO + 2\,s$	4.45895E+09	0.50	165.31
587	$N_2 + 2\,s \rightarrow N_2(s_2)$	6.65374E+08	0.00	0.00
588	$N_2(s_2) \rightarrow N_2 + 2\,s$	1.10244E+10	1.00	45.23
589	$N_2 + 2\,s \rightarrow 2\,N(s)$	2.75883E+08	0.00	86.05
590	$2\,N(s) \rightarrow N_2 + 2\,s$	4.64959E+09	0.50	93.14
591	$N_2(s_2) \rightarrow 2\,N(s)$	2.08366E+10	1.00	131.28
592	$2\,N(s) \rightarrow N_2(s_2)$	4.64959E+09	0.50	93.14
593	$s + NO_2 \rightarrow NO_2(s)$	1.34133E+09	-0.50	0.00
594	$NO_2(s) \rightarrow NO_2 + s$	1.48835E+10	1.00	41.16
595	$NO_2(s) + 3\,s \rightarrow NO(s_3) + O(s)$	9.01317E+07	0.50	0.00
596	$O(s) + NO(s_3) \rightarrow NO_2(s) + 3\,s$	4.46634E+09	0.50	60.15
597	$s + N \rightarrow N(s)$	1.89986E+08	1.00	0.00
598	$N(s) \rightarrow N + s$	3.29696E+10	1.00	485.33
599	$N_2O(s_2) + O \rightarrow N(s) + NO_2(s)$	2.04982E+09	1.00	32.31
600	$N(s) + NO_2(s) \rightarrow N_2O(s_2) + O$	4.79495E+09	0.50	7.62
601	$O_2(s_2) + NO \rightarrow NO_2(s) + O(s)$	3.78737E+09	0.00	0.00
602	$O(s) + NO_2(s) \rightarrow NO + O_2(s_2)$	4.52578E+09	0.50	56.70
603	$N_2(s_2) + O \rightarrow N_2O(s_2)$	3.16605E+10	1.00	251.05
604	$N_2O(s_2) \rightarrow N_2(s_2) + O$	2.08366E+10	1.00	0.00
605	$O(s) + NO_2(s) + 3\,s \rightarrow NO(s_3) + O_2(s_2)$	1.67622E+08	0.50	56.70
606	$O_2(s_2) + NO(s_3) \rightarrow NO_2(s) + O(s) + 3\,s$	4.33016E+09	0.50	0.00
607	$N(s) + NO_2(s) + 4\,s \rightarrow 2\,NO(s_3)$	1.87303E+07	0.50	64.21
608	$2\,NO(s_3) \rightarrow N(s) + NO_2(s) + 4\,s$	4.33450E+09	0.50	0.00
609	$s + O(s) + N_2O(s_2) \rightarrow N_2(s_2) + O_2(s_2)$	4.69799E+09	0.50	0.00
610	$O_2(s_2) + N_2(s_2) \rightarrow N_2O(s_2) + O(s) + s$	4.47063E+09	0.50	66.39
611	$N(s) + N_2O(s_2) + 2\,s \rightarrow N_2(s_2) + NO(s_3)$	1.24337E+09	0.50	0.00
612	$N_2(s_2) + NO(s_3) \rightarrow N_2O(s_2) + N(s) + 2\,s$	4.47357E+09	0.50	59.66
613	$NO(s_3) \rightarrow N(s) + O(s) + s$	2.08366E+10	1.00	10.68
614	$s + N(s) + O(s) \rightarrow NO(s_3)$	4.45895E+09	0.50	165.31
615	$N(s) + NO(s_3) \rightarrow N_2(s_2) + O(s) + s$	4.70745E+09	0.50	0.00
616	$s + O(s) + N_2(s_2) \rightarrow N(s) + NO(s_3)$	4.59599E+09	0.50	124.88
617	$O(s) + NO(s_3) \rightarrow N(s) + O_2(s_2) + s$	4.46634E+09	0.50	13.68
618	$s + N(s) + O_2(s_2) \rightarrow NO(s_3) + O(s)$	4.74084E+09	0.50	22.97
619	$C_3H_6 + 2\,s \rightarrow C_3H_6(s_2)$	1.33006E+14	-0.50	39.40
620*	$C_3H_6(s_2) \rightarrow C_3H_6 + 2\,s$	1.25250E-09	1.00	39.13
621	$C_3H_6(s_2) \rightarrow CH_3(s) + CHCH_2(s)$	2.08366E+10	1.00	100.47
622*	$CH_3(s) + CHCH_2(s) \rightarrow C_3H_6(s_2)$	6.13949E-09	0.50	0.00
623	$s + C_3H_5a \rightarrow C_3H_5(s)$	4.21289E+09	-0.50	0.00
624	$C_3H_5(s) \rightarrow C_3H_5a + s$	1.10134E+11	1.00	41.52

*Removed reaction

#	Reaction	A	β	E_A
625	$C_3H_5(s) + 4\,s \rightarrow CCH_3(s_3) + CH_2(s_2)$	1.32573E+07	0.50	113.74
626	$CH_2(s_2) + CCH_3(s_3) \rightarrow C_3H_5(s) + 4\,s$	6.02307E+09	0.50	47.31
627	$C_3H_5(s) + 2\,s \rightarrow CH_2(s_2) + CHCH_2(s)$	8.48464E+08	0.50	85.98
628	$CH_2(s_2) + CHCH_2(s) \rightarrow C_3H_5(s) + 2\,s$	6.28757E+09	0.50	26.16
629	$C_3H_5(s) + 3\,s \rightarrow C_2H_2(s_3) + CH_3(s)$	1.25698E+08	0.50	0.00
630	$CH_3(s) + C_2H_2(s_3) \rightarrow C_3H_5(s) + 2\,s$	6.35120E+09	0.50	65.12
631	$C_3H_5(s) + 3\,s \rightarrow C(s_3) + CH_2CH_3(s)$	1.25698E+08	0.50	6.70
632	$C(s_3) + CH_2CH_3(s) \rightarrow C_3H_5(s) + 3\,s$	6.03919E+09	0.50	104.20
633	$O(s) + C_3H_5a + 3\,s \rightarrow C_2H_4(s) + COH(s_3)$	4.69320E+08	-0.50	0.00
634	$C_2H_4(s) + COH(s_3) \rightarrow C_3H_5a + O(s) + 3\,s$	5.37732E+09	0.50	101.82
635	$OH(s) + C_3H_5a + 3\,s \rightarrow CHCH_3(s_2) + CHOH(s_2)$	3.89821E+07	-0.50	34.44
636	$CHCH_3(s_2) + CHOH(s_2) \rightarrow C_3H_5a + OH(s) + 3\,s$	5.38703E+09	0.50	37.29
637	$OH(s) + C_3H_5(s) \rightarrow C_3H_6 + O(s) + s$	6.38270E+09	0.50	0.00
638	$s + O(s) + C_3H_6 \rightarrow C_3H_5(s) + OH(s)$	1.70040E+10	-0.50	15.39
639	$C_3H_6(s_2) \rightarrow C_3H_5(s) + H(s)$	2.08366E+10	1.00	87.68
640	$H(s) + C_3H_5(s) \rightarrow C_3H_6(s_2)$	1.97271E+10	0.50	0.00

Table A.2: Surface reaction mechanism corresponding to $\theta = 20\%$ [100] of the magnitude of $Q_{C,H,O,N}$. The global catalytic C_3H_6 step sub-mechanism is considered.

#	Reaction	A	β	E_A
1	$C_2H_6 + 2\,s \rightarrow C_2H_6(s_2)$	4.76569E+10	-0.50	0.00
2	$C_2H_6(s_2) \rightarrow C_2H_6 + 2\,s$	4.06295E+11	1.00	36.10
3	$s + O(s) + C_2H_6 \rightarrow CH_2CH_3(s) + OH(s)$	2.39624E+09	-0.50	0.00
4	$CH_2CH_3(s) + OH(s) \rightarrow C_2H_6 + O(s) + s$	5.55266E+09	0.50	35.27
5	$s + OH(s) + C_2H_6 \rightarrow CH_2CH_3(s) + H_2O(s)$	2.86372E+09	-0.50	3.29
6	$CH_2CH_3(s) + H_2O(s) \rightarrow C_2H_6 + OH(s) + s$	5.59873E+09	0.50	13.53
7	$C_2H_6 + 2\,s \rightarrow 2\,CH_3(s)$	2.29579E+08	-0.50	50.31
8	$2\,CH_3(s) \rightarrow C_2H_6 + 2\,s$	6.05457E+09	0.50	0.00
9	$C_2H_6 + 2\,s \rightarrow CH_2CH_3(s) + H(s)$	5.00971E+08	-0.50	32.91
10	$CH_2CH_3(s) + H(s) \rightarrow C_2H_6 + 2\,s$	1.58541E+10	0.50	35.72
11	$s + C_2H_5 \rightarrow CH_2CH_3(s)$	2.34877E+08	-0.50	0.00
12	$CH_2CH_3(s) \rightarrow C_2H_5 + s$	2.60107E+10	1.00	163.00
13	$C_2H_5 + 2\,s \rightarrow C_2H_4(s) + H(s)$	3.23465E+07	-0.50	0.00
14	$C_2H_4(s) + H(s) \rightarrow C_2H_5 + 2\,s$	1.58188E+10	0.50	27.05
15	$C_2H_5 + 3\,s \rightarrow C_2H_4(s_2) + H(s)$	3.51341E+07	-0.50	0.00
16	$C_2H_4(s_2) + H(s) \rightarrow C_2H_5 + 3\,s$	1.50167E+10	0.50	46.14
17	$C_2H_5 + 3\,s \rightarrow CH_2(s_2) + CH_3(s)$	3.98655E+06	-0.50	139.22
18	$CH_3(s) + CH_2(s_2) \rightarrow C_2H_5 + 3\,s$	6.16870E+09	0.50	0.00
19	$H(s) + C_2H_5 + 2\,s \rightarrow CHCH_3(s_2) + H_2(s)$	1.55736E+08	-0.50	131.54
20	$CHCH_3(s_2) + H_2(s) \rightarrow C_2H_5 + H(s) + 2\,s$	1.20373E+10	0.50	0.00
21	$C_2H_4 + 2\,s \rightarrow CHCH_3(s_2)$	3.13138E+10	-0.50	0.00
22	$CHCH_3(s_2) \rightarrow C_2H_4 + 2\,s$	2.05882E+10	1.00	294.00
23	$C_2H_3 + 3\,s \rightarrow CCH_3(s_3)$	1.94448E+09	-0.50	0.00
24	$CCH_3(s_3) \rightarrow C_2H_3 + 3\,s$	1.92432E+09	1.00	405.00
25	$s + C_2H_3 \rightarrow CHCH_2(s)$	8.26077E+08	-0.50	0.00
26	$CHCH_2(s) \rightarrow C_2H_3 + s$	2.93508E+10	1.00	184.00
27	$C_2H_3 + 3\,s \rightarrow CHCH_2(s_3)$	9.44764E+08	-0.50	0.00

#	Reaction	A	β	E_A
28	$CHCH_2(s_3) \rightarrow C_2H_3 + 3\ s$	1.07488E+10	1.00	129.00
29	$C_2H_3 + 3\ s \rightarrow CCH_2(s_2) + H(s)$	1.00172E+08	-0.50	78.09
30	$CCH_2(s_2) + H(s) \rightarrow C_2H_3 + 3\ s$	1.48937E+10	0.50	46.18
31	$C_2H_3 + 4\ s \rightarrow C_2H_2(s_3) + H(s)$	1.26275E+08	-0.50	59.61
32	$C_2H_2(s_3) + H(s) \rightarrow C_2H_3 + 4\ s$	1.63611E+10	0.50	29.11
33	$C_2H_3 + 4\ s \rightarrow C(s_3) + CH_3(s)$	2.16839E+06	-0.50	77.76
34	$CH_3(s) + C(s_3) \rightarrow C_2H_3 + 4\ s$	5.82816E+09	0.50	42.21
35	$C_2H_3 + 5\ s \rightarrow CH_2(s_2) + CH(s_3)$	3.34229E+05	-0.50	299.38
36	$CH_2(s_2) + CH(s_3) \rightarrow C_2H_3 + 5\ s$	6.25503E+09	0.50	0.00
37	$C_2H_2 + 2\ s \rightarrow CCH_2(s_2)$	7.84804E+08	0.00	0.00
38	$CCH_2(s_2) \rightarrow C_2H_2 + 2\ s$	2.22914E+10	1.00	299.00
39	$C_2H_2 + 3\ s \rightarrow CCH_2(s_3)$	1.00146E+09	0.00	0.00
40	$CCH_2(s_3) \rightarrow C_2H_2 + 3\ s$	1.97263E+09	1.00	149.00
41	$s + CH_3 \rightarrow CH_3(s)$	2.07540E+10	-0.50	0.00
42	$CH_3(s) \rightarrow CH_3 + s$	3.21604E+10	1.00	159.00
43	$CH_3 + 3\ s \rightarrow CH_2(s_2) + H(s)$	1.44628E+09	-0.50	84.47
44	$CH_2(s_2) + H(s) \rightarrow CH_3 + 3\ s$	1.35262E+10	0.50	44.54
45	$CH_2t + 2\ s \rightarrow CH_2(s_2)$	1.12362E+10	-0.50	0.00
46	$CH_2(s_2) \rightarrow CH_2t + 2\ s$	2.24567E+10	1.00	283.00
47	$CH_2t + 4\ s \rightarrow CH(s_3) + H(s)$	1.63237E+09	-0.50	43.57
48	$CH(s_3) + H(s) \rightarrow CH_2t + 4\ s$	1.31483E+10	0.50	59.81
49	$CH + 3\ s \rightarrow CH(s_3)$	2.83595E+09	0.00	0.00
50	$CH(s_3) \rightarrow CH + 3\ s$	6.42738E+09	1.00	407.00
51	$CH + 4\ s \rightarrow C(s_3) + H(s)$	1.77138E+08	0.00	0.00
52	$C(s_3) + H(s) \rightarrow CH + 4\ s$	1.19364E+10	0.50	132.12
53	$C1 + 3\ s \rightarrow C(s_3)$	8.12015E+07	1.00	0.00
54	$C(s_3) \rightarrow C1 + 3\ s$	9.19010E+09	1.00	628.00
55	$s + O(s) + CO \rightarrow CO_2(s_2)$	4.87946E+09	0.00	0.00
56	$CO_2(s_2) \rightarrow CO + O(s) + s$	2.08366E+10	1.00	77.30
57	$OH(s) + CO + 2\ s \rightarrow CO_2(s_2) + H(s)$	1.45784E+09	0.00	8.62
58	$CO_2(s_2) + H(s) \rightarrow CO + OH(s) + 2\ s$	1.53187E+10	0.50	34.87
59	$s + CH_2O(s) + CO \rightarrow 2\ CHO(s)$	1.61064E+09	0.00	150.39
60	$2\ CHO(s) \rightarrow CH_2O(s) + CO + s$	4.90873E+09	0.50	0.00
61	$CH_2O(s) + CO + 3\ s \rightarrow CH_2(s_2) + CO_2(s_2)$	3.60274E+08	0.00	99.39
62	$CO_2(s_2) + CH_2(s_2) \rightarrow CH_2O(s) + CO + 3\ s$	5.74322E+09	0.50	0.00
63	$C_2H_6(s_2) + CO \rightarrow CH_2CH_3(s) + CHO(s)$	3.76156E+09	0.00	4.95
64	$CHO(s) + CH_2CH_3(s) \rightarrow C_2H_6(s_2) + CO$	5.29470E+09	0.50	0.00
65	$s + H_2O(s) + CO \rightarrow CHO(s) + OH(s)$	1.01333E+09	0.00	11.88
66	$CHO(s) + OH(s) \rightarrow CO + H_2O(s) + s$	5.09820E+09	0.50	0.00
67	$CH_2CH_3(s) + CO + 2\ s \rightarrow C_2H_4(s_2) + CHO(s)$	5.00147E+08	0.00	117.67
68	$CHO(s) + C_2H_4(s_2) \rightarrow CH_2CH_3(s) + CO + 2\ s$	5.12390E+09	0.50	0.00
69	$CHCH_3(s_2) + CO + 2\ s \rightarrow CCH_3(s_3) + CHO(s)$	4.33680E+08	0.00	3.04
70	$CHO(s) + CCH_3(s_3) \rightarrow CHCH_3(s_2) + CO + 2\ s$	5.16949E+09	0.50	0.00
71	$s + CH_3OH(s) + CO \rightarrow CH_2OH(s) + CHO(s)$	4.44638E+09	0.00	0.81
72	$CH_2OH(s) + CHO(s) \rightarrow CH_3OH(s) + CO + s$	4.86242E+09	0.50	0.00
73	$s + CH_2CH_3(s) + CO \rightarrow C_2H_4(s) + CHO(s)$	2.00059E+09	0.00	148.67
74	$CHO(s) + C_2H_4(s) \rightarrow CH_2CH_3(s) + CO + s$	5.33279E+09	0.50	0.00
75	$s + OH(s) + CO \rightarrow CHO(s) + O(s)$	9.65546E+08	0.00	34.19
76	$O(s) + CHO(s) \rightarrow CO + OH(s) + s$	4.79132E+09	0.50	0.00
77	$s + C(s_3) + CO_2 \rightarrow 2\ CO(s_2)$	9.77443E+08	0.00	0.00
78	$2\ CO(s_2) \rightarrow C(s_3) + CO_2 + s$	4.70876E+09	0.50	77.22

#	Reaction			A	β	E_A
79	s + O(s) + CH_2O	→	CHO(s) + OH(s)	2.12670E+09	-0.50	0.00
80	CHO(s) + OH(s)	→	CH_2O + O(s) + s	5.09820E+09	0.50	49.81
81	s + OH(s) + CH_2O	→	CHO(s) + H_2O(s)	2.54159E+09	-0.50	0.00
82	CHO(s) + H_2O(s)	→	CH_2O + OH(s) + s	5.15363E+09	0.50	33.83
83	CH_2O + 2 s	→	CHO(s) + H(s)	4.44619E+08	-0.50	0.53
84	CHO(s) + H(s)	→	CH_2O + 2 s	1.43087E+10	0.50	47.96
85	s + CHO	→	CHO(s)	1.66541E+09	-0.50	0.00
86	CHO(s)	→	CHO + s	2.52417E+10	1.00	167.00
87	CHO + 3 s	→	CO(s_2) + H(s)	1.57308E+08	-0.50	0.00
88	CO(s_2) + H(s)	→	CHO + 3 s	1.37609E+10	0.50	102.88
89	H(s) + CHO + 2 s	→	CO(s_2) + H_2(s)	7.91383E+08	-0.50	0.00
90	CO(s_2) + H_2(s)	→	CHO + H(s) + 2 s	1.05821E+10	0.50	97.72
91	s + CH_3OH	→	CH_3OH(s)	1.12314E+09	-0.50	0.00
92	CH_3OH(s)	→	CH_3OH + s	3.29727E+10	1.00	44.10
93	s + O(s) + CH_3OH	→	CH_2OH(s) + OH(s)	9.34579E+08	-0.50	0.00
94	CH_2OH(s) + OH(s)	→	CH_3OH + O(s) + s	5.07843E+09	0.50	37.95
95	s + O(s) + CH_3OH	→	CH_3O(s) + OH(s)	9.22896E+08	-0.50	1.87
96	CH_3O(s) + OH(s)	→	CH_3OH + O(s) + s	5.06500E+09	0.50	49.41
97	s + CH_3O	→	CH_3O(s)	3.94297E+09	-0.50	0.00
98	CH_3O(s)	→	CH_3O + s	2.64242E+10	1.00	173.00
99	CH_3O + 2 s	→	CH_3(s) + O(s)	2.89297E+08	-0.50	31.88
100	CH_3(s) + O(s)	→	CH_3O + 2 s	5.15078E+09	0.50	41.64
101	CH_3O + 2 s	→	CH_2O(s) + H(s)	4.24720E+08	-0.50	0.00
102	CH_2O(s) + H(s)	→	CH_3O + 2 s	1.44089E+10	0.50	33.05
103	CO(s_2) + CH_3O	→	CH_2O(s) + CHO(s)	2.54115E+09	-0.50	116.55
104	CH_2O(s) + CHO(s)	→	CH_3O + CO(s_2)	4.89255E+09	0.50	0.00
105	H(s) + CH_3O	→	CH_3OH(s)	4.27655E+09	-0.50	0.00
106	CH_3OH(s)	→	CH_3O + H(s)	2.08366E+10	1.00	79.57
107	s + C_2H	→	CCH(s)	9.06087E+08	0.00	0.00
108	CCH(s)	→	C_2H + s	2.85007E+10	1.00	287.00
109	C_2 + 6 s	→	2 C(s_3)	2.22964E+05	0.00	0.00
110	2 C(s_3)	→	C_2 + 6 s	5.50717E+09	0.50	361.88
111	C_2H_6(s_2)	→	2 CH_3(s)	2.08366E+10	1.00	86.42
112	2 CH_3(s)	→	C_2H_6(s_2)	6.05457E+09	0.50	0.00
113	H(s) + C_2H_6(s_2)	→	CH_2CH_3(s) + H_2(s) + s	1.54829E+10	0.50	50.55
114	s + CH_2CH_3(s) + H_2(s)	→	C_2H_6(s_2) + H(s)	1.20294E+10	0.50	0.00
115	H(s) + C_2H_6(s_2)	→	CH_3(s) + CH_4 + 2 s	1.54829E+10	0.50	31.49
116	CH_3(s) + CH_4 + 2 s	→	C_2H_6(s_2) + H(s)	3.13089E+12	-0.50	0.00
117	C_2H_6(s_2) + O(s)	→	C_2H_5 + OH(s) + 2 s	5.11340E+09	0.50	11.32
118	OH(s) + C_2H_5 + 2 s	→	C_2H_6(s_2) + O(s)	7.98272E+09	-0.50	27.29
119	O(s) + C_2H_6(s_2)	→	CH_2CH_3(s) + OH(s) + s	5.11340E+09	0.50	11.32
120	s + CH_2CH_3(s) + OH(s)	→	C_2H_6(s_2) + O(s)	5.55266E+09	0.50	35.27
121	OH(s) + C_2H_6(s_2)	→	CH_2CH_3(s) + H_2O(s) + s	5.40841E+09	0.50	15.38
122	s + CH_2CH_3(s) + H_2O(s)	→	C_2H_6(s_2) + OH(s)	5.59873E+09	0.50	13.53
123	CH_3(s) + C_2H_6(s_2)	→	CH_2CH_3(s) + CH_4 + 2 s	5.92480E+09	0.50	10.68
124	CH_2CH_3(s) + CH_4 + 2 s	→	C_2H_6(s_2) + CH_3(s)	4.58655E+12	-0.50	10.79
125	C_2H_6(s_2)	→	CH_2CH_3(s) + H(s)	2.08366E+10	1.00	69.01
126	CH_2CH_3(s) + H(s)	→	C_2H_6(s_2)	1.58541E+10	0.50	35.72
127	O(s) + C_2H_6(s_2)	→	CH_3(s) + CH_3O(s) + s	5.11340E+09	0.50	63.07
128	s + CH_3O(s) + CH_3(s)	→	C_2H_6(s_2) + O(s)	5.56880E+09	0.50	27.66
129	OH(s) + C_2H_6(s_2)	→	CH_2CH_3(s) + H_2O + 2 s	5.40841E+09	0.50	15.38

#	Reaction			A	β	E_A
130	$CH_2CH_3(s) + H_2O + 2\ s$	$\rightarrow$	$C_2H_6(s_2) + OH(s)$	3.88003E+12	-0.50	0.00
131	$CH_2CH_3(s)$	$\rightarrow$	$C_2H_4 + H(s)$	2.08366E+10	1.00	22.76
132	$H(s) + C_2H_4$	$\rightarrow$	$CH_2CH_3(s)$	2.62333E+09	-0.50	8.17
133	$H(s) + CH_2CH_3(s)$	$\rightarrow$	$2\ CH_3(s)$	1.58541E+10	0.50	64.39
134	$2\ CH_3(s)$	$\rightarrow$	$CH_2CH_3(s) + H(s)$	6.05457E+09	0.50	27.90
135	$O(s) + CH_2CH_3(s)$	$\rightarrow$	$C_2H_4 + OH(s) + s$	5.25663E+09	0.50	37.05
136	$s + OH(s) + C_2H_4$	$\rightarrow$	$CH_2CH_3(s) + O(s)$	5.03010E+09	-0.50	24.92
137	$O(s) + CH_2CH_3(s)$	$\rightarrow$	$C_2H_4(s) + OH(s)$	5.25663E+09	0.50	37.05
138	$C_2H_4(s) + OH(s)$	$\rightarrow$	$CH_2CH_3(s) + O(s)$	5.57766E+09	0.50	79.56
139	$s + O(s) + CH_2CH_3(s)$	$\rightarrow$	$C_2H_4(s_2) + OH(s)$	5.25663E+09	0.50	41.82
140	$C_2H_4(s_2) + OH(s)$	$\rightarrow$	$CH_2CH_3(s) + O(s) + s$	5.33523E+09	0.50	91.85
141	$O(s) + CH_2CH_3(s)$	$\rightarrow$	$CH_2O(s) + CH_3(s)$	5.25663E+09	0.50	45.99
142	$CH_2O(s) + CH_3(s)$	$\rightarrow$	$CH_2CH_3(s) + O(s)$	5.60134E+09	0.50	55.45
143	$s + OH(s) + CH_2CH_3(s)$	$\rightarrow$	$C_2H_4(s_2) + H_2O(s)$	5.55266E+09	0.50	32.92
144	$C_2H_4(s_2) + H_2O(s)$	$\rightarrow$	$CH_2CH_3(s) + OH(s) + s$	5.38793E+09	0.50	77.57
145	$CH_2CH_3(s) + 2\ s$	$\rightarrow$	$C_2H_4(s_2) + H(s)$	8.22089E+08	0.50	16.07
146	$C_2H_4(s_2) + H(s)$	$\rightarrow$	$CH_2CH_3(s) + 2\ s$	1.50167E+10	0.50	46.14
147	$s + H(s) + CH_2CH_3(s)$	$\rightarrow$	$C_2H_4(s_2) + H_2(s)$	1.58541E+10	0.50	47.81
148	$C_2H_4(s_2) + H_2(s)$	$\rightarrow$	$CH_2CH_3(s) + H(s) + s$	1.14546E+10	0.50	39.88
149	$C_2H_4(s) + H(s)$	$\rightarrow$	$CH_2CH_3(s) + s$	1.58188E+10	0.50	27.05
150	$s + CH_2CH_3(s)$	$\rightarrow$	$C_2H_4(s) + H(s)$	3.28836E+09	0.50	22.76
151	$C_2H_4(s)$	$\rightarrow$	$C_2H_4 + s$	5.00567E+10	1.00	68.00
152	$s + C_2H_4$	$\rightarrow$	$C_2H_4(s)$	1.93895E+09	-0.50	0.00
153	$s + O(s) + C_2H_4(s)$	$\rightarrow$	$CH_2(s_2) + CH_2O(s)$	5.27779E+09	0.50	55.04
154	$CH_2O(s) + CH_2(s_2)$	$\rightarrow$	$C_2H_4(s) + O(s) + s$	5.74122E+09	0.50	0.00
155	$OH(s) + C_2H_4(s)$	$\rightarrow$	$CH_2O(s) + CH_3(s)$	5.57766E+09	0.50	45.57
156	$CH_2O(s) + CH_3(s)$	$\rightarrow$	$C_2H_4(s) + OH(s)$	5.60134E+09	0.50	0.00
157	$s + C_2H_4(s)$	$\rightarrow$	$CHCH_2(s) + H(s)$	3.34198E+09	0.50	98.96
158	$CHCH_2(s) + H(s)$	$\rightarrow$	$C_2H_4(s) + s$	1.58249E+10	0.50	37.31
159	$C_2H_4(s) + 3\ s$	$\rightarrow$	$CHCH_2(s_3) + H(s)$	1.23777E+08	0.50	115.86
160	$H(s) + CHCH_2(s_3)$	$\rightarrow$	$C_2H_4(s) + 3\ s$	1.50255E+10	0.50	0.00
161	$OH(s) + C_2H_4(s)$	$\rightarrow$	$CHCH_2(s) + H_2O(s)$	5.57766E+09	0.50	45.20
162	$CHCH_2(s) + H_2O(s)$	$\rightarrow$	$C_2H_4(s) + OH(s)$	5.66776E+09	0.50	0.00
163	$C_2H_4(s_2) + H_2O$	$\rightarrow$	$CH_2CH_3(s) + OH(s)$	1.53139E+11	-0.50	46.13
164	$OH(s) + CH_2CH_3(s)$	$\rightarrow$	$C_2H_4(s_2) + H_2O$	5.55266E+09	0.50	32.92
165	$C_2H_4(s_2)$	$\rightarrow$	$C_2H_4 + 2\ s$	1.40786E+11	1.00	99.00
166	$C_2H_4 + 2\ s$	$\rightarrow$	$C_2H_4(s_2)$	3.55395E+10	-0.50	0.00
167	$C_2H_4(s_2)$	$\rightarrow$	$CHCH_2(s) + H(s)$	2.08366E+10	1.00	114.46
168	$CHCH_2(s) + H(s)$	$\rightarrow$	$C_2H_4(s_2)$	1.58249E+10	0.50	0.00
169	$O(s) + C_2H_4(s_2)$	$\rightarrow$	$CH_2(s_2) + CH_2O(s)$	5.03030E+09	0.50	76.49
170	$CH_2O(s) + CH_2(s_2)$	$\rightarrow$	$C_2H_4(s_2) + O(s)$	5.74122E+09	0.50	0.00
171	$OH(s) + C_2H_4(s_2)$	$\rightarrow$	$CH_2O(s) + CH_3(s) + s$	5.33523E+09	0.50	65.76
172	$s + CH_2O(s) + CH_3(s)$	$\rightarrow$	$C_2H_4(s_2) + OH(s)$	5.60134E+09	0.50	0.00
173	$C_2H_4(s_2) + 2\ s$	$\rightarrow$	$CHCH_2(s_3) + H(s)$	7.98328E+08	0.50	131.36
174	$H(s) + CHCH_2(s_3)$	$\rightarrow$	$C_2H_4(s_2) + 2\ s$	1.50255E+10	0.50	0.00
175	$CHCH_3(s_2) + H(s)$	$\rightarrow$	$C_2H_5 + 3\ s$	1.58531E+10	0.50	45.40
176	$C_2H_5 + 3\ s$	$\rightarrow$	$CHCH_3(s_2) + H(s)$	3.09566E+07	-0.50	84.31
177	$CHCH_3(s_2) + H(s)$	$\rightarrow$	$CH_2CH_3(s) + 2\ s$	1.58531E+10	0.50	45.40
178	$CH_2CH_3(s) + 2\ s$	$\rightarrow$	$CHCH_3(s_2) + H(s)$	8.22089E+08	0.50	110.43
179	$CHCH_3(s_2)$	$\rightarrow$	$C_2H_4(s_2)$	2.08366E+10	1.00	0.00
180	$C_2H_4(s_2)$	$\rightarrow$	$CHCH_3(s_2)$	2.08366E+10	1.00	176.52

#	Reaction	A	β	E_A
181	$CHCH_3(s_2) + 2\ s \rightarrow CHCH_2(s_3) + H(s)$	8.37085E+08	0.50	69.62
182	$H(s) + CHCH_2(s_3) \rightarrow CHCH_3(s_2) + 2\ s$	1.50255E+10	0.50	28.45
183	$s + H(s) + CHCH_3(s_2) \rightarrow CCH_3(s_3) + H_2(s)$	1.58531E+10	0.50	77.64
184	$CCH_3(s_3) + H_2(s) \rightarrow CHCH_3(s_2) + H(s) + s$	1.14559E+10	0.50	38.77
185	$CHCH_3(s_2) + 2\ s \rightarrow CCH_3(s_3) + H(s)$	8.37085E+08	0.50	77.74
186	$CCH_3(s_3) + H(s) \rightarrow CHCH_3(s_2) + 2\ s$	1.50058E+10	0.50	71.58
187	$CHCH_3(s_2) \rightarrow CHCH_2(s) + H(s)$	2.08366E+10	1.00	52.73
188	$H(s) + CHCH_2(s) \rightarrow CHCH_3(s_2)$	1.58249E+10	0.50	49.12
189	$CCH_3(s_3) \rightarrow CHCH_2(s) + 2\ s$	2.08366E+10	1.00	0.00
190	$CHCH_2(s) + 2\ s \rightarrow CCH_3(s_3)$	8.51652E+08	0.50	77.94
191	$CHCH_2(s) + H(s) \rightarrow C_2H_4 + 2\ s$	1.58249E+10	0.50	37.31
192	$C_2H_4 + 2\ s \rightarrow CHCH_2(s) + H(s)$	6.00099E+08	-0.50	30.96
193	$CHCH_2(s) + 3\ s \rightarrow C(s_3) + CH_3(s)$	1.26171E+08	0.50	44.81
194	$CH_3(s) + C(s_3) \rightarrow CHCH_2(s) + 3\ s$	5.82816E+09	0.50	70.10
195	$s + H(s) + CHCH_2(s) \rightarrow CCH_2(s_2) + H_2(s)$	1.58249E+10	0.50	51.91
196	$CCH_2(s_2) + H_2(s) \rightarrow CHCH_2(s) + H(s) + s$	1.13873E+10	0.50	41.77
197	$O(s) + CHCH_2(s) \rightarrow C_2H_2 + OH(s) + s$	5.31391E+09	0.50	48.50
198	$s + OH(s) + C_2H_2 \rightarrow CHCH_2(s) + O(s)$	1.37021E+09	0.00	121.26
199	$OH(s) + CHCH_2(s) \rightarrow C_2H_2 + H_2O(s) + s$	5.61761E+09	0.50	37.00
200	$s + H_2O(s) + C_2H_2 \rightarrow CHCH_2(s) + OH(s)$	1.43802E+09	0.00	90.69
201	$CHCH_2(s) + 2\ s \rightarrow CCH_2(s_2) + H(s)$	8.51652E+08	0.50	50.35
202	$H(s) + CCH_2(s_2) \rightarrow CHCH_2(s) + 2\ s$	1.48937E+10	0.50	74.81
203	$CHCH_2(s) + 3\ s \rightarrow C_2H_2(s_3) + H(s)$	1.26171E+08	0.50	16.22
204	$H(s) + C_2H_2(s_3) \rightarrow CHCH_2(s) + 3\ s$	1.63611E+10	0.50	59.61
205	$H(s) + CHCH_2(s) \rightarrow C_2H_2 + H_2(s) + s$	1.58249E+10	0.50	46.29
206	$s + H_2(s) + C_2H_2 \rightarrow CHCH_2(s) + H(s)$	9.78993E+08	0.00	8.16
207	$O(s) + C_2H_2(s_3) \rightarrow CH(s_3) + CHO(s)$	5.51825E+09	0.50	80.83
208	$CH(s_3) + CHO(s) \rightarrow C_2H_2(s_3) + O(s)$	5.76374E+09	0.50	39.26
209	$s + O(s) + C_2H_2(s_3) \rightarrow C(s_3) + CHOH(s_2)$	5.51825E+09	0.50	66.34
210	$C(s_3) + CHOH(s_2) \rightarrow C_2H_2(s_3) + O(s) + s$	5.61672E+09	0.50	66.81
211	$O(s) + C_2H_2(s_3) \rightarrow CH_2(s_2) + CO(s_2)$	5.51825E+09	0.50	0.00
212	$CH_2(s_2) + CO(s_2) \rightarrow C_2H_2(s_3) + O(s)$	5.59733E+09	0.50	92.17
213	$O(s) + C_2H_2(s_3) \rightarrow C(s_3) + CH_2O(s)$	5.51825E+09	0.50	0.00
214	$C(s_3) + CH_2O(s) \rightarrow C_2H_2(s_3) + O(s)$	5.53252E+09	0.50	40.50
215	$O(s) + C_2H_2(s_3) + 2\ s \rightarrow CH(s_3) + COH(s_3)$	1.37956E+09	0.50	112.12
216	$CH(s_3) + COH(s_3) \rightarrow C_2H_2(s_3) + O(s) + 2\ s$	5.81989E+09	0.50	64.41
217	$O(s) + C_2H_2(s_3) \rightarrow CCH(s) + OH(s) + 2\ s$	5.51825E+09	0.50	90.46
218	$OH(s) + CCH(s) + 2\ s \rightarrow C_2H_2(s_3) + O(s)$	1.38112E+09	0.50	44.04
219	$CHCH_2(s) + 3\ s \rightarrow CCH_2(s_3) + H(s)$	1.26171E+08	0.50	103.57
220	$H(s) + CCH_2(s_3) \rightarrow CHCH_2(s) + 3\ s$	1.50168E+10	0.50	0.00
221	$H(s) + CHCH_2(s_3) \rightarrow C_2H_4 + 4\ s$	1.50255E+10	0.50	0.00
222	$C_2H_4 + 4\ s \rightarrow CHCH_2(s_3) + H(s)$	2.89540E+08	-0.50	47.86
223	$CHCH_2(s_3) \rightarrow CHCH_2(s) + 2\ s$	2.08366E+10	1.00	0.00
224	$CHCH_2(s) + 2\ s \rightarrow CHCH_2(s_3)$	8.51652E+08	0.50	0.00
225	$CHCH_2(s_3) \rightarrow CCH_3(s_3)$	2.08366E+10	1.00	20.57
226	$CCH_3(s_3) \rightarrow CHCH_2(s_3)$	2.08366E+10	1.00	0.00
227	$CHCH_2(s_3) \rightarrow CCH_2(s_2) + H(s)$	2.08366E+10	1.00	22.86
228	$CCH_2(s_2) + H(s) \rightarrow CHCH_2(s_3)$	1.48937E+10	0.50	95.41
229	$s + CHCH_2(s_3) \rightarrow C(s_3) + CH_3(s)$	3.25564E+09	0.50	17.31
230	$CH_3(s) + C(s_3) \rightarrow CHCH_2(s_3) + s$	5.82816E+09	0.50	90.94
231	$H(s) + CHCH_2(s_3) \rightarrow C_2H_2 + H_2(s) + 3\ s$	1.50255E+10	0.50	28.58

#	Reaction	A	β	E_A
232	$H_2(s) + C_2H_2 + 3\,s \rightarrow CHCH_2(s_3) + H(s)$	1.11965E+09	0.00	63.16
233	$H(s) + CHCH_2(s_3) \rightarrow C_2H_2(s_3) + H_2(s)$	1.50255E+10	0.50	28.58
234	$C_2H_2(s_3) + H_2(s) \rightarrow CHCH_2(s_3) + H(s)$	1.24112E+10	0.50	67.39
235	$H(s) + CHCH_2(s_3) \rightarrow CCH_2(s_2) + H_2(s) + s$	1.50255E+10	0.50	29.11
236	$s + H_2(s) + CCH_2(s_2) \rightarrow CHCH_2(s_3) + H(s)$	1.13873E+10	0.50	57.92
237	$H(s) + CHCH_2(s_3) \rightarrow CCH_2(s_2) + H_2 + 2\,s$	1.50255E+10	0.50	29.11
238	$CCH_2(s_2) + H_2 + 2\,s \rightarrow CHCH_2(s_3) + H(s)$	7.07027E+11	0.00	38.37
239	$H(s) + CHCH_2(s_3) \rightarrow C_2H_2(s_3) + H_2 + s$	1.50255E+10	0.50	28.58
240	$s + C_2H_2(s_3) + H_2 \rightarrow CHCH_2(s_3) + H(s)$	4.34190E+12	0.00	47.61
241	$s + CCH_3(s_3) \rightarrow C(s_3) + CH_3(s)$	3.25193E+09	0.50	44.60
242	$CH_3(s) + C(s_3) \rightarrow CCH_3(s_3) + s$	5.82816E+09	0.50	70.25
243	$H(s) + CCH_3(s_3) \rightarrow C(s_3) + CH_4 + s$	1.50058E+10	0.50	52.65
244	$s + C(s_3) + CH_4 \rightarrow CCH_3(s_3) + H(s)$	4.22250E+12	-0.50	96.67
245	$CCH_3(s_3) + H(s) \rightarrow CCH_2(s_2) + H_2(s) + s$	1.50058E+10	0.50	74.34
246	$s + H_2(s) + CCH_2(s_2) \rightarrow CCH_3(s_3) + H(s)$	1.13873E+10	0.50	65.79
247	$H(s) + CCH_2(s_2) \rightarrow CCH_3(s_3)$	1.48937E+10	0.50	74.96
248	$CCH_3(s_3) \rightarrow CCH_2(s_2) + H(s)$	2.08366E+10	1.00	50.14
249	$CCH_2(s_2) \rightarrow CCH(s) + H(s)$	2.08366E+10	1.00	133.72
250	$CCH(s) + H(s) \rightarrow CCH_2(s_2)$	1.52488E+10	0.50	52.77
251	$s + H(s) + CCH_2(s_2) \rightarrow C(s_3) + CH_3(s)$	1.48937E+10	0.50	59.45
252	$CH_3(s) + C(s_3) \rightarrow CCH_2(s_2) + H(s) + s$	5.82816E+09	0.50	57.90
253	$s + O(s) + CCH_2(s_2) \rightarrow CH_2(s_2) + CO(s_2)$	5.05950E+09	0.50	57.59
254	$CO(s_2) + CH_2(s_2) \rightarrow CCH_2(s_2) + O(s) + s$	5.59733E+09	0.50	130.00
255	$O(s) + CCH_2(s_2) \rightarrow CCH(s) + OH(s) + s$	5.05950E+09	0.50	96.60
256	$s + OH(s) + CCH(s) \rightarrow CCH_2(s_2) + O(s)$	5.52448E+09	0.50	50.67
257	$s + O(s) + CCH_2(s_2) \rightarrow C(s_3) + CH_2O(s)$	5.05950E+09	0.50	56.82
258	$CH_2O(s) + C(s_3) \rightarrow CCH_2(s_2) + O(s) + s$	5.53252E+09	0.50	104.60
259	$O(s) + CCH_2(s_2) \rightarrow CH_2(s_2) + CO + s$	5.05950E+09	0.50	57.59
260	$s + CH_2(s_2) + CO \rightarrow CCH_2(s_2) + O(s)$	5.00710E+09	0.00	18.35
261	$O(s) + CCH_2(s_2) \rightarrow C(s_3) + CH_2O$	5.05950E+09	0.50	56.82
262	$C(s_3) + CH_2O \rightarrow CCH_2(s_2) + O(s)$	1.13438E+10	-0.50	70.80
263	$s + OH(s) + CCH_2(s_2) \rightarrow C(s_3) + CH_2OH(s)$	5.37310E+09	0.50	61.90
264	$CH_2OH(s) + C(s_3) \rightarrow CCH_2(s_2) + OH(s) + s$	5.52043E+09	0.50	55.54
265	$CCH_2(s_2) + 3\,s \rightarrow C(s_3) + CH_2(s_2)$	1.22021E+08	0.50	139.61
266	$CH_2(s_2) + C(s_3) \rightarrow CCH_2(s_2) + 3\,s$	5.92507E+09	0.50	68.66
267	$CCH_2(s_3) + H(s) \rightarrow C_2H_3 + 4\,s$	1.50168E+10	0.50	0.00
268	$C_2H_3 + 4\,s \rightarrow CCH_2(s_3) + H(s)$	9.10007E+07	-0.50	228.09
269	$CCH_2(s_3) \rightarrow CCH_2(s_2) + s$	2.08366E+10	1.00	0.00
270	$s + CCH_2(s_2) \rightarrow CCH_2(s_3)$	3.29456E+09	0.50	0.00
271	$H(s) + CCH_2(s_3) \rightarrow CHCH_2(s_3) + s$	1.50168E+10	0.50	31.27
272	$s + CHCH_2(s_3) \rightarrow CCH_2(s_3) + H(s)$	3.25564E+09	0.50	76.07
273	$H(s) + CCH_2(s_3) \rightarrow CCH_3(s_3) + s$	1.50168E+10	0.50	0.00
274	$s + CCH_3(s_3) \rightarrow CCH_2(s_3) + H(s)$	3.25193E+09	0.50	103.35
275	$H(s) + CCH_2(s_3) \rightarrow CCH(s) + H_2 + 3\,s$	1.50168E+10	0.50	52.68
276	$CCH(s) + H_2 + 3\,s \rightarrow CCH_2(s_3) + H(s)$	8.95897E+10	0.00	5.40
277	$H(s) + CCH_2(s_3) \rightarrow C(s_3) + CH_3(s)$	1.50168E+10	0.50	0.00
278	$CH_3(s) + C(s_3) \rightarrow CCH_2(s_3) + H(s)$	5.82816E+09	0.50	115.06
279	$C_2H_2(s_3) + H(s) \rightarrow CHCH_2(s_3) + s$	1.63611E+10	0.50	82.37
280	$s + CHCH_2(s_3) \rightarrow C_2H_2(s_3) + H(s)$	3.25564E+09	0.50	0.00
281	$C_2H_2(s_3) \rightarrow CCH_2(s_2) + s$	2.08366E+10	1.00	73.96
282	$s + CCH_2(s_2) \rightarrow C_2H_2(s_3)$	3.29456E+09	0.50	0.00

#	Reaction	A	β	E_A
283	$C_2H_2(s_3) \rightarrow C_2H_2 + 3\ s$	3.91827E+10	1.00	134.00
284	$C_2H_2 + 3\ s \rightarrow C_2H_2(s_3)$	1.38965E+09	0.00	0.00
285	$s + CCH(s) + H(s) \rightarrow CCH_2(s_3)$	1.52488E+10	0.50	67.07
286	$CCH_2(s_3) \rightarrow CCH(s) + H(s) + s$	2.08366E+10	1.00	58.72
287	$H_2O(s) + CCH(s) + 2\ s \rightarrow C_2H_2(s_3) + OH(s)$	1.39557E+09	0.50	0.00
288	$OH(s) + C_2H_2(s_3) \rightarrow CCH(s) + H_2O(s) + 2\ s$	5.82278E+09	0.50	62.60
289	$H_2O(s) + CCH(s) \rightarrow C_2H_2 + OH(s) + s$	5.58227E+09	0.50	0.00
290	$s + OH(s) + C_2H_2 \rightarrow CCH(s) + H_2O(s)$	2.11772E+09	0.00	115.60
291	$H(s) + CCH(s) \rightarrow C_2H_2 + 2\ s$	1.52488E+10	0.50	0.00
292	$C_2H_2 + 2\ s \rightarrow CCH(s) + H(s)$	3.70468E+08	0.00	8.96
293	$s + H(s) + CCH(s) \rightarrow C_2H_2(s_3)$	1.52488E+10	0.50	0.00
294	$C_2H_2(s_3) \rightarrow CCH(s) + H(s) + s$	2.08366E+10	1.00	142.96
295	$s + O(s) + CCH(s) \rightarrow CH(s_3) + CO$	5.20866E+09	0.50	0.00
296	$CH(s_3) + CO \rightarrow CCH(s) + O(s) + s$	2.03430E+09	0.00	60.97
297	$s + O(s) + CCH(s) \rightarrow C(s_3) + CHO$	5.20866E+09	0.50	0.00
298	$C(s_3) + CHO \rightarrow CCH(s) + O(s) + s$	5.01442E+09	-0.50	18.13
299	$O(s) + CCH(s) + 2\ s \rightarrow C(s_3) + CHO(s)$	1.30216E+09	0.50	0.00
300	$CHO(s) + C(s_3) \rightarrow CCH(s) + O(s) + 2\ s$	5.52482E+09	0.50	155.77
301	$s + H_2O(s) + CCH(s) \rightarrow CCH_2(s_2) + OH(s)$	5.58227E+09	0.50	16.96
302	$CCH_2(s_2) + OH(s) \rightarrow CCH(s) + H_2O(s) + s$	5.37310E+09	0.50	96.47
303	$s + H_2(s) + CCH(s) \rightarrow CCH_2(s_2) + H(s)$	1.16456E+10	0.50	0.00
304	$CCH_2(s_2) + H(s) \rightarrow CCH(s) + H_2(s) + s$	1.48937E+10	0.50	131.95
305	$CCH(s) + 5\ s \rightarrow C(s_3) + CH(s_3)$	1.09826E+06	0.50	121.12
306	$CH(s_3) + C(s_3) \rightarrow CCH(s) + 5\ s$	5.87571E+09	0.50	113.93
307	$CH_3(s) + OH(s) \rightarrow CH_3OH + 2\ s$	5.53948E+09	0.50	38.02
308	$CH_3OH + 2\ s \rightarrow CH_3(s) + OH(s)$	5.87013E+07	-0.50	15.30
309	$CH_3(s) + H_2O(s) \rightarrow CH_3OH + H(s) + s$	5.63757E+09	0.50	21.19
310	$s + H(s) + CH_3OH \rightarrow CH_3(s) + H_2O(s)$	2.57065E+08	-0.50	0.00
311	$H(s) + CH_3(s) \rightarrow CH_4 + 2\ s$	1.34946E+10	0.50	33.48
312	$CH_4 + 2\ s \rightarrow CH_3(s) + H(s)$	7.46193E+09	-0.50	48.55
313	$s + H(s) + CH_3(s) \rightarrow CH_2(s_2) + H_2(s)$	1.34946E+10	0.50	65.09
314	$H_2(s) + CH_2(s_2) \rightarrow CH_3(s) + H(s) + s$	1.06151E+10	0.50	0.00
315	$O(s) + CH_3(s) \rightarrow CH_2O + H(s) + s$	5.15078E+09	0.50	36.43
316	$s + H(s) + CH_2O \rightarrow CH_3(s) + O(s)$	1.04152E+09	-0.50	44.34
317	$O(s) + CH_3(s) \rightarrow CH_2OH(s) + s$	5.15078E+09	0.50	37.40
318	$s + CH_2OH(s) \rightarrow CH_3(s) + O(s)$	2.94435E+09	0.50	83.39
319	$O(s) + CH_3(s) \rightarrow CH_3O(s) + s$	5.15078E+09	0.50	41.64
320	$s + CH_3O(s) \rightarrow CH_3(s) + O(s)$	2.93637E+09	0.50	70.89
321	$O(s) + CH_3(s) \rightarrow CH_2O(s) + H(s)$	5.15078E+09	0.50	36.43
322	$CH_2O(s) + H(s) \rightarrow CH_3(s) + O(s)$	1.44089E+10	0.50	79.92
323	$OH(s) + CH_3(s) \rightarrow CH_4 + O(s) + s$	5.53948E+09	0.50	49.34
324	$s + O(s) + CH_4 \rightarrow CH_3(s) + OH(s)$	3.32184E+10	-0.50	15.02
325	$H_2O(s) + CH_3(s) \rightarrow CH_4 + OH(s) + s$	5.63757E+09	0.50	10.69
326	$s + OH(s) + CH_4 \rightarrow CH_3(s) + H_2O(s)$	5.83150E+10	-0.50	14.08
327	$OH(s) + CH_3(s) \rightarrow CH_3OH(s) + s$	5.53948E+09	0.50	38.02
328	$s + CH_3OH(s) \rightarrow CH_3(s) + OH(s)$	3.05521E+09	0.50	59.40
329	$s + CH_3(s) + H_2O \rightarrow CH_3OH(s) + H(s)$	2.27206E+11	-0.50	13.22
330	$H(s) + CH_3OH(s) \rightarrow CH_3(s) + H_2O + s$	1.53610E+10	0.50	13.76
331	$H_2O(s) + CH_3(s) \rightarrow CH_3OH(s) + H(s)$	5.63757E+09	0.50	21.19
332	$H(s) + CH_3OH(s) \rightarrow CH_3(s) + H_2O(s)$	1.53610E+10	0.50	13.76
333	$CH_2(s_2) + H_2O(s) \rightarrow CH_3(s) + OH(s) + s$	5.75301E+09	0.50	20.17

#	Reaction	A	β	E_A
334	$s + OH(s) + CH_3(s) \rightarrow CH_2(s_2) + H_2O(s)$	5.53948E+09	0.50	61.08
335	$CH_2(s_2) + OH(s) \rightarrow CH_2OH + 3\ s$	5.64976E+09	0.50	44.20
336	$CH_2OH + 3\ s \rightarrow CH_2(s_2) + OH(s)$	1.26734E+07	-0.50	75.47
337	$H(s) + CH_2(s_2) \rightarrow CH_3(s) + 2\ s$	1.35262E+10	0.50	44.54
338	$CH_3(s) + 2\ s \rightarrow CH_2(s_2) + H(s)$	9.79879E+08	0.50	109.30
339	$O(s) + CH_2(s_2) \rightarrow CHO + H(s) + 2\ s$	5.25018E+09	0.50	0.00
340	$H(s) + CHO + 2\ s \rightarrow CH_2(s_2) + O(s)$	2.43827E+08	-0.50	163.08
341	$OH(s) + CH_2(s_2) \rightarrow CH_2O + H(s) + 2\ s$	5.64976E+09	0.50	43.73
342	$H(s) + CH_2O + 2\ s \rightarrow CH_2(s_2) + OH(s)$	2.69922E+08	-0.50	64.63
343	$CH_2(s_2) + H_2O(s) \rightarrow CH_3OH(s) + 2\ s$	5.75301E+09	0.50	0.00
344	$CH_3OH(s) + 2\ s \rightarrow CH_2(s_2) + H_2O(s)$	7.63801E+08	0.50	53.23
345	$OH(s) + CH_2(s_2) \rightarrow CH_2O(s) + H(s) + s$	5.64976E+09	0.50	43.73
346	$s + H(s) + CH_2O(s) \rightarrow CH_2(s_2) + OH(s)$	1.44089E+10	0.50	99.46
347	$s + CH_2(s_2) + H(s) \rightarrow CH(s_3) + H_2(s)$	1.35262E+10	0.50	93.47
348	$H_2(s) + CH(s_3) \rightarrow CH_2(s_2) + H(s) + s$	1.03779E+10	0.50	17.99
349	$OH(s) + CH_2(s_2) \rightarrow CH_2OH(s) + 2\ s$	5.64976E+09	0.50	44.20
350	$CH_2OH(s) + 2\ s \rightarrow CH_2(s_2) + OH(s)$	7.36089E+08	0.50	103.68
351	$CH_2(s_2) + H_2O(s) \rightarrow CH_2OH(s) + H(s) + s$	5.75301E+09	0.50	24.18
352	$s + H(s) + CH_2OH(s) \rightarrow CH_2(s_2) + H_2O(s)$	1.44461E+10	0.50	58.41
353	$CH(s_3) + H(s) \rightarrow CH_2(s_2) + 2\ s$	1.31483E+10	0.50	59.81
354	$CH_2(s_2) + 2\ s \rightarrow CH(s_3) + H(s)$	1.01650E+09	0.50	100.17
355	$H(s) + CH(s_3) \rightarrow C(s_3) + H_2(s)$	1.31483E+10	0.50	52.53
356	$C(s_3) + H_2(s) \rightarrow CH(s_3) + H(s)$	9.54955E+09	0.50	114.65
357	$H(s) + CH(s_3) \rightarrow C(s_3) + H_2 + s$	1.31483E+10	0.50	52.53
358	$s + C(s_3) + H_2 \rightarrow CH(s_3) + H(s)$	9.82745E+11	0.00	96.55
359	$O(s) + CH(s_3) \rightarrow CHO + 4\ s$	5.21415E+09	0.50	0.00
360	$CHO + 4\ s \rightarrow CH(s_3) + O(s)$	5.11175E+06	-0.50	31.28
361	$OH(s) + CH(s_3) \rightarrow CHO + H(s) + 3\ s$	5.62821E+09	0.50	56.25
362	$H(s) + CHO + 3\ s \rightarrow CH(s_3) + OH(s)$	3.74463E+07	-0.50	140.78
363	$OH(s) + CH(s_3) \rightarrow CHO(s) + H(s) + 2\ s$	5.62821E+09	0.50	56.25
364	$CHO(s) + H(s) + 2\ s \rightarrow CH(s_3) + OH(s)$	3.57717E+09	0.50	124.25
365	$OH(s) + C(s_3) \rightarrow CHO + 4\ s$	5.31413E+09	0.50	79.67
366	$CHO + 4\ s \rightarrow C(s_3) + OH(s)$	5.29908E+06	-0.50	3.63
367	$C(s_3) + H(s) \rightarrow CH(s_3) + s$	1.19364E+10	0.50	132.12
368	$s + CH(s_3) \rightarrow C(s_3) + H(s)$	4.11933E+09	0.50	22.10
369	$O(s) + C(s_3) \rightarrow CO + 4\ s$	4.87970E+09	0.50	90.45
370	$CO + 4\ s \rightarrow C(s_3) + O(s)$	2.07378E+06	0.00	92.77
371	$O(s) + C(s_3) \rightarrow CO(s_2) + 2\ s$	4.87970E+09	0.50	90.45
372	$CO(s_2) + 2\ s \rightarrow C(s_3) + O(s)$	7.44321E+08	0.50	226.77
373	$OH(s) + C(s_3) \rightarrow CHO(s) + 3\ s$	5.31413E+09	0.50	79.67
374	$CHO(s) + 3\ s \rightarrow C(s_3) + OH(s)$	1.11978E+08	0.50	90.45
375	$OH(s) + C(s_3) \rightarrow CO + H(s) + 3\ s$	5.31413E+09	0.50	64.29
376	$H(s) + CO + 3\ s \rightarrow C(s_3) + OH(s)$	1.51916E+07	0.00	34.87
377	$OH(s) + C(s_3) \rightarrow CO(s_2) + H(s) + s$	5.31413E+09	0.50	64.29
378	$s + CO(s_2) + H(s) \rightarrow C(s_3) + OH(s)$	1.37609E+10	0.50	145.84
379	$C(s_3) + O_2 \rightarrow CO(s_2) + O(s)$	3.95122E+09	0.00	0.00
380	$CO(s_2) + O(s) \rightarrow C(s_3) + O_2$	4.65178E+09	0.50	191.36
381	$H_2O(s) + C(s_3) \rightarrow CH(s_3) + OH(s)$	5.43728E+09	0.50	150.53
382	$OH(s) + CH(s_3) \rightarrow C(s_3) + H_2O(s)$	5.62821E+09	0.50	0.00
383	$CH_2O(s) + C(s_3) \rightarrow CH_2(s_2) + CO(s_2)$	5.53252E+09	0.50	0.00
384	$CO(s_2) + CH_2(s_2) \rightarrow C(s_3) + CH_2O(s)$	5.59733E+09	0.50	48.68

#	**Reaction**	A	β	E_A
385	$CO(s_2) \rightarrow CO + 2\ s$	1.89929E+10	1.00	187.00
386	$CO + 2\ s \rightarrow CO(s_2)$	4.30773E+08	0.00	0.00
387	$O(s) + CO(s_2) \rightarrow CO_2(s_2) + s$	4.65178E+09	0.50	32.52
388	$s + CO_2(s_2) \rightarrow CO(s_2) + O(s)$	2.62137E+09	0.50	77.30
389	$O(s) + CO(s_2) \rightarrow CO_2 + 3\ s$	4.65178E+09	0.50	32.52
390	$CO_2 + 3\ s \rightarrow CO(s_2) + O(s)$	2.42025E+07	0.00	62.20
391	$OH(s) + CO(s_2) \rightarrow CO_2(s_2) + H(s)$	4.96572E+09	0.50	42.27
392	$CO_2(s_2) + H(s) \rightarrow CO(s_2) + OH(s)$	1.53187E+10	0.50	34.87
393	$s + CO(s_2) + O_2 \rightarrow CO_2(s_2) + O(s)$	9.35703E+09	0.00	0.00
394	$CO_2(s_2) + O(s) \rightarrow CO(s_2) + O_2 + s$	4.81019E+09	0.50	124.64
395	$CH_3O(s) + CO(s_2) \rightarrow CH_3(s) + CO_2(s_2)$	4.75611E+09	0.50	27.88
396	$CO_2(s_2) + CH_3(s) \rightarrow CH_3O(s) + CO(s_2)$	5.58743E+09	0.50	46.01
397	$OH(s) + CO(s_2) \rightarrow COOH(s) + 2\ s$	4.96572E+09	0.50	48.96
398	$COOH(s) + 2\ s \rightarrow CO(s_2) + OH(s)$	6.48603E+08	0.50	29.32
399	$s + H_2(s) + CO(s_2) \rightarrow COH(s_3) + H(s)$	1.05821E+10	0.50	122.55
400	$H(s) + COH(s_3) \rightarrow CO(s_2) + H_2(s) + s$	1.44796E+10	0.50	49.27
401	$CO_2(s_2) \rightarrow CO_2 + 2\ s$	4.99858E+07	1.00	15.10
402	$CO_2 + 2\ s \rightarrow CO_2(s_2)$	3.86874E+08	0.00	0.00
403	$H(s) + CH_3OH(s) \rightarrow CH_4 + OH(s) + s$	1.53610E+10	0.50	12.52
404	$s + OH(s) + CH_4 \rightarrow CH_3OH(s) + H(s)$	1.89891E+11	-0.50	7.35
405	$H(s) + CH_3OH(s) \rightarrow CH_2OH(s) + H_2(s)$	1.53610E+10	0.50	49.11
406	$CH_2OH(s) + H_2(s) \rightarrow CH_3OH(s) + H(s)$	1.10366E+10	0.50	0.00
407	$O(s) + CH_3OH(s) \rightarrow CH_2OH(s) + OH(s)$	5.03071E+09	0.50	14.03
408	$CH_2OH(s) + OH(s) \rightarrow CH_3OH(s) + O(s)$	5.07843E+09	0.50	37.95
409	$H(s) + CH_3O(s) \rightarrow CH_3OH + 2\ s$	1.44009E+10	0.50	34.79
410	$CH_3OH + 2\ s \rightarrow CH_3O(s) + H(s)$	1.92946E+08	-0.50	35.47
411	$H(s) + CH_3O(s) \rightarrow CH_3(s) + OH(s)$	1.44009E+10	0.50	38.18
412	$CH_3(s) + OH(s) \rightarrow CH_3O(s) + H(s)$	5.53948E+09	0.50	57.77
413	$CH_3O(s) + H_2O(s) \rightarrow CH_3OH(s) + OH(s)$	5.11649E+09	0.50	11.21
414	$OH(s) + CH_3OH(s) \rightarrow CH_3O(s) + H_2O(s)$	5.32122E+09	0.50	24.30
415	$H(s) + CH_3O(s) \rightarrow CH_4 + O(s) + s$	1.44009E+10	0.50	42.02
416	$s + O(s) + CH_4 \rightarrow CH_3O(s) + H(s)$	1.09186E+11	-0.50	35.18
417	$H(s) + CH_3O(s) \rightarrow CH_3OH(s) + s$	1.44009E+10	0.50	34.79
418	$s + CH_3OH(s) \rightarrow CH_3O(s) + H(s)$	3.05521E+09	0.50	79.57
419	$CH_3O(s) \rightarrow CH_2O + H(s)$	2.08366E+10	1.00	0.00
420	$H(s) + CH_2O \rightarrow CH_3O(s)$	3.54884E+09	-0.50	40.29
421	$H(s) + CH_3O(s) \rightarrow CH_2O(s) + H_2(s)$	1.44009E+10	0.50	49.10
422	$CH_2O(s) + H_2(s) \rightarrow CH_3O(s) + H(s)$	1.10178E+10	0.50	42.94
423	$s + CH_3O(s) \rightarrow CH_2O(s) + H(s)$	2.93637E+09	0.50	0.00
424	$CH_2O(s) + H(s) \rightarrow CH_3O(s) + s$	1.44089E+10	0.50	33.05
425	$H(s) + CH_2OH(s) \rightarrow CH_3OH + 2\ s$	1.44461E+10	0.50	36.70
426	$CH_3OH + 2\ s \rightarrow CH_2OH(s) + H(s)$	1.95388E+08	-0.50	20.59
427	$CH_2OH(s) \rightarrow CH_2OH + s$	2.36220E+10	1.00	160.00
428	$s + CH_2OH \rightarrow CH_2OH(s)$	1.13896E+09	-0.50	0.00
429	$H(s) + CH_2OH(s) \rightarrow CH_3(s) + OH(s)$	1.44461E+10	0.50	42.16
430	$OH(s) + CH_3(s) \rightarrow CH_2OH(s) + H(s)$	5.53948E+09	0.50	47.39
431	$CH_2OH(s) + H_2O(s) \rightarrow CH_3OH(s) + OH(s)$	5.12966E+09	0.50	17.78
432	$OH(s) + CH_3OH(s) \rightarrow CH_2OH(s) + H_2O(s)$	5.32122E+09	0.50	15.83
433	$H(s) + CH_2OH(s) \rightarrow CH_3OH(s) + s$	1.44461E+10	0.50	36.70
434	$s + CH_3OH(s) \rightarrow CH_2OH(s) + H(s)$	3.05521E+09	0.50	64.69
435	$CH_2OH(s) \rightarrow CH_2O + H(s)$	2.08366E+10	1.00	12.09

#	**Reaction**			A	β	E_A
436	$H(s) + CH_2O$	$\rightarrow$	$CH_2OH(s)$	3.59376E+09	-0.50	15.29
437	$H(s) + CH_2OH(s)$	$\rightarrow$	$CH_2O(s) + H_2(s)$	1.44461E+10	0.50	55.41
438	$CH_2O(s) + H_2(s)$	$\rightarrow$	$CH_2OH(s) + H(s)$	1.10178E+10	0.50	28.69
439	$O(s) + CH_2OH(s)$	$\rightarrow$	$CH_2O + OH(s) + s$	4.77901E+09	0.50	36.81
440	$s + OH(s) + CH_2O$	$\rightarrow$	$CH_2OH(s) + O(s)$	6.89087E+09	-0.50	49.07
441	$CH_2OH(s) + 2\,s$	$\rightarrow$	$CHOH(s_2) + H(s)$	7.36089E+08	0.50	79.28
442	$H(s) + CHOH(s_2)$	$\rightarrow$	$CH_2OH(s) + 2\,s$	1.46587E+10	0.50	39.75
443	$s + H(s) + CH_2OH(s)$	$\rightarrow$	$CHOH(s_2) + H_2(s)$	1.44461E+10	0.50	79.54
444	$H_2(s) + CHOH(s_2)$	$\rightarrow$	$CH_2OH(s) + H(s) + s$	1.11917E+10	0.50	8.05
445	$s + CH_2OH(s)$	$\rightarrow$	$CH_2O(s) + H(s)$	2.94435E+09	0.50	12.09
446	$CH_2O(s) + H(s)$	$\rightarrow$	$CH_2OH(s) + s$	1.44089E+10	0.50	23.14
447	$CH_2O(s) + H(s)$	$\rightarrow$	$CH_2OH + 2\,s$	1.44089E+10	0.50	23.14
448	$CH_2OH + 2\,s$	$\rightarrow$	$CH_2O(s) + H(s)$	1.21150E+08	-0.50	0.00
449	$CH_2O(s)$	$\rightarrow$	$CH_2O + s$	2.52101E+10	1.00	46.70
450	$s + CH_2O$	$\rightarrow$	$CH_2O(s)$	2.05161E+09	-0.50	0.00
451	$s + CH_2O(s)$	$\rightarrow$	$CHO(s) + H(s)$	2.98841E+09	0.50	47.23
452	$CHO(s) + H(s)$	$\rightarrow$	$CH_2O(s) + s$	1.43087E+10	0.50	47.96
453	$H(s) + CH_2O(s)$	$\rightarrow$	$CHO(s) + H_2(s)$	1.44089E+10	0.50	33.26
454	$CHO(s) + H_2(s)$	$\rightarrow$	$CH_2O(s) + H(s)$	1.09557E+10	0.50	0.00
455	$O(s) + CH_2O(s)$	$\rightarrow$	$CHO(s) + OH(s)$	4.79404E+09	0.50	0.00
456	$CHO(s) + OH(s)$	$\rightarrow$	$CH_2O(s) + O(s)$	5.09820E+09	0.50	49.81
457	$OH(s) + CH_2O(s)$	$\rightarrow$	$CHO(s) + H_2O(s)$	5.09689E+09	0.50	0.00
458	$CHO(s) + H_2O(s)$	$\rightarrow$	$CH_2O(s) + OH(s)$	5.15363E+09	0.50	33.83
459	$OH(s) + CH_2O(s)$	$\rightarrow$	$CHO(s) + H_2O + s$	5.09689E+09	0.50	0.00
460	$s + CHO(s) + H_2O$	$\rightarrow$	$CH_2O(s) + OH(s)$	6.80071E+10	-0.50	0.31
461	$CHOH(s_2) + 2\,s$	$\rightarrow$	$COH(s_3) + H(s)$	7.58334E+08	0.50	41.43
462	$H(s) + COH(s_3)$	$\rightarrow$	$CHOH(s_2) + 2\,s$	1.44796E+10	0.50	87.34
463	$CHOH(s_2)$	$\rightarrow$	$CHO(s) + H(s)$	2.08366E+10	1.00	16.35
464	$H(s) + CHO(s)$	$\rightarrow$	$CHOH(s_2)$	1.43087E+10	0.50	70.28
465	$s + H(s) + CHOH(s_2)$	$\rightarrow$	$COH(s_3) + H_2(s)$	1.46587E+10	0.50	46.74
466	$H_2(s) + COH(s_3)$	$\rightarrow$	$CHOH(s_2) + H(s) + s$	1.10747E+10	0.50	56.33
467	$H(s) + CHOH(s_2)$	$\rightarrow$	$CHO(s) + H_2(s) + s$	1.46587E+10	0.50	45.20
468	$s + H_2(s) + CHO(s)$	$\rightarrow$	$CHOH(s_2) + H(s)$	1.09557E+10	0.50	59.55
469	$CHO(s) + 2\,s$	$\rightarrow$	$CO(s_2) + H(s)$	7.55853E+08	0.50	0.00
470	$CO(s_2) + H(s)$	$\rightarrow$	$CHO(s) + 2\,s$	1.37609E+10	0.50	102.88
471	$H(s) + CHO(s)$	$\rightarrow$	$CO + H_2(s) + s$	1.43087E+10	0.50	0.00
472	$s + H_2(s) + CO$	$\rightarrow$	$CHO(s) + H(s)$	6.89865E+08	0.00	109.61
473	$s + H(s) + CHO(s)$	$\rightarrow$	$CO(s_2) + H_2(s)$	1.43087E+10	0.50	0.00
474	$CO(s_2) + H_2(s)$	$\rightarrow$	$CHO(s) + H(s) + s$	1.05821E+10	0.50	97.72
475	$H(s) + CHO(s)$	$\rightarrow$	$CO(s_2) + H_2$	1.43087E+10	0.50	0.00
476	$CO(s_2) + H_2$	$\rightarrow$	$CHO(s) + H(s)$	6.41855E+10	0.00	78.46
477	$s + O(s) + CHO(s)$	$\rightarrow$	$CO(s_2) + OH(s)$	4.79132E+09	0.50	0.00
478	$CO(s_2) + OH(s)$	$\rightarrow$	$CHO(s) + O(s) + s$	4.96572E+09	0.50	145.34
479	$s + OH(s) + CHO(s)$	$\rightarrow$	$CO(s_2) + H_2O(s)$	5.09820E+09	0.50	0.00
480	$CO(s_2) + H_2O(s)$	$\rightarrow$	$CHO(s) + OH(s) + s$	5.02610E+09	0.50	135.45
481	$COH(s_3)$	$\rightarrow$	$CO(s_2) + H(s)$	2.08366E+10	1.00	0.00
482	$H(s) + CO(s_2)$	$\rightarrow$	$COH(s_3)$	1.37609E+10	0.50	67.43
483	$COOH(s) + 2\,s$	$\rightarrow$	$CO_2(s_2) + H(s)$	6.48603E+08	0.50	0.00
484	$H(s) + CO_2(s_2)$	$\rightarrow$	$COOH(s) + 2\,s$	1.53187E+10	0.50	14.10
485	$s + H(s) + COOH(s)$	$\rightarrow$	$CO(s_2) + H_2O(s)$	1.53322E+10	0.50	39.14
486	$H_2O(s) + CO(s_2)$	$\rightarrow$	$COOH(s) + H(s) + s$	5.02610E+09	0.50	80.41

#	**Reaction**			A	β	E_A
487	s + O(s) + COOH(s)	→	$CO_2(s_2)$ + OH(s)	4.80082E+09	0.50	44.20
488	OH(s) + $CO_2(s_2)$	→	COOH(s) + O(s) + s	5.07670E+09	0.50	104.24
489	s + OH(s) + COOH(s)	→	$CO_2(s_2)$ + H_2O(s)	5.06567E+09	0.50	39.44
490	H_2O(s) + $CO_2(s_2)$	→	COOH(s) + OH(s) + s	5.10838E+09	0.50	80.68
491	s + H_2	→	H_2(s)	3.48078E+10	0.00	0.00
492	H_2(s)	→	H_2 + s	3.16156E+10	1.00	26.80
493	s + O(s) + H_2	→	H(s) + OH(s)	4.17970E+10	0.00	0.00
494	OH(s) + H(s)	→	H_2 + O(s) + s	1.24298E+10	0.50	98.82
495	$O_2(s_2)$ + H_2	→	H(s) + OOH(s)	1.32798E+11	0.00	0.00
496	OOH(s) + H(s)	→	H_2 + $O_2(s_2)$	1.39551E+10	0.50	112.76
497	O_2 + 2 s	→	$O_2(s_2)$	7.92136E+08	0.00	0.00
498	$O_2(s_2)$	→	O_2 + 2 s	1.91839E+10	1.00	44.30
499	s + H(s) + O_2	→	O(s) + OH(s)	6.28814E+08	0.00	0.00
500	OH(s) + O(s)	→	H(s) + O_2 + s	4.66121E+09	0.50	159.53
501	O_2 + 2 s	→	2 O(s)	2.03469E+08	0.00	0.00
502	2 O(s)	→	O_2 + 2 s	4.26627E+09	0.50	143.87
503	H(s) + O_2	→	OOH(s)	1.30300E+09	0.00	0.00
504	OOH(s)	→	H(s) + O_2	2.08366E+10	1.00	73.94
505	s + OH	→	OH(s)	5.32909E+09	0.00	0.00
506	OH(s)	→	OH + s	3.25484E+10	1.00	247.00
507	s + O	→	O(s)	1.89986E+08	1.00	0.00
508	O(s)	→	O + s	3.12808E+10	1.00	356.00
509	s + O(s) + H_2O	→	2 OH(s)	2.81013E+10	-0.50	6.26
510	2 OH(s)	→	H_2O + O(s) + s	5.03981E+09	0.50	66.24
511	s + H(s) + H_2O	→	H_2(s) + OH(s)	1.75147E+10	-0.50	13.15
512	OH(s) + H_2(s)	→	H_2O + H(s) + s	9.77616E+09	0.50	0.00
513	s + HO_2	→	OOH(s)	2.05387E+09	-0.50	0.00
514	OOH(s)	→	HO_2 + s	2.60085E+10	1.00	204.00
515	HO_2 + 2 s	→	O(s) + OH(s)	2.47795E+08	-0.50	0.00
516	OH(s) + O(s)	→	HO_2 + 2 s	4.66121E+09	0.50	112.23
517	HO_2 + 3 s	→	H(s) + $O_2(s_2)$	1.37866E+08	-0.50	110.13
518	H(s) + $O_2(s_2)$	→	HO_2 + 3 s	1.35635E+10	0.50	0.00
519	H_2O_2 + 2 s	→	$H_2O_2(s_2)$	2.70654E+09	-0.50	0.00
520	$H_2O_2(s_2)$	→	H_2O_2 + 2 s	7.12037E+09	1.00	27.10
521	s + H(s) + H_2O_2	→	H_2O(s) + OH(s)	4.59391E+08	-0.50	0.00
522	H_2O(s) + OH(s)	→	H_2O_2 + H(s) + s	5.13543E+09	0.50	146.51
523	H_2O_2 + 2 s	→	2 OH(s)	1.04903E+08	-0.50	0.00
524	2 OH(s)	→	H_2O_2 + 2 s	5.03981E+09	0.50	160.96
525	H_2O_2 + 2 s	→	H_2O(s) + O(s)	1.54095E+08	-0.50	0.00
526	H_2O(s) + O(s)	→	H_2O_2 + 2 s	4.76774E+09	0.50	119.41
527	s + H(s) + H_2O_2	→	H_2(s) + OOH(s)	6.48039E+08	-0.50	0.00
528	OOH(s) + H_2(s)	→	H_2O_2 + H(s) + s	1.06844E+10	0.50	17.72
529	O(s) + H_2(s)	→	H(s) + OH(s)	8.84834E+09	0.50	8.52
530	OH(s) + H(s)	→	H_2(s) + O(s)	1.24298E+10	0.50	98.82
531	s + H_2(s)	→	2 H(s)	8.92735E+09	0.50	40.13
532	2 H(s)	→	H_2(s) + s	1.34184E+10	0.50	73.96
533	H(s) + $O_2(s_2)$	→	O(s) + OH(s) + s	1.35635E+10	0.50	0.00
534	s + OH(s) + O(s)	→	H(s) + $O_2(s_2)$	4.66121E+09	0.50	159.53
535	$O_2(s_2)$	→	2 O(s)	2.08366E+10	1.00	4.33
536	2 O(s)	→	$O_2(s_2)$	4.26627E+09	0.50	143.87
537	H(s) + $O_2(s_2)$	→	OOH(s) + 2 s	1.35635E+10	0.50	0.00

#	**Reaction**	A	β	E_A
538	$OOH(s) + 2\,s \rightarrow H(s) + O_2(s_2)$	6.94856E+08	0.50	73.94
539	$O(s) + H(s) \rightarrow OH + 2\,s$	1.10870E+10	0.50	52.01
540	$OH + 2\,s \rightarrow H(s) + O(s)$	1.28517E+09	0.00	65.87
541	$H_2O(s) + O(s) \rightarrow 2\,OH(s)$	4.76774E+09	0.50	38.87
542	$2\,OH(s) \rightarrow H_2O(s) + O(s)$	5.03981E+09	0.50	66.24
543	$O(s) + H(s) \rightarrow OH(s) + s$	1.10870E+10	0.50	52.01
544	$s + OH(s) \rightarrow H(s) + O(s)$	3.46268E+09	0.50	107.22
545	$OH(s) + H(s) \rightarrow H_2O(s) + s$	1.24298E+10	0.50	47.77
546	$s + H_2O(s) \rightarrow H(s) + OH(s)$	3.47731E+09	0.50	80.38
547	$OH(s) + H(s) \rightarrow H_2O + 2\,s$	1.24298E+10	0.50	47.77
548	$H_2O + 2\,s \rightarrow H(s) + OH(s)$	5.87502E+09	-0.50	40.18
549	$2\,H(s) \rightarrow H_2 + 2\,s$	1.34184E+10	0.50	73.96
550	$H_2 + 2\,s \rightarrow 2\,H(s)$	8.42938E+09	0.00	13.34
551	$H(s) \rightarrow H + s$	3.51899E+10	1.00	255.00
552	$s + H \rightarrow H(s)$	1.89986E+08	1.00	0.00
553	$H_2O_2(s_2) + H(s) \rightarrow H_2O + OH(s) + 2\,s$	1.43342E+10	0.50	0.00
554	$OH(s) + H_2O + 2\,s \rightarrow H_2O_2(s_2) + H(s)$	2.16617E+11	-0.50	117.91
555	$OOH(s) + H(s) \rightarrow H_2O + O(s) + s$	1.39551E+10	0.50	0.00
556	$s + O(s) + H_2O \rightarrow H(s) + OOH(s)$	5.82302E+10	-0.50	96.65
557	$OOH(s) + H(s) \rightarrow H_2O_2 + 2\,s$	1.39551E+10	0.50	74.58
558	$H_2O_2 + 2\,s \rightarrow H(s) + OOH(s)$	2.17374E+08	-0.50	0.00
559	$H_2O(s) + H(s) \rightarrow H_2(s) + OH(s)$	1.29285E+10	0.50	45.20
560	$OH(s) + H_2(s) \rightarrow H_2O(s) + H(s)$	9.77616E+09	0.50	0.00
561	$OOH(s) + H(s) \rightarrow H_2O(s) + O(s)$	1.39551E+10	0.50	0.00
562	$H_2O(s) + O(s) \rightarrow H(s) + OOH(s)$	4.76774E+09	0.50	125.16
563	$H_2O_2(s_2) + H(s) \rightarrow H_2O(s) + OH(s) + s$	1.43342E+10	0.50	0.00
564	$s + H_2O(s) + OH(s) \rightarrow H_2O_2(s_2) + H(s)$	5.13543E+09	0.50	146.51
565	$OOH(s) + H(s) \rightarrow 2\,OH(s)$	1.39551E+10	0.50	0.00
566	$2\,OH(s) \rightarrow H(s) + OOH(s)$	5.03981E+09	0.50	126.95
567	$OOH(s) + H(s) \rightarrow H_2O_2(s_2)$	1.39551E+10	0.50	74.58
568	$H_2O_2(s_2) \rightarrow H(s) + OOH(s)$	2.08366E+10	1.00	23.92
569	$H_2O(s) \rightarrow H_2O + s$	3.23181E+10	1.00	40.20
570	$s + H_2O \rightarrow H_2O(s)$	3.45201E+10	-0.50	0.00
571	$s + OOH(s) \rightarrow O(s) + OH(s)$	2.77942E+09	0.50	10.38
572	$OH(s) + O(s) \rightarrow OOH(s) + s$	4.66121E+09	0.50	112.23
573	$H_2O_2(s_2) \rightarrow 2\,OH(s)$	2.08366E+10	1.00	0.00
574	$2\,OH(s) \rightarrow H_2O_2(s_2)$	5.03981E+09	0.50	160.96
575	$H_2O_2(s_2) \rightarrow H_2O(s) + O(s)$	2.08366E+10	1.00	0.00
576	$H_2O(s) + O(s) \rightarrow H_2O_2(s_2)$	4.76774E+09	0.50	119.41
577	$N_2O + 2\,s \rightarrow N_2O(s_2)$	7.16064E+09	-0.50	0.00
578	$N_2O(s_2) \rightarrow N_2O + 2\,s$	1.34252E+10	1.00	72.57
579	$N_2O(s_2) + 2\,s \rightarrow N(s) + NO(s_3)$	6.40833E+08	0.50	7.69
580	$NO(s_3) + N(s) \rightarrow N_2O(s_2) + 2\,s$	4.70745E+09	0.50	45.49
581	$N_2O + 3\,s \rightarrow N_2(s_2) + O(s)$	2.86198E+07	-0.50	0.00
582	$O(s) + N_2(s_2) \rightarrow N_2O + 3\,s$	4.59599E+09	0.50	132.73
583	$NO + 3\,s \rightarrow NO(s_3)$	1.94052E+10	0.00	0.00
584	$NO(s_3) \rightarrow NO + 3\,s$	2.17814E+09	1.00	71.76
585	$NO + 2\,s \rightarrow N(s) + O(s)$	1.18545E+08	0.00	0.00
586	$O(s) + N(s) \rightarrow NO + 2\,s$	4.45895E+09	0.50	161.29
587	$N_2 + 2\,s \rightarrow N_2(s_2)$	6.65374E+08	0.00	0.00
588	$N_2(s_2) \rightarrow N_2 + 2\,s$	1.10244E+10	1.00	45.23

#	Reaction	A	β	E_A
589	$N_2 + 2\,s \rightarrow 2\,N(s)$	2.75883E+08	0.00	86.05
590	$2\,N(s) \rightarrow N_2 + 2\,s$	4.64959E+09	0.50	104.72
591	$N_2(s_2) \rightarrow 2\,N(s)$	2.08366E+10	1.00	131.28
592	$2\,N(s) \rightarrow N_2(s_2)$	4.64959E+09	0.50	104.72
593	$s + NO_2 \rightarrow NO_2(s)$	1.34133E+09	-0.50	0.00
594	$NO_2(s) \rightarrow NO_2 + s$	1.48835E+10	1.00	41.16
595	$NO_2(s) + 3\,s \rightarrow NO(s_3) + O(s)$	9.01317E+07	0.50	0.00
596	$O(s) + NO(s_3) \rightarrow NO_2(s) + 3\,s$	4.46634E+09	0.50	57.91
597	$s + N \rightarrow N(s)$	1.89986E+08	1.00	0.00
598	$N(s) \rightarrow N + s$	3.29696E+10	1.00	485.33
599	$N_2O(s_2) + O \rightarrow N(s) + NO_2(s)$	2.04982E+09	1.00	32.31
600	$N(s) + NO_2(s) \rightarrow N_2O(s_2) + O$	4.79495E+09	0.50	13.24
601	$O_2(s_2) + NO \rightarrow NO_2(s) + O(s)$	3.78737E+09	0.00	0.00
602	$O(s) + NO_2(s) \rightarrow NO + O_2(s_2)$	4.52578E+09	0.50	54.20
603	$N_2(s_2) + O \rightarrow N_2O(s_2)$	3.16605E+10	1.00	251.05
604	$N_2O(s_2) \rightarrow N_2(s_2) + O$	2.08366E+10	1.00	0.00
605	$O(s) + NO_2(s) + 3\,s \rightarrow NO(s_3) + O_2(s_2)$	1.67622E+08	0.50	54.20
606	$O_2(s_2) + NO(s_3) \rightarrow NO_2(s) + O(s) + 3\,s$	4.33016E+09	0.50	0.00
607	$N(s) + NO_2(s) + 4\,s \rightarrow 2\,NO(s_3)$	1.87303E+07	0.50	61.40
608	$2\,NO(s_3) \rightarrow N(s) + NO_2(s) + 4\,s$	4.33450E+09	0.50	0.00
609	$s + O(s) + N_2O(s_2) \rightarrow N_2(s_2) + O_2(s_2)$	4.69799E+09	0.50	0.00
610	$O_2(s_2) + N_2(s_2) \rightarrow N_2O(s_2) + O(s) + s$	4.47063E+09	0.50	64.05
611	$N(s) + N_2O(s_2) + 2\,s \rightarrow N_2(s_2) + NO(s_3)$	1.24337E+09	0.50	0.00
612	$N_2(s_2) + NO(s_3) \rightarrow N_2O(s_2) + N(s) + 2\,s$	4.47357E+09	0.50	57.22
613	$NO(s_3) \rightarrow N(s) + O(s) + s$	2.08366E+10	1.00	10.68
614	$s + N(s) + O(s) \rightarrow NO(s_3)$	4.45895E+09	0.50	161.29
615	$N(s) + NO(s_3) \rightarrow N_2(s_2) + O(s) + s$	4.70745E+09	0.50	0.00
616	$s + O(s) + N_2(s_2) \rightarrow N(s) + NO(s_3)$	4.59599E+09	0.50	120.61
617	$O(s) + NO(s_3) \rightarrow N(s) + O_2(s_2) + s$	4.46634E+09	0.50	20.04
618	$s + N(s) + O_2(s_2) \rightarrow NO(s_3) + O(s)$	4.74084E+09	0.50	23.42
619	$C_3H_6 + 2\,s \rightarrow C_3H_6(s_2)$	1.33006E+14	-0.50	39.40
620*	$C_3H_6(s_2) \rightarrow C_3H_6 + 2\,s$	1.25250E-09	1.00	39.13
621	$C_3H_6(s_2) \rightarrow CH_3(s) + CHCH_2(s)$	2.08366E+10	1.00	100.47
622*	$CH_3(s) + CHCH_2(s) \rightarrow C_3H_6(s_2)$	6.13949E-09	0.50	0.00
623	$s + C_3H_5a \rightarrow C_3H_5(s)$	4.21289E+09	-0.50	0.00
624	$C_3H_5(s) \rightarrow C_3H_5a + s$	1.10134E+11	1.00	41.52
625	$C_3H_5(s) + 4\,s \rightarrow CCH_3(s_3) + CH_2(s_2)$	1.32573E+07	0.50	113.74
626	$CH_2(s_2) + CCH_3(s_3) \rightarrow C_3H_5(s) + 4\,s$	6.02307E+09	0.50	60.54
627	$C_3H_5(s) + 2\,s \rightarrow CH_2(s_2) + CHCH_2(s)$	8.48464E+08	0.50	85.98
628	$CH_2(s_2) + CHCH_2(s) \rightarrow C_3H_5(s) + 2\,s$	6.28757E+09	0.50	37.66
629	$C_3H_5(s) + 3\,s \rightarrow C_2H_2(s_3) + CH_3(s)$	1.25698E+08	0.50	0.00
630	$CH_3(s) + C_2H_2(s_3) \rightarrow C_3H_5(s) + 2\,s$	6.35120E+09	0.50	63.07
631	$C_3H_5(s) + 3\,s \rightarrow C(s_3) + CH_2CH_3(s)$	1.25698E+08	0.50	6.70
632	$C(s_3) + CH_2CH_3(s) \rightarrow C_3H_5(s) + 3\,s$	6.03919E+09	0.50	101.66
633	$O(s) + C_3H_5a + 3\,s \rightarrow C_2H_4(s) + COH(s_3)$	4.69320E+08	-0.50	0.00
634	$C_2H_4(s) + COH(s_3) \rightarrow C_3H_5a + O(s) + 3\,s$	5.37732E+09	0.50	97.43
635	$OH(s) + C_3H_5a + 3\,s \rightarrow CHCH_3(s_2) + CHOH(s_2)$	3.89821E+07	-0.50	34.44
636	$CHCH_3(s_2) + CHOH(s_2) \rightarrow C_3H_5a + OH(s) + 3\,s$	5.38703E+09	0.50	45.46
637	$OH(s) + C_3H_5(s) \rightarrow C_3H_6 + O(s) + s$	6.38270E+09	0.50	0.00

*Removed reaction

#	Reaction	A	β	E_A
638	$s + O(s) + C_3H_6 \rightarrow C_3H_5(s) + OH(s)$	1.70040E+10	-0.50	15.39
639	$C_3H_6(s_2) \rightarrow C_3H_5(s) + H(s)$	2.08366E+10	1.00	87.68
640	$H(s) + C_3H_5(s) \rightarrow C_3H_6(s_2)$	1.97271E+10	0.50	0.00

Table A.3: Detailed C_3H_6 reaction sub-mechanism corresponding to $\theta = 12\%$ [99] of the magnitude of $Q_{C,H,O,N}$.

#	Reaction	A	β	E_A
1	$C_3H_6 + 2\,s \rightarrow C_3H_6(s_2)$	3.55043E+10	-0.50	0.00
2	$C_3H_6(s_2) \rightarrow C_3H_6 + 2\,s$	1.25250E+09	1.00	39.13
3	$C_3H_6(s_2) \rightarrow CH_3(s) + CHCH_2(s)$	2.08366E+10	1.00	100.47
4	$CH_3(s) + CHCH_2(s) \rightarrow C_3H_6(s_2)$	6.13949E+09	0.50	0.00
5	$s + C_3H_5a \rightarrow C_3H_5(s)$	4.21289E+09	-0.50	0.00
6	$C_3H_5(s) \rightarrow C_3H_5a + s$	1.10134E+11	1.00	41.52
7	$C_3H_5(s) + 4\,s \rightarrow CCH_3(s_3) + CH_2(s_2)$	1.32573E+07	0.50	113.74
8	$CH_2(s_2) + CCH_3(s_3) \rightarrow C_3H_5(s) + 4\,s$	6.02307E+09	0.50	47.31
9	$C_3H_5(s) + 2\,s \rightarrow CH_2(s_2) + CHCH_2(s)$	8.48464E+08	0.50	85.98
10	$CH_2(s_2) + CHCH_2(s) \rightarrow C_3H_5(s) + 2\,s$	6.28757E+09	0.50	26.16
11	$C_3H_5(s) + 3\,s \rightarrow C_2H_2(s_3) + CH_3(s)$	1.25698E+08	0.50	0.00
12	$CH_3(s) + C_2H_2(s_3) \rightarrow C_3H_5(s) + 2\,s$	6.35120E+09	0.50	65.12
13	$C_3H_5(s) + 3\,s \rightarrow C(s_3) + CH_2CH_3(s)$	1.25698E+08	0.50	6.70
14	$C(s_3) + CH_2CH_3(s) \rightarrow C_3H_5(s) + 3\,s$	6.03919E+09	0.50	104.20
15	$O(s) + C_3H_5a + 3\,s \rightarrow C_2H_4(s) + COH(s_3)$	4.69320E+08	-0.50	0.00
16	$C_2H_4(s) + COH(s_3) \rightarrow C_3H_5a + O(s) + 3\,s$	5.37732E+09	0.50	101.82
17	$OH(s) + C_3H_5a + 3\,s \rightarrow CHCH_3(s_2) + CHOH(s_2)$	3.89821E+07	-0.50	34.44
18	$CHCH_3(s_2) + CHOH(s_2) \rightarrow C_3H_5a + OH(s) + 3\,s$	5.38703E+09	0.50	37.29
19	$OH(s) + C_3H_5(s) \rightarrow C_3H_6 + O(s) + s$	6.38270E+09	0.50	0.00
20	$s + O(s) + C_3H_6 \rightarrow C_3H_5(s) + OH(s)$	1.70040E+10	-0.50	15.39
21	$C_3H_6(s_2) \rightarrow C_3H_5(s) + H(s)$	2.08366E+10	1.00	87.68
22	$H(s) + C_3H_5(s) \rightarrow C_3H_6(s_2)$	1.97271E+10	0.50	0.00
23	$C_3H_6 + 2\,s \rightarrow C_2H_5CH(s_2)$	9.82480E+10	-0.50	0.00
24	$C_2H_5CH(s_2) \rightarrow C_3H_6 + 2\,s$	1.35849E+10	1.00	84.33
25*	$C_3H_6(s_2) \rightarrow C_2H_5CH(s_2)$	2.08366E-10	1.00	0.00
26*	$C_2H_5CH(s_2) \rightarrow C_3H_6(s_2)$	2.08366E-10	1.00	0.00
27	$C_2H_5CH(s_2) + 2\,s \rightarrow CH_2CH_3(s) + CH(s_3)$	8.22495E+08	0.50	47.67
28	$CH(s_3) + CH_2CH_3(s) \rightarrow C_2H_5CH(s_2) + 2\,s$	6.26159E+09	0.50	56.93
29	$C_2H_5CH(s_2) + 2\,s \rightarrow C_2H_5C(s_3) + H(s)$	8.22495E+08	0.50	104.79
30	$H(s) + C_2H_5C(s_3) \rightarrow C_2H_5CH(s_2) + 2\,s$	2.07501E+10	0.50	0.00
31	$s + C_2H_5C(s_3) \rightarrow C(s_3) + CH_2CH_3(s)$	3.55218E+09	0.50	0.00
32	$C(s_3) + CH_2CH_3(s) \rightarrow C_2H_5C(s_3) + s$	6.03919E+09	0.50	185.95
33	$C_3H_6 + 4\,s \rightarrow C_2H_5C(s_3) + H(s)$	5.41354E+09	-0.50	156.58
34	$H(s) + C_2H_5C(s_3) \rightarrow C_3H_6 + 4\,s$	2.07501E+10	0.50	0.00
35	$O(s) + C_2H_5CH(s_2) \rightarrow CH_2CH_3(s) + CHO(s) + s$	6.00026E+09	0.50	0.00
36	$s + CHO(s) + CH_2CH_3(s) \rightarrow C_2H_5CH(s_2) + O(s)$	5.29470E+09	0.50	132.81
37	$OH(s) + C_2H_5CH(s_2) \rightarrow CH_2CH_3(s) + CH_2O(s) + s$	6.24300E+09	0.50	0.00
38	$s + CH_2O(s) + CH_2CH_3(s) \rightarrow C_2H_5CH(s_2) + OH(s)$	5.27471E+09	0.50	101.70
39	$O(s) + C_2H_5C(s_3) \rightarrow CH_2CH_3(s) + CO(s_2) + s$	6.43992E+09	0.50	0.00

*Removed reaction

#	Reaction			A	β	E_A
40	s + $CO(s_2)$ + $CH_2CH_3(s)$	→	$C_2H_5C(s_3)$ + O(s)	5.20069E+09	0.50	285.20
41	OH(s) + $C_2H_5C(s_3)$	→	$CH_2CH_3(s)$ + CHO(s) + 2 s	6.67484E+09	0.50	0.00
42	CHO(s) + $CH_2CH_3(s)$ + 2 s	→	$C_2H_5C(s_3)$ + OH(s)	1.32368E+09	0.50	169.33

Table A.4: Detailed C_3H_6 reaction sub-mechanism corresponding to $\theta = 20\%$ [100] of the magnitude of $Q_{C,H,O,N}$.

#	Reaction			A	β	E_A
1	C_3H_6 + 2 s	→	$C_3H_6(s_2)$	3.55043E+10	-0.50	0.00
2	$C_3H_6(s_2)$	→	C_3H_6 + 2 s	1.25250E+09	1.00	39.13
3	$C_3H_6(s_2)$	→	$CH_3(s)$ + $CHCH_2(s)$	2.08366E+10	1.00	100.47
4	$CH_3(s)$ + $CHCH_2(s)$	→	$C_3H_6(s_2)$	6.13949E+09	0.50	0.00
5	s + C_3H_5a	→	$C_3H_5(s)$	4.21289E+09	-0.50	0.00
6	$C_3H_5(s)$	→	C_3H_5a + s	1.10134E+11	1.00	41.52
7	$C_3H_5(s)$ + 4 s	→	$CCH_3(s_3)$ + $CH_2(s_2)$	1.32573E+07	0.50	113.74
8	$CH_2(s_2)$ + $CCH_3(s_3)$	→	$C_3H_5(s)$ + 4 s	6.02307E+09	0.50	60.54
9	$C_3H_5(s)$ + 2 s	→	$CH_2(s_2)$ + $CHCH_2(s)$	8.48464E+08	0.50	85.98
10	$CH_2(s_2)$ + $CHCH_2(s)$	→	$C_3H_5(s)$ + 2 s	6.28757E+09	0.50	37.66
11	$C_3H_5(s)$ + 3 s	→	$C_2H_2(s_3)$ + $CH_3(s)$	1.25698E+08	0.50	0.00
12	$CH_3(s)$ + $C_2H_2(s_3)$	→	$C_3H_5(s)$ + 2 s	6.35120E+09	0.50	63.07
13	$C_3H_5(s)$ + 3 s	→	$C(s_3)$ + $CH_2CH_3(s)$	1.25698E+08	0.50	6.70
14	$C(s_3)$ + $CH_2CH_3(s)$	→	$C_3H_5(s)$ + 3 s	6.03919E+09	0.50	101.66
15	O(s) + C_3H_5a + 3 s	→	$C_2H_4(s)$ + $COH(s_3)$	4.69320E+08	-0.50	0.00
16	$C_2H_4(s)$ + $COH(s_3)$	→	C_3H_5a + O(s) + 3 s	5.37732E+09	0.50	97.43
17	OH(s) + C_3H_5a + 3 s	→	$CHCH_3(s_2)$ + $CHOH(s_2)$	3.89821E+07	-0.50	34.44
18	$CHCH_3(s_2)$ + $CHOH(s_2)$	→	C_3H_5a + OH(s) + 3 s	5.38703E+09	0.50	45.46
19	OH(s) + $C_3H_5(s)$	→	C_3H_6 + O(s) + s	6.38270E+09	0.50	0.00
20	s + O(s) + C_3H_6	→	$C_3H_5(s)$ + OH(s)	1.70040E+10	-0.50	15.39
21	$C_3H_6(s_2)$	→	$C_3H_5(s)$ + H(s)	2.08366E+10	1.00	87.68
22	H(s) + $C_3H_5(s)$	→	$C_3H_6(s_2)$	1.97271E+10	0.50	0.00
23	C_3H_6 + 2 s	→	$C_2H_5CH(s_2)$	9.82480E+10	-0.50	0.00
24	$C_2H_5CH(s_2)$	→	C_3H_6 + 2 s	1.35849E+10	1.00	84.33
25*	$C_3H_6(s_2)$	→	$C_2H_5CH(s_2)$	2.08366E-10	1.00	0.00
26*	$C_2H_5CH(s_2)$	→	$C_3H_6(s_2)$	2.08366E-10	1.00	0.00
27	$C_2H_5CH(s_2)$ + 2 s	→	$CH_2CH_3(s)$ + $CH(s_3)$	8.22495E+08	0.50	47.67
28	$CH(s_3)$ + $CH_2CH_3(s)$	→	$C_2H_5CH(s_2)$ + 2 s	6.26159E+09	0.50	59.76
29	$C_2H_5CH(s_2)$ + 2 s	→	$C_2H_5C(s_3)$ + H(s)	8.22495E+08	0.50	104.79
30	H(s) + $C_2H_5C(s_3)$	→	$C_2H_5CH(s_2)$ + 2 s	2.07501E+10	0.50	0.00
31	s + $C_2H_5C(s_3)$	→	$C(s_3)$ + $CH_2CH_3(s)$	3.55218E+09	0.50	0.00
32	$C(s_3)$ + $CH_2CH_3(s)$	→	$C_2H_5C(s_3)$ + s	6.03919E+09	0.50	177.76
33	C_3H_6 + 4 s	→	$C_2H_5C(s_3)$ + H(s)	5.41354E+09	-0.50	156.58
34	H(s) + $C_2H_5C(s_3)$	→	C_3H_6 + 4 s	2.07501E+10	0.50	0.00
35	O(s) + $C_2H_5CH(s_2)$	→	$CH_2CH_3(s)$ + CHO(s) + s	6.00026E+09	0.50	0.00
36	s + CHO(s) + $CH_2CH_3(s)$	→	$C_2H_5CH(s_2)$ + O(s)	5.29470E+09	0.50	126.98
37	OH(s) + $C_2H_5CH(s_2)$	→	$CH_2CH_3(s)$ + $CH_2O(s)$ + s	6.24300E+09	0.50	0.00
38	s + $CH_2O(s)$ + $CH_2CH_3(s)$	→	$C_2H_5CH(s_2)$ + OH(s)	5.27471E+09	0.50	98.01
39	O(s) + $C_2H_5C(s_3)$	→	$CH_2CH_3(s)$ + $CO(s_2)$ + s	6.43992E+09	0.50	0.00

*Removed reaction

#	**Reaction**			A	β	E_A
40	s + $CO(s_2)$ + CH_2CH_3(s)	$\rightarrow$	$C_2H_5C(s_3)$ + O(s)	5.20069E+09	0.50	276.71
41	OH(s) + $C_2H_5C(s_3)$	$\rightarrow$	CH_2CH_3(s) + CHO(s) + 2 s	6.67484E+09	0.50	0.00
42	CHO(s) + CH_2CH_3(s) + 2 s	$\rightarrow$	$C_2H_5C(s_3)$ + OH(s)	1.32368E+09	0.50	162.29

Appendix B

Surface species data

The current Appendix includes the surface species data applied in Chapter 4 for the evaluation of the surface mechanism presented in Appendix A. The -N and -C_3 containing surface species data are omitted from Chapter 5 due to the scarcity of related experimental data. The left column corresponds to adsorbed species' data, while the right one is related to the transition states. The units of vibrational frequencies v_i and rotational constants I, are given below in cm^{-1} and Hz, respectively. The rotational symmetry number σ and the Pitzer-Gwinn hindered rotor correction ν_{corr} are unitless. The heat of adsorption Q_A and the total bond energy E are both in kJ/mol. The surface area of the platinum site A_{Pt} is presented in Å^2. The Q_A, E and A_{Pt} have the same value for the adsorbed and transition state.

Adsorbed species		**Transition state**	
	$C_2H_2(s_3)$		
$\{v_i\}$:	46.0, 68.9, 155.2, 275.5, 442.6, 445.7, 582.9, 614.1, 784.0, 826.1, 929.6, 1073.2, 1279.2, 3091.5, 3110.2 [cm^{-1}]	$\{v_i\}$:	-161.7, 53.9, 64.8, 154.9, 259.2, 364.6, 541.0, 586.3, 708.3, 775.6, 887.3, 1024.7, 1331.0, 3071.7, 3188.1 [cm^{-1}]
I:	0.69, 0.47, 0.29 [Hz]	I:	0.68, 0.46, 0.29 [Hz]
σ:	2.0, v_{corr}: 1.000	σ:	1.0, v_{corr}: 1.000
	Q_A: 134.0 kJ/mol, E: 1641.0 kJ/mol, A_{Pt}: 15.3 Å^2		
	$C_2H_4(s)$		
$\{v_i\}$:	469.0, 495.6, 685.3, 795.5, 895.0, 985.7, 1003.2, 1188.6, 1203.0, 1420.6, 1498.7, 3083.4, 3089.7, 3162.7, 3182.6 [cm^{-1}]	$\{v_i\}$:	-27.5, 420.6, 513.0, 790.2, 911.4, 926.4, 960.6, 1199.0, 1222.0, 1414.8, 1506.5, 3063.1, 3136.4, 3147.9, 3242.8 [cm^{-1}]
I:	23.16, 5.13, 4.45 [Hz]	I:	25.42, 3.94, 3.58 [Hz]
σ:	4.0, v_{corr}: 1.000	σ:	2.0, v_{corr}: 1.000
	Q_A: 68.0 kJ/mol, E: 2252.7 kJ/mol, A_{Pt}: 18.1 Å^2		

	Adsorbed species		**Transition state**
	$C_2H_4(s_2)$		
$\{v_i\}$:	-24.4, 170.8, 243.5, 553.0, 613.4, 639.3, 796.7, 947.1, 1046.1, 1057.1, 1104.3, 1203.9, 1397.2, 1435.6, 3005.0, 3011.6, 3075.8, 3096.3 [cm^{-1}]	$\{v_i\}$:	-49.4, 72.4, 165.6, 294.7, 564.5, 590.8, 794.0, 904.0, 904.4, 1057.4, 1112.9, 1207.9, 1401.7, 1458.7, 3000.7, 3079.3, 3103.5, 3207.8 [cm^{-1}]
I:	4.65, 0.75, 0.65 [Hz]	I:	3.96, 0.74, 0.63 [Hz]
σ:	4.0, v_{corr}: 1.000	σ:	2.0, v_{corr}: 1.000
	Q_A: 99.0 kJ/mol, E: 2252.7 kJ/mol, A_{Pt}: 16.9 Å^2		
	$C_2H_5CH(s_2)$		
$\{v_i\}$:	67.5, 140.8, 160.0, 178.8, 246.0, 440.3, 492.0, 615.5, 736.7, 893.0, 901.7, 1013.7, 1055.4, 1106.6, 1237.0, 1260.4, 1340.4, 1391.6, 1414.6, 1457.0, 1467.7, 2971.2, 3005.5, 3014.5, 3020.5, 3103.8, 3104.5 [cm^{-1}]	$\{v_i\}$:	-66.9, 45.5, 83.4, 158.8, 241.9, 302.1, 452.2, 713.8, 742.1, 879.8, 983.6, 1039.8, 1051.3, 1175.0, 1259.2, 1320.5, 1382.9, 1416.6, 1458.4, 1465.0, 1496.2, 2826.8, 2967.2, 3016.2, 3017.3, 3097.3, 3101.5 [cm^{-1}]
I:	1.81, 0.74, 0.57 [Hz]	I:	1.94, 0.74, 0.58 [Hz]
σ:	3.0, v_{corr}: 3.197	σ:	6.0, v_{corr}: 3.117
	Q_A: 84.3 kJ/mol, E: 3208.0 kJ/mol, A_{Pt}: 25.1 Å^2		
	$C_2H_5C(s_3)$		
$\{v_i\}$:	22.0, 31.5, 76.1, 102.0, 145.0, 168.0, 277.8, 291.1, 352.9, 376.3, 405.8, 478.1, 534.3, 647.3, 801.8, 986.0, 1004.7, 1022.8, 1231.8, 1292.9, 1410.2, 1634.7, 2102.3, 2291.7, 3115.2, 3149.4, 3225.3 [cm^{-1}]	$\{v_i\}$:	-60.2, 30.9, 36.7, 81.3, 96.3, 124.0, 191.6, 203.6, 232.8, 285.5, 410.3, 436.8, 465.4, 552.3, 627.2, 867.9, 915.2, 989.9, 1203.8, 1299.0, 1388.0, 1497.7, 2334.6, 2388.6, 3122.6, 3133.2, 3240.9 [cm^{-1}]
I:	1.30, 0.19, 0.18 [Hz]	I:	1.07, 0.20, 0.17 [Hz]
σ:	1.0, v_{corr}: 1.000	σ:	2.0, v_{corr}: 1.000
	Q_A: 115.0 kJ/mol, E: 2792.0 kJ/mol, A_{Pt}: 29.6 Å^2		

	Adsorbed species		**Transition state**
	$C_2H_6(s_2)$		
$\{v_i\}$:	-252.0, -85.6, 86.1, 108.2, 187.7, 213.6, 342.7, 748.0, 821.1, 1001.7, 1109.1, 1196.1, 1285.8, 1378.5, 1420.7, 1451.0, 1453.6, 1547.5, 2484.6, 3013.7, 3028.0, 3083.6, 3095.0, 3114.9 [cm^{-1}]	$\{v_i\}$:	-60.9, 12.4, 123.9, 157.3, 199.1, 222.7, 349.3, 777.3, 819.9, 1030.0, 1146.3, 1199.8, 1332.0, 1386.7, 1439.9, 1448.8, 1455.2, 1476.2, 2751.5, 2907.3, 3036.2, 3061.0, 3081.5, 3114.7 [cm^{-1}]
I:	2.15, 0.84, 0.61 [Hz]	I:	1.91, 0.86, 0.60 [Hz]
σ:	6.0, v_{corr}: 1.000	σ:	3.0, v_{corr}: 1.000
	Q_A: 36.1 kJ/mol, E: 2825.0 kJ/mol, A_{Pt}: 17.7 Å^2		
	$C_3H_5(s)$		
$\{v_i\}$:	122.4, 182.5, 214.3, 336.7, 535.1, 625.5, 704.1, 754.1, 766.5, 956.9, 964.7, 1176.1, 1191.8, 1252.0, 1413.8, 1483.2, 2343.7, 3081.8, 3127.3, 3138.6, 3232.9 [cm^{-1}]	$\{v_i\}$:	-574.2, 11.2, 156.1, 203.1, 487.3, 549.6, 658.1, 799.0, 953.4, 976.0, 1116.9, 1186.7, 1257.2, 1385.0, 1484.5, 1777.9, 2330.5, 3096.0, 3118.8, 3136.1, 3227.4 [cm^{-1}]
I:	35.56, 1.47, 1.41 [Hz]	I:	24.95, 1.33, 1.26 [Hz]
σ:	1.0, v_{corr}: 1.015	σ:	2.0, v_{corr}: 1.015
	Q_A: 41.5 kJ/mol, E: 3038.0 kJ/mol, A_{Pt}: 23.9 Å^2		
	$C_3H_6(s)$		
$\{v_i\}$:	209.7, 225.3, 397.6, 454.3, 497.3, 768.6, 877.1, 914.2, 973.3, 980.9, 1051.8, 1170.8, 1214.4, 1369.0, 1398.6, 1447.7, 1457.4, 1499.0, 3005.0, 3077.8, 3079.6, 3093.7, 3116.8, 3167.5 [cm^{-1}]	$\{v_i\}$:	-10.9, 112.3, 121.2, 231.4, 320.3, 423.4, 540.3, 644.4, 865.1, 918.6, 941.6, 1041.0, 1115.4, 1223.1, 1389.0, 1427.2, 1454.1, 1701.5, 2395.3, 2992.2, 3056.6, 3075.5, 3090.7, 3227.7 [cm^{-1}]
I:	9.97, 2.60, 2.23 [Hz]	I:	10.52, 1.69, 1.47 [Hz]
σ:	3.0, v_{corr}: 1.071	σ:	6.0, v_{corr}: 1.175
	Q_A: 37.2 kJ/mol, E: 3435.0 kJ/mol, A_{Pt}: 26.6 Å^2		

	Adsorbed species		**Transition state**
	$C_3H_6(s_2)$		
$\{v_i\}$:	33.6, 65.4, 149.7, 165.7, 171.5, 190.1, 335.9, 343.6, 460.0, 633.2, 676.3, 892.9, 929.6, 1022.2, 1040.4, 1185.4, 1289.5, 1379.9, 1442.7, 1451.2, 1655.1, 2425.7, 3005.4, 3069.8, 3079.4, 3097.6, 3108.4 [cm^{-1}]	$\{v_i\}$:	-71.2, 83.3, 159.9, 170.1, 179.7, 353.2, 396.5, 448.9, 536.9, 624.8, 707.6, 920.7, 924.7, 1026.7, 1044.6, 1189.0, 1296.3, 1381.5, 1444.5, 1445.0, 1626.2, 2341.1, 3009.5, 3073.1 [cm^{-1}]
I:	1.74, 0.66, 0.51 [Hz]	I:	1.79, 0.73, 0.56 [Hz]
σ:	3.0, v_{corr}: 1.121	σ:	6.0, v_{corr}: 2.220
	Q_A: 39.4 kJ/mol, E: 3435.0 kJ/mol, A_{Pt}: 26.2 Å^2		
	$C_3H_6(s_3)$		
$\{v_i\}$:	16.4, 39.2, 58.2, 104.5, 130.8, 169.4, 173.5, 193.7, 302.3, 453.7, 465.4, 511.9, 606.6, 683.0, 866.8, 906.7, 982.3, 1002.8, 1009.5, 1076.5, 1298.6, 1313.4, 1401.8, 1539.5, 1643.2, 2175.2, 3049.0, 3109.9, 3122.6, 3227.2 [cm^{-1}]	$\{v_i\}$:	-202.7, 29.0, 37.8, 65.5, 107.2, 141.1, 174.7, 180.7, 191.8, 252.8, 467.7, 503.3, 519.5, 644.0, 684.1, 905.8, 986.1, 1001.7, 1009.3, 1081.4, 1300.4, 1317.9, 1403.0, 1643.8, 2006.7, 2169.4, 3048.1, 3117.1, 3127.3, 3230.1 [cm^{-1}]
I:	0.69, 0.36, 0.25 [Hz]	I:	0.71, 0.36, 0.25 [Hz]
σ:	3.0, v_{corr}: 1.000	σ:	6.0, v_{corr}: 1.000
	Q_A: 39.8 kJ/mol, E: 3435.0 kJ/mol, A_{Pt}: 21.8 Å^2		
	$CCH_2(s_2)$		
$\{v_i\}$:	161.9, 193.9, 320.6, 375.3, 491.7, 550.7, 771.8, 925.5, 1329.3, 1664.3, 3102.4, 3189.8 [cm^{-1}]	$\{v_i\}$:	-160.5, 157.0, 201.2, 301.0, 361.6, 525.3, 782.1, 840.0, 1308.4, 1695.1, 3101.4, 3199.3 [cm^{-1}]
I:	3.93, 0.77, 0.64 [Hz]	I:	3.30, 0.76, 0.62 [Hz]
σ:	2.0, v_{corr}: 1.000	σ:	2.0, v_{corr}: 1.000
	Q_A: 299.0 kJ/mol, E: 1457.6 kJ/mol, A_{Pt}: 9.9 Å^2		
	$CCH_2(s_3)$		
$\{v_i\}$:	10.5, 62.5, 154.9, 175.1, 361.1, 462.1, 544.1, 567.1, 685.7, 908.2, 962.1, 1288.5, 1424.5, 3073.5, 3164.2 [cm^{-1}]	$\{v_i\}$:	-95.0, 55.7, 121.3, 160.4, 183.2, 444.1, 467.5, 515.2, 533.7, 798.2, 950.5, 1304.0, 1454.4, 3113.7, 3220.1 [cm^{-1}]
I:	0.69, 0.42, 0.28 [Hz]	I:	0.66, 0.50, 0.32 [Hz]
σ:	2.0, v_{corr}: 1.000	σ:	2.0, v_{corr}: 1.000
	Q_A: 149.0 kJ/mol, E: 1457.6 kJ/mol, A_{Pt}: 15.9 Å^2		

	Adsorbed species		**Transition state**
	$CCH_3(s_3)$		
$\{v_i\}$:	25.2, 93.8, 153.2, 156.0, 183.9, 192.6, 445.2, 515.8, 600.6, 972.1, 1009.0, 1146.8, 1351.8, 1415.4, 1422.7, 3002.5, 3084.1, 3092.2 [cm^{-1}]	$\{v_i\}$:	-49.0, 48.0, 120.4, 136.0, 163.9, 211.2, 289.7, 500.0, 566.6, 914.6, 957.9, 968.6, 1305.8, 1413.4, 1419.2, 3013.4, 3101.7, 3130.3 [cm^{-1}]
I:	0.62, 0.53, 0.33 [Hz]	I:	0.61, 0.55, 0.34 [Hz]
σ:	3.0, v_{corr}: 3.425	σ:	3.0, v_{corr}: 1.000
	Q_A: 405.0 kJ/mol, E: 1569.2 kJ/mol, A_{Pt}: 10.7 Å^2		
	$CCH(s)$		
$\{v_i\}$:	194.8, 233.9, 500.4, 521.7, 701.9, 1851.4, 3413.6 [cm^{-1}]	$\{v_i\}$:	-140.1, 217.9, 217.9, 666.8, 666.8, 2063.0, 3430.8 [cm^{-1}]
I:	3.26 [Hz]	I:	2.04 [Hz]
σ:	1.0, v_{corr}: 1.000	σ:	1.0, v_{corr}: 1.000
	Q_A: 287.0 kJ/mol, E: 1082.1 kJ/mol, A_{Pt}: 9.3 Å^2		
	$CH_2CH_3(s)$		
$\{v_i\}$:	236.9, 245.7, 517.7, 673.7, 923.6, 944.1, 1043.9, 1183.4, 1224.8, 1379.4, 1429.3, 1456.2, 1464.2, 2999.6, 3023.2, 3076.7, 3077.3, 3108.7 [cm^{-1}]	$\{v_i\}$:	-20.7, 240.9, 247.8, 625.6, 844.2, 881.0, 1020.0, 1091.4, 1204.4, 1375.3, 1441.6, 1445.4, 1461.6, 2974.5, 3077.5, 3102.6, 3121.8, 3190.5 [cm^{-1}]
I:	30.56, 2.96, 2.79 [Hz]	I:	27.68, 2.29, 2.18 [Hz]
σ:	1.0, v_{corr}: 1.058	σ:	1.0, v_{corr}: 1.054
	Q_A: 163.0 kJ/mol, E: 2404.5 kJ/mol, A_{Pt}: 18.0 Å^2		
	$CH_2OH(s)$		
$\{v_i\}$:	216.4, 404.1, 577.9, 720.7, 1091.0, 1112.7, 1202.9, 1359.0, 1442.1, 2960.2, 3073.0, 3878.2 [cm^{-1}]	$\{v_i\}$:	-35.4, 286.1, 429.2, 691.8, 981.0, 1097.1, 1225.5, 1371.3, 1474.1, 3089.1, 3211.0, 3879.3 [cm^{-1}]
I:	35.64, 3.19, 3.01 [Hz]	I:	35.74, 2.22, 2.13 [Hz]
σ:	1.0, v_{corr}: 2.157	σ:	1.0, v_{corr}: 2.138
	Q_A: 160.0 kJ/mol, E: 1636.8 kJ/mol, A_{Pt}: 14.5 Å^2		

	Adsorbed species		**Transition state**
	$CH_2O(s)$		
$\{v_i\}$:	379.8, 435.9, 672.0, 1061.0, 1183.2, 1364.5, 1530.8, 2942.7, 3031.3 [cm^{-1}]	$\{v_i\}$:	-113.3, 347.4, 388.6, 1042.2, 1207.6, 1447.9, 1594.0, 2947.7, 3042.3 [cm^{-1}]
I:	31.31, 4.81, 4.30 [Hz]	I:	35.65, 3.77, 3.49 [Hz]
σ:	2.0, v_{corr}: 1.000	σ:	2.0, v_{corr}: 1.000
	Q_A: 46.7 kJ/mol, E: 1510.4 kJ/mol, A_{Pt}: 14.5 Å^2		
	$CH_2(s_2)$		
$\{v_i\}$:	172.3, 499.1, 667.2, 709.5, 713.5, 982.8, 1349.6, 3011.5, 3098.7 [cm^{-1}]	$\{v_i\}$:	-84.3, 170.8, 542.2, 666.4, 729.8, 873.4, 1319.3, 3067.7, 3184.1 [cm^{-1}]
I:	13.97, 0.79, 0.75 [Hz]	I:	11.27, 0.78, 0.74 [Hz]
σ:	2.0, v_{corr}: 1.000	σ:	2.0, v_{corr}: 1.000
	Q_A: 283.0 kJ/mol, E: 761.4 kJ/mol, A_{Pt}: 10.5 Å^2		
	$CH_3OH(s)$		
$\{v_i\}$:	175.4, 199.6, 325.5, 498.2, 1048.0, 1064.1, 1164.7, 1326.2, 1440.3, 1455.6, 1465.5, 3013.3, 3098.8, 3151.8, 3870.1 [cm^{-1}]	$\{v_i\}$:	-93.7, 132.9, 173.5, 377.2, 1051.7, 1075.1, 1166.2, 1334.1, 1452.4, 1459.8, 1470.4, 2998.6, 3071.6, 3128.9, 3897.0 [cm^{-1}]
I:	36.08, 2.66, 2.53 [Hz]	I:	30.60, 2.06, 1.97 [Hz]
σ:	1.0, v_{corr}: 1.094	σ:	1.0, v_{corr}: 1.095
	Q_A: 44.1 kJ/mol, E: 2038.7 kJ/mol, A_{Pt}: 14.7 Å^2		
	$CH_3O(s)$		
$\{v_i\}$:	121.8, 247.0, 561.3, 1058.1, 1152.8, 1210.5, 1423.8, 1435.6, 1444.2, 2973.8, 3062.3, 3064.9 [cm^{-1}]	$\{v_i\}$:	-212.7, 175.8, 182.0, 1047.6, 1051.0, 1148.6, 1371.3, 1387.1, 1474.9, 2898.0, 2952.1, 2961.5 [cm^{-1}]
I:	47.34, 3.17, 3.03 [Hz]	I:	36.84, 2.35, 2.25 [Hz]
σ:	3.0, v_{corr}: 1.169	σ:	3.0, v_{corr}: 1.117
	Q_A: 173.0 kJ/mol, E: 1598.8 kJ/mol, A_{Pt}: 12.3 Å^2		

	Adsorbed species		**Transition state**
	CH_3(s)		
$\{v_i\}$:	558.7, 772.0, 773.8, 1192.7, 1416.9, 1419.6, 3024.3, 3134.3, 3139.5 [cm^{-1}]	$\{v_i\}$:	-156.2, 632.6, 640.5, 942.1, 1388.9, 1393.0, 3082.3, 3252.1, 3255.5 [cm^{-1}]
I:	155.17, 7.94, 7.94 [Hz]	I:	147.94, 5.19, 5.19 [Hz]
σ:	3.0, v_{corr}: 1.000	σ:	3.0, v_{corr}: 1.000
	Q_A: 159.0 kJ/mol, E: 1224.9 kJ/mol, A_{Pt}: 12.3 Å^2		
	$CHCH_2$(s)		
$\{v_i\}$:	247.9, 469.8, 530.1, 933.9, 968.2, 1008.9, 1180.3, 1330.9, 1508.5, 3088.9, 3126.8, 3198.3 [cm^{-1}]	$\{v_i\}$:	-121.4, 262.2, 443.7, 860.5, 876.7, 933.5, 1062.8, 1359.2, 1651.4, 3067.4, 3186.4, 3211.4 [cm^{-1}]
I:	52.20, 3.40, 3.19 [Hz]	I:	47.88, 2.31, 2.21 [Hz]
σ:	1.0, v_{corr}: 1.000	σ:	1.0, v_{corr}: 1.000
	Q_A: 184.0 kJ/mol, E: 1790.6 kJ/mol, A_{Pt}: 14.5 Å^2		
	$CHCH_2$(s_3)		
$\{v_i\}$:	31.9, 92.6, 149.0, 238.5, 292.3, 500.3, 563.6, 619.0, 659.1, 774.3, 943.8, 1028.8, 1097.1, 1131.8, 1404.6, 2992.2, 3010.6, 3064.6 [cm^{-1}]	$\{v_i\}$:	-271.0, 70.2, 99.8, 153.4, 204.3, 278.2, 477.3, 519.4, 592.4, 756.8, 858.5, 942.4, 1099.3, 1196.2, 1418.5, 2972.1, 3072.3, 3171.6 [cm^{-1}]
I:	0.63, 0.57, 0.33 [Hz]	I:	0.63, 0.56, 0.34 [Hz]
σ:	1.0, v_{corr}: 1.000	σ:	1.0, v_{corr}: 1.000
	Q_A: 129.0 kJ/mol, E: 1790.6 kJ/mol, A_{Pt}: 15.9 Å^2		
	$CHCH_3$(s_2)		
$\{v_i\}$:	167.2, 171.0, 190.4, 288.7, 491.0, 583.4, 859.2, 948.1, 998.1, 1084.3, 1257.7, 1357.9, 1432.4, 1447.0, 2984.2, 3027.4, 3043.7, 3123.9 [cm^{-1}]	$\{v_i\}$:	-29.9, 158.1, 174.5, 204.4, 288.8, 592.4, 775.8, 933.3, 957.1, 1112.0, 1243.8, 1357.1, 1428.2, 1441.7, 2984.0, 3051.1, 3082.8, 3133.2 [cm^{-1}]
I:	3.56, 0.77, 0.65 [Hz]	I:	3.19, 0.75, 0.62 [Hz]
σ:	1.0, v_{corr}: 1.098	σ:	1.0, v_{corr}: 1.106
	Q_A: 294.0 kJ/mol, E: 1934.2 kJ/mol, A_{Pt}: 15.6 Å^2		

	Adsorbed species		**Transition state**
	CHOH(s_2)		
$\{v_i\}$:	165.2, 190.6, 313.0, 326.8, 534.1, 607.1, 922.5, 1157.5, 1202.3, 1380.8, 2980.2, 3833.0 [cm^{-1}]	$\{v_i\}$:	-81.9, 164.7, 246.7, 322.1, 412.4, 626.7, 835.7, 1192.6, 1240.3, 1389.0, 3039.2, 3813.3 [cm^{-1}]
I:	3.67, 0.77, 0.65 [Hz]	I:	3.25, 0.76, 0.63 [Hz]
σ:	1.0, v_{corr}: 3.394	σ:	1.0, v_{corr}: 3.226
	Q_A: 200.0 kJ/mol, E: 1295.3 kJ/mol, A_{Pt}: 13.0 Å^2		
	CHO(s)		
$\{v_i\}$:	266.3, 571.8, 803.7, 1188.5, 1835.1, 2775.0 [cm^{-1}]	$\{v_i\}$:	-53.0, 343.8, 759.0, 1136.5, 1914.9, 2860.6 [cm^{-1}]
I:	77.88, 3.47, 3.33 [Hz]	I:	69.73, 2.54, 2.45 [Hz]
σ:	1.0, v_{corr}: 1.000	σ:	1.0, v_{corr}: 1.000
	Q_A: 167.0 kJ/mol, E: 1141.5 kJ/mol, A_{Pt}: 12.4 Å^2		
	CH(s_3)		
$\{v_i\}$:	23.9, 91.3, 156.6, 500.8, 603.9, 657.7, 864.4, 865.4, 3072.4 [cm^{-1}]	$\{v_i\}$:	-246.2, 63.4, 109.3, 162.2, 622.2, 667.9, 732.7, 890.4, 3132.5 [cm^{-1}]
I:	0.71, 0.59, 0.33 [Hz]	I:	0.75, 0.59, 0.34 [Hz]
σ:	1.0, v_{corr}: 1.000	σ:	1.0, v_{corr}: 1.000
	Q_A: 407.0 kJ/mol, E: 338.8 kJ/mol, A_{Pt}: 9.1 Å^2		
	CO_2(s_2)		
$\{v_i\}$:	14.5, 32.5, 67.0, 75.5, 213.7, 676.8, 687.0, 1410.5, 2502.5 [cm^{-1}]	$\{v_i\}$:	-0.3, 127.5, 155.9, 263.9, 342.7, 611.0, 742.5, 1199.9, 1840.3 [cm^{-1}]
I:	1.02, 0.83, 0.46 [Hz]	I:	2.62, 0.69, 0.54 [Hz]
σ:	2.0, v_{corr}: 1.000	σ:	2.0, v_{corr}: 1.000
	Q_A: 15.1 kJ/mol, E: 1608.5 kJ/mol, A_{Pt}: 14.3 Å^2		

	Adsorbed species		**Transition state**
	COH(s_3)		
$\{v_i\}$:	6.0, 92.8, 152.4, 206.2, 231.4, 338.6, 440.4, 550.4, 668.8, 1200.6, 1291.9, 3797.1 [cm^{-1}]	$\{v_i\}$:	-211.3, 54.8, 116.7, 164.1, 217.8, 229.6, 374.1, 494.8, 714.9, 1208.1, 1396.3, 3789.1 [cm^{-1}]
I:	0.63, 0.52, 0.32 [Hz]	I:	0.64, 0.54, 0.34 [Hz]
σ:	3.0, v_{corr}: 3.408	σ:	1.0, v_{corr}: 3.361
	Q_A: 337.0 kJ/mol, E: 965.6 kJ/mol, A_{Pt}: 9.9 Å^2		
	COOH(s)		
$\{v_i\}$:	281.2, 304.0, 461.9, 600.1, 701.9, 1124.2, 1258.2, 1900.2, 3829.0 [cm^{-1}]	$\{v_i\}$:	-21.6, 216.1, 446.2, 585.8, 590.1, 1121.3, 1247.8, 2000.8, 3809.4 [cm^{-1}]
I:	11.82, 2.28, 1.91 [Hz]	I:	11.69, 1.66, 1.45 [Hz]
σ:	1.0, v_{corr}: 1.018	σ:	1.0, v_{corr}: 1.016
	Q_A: 213.0 kJ/mol, E: 1646.0 kJ/mol, A_{Pt}: 14.4 Å^2		
	CO(s)		
$\{v_i\}$:	154.9, 229.3, 416.6, 456.7, 582.6, 1950.2 [cm^{-1}]	$\{v_i\}$:	314.0, 314.0, 2157.3 [cm^{-1}]
I:	4.11, 0.75, 0.63 [Hz]	I:	2.57 [Hz]
σ:	1.0, v_{corr}: 1.000	σ:	1.0, v_{corr}: 1.000
	Q_A: 134.0 kJ/mol, E: 1076.3 kJ/mol, A_{Pt}: 9.1 Å^2		
	CO(s_2)		
$\{v_i\}$:	154.9, 229.3, 416.6, 456.7, 582.6, 1950.2 [cm^{-1}]	$\{v_i\}$:	-48.9, 148.8, 291.4, 406.6, 540.2, 2027.6 [cm^{-1}]
I:	4.11, 0.75, 0.63 [Hz]	I:	3.60, 0.74, 0.61 [Hz]
σ:	1.0, v_{corr}: 1.000	σ:	1.0, v_{corr}: 1.000
	Q_A: 134.0 kJ/mol, E: 1076.3 kJ/mol, A_{Pt}: 9.1 Å^2		
	C(s_3)		
$\{v_i\}$:	36.8, 123.8, 219.2, 249.0, 618.8, 1011.1 [cm^{-1}]	$\{v_i\}$:	-46.8, 57.7, 151.1, 277.9, 692.3, 702.0 [cm^{-1}]
I:	0.76, 0.39, 0.26 [Hz]	I:	0.75, 0.31, 0.22 [Hz]
σ:	1.0, v_{corr}: 1.000	σ:	1.0, v_{corr}: 1.000
	Q_A: 628.0 kJ/mol, E: 0.0 kJ/mol, A_{Pt}: 9.1 Å^2		

	Adsorbed species		**Transition state**
	$H_2O_2(s_2)$		
$\{v_i\}$:	38.7, 104.3, 134.2, 174.7, 293.8, 527.2, 603.8, 641.6, 983.9, 1108.3, 3695.3, 3816.4 [cm^{-1}]	$\{v_i\}$:	-51.6, 111.1, 117.4, 168.6, 181.5, 302.0, 493.8, 608.0, 920.3, 987.3, 3723.0, 3824.1 [cm^{-1}]
I:	4.27, 0.72, 0.63 [Hz]	I:	3.40, 0.72, 0.62 [Hz]
σ:	1.0, v_{corr}: 1.009	σ:	1.0, v_{corr}: 1.009
	Q_A: 27.1 kJ/mol, E: 1070.2 kJ/mol, A_{Pt}: 12.9 Å^2		
	$H_2O(s)$		
$\{v_i\}$:	331.9, 490.6, 548.0, 1565.0, 3816.3, 3927.4 [cm^{-1}]	$\{v_i\}$:	-102.2, 339.2, 350.1, 1579.5, 3845.7, 3961.0 [cm^{-1}]
I:	299.70, 6.32, 6.26 [Hz]	I:	282.81, 4.28, 4.26 [Hz]
σ:	2.0, v_{corr}: 1.000	σ:	2.0, v_{corr}: 1.000
	Q_A: 40.2 kJ/mol, E: 927.0 kJ/mol, A_{Pt}: 9.1 Å^2		
	$H_2(s)$		
$\{v_i\}$:	700.7, 2328.5, 2386.4 [cm^{-1}]	$\{v_i\}$:	-235.1, 717.4, 2453.4 [cm^{-1}]
I:	245.92, 193.45, 108.28 [Hz]	I:	228.19, 122.41, 79.67 [Hz]
σ:	2.0, v_{corr}: 1.000	σ:	2.0, v_{corr}: 1.000
	Q_A: 26.8 kJ/mol, E: 436.0 kJ/mol, A_{Pt}: 6.2 Å^2		
	$H(s)$		
$\{v_i\}$:	2227.0 [cm^{-1}]	$\{v_i\}$:	-83.6 [cm^{-1}]
I:	213.78 [Hz]	I:	126.58 [Hz]
σ:	1.0, v_{corr}: 1.000	σ:	1.0, v_{corr}: 1.000
	Q_A: 255.0 kJ/mol, E: 0.0 kJ/mol, A_{Pt}: 4.5 Å^2		
	$N_2O(s_2)$		
$\{v_i\}$:	90.7, 127.2, 144.2, 145.0, 319.4, 432.6, 548.1, 1277.2, 2095.8 [cm^{-1}]	$\{v_i\}$:	-274.1, 41.5, 103.0, 276.0, 324.8, 420.0, 850.5, 1415.5, 1774.1 [cm^{-1}]
I:	1.56, 0.72, 0.49 [Hz]	I:	1.84, 0.73, 0.52 [Hz]
σ:	2.0, v_{corr}: 3.232	σ:	2.0, v_{corr}: 3.164
	Q_A: 72.6 kJ/mol, E: 1022.9 kJ/mol, A_{Pt}: 15.0 Å^2		

	Adsorbed species		**Transition state**
	$N_2(s_2)$		
$\{v_i\}$:	132.0, 312.2, 328.0, 458.5, 532.3, 1841.1 [cm^{-1}]	$\{v_i\}$:	-103.1, 220.6, 257.8, 462.3, 1130.3, 1797.3 [cm^{-1}]
I:	5.79, 0.71, 0.63 [Hz]	I:	7.18, 0.68, 0.62 [Hz]
σ:	2.0, v_{corr}: 1.000	σ:	2.0, v_{corr}: 1.000
	Q_A: 45.2 kJ/mol, E: 945.3 kJ/mol, A_{Pt}: 11.3 Å^2		
	$NO_2(s)$		
$\{v_i\}$:	123.1, 144.0, 372.5, 791.8, 847.3, 1723.0 [cm^{-1}]	$\{v_i\}$:	-108.6, 89.4, 252.1, 572.0, 1039.6, 1931.6 [cm^{-1}]
I:	52.97, 1.58, 1.53 [Hz]	I:	58.41, 1.61, 1.56 [Hz]
σ:	2.0, v_{corr}: 1.028	σ:	2.0, v_{corr}: 1.000
	Q_A: 41.2 kJ/mol, E: 892.7 kJ/mol, A_{Pt}: 14.4 Å^2		
	$NO(s_3)$		
$\{v_i\}$:	27.9, 38.2, 111.7, 196.3, 244.1, 390.1, 461.0, 703.7, 1790.1 [cm^{-1}]	$\{v_i\}$:	-23.5, 39.7, 112.2, 195.9, 272.9, 377.1, 498.9, 827.1, 1766.0 [cm^{-1}]
I:	3.61, 0.19, 0.18 [Hz]	I:	4.20, 0.19, 0.18 [Hz]
σ:	1.0, v_{corr}: 1.000	σ:	1.0, v_{corr}: 1.000
	Q_A: 71.8 kJ/mol, E: 585.6 kJ/mol, A_{Pt}: 10.8 Å^2		
	N(s)		
$\{v_i\}$:	899.0 [cm^{-1}]	$\{v_i\}$:	-409.4 [cm^{-1}]
I:	13.34 [Hz]	I:	8.32 [Hz]
σ:	1.0, v_{corr}: 1.000	σ:	1.0, v_{corr}: 1.000
	Q_A: 485.3 kJ/mol, E: 0.0 kJ/mol, A_{Pt}: 7.5 Å^2		
	$O_2(s_2)$		
$\{v_i\}$:	144.5, 208.6, 283.9, 528.0, 635.6, 941.6 [cm^{-1}]	$\{v_i\}$:	-152.7, 148.0, 236.0, 328.1, 567.6, 1091.1 [cm^{-1}]
I:	5.08, 0.74, 0.65 [Hz]	I:	4.06, 0.73, 0.62 [Hz]
σ:	2.0, v_{corr}: 1.000	σ:	2.0, v_{corr}: 1.000
	Q_A: 44.3 kJ/mol, E: 498.4 kJ/mol, A_{Pt}: 11.1 Å^2		

	Adsorbed species		**Transition state**
	OH(s)		
$\{v_i\}$:	613.0, 884.9, 3806.5 [cm^{-1}]	$\{v_i\}$:	-96.0, 692.3, 3831.1 [cm^{-1}]
I:	637.69, 8.69, 8.57 [Hz]	I:	584.20, 5.62, 5.57 [Hz]
σ:	1.0, v_{corr}: 1.000	σ:	1.0, v_{corr}: 1.000
	Q_A: 247.0 kJ/mol, E: 429.9 kJ/mol, A_{Pt}: 8.7 Å^2		
	OOH(s)		
$\{v_i\}$:	205.1, 305.2, 599.3, 940.5, 1350.9, 3799.7 [cm^{-1}]	$\{v_i\}$:	-130.6, 200.7, 328.3, 1021.9, 1397.9, 3725.8 [cm^{-1}]
I:	51.99, 3.15, 2.99 [Hz]	I:	41.98, 2.57, 2.44 [Hz]
σ:	1.0, v_{corr}: 1.063	σ:	1.0, v_{corr}: 1.051
	Q_A: 204.0 kJ/mol, E: 703.8 kJ/mol, A_{Pt}: 8.4 Å^2		
	O(s)		
$\{v_i\}$:	803.4 [cm^{-1}]	$\{v_i\}$:	-121.5 [cm^{-1}]
I:	10.99 [Hz]	I:	7.17 [Hz]
σ:	1.0, v_{corr}: 1.000	σ:	1.0, v_{corr}: 1.000
	Q_A: 356.0 kJ/mol, E: 0.0 kJ/mol, A_{Pt}: 7.3 Å^2		

Appendix C

Gas phase reaction mechanisms

The following Tables contain the rate parameters, the modified collision dependencies and the fall-off parameters for the gas phase mechanisms used in this work. The C_1-C_2-C_3 mechanism listed in Table C.1 is applied in Chapters 4 and 5, while the additional gas phase reactions presented in Tables C.4 and C.7 are implemented in Chapters 4 and 5, respectively.

The modified collision dependencies and the fall-off parameters for the C_1 - C_2 - C_3, -N and -C_4 containing gas phase reactions are shown in Tables C.2 - C.3, C.5 - C.6 and C.8 - C.9, respectively. The units of the pre-exponential factors are in [kmol, m^3, s], depending on the reaction order and the activation barriers are given in [kJ/mol]. The number (#) of the reactions accompanied by an asterisk (∗), corresponds to the reactions that have been removed from the current gas phase reaction mechanisms.

Table C.1: Gas phase mechanism (C_1 - C_2 - C_3) implemented in Chapters 4 and 5.

#	Reaction	A	β	E_A
1	$O_2 + H \rightarrow O + OH$	3.55000E+12	-0.41	69.50
2	$O + H_2 \rightarrow H + OH$	5.12000E+01	2.67	26.30
3	$OH + H_2 \rightarrow H + H_2O$	1.00000E+05	1.60	13.80
4	$2\ OH \rightarrow H_2O + O$	3.57000E+01	2.40	-8.84
5	$O_2 + H \rightarrow HO_2$	4.65000E+09	0.40	0.00
6	$O_2 + H \rightarrow HO_2$	4.65000E+09	0.40	0.00
7	$H + HO_2 \rightarrow 2\ OH$	6.00000E+10	0.00	1.23
8	$H + HO_2 \rightarrow H_2 + O_2$	1.66000E+10	0.00	3.43
9	$OH + HO_2 \rightarrow H_2O + O_2$	2.89000E+10	0.00	-2.08
10	$H + HO_2 \rightarrow H_2O + O$	3.00000E+10	0.00	7.20
11	$O + HO_2 \rightarrow O_2 + OH$	3.19000E+10	0.00	0.00
12	$2\ HO_2 \rightarrow H_2O_2 + O_2$	1.86000E+09	0.00	6.44
13	$H_2O_2 + H \rightarrow H_2O + OH$	1.00000E+10	0.00	15.00
14	$H_2O_2 + H \rightarrow H_2 + HO_2$	4.82000E+10	0.00	33.28
15	$H_2O_2 + O \rightarrow HO_2 + OH$	6.60000E+08	0.00	16.60
16	$H_2O_2 + OH \rightarrow H_2O + HO_2$	1.75000E+09	0.00	1.33
17	$H_2O_2 \rightarrow 2\ OH$	2.95000E+14	0.00	202.64
18	$M + 2\ H \rightarrow H_2 + M$	6.53000E+11	-1.00	0.00
19	$M + 2\ H \rightarrow H_2 + M$	9.20000E+10	-0.60	0.00
20	$M + 2\ H \rightarrow H_2 + M$	6.00000E+13	-1.25	0.00

#	**Reaction**			A	β	E_A
21	M + 2 H	→	H_2 + M	5.49000E+14	-2.00	0.00
22	OH + M + H	→	H_2O + M	2.20000E+16	-2.00	0.00
23	M + 2 O	→	M + O_2	1.00000E+11	-1.00	0.00
24	OH + C1	→	CO + H	5.00000E+10	0.00	0.00
25	O_2 + C1	→	CO + O	1.20000E+11	0.00	16.71
26	M + 2 C1	→	C_2 + M	1.80000E+15	-1.60	0.00
27	M + CH	→	C1 + H + M	1.00000E+11	0.00	267.95
28	CH + H	→	C1 + H_2	3.00000E+10	0.00	0.00
29	O + CH	→	CO + H	4.00000E+10	0.00	0.00
30	OH + CH	→	C1 + H_2O	4.00000E+04	2.00	12.55
31	OH + CH	→	CHO + H	3.00000E+10	0.00	0.00
32	CH + O_2	→	CHO + O	7.50000E+10	0.00	0.00
33	H_2O + CH	→	CH_2OH	5.73000E+09	0.00	-3.15
34	CO_2 + CH	→	CHO + CO	3.40000E+09	0.00	2.90
35	CH_2s + M	→	CH_2t + M	1.00000E+10	0.00	0.00
36	CH_2s + H	→	CH + H_2	7.00000E+10	0.00	0.00
37	O + CH_2s	→	CO + 2 H	1.50000E+10	0.00	0.00
38	O + CH_2s	→	CO + H_2	1.50000E+10	0.00	0.00
39	OH + CH_2s	→	CH_2O + H	3.00000E+10	0.00	0.00
40	CH_2s + H_2	→	CH_3 + H	7.23000E+10	0.00	0.00
41	CH_2s + O_2	→	CO + H + OH	3.00000E+10	0.00	0.00
42	CO_2 + CH_2s	→	CH_2O + CO	3.00000E+09	0.00	0.00
43	M + CH_2t	→	C1 + H_2 + M	1.14800E+11	0.00	233.70
44	CH_2t + H	→	CH + H_2	1.10000E+11	0.00	0.00
45	O + CH_2t	→	CO + 2 H	4.88000E+10	0.00	0.00
46	O + CH_2t	→	CO + H_2	3.25000E+10	0.00	0.00
47	OH + CH_2t	→	CH + H_2O	1.13000E+04	2.00	12.56
48	OH + CH_2t	→	CH_2O + H	2.50000E+10	0.00	0.00
49	CH_2t + C1	→	C_2H + H	5.00000E+10	0.00	0.00
50	CH_2t + CH	→	C_2H_2 + H	4.00000E+10	0.00	0.00
51	2 CH_2t	→	C_2H_2 + 2 H	1.20000E+11	0.00	3.32
52	CH_2t + H_2	→	CH_3 + H	3.00000E+06	0.00	0.00
53	CH_2t + O_2	→	CO + H + OH	1.64200E+18	-3.30	12.00
54	CH_2t + O_2	→	CO + H_2O	2.24000E+19	-3.30	12.00
55	CH_2t + O_2	→	CO_2 + 2 H	3.28500E+18	-3.30	12.00
56	CH_2t + O_2	→	CO_2 + H_2	2.63000E+18	-3.30	12.00
57	CH_2t + O_2	→	CH_2O + O	3.28500E+18	-3.30	12.00
58	CO + CH_2t	→	C_2H_2O	6.03000E+05	0.00	0.00
59	CO_2 + CH_2t	→	CH_2O + CO	1.10000E+08	0.00	4.18
60	CH_3 + M	→	CH_2s + H + M	1.90000E+13	0.00	382.44
61	CH_3 + H	→	CH_4	2.10000E+11	0.00	0.00
62	O + CH_3	→	CH_2O + H	8.43000E+10	0.00	0.00
63	OH + CH_3	→	CH_2s + H_2O	4.00000E+10	0.00	10.47
64	OH + CH_3	→	CH_2O + H_2	1.02400E+09	0.00	0.00
65	OH + CH_3	→	CH_2OH + H	1.50000E+11	0.00	34.46
66	OH + CH_3	→	CH_3O + H	5.74000E+09	-0.23	58.28
67	OH + CH_3	→	CH_3OH	6.00000E+10	0.00	0.00
68	CH_3 + HO_2	→	CH_3O + OH	1.80000E+11	0.00	0.00
69	CH_3 + C1	→	C_2H_2 + H	5.00000E+10	0.00	0.00
70	CH_3 + CH	→	C_2H_3 + H	3.00000E+10	0.00	0.00
71	CH_3 + CH_2s	→	C_2H_4 + H	1.80000E+10	0.00	0.00

#	Reaction	A	β	E_A
72	$CH_3 + CH_2t \rightarrow C_2H_4 + H$	4.00000E+10	0.00	0.00
73	$2\ CH_3 \rightarrow C_2H_5 + H$	8.02000E+11	0.00	111.00
74	$2\ CH_3 \rightarrow C_2H_6$	2.27600E+12	-0.69	0.73
75	$CH_3 + O_2 \rightarrow CH_2O + OH$	1.10000E+08	0.00	37.41
76	$CH_3 + O_2 \rightarrow CH_3O + O$	1.32000E+11	0.00	131.36
77	$CH_3 + O_2 \rightarrow CH_3OO$	2.06000E+06	1.10	0.00
78	$CH_4 + H \rightarrow CH_3 + H_2$	3.86000E+03	2.11	32.42
79	$O + CH_4 \rightarrow CH_3 + OH$	9.03300E+05	1.56	35.50
80	$OH + CH_4 \rightarrow CH_3 + H_2O$	1.56000E+04	1.83	11.60
81	$CH_4 + HO_2 \rightarrow CH_3 + H_2O_2$	9.03300E+09	0.00	103.09
82	$CH_4 + CH \rightarrow C_2H_4 + H$	6.00000E+10	0.00	0.00
83	$CH_4 + CH_2s \rightarrow 2\ CH_3$	4.27000E+10	0.00	0.00
84	$CH_4 + O_2 \rightarrow CH_3 + HO_2$	3.97000E+10	0.00	238.00
85	$O + CO + M \rightarrow CO_2 + M$	3.00000E+08	0.00	12.55
86	$OH + CO \rightarrow CO_2 + H$	1.00000E+10	0.00	66.89
87	$OH + CO \rightarrow CO_2 + H$	9.00000E+08	0.00	19.11
88	$OH + CO \rightarrow CO_2 + H$	1.01000E+08	0.00	0.25
89	$CO + HO_2 \rightarrow CO_2 + OH$	1.15000E+02	2.28	73.37
90	$CO + O_2 \rightarrow CO_2 + O$	2.50000E+09	0.00	200.00
91	$CHO + M \rightarrow CO + H + M$	1.86000E+14	-1.00	71.13
92	$CHO + H \rightarrow CO + H_2$	1.11000E+11	0.00	0.00
93	$CHO + O \rightarrow CO + OH$	3.00000E+10	0.00	0.00
94	$CHO + O \rightarrow CO_2 + H$	3.00000E+10	0.00	0.00
95	$CHO + OH \rightarrow CO + H_2O$	1.00000E+11	0.00	0.00
96	$CHO + CH_3 \rightarrow CH_4 + CO$	1.20000E+11	0.00	0.00
97	$CHO + O_2 \rightarrow CO + HO_2$	1.20000E+07	0.81	-3.04
98	$M + CH_2O \rightarrow CHO + H + M$	1.26000E+13	0.00	326.00
99	$H + CH_2O \rightarrow CHO + H_2$	1.26000E+05	1.62	9.06
100	$O + CH_2O \rightarrow CHO + OH$	4.15000E+08	0.57	11.56
101	$OH + CH_2O \rightarrow CHO + H_2O$	3.43000E+06	1.18	-1.87
102	$HO_2 + CH_2O \rightarrow CHO + H_2O_2$	2.00000E+09	0.00	48.97
103	$CH + CH_2O \rightarrow C_2H_2O + H$	9.46000E+10	0.00	-2.16
104	$CH_3 + CH_2O \rightarrow CH_4 + CHO$	4.09000E+09	0.00	37.00
105	$O_2 + CH_2O \rightarrow CHO + HO_2$	6.00000E+10	0.00	170.00
106	$CH_2OH + M \rightarrow CH_2O + H + M$	4.40000E+12	0.00	125.52
107	$CH_2OH + H \rightarrow CH_2O + H_2$	3.00000E+10	0.00	0.00
108	$O + CH_2OH \rightarrow CH_2O + OH$	4.22000E+10	0.00	0.00
109	$OH + CH_2OH \rightarrow CH_2O + H_2O$	2.40000E+10	0.00	0.00
110*	$CH_2OH + O_2 \rightarrow CH_2O + HO_2$	4.56000E–09	5.94	-18.99
111	$M + CH_3O \rightarrow CH_2O + H + M$	5.45000E+10	0.00	56.50
112	$M + CH_3O \rightarrow CH_2OH + M$	3.01000E+08	0.00	17.04
113	$H + CH_3O \rightarrow CH_2O + H_2$	2.00000E+10	0.00	0.00
114	$O + CH_3O \rightarrow CH_2O + OH$	6.00000E+09	0.00	0.00
115	$OH + CH_3O \rightarrow CH_2O + H_2O$	1.80000E+10	0.00	0.00
116	$O_2 + CH_3O \rightarrow CH_2O + HO_2$	6.60000E+07	0.00	10.88
117	$M + CH_3OH \rightarrow CH_2s + H_2O + M$	7.00000E+12	0.00	277.99
118	$M + CH_3OH \rightarrow CH_2OH + H + M$	2.00000E+14	0.00	315.89
119	$CH_3OH + H \rightarrow CH_2OH + H_2$	1.44000E+10	0.00	25.50
120	$CH_3OH + H \rightarrow CH_3O + H_2$	4.00000E+09	0.00	25.50

*Removed reaction

#	Reaction	A	β	E_A
121	$O + CH_3OH \rightarrow CH_2OH + OH$	3.88000E+02	2.50	12.90
122	$O + CH_3OH \rightarrow CH_3O + OH$	1.00000E+10	0.00	19.59
123	$OH + CH_3OH \rightarrow CH_2OH + H_2O$	3.00000E+01	2.65	-3.70
124	$OH + CH_3OH \rightarrow CH_3O + H_2O$	5.30000E+00	2.65	-3.70
125*	$CH_3 + CH_3OH \rightarrow CH_2OH + CH_4$	3.19000E–02	3.20	30.00
126	$O_2 + CH_3OH \rightarrow CH_2OH + HO_2$	2.05000E+10	0.00	188.00
127	$CH_3OH + HO_2 \rightarrow CH_2OH + H_2O_2$	3.98000E+10	0.00	81.22
128	$CH_3OO + CH_4 \rightarrow CH_3 + CH_3OOH$	3.00000E+09	0.00	95.00
129	$CH_3OO + CH_2O \rightarrow CH_3OOH + CHO$	3.00000E+09	0.00	52.00
130	$CH_3OO + HO_2 \rightarrow CH_3OOH + O_2$	2.47000E+08	0.00	-6.57
131	$2\ CH_3OO \rightarrow 2\ CH_3O + O_2$	5.48000E+07	0.00	-3.49
132	$CH_3 + CH_3OO \rightarrow 2\ CH_3O$	1.00000E+10	0.00	0.00
133	$C_2H_6 + CH_3OO \rightarrow C_2H_5 + CH_3OOH$	3.00000E+08	0.00	62.50
134	$CH_3OOH \rightarrow CH_3O + OH$	6.00000E+14	0.00	177.09
135	$C_2 + O \rightarrow C1 + CO$	3.61000E+11	0.00	0.00
136	$C_2 + O_2 \rightarrow 2\ CO$	8.97000E+09	0.00	4.10
137	$O + C_2H \rightarrow CH + CO$	1.00000E+10	0.00	0.00
138	$OH + C_2H \rightarrow C_2HO + H$	2.00000E+10	0.00	0.00
139	$H_2 + C_2H \rightarrow C_2H_2 + H$	5.67000E+07	0.90	8.34
140	$O_2 + C_2H \rightarrow 2\ CO + H$	9.04000E+09	0.00	-1.91
141	$H_2O + C_2H \rightarrow C_2H_2O + H$	1.14000E+10	0.00	1.66
142	$H + C_2H \rightarrow C_2 + H_2$	3.61000E+10	0.00	118.25
143	$2\ C_2H \rightarrow C_2 + C_2H_2$	1.81000E+09	0.00	0.00
144	$M + C_2H_2 \rightarrow C_2H + H + M$	4.20000E+13	0.00	448.00
145	$M + C_2H_2 \rightarrow H_2C_2 + M$	2.50000E+12	-0.64	207.95
146	$O + C_2H_2 \rightarrow CH_2t + CO$	2.89300E+03	2.09	6.53
147	$O + C_2H_2 \rightarrow C_2HO + H$	4.33900E+03	2.09	6.53
148	$OH + C_2H_2 \rightarrow C_2H + H_2O$	3.37000E+04	2.00	58.57
149	$OH + C_2H_2 \rightarrow C_2H_2O + H$	3.75000E+03	1.70	4.18
150	$C_2H_2 + HO_2 \rightarrow C_2H_2O + OH$	6.00000E+06	0.00	33.52
151	$O_2 + C_2H_2 \rightarrow C_2H + HO_2$	1.20000E+10	0.00	311.70
152	$H_2C_2 + O_2 \rightarrow CH_2t + CO_2$	5.00000E+10	0.00	0.00
153	$O + H_2C_2 \rightarrow CH_2t + CO$	3.00000E+10	0.00	0.00
154	$OH + H_2C_2 \rightarrow CH_2t + CHO$	2.00000E+10	0.00	0.00
155	$H_2C_2 + O_2 \rightarrow 2\ CHO$	1.00000E+10	0.00	0.00
156	$C_2H_3 \rightarrow C_2H_2 + H$	2.00000E+14	0.00	166.28
157	$C_2H_3 + H \rightarrow C_2H_2 + H_2$	3.00000E+10	0.00	0.00
158	$O + C_2H_3 \rightarrow C_2H_2O + H$	3.00000E+10	0.00	0.00
159	$OH + C_2H_3 \rightarrow C_2H_2 + H_2O$	2.00000E+10	0.00	0.00
160	$C_2H_3 + HO_2 \rightarrow CH_3CO + OH$	3.00000E+10	0.00	0.00
161	$CH + C_2H_3 \rightarrow C_2H_2 + CH_2t$	5.00000E+10	0.00	0.00
162	$C_2H_3 + C_2H \rightarrow 2\ C_2H_2$	3.00000E+10	0.00	0.00
163	$O_2 + C_2H_3 \rightarrow CH_2O + CHO$	1.64000E+18	-2.78	10.56
164	$O_2 + C_2H_3 \rightarrow C_2H_2 + HO_2$	1.66000E+11	-0.83	10.63
165	$O_2 + C_2H_3 \rightarrow CH_2CHO + O$	2.50000E+09	0.06	3.97
166	$O_2 + C_2H_3 \rightarrow CH_3CO + O$	1.50000E+08	0.00	-1.00
167	$C_2H_4 + M \rightarrow C_2H_3 + H + M$	2.60000E+14	0.00	404.00
168	$C_2H_4 + H \rightarrow C_2H_3 + H_2$	4.00000E+03	2.53	51.22
169	$C_2H_4 + H \rightarrow C_2H_5$	3.97400E+06	1.28	5.40

*Removed reaction

#	Reaction	A	β	E_A
170	$C_2H_4 + O \rightarrow CH_3 + CHO$	8.10000E+03	1.88	0.76
171	$C_2H_4 + O \rightarrow CH_2CHO + H$	4.70000E+03	1.88	0.76
172	$C_2H_4 + O \rightarrow C_2H_2O + H_2$	6.75000E+02	1.88	0.76
173	$C_2H_4 + OH \rightarrow C_2H_3 + H_2O$	2.05000E+10	0.00	24.86
174	$C_2H_4 + HO_2 \rightarrow C_2H_3 + H_2O_2$	1.12000E+10	0.00	127.30
175	$C_2H_4 + HO_2 \rightarrow CH_3CHO + OH$	6.03000E+06	0.00	33.26
176	$C_2H_4 + HO_2 \rightarrow C_2H_4O + OH$	2.23000E+09	0.00	71.90
177	$C_2H_4 + O_2 \rightarrow C_2H_3 + HO_2$	4.22000E+10	0.00	241.12
178	$2\ C_2H_4 \rightarrow C_2H_3 + C_2H_5$	5.01000E+11	0.00	271.00
179	$H + C_2H_5 \rightarrow C_2H_4 + H_2$	4.50000E+10	0.00	0.00
180	$O + C_2H_5 \rightarrow CH_2O + CH_3$	6.60000E+10	0.00	0.00
181	$O + C_2H_5 \rightarrow C_2H_4 + OH$	3.06000E+10	0.00	0.00
182	$O + C_2H_5 \rightarrow CH_3CHO + H$	6.60000E+10	0.00	0.00
183	$O_2 + C_2H_5 \rightarrow CH_3CHO + OH$	1.94620E+09	-0.48	32.47
184	$O_2 + C_2H_5 \rightarrow C_2H_4 + HO_2$	2.43000E+14	-1.90	18.52
185	$O_2 + C_2H_5 \rightarrow C_2H_4 + HO_2$	1.02000E+17	-2.97	36.13
186	$O_2 + C_2H_5 \rightarrow C_2H_4O + OH$	1.93900E+17	-3.08	36.13
187	$O_2 + C_2H_5 \rightarrow C_2H_4OOH$	8.84000E+34	-9.33	42.48
188	$O_2 + C_2H_5 \rightarrow C_2H_5OO$	9.42000E+33	-8.01	25.50
189	$2\ C_2H_5 \rightarrow C_2H_4 + C_2H_6$	1.72322E+14	-1.66	4.59
190	$C_2H_6 \rightarrow C_2H_5 + H$	8.85000E+20	-1.23	427.70
191	$C_2H_6 + H \rightarrow C_2H_5 + H_2$	1.44500E+06	1.50	31.00
192	$O + C_2H_6 \rightarrow C_2H_5 + OH$	1.00000E+06	1.50	24.30
193	$OH + C_2H_6 \rightarrow C_2H_5 + H_2O$	7.22600E+03	2.00	3.61
194	$C_2H_6 + CH_2s \rightarrow C_2H_5 + CH_3$	1.14000E+11	0.00	0.00
195	$C_2H_6 + O_2 \rightarrow C_2H_5 + HO_2$	6.02300E+10	0.00	217.00
196	$C_2H_6 + HO_2 \rightarrow C_2H_5 + H_2O_2$	1.32000E+10	0.00	85.64
197*	$CH_3 + C_2H_6 \rightarrow C_2H_5 + CH_4$	1.50000E–10	6.00	25.27
198	$C_2O + H \rightarrow CH + CO$	5.00000E+10	0.00	0.00
199	$C_2O + O \rightarrow 2\ CO$	5.00000E+10	0.00	0.00
200	$C_2O + OH \rightarrow 2\ CO + H$	2.00000E+10	0.00	0.00
201	$C_2O + O_2 \rightarrow 2\ CO + O$	2.00000E+10	0.00	0.00
202	$C_2HO + H \rightarrow CH_2s + CO$	1.00000E+11	0.00	0.00
203	$O + C_2HO \rightarrow 2\ CO + H$	9.63500E+10	0.00	0.00
204	$OH + C_2HO \rightarrow C_2O + H_2O$	3.00000E+10	0.00	0.00
205	$CH + C_2HO \rightarrow C_2H_2 + CO$	5.00000E+10	0.00	0.00
206	$CH_2t + C_2HO \rightarrow C_2H_3 + CO$	3.00000E+10	0.00	0.00
207	$2\ C_2HO \rightarrow C_2H_2 + 2\ CO$	1.00000E+10	0.00	0.00
208	$O_2 + C_2HO \rightarrow 2\ CO + OH$	1.00000E+10	0.00	0.00
209	$O_2 + C_2HO \rightarrow CO + CO_2 + H$	1.00000E+10	0.00	0.00
210	$C_2H_2O + H \rightarrow CH_3 + CO$	1.11000E+04	2.00	8.36
211	$C_2H_2O + H \rightarrow C_2HO + H_2$	1.80000E+11	0.00	35.98
212	$O + C_2H_2O \rightarrow CH_2t + CO_2$	2.00000E+10	0.00	9.60
213	$O + C_2H_2O \rightarrow C_2HO + OH$	2.00000E+04	2.00	41.68
214	$OH + C_2H_2O \rightarrow CH_2OH + CO$	1.02000E+10	0.00	0.00
215	$C_2H_2O + CH_2s \rightarrow C_2H_4 + CO$	1.26000E+11	0.00	0.00
216	$CH_3 + C_2H_2O \rightarrow C_2H_5 + CO$	9.00000E+07	0.00	0.00
217	$CH_3 + C_2H_2O \rightarrow C_2HO + CH_4$	7.50000E+09	0.00	54.39
218	$OH + C_2H_2O \rightarrow C_2HO + H_2O$	1.00000E+04	2.00	12.56

*Removed reaction

#	Reaction	A	β	E_A
219	$CHCH_2O \rightarrow CH_3CO$	8.50000E+14	0.00	58.60
220	$CHCH_2O \rightarrow CH_2CHO$	1.00000E+14	0.00	58.60
221	$CH_2CHO \rightarrow CH_3CO$	1.00000E+13	0.00	184.10
222	$CH_2CHO \rightarrow C_2H_2O + H$	1.58000E+13	0.00	196.65
223	$OH + CH_2CHO \rightarrow C_2H_2O + H_2O$	1.00000E+10	0.00	0.00
224	$O + CH_2CHO \rightarrow C_2H_2O + OH$	1.00000E+11	0.00	0.00
225	$CH_2CHO + O_2 \rightarrow CH_2O + CO + OH$	1.81000E+07	0.00	0.00
226	$CH_3 + CH_2CHO \rightarrow C_2H_6 + CO$	6.10000E+09	0.00	0.00
227	$CH_3CHO + M \rightarrow CH_3 + CHO + M$	7.08000E+15	0.00	342.15
228	$CH_3CHO + H \rightarrow CH_3CO + H_2$	2.10000E+06	1.16	10.09
229	$O + CH_3CHO \rightarrow CH_3CO + OH$	5.00000E+09	0.00	7.50
230	$OH + CH_3CHO \rightarrow CH_3CO + H_2O$	2.30000E+07	0.73	-4.66
231	$CH_3CHO + HO_2 \rightarrow CH_3CO + H_2O_2$	3.00000E+09	0.00	49.87
232	$CH_3CHO + CH_2t \rightarrow CH_3 + CH_3CO$	2.50000E+09	0.00	15.89
233*	$CH_3 + CH_3CHO \rightarrow CH_3CO + CH_4$	2.00000E–09	5.64	10.31
234	$CH_3CHO + O_2 \rightarrow CH_3CO + HO_2$	4.00000E+10	0.00	164.19
235	$CH_3CO \rightarrow CH_3 + CO$	2.80000E+13	0.00	71.75
236	$H + CH_3CO \rightarrow C_2H_2O + H_2$	1.15000E+10	0.00	0.00
237	$H + CH_3CO \rightarrow CH_3 + CHO$	2.15000E+10	0.00	0.00
238	$OH + CH_3CO \rightarrow C_2H_2O + H_2O$	1.21000E+10	0.00	0.00
239	$O + CH_3CO \rightarrow CH_3 + CO_2$	1.54400E+11	0.00	0.00
240	$O + CH_3CO \rightarrow C_2H_2O + OH$	3.86000E+10	0.00	0.00
241	$CH_3 + CH_3CO \rightarrow C_2H_6 + CO$	5.00000E+10	0.00	0.00
242	$C_2H_4O \rightarrow CH_3 + CHO$	3.40000E+13	0.00	241.90
243	$C_2H_4O \rightarrow CH_3CHO$	5.84000E+11	0.00	219.10
244	$C_2H_4O + H \rightarrow CHCH_2O + H_2$	7.90000E+10	0.00	41.00
245	$OH + C_2H_4O \rightarrow CHCH_2O + H_2O$	1.78000E+10	0.00	15.10
246	$C_2H_4O + HO_2 \rightarrow CHCH_2O + H_2O_2$	1.12000E+10	0.00	127.30
247	$C_2H_4O + HO_2 \rightarrow CH_3 + CO + H_2O_2$	4.00000E+09	0.00	71.20
248	$CH_3 + C_2H_4O \rightarrow CH_4 + CHCH_2O$	1.07000E+09	0.00	49.50
249	$C_2H_4O + CH_3O \rightarrow CH_3OH + CHCH_2O$	1.20000E+08	0.00	28.30
250	$CH_3OO + C_2H_4O \rightarrow CH_3OOH + CHCH_2O$	1.12000E+10	0.00	127.30
251	$C_2H_4OOH \rightarrow C_2H_4O + OH$	1.49000E+41	-9.51	94.47
252	$C_2H_4OOH \rightarrow C_2H_4 + HO_2$	6.58000E+41	-9.70	96.28
253	$C_2H_4OOH \rightarrow C_2H_4 + HO_2$	5.65000E+41	-10.90	110.78
254	$C_2H_4OOH \rightarrow CH_3CHO + OH$	3.10000E+37	-10.10	119.56
255	$C_2H_5O \rightarrow CH_2O + CH_3$	1.00000E+15	0.00	90.40
256	$C_2H_5O \rightarrow CH_3CHO + H$	2.51000E+14	0.00	97.90
257	$O_2 + C_2H_5O \rightarrow CH_3CHO + HO_2$	6.03000E+07	0.00	6.90
258	$C_2H_5OO \rightarrow C_2H_4OOH$	4.55400E+51	-13.30	184.53
259	$C_2H_5OO \rightarrow C_2H_4 + HO_2$	6.46300E+30	-6.06	146.98
260	$C_2H_5OO \rightarrow C_2H_4 + HO_2$	4.47000E+42	-10.10	187.08
261	$C_2H_5OO \rightarrow C_2H_4O + OH$	3.01500E+42	-10.00	188.66
262	$C_2H_5OO \rightarrow CH_3CHO + OH$	2.13400E+41	-9.81	192.03
263	$HO_2 + C_2H_5OO \rightarrow C_2H_5OOH + O_2$	1.63000E+08	0.00	-8.31
264	$CH_2O + C_2H_5OO \rightarrow C_2H_5OOH + CHO$	2.00000E+09	0.00	48.80
265	$CH_4 + C_2H_5OO \rightarrow C_2H_5OOH + CH_3$	1.12000E+10	0.00	103.20
266	$C_2H_4 + C_2H_5OO \rightarrow C_2H_4O + C_2H_5O$	2.82000E+09	0.00	71.60
267	$C_2H_4 + C_2H_5OO \rightarrow C_2H_3 + C_2H_5OOH$	1.12000E+10	0.00	127.30

*Removed reaction

#	**Reaction**			A	β	E_A
268	$C_2H_6 + C_2H_5OO$	$\rightarrow$	$C_2H_5 + C_2H_5OOH$	1.70000E+10	0.00	85.60
269	$C_2H_4O + C_2H_5OO$	$\rightarrow$	$C_2H_5OOH + CHCH_2O$	1.12000E+10	0.00	127.30
270	C_2H_5OOH	$\rightarrow$	$C_2H_5O + OH$	4.00000E+15	0.00	179.60
271	$CH_2OH + C_2H_5OOH$	$\rightarrow$	$C_2H_5OO + CH_3OH$	3.01060E+06	0.00	10.80
272	$CH + C_2H_2$	$\rightarrow$	$C_3H + H_2$	3.15000E+10	0.00	-0.51
273	$CH + C_2H_2$	$\rightarrow$	$C_3H_2 + H$	1.78500E+11	0.00	-0.51
274	$CH_2s + C_2H_2$	$\rightarrow$	$C_3H_3 + H$	8.00000E+10	0.00	0.00
275	$CH_2s + C_2H_2$	$\rightarrow$	C_3H_4b	8.00000E+10	0.00	0.00
276	$C_2H_4 + CH_2s$	$\rightarrow$	C_3H_6	6.60000E+10	0.00	0.00
277	$CH_2t + C_2H_2$	$\rightarrow$	C_3H_4b	1.20000E+10	0.00	27.70
278	$C_2H_4 + CH_2t$	$\rightarrow$	C_3H_6	1.80000E+07	0.00	0.00
279	$CH_2CHO + CH_3$	$\rightarrow$	$C_2H_6 + CO$	0.00000E+00	0.00	0.00
280	$CH_3 + C_2H$	$\rightarrow$	$C_3H_3 + H$	2.41000E+10	0.00	0.00
281	$C_2HO + C_2H_2$	$\rightarrow$	$C_3H_3 + CO$	1.00000E+08	0.00	12.60
282	$CH_3 + C_2H_2$	$\rightarrow$	$C_3H_4a + H$	9.68000E+10	0.00	117.13
283	$C_3H_4p + H$	$\rightarrow$	$C_2H_2 + CH_3$	4.26000E+07	1.00	28.90
284	$CH_3 + C_2H_2$	$\rightarrow$	C_3H_5s	1.61000E+37	-8.58	85.06
285	$CH_3 + C_2H_2$	$\rightarrow$	C_3H_5a	2.68000E+50	-12.82	150.00
286	$CH + C_2H_3$	$\rightarrow$	$C_3H_2 + H_2$	3.15000E+10	0.00	-0.51
287	$CH + C_2H_3$	$\rightarrow$	$C_3H_3 + H$	1.78500E+11	0.00	-0.51
288	$CH_2s + C_2H_3$	$\rightarrow$	$C_3H_3 + H_2$	8.00000E+10	0.00	0.00
289	$CH_2s + C_2H_3$	$\rightarrow$	$C_3H_4b + H$	8.00000E+10	0.00	0.00
290	$CH_2t + C_2H_3$	$\rightarrow$	$C_3H_4b + H$	1.20000E+10	0.00	27.70
291	$C_2H_4 + CH$	$\rightarrow$	$C_3H_3 + H_2$	3.15000E+10	0.00	-0.51
292	$C_2H_4 + CH$	$\rightarrow$	$C_3H_4b + H$	1.78500E+11	0.00	-0.51
293	$C_2H_4 + CH_2s$	$\rightarrow$	$C_3H_4b + H_2$	8.00000E+10	0.00	0.00
294	$C_2H_4 + CH_2s$	$\rightarrow$	$C_3H_5b + H$	8.00000E+10	0.00	0.00
295	$C_2H_4 + CH_2t$	$\rightarrow$	$C_3H_5b + H$	1.20000E+10	0.00	27.70
296	$O + C_3H$	$\rightarrow$	$C_2H + CO$	6.80000E+10	0.00	0.00
297	$OH + C_3H$	$\rightarrow$	$C_2H_2 + CO$	6.80000E+10	0.00	0.00
298	$O_2 + C_3H$	$\rightarrow$	$C_2H + CO_2$	9.04000E+09	0.00	-1.91
299	$H_2O + C_3H$	$\rightarrow$	$C_3H_2O + H$	1.15000E+10	0.00	1.66
300	C_3H_2	$\rightarrow$	C_3H_2l	1.00000E+13	0.00	272.00
301	$C_3H_2 + H$	$\rightarrow$	$C_3H + H_2$	1.00000E+11	0.00	0.00
302	$H_2O + C_3H_2$	$\rightarrow$	$C_3H_2O + H_2$	5.73000E+09	0.00	-3.16
303	$O + C_3H_2$	$\rightarrow$	$C_2H + CO + H$	1.40000E+11	0.00	0.00
304	$OH + C_3H_2$	$\rightarrow$	$C_3H + H_2O$	6.00000E+10	0.00	0.00
305	$C_3H_2 + O_2$	$\rightarrow$	$C_2H_2 + CO_2$	2.00000E+09	0.00	0.00
306	$C_3H_2 + O_2$	$\rightarrow$	$C_3H_2O + O$	2.00000E+09	0.00	0.00
307	$C_3H_2l + H$	$\rightarrow$	$C_3H + H_2$	1.00000E+11	0.00	0.00
308	$OH + C_3H_2l$	$\rightarrow$	$C_3H + H_2O$	2.00000E+10	0.00	0.00
309	$C_3H_3 + H$	$\rightarrow$	$C_3H_2l + H_2$	1.00000E+10	0.00	9.00
310	$O + C_3H_3$	$\rightarrow$	$C_3H_2O + H$	1.40000E+11	0.00	0.00
311	$OH + C_3H_3$	$\rightarrow$	$C_3H_2O + H_2$	4.00000E+10	0.00	0.00
312	$C_3H_3 + O_2$	$\rightarrow$	$C_2H_2O + CHO$	3.00000E+07	0.00	12.00
313	$H_2O + C_3H_3$	$\rightarrow$	$C_3H_4O + H$	1.15000E+10	0.00	100.66
314	$C_3H_4a + H$	$\rightarrow$	C_3H_5t	8.50000E+09	0.00	8.37
315	$C_3H_4a + H$	$\rightarrow$	C_3H_5a	4.67000E+48	-11.50	89.30
316	$C_3H_4a + H$	$\rightarrow$	$C_3H_3 + H_2$	1.00000E+09	0.00	6.28

#	Reaction	A	β	E_A
317*	$C_3H_4a + O \rightarrow C_2H_3 + CHO$	1.10000E–05	4.61	-17.80
318	$OH + C_3H_4a \rightarrow C_2H_2O + CH_3$	3.12000E+09	0.00	-1.66
319	$OH + C_3H_4a \rightarrow C_3H_3 + H_2O$	1.00000E+09	0.00	6.28
320	$C_3H_4a + O_2 \rightarrow C_3H_3 + HO_2$	4.00000E+10	0.00	257.50
321	$C_3H_4a + CH_3 \rightarrow C_3H_3 + CH_4$	2.00000E+09	0.00	32.20
322	$C_3H_4a + C_2H \rightarrow C_2H_2 + C_3H_3$	1.00000E+10	0.00	0.00
323	$2\ C_3H_4a \rightarrow C_3H_3 + C_3H_5a$	5.00000E+11	0.00	270.88
324	$C_3H_4a + M \rightarrow C_3H_3 + H + M$	2.00000E+15	0.00	334.72
325	$C_3H_4b \rightarrow C_3H_4a$	1.51300E+14	0.00	211.00
326	$C_3H_4b \rightarrow C_3H_4p$	7.08000E+13	0.00	182.96
327	$C_3H_4p + H \rightarrow C_3H_5t$	6.50000E+09	0.00	8.37
328	$C_3H_4p + H \rightarrow C_3H_5s$	5.80000E+09	0.00	12.98
329	$C_3H_4p + H \rightarrow C_3H_3 + H_2$	1.00000E+09	0.00	6.28
330	$C_3H_4p + O \rightarrow C_2H_2O + CH_2t$	6.40000E+09	0.00	8.41
331	$C_3H_4p \rightarrow C_3H_4a$	5.15000E+60	-13.93	381.49
332	$C_3H_4p + M \rightarrow C_3H_4a + M$	6.27000E+14	-0.91	42.20
333	$C_3H_4p + O \rightarrow C_2H_3 + CHO$	3.20000E+09	0.00	8.41
334	$C_3H_4p + O \rightarrow C_2HO + CH_3$	6.30000E+09	0.00	8.41
335*	$C_3H_4p + OH \rightarrow C_2H_4 + CHO$	5.00000E–07	4.50	-4.19
336	$C_3H_4p + OH \rightarrow C_3H_3 + H_2O$	3.00000E+00	3.00	0.84
337	$C_3H_4p + O_2 \rightarrow C_2HO + CH_2t + OH$	6.15385E+04	1.50	126.00
338	$C_3H_4p + O_2 \rightarrow C_3H_3 + HO_2$	5.00000E+09	0.00	213.00
339	$C_3H_4p + CH_3 \rightarrow C_3H_3 + CH_4$	2.00000E+09	0.00	32.20
340	$C_3H_4p + C_2H \rightarrow C_2H_2 + C_3H_3$	1.00000E+10	0.00	0.00
341	$C_3H_4p + M \rightarrow C_3H_3 + H + M$	4.70000E+15	0.00	334.17
342	$C_3H_5a + H \rightarrow C_3H_4a + H_2$	1.81000E+10	0.00	0.00
343	$C_3H_5a + O \rightarrow C_3H_4O + H$	6.00000E+10	0.00	0.00
344	$C_3H_5a + O_2 \rightarrow C_3H_4a + HO_2$	1.21000E+09	0.00	56.70
345	$C_3H_5a + O_2 \rightarrow C_3H_4O + OH$	8.42000E+05	0.00	-9.62
346	$C_3H_5a + O_2 \rightarrow CH_2O + CH_3CO$	1.19000E+12	-1.01	84.27
347	$C_3H_5a + CH_3 \rightarrow C_3H_4a + CH_4$	3.00000E+09	-0.32	-0.55
348	$C_3H_5a + HO_2 \rightarrow C_2H_3 + CH_2O + OH$	6.60000E+09	0.00	0.00
349	$C_3H_5a + C_2H_3 \rightarrow C_2H_4 + C_3H_4a$	2.41000E+09	0.00	0.00
350	$C_3H_5a + C_2H_5 \rightarrow C_2H_6 + C_3H_4a$	9.60000E+08	0.00	-0.55
351	$2\ C_3H_5a \rightarrow C_3H_4a + C_3H_6$	8.43000E+07	0.00	-1.10
352	$C_3H_5a + H \rightarrow C_3H_6$	2.29000E+10	0.00	0.20
353	$C_3H_5a + OH \rightarrow C_2H_2 + CH_2O + H_2$	1.50000E+10	0.00	0.00
354	$C_3H_5a + HO_2 \rightarrow C_3H_5O + OH$	4.45500E+09	0.00	0.00
355	$C_3H_5s + H \rightarrow C_3H_4a + H_2$	1.81000E+10	0.00	0.00
356	$O + C_3H_5s \rightarrow C_2H_2O + CH_3$	1.80700E+11	0.00	0.00
357	$C_3H_5s + O_2 \rightarrow C_3H_4O + OH$	2.17000E+09	0.00	0.00
358	$CH_3 + C_3H_5s \rightarrow C_3H_4a + CH_4$	1.00000E+08	0.00	0.00
359	$C_3H_5s + C_2H_3 \rightarrow C_2H_4 + C_3H_4a$	1.00000E+08	0.00	0.00
360	$C_3H_5s + C_2H_5 \rightarrow C_2H_6 + C_3H_4a$	1.00000E+08	0.00	0.00
361	$C_3H_5s + O_2 \rightarrow CH_2O + CH_3CO$	2.17000E+09	0.00	0.00
362	$O_2 + C_3H_5t \rightarrow CH_2O + CH_3CO$	2.17000E+09	0.00	0.00
363	$C_3H_5t + H \rightarrow C_3H_4a + H_2$	1.81000E+10	0.00	0.00
364	$O + C_3H_5t \rightarrow C_2HO + CH_3 + H$	1.80700E+11	0.00	0.00
365	$O_2 + C_3H_5t \rightarrow C_3H_4O + OH$	2.17000E+09	0.00	0.00

*Removed reaction

#	Reaction	A	β	E_A
366	$CH_3 + C_3H_5t \rightarrow C_3H_4a + CH_4$	1.00000E+08	0.00	0.00
367	$C_2H_3 + C_3H_5t \rightarrow C_2H_4 + C_3H_4a$	1.00000E+08	0.00	0.00
368	$C_3H_5t + C_2H_5 \rightarrow C_2H_6 + C_3H_4a$	1.00000E+08	0.00	0.00
369	$C_3H_5b \rightarrow C_3H_5a$	1.00000E+10	0.00	0.00
370	$C_3H_5b + H \rightarrow C_3H_4b + H_2$	1.00000E+11	0.00	0.00
371	$OH + C_3H_5b \rightarrow C_3H_4b + H_2O$	2.00000E+10	0.00	0.00
372	$O + C_3H_5b \rightarrow C_3H_4b + OH$	3.67000E+10	0.00	0.00
373	$O + C_3H_5b \rightarrow C_2H_4 + CHO$	1.10000E+11	0.00	0.00
374	$OH + C_3H_6 \rightarrow CH_3 + CH_3CHO$	3.46000E+08	0.00	0.00
375	$HO_2 + C_3H_6 \rightarrow C_3H_5a + H_2O_2$	9.64000E+00	2.60	58.20
376	$M + C_3H_6 \rightarrow C_2H_3 + CH_3 + M$	1.10000E+21	-1.20	408.84
377	$C_3H_6 \rightarrow C_3H_5s + H$	7.59000E+14	0.00	424.12
378	$C_3H_6 \rightarrow C_3H_5t + H$	1.45000E+15	0.00	410.56
379	$H + C_3H_6 \rightarrow C_3H_5a + H_2$	1.72800E+02	2.50	10.43
380	$H + C_3H_6 \rightarrow C_3H_5s + H_2$	4.10000E+02	2.50	40.98
381	$H + C_3H_6 \rightarrow C_3H_5t + H_2$	8.03600E+02	2.50	51.39
382	$O + C_3H_6 \rightarrow C_2H_5 + CHO$	5.21700E+04	1.57	-2.63
383	$O + C_3H_6 \rightarrow C_2H_4 + CH_2O$	3.48400E+04	1.57	-2.63
384	$O + C_3H_6 \rightarrow 2\ CH_3 + CO$	6.96000E+04	1.57	-2.63
385	$OH + C_3H_6 \rightarrow C_3H_5a + H_2O$	3.10000E+03	2.00	-1.25
386	$OH + C_3H_6 \rightarrow C_3H_5s + H_2O$	4.10000E+09	0.00	28.87
387	$OH + C_3H_6 \rightarrow C_3H_5t + H_2O$	4.10000E+09	0.00	28.87
388	$O_2 + C_3H_6 \rightarrow C_3H_5a + HO_2$	1.95000E+09	0.00	163.28
389	$O_2 + C_3H_6 \rightarrow C_3H_5s + HO_2$	2.00000E+10	0.00	199.29
390	$O_2 + C_3H_6 \rightarrow C_3H_5t + HO_2$	2.00000E+10	0.00	184.22
391*	$CH_3 + C_3H_6 \rightarrow C_3H_5a + CH_4$	2.21600E–03	3.50	23.74
392*	$CH_3 + C_3H_6 \rightarrow C_3H_5s + CH_4$	8.42000E–04	3.50	48.77
393*	$CH_3 + C_3H_6 \rightarrow C_3H_5t + CH_4$	1.35100E–03	3.50	53.76
394*	$C_2H_5 + C_3H_6 \rightarrow C_2H_6 + C_3H_5a$	2.22000E–03	3.50	27.77
395	$H + C_3H_6 \rightarrow C_2H_4 + CH_3$	2.60000E+05	1.50	8.36
396	$HO_2 + C_3H_6 \rightarrow C_3H_6O + OH$	1.29000E+09	0.00	62.38
397*	$OH + C_3H_6 \rightarrow C_3H_6OH$	2.75000E–11	0.00	-4.35
398	$H + C_3H_6 \rightarrow C_3H_7n$	7.23000E+09	0.00	12.14
399	$C_3H_6 \rightarrow C_3H_5s + H$	0.00000E+00	0.00	0.00
400	$C_3H_6b \rightarrow C_3H_6$	8.04000E+14	0.00	267.50
401	$C_3H_6b + H \rightarrow C_3H_5b + H_2$	1.62000E+11	0.00	49.00
402	$C_3H_6b + OH \rightarrow C_3H_5b + H_2O$	7.04000E+04	1.50	4.33
403	$C_3H_6b + O \rightarrow C_2H_6 + CO$	6.30000E+05	1.45	-3.59
404	$C_3H_7n + H \rightarrow C_3H_6 + H_2$	1.81000E+09	0.00	0.00
405	$OH + C_3H_7n \rightarrow C_3H_6 + H_2O$	2.41000E+10	0.00	0.00
406	$O + C_3H_7n \rightarrow C_3H_6Op + H$	8.30000E+10	0.00	0.00
407	$O + C_3H_7n \rightarrow C_2H_5 + CH_2O$	1.40000E+10	0.00	0.00
408	$O_2 + C_3H_7n \rightarrow C_3H_7OOn$	1.00000E+09	0.00	0.00
409	$C_3H_7n + H \rightarrow C_3H_8$	2.00000E+10	0.00	0.00
410	$O_2 + C_3H_7n \rightarrow C_3H_6 + HO_2$	1.00000E+09	0.00	20.91
411	$M + C_3H_7n \rightarrow C_2H_4 + CH_3 + M$	1.23000E+13	-0.10	126.37
412	$C_3H_7i + H \rightarrow C_3H_8$	2.00000E+10	0.00	0.00
413	$C_3H_7i + O_2 \rightarrow C_3H_6 + HO_2$	1.00000E+09	0.00	12.50
414	$C_3H_7i \rightarrow C_2H_4 + CH_3$	2.00000E+10	0.00	123.50

*Removed reaction

#	Reaction	A	β	E_A
415	$C_3H_7i + M \rightarrow C_3H_6 + H + M$	8.76000E+07	1.76	148.57
416	$C_3H_7i + O_2 \rightarrow C_3H_7OOi$	6.62000E+09	0.00	0.00
417	$OH + C_3H_7i \rightarrow C_3H_6 + H_2O$	2.41000E+10	0.00	0.00
418	$C_3H_7i + H \rightarrow C_3H_6 + H_2$	3.61000E+09	0.00	0.00
419	$O + C_3H_7i \rightarrow C_3H_6Oa + H$	4.82000E+10	0.00	0.00
420	$O + C_3H_7i \rightarrow CH_3 + CH_3CHO$	4.82000E+10	0.00	0.00
421	$O_2 + C_3H_8 \rightarrow C_3H_7i + HO_2$	3.97000E+10	0.00	199.54
422	$O_2 + C_3H_8 \rightarrow C_3H_7n + HO_2$	3.97000E+10	0.00	212.85
423	$M + C_3H_8 \rightarrow C_2H_5 + CH_3 + M$	1.10000E+17	0.00	353.00
424	$C_3H_8 + H \rightarrow C_3H_7n + H_2$	1.30000E+11	0.00	40.60
425	$C_3H_8 + H \rightarrow C_3H_7i + H_2$	1.00000E+11	0.00	34.90
426	$O + C_3H_8 \rightarrow C_3H_7n + OH$	3.00000E+10	0.00	24.10
427	$O + C_3H_8 \rightarrow C_3H_7i + OH$	2.60000E+10	0.00	18.70
428	$OH + C_3H_8 \rightarrow C_3H_7n + H_2O$	5.75400E+05	1.40	3.56
429	$OH + C_3H_8 \rightarrow C_3H_7i + H_2O$	4.78600E+05	1.40	3.56
430*	$CH_3 + C_3H_8 \rightarrow C_3H_7n + CH_4$	9.03300E–04	3.65	29.90
431*	$CH_3 + C_3H_8 \rightarrow C_3H_7i + CH_4$	1.50550E–03	3.46	22.90
432	$C_3H_2O \rightarrow C_2H_2 + CO$	8.51000E+14	0.00	297.00
433	$C_3H_2O + O \rightarrow C_2HO + CHO$	1.00000E+10	0.00	0.00
434	$OH + C_3H_2O \rightarrow C_2H_2O + CHO$	1.00000E+10	0.00	0.00
435	$C_3H_3O \rightarrow C_2H_3 + CO$	1.00000E+12	0.00	138.27
436	$C_3H_3O + H \rightarrow C_3H_2O + H_2$	6.00000E+10	0.00	0.00
437	$C_3H_3O + O \rightarrow C_3H_2O + OH$	7.83000E+10	0.00	0.00
438	$C_3H_4O \rightarrow C_2H_3 + CHO$	1.00000E+14	0.00	422.00
439	$H + C_3H_4O \rightarrow C_3H_3O + H_2$	3.98000E+10	0.00	17.58
440	$O + C_3H_4O \rightarrow C_3H_3O + OH$	5.00000E+09	0.00	7.50
441	$OH + C_3H_4O \rightarrow C_3H_3O + H_2O$	1.00000E+10	0.00	0.00
442	$HO_2 + C_3H_4O \rightarrow C_3H_3O + H_2O_2$	1.69800E+09	0.00	44.80
443	$C_3H_5O \rightarrow C_2H_2O + CH_3$	1.51000E+14	0.00	250.62
444	$C_3H_5O \rightarrow C_2H_4 + CHO$	2.45000E+14	0.00	244.76
445	$C_3H_5O \rightarrow C_2H_3 + CH_2O$	3.24000E+13	0.00	246.02
446	$C_3H_5O \rightarrow C_3H_5Op$	1.84000E+14	0.00	244.76
447	$C_3H_5O \rightarrow C_3H_5Ot$	1.84000E+14	0.00	244.76
448	$C_3H_5Op \rightarrow C_2H_2O + CH_3$	8.00000E+13	0.00	125.52
449	$C_3H_5Ot \rightarrow C_2H_4 + CHO$	8.00000E+13	0.00	83.68
450	$C_3H_5Ot + O_2 \rightarrow C_3H_4O + HO_2$	1.73700E+08	0.00	7.33
451	$C_3H_5Oa \rightarrow C_2H_2O + CH_3$	8.00000E+13	0.00	108.78
452	$C_3H_6O \rightarrow C_3H_5O + H$	8.00000E+14	0.00	383.92
453	$C_3H_6O \rightarrow CH_3 + CH_3CO$	8.00000E+15	0.00	384.93
454	$C_3H_6O + H \rightarrow C_3H_5O + H_2$	5.00000E+09	0.00	6.28
455	$OH + C_3H_6O \rightarrow C_3H_5O + H_2O$	2.00000E+10	0.00	12.80
456	$O + C_3H_6O \rightarrow C_3H_5O + OH$	3.00000E+10	0.00	21.76
457	$C_3H_6O \rightarrow C_3H_6Oa$	1.01000E+14	0.00	250.62
458	$C_3H_6O \rightarrow C_3H_6Op$	1.84000E+14	0.00	244.76
459	$C_3H_6O + HO_2 \rightarrow C_3H_5O + H_2O_2$	3.24000E+08	0.00	62.34
460	$C_3H_6Oa + M \rightarrow CH_3 + CH_3CO + M$	2.48000E+16	0.00	340.58
461	$C_3H_6Oa + H \rightarrow C_3H_5Oa + H_2$	2.00000E+11	0.00	37.66
462	$OH + C_3H_6Oa \rightarrow C_3H_5Oa + H_2O$	1.02000E+09	0.00	4.99
463	$C_3H_6Oa + O \rightarrow C_3H_5Oa + OH$	1.00000E+10	0.00	24.94

*Removed reaction

#	Reaction	A	β	E_A
464	$C_3H_6Oa + CH_3 \rightarrow C_3H_5Oa + CH_4$	5.00000E+09	0.00	33.47
465	$C_3H_6Op + M \rightarrow C_2H_5 + CHO + M$	7.25000E+16	0.00	344.76
466	$C_3H_6Op + M \rightarrow CH_3 + CH_3CO + M$	4.78000E+16	0.00	351.46
467	$C_3H_6Op + H \rightarrow C_3H_5Op + H_2$	1.00000E+11	0.00	37.66
468	$C_3H_6Op + H \rightarrow C_3H_5Ot + H_2$	1.00000E+11	0.00	37.66
469	$C_3H_6Op + O \rightarrow C_3H_5Op + OH$	5.68000E+09	0.00	6.45
470	$C_3H_6Op + O \rightarrow C_3H_5Ot + OH$	5.68000E+09	0.00	6.45
471	$C_3H_6Op + OH \rightarrow C_3H_5Op + H_2O$	1.21000E+10	0.00	0.00
472	$C_3H_6Op + OH \rightarrow C_3H_5Ot + H_2O$	1.21000E+10	0.00	0.00
473	$C_3H_6Op + CH_3 \rightarrow C_3H_5Op + CH_4$	5.00000E+09	0.00	33.47
474	$C_3H_6Op + CH_3 \rightarrow C_3H_5Ot + CH_4$	5.00000E+09	0.00	33.47
475	$C_3H_6OH \rightarrow C_2H_5 + CH_2O$	1.41000E+09	0.00	72.00
476	$C_3H_6OH \rightarrow CH_3 + CH_3CHO$	1.00000E+09	0.00	72.00
477*	$C_3H_6OH + O_2 \rightarrow CH_2O + CH_3CHO + OH$	1.00000E–11	0.00	-4.60
478	$C_3H_6OOH \rightarrow C_3H_6O + OH$	3.98100E+15	0.00	179.91
479	$O_2 + C_3H_7On \rightarrow C_3H_6O + HO_2$	3.16200E+08	0.00	16.74
480	$O_2 + C_3H_7On \rightarrow C_3H_6Op + HO_2$	3.16200E+08	0.00	16.74
481	$C_3H_7On \rightarrow C_2H_5 + CH_2O$	3.98100E+14	0.00	71.96
482	$C_3H_7Oi + O_2 \rightarrow C_3H_6Op + HO_2$	3.16200E+08	0.00	16.74
483	$C_3H_7Oi + O_2 \rightarrow C_3H_6Oa + HO_2$	3.16200E+08	0.00	16.74
484	$C_3H_7Oi \rightarrow CH_3 + CH_3CHO$	3.98100E+14	0.00	71.96
485	$C_3H_7OOi \rightarrow CH_3CHO + CH_3O$	1.00000E+13	0.00	104.60
486	$C_3H_8 + C_3H_7OOi \rightarrow C_3H_7OOHi + C_3H_7i$	1.00000E+09	0.00	71.55
487	$C_3H_8 + C_3H_7OOi \rightarrow C_3H_7OOHi + C_3H_7n$	1.00000E+09	0.00	81.17
488	$CH_3CHO + C_3H_7OOi \rightarrow C_3H_7OOHi + CH_3CO$	1.00000E+09	0.00	37.66
489	$C_3H_7OOn \rightarrow C_3H_6OOH$	1.25900E+12	0.00	158.99
490	$C_3H_7OOn + C_3H_8 \rightarrow C_3H_7OOHn + C_3H_7n$	1.00000E+09	0.00	81.17
491	$C_3H_7OOn + C_3H_8 \rightarrow C_3H_7OOHn + C_3H_7i$	1.00000E+09	0.00	71.55
492	$C_3H_7OOn + CH_3CHO \rightarrow C_3H_7OOHn + CH_3CO$	1.00000E+09	0.00	37.66
493	$C_3H_7OOHn \rightarrow C_3H_7On + OH$	3.98100E+15	0.00	179.91
494	$C_3H_7OOHi \rightarrow C_3H_7Oi + OH$	3.98100E+15	0.00	179.91
495	$C_3H_4p + H \rightarrow C_2H_2 + CH_3$	0.00000E+00	0.00	16.63
496	$CH_3 + C_2H_2 \rightarrow C_2H + CH_4$	1.81000E+08	0.00	72.34
497	$OH + C_3H_3 \rightarrow C_2H_3 + CHO$	0.00000E+00	0.00	0.00
498	$OH + C_3H_3 \rightarrow C_2H_4 + CO$	0.00000E+00	0.00	0.00
499	$C_3H_4a + H \rightarrow C_3H_5a$	3.32000E+30	-5.80	89.30
500	$C_2H_3 + C_3H_8 \rightarrow C_2H_4 + C_3H_7i$	0.00000E+00	0.00	0.00
501	$C_2H_3 + C_3H_8 \rightarrow C_2H_4 + C_3H_7n$	0.00000E+00	0.00	0.00
502	$C_3H_8 + C_2H_5 \rightarrow C_2H_6 + C_3H_7i$	0.00000E+00	0.00	0.00
503	$C_3H_8 + C_2H_5 \rightarrow C_2H_6 + C_3H_7n$	0.00000E+00	0.00	0.00
504	$C_3H_8 + HO_2 \rightarrow C_3H_7n + H_2O_2$	0.00000E+00	0.00	0.00
505	$C_3H_8 + HO_2 \rightarrow C_3H_7i + H_2O_2$	0.00000E+00	0.00	0.00
506	$HO_2 + C_2H_5 \rightarrow C_2H_5O + OH$	3.20000E+10	0.00	0.00
507	$CH_3OO + C_2H_5 \rightarrow C_2H_5O + CH_3O$	7.00000E+09	0.00	-4.18
508*	$C_3H_6OH \rightarrow C_3H_6 + OH$	2.28100E–42	-9.47	146.61

*Removed reaction

Table C.2: Modified collision dependencies. The numbering in the first column refers to the corresponding reactions shown in Table C.1. The default value of the collision dependency is 1.0 unless otherwise stated.

#	Modified collision dependencies
5	H_2: 1.49, CO: 1.9, CO_2: 2.4, H_2O: 0
6	Default: 0.0, H_2O: 1.0
17	H_2: 2.5, CO: 1.9, CO_2: 3.8, H_2O: 12.0
18	H_2: 0.0, CO_2: 0.0, H_2O: 0.0
19	Default: 0.0, H_2: 1.0
20	Default: 0.0, H_2O: 1.0
21	Default: 0.0, CO_2: 1.0
22	H_2: 3.0, CO: 2.0, CO_2: 5.0, H_2O: 6.5, O_2: 2.5
23	H_2: 2.5, CO: 1.9, CO_2: 3.8, H_2O: 6.5
35	N_2: 0.36, CO: 0.36, CO_2: 0.36, H_2O: 4.0, CH_4: 0.7, C_2H_2: 5.0, C_2H_4: 1.4, C_2H_6: 2.2
61	H_2: 2.0, O_2: 1.5, CO: 1.5, CO_2: 3.0, H_2O: 6.0
85	H_2: 2.5, CO: 1.9, CO_2: 3.8, H_2O: 12.0
91	H_2: 1.89, CO: 2.5, CO_2: 2.5, H_2O: 6.5
111	CH_3OH: 1.0
156	H_2: 2.0, CO: 2.0, CO_2: 3.0, H_2O: 5.0, O_2: 1.5
169	N_2: 0.36, CO: 0.36, CO_2: 0.36, H_2O: 4.0, CH_4: 0.7, C_2H_2: 5.0, C_2H_4: 1.4, C_2H_6: 2.2
190	H_2: 1.1, N_2: 1.6, O_2: 1.9, CO: 1.9, CO_2: 3.3, H_2O: 5.7
332	Default:0.0, H: 1.0

Table C.3: Fall-off parameters. The numbering in the first column refers to the corresponding pressure dependency reactions listed in Table C.1. The units of the pre-exponential factors are in [kmol, m^3, s] depending on the reaction order and the activation barriers are given in [kJ/mol].

#	Fall-off parameters	A	β	E_A
5	$F_c = 0.57$	2.65000E+13	-1.30	0.00
6	$F_c = 0.81$	3.63000E+13	-1.00	0.00
17	$F_c = 0.50$	1.20000E+14	0.00	190.37
61	$F_c = 0.63e^{(-T/3315.0)} + 0.37e^{(-T/61.0)}$	6.30000E+17	-1.80	0.00
67	$F_c = 0.18e^{(-T/200.0)} + 0.82e^{(-T/1438.0)}$	1.59500E+38	-8.20	0.00
74	$F_c = e^{(-T/570)} + 0.00e^{(-T/1.00)}$	8.04800E+25	-3.75	4.11
77	$F_c = 0.27$	5.31000E+19	-3.30	0.00
156	$F_c = 0.35$	4.16000E+38	-7.50	190.40
169	$F_c = 0.24e^{(-T/40.0)} + 0.76e^{(-T/1025.0)}$	4.71400E+12	0.00	3.16
190	$F_c = -46.6e^{(-T/16182.0)} + 47.6e^{(-T/3371.0)}$	4.90000E+39	-6.43	448.40
235	$F_c = 1.000$	6.03000E+12	0.00	58.86
376	$F_c = 0.30e^{(T/1600.0)} + e^{(-1400/T)}$	0.20000E+12	0.00	0.00
411	$F_c = 2.17e^{(-251.0/T)} + e^{(-T/1.0)}$	5.40000E+46	-12.00	149.65
415	$F_c = 0.35$	2.16000E+14	0.00	118.06
423	$F_c = 0.76e^{(-T/38.0)} + 0.24e^{(-T/1946.0)}$	7.82800E+15	0.00	217.19

Table C.4: Additional gas phase mechanism (-N) implemented in Chapter 4.

#	Reaction	A	β	E_A
1	$M + NH_3 \rightarrow H + M + NH_2$	1.40000E+13	0.06	380.52
2	$NH_3 + H \rightarrow H_2 + NH_2$	6.36000E+02	2.39	42.72
3	$OH + NH_3 \rightarrow H_2O + NH_2$	2.04000E+03	2.04	2.38
4	$O + NH_3 \rightarrow NH_2 + OH$	2.10000E+10	0.00	37.80
5*	$NO_2 + NH_3 \rightarrow HNO_2 + NH_2$	2.45100E–03	3.41	125.00
6	$H + NH_2 \rightarrow H_2 + NH$	5.67000E+08	0.59	15.32
7	$OH + NH_2 \rightarrow H_2O + NH$	9.00000E+04	1.50	-1.92
8	$O + NH_2 \rightarrow NH + OH$	7.00000E+09	0.00	0.00
9	$O + NH_2 \rightarrow H + HNO$	9.90000E+11	-0.50	0.00
10	$O + NH_2 \rightarrow H_2 + NO$	5.00000E+09	0.00	0.00
11	$N + NH_2 \rightarrow 2\ H + N_2$	7.20000E+10	0.00	0.00
12	$NO + NH_2 \rightarrow H_2O + N_2$	2.77000E+17	-2.65	-5.26
13	$NO + NH_2 \rightarrow NNH + OH$	3.10000E+10	-0.48	4.94
14	$NO + NH_2 \rightarrow H_2 + N_2O$	5.00000E+10	0.00	102.82
15	$O_2 + NH_2 \rightarrow HNO + OH$	1.51000E+09	-0.39	151.62
16	$O_2 + NH_2 \rightarrow HO_2 + NH$	1.00000E+11	0.00	209.99
17	$NH_2 + HO_2 \rightarrow NH_3 + O_2$	4.52000E+10	0.00	0.00
18	$NH_2 + NH \rightarrow H + N_2H_2$	1.00000E+12	-0.50	0.00
19	$2\ NH_2 \rightarrow H_2 + N_2H_2$	4.00000E+10	0.00	49.74
20	$2\ NH_2 \rightarrow NH + NH_3$	5.00000E+10	0.00	41.73
21	$H + NH \rightarrow H_2 + N$	1.00000E+10	0.00	0.00
22	$O + NH \rightarrow H + NO$	7.00000E+10	0.00	0.00
23	$O + NH \rightarrow N + OH$	7.00000E+09	0.00	0.00
24	$OH + NH \rightarrow H_2O + N$	2.00000E+06	1.20	0.03
25	$OH + NH \rightarrow H + HNO$	4.00000E+10	0.00	0.00
26	$O_2 + NH \rightarrow NO + OH$	1.00000E+10	-0.20	20.12
27	$O_2 + NH \rightarrow HNO + O$	4.61000E+02	2.00	27.30
28	$N + NH \rightarrow H + N_2$	3.00000E+10	0.00	0.00
29	$NO + NH \rightarrow H + N_2O$	2.94000E+11	-0.40	0.00
30	$NO + NH \rightarrow N_2 + OH$	2.16000E+10	-0.23	0.00
31	$NO + NH \rightarrow NNH + O$	5.60000E+09	0.21	45.65
32	$2\ NH \rightarrow 2\ H + N_2$	2.54000E+10	0.00	0.00
33	$N + O_2 \rightarrow NO + O$	6.40000E+06	1.00	26.38
34	$N + OH \rightarrow H + NO$	3.80000E+10	0.00	0.00
35	$N + NO \rightarrow N_2 + O$	3.30000E+09	0.30	0.00
36	$N_3 + O_2 \rightarrow N_2O + NO$	3.61300E+01	0.00	0.00
37	$O + N_3 \rightarrow N_2 + NO$	6.74500E+09	0.00	0.00
38	$2\ N_3 \rightarrow 3\ N_2$	9.03300E+08	0.00	0.00
39*	$NO + O_2 \rightarrow NO_3$	3.40300E–16	-1.75	0.00
40	$M + N_2H_2 \rightarrow H + M + NNH$	1.17000E+14	0.00	210.00
41	$N_2H_2 + H \rightarrow H_2 + NNH$	5.00000E+10	0.00	4.20
42	$NO + N_2H_2 \rightarrow N_2O + NH_2$	3.00000E+09	0.00	0.00
43	$NNH + M \rightarrow H + M + N_2$	1.70000E+09	0.00	60.09
44	$NNH + OH \rightarrow H_2O + N_2$	5.00000E+10	0.00	0.00
45	$NNH + NO \rightarrow HNO + N_2$	9.10000E+08	0.00	0.00
46	$NNH + NH \rightarrow N_2 + NH_2$	5.00000E+10	0.00	0.00
47	$NNH + O \rightarrow N_2 + OH$	1.00000E+10	0.00	21.00

*Removed reaction

#	Reaction	A	β	E_A
48	$H + N_2O \rightarrow N_2 + OH$	2.23000E+11	0.00	70.35
49	$H + N_2O \rightarrow NNH + O$	2.40000E+16	-1.26	197.80
50	$O + N_2O \rightarrow 2\ NO$	2.90000E+10	0.00	97.30
51	$O + N_2O \rightarrow N_2 + O_2$	1.40000E+09	0.00	45.39
52	$M + N_2O \rightarrow M + N_2 + O$	1.30000E+11	0.00	250.37
53*	$OH + N_2O \rightarrow HO_2 + N_2$	1.30000E–05	4.72	153.55
54	$HNO + M \rightarrow H + M + NO$	1.26000E+13	-0.43	207.03
55	$HNO + H \rightarrow H_2 + NO$	4.50000E+08	0.72	2.75
56	$OH + HNO \rightarrow H_2O + NO$	1.30000E+04	1.88	-4.01
57	$HNO + O \rightarrow NO + OH$	3.60000E+10	0.00	0.00
58	$2\ HNO \rightarrow H_2O + N_2O$	3.90000E+09	0.00	210.00
59	$HNO + NH_2 \rightarrow NH_3 + NO$	2.00000E+10	0.00	4.20
60	$NO + HNO \rightarrow N_2O + OH$	2.00000E+09	0.00	109.20
61	$HNO + O_2 \rightarrow HO_2 + NO$	3.16000E+09	0.00	12.60
62	$HNO + NO_2 \rightarrow HNO_2 + NO$	6.02200E+08	0.00	8.35
63	$NO + HO_2 \rightarrow NO_2 + OH$	2.17000E+09	0.00	-2.25
64	$NO + O + M \rightarrow M + NO_2$	3.26000E+09	0.30	0.00
65	$NO_2 + H \rightarrow NO + OH$	2.41000E+11	0.00	2.84
66	$O + NO_2 \rightarrow NO + O_2$	3.90000E+09	0.00	-1.00
67	$2\ NO_2 \rightarrow 2\ NO + O_2$	1.62600E+09	0.00	109.72
68	$NO_2 + HO_2 \rightarrow HNO_2 + O_2$	4.64000E+08	0.00	-2.02
69	$NO + NO_2 \rightarrow N_2O + O_2$	1.00000E+09	0.00	252.96
70	$N_3 + NO_2 \rightarrow 2\ N_2O$	1.20400E+08	0.00	0.00
71	$N_3 + NO_2 \rightarrow N_2 + 2\ NO$	3.61300E+08	0.00	0.00
72*	$O + M + NO_2 \rightarrow M + NO_3$	4.09900E–07	-1.50	0.00
73	$O + NO_2 \rightarrow NO_3$	3.52400E+09	0.24	0.00
74	$NO_2 + NO_3 \rightarrow N_2O5$	3.73000E+07	0.60	0.00
75	$NO + NO_2 \rightarrow N_2O_3$	1.60500E+06	0.00	0.00
76	$H_2O + N_2O_3 \rightarrow 2\ HNO_2$	1.29000E+07	0.00	37.17
77*	$H_2O + N_2O5 \rightarrow 2\ HNO_3$	5.10000E–05	0.00	0.00
78	$2\ NO_2 \rightarrow N_2O4$	6.02200E+05	0.00	0.00
79*	$NO + H_2O + NO_2 \rightarrow 2\ HNO_2$	5.15300E–10	0.00	0.00
80*	$N_2 + NH \rightarrow HN_3$	6.02200E–18	0.00	0.00
81	$N_3 + C1 \rightarrow CN + N_2$	6.62400E+10	0.00	0.00
82	$N_3 + CO \rightarrow N_2 + NCO$	1.07800E+09	0.00	0.00
83	$NO + M + OH \rightarrow HNO_2 + M$	1.99000E+11	-0.05	3.03
84	$HNO_2 + H \rightarrow H_2 + NO_2$	1.20000E+10	0.00	25.04
85	$OH + HNO_2 \rightarrow H_2O + NO_2$	1.51000E+09	0.00	-2.17
86	$O + HNO_2 \rightarrow NO_2 + OH$	1.20000E+10	0.00	30.88
87	$NO + C1 \rightarrow CO + N$	2.80000E+10	0.00	0.00
88	$NO + C1 \rightarrow CN + O$	2.00000E+10	0.00	0.00
89	$NO + CH \rightarrow HCN + O$	4.80000E+10	0.00	0.00
90	$NO + CH \rightarrow CO + NH$	5.00000E+09	0.00	0.00
91	$NO + CH \rightarrow H + NCO$	1.80000E+10	0.00	0.00
92	$NO + CH \rightarrow CHO + N$	2.60000E+10	0.00	0.00
93	$NO + CH_2t \rightarrow H + HCNO$	2.50000E+09	0.00	25.10
94	$NO + CH_2t \rightarrow HCN + OH$	5.01200E+08	0.00	12.05
95	$NO + CH_2s \rightarrow HCN + OH$	3.30000E+09	0.00	0.00
96	$NO + CH_2s \rightarrow H + HCNO$	6.60000E+09	0.00	0.00

*Removed reaction

#	Reaction			A	β	E_A
97	$NO + CH_3$	$\rightarrow$	$H_2O + HCN$	1.20000E+11	0.00	121.76
98	$NO + CHO$	$\rightarrow$	$CO + HNO$	1.08500E+09	0.10	-2.01
99	$NO + CH_2O$	$\rightarrow$	$CHO + HNO$	1.02300E+10	0.00	171.42
100	$NO + CH_3O$	$\rightarrow$	$CH_2O + HNO$	1.30000E+11	-0.70	0.00
101	$NO + C_2HO$	$\rightarrow$	$CO_2 + HCN$	1.63000E+12	-0.74	4.36
102	$NO + C_2HO$	$\rightarrow$	$CO + HCNO$	5.65200E+10	0.00	3.55
103	$NO + C_2H$	$\rightarrow$	$CO + HCN$	6.00000E+10	0.00	2.40
104	$CH + NO_2$	$\rightarrow$	$CHO + NO$	1.01000E+11	0.00	0.00
105	$CH_3 + NO_2$	$\rightarrow$	$CH_3O + NO$	1.30000E+10	0.00	0.00
106	$CH_4 + NO_2$	$\rightarrow$	$CH_3 + HNO_2$	1.20000E+10	0.00	126.00
107	$CHO + NO_2$	$\rightarrow$	$CO + HNO_2$	1.70000E+10	0.00	0.00
108	$CO + NO_2$	$\rightarrow$	$CO_2 + NO$	9.03300E+10	0.00	141.88
109	$C1 + N_2O$	$\rightarrow$	$CN + NO$	1.00000E+10	0.00	0.00
110	$CO + N_2O$	$\rightarrow$	$CO_2 + N_2$	3.20000E+08	0.00	85.32
111	$N_2 + CH$	$\rightarrow$	$HCN + N$	3.68000E+04	1.42	87.04
112	$N_2 + CH_2t$	$\rightarrow$	$HCN + NH$	1.00000E+09	0.00	310.18
113	$N + CH$	$\rightarrow$	$CN + H$	1.30000E+10	0.00	0.00
114	$N + CH_2t$	$\rightarrow$	$H + HCN$	5.00000E+10	0.00	0.00
115	$N + CH_3$	$\rightarrow$	$H_2 + HCN$	7.00000E+09	0.00	0.00
116	$N + CH_4$	$\rightarrow$	$CH_3 + NH$	1.00000E+10	0.00	100.80
117	$CH + NH$	$\rightarrow$	$H + HCN$	5.00000E+10	0.00	0.00
118	$CH_2t + NH$	$\rightarrow$	$H + H_2CN$	3.00000E+10	0.00	0.00
119	$O + HCN$	$\rightarrow$	$CN + OH$	4.20000E+07	0.40	86.83
120	$O + HCN$	$\rightarrow$	$CO + NH$	5.40000E+05	1.21	31.46
121	$O + HCN$	$\rightarrow$	$H + NCO$	2.00000E+05	1.47	31.88
122	$OH + HCN$	$\rightarrow$	$CN + H_2O$	3.90000E+03	1.83	43.22
123	$OH + HCN$	$\rightarrow$	$H + HNCO$	4.80000E+08	0.00	46.20
124	$OH + HCN$	$\rightarrow$	$H + HOCN$	9.20000E+09	0.00	63.00
125*	$OH + HCN$	$\rightarrow$	$CO + NH_2$	7.83000E–07	4.00	16.80
126	$O + CN$	$\rightarrow$	$CO + N$	7.70000E+10	0.00	0.00
127	$CN + H_2$	$\rightarrow$	$H + HCN$	3.00000E+02	2.45	9.40
128	$OH + CN$	$\rightarrow$	$H + NCO$	6.00000E+10	0.00	0.00
129	$CN + O_2$	$\rightarrow$	$NCO + O$	6.62000E+09	0.00	-1.71
130	$CN + NO_2$	$\rightarrow$	$NCO + NO$	3.00000E+10	0.00	0.00
131	$CN + N_2O$	$\rightarrow$	$N_2 + NCO$	1.00000E+10	0.00	0.00
132	$CN + CH_4$	$\rightarrow$	$CH_3 + HCN$	2.17000E+10	0.00	5.14
133	$N + CN$	$\rightarrow$	$C1 + N_2$	1.04000E+12	-0.50	0.00
134	$NO + CN$	$\rightarrow$	$CO + N_2$	1.08000E+11	0.00	33.72
135	$NO + CN$	$\rightarrow$	$N + NCO$	9.64000E+10	0.00	176.94
136	$NCO + M$	$\rightarrow$	$CO + M + N$	1.02000E+12	0.00	196.14
137	$NCO + H$	$\rightarrow$	$CO + NH$	5.00000E+10	0.00	0.00
138	$NCO + O$	$\rightarrow$	$CO + NO$	5.60000E+10	0.00	0.00
139	$NCO + OH$	$\rightarrow$	$CHO + NO$	5.00000E+09	0.00	63.04
140	$NCO + NO$	$\rightarrow$	$CO + N_2O$	6.20000E+14	-1.73	3.21
141	$NCO + NO$	$\rightarrow$	$CO_2 + N_2$	7.80000E+14	-1.73	3.21
142	$NCO + N$	$\rightarrow$	$CO + N_2$	2.00000E+10	0.00	0.00
143	$NCO + HNO$	$\rightarrow$	$HNCO + NO$	1.80000E+10	0.00	0.00
144	$2\ NCO$	$\rightarrow$	$2\ CO + N_2$	1.80000E+10	0.00	0.00
145	$NCO + O_2$	$\rightarrow$	$CO_2 + NO$	2.00000E+09	0.00	84.06

*Removed reaction

#	Reaction	A	β	E_A
146	M + HNCO → H + M + NCO	5.00000E+12	0.00	500.75
147	H + HNCO → H_2 + NCO	5.50000E+11	0.00	114.34
148	H + HNCO → CO + NH_2	2.08900E+11	0.00	70.94
149	O + HNCO → NCO + OH	2.23000E+03	2.11	47.99
150	O + HNCO → CO_2 + NH	9.60000E+04	1.41	35.81
151	O + HNCO → CO + HNO	1.50000E+05	1.57	184.97
152	OH + HNCO → H_2O + NCO	3.45000E+04	1.50	15.10
153	OH + HNCO → CO_2 + NH_2	3.63000E+03	1.50	15.10
154	CN + HNCO → HCN + NCO	1.50000E+10	0.00	0.00
155	NH + HNCO → NCO + NH_2	2.00000E+10	0.00	50.06
156	M + HOCN → HNCO + M	3.10000E+05	0.84	8.05
157	H + HOCN → CO + NH_2	1.20000E+05	0.61	8.72
158	H + HOCN → H_2 + NCO	2.40000E+05	1.50	27.79
159	O + HOCN → NCO + OH	1.70000E+05	1.50	17.36
160	OH + HOCN → H_2O + NCO	1.20000E+03	2.00	-1.04
161	HCNO + M → HNCO + M	2.10000E+12	-0.69	11.98
162	HCNO + M → HOCN + M	1.40000E+08	-0.19	10.43
163	HCNO + H → HCN + OH	2.70000E+08	0.18	8.89
164	HCNO + H → CO + NH_2	1.70000E+11	-0.75	12.14
165	HCNO + O → CHO + NO	7.00000E+10	0.00	0.00
166	OH + HCNO → CH_2O + NO	4.00000E+10	0.00	0.00
167	N + CH_3 → H + H_2CN	7.10000E+10	0.00	0.00
168	NO + CH_3 → H_2CN + OH	5.20000E+09	0.00	101.82
169	CH_3 + NH → H_2 + H_2CN	7.10000E+10	0.00	0.00
170	H_2CN + H → H_2 + HCN	1.00000E+11	0.00	0.00
171	OH + H_2CN → H_2O + HCN	1.00000E+11	0.00	0.00
172	H_2CN + M → H + HCN + M	3.00000E+11	0.00	92.40
173	N + H_2CN → CH_2t + N_2	2.00000E+10	0.00	0.00
174	HCN + M → HNC + M	1.60000E+23	-3.23	208.23
175	O + HNC → CO + NH	4.60000E+09	0.00	9.18
176	OH + HNC → H + HNCO	2.80000E+10	0.00	15.52
177	CH_3NO_2 → CH_3 + NO_2	1.03300E+48	-10.33	284.81
178	CH_3NO_2 → CH_3O + NO	4.93200E+47	-10.64	280.92
179	CH_3NO_2 + H → CH_3 + HNO_2	3.30000E+09	0.00	15.61
180	CH_3 + CH_2NO_2 → C_2H_5 + NO_2	5.00000E+10	0.00	0.00
181	O + CH_3NO_2 → CH_2NO_2 + OH	1.51000E+10	0.00	0.00
182	OH + CH_3NO_2 → CH_2NO_2 + H_2O	5.00000E+02	2.00	4.18
183	OH + CH_3NO_2 → CH_3OH + NO_2	2.00000E+07	0.00	-4.18
184	CH_3NO_2 + O_2 → CH_2NO_2 + HO_2	2.00000E+10	0.00	238.50
185	CH_2t + CH_3NO_2 → CH_2NO_2 + CH_3	6.50000E+09	0.00	33.06
186	CH_3NO_2 + H → CH_2NO_2 + H_2	7.50000E+09	0.00	41.84
187	CH_3 + CH_3NO_2 → CH_2NO_2 + CH_4	7.08000E+08	0.00	46.61
188	CH_3NO_2 + CH_3O → CH_2NO_2 + CH_3OH	3.00000E+08	0.00	29.29
189	CH_3NO_2 + C_2H_5 → C_2H_6 + CH_2NO_2	3.00000E+08	0.00	48.96
190	CH_3NO_2 + HO_2 → CH_2NO_2 + H_2O_2	1.50000E+08	0.00	62.76
191	CH_2NO_2 → CH_2O + NO	1.00000E+13	0.00	150.63
192	H + CH_2NO_2 → CH_3 + NO_2	5.00000E+10	0.00	0.00
193	O + CH_2NO_2 → CH_2O + NO_2	5.00000E+10	0.00	0.00
194	OH + CH_2NO_2 → CH_2OH + NO_2	1.00000E+10	0.00	0.00

Table C.5: Modified collision dependencies. The numbering in the first column refers to the corresponding reactions shown in Table C.4. The default value of the collision dependency is 1.0 unless otherwise stated.

#	Modified collision dependencies
1	Default: 0.0, H_2O: 6.5
52	Default: 0.0, N_2O: 5.0, H_2O: 5.0
54	Default: 0.0, H_2: 1.25, H_2O: 4.1
156	Default: 0.0, H: 1.0
161	Default: 0.0, H: 1.0
162	Default: 0.0, H: 1.0

Table C.6: Fall-off parameters. The numbering in the first column refers to the corresponding pressure dependency reactions listed in Table C.4. The units of the pre-exponential factors are in [kmol, m^3, s] depending on the reaction order and the activation barriers are given in [kJ/mol].

#	Fall-off parameters	A	β	E_A
52	$F_c = 1.17815e^{(-T/7995.95)} - 0.17815e^{(-T/0.1)}$	7.20000E+14	-0.73	263.70
64	$F_c = 0.95874e^{(-T/8159.75)} + 0.04126e^{(-T/0.1)}$	3.30000E+14	-1.60	0.00
83	$F_c = e^{(-T/1420.00)}$	5.08000E+17	-2.51	0.2841

Table C.7: Additional gas phase mechanism (-C_4) implemented in Chapter 5.

#	**Reaction**	A	β	E_A
1	$2\ C_2H \rightarrow C_4H + H$	1.00000E+11	0.00	0.00
2	$2\ C_2H_2 \rightarrow C_4H_3n + H$	1.00000E+09	0.00	276.14
3	$2\ C_2H_2 \rightarrow C_4H_3i + H$	2.00000E+09	0.00	268.00
4	$C_2H_2 + C_2H \rightarrow C_4H_2 + H$	1.20000E+11	0.00	0.00
5	$C_2H_3 + C_2H \rightarrow C_4H_4$	1.00000E+11	0.00	0.00
6	$C_2H_3 + C_2H_2 \rightarrow C_4H_4 + H$	4.68000E+09	0.00	21.70
7	$2\ C_2H_3 \rightarrow C_4H_6t$	1.00000E+10	0.00	0.00
8	$C_2H_4 + C_2H \rightarrow C_4H_4 + H$	1.21000E+10	0.00	0.00
9	$2\ C_2H_5 \rightarrow C_4H_10n$	6.89290E+14	-1.66	4.59
10*	$C_2H_4 + C_2H_5 \rightarrow C_4H_9n$	7.93436E–01	2.44	22.43
11	$CH + C_3H \rightarrow C_4H + H$	7.00000E+10	0.00	0.00
12	$CH_2s + C_3H \rightarrow C_4H_2 + H$	8.00000E+10	0.00	0.00
13	$CH_2t + C_3H \rightarrow C_4H_2 + H$	8.00000E+10	0.00	0.00
14	$CH_3 + C_3H \rightarrow C_4H_3i + H$	4.00000E+10	0.00	0.00
15	$CH_3 + C_3H_2 \rightarrow C_4H_4 + H$	4.00000E+10	0.00	0.00
16	$C_3H_2 + CH_2s \rightarrow C_4H_3i + H$	8.00000E+10	0.00	0.00
17	$C_3H_2 + CH \rightarrow C_4H_2 + H$	7.00000E+10	0.00	0.00
18	$C_3H_2 + CH_2t \rightarrow C_4H_3i + H$	8.00000E+10	0.00	0.00
19	$C_3H_3 + CH \rightarrow C_4H_3n + H$	7.00000E+10	0.00	0.00
20	$C_3H_3 + CH \rightarrow C_4H_3i + H$	7.00000E+10	0.00	0.00
21	$CH_2t + C_3H_3 \rightarrow C_4H_4 + H$	8.00000E+10	0.00	0.00
22	$CH_2s + C_3H_3 \rightarrow C_4H_4 + H$	8.00000E+10	0.00	0.00
23	$C_3H_4a + CH \rightarrow C_4H_4 + H$	2.77000E+11	0.00	0.00

*Removed reaction

#	Reaction			A	β	E_A
24	$C_3H_4a + CH_2s$	$\rightarrow$	C_4H_6b	1.60000E+11	0.00	0.00
25	$C_3H_4a + CH_2t$	$\rightarrow$	C_4H_6b	1.60000E+10	0.00	0.00
26	$C_3H_4p + CH_2s$	$\rightarrow$	C_4H_6b	1.60000E+11	0.00	0.00
27	$C_3H_4p + CH$	$\rightarrow$	$C_4H_4 + H$	2.77000E+11	0.00	0.00
28	$C_3H_4p + CH_2t$	$\rightarrow$	C_4H_6b	1.60000E+10	0.00	0.00
29	$C_4H + H_2$	$\rightarrow$	$C_4H_2 + H$	4.07400E+02	2.40	0.84
30	C_4H_2	$\rightarrow$	$C_4H + H$	7.80000E+14	0.00	502.40
31	$C_4H_2 + O$	$\rightarrow$	$C_3H_2 + CO$	9.00000E+08	0.00	0.00
32	$C_4H_2 + OH$	$\rightarrow$	$C_4H_2O + H$	6.69000E+09	0.00	-1.72
33	$M + C_4H_3n$	$\rightarrow$	$C_4H_2 + H + M$	1.00000E+14	0.00	150.72
34	$C_4H_3n + H$	$\rightarrow$	$C_4H_2 + H_2$	3.00000E+10	0.00	0.00
35	$OH + C_4H_3n$	$\rightarrow$	$C_4H_2 + H_2O$	3.00000E+10	0.00	0.00
36	C_4H_3i	$\rightarrow$	C_4H_3n	1.50000E+13	0.00	283.45
37	$C_4H_3i + M$	$\rightarrow$	$C_4H_2 + H + M$	1.00000E+14	0.00	150.62
38	$C_4H_3i + H$	$\rightarrow$	$C_4H_2 + H_2$	3.00000E+10	0.00	0.00
39	$O + C_4H_3i$	$\rightarrow$	$C_4H_2 + OH$	2.00000E+10	0.00	0.00
40	$OH + C_4H_3i$	$\rightarrow$	$C_4H_2 + H_2O$	3.00000E+10	0.00	0.00
41	$C_4H_3i + O_2$	$\rightarrow$	$C_4H_2 + HO_2$	1.00000E+09	0.00	12.55
42	C_4H_4	$\rightarrow$	$C_4H_3i + H$	8.63000E+09	0.00	246.86
43	$H + C_4H_4$	$\rightarrow$	$C_4H_3n + H_2$	2.00000E+04	2.00	25.17
44	$O + C_4H_4$	$\rightarrow$	$C_3H_4a + CO$	2.95000E+09	0.00	0.00
45	$OH + C_4H_4$	$\rightarrow$	$C_4H_3n + H_2O$	1.00000E+04	2.00	12.60
46	$C_4H_4 + C_2H$	$\rightarrow$	$C_2H_2 + C_4H_3i$	3.98000E+10	0.00	0.00
47	$M + C_4H_5s$	$\rightarrow$	$C_4H_4 + H + M$	1.00000E+14	0.00	209.20
48	$H + C_4H_5s$	$\rightarrow$	$C_4H_4 + H_2$	1.00000E+11	0.00	0.00
49	$OH + C_4H_5s$	$\rightarrow$	$C_4H_4 + H_2O$	2.00000E+04	2.00	4.18
50	C_4H_5s	$\rightarrow$	C_4H_5t	1.50000E+13	0.00	283.45
51	$O_2 + C_4H_5s$	$\rightarrow$	$C_3H_3O + CH_2O$	4.15000E+07	0.00	10.50
52	$O + C_4H_5s$	$\rightarrow$	$C_2H_2O + C_2H_3$	1.80700E+11	0.00	0.00
53	$C_4H_5t + M$	$\rightarrow$	$C_4H_4 + H + M$	1.00000E+14	0.00	154.90
54	$C_2H_3 + C_2H_2$	$\rightarrow$	C_4H_5t	9.30000E+35	-8.76	50.21
55	$C_4H_5t + O_2$	$\rightarrow$	$C_4H_5Oy + O$	3.00000E+08	0.29	0.05
56	$C_4H_5t + H$	$\rightarrow$	$C_4H_4 + H_2$	1.00000E+11	0.00	0.00
57	$C_4H_5t + OH$	$\rightarrow$	$C_4H_4 + H_2O$	2.00000E+04	2.00	4.18
58	$C_4H_5t + O_2$	$\rightarrow$	$C_2H_2O + CH_3CO$	2.00000E+09	0.00	0.00
59	$C_4H_5t + O_2$	$\rightarrow$	$C_3H_4O + CHO$	5.00000E+08	0.00	0.00
60	$C_4H_5t + O$	$\rightarrow$	$C_3H_4a + CHO$	1.80700E+11	0.00	0.00
61	$C_4H_5t + O_2$	$\rightarrow$	$C_4H_4O + OH$	5.00000E+08	0.00	0.00
62	$C_4H_5t + HO_2$	$\rightarrow$	$C_3H_4a + CHO + OH$	8.91000E+09	0.00	0.00
63	$C_4H_5t + O_2$	$\rightarrow$	$C_4H_4 + HO_2$	1.00000E+10	0.00	0.00
64	$C_4H_5t + H$	$\rightarrow$	$C_4H_4 + H_2$	0.00000E+00	0.00	0.00
65	$O_2 + C_4H_5i$	$\rightarrow$	$C_4H_4 + HO_2$	1.66000E+11	-0.83	10.63
66	$O_2 + C_4H_5i$	$\rightarrow$	$C_2H_2O + CH_3CO$	4.15000E+07	0.00	10.50
67	$O + C_4H_5i$	$\rightarrow$	$C_2H_2O + C_2H_3$	1.80700E+11	0.00	0.00
68	C_4H_5i	$\rightarrow$	C_4H_5t	1.50000E+13	0.00	283.45
69	$M + C_4H_5i$	$\rightarrow$	$C_4H_4 + H + M$	1.00000E+14	0.00	209.34
70	$C_4H_5i + H$	$\rightarrow$	$C_4H_4 + H_2$	1.00000E+11	0.00	0.00
71	$OH + C_4H_5i$	$\rightarrow$	$C_4H_4 + H_2O$	2.00000E+04	2.00	4.18
72	C_4H_6t	$\rightarrow$	$C_4H_5i + H$	4.40000E+15	0.00	397.92
73	$C_4H_6t + H$	$\rightarrow$	$C_4H_5t + H_2$	6.30000E+07	0.70	25.10
74	$C_4H_6t + H$	$\rightarrow$	$C_2H_3 + C_2H_4$	2.00000E+10	0.00	20.92

#	Reaction			A	β	E_A
75	$OH + C_4H_6t$	$\rightarrow$	$C_4H_5t + H_2O$	2.00000E+04	2.00	20.93
76	$C_4H_6t + O_2$	$\rightarrow$	$C_4H_5t + HO_2$	4.00000E+10	0.00	242.00
77	$C_4H_6t + C_2H_3$	$\rightarrow$	$C_2H_4 + C_4H_5t$	6.31000E+10	0.00	60.70
78	$C_4H_6t + C_3H_3$	$\rightarrow$	$C_3H_4a + C_4H_5t$	2.00000E+09	0.00	75.31
79	$C_4H_6t + C_3H_3$	$\rightarrow$	$C_3H_4p + C_4H_5t$	1.00000E+10	0.00	75.31
80	$C_4H_6t + H$	$\rightarrow$	$C_3H_4a + CH_3$	6.00000E+09	0.00	29.71
81	$OH + C_4H_6t$	$\rightarrow$	$C_3H_5a + CH_2O$	2.81000E+09	0.00	-3.66
82	$OH + C_4H_6t$	$\rightarrow$	$C_3H_4O + CH_3$	2.81000E+09	0.00	-3.66
83	$OH + C_4H_6t$	$\rightarrow$	$C_2H_4 + CH_3CO$	2.81000E+09	0.00	-3.66
84	$O + C_4H_6t$	$\rightarrow$	$C_2H_2O + C_2H_4$	1.00000E+09	0.00	0.00
85	$O + C_4H_6t$	$\rightarrow$	$C_3H_4p + CH_2O$	1.00000E+09	0.00	0.00
86	$C_4H_6t + HO_2$	$\rightarrow$	$C_3H_4O + CH_2O + H$	1.30000E+09	0.00	62.60
87	$O + C_4H_6t$	$\rightarrow$	$C_4H_5t + OH$	2.27000E+12	-0.48	29.42
88	C_4H_6t	$\rightarrow$	$C_4H_5t + H$	7.00000E+14	0.00	397.46
89	$C_4H_6t + O_2$	$\rightarrow$	$C_4H_5i + HO_2$	1.40000E+09	0.00	211.85
90	$O + C_4H_6t$	$\rightarrow$	$C_4H_5i + OH$	4.53000E+12	-0.47	29.42
91	$OH + C_4H_6t$	$\rightarrow$	$C_4H_5i + H_2O$	3.10000E+03	2.00	1.80
92	$C_4H_6t + H$	$\rightarrow$	$C_4H_5i + H_2$	6.65000E+02	2.53	38.69
93	$O + C_4H_6t$	$\rightarrow$	$C_4H_5Ox + H$	1.50000E+05	1.45	-3.60
94	C_4H_6t	$\rightarrow$	C_4H_6m	2.10000E+13	0.00	304.29
95	C_4H_6t	$\rightarrow$	C_4H_6s	2.18776E+75	-17.56	484.46
96	C_4H_6t	$\rightarrow$	C_4H_6b	4.20000E+11	0.00	178.75
97	C_4H_6s	$\rightarrow$	C_4H_6m	7.00000E+12	0.00	263.72
98	C_4H_6s	$\rightarrow$	$C_3H_3 + CH_3$	2.00000E+11	0.00	248.95
99	C_4H_6s	$\rightarrow$	$C_4H_5i + H$	4.20000E+15	0.00	387.10
100	$C_4H_6s + H$	$\rightarrow$	$C_2H_3 + C_2H_4$	4.00000E+08	0.00	0.00
101	$C_4H_6s + H$	$\rightarrow$	$C_4H_5s + H_2$	1.00000E+11	0.00	60.71
102	$OH + C_4H_6s$	$\rightarrow$	$C_4H_5s + H_2O$	1.62000E+10	0.00	0.00
103	$CH_3 + C_4H_6s$	$\rightarrow$	$C_4H_5s + CH_4$	7.00000E+10	0.00	25.00
104	$C_3H_3 + C_4H_6s$	$\rightarrow$	$C_3H_4a + C_4H_5s$	1.00000E+10	0.00	25.00
105	$C_3H_3 + C_4H_6s$	$\rightarrow$	$C_3H_4p + C_4H_5s$	1.00000E+10	0.00	25.00
106	$C_4H_6s + H$	$\rightarrow$	$C_3H_4a + CH_3$	6.00000E+09	0.00	8.79
107	$O + C_4H_6s$	$\rightarrow$	$C_3H_3O + CH_3$	3.58000E+09	0.00	0.00
108	C_4H_6b	$\rightarrow$	C_4H_6s	3.00000E+13	0.00	183.00
109	C_4H_6b	$\rightarrow$	C_4H_6m	5.25000E+12	0.00	158.00
110	C_4H_6b	$\rightarrow$	$C_2H_2 + C_2H_4$	1.40000E+15	0.00	301.80
111	$C_4H_6m + H$	$\rightarrow$	$C_3H_4p + CH_3$	6.50000E+01	2.50	4.18
112	$O + C_4H_6m$	$\rightarrow$	$C_3H_6 + CO$	6.00000E+10	0.00	7.48
113	C_4H_6f	$\rightarrow$	C_4H_6s	2.50000E+13	0.00	271.96
114	$C_4H_6f + H$	$\rightarrow$	$C_3H_4a + CH_3$	1.30000E+02	2.50	4.18
115	$C_4H_6f + H$	$\rightarrow$	$C_2H_2 + C_2H_5$	6.50000E+01	2.50	4.18
116	C_4H_6f	$\rightarrow$	$C_3H_3 + CH_3$	3.00000E+13	0.00	317.15
117	$C_4H_6f + O$	$\rightarrow$	$C_3H_6 + CO$	2.00000E+10	0.00	6.94
118	$C_4H_7n + O_2$	$\rightarrow$	$C_4H_6t + HO_2$	1.00000E+08	0.00	0.00
119	C_4H_7n	$\rightarrow$	$C_2H_3 + C_2H_4$	5.00000E+13	0.00	159.10
120	$C_4H_7n + H$	$\rightarrow$	$C_4H_6t + H_2$	3.16000E+09	0.00	0.00
121	C_4H_7n	$\rightarrow$	$C_4H_6t + H$	2.48000E+53	-12.30	217.57
122	$C_4H_7n + OH$	$\rightarrow$	$C_4H_6t + H_2O$	4.00000E+10	0.00	0.00
123	$C_4H_7n + O$	$\rightarrow$	$C_4H_6t + OH$	4.00000E+10	0.00	0.00
124	$C_4H_7n + M + H$	$\rightarrow$	$C_4H_8n + M$	3.60000E+10	0.00	0.00
125	$HO_2 + C_4H_7i$	$\rightarrow$	$C_4H_7Ox + OH$	4.50000E+09	0.00	0.00

#	Reaction	A	β	E_A
126	$CH_3OO + C_4H_7i \rightarrow C_4H_7Ox + CH_3O$	2.00000E+09	0.00	-5.02
127	$C_4H_7i \rightarrow C_3H_4a + CH_3$	2.00000E+13	0.00	209.52
128	$C_4H_7s + H \rightarrow C_4H_6s + H_2$	3.16000E+09	0.00	0.00
129	$OH + C_4H_7s \rightarrow C_4H_6s + H_2O$	4.00000E+10	0.00	0.00
130	$O + C_4H_7s \rightarrow C_4H_6s + OH$	4.00000E+10	0.00	0.00
131	$C_4H_8i \rightarrow C_3H_5t + CH_3$	3.30000E+21	-1.20	408.86
132	$C_4H_8i \rightarrow C_4H_7i + H$	1.06000E+47	-9.30	437.44
133	$C_4H_8i + O_2 \rightarrow C_4H_7i + HO_2$	1.44000E+10	0.00	161.21
134	$C_4H_8i + HO_2 \rightarrow C_4H_7i + H_2O_2$	3.00000E+08	0.00	59.37
135	$C_4H_8i + HO_2 \rightarrow C_4H_8Ox + OH$	1.02000E+09	0.00	62.61
136	$C_4H_8i + OH \rightarrow C_4H_7i + H_2O$	6.00000E+03	2.00	-0.25
137	$C_4H_8i + OH \rightarrow C_4H_8OHi$	3.40000E+20	-3.59	8.71
138	$C_4H_8i + O \rightarrow C_4H_7i + OH$	3.00000E+05	1.28	-4.51
139	$C_4H_8i + O \rightarrow C_3H_7i + CHO$	5.00000E+05	1.28	-4.51
140	$C_4H_8i + O \rightarrow C_4H_8Ox$	1.00000E+05	1.28	-4.51
141	$C_4H_8i + H \rightarrow C_4H_7i + H_2$	1.72000E+11	0.00	33.47
142	$C_4H_8i + H \rightarrow C_3H_6 + CH_3$	1.72000E+10	0.00	15.06
143*	$C_4H_8i + CH_3 \rightarrow C_4H_7i + CH_4$	4.42000E–03	3.50	18.49
144	$C_4H_8i + CHO \rightarrow C_4H_7i + CH_2O$	3.30000E+08	0.00	25.98
145	$C_4H_8i + C_2H_3 \rightarrow C_2H_4 + C_4H_7i$	1.00000E+10	0.00	54.39
146	$C_4H_8i + C_3H_5a \rightarrow C_3H_6 + C_4H_7i$	7.94000E+08	0.00	85.77
147	$C_4H_8i + C_3H_5s \rightarrow C_3H_6 + C_4H_7i$	7.94000E+08	0.00	85.77
148	$C_4H_8i + C_3H_5t \rightarrow C_3H_6 + C_4H_7i$	7.94000E+08	0.00	85.77
149	$C_4H_8i + CH_3OO \rightarrow C_4H_8Ox + CH_3O$	4.00000E+08	0.00	50.21
150	$O_2 + C_4H_8n \rightarrow C_4H_7n + HO_2$	1.44000E+10	0.00	250.21
151	$O_2 + C_4H_8n \rightarrow C_2H_4 + 2\ CH_2O$	0.00000E+00	0.00	10.00
152	$HO_2 + C_4H_8n \rightarrow C_4H_7n + H_2O_2$	3.00000E+08	0.00	148.37
153	$C_4H_8n \rightarrow C_3H_5a + CH_3$	1.00000E+16	0.00	305.43
154	$OH + C_4H_8n \rightarrow C_4H_7n + H_2O$	6.00000E+03	2.00	-0.25
155	$O + C_4H_8n \rightarrow C_4H_7n + OH$	3.00000E+05	1.28	-4.51
156	$O + C_4H_8n \rightarrow C_3H_7n + CHO$	5.00000E+05	1.28	-4.51
157	$H + C_4H_8n \rightarrow C_4H_7n + H_2$	1.72000E+11	0.00	88.47
158	$H + C_4H_8n \rightarrow C_3H_6 + CH_3$	1.72000E+10	0.00	32.06
159*	$CH_3 + C_4H_8n \rightarrow C_4H_7n + CH_4$	4.42000E–03	3.50	73.49
160	$CHO + C_4H_8n \rightarrow C_4H_7n + CH_2O$	3.30000E+08	0.00	80.98
161	$C_2H_3 + C_4H_8n \rightarrow C_2H_4 + C_4H_7n$	1.00000E+10	0.00	109.92
162	$C_3H_5a + C_4H_8n \rightarrow C_3H_6 + C_4H_7n$	7.94000E+08	0.00	140.77
163	$C_3H_5s + C_4H_8n \rightarrow C_3H_6 + C_4H_7n$	7.94000E+08	0.00	140.77
164	$C_3H_5t + C_4H_8n \rightarrow C_3H_6 + C_4H_7n$	7.94000E+08	0.00	140.77
165	$C_4H_8s + O_2 \rightarrow C_4H_7s + HO_2$	1.44000E+10	0.00	250.21
166	$C_4H_8s + HO_2 \rightarrow C_4H_7s + H_2O_2$	3.00000E+08	0.00	148.37
167	$C_4H_8s \rightarrow C_4H_7s + H$	3.98000E+15	0.00	356.05
168	$C_4H_8s \rightarrow C_3H_5s + CH_3$	3.16000E+17	0.00	415.46
169	$OH + C_4H_8s \rightarrow C_4H_7s + H_2O$	6.00000E+03	2.00	-0.25
170	$O + C_4H_8s \rightarrow C_4H_7s + OH$	3.00000E+05	1.28	-4.51
171	$O + C_4H_8s \rightarrow C_3H_7i + CHO$	5.00000E+05	1.28	-4.51
172	$C_4H_8s + H \rightarrow C_4H_7s + H_2$	1.72000E+11	0.00	88.47
173	$C_4H_8s + H \rightarrow C_3H_6 + CH_3$	1.72000E+10	0.00	32.06
174*	$CH_3 + C_4H_8s \rightarrow C_4H_7s + CH_4$	4.42000E–03	3.50	73.49

*Removed reaction

#	Reaction	A	β	E_A
175	$CHO + C_4H_8s \rightarrow C_4H_7s + CH_2O$	3.30000E+08	0.00	80.98
176	$C_4H_8s + C_2H_3 \rightarrow C_2H_4 + C_4H_7s$	1.00000E+10	0.00	109.92
177	$C_3H_5a + C_4H_8s \rightarrow C_3H_6 + C_4H_7s$	7.94000E+08	0.00	140.77
178	$C_3H_5s + C_4H_8s \rightarrow C_3H_6 + C_4H_7s$	7.94000E+08	0.00	140.77
179	$C_4H_8s + C_3H_5t \rightarrow C_3H_6 + C_4H_7s$	7.94000E+08	0.00	140.77
180	$C_4H_9s + M \rightarrow C_3H_6 + CH_3 + M$	2.67000E+10	1.06	129.48
181	$C_4H_9s \rightarrow C_4H_8s + H$	3.16000E+12	0.00	154.38
182	$C_4H_9s \rightarrow C_4H_8n + H$	1.58000E+13	0.00	165.68
183	$C_4H_9s + O_2 \rightarrow C_4H_8n + HO_2$	5.11000E+07	0.00	0.00
184	$C_4H_9s + O_2 \rightarrow C_4H_8s + HO_2$	7.80000E+07	0.00	0.00
185	$OH + C_4H_9s \rightarrow C_4H_8n + H_2O$	1.80000E+10	0.00	0.00
186	$OH + C_4H_9s \rightarrow C_4H_8s + H_2O$	1.80000E+10	0.00	0.00
187	$C_4H_9s + H \rightarrow C_4H_8n + H_2$	5.40000E+09	0.00	0.00
188	$C_4H_9s + H \rightarrow C_4H_8s + H_2$	5.40000E+09	0.00	0.00
189	$O + C_4H_9s \rightarrow C_4H_8n + OH$	4.16000E+11	0.00	0.00
190	$O + C_4H_9s \rightarrow C_4H_8s + OH$	4.16000E+11	0.00	0.00
191	$CH_3 + C_4H_9s \rightarrow C_4H_8n + CH_4$	1.26000E+10	0.00	-2.49
192	$CH_3 + C_4H_9s \rightarrow C_4H_8s + CH_4$	1.26000E+10	0.00	-2.49
193	$C_4H_9i \rightarrow C_3H_6 + CH_3$	2.00000E+13	0.00	125.31
194	$C_4H_9i \rightarrow C_4H_8i + H$	1.91000E+29	-5.25	166.35
195	$C_4H_9i + O_2 \rightarrow C_4H_8i + HO_2$	2.40000E+07	0.00	0.00
196	$C_4H_9i + HO_2 \rightarrow C_3H_7i + CH_2O + OH$	2.41000E+10	0.00	0.00
197	$C_4H_9t \rightarrow C_4H_8i + H$	2.90000E+51	-11.53	220.16
198	$CH_3OO + C_4H_9t \rightarrow C_3H_6Oa + CH_3 + CH_3O$	1.30000E+10	0.00	0.00
199	$C_4H_9t \rightarrow C_3H_6 + CH_3$	3.00000E+14	0.00	193.72
200	$C_4H_9t + O_2 \rightarrow C_4H_8i + HO_2$	4.80000E+08	0.00	0.00
201	$C_4H_9t + HO_2 \rightarrow C_3H_6Oa + CH_3 + OH$	1.80000E+10	0.00	0.00
202	$OH + C_4H_9t \rightarrow C_4H_8i + H_2O$	1.80000E+10	0.00	0.00
203	$C_4H_9t + H \rightarrow C_4H_8i + H_2$	5.40000E+09	0.00	0.00
204	$O + C_4H_9t \rightarrow C_4H_8i + OH$	4.16000E+11	0.00	0.00
205	$O + C_4H_9t \rightarrow C_3H_6Oa + CH_3$	1.04000E+11	0.00	0.00
206	$CH_3 + C_4H_9t \rightarrow C_4H_8i + CH_4$	1.26000E+10	0.00	-2.49
207	$OH + C_4H_9n \rightarrow C_4H_8n + H_2O$	1.80000E+10	0.00	0.00
208	$C_4H_9n \rightarrow C_3H_6 + CH_3$	1.26000E+12	0.00	113.38
209	$C_4H_9n \rightarrow C_4H_8n + H$	1.00000E+14	0.00	160.24
210	$O_2 + C_4H_9n \rightarrow C_4H_8n + HO_2$	2.70000E+08	0.00	0.00
211	$H + C_4H_9n \rightarrow C_4H_8n + H_2$	5.40000E+09	0.00	0.00
212	$O + C_4H_9n \rightarrow C_4H_8n + OH$	4.16000E+11	0.00	0.00
213	$CH_3 + C_4H_9n \rightarrow C_4H_8n + CH_4$	1.26000E+10	0.00	-2.49
214	$C_4H_10i \rightarrow C_3H_7i + CH_3$	1.10000E+26	-2.61	377.99
215	$H + C_4H_10i \rightarrow C_4H_9i + H_2$	1.81000E+03	2.54	28.27
216	$H + C_4H_10i \rightarrow C_4H_9t + H_2$	6.02000E+02	2.40	10.81
217	$OH + C_4H_10i \rightarrow C_4H_9i + H_2O$	2.29000E+05	1.53	3.24
218	$OH + C_4H_10i \rightarrow C_4H_9t + H_2O$	5.73000E+07	0.51	0.27
219	$O + C_4H_10i \rightarrow C_4H_9i + OH$	4.28000E+02	2.50	15.25
220	$O + C_4H_10i \rightarrow C_4H_9t + OH$	1.56000E+02	2.50	4.66
221	$C_4H_10i + HO_2 \rightarrow C_4H_9i + H_2O_2$	3.01000E+01	2.55	64.85
222	$C_4H_10i + HO_2 \rightarrow C_4H_9t + H_2O_2$	3.61000E+00	2.55	44.07
223	$C_4H_10n \rightarrow C_4H_9n + H$	1.58000E+16	0.00	410.02
224	$C_4H_10n \rightarrow C_4H_9s + H$	1.00000E+16	0.00	397.46
225	$C_4H_10n \rightarrow C_3H_7n + CH_3$	1.00000E+17	0.00	354.37

#	**Reaction**			A	β	E_A
226	$C_4H_10n + H$	$\rightarrow$	$C_4H_9n + H_2$	5.62000E+04	2.00	32.22
227	$C_4H_10n + H$	$\rightarrow$	$C_4H_9s + H_2$	2.00000E+11	0.00	34.90
228	$OH + C_4H_10n$	$\rightarrow$	$C_4H_9n + H_2O$	4.13000E+04	1.73	3.15
229	$OH + C_4H_10n$	$\rightarrow$	$C_4H_9s + H_2O$	2.57000E+06	1.25	2.93
230	$C_4H_10n + O$	$\rightarrow$	$C_4H_9n + OH$	3.00000E+10	0.00	24.00
231	$C_4H_10n + O$	$\rightarrow$	$C_4H_9s + OH$	5.20000E+10	0.00	18.60
232	$C_4H_10n + HO_2$	$\rightarrow$	$C_4H_9n + H_2O_2$	1.12000E+10	0.00	81.16
233	$C_4H_10n + HO_2$	$\rightarrow$	$C_4H_9s + H_2O_2$	5.00000E+08	0.00	43.92
234	$C_4H_10n + O_2$	$\rightarrow$	$C_4H_9n + HO_2$	2.51000E+10	0.00	205.00
235	$C_4H_10n + O_2$	$\rightarrow$	$C_4H_9s + HO_2$	3.98000E+10	0.00	199.00
236	$OH + C_4H_2O$	$\rightarrow$	$C_2H_2 + 2\ CO + H$	1.00000E+12	0.00	0.00
237	C_4H_4O	$\rightarrow$	$C_3H_4p + CO$	1.78000E+15	0.00	324.26
238	C_4H_4O	$\rightarrow$	$C_2H_2 + C_2H_2O$	5.01000E+14	0.00	324.26
239	C_4H_5Ox	$\rightarrow$	$C_3H_5s + CO$	1.00000E+14	0.00	125.60
240	C_4H_5Oy	$\rightarrow$	$C_3H_5a + CO$	1.00000E+14	0.00	104.67
241	C_4H_6Oa	$\rightarrow$	C_4H_6Ob	1.35000E+15	0.00	211.71
242	C_4H_6Oa	$\rightarrow$	$C_2H_3 + CH_3CO$	1.00000E+16	0.00	284.51
243	C_4H_6Ob	$\rightarrow$	$C_3H_6 + CO$	1.09000E+16	0.00	305.43
244	C_4H_6Ob	$\rightarrow$	$C_4H_5t + OH$	0.00000E+00	0.00	203.06
245	C_4H_6Ob	$\rightarrow$	$C_4H_4O + H_2$	5.30000E+12	0.00	203.06
246	$C_4H_7Om + M$	$\rightarrow$	$C_3H_7i + CO + M$	8.64000E+12	0.00	60.25
247	C_4H_7Ox	$\rightarrow$	$C_3H_5t + CH_2O$	5.00000E+15	0.00	104.60
248	C_4H_7Ox	$\rightarrow$	$C_3H_5a + CH_2O$	1.00000E+15	0.00	104.60
249	C_4H_8Ox	$\rightarrow$	C_4H_8Om	4.00000E+13	0.00	239.32
250	C_4H_8Ox	$\rightarrow$	$C_3H_7i + CHO$	6.00000E+13	0.00	239.32
251	C_4H_8Om	$\rightarrow$	$C_3H_7i + CHO$	2.44000E+16	0.00	351.99
252	$C_4H_8Om + O_2$	$\rightarrow$	$C_4H_7Om + HO_2$	3.01000E+10	0.00	163.79
253	$C_4H_8Om + HO_2$	$\rightarrow$	$C_4H_7Om + H_2O_2$	3.01000E+09	0.00	49.89
254	$C_4H_8Om + OH$	$\rightarrow$	$C_4H_7Om + H_2O$	3.37000E+09	0.00	-2.58
255	$C_4H_8Om + O$	$\rightarrow$	$C_4H_7Om + OH$	5.00000E+09	0.00	7.50
256	$C_4H_8Om + H$	$\rightarrow$	$C_4H_7Om + H_2$	4.00000E+10	0.00	17.60
257	$C_4H_8OHi + O_2$	$\rightarrow$	$O_2C_4H_9O$	3.25000E+23	-4.69	17.97
258	$O_2C_4H_9O$	$\rightarrow$	$C_3H_6Oa + CH_2O + OH$	1.00000E+16	0.00	104.60
259	$CH_2t + C_3H_3$	$\rightarrow$	C_4H_5i	8.00000E+10	0.00	0.00
260	$CH_2s + C_3H_3$	$\rightarrow$	C_4H_5i	8.00000E+10	0.00	0.00

Table C.8: Modified collision dependencies. The numbering in the first column refers to the corresponding reaction shown in Table C.7. The default value of the collision dependency is 1.0 unless otherwise stated.

#	Modified collision dependencies
124	H_2: 2.0, CO: 1.5, CO_2: 2.0, H_2O: 6.0, CH_4: 2.0, C_2H_6: 3.0

Table C.9: Fall-off parameters. The numbering in the first column refers to the corresponding pressure dependency reactions listed in Table C.7. The units of the pre-exponential factors are in [kmol, m^3, s] depending on the reaction order and the activation barriers are given in [kJ/mol].

#	Fall-off parameters	A	β	E_A
33	$F_c = 1.00$	1.00000E+11	0.00	125.52
37	$F_c = 1.00$	1.00000E+11	0.00	125.52
47	$F_c = 1.00$	2.00000E+12	0.00	175.73
53	$F_c = 1.00$	1.00000E+11	0.00	125.52
69	$F_c = 1.00$	2.00000E+12	0.00	175.73
124	$F_c = e^{(-1314.0/T)} + e^{(-T/1.0)}$	3.01000E+42	-9.32	24.41
180	$F_c = 1.01e^{(-206.0/T)} + e^{(-T/0.196)}$	2.30000E+60	-14.30	153.80

Appendix D

Gas phase transport and thermochemical properties

This Appendix illustrates the gas phase transport and thermochemical properties as applied in Chapters 4 and 5. The gas phase transport and thermochemical properties shown in Tables D.1 and D.4 are implemented in both Chapters 4 and 5, while the ones presented in Tables D.2 and D.5 are exclusively included in Chapter 4. The additional -C_4 containing gas phase transport and thermochemical properties, shown in Tables D.3 and D.6, are applied in Chapter 5. Finally, the thermochemical data are represented as the high and low temperature JANAF polynomials, described in Section 2.2.

Table D.1: Gas phase (C_1 - C_2 - C_3) transport properties implemented in Chapters 4 and 5.

Species	σ_{LJ}	ϵ_{LJ}	Z_{rot}	C_{rot}	μ_i
H_2	2.83	59.7	280	1	8.92E-06
O_2	3.46	107.4	3.8	2	2.06E-05
H	2.71	37	1000	1	7.49E-06
OH	2.75	80	10	1	1.97E-05
O	2.75	80	1000	1	1.89E-05
H_2O	2.61	572	4	1	1.10E-05
HO_2	3.46	107.4	3	1	9.82E-06
H_2O_2	3.46	107.4	3	2	9.82E-06
C_2H_6	4.30	252.3	2	1.5	9.47E-06
C_2H_5	4.30	252.3	2	1.5	1.02E-05
C_2H_4	3.97	280.8	2	1.5	1.02E-05
C_2H_2	4.1	209	2.5	1.5	1.03E-05
CH_4	3.75	141	13	1	1.12E-05

Species	σ_{LJ}	ϵ_{LJ}	Z_{rot}	C_{rot}	μ_i
CH_3	3.8	144	13	1.5	1.12E-05
CH_2s	3.8	144	13	1	1.12E-05
CH_2t	3.8	144	13	1	1.12E-05
CH	2.75	80	2	1	1.55E-05
C_1	2.75	80	2	1	1.55E-05
CO	3.65	98	1.8	4	1.77E-05
CO_2	3.76	244	2.1	1.5	1.52E-05
CH_2O	3.59	498	2	1.5	1.83E-05
CHO	3.59	498	2	1.5	1.83E-05
CH_3OH	3.63	481.8	1	1.5	9.82E-06
CH_3O	3.59	498	2	1.5	1.83E-05
CH_2OH	3.59	498	2	1.5	1.83E-05
C_2O	2.5	150	2	1.5	8.74E-06
C_2H	4.1	209	2.5	1.5	1.03E-05
C_2HO	2.5	150	2	1.5	8.74E-06
C_2H_2O	3.97	436	2	1.5	8.74E-06
C_2H_3	4.1	209	2	1.5	1.03E-05
CH_3CHO	3.97	280.8	2	1.5	1.02E-05
CH_3CO	3.97	280.8	2	1.5	1.02E-05
C_2	3.91	78.8	1	1	1.52E-05
CH_2CHO	3.97	280.8	2	1.5	1.02E-05
H_2C_2	4.1	209	2.5	1.5	1.03E-05
CH_3OO	3.63	481.8	1	1.5	9.82E-06
CH_3OOH	3.63	481.8	1	1.5	9.82E-06
$CHCH_2O$	3.63	481.8	1	1.5	9.82E-06
C_2H_4O	3.63	481.8	1	1.5	9.82E-06
C_2H_4OOH	3.63	481.8	1	1.5	9.82E-06
C_2H_5O	3.63	481.8	1	1.5	9.82E-06
C_2H_5OO	3.63	481.8	1	1.5	9.82E-06
C_2H_5OOH	3.63	481.8	1	1.5	9.82E-06
C_3H	4.1	209	1	1.5	8.86E-06
C_3H_2	4.1	209	1	1.5	8.86E-06
C_3H_2l	4.1	209	1	1.5	8.86E-06

Species	σ_{LJ}	ϵ_{LJ}	Z_{rot}	C_{rot}	μ_i
C_3H_3	4.76	252	1	1.5	8.86E-06
C_3H_4a	4.76	252	1	1.5	8.86E-06
C_3H_4p	4.76	252	1	1.5	8.86E-06
C_3H_4b	4.76	252	1	1.5	8.86E-06
C_3H_5a	4.76	252	1	1.5	8.86E-06
C_3H_5s	4.76	252	1	1.5	8.86E-06
C_3H_5t	4.76	252	1	1.5	8.86E-06
C_3H_5b	4.76	252	1	1.5	8.86E-06
C_3H_6b	4.76	252	1	1.5	8.86E-06
C_3H_6	4.98	266.8	1	1.5	8.95E-06
C_3H_7n	4.98	266.8	1	1.5	8.27E-06
C_3H_7i	4.98	266.8	1	1.5	8.27E-06
C_3H_8	4.98	266.8	1	1.5	8.27E-06
C_3H_2O	4.1	209	1	1.5	8.86E-06
C_3H_3O	4.76	252	1	1.5	8.86E-06
C_3H_4O	4.76	252	1	1.5	8.86E-06
C_3H_5O	4.76	252	1	1.5	8.86E-06
C_3H_5Op	4.76	252	1	1.5	8.86E-06
C_3H_5Ot	4.76	252	1	1.5	8.86E-06
C_3H_5Oa	4.76	252	1	1.5	8.86E-06
C_3H_6O	4.76	252	1	1.5	8.86E-06
C_3H_6Oa	4.76	252	1	1.5	8.86E-06
C_3H_6Op	4.76	252	1	1.5	8.86E-06
C_3H_7Oi	4.76	252	1	1.5	8.86E-06
C_3H_7On	4.76	252	1	1.5	8.86E-06
C_3H_6OH	4.76	252	1	1.5	8.86E-06
C_3H_7OOHi	4.76	252	1	1.5	8.86E-06
C_3H_7OOHn	4.76	252	1	1.5	8.86E-06
C_3H_7OOi	4.76	252	1	1.5	8.86E-06
C_3H_7OOn	4.76	252	1	1.5	8.86E-06
C_3H_6OOH	4.76	252	1	1.5	8.86E-06

Table D.2: Additional gas phase (-N) transport properties implemented in Chapter 4.

Species	σ_{LJ}	ϵ_{LJ}	Z_{rot}	C_{rot}	μ_i
NH_3	2.92	481	10	1	9.19E-06
NH_2	2.65	80	4	1	9.19E-06
NH	2.65	80	4	1	1.89E-05
N	3.30	71.4	1	1	1.89E-05
N_2H_2	3.80	71.4	1	1	9.19E-06
NNH	3.80	71.4	1	1	9.19E-06
HNO	3.49	116.7	1	1	1.78E-05
NO	3.62	97.53	4	1	1.78E-05
NO_2	3.5	200	1	1	1.33E-10
N_2O	3.83	232.4	1	1	1.36E-05
HCN	3.63	569	1	1	2.01E-05
CN	3.86	75	1	1	2.01E-05
NCO	3.83	232.4	1	1	2.01E-05
HNCO	3.83	232.4	1	1	2.01E-05
HOCN	3.83	232.4	1	1	2.01E-05
HNO_2	3.5	200	1	1	1.33E-10
H_2CN	3.63	569	1	1	2.01E-05
HCNO	3.83	232.4	1	1	2.01E-05
HNC	3.86	75	1	1	2.01E-05
CH_3NO_2	3.63	481.8	1	1.5	0
CH_2NO_2	3.63	481.8	1	1.5	0
N_2	3.62	97.53	4	1	0
N_3	3.83	232.4	1	1	2.01E-05
NO_3	4.11	390	1.5	2.1	1.6E-05
N_2O_5	4.11	390	1.5	2.1	1.6E-05
N_2O_3	4.11	390	1.5	2.1	1.6E-05
HNO_3	4.11	390	2.1	1.5	1.6E-05
N_2O_4	4.11	390	1.5	2.1	1.6E-05
HN_3	3.83	232.4	1	1	2.01E-05

Table D.3: Additional gas phase (-C_4) transport properties implemented in Chapter 5.

Species	σ_{LJ}	ϵ_{LJ}	Z_{rot}	C_{rot}	μ_i
C_4H	5.18	357	1	1.5	7.55E-06
C_4H_2	5.18	357	1	1.5	7.55E-06
C_4H_3n	5.18	357	1	1.5	7.55E-06
C_4H_3i	5.18	357	1	1.5	7.55E-06
C_4H_4	5.18	357	1	1.5	7.55E-06
C_4H_5s	5.18	357	1	1.5	7.55E-06
C_4H_5t	5.18	357	1	1.5	7.55E-06
C_4H_5i	5.28	330	1	1.5	7.55E-06
C_4H_6s	5.28	330	1	1.5	7.55E-06
C_4H_6t	5.28	330	1	1.5	7.55E-06
C_4H_6f	5.28	330	1	1.5	7.55E-06
C_4H_6b	5.28	330	1	1.5	7.55E-06
C_4H_6m	5.28	330	1	1.5	7.55E-06
C_4H_7i	5.28	330	1	1.5	7.55E-06
C_4H_7n	5.28	330	1	1.5	7.55E-06
C_4H_7s	5.28	330	1	1.5	7.55E-06
C_4H_8i	5.28	330	1	1.5	7.55E-06
C_4H_8n	5.28	330	1	1.5	7.55E-06
C_4H_8s	5.28	330	1	1.5	7.55E-06
C_4H_9i	5.28	330	1	1.5	7.55E-06
C_4H_9t	5.28	330	1	1.5	7.55E-06
C_4H_9n	5.28	330	1	1.5	7.55E-06
C_4H_9s	5.28	330	1	1.5	7.55E-06
$C_4H_{10}n$	5.28	330	1	1.5	7.55E-06
$C_4H_{10}i$	5.28	330	1	1.5	7.55E-06
C_4H_2O	5.49	374	1	1.5	7.18E-06
C_4H_4O	5.49	374	1	1.5	7.18E-06
C_4H_5Ox	5.49	374	1	1.5	7.18E-06
C_4H_5Oy	5.49	374	1	1.5	7.18E-06
C_4H_6Ob	5.49	374	1	1.5	7.18E-06
C_4H_6Oa	5.49	374	1	1.5	7.18E-06
C_4H_7Ox	5.49	374	1	1.5	7.18E-06

Species	σ_{LJ}	ϵ_{LJ}	Z_{rot}	C_{rot}	μ_i
C_4H_7Om	5.49	374	1	1.5	7.18E-06
C_4H_8Ox	5.49	374	1	1.5	7.18E-06
C_4H_8Om	5.49	374	1	1.5	7.18E-06
C_4H_8OHi	5.49	374	1	1.5	7.18E-06
$O_2C_4H_9O$	5.49	374	1	1.5	7.18E-06

Table D.4: Gas phase thermochemical properties implemented in Chapters 4 and 5.

	H_2
$T > 1000K$	0.29328305E+01 0.82659802E-03 -0.14640057E-06 0.15409851E-10 -0.68879615E-15 -0.813055820E+03 -0.102431640E+01
$T \leq 1000K$	0.23443029E+01 0.79804248E-02 -0.19477917E-04 0.20156967E-07 -0.73760289E-11 -0.91792413E+03 0.68300218E+00
	O_2
$T > 1000K$	3.66096083E+00 6.56365523E-04 -1.41149485E-07 2.05797658E-11 -1.29913248E-15 -1.21597725E+03 3.41536184E+00
$T \leq 1000K$	3.78245636E+00 -2.99673415E-03 9.84730200E-06 -9.68129508E-09 3.24372836E-12 -1.06394356E+03 3.65767573E+00
	H
$T > 1000K$	0.25000000E+01 0.0000000E+00 0.0000000E+00 0.00000000E+00 0.00000000E+00 0.25473660E+05 -0.44668285E+00
$T \leq 1000K$	0.25000000E+01 0.0000000E+00 0.0000000E+00 0.00000000E+00 0.00000000E+00 0.25473660E+05 -0.44668285E+00
	OH
$T > 1000K$	2.83853033E+00 1.10741289E-03 -2.94000209E-07 4.20698729E-11 -2.42289890E-15 3.69780808E+03 5.84494652E+00
$T \leq 1000K$	3.99198424E+00 -2.40106655E-03 4.61664033E-06 -3.87916306E-09 1.36319502E-12 3.36889836E+03 -1.03998477E-01
	O
$T > 1000K$	0.25420597E+01 -0.27550619E-04 -0.31028033E-08 0.45510674E-11 -0.43680515E-15 0.29230803E+05 0.49203081E+01
$T \leq 1000K$	0.29464288E+01 -0.16381665E-02 0.24210317E-05 -0.16028432E-08 0.38906963E-12 0.29147644E+05 0.29639949E+01

H_2O	
$T > 1000$K	0.26770389E+01 0.29731816E-02 -0.77376889E-06 0.94433514E-10 -0.42689991E-14 -0.29885894E+05 0.68825500E+01
$T \leq 1000$K	0.41986352E+01 -0.20364017E-02 0.65203416E-05 -0.54879269E-08 0.17719680E-11 -0.30293726E+05 -0.84900901E+00
HO_2	
$T > 1000$K	0.41722659E+01 0.18812098E-02 -0.34629297E-06 0.19468516E-10 0.17609153E-15 0.61818851E+02 0.29577974E+01
$T \leq 1000$K	0.43017880E+01 -0.47490201E-02 0.21157953E-04 -0.24275961E-07 0.92920670E-11 0.29480876E+03 0.37167010E+01
H_2O_2	
$T > 1000$K	4.57977305E+00 4.05326003E-03 -1.29844730E-06 1.98211400E-10 -1.13968792E-14 -1.80071775E+04 6.64970694E-01
$T \leq 1000$K	4.31515149E+00 -8.47390622E-04 1.76404323E-05 -2.26762944E-08 9.08950158E-12 -1.77067437E+04 3.27373319E+00
C_2H_6	
$T > 1000$K	4.04666411E+00 1.53538802E-02 -5.47039485E-06 8.77826544E-10 -5.23167531E-14 -1.24473499E+04 -9.68698313E-01
$T \leq 1000$K	4.29142572E+00 -5.50154901E-03 5.99438458E-05 -7.08466469E-08 2.68685836E-11 -1.15222056E+04 2.66678994E+00
C_2H_5	
$T > 1000$K	0.42878814E+01 0.12433893E-01 -0.44139119E-05 0.70654102E-09 -0.42035136E-13 0.12056455E+05 0.84602583E+00
$T \leq 1000$K	0.43058580E+01 -0.41833638E-02 0.49707270E-04 -0.59905874E-07 0.23048478E-10 0.12841714E+05 0.47100236E+01
C_2H_4	
$T > 1000$K	3.99182724E+00 1.04833908E-02 -3.71721342E-06 5.94628366E-10 -3.53630386E-14 4.26865851E+03 -2.69081762E-01
$T \leq 1000$K	3.95920063E+00 -7.57051373E-03 5.70989993E-05 -6.91588352E-08 2.69884190E-11 5.08977598E+03 4.09730213E+00
C_2H_2	
$T > 1000$K	4.65878489E+00 4.88396667E-03 -1.60828888E-06 2.46974544E-10 -1.38605959E-14 2.57594042E+04 -3.99838194E+00
$T \leq 1000$K	8.08679682E-01 2.33615762E-02 -3.55172234E-05 2.80152958E-08 -8.50075165E-12 2.64289808E+04 1.39396761E+01

CH_4	
$T > 1000$K	1.65326226E+00 1.00263099E-02 -3.31661238E-06 5.36483138E-10 -3.14696758E-14 -1.00095936E+04 9.90506283E+00
$T \leq 1000$K	5.14911468E+00 -1.36622009E-02 4.91453921E-05 -4.84246767E-08 1.66603441E-11 -1.02465983E+04 -4.63848842E+00
CH_3	
$T > 1000$K	0.28440516E+01 0.61379741E-02 -0.22303452E-05 0.37851608E-09 -0.24521590E-13 0.16437808E+05 0.54526973E+01
$T \leq 1000$K	0.24304428E+01 0.11124099E-01 -0.16802203E-04 0.16218287E-07 -0.58649526E-11 0.16423781E+05 0.67897939E+01
CH_2s	
$T > 1000$K	3.13501686E+00 2.89593926E-03 -8.16668090E-07 1.13572697E-10 -6.36262835E-15 5.05040504E+04 4.06030621E+00
$T \leq 1000$K	4.19331325E+00 -2.33105184E-03 8.15676451E-06 -6.62985981E-09 1.93233199E-12 5.03662246E+04 -7.46734310E-01
CH_2t	
$T > 1000$K	3.14631886E+00 3.03671259E-03 -9.96474439E-07 1.50483580E-10 -8.57335515E-15 4.60412605E+04 4.72341711E+00
$T \leq 1000$K	3.71757846E+00 1.27391260E-03 2.17347251E-06 -3.48858500E-09 1.65208866E-12 4.58723866E+04 1.75297945E+00
CH	
$T > 1000$K	0.25209369E+01 0.17653639E-02 -0.46147660E-06 0.59289675E-10 -0.33474501E-14 0.70946769E+05 0.74051829E+01
$T \leq 1000$K	0.34897583E+01 0.32432160E-03 -0.16899751E-05 0.31628420E-08 -0.14061803E-11 0.70612646E+05 0.20842841E+01
C_1	
$T > 1000$K	0.26055830E+01 -0.19593434E-03 0.10673722E-06 -0.16423940E-10 0.81870580E-15 0.85411742E+05 0.41923868E+01
$T \leq 1000$K	0.25542395E+01 -0.32153772E-03 0.73379223E-06 -0.73223487E-09 0.26652144E-12 0.85442681E+05 0.45313085E+01
CO	
$T > 1000$K	0.30484859E+01 0.13517281E-02 -0.48579405E-06 0.78853644E-10 -0.46980746E-14 -0.14266117E+05 0.60170977E+01
$T \leq 1000$K	0.35795335E+01 -0.61035369E-03 0.10168143E-05 0.90700586E-09 -0.90442449E-12 -0.14344086E+05 0.35084093E+01

CO_2	
$T > 1000$K	0.46365111E+01 0.27414569E-02 -0.99589759E-06 0.16038666E-09 -0.91619857E-14 -0.49024904E+05 -0.19348955E+01
$T \leq 1000$K	0.23568130E+01 0.89841299E-02 -0.71220632E-05 0.24573008E-08 -0.14288548E-12 -0.48371971E+05 0.99009035E+01
CH_2O	
$T > 1000$K	0.31694807E+01 0.61932742E-02 -0.22505981E-05 0.36598245E-09 -0.22015410E-13 -0.14478425E+05 0.60423533E+01
$T \leq 1000$K	0.47937036E+01 -0.99081518E-02 0.37321459E-04 -0.37927902E-07 0.13177015E-10 -0.14308955E+05 0.60288702E+00
CHO	
$T > 1000$K	3.92001542E+00 2.52279324E-03 -6.71004164E-07 1.05615948E-10 -7.43798261E-15 3.65342928E+03 3.58077056E+00
$T \leq 1000$K	4.23754610E+00 -3.32075257E-03 1.40030264E-05 -1.34239995E-08 4.37416208E-12 3.87241185E+03 3.30834869E+00
CH_3OH	
$T > 1000$K	0.36012593E+01 0.10243223E-01 -0.35999217E-05 0.57251951E-09 -0.33912719E-13 -0.25997155E+05 0.47056025E+01
$T \leq 1000$K	0.57153948E+01 -0.15230920E-01 0.65244182E-04 -0.71080873E-07 0.26135383E-10 -0.25642765E+05 -0.15040970E+01
CH_3O	
$T > 1000$K	4.75779238E+00 7.44142474E-03 -2.69705176E-06 4.38090504E-10 -2.63537098E-14 3.78111940E+02 -1.96680028E+00
$T \leq 1000$K	3.71180502E+00 -2.80463306E-03 3.76550971E-05 -4.73072089E-08 1.86588420E-11 1.29569760E+03 6.57240864E+00
CH_2OH	
$T > 1000$K	5.09314370E+00 5.94761260E-03 -2.06497460E-06 3.23008173E-10 -1.88125902E-14 -4.03409640E+03 -1.84691493E+00
$T \leq 1000$K	4.47834367E+00 -1.35070310E-03 2.78484980E-05 -3.64869060E-08 1.47907450E-11 -3.50072890E+03 3.30913500E+00
C_2O	
$T > 1000$K	5.42468378E+00 1.85393945E-03 -5.17932956E-07 6.77646230E-11 -3.53315237E-15 3.31537194E+04 -3.69608405E+00
$T \leq 1000$K	2.86278214E+00 1.19701204E-02 -1.80851222E-05 1.52777730E-08 -5.20063163E-12 3.37501779E+04 8.89759099E+00

C_2H						
$T > 1000$K	0.36646060E+01	0.38218694E-02	-0.13650743E-05	0.21324828E-09	-0.12309430E-13	0.67297055E+05 0.39134973E+01
$T \leq 1000$K	0.29018020E+01	0.13285982E-01	-0.28050886E-04	0.28930184E-07	-0.10744742E-10	0.67190326E+05 0.61723506E+01

C_2HO						
$T > 1000$K	5.80668033E+00	3.63140881E-03	-1.28197024E-06	2.04562706E-10	-1.21475486E-14	1.94243191E+04 -4.44501759E+00
$T \leq 1000$K	2.50499402E+00	1.94889354E-02	-3.30041888E-05	2.96410713E-08	-1.02822778E-11	2.00662139E+04 1.11211692E+01

C_2H_2O						
$T > 1000$K	0.57577901E+01	0.63496507E-02	-0.22584407E-05	0.36208462E-09	-0.21569030E-13	-0.79786113E+04 -0.61064037E+01
$T \leq 1000$K	0.21401165E+01	0.18088368E-01	-0.17324216E-04	0.92767477E-08	-0.19915011E-11	-0.70430509E+04 0.12198699E+02

C_2H_3						
$T > 1000$K	4.15026763E+00	7.54021341E-03	-2.62997847E-06	4.15974048E-10	-2.45407509E-14	3.38566380E+04 1.72812235E+00
$T \leq 1000$K	3.36377642E+00	2.65765722E-04	2.79620704E-05	-3.72986942E-08	1.51590176E-11	3.44749589E+04 7.91510092E+00

CH_3CHO						
$T > 1000$K	5.25190093E+00	1.18574124E-02	-4.27442759E-06	6.91482701E-10	-4.14491372E-14	-2.24327033E+04 -2.48438587E+00
$T \leq 1000$K	5.08801432E+00	-6.39393756E-03	5.50299788E-05	-6.47002177E-08	2.44610814E-11	-2.14638582E+04 2.91845026E+00

CH_3CO						
$T > 1000$K	0.53137165E+01	0.91737793E-02	-0.33220386E-05	0.53947456E-09	-0.32452368E-13	-0.36450414E+04 -0.16757558E+01
$T \leq 1000$K	0.40358705E+01	0.87729487E-03	0.30710010E-04	-0.39247565E-07	0.15296869E-10	-0.26820738E+04 0.78617682E+01

C_2						
$T > 1000$K	4.12492246E+00	1.08348338E-04	1.57252585E-07	-4.24046828E-11	3.25059373E-15	9.81882961E+04 7.97432262E-01
$T \leq 1000$K	-1.96261001E+00	5.76822247E-02	-1.58039636E-04	1.72462711E-07	-6.57913199E-11	9.82538219E+04 2.33201223E+01

CH_2CHO	
$T > 1000$K	0.59756699E+01 0.81305914E-02 -0.27436245E-05 0.40703041E-09 -0.21760171E-13 0.49032178E+03 -0.50320879E+01
$T \leq 1000$K	0.34090624E+01 0.10738574E-01 0.18914925E-05 0.71585831E-08 0.28673851E-11 0.15214766E+04 0.95714535E+01
H_2C_2	
$T > 1000$K	0.42780340E+01 0.47562804E-02 -0.16301009E-05 0.25462806E-09 -0.14886379E-13 0.48316688E+05 0.64023701E+00
$T \leq 1000$K	0.32815483E+01 0.69764791E-02 -0.23855244E-05 -0.12104432E-08 0.98189545E-12 0.48621794E+05 0.59203910E+01
CH_3OO	
$T > 1000$K	5.92505819E+00 9.00194542E-03 -3.24254309E-06 5.24362718E-10 -3.14263003E-14 -1.53258958E+03 -4.93669747E+00
$T \leq 1000$K	4.76597792E+00 -3.51077148E-03 4.54394152E-05 -5.66763729E-08 2.21591482E-11 -4.82401289E+02 4.76095141E+00
CH_3OOH	
$T > 1000$K	7.76538058E+00 8.61499712E-03 -2.98006935E-06 4.68638071E-10 -2.75339255E-14 -1.82979984E+04 -1.43992663E+01
$T \leq 1000$K	2.90540897E+00 1.74994735E-02 5.28243630E-06 -2.52827275E-08 1.34368212E-11 -1.68894632E+04 1.13741987E+01
$CHCH_2O$	
$T > 1000$K	1.07995416E+01 5.72671347E-04 8.02782550E-07 -2.53454280E-10 2.09044767E-14 1.52021967E+04 -3.37254674E+01
$T \leq 1000$K	2.67776365E+00 9.77160821E-03 1.10328958E-05 -1.85799046E-08 7.04008273E-12 1.84922455E+04 1.24178161E+01
C_2H_4O	
$T > 1000$K	0.54887641E+01 0.12046190E-01 -0.43336931E-05 0.70028311E-09 -0.41949088E-13 -0.91804251E+04 -0.70799605E+01
$T \leq 1000$K	0.37590532E+01 -0.94412180E-02 0.80309721E-04 -0.10080788E-06 0.40039921E-10 -0.75608143E+04 0.78497475E+01
C_2H_4OOH	
$T > 1000$K	9.74660000E+00 0.01084240E+00 -3.13022000E-06 3.83694000E-10 -1.60474000E-14 -3.94819063E+02 -2.07656245E+01
$T \leq 1000$K	2.10863000E+00 0.03341860E+00 -2.66198000E-05 1.03835000E-08 -1.41770000E-12 1.56528996E+03 1.81813376E+01

C_2H_5O	
$T > 1000$K	0.66889982E+01 0.13125676E-01 -0.47038840E-05 0.75858552E-09 -0.45413306E-13 -0.47457832E+04 -0.96983755E+01
$T \leq 1000$K	0.43074268E+01 0.64147205E-02 0.31139714E-04 -0.43314083E-07 0.17276184E-10 -0.34027524E+04 0.59025837E+01
C_2H_5OO	
$T > 1000$K	8.05957692E+00 1.52921019E-02 -5.54442603E-06 9.00496195E-10 -5.41302799E-14 -7.31028500E+03 -1.59992904E+01
$T \leq 1000$K	5.21694144E+00 1.24160003E-04 6.15529492E-05 -7.94505636E-08 3.12101317E-11 -5.41455775E+03 4.22381533E+00
C_2H_5OOH	
$T > 1000$K	8.99519146E+00 1.52768090E-02 -5.42345537E-06 8.64392953E-10 -5.12061321E-14 -2.34335955E+04 -1.78995702E+01
$T \leq 1000$K	6.95135129E+00 2.46459348E-03 5.06621132E-05 -6.73457524E-08 2.69294264E-11 -2.20224273E+04 -3.02023422E+00
C_3H	
$T > 1000$K	6.14184491E+00 3.39661013E-03 -1.21915444E-06 1.97782838E-10 -1.18312807E-14 8.44225753E+04 -6.44480148E+00
$T \leq 1000$K	3.34917187E+00 1.65822626E-02 -2.77115653E-05 2.51382364E-08 -8.85285352E-12 8.49863168E+04 6.80362439E+00
C_3H_2	
$T > 1000$K	5.69445684E+00 6.53821901E-03 -2.35907266E-06 3.82037384E-10 -2.29227460E-14 5.49264274E+04 -6.96163733E+00
$T \leq 1000$K	3.18167129E+00 -3.37611741E-04 3.95343765E-05 -5.49792422E-08 2.28335240E-11 5.61816758E+04 9.06482468E+00
C_3H_2l	
$T > 1000$K	6.42557170E+00 5.57113530E-03 -1.93729414E-06 3.05883061E-10 -1.80270714E-14 6.99539184E+04 -8.83877867E+00
$T \leq 1000$K	2.51874113E+00 1.96318981E-02 -2.17479988E-05 1.29990854E-08 -3.05445698E-12 7.08679212E+04 1.05212804E+01
C_3H_3	
$T > 1000$K	7.14221719E+00 7.61902211E-03 -2.67460030E-06 4.24914904E-10 -2.51475443E-14 3.95709594E+04 -1.25848690E+01
$T \leq 1000$K	1.35110873E+00 3.27411291E-02 -4.73827407E-05 3.76310220E-08 -1.18541128E-11 4.07679941E+04 1.52058598E+01

C_3H_4a						
$T > 1000$K	0.63168722E+01	0.11133728E-01	-0.39629378E-05	0.63564238E-09	-0.37875540E-13	0.20117495E+05 -0.10995766E+02
$T \leq 1000$K	0.26130445E+01	0.12122575E-01	0.18539880E-04	-0.34525149E-07	0.15335079E-10	0.21541567E+05 0.10226139E+02

C_3H_4p						
$T > 1000$K	0.60252400E+01	0.11336542E-01	-0.40223391E-05	0.64376063E-09	-0.38299635E-13	0.19620942E+05 -0.86043785E+01
$T \leq 1000$K	0.26803869E+01	0.15799651E-01	0.25070596E-05	-0.13657623E-07	0.66154285E-11	0.20802374E+05 0.98769351E+01

C_3H_4b						
$T > 1000$K	6.28078872E+00	1.12393798E-02	-4.01957416E-06	6.46920405E-10	-3.86433056E-14	3.03415080E+04 -1.11420363E+01
$T \leq 1000$K	2.24666571E+00	5.76237942E-03	4.42080338E-05	-6.62906810E-08	2.81824735E-11	3.21284389E+04 1.33451493E+01

C_3H_5a						
$T > 1000$K	7.05019790E+00	1.30417133E-02	-4.62341683E-06	7.39605232E-10	-4.39893394E-14	1.69162444E+04 -1.41334291E+01
$T \leq 1000$K	1.36322505E+00	2.00030606E-02	1.22366530E-05	-3.34032456E-08	1.59644171E-11	1.88365517E+04 1.71382540E+01

C_3H_5s						
$T > 1000$K	6.05091412E+00	1.34052084E-02	-4.73450586E-06	7.55380897E-10	-4.48421084E-14	2.90860210E+04 -6.73692060E+00
$T \leq 1000$K	3.33277282E+00	1.06102499E-02	2.17559727E-05	-3.47145235E-08	1.44476835E-11	3.03404530E+04 9.78922358E+00

C_3H_5t						
$T > 1000$K	6.17467558E+00	1.35842068E-02	-4.86523676E-06	7.83574439E-10	-4.68222090E-14	2.72013596E+04 -7.02846541E+00
$T \leq 1000$K	4.82883324E+00	8.99954001E-04	4.44768198E-05	-5.67019197E-08	2.21267105E-11	2.83786431E+04 3.89995688E+00

C_3H_5b						
$T > 1000$K	6.62512238E+00	1.36577057E-02	-4.90066661E-06	7.90436486E-10	-4.72860275E-14	3.03239999E+04 -1.31845240E+01
$T \leq 1000$K	2.15143774E+00	3.80171682E-03	6.14538989E-05	-8.83383102E-08	3.70565687E-11	3.24689062E+04 1.48309194E+01

C_3H_6b	
$T > 1000$K	6.33778554E+00 1.64174480E-02 -5.85359278E-06 9.40111948E-10 -5.60727359E-14 3.28971390E+03 -1.41848666E+01
$T \leq 1000$K	2.57234000E+00 -2.50916956E-03 8.62737013E-05 -1.16111392E-07 4.75602007E-11 5.54899161E+03 1.18019800E+01
C_3H_6	
$T > 1000$K	5.86511931E+00 1.62909053E-02 -5.78250953E-06 9.25734966E-10 -5.50869091E-14 -6.52412479E+02 -7.28859556E+00
$T \leq 1000$K	4.14122102E+00 1.04671677E-03 5.52224672E-05 -7.11940972E-08 2.80278554E-11 7.71957427E+02 6.38058062E+00
C_3H_7n	
$T > 1000$K	6.49636579E+00 1.77337992E-02 -6.24898046E-06 9.95389495E-10 -5.90199770E-14 8.85973885E+03 -8.56389710E+00
$T \leq 1000$K	4.08211458E+00 5.23240341E-03 5.13554466E-05 -6.99343598E-08 2.81819493E-11 1.04074558E+04 8.39534919E+00
C_3H_7i	
$T > 1000$K	6.10103510E+00 1.85252265E-02 -6.63451675E-06 1.06844391E-09 -6.38396464E-14 7.53376696E+03 -6.77594633E+00
$T \leq 1000$K	7.17878202E+00 -1.63182405E-02 9.96703136E-05 -1.15074793E-07 4.35402866E-11 8.75779397E+03 -4.71632586E+00
C_3H_8	
$T > 1000$K	6.46876392E+00 2.07740138E-02 -7.41974628E-06 1.19269771E-09 -7.11713650E-14 -1.61396855E+04 -1.15613433E+01
$T \leq 1000$K	4.34772075E+00 3.58595707E-03 6.14128031E-05 -7.96781660E-08 3.12762429E-11 -1.44205640E+04 4.98218695E+00
C_3H_2O	
$T > 1000$K	8.31837925E+00 6.29241735E-03 -2.23673278E-06 3.58419038E-10 -2.13415819E-14 1.24699728E+04 -1.64469649E+01
$T \leq 1000$K	3.31113539E-01 4.22486648E-02 -6.51735418E-05 4.99681989E-08 -1.46632942E-11 1.39839966E+04 2.13631640E+01
C_3H_3O	
$T > 1000$K	6.90703955E+00 1.02341927E-02 -3.65649593E-06 5.87914100E-10 -3.51359226E-14 7.62708561E+03 -7.29856114E+00
$T \leq 1000$K	4.11237192E+00 5.05829116E-03 3.17832265E-05 -4.55489258E-08 1.86325507E-11 8.99713585E+03 1.01743843E+01

C_3H_4O	
$T > 1000$K	7.31820729E+00 1.27398510E-02 -4.60112009E-06 7.44735077E-10 -4.46993049E-14 -1.16137229E+04 -1.11884734E+01
$T \leq 1000$K	3.98487241E+00 3.40751550E-03 4.81227535E-05 -6.61399005E-08 2.67817331E-11 -9.83297241E+03 1.03960574E+01
C_3H_5O	
$T > 1000$K	8.79584189E+00 1.43678209E-02 -5.15086817E-06 8.30425063E-10 -4.96670802E-14 4.54840599E+03 -2.22910017E+01
$T \leq 1000$K	1.70176691E+00 1.81714690E-02 3.24069942E-05 -6.06152090E-08 2.71285315E-11 7.14713827E+03 1.78178812E+01
C_3H_5Op	
$T > 1000$K	6.52325448E+00 1.54211952E-02 -5.50898157E-06 8.85889862E-10 -5.28846399E-14 -7.19631634E+03 -5.19862218E+00
$T \leq 1000$K	6.25722402E+00 -9.17612184E-03 7.61190493E-05 -9.05514997E-08 3.46198215E-11 -5.91616484E+03 2.23330599E+00
C_3H_5Ot	
$T > 1000$K	8.19121321E+00 1.40061388E-02 -5.00831912E-06 8.03961104E-10 -4.79449403E-14 -1.02130206E+03 -1.33490112E+01
$T \leq 1000$K	7.54792894E+00 -7.02219530E-03 6.80989676E-05 -8.26664815E-08 3.19868293E-11 2.27709482E+02 -4.61588282E+00
C_3H_5Oa	
$T > 1000$K	7.54410697E+00 1.43443222E-02 -5.08381081E-06 8.13200521E-10 -4.83673315E-14 -7.48672286E+03 -1.14792587E+01
$T \leq 1000$K	4.70187196E+00 5.51653762E-03 4.27505858E-05 -5.94680816E-08 2.40685378E-11 -5.92845491E+03 7.12932590E+00
C_3H_6O	
$T > 1000$K	8.95739587E+00 1.60217198E-02 -5.65131014E-06 9.01550505E-10 -5.35370086E-14 -1.65852904E+04 -2.45939234E+01
$T \leq 1000$K	2.12818440E+00 8.44261433E-03 6.99012101E-05 -1.04542243E-07 4.42460530E-11 -1.36496693E+04 1.64564771E+01
C_3H_6Oa	
$T > 1000$K	7.34483390E+00 1.74962257E-02 -6.28532764E-06 1.01447594E-09 -6.07151779E-14 -3.01532755E+04 -1.27759736E+01
$T \leq 1000$K	5.14509588E+00 4.67026325E-04 6.25054589E-05 -7.97481327E-08 3.11400443E-11 -2.84186997E+04 4.17376406E+00

C_3H_6Op	
$T > 1000$K	7.46481253E+00 1.73054253E-02 -6.18909444E-06 9.94186575E-10 -5.93176585E-14 -2.56962482E+04 -1.18908315E+01
$T \leq 1000$K	7.04863211E+00 -9.12731989E-04 5.08259482E-05 -5.85807754E-08 2.11349394E-11 -2.45211143E+04 -4.74556661E+00
C_3H_7Oi	
$T > 1000$K	8.80421897E+00 1.88114477E-02 -6.74383714E-06 1.08690817E-09 -6.49826929E-14 -9.96635265E+03 -2.04194805E+01
$T \leq 1000$K	4.06975593E+00 1.57818571E-02 3.26769683E-05 -5.24145601E-08 2.17797338E-11 -7.85093901E+03 7.97686302E+00
C_3H_7On	
$T > 1000$K	8.87053269E+00 1.87153354E-02 -6.69616386E-06 1.07443755E-09 -6.40016274E-14 -8.85691524E+03 -1.96438956E+01
$T \leq 1000$K	4.09403015E+00 1.14654143E-02 4.94218617E-05 -7.37440702E-08 3.06629042E-11 -6.60221489E+03 9.79969944E+00
C_3H_6OH	
$T > 1000$K	8.21028051E+00 1.85492319E-02 -6.56857220E-06 1.04665387E-09 -6.20423973E-14 -1.09219055E+04 -1.24556007E+01
$T \leq 1000$K	6.27529305E+00 5.74998842E-03 4.43255747E-05 -5.66432538E-08 2.14679493E-11 -9.43553334E+03 2.11046046E+00
C_3H_7OOHi	
$T > 1000$K	1.20456150E+01 2.00609758E-02 -7.14988442E-06 1.14410241E-09 -6.79756845E-14 -2.93586148E+04 -3.37253315E+01
$T \leq 1000$K	5.33794019E+00 2.76687712E-02 1.27589136E-05 -3.73171105E-08 1.75843187E-11 -2.70062593E+04 3.45478108E+00
C_3H_7OOHn	
$T > 1000$K	1.13659898E+01 2.09104854E-02 -7.54558182E-06 1.21408112E-09 -7.23348512E-14 -2.69948187E+04 -2.79668904E+01
$T \leq 1000$K	7.72592798E+00 7.00071376E-03 6.31053345E-05 -8.74966515E-08 3.55373150E-11 -2.48944233E+04 -3.57008863E+00
C_3H_7OOi	
$T > 1000$K	1.01751084E+01 1.99154854E-02 -7.17577191E-06 1.15641116E-09 -6.90571155E-14 -1.24254561E+04 -2.34403543E+01
$T \leq 1000$K	6.27854157E+00 9.67831116E-03 4.97219807E-05 -6.92781488E-08 2.76014913E-11 -1.03016894E+04 1.82502336E+00

C_3H_7OOn	
$T > 1000$K	1.00126671E+01 2.02489787E-02 -7.37478477E-06 1.19344117E-09 -7.13933622E-14 -9.88113441E+03 -2.09357644E+01
$T \leq 1000$K	7.01899874E+00 -3.60956122E-04 7.97640943E-05 -1.03233840E-07 4.08206117E-11 -7.70037244E+03 1.37035175E+00
C_3H_6OOH	
$T > 1000$K	1.12645108E+01 1.83702458E-02 -6.64465781E-06 1.07024893E-09 -6.38038186E-14 -2.96405270E+03 -2.41355971E+01
$T \leq 1000$K	1.08227752E+01 -1.44735606E-02 1.06410370E-04 -1.29121248E-07 5.03582068E-11 -1.32195120E+03 -1.39762404E+01

Table D.5: Additional gas phase thermochemical properties implemented in Chapter 4.

NH_3	
$T > 1000$K	0.24619040E+01 0.60591660E-02 -0.20049765E-05 0.31360031E-09 -0.19383170E-13 -0.64932695E+04 0.74720969E+01
$T \leq 1000$K	0.22043516E+01 0.10114765E-01 -0.14652648E-04 0.14472350E-07 -0.53285089E-11 -0.65254883E+04 0.81271381E+01
NH_2	
$T > 1000$K	0.29613111E+01 0.29326989E-02 -0.90636001E-06 0.16172574E-09 -0.12042002E-13 0.21919767E+05 0.57778778E+01
$T \leq 1000$K	0.34324929E+01 0.32995399E-02 -0.66136003E-05 0.85909466E-08 -0.35720467E-11 0.21772277E+05 0.30901105E+01
NH	
$T > 1000$K	0.27602491E+01 0.13753462E-02 -0.44519143E-06 0.76927915E-10 -0.50175923E-14 0.42078281E+05 0.58571992E+01
$T \leq 1000$K	0.33397579E+01 0.12530086E-02 -0.34916459E-05 0.42188119E-08 -0.15576178E-11 0.41850473E+05 0.25071807E+01
N	
$T > 1000$K	0.24502683E+01 0.10661458E-03 -0.74653371E-07 0.18796523E-10 -0.10259839E-14 0.56116039E+05 0.44487581E+01
$T \leq 1000$K	0.25030713E+01 -0.21800181E-04 0.54205287E-07 -0.56475602E-10 0.20999044E-13 0.56098902E+05 0.41675663E+01
N_2H_2	
$T > 1000$K	0.33711853E+01 0.60399682E-02 -0.23038535E-05 0.40627889E-09 -0.27131444E-13 0.24181719E+05 0.49805851E+01
$T \leq 1000$K	0.16179994E+01 0.13063121E-01 -0.17157115E-04 0.16056079E-07 -0.60936386E-11 0.24675263E+05 0.13794670E+02

		NNH			
$T > 1000$K	0.44153423E+01	0.16143878E-02	-0.16328943E-06	-0.85598459E-10	0.16147909E-13
	0.27880293E+05	0.90428883E+00			
$T \leq 1000$K	0.35013444E+01	0.20535865E-02	0.71704096E-06	0.49213477E-09	-0.96711701E-12
	0.28333468E+05	0.63918371E+01			
		HNO			
$T > 1000$K	0.36151440E+01	0.32124857E-02	-0.12603369E-05	0.22672976E-09	-0.15362357E-13
	0.10661911E+05	0.48102636E+01			
$T \leq 1000$K	0.27844026E+01	0.66096461E-02	-0.93002227E-05	0.94379802E-08	-0.37531462E-11
	0.10918779E+05	0.90356293E+01			
		NO			
$T > 1000$K	0.32454355E+01	0.12691383E-02	-0.50158900E-06	0.91692834E-10	-0.62754193E-14
	0.98008398E+04	0.64172935E+01			
$T \leq 1000$K	0.33765416E+01	0.12530633E-02	-0.33027506E-05	0.52178102E-08	-0.24462628E-11
	0.98179609E+04	0.58295898E+01			
		NO_2			
$T > 1000$K	0.46828589E+01	0.24624290E-02	-0.10422585E-05	0.19769024E-09	-0.13917168E-13
	0.22612922E+04	0.98859846E+00			
$T \leq 1000$K	0.26706004E+01	0.78385006E-02	-0.80638647E-05	0.61617147E-08	-0.23201501E-11
	0.28962905E+04	0.11612071E+02			
		N_2O			
$T > 1000$K	0.47189769E+01	0.28737138E-02	-0.11974957E-05	0.22505515E-09	-0.15753369E-13
	0.81658110E+04	-0.16572504E+01			
$T \leq 1000$K	0.25430577E+01	0.94921933E-02	-0.97927750E-05	0.62638445E-08	-0.19018259E-11
	0.87650996E+04	0.95112219E+01			
		HCN			
$T > 1000$K	0.36500778E+01	0.34609979E-02	-0.12742787E-05	0.22176556E-09	-0.14771773E-13
	0.14767374E+05	0.23932204E+01			
$T \leq 1000$K	0.24904623E+01	0.86112805E-02	-0.10310342E-04	0.74814981E-08	-0.22291095E-11
	0.14991802E+05	0.79049816E+01			
		CN			
$T > 1000$K	0.37201197E+01	0.15183506E-03	0.19873811E-06	-0.37983713E-10	0.13282296E-14
	0.51619846E+05	0.28885972E+01			
$T \leq 1000$K	0.36632042E+01	-0.11565291E-02	0.21634089E-05	0.18542082E-09	-0.82146952E-12
	0.51784763E+05	0.37390156E+01			

NCO	
$T > 1000$K	0.50120454E+01 0.26267732E-02 -0.11082433E-05 0.20938602E-09 -0.14603469E-13 0.14058271E+05 -0.18300752E+01
$T \leq 1000$K	0.28303203E+01 0.88714901E-02 -0.89456362E-05 0.58769185E-08 -0.19077346E-11 0.14691845E+05 0.94988308E+01
HNCO	
$T > 1000$K	0.62118668E+01 0.22971372E-02 -0.22161288E-06 -0.12220437E-09 0.22724061E-13 -0.16447649E+05 -0.80166330E+01
$T \leq 1000$K	0.36940591E+01 0.66572362E-02 -0.50544681E-07 -0.34734115E-08 0.13605694E-11 -0.15596693E+05 0.57127418E+01
HOCN	
$T > 1000$K	0.56456074E+01 0.22982065E-02 -0.21626292E-06 -0.12148013E-09 0.22386362E-13 -0.22525005E+04 -0.35902631E+01
$T \leq 1000$K	0.36282923E+01 0.56641842E-02 -0.11702056E-06 -0.23486386E-08 0.80164022E-12 -0.15503163E+04 0.74768252E+01
HNO_2	
$T > 1000$K	0.54868927E+01 0.42180647E-02 -0.16491426E-05 2.97187663E-10 -2.02114801E-14 -1.12686465E+04 -2.99700189E+00
$T \leq 1000$K	2.29041290E+00 1.40992226E-02 -1.36787176E-05 7.49878026E-09 -1.87690532E-12 -1.04319453E+04 1.32807694E+01
H_2CN	
$T > 1000$K	0.34037385E+01 0.40840562E-02 -0.18275330E-05 0.42478668E-09 -0.41025766E-13 0.28581176E+05 0.36877346E+01
$T \leq 1000$K	0.26118708E+01 0.77789519E-02 -0.83243649E-05 0.54564659E-08 -0.14789024E-11 0.28720859E+05 0.73935413E+01
HCNO	
$T > 1000$K	5.91979744E+00 4.00114600E-03 -1.42063343E-06 2.27569621E-10 -1.35504870E-14 1.80385534E+04 -8.26935223E+00
$T \leq 1000$K	6.07949401E-01 2.82182431E-02 -4.60451618E-05 3.82559486E-08 -1.23226501E-11 1.90714209E+04 1.69199098E+01
HNC	
$T > 1000$K	0.36500778E+01 0.34609979E-02 -0.12742787E-05 0.22176556E-09 -0.14771773E-13 0.22320564E+05 0.23932204E+01
$T \leq 1000$K	0.24904623E+01 0.86112805E-02 -0.10310342E-04 0.74814981E-08 -0.22291095E-11 0.22544992E+05 0.79049816E+01

CH_3NO_2	
$T > 1000$K	0.72579584E+01 0.97425506E-02 -0.32998314E-05 0.49756554E-09 -0.27304449E-13 -0.12274141E+05 -0.12651306E+02
$T \leq 1000$K	0.16658440E+01 0.18138818E-01 0.12019345E-05 -0.12436082E-07 0.56004723E-11 -0.10272887E+05 0.18234782E+02
CH_2NO_2	
$T > 1000$K	7.67214886E+00 7.04674142E-03 -2.55301211E-06 4.14646979E-10 -2.49316782E-14 1.52307521E+04 -1.22510821E+01
$T \leq 1000$K	2.46754293E+00 1.56130407E-02 4.71686464E-06 -2.05123642E-08 1.02705094E-11 1.69015807E+04 1.59016345E+01
N_2	
$T > 1000$K	2.95257637E+00 1.39690040E-03 -4.92631603E-07 7.86010195E-11 -4.60755204E-15 -9.23948688E+02 5.87188762E+00
$T \leq 1000$K	3.53100528E+00 -1.23660988E-04 -5.02999433E-07 2.43530612E-09 -1.40881235E-12 -1.04697628E+03 2.96747038E+00
N_3	
$T > 1000$K	4.64110774E+00 2.76960647E-03 -1.04917579E-06 1.75340743E-10 -1.07482727E-14 5.28079884E+04 -9.40233115E-01
$T \leq 1000$K	2.86063087E+00 4.24883043E-03 5.14574004E-06 -1.01478684E-08 4.41879795E-12 5.34787743E+04 9.11586663E+00
NO_3	
$T > 1000$K	7.48347734E+00 2.57772041E-03 -1.00945831E-06 1.72314072E-10 -1.07154015E-14 5.70919428E+03 -1.41618155E+01
$T \leq 1000$K	2.17359310E+00 1.04902697E-02 1.10472650E-05 -2.81561854E-08 1.36583958E-11 7.39219877E+03 1.46022098E+01
N_2O_5	
$T > 1000$K	1.31108082E+01 4.87435791E-03 -1.87548389E-06 3.16374121E-10 -1.95926845E-14 -3.11634700E+03 -3.46877692E+01
$T \leq 1000$K	3.68767444E+00 3.92120798E-02 -5.53770029E-05 4.20097833E-08 -1.31260710E-11 -8.30291184E+02 1.21967866E+01
N_2O_3	
$T > 1000$K	9.08583845E+00 3.37756330E-03 -1.31583890E-06 2.30762329E-10 -1.47151267E-14 7.27160146E+03 -1.55361904E+01
$T \leq 1000$K	5.81083964E+00 1.43330962E-02 -1.96208597E-05 1.73060735E-08 -6.46553954E-12 8.19184453E+03 1.20461321E+00

HNO_3						
$T > 1000$K	8.03098942E+00	4.46958589E-03	-1.72459491E-06	2.91556153E-10	-1.80102702E-14	-1.93138183E+04 -1.62616537E+01
$T \leq 1000$K	1.69329154E+00	1.90167702E-02	-8.25176697E-06	-6.06113827E-09	4.65236978E-12	-1.74198909E+04 1.71839838E+01
N_2O_4						
$T > 1000$K	1.15752899E+01	4.01616086E-03	-1.57178323E-06	2.68274309E-10	-1.66922019E-14	-2.92191226E+03 -3.19488439E+01
$T \leq 1000$K	3.02002308E+00	2.95904321E-02	-3.01342458E-05	1.42360407E-08	-2.44100049E-12	-6.40040162E+02 1.18059606E+01
HN_3						
$T > 1000$K	5.14700198E+00	4.30561405E-03	-1.52704650E-06	2.46295940E-10	-1.47144292E-14	3.31533377E+04 -2.25528569E+00
$T \leq 1000$K	2.88510835E+00	9.44343949E-03	-3.87921021E-06	-1.89401832E-09	1.60183173E-12	3.38421425E+04 9.71687992E+00

Table D.6: Additional gas phase thermochemical properties implemented in Chapter 5.

C_4H						
$T > 1000$K	6.80958026E+00	5.53720360E-03	-1.99731156E-06	3.23402907E-10	-1.94028936E-14	9.55410750E+04 -9.27742185E+00
$T \leq 1000$K	1.61853523E+00	2.42334896E-02	-2.92435255E-05	1.90475677E-08	-5.00259472E-12	9.67816455E+04 1.65122775E+01
C_4H_2						
$T > 1000$K	8.68978130E+00	6.69732229E-03	-2.34774865E-06	3.72759231E-10	-2.20554548E-14	5.19942624E+04 -2.20010465E+01
$T \leq 1000$K	-5.84768273E-01	5.33506727E-02	-9.50805952E-05	8.37959674E-08	-2.80912179E-11	5.36111160E+04 2.09878997E+01
C_4H_3n						
$T > 1000$K	8.67518979E+00	8.99760032E-03	-3.18870421E-06	5.10080852E-10	-3.03404906E-14	6.19699844E+04 -1.87973407E+01
$T \leq 1000$K	7.12909471E-01	3.86307007E-02	-4.72486887E-05	3.09706868E-08	-8.10178201E-12	6.38015128E+04 2.04653602E+01
C_4H_3i						
$T > 1000$K	8.51181244E+00	9.03337808E-03	-3.17602594E-06	5.05276458E-10	-2.99379699E-14	5.71046116E+04 -1.51017769E+01
$T \leq 1000$K	3.37964170E+00	2.70498840E-02	-2.90761572E-05	1.83027765E-08	-4.81164203E-12	5.83688723E+04 1.05464883E+01

		C_4H_4			
$T > 1000$K	7.98456038E+00	1.20558816E-02	-4.23587475E-06	6.73646140E-10	-3.99059864E-14
	3.11993029E+04	-1.67958975E+01			
$T \leq 1000$K	1.37368786E+00	2.88801256E-02	-1.46863874E-05	-3.91045446E-09	4.78133572E-12
	3.30633344E+04	1.75941274E+01			
		C_4H_5s			
$T > 1000$K	8.40733458E+00	1.40059672E-02	-4.95807494E-06	7.92402949E-10	-4.71000236E-14
	3.44768074E+04	-1.65735377E+01			
$T \leq 1000$K	3.28671229E+00	2.27907195E-02	-8.19784841E-07	-1.48809448E-08	7.82382760E-12
	3.61697749E+04	1.12012879E+01			
		C_4H_5t			
$T > 1000$K	1.05908873E+01	1.20520192E-02	-4.25436532E-06	6.78465925E-10	-4.03132920E-14
	3.85927282E+04	-3.08524262E+01			
$T \leq 1000$K	1.91541514E+00	2.07457141E-02	3.19954425E-05	-6.69258254E-08	3.12959476E-11
	4.14719044E+04	1.69577125E+01			
		C_4H_5i			
$T > 1000$K	8.84861310E+00	1.41333440E-02	-5.02167996E-06	8.04623264E-10	-4.79136957E-14
	3.37711137E+04	-2.10173757E+01			
$T \leq 1000$K	1.87535071E+00	2.65030231E-02	1.96342023E-06	-2.45970811E-08	1.29722739E-11
	3.59775585E+04	1.65021732E+01			
		C_4H_6s			
$T > 1000$K	7.91693669E+00	1.72036050E-02	-6.12682850E-06	9.83121060E-10	-5.85980280E-14
	1.56644026E+04	-1.64630702E+01			
$T \leq 1000$K	3.97325190E+00	1.19311387E-02	3.67647333E-05	-5.58850964E-08	2.31342088E-11
	1.75256264E+04	7.76349546E+00			
		C_4H_6t			
$T > 1000$K	1.04197067E+01	1.47876391E-02	-5.21635362E-06	8.31059701E-10	-4.93320213E-14
	8.54812076E+03	-3.23589750E+01			
$T \leq 1000$K	3.42577713E+00	4.55942735E-03	8.23041857E-05	-1.20416724E-07	5.09000540E-11
	1.16047119E+04	1.00999028E+01			
		C_4H_6f			
$T > 1000$K	8.43880732E+00	1.65900125E-02	-5.87209474E-06	9.38337857E-10	-5.57662624E-14
	1.61699434E+04	-1.92895245E+01			
$T \leq 1000$K	2.32743471E+00	2.59076877E-02	4.14601953E-06	-2.47406550E-08	1.23988097E-11
	1.82119400E+04	1.40456299E+01			

C_4H_6b						
$T > 1000$K	8.20335300E+00	1.69495299E-02	-6.03753174E-06	9.69060562E-10	-5.77756231E-14	2.65189274E+04 -1.93243077E+01
$T \leq 1000$K	2.96302031E+00	1.31820550E-02	4.22616015E-05	-6.65521728E-08	2.81721321E-11	2.87776133E+04 1.19421372E+01

C_4H_6m						
$T > 1000$K	7.16249995E+00	1.79678340E-02	-6.42169543E-06	1.03280570E-09	-6.16552906E-14	1.42079893E+04 -1.33397082E+01
$T \leq 1000$K	5.45022262E+00	2.76407277E-03	5.23661192E-05	-6.66978269E-08	2.57972012E-11	1.56870959E+04 4.10301778E-01

C_4H_7i						
$T > 1000$K	8.97924987E+00	1.89314502E-02	-6.74883879E-06	1.08370764E-09	-6.46277001E-14	1.19605358E+04 -2.22521993E+01
$T \leq 1000$K	1.01003603E+00	3.02533518E-02	9.27971616E-06	-3.58385260E-08	1.74763632E-11	1.46483074E+04 2.13831640E+01

C_4H_7n						
$T > 1000$K	8.49073768E+00	1.91056974E-02	-6.74370664E-06	1.07343267E-09	-6.36251837E-14	2.04659294E+04 -1.74555814E+01
$T \leq 1000$K	5.07355313E+00	5.27619329E-03	6.23441322E-05	-8.54203458E-08	3.45890031E-11	2.24615054E+04 5.60318035E+00

C_4H_7s						
$T > 1000$K	8.77047624E+00	1.92187729E-02	-6.87542705E-06	1.10663532E-09	-6.61028746E-14	1.20695085E+04 -2.08842606E+01
$T \leq 1000$K	4.16630233E+00	8.96330982E-03	5.79781450E-05	-8.30895850E-08	3.41361824E-11	1.43921546E+04 8.26375850E+00

C_4H_8i						
$T > 1000$K	8.06269034E+00	2.20765179E-02	-7.90114313E-06	1.27198170E-09	-7.59864193E-14	-6.16389292E+03 -1.83725208E+01
$T \leq 1000$K	5.16031440E+00	5.63178326E-03	6.25749118E-05	-8.20550258E-08	3.21220767E-11	-4.13902874E+03 2.60924249E+00

C_4H_8n						
$T > 1000$K	8.37176539E+00	2.17689316E-02	-7.77572559E-06	1.24747571E-09	-7.43321930E-14	-4.28560037E+03 -1.81843440E+01
$T \leq 1000$K	5.48963814E+00	1.37802066E-03	7.79778572E-05	-1.01585586E-07	4.02781850E-11	-2.15478324E+03 3.42836316E+00

C_4H_8s	
$T > 1000$K	7.88750247E+00 2.22988814E-02 -7.99637187E-06 1.28899533E-09 -7.70725949E-14 -5.45955297E+03 -1.70739220E+01
$T \leq 1000$K	6.85844649E+00 -6.51094213E-03 9.08047195E-05 -1.09617044E-07 4.18667549E-11 -3.62153801E+03 -4.07345440E+00
C_4H_9i	
$T > 1000$K	9.61250942E+00 2.28581786E-02 -8.06391309E-06 1.28556553E-09 -7.62730799E-14 4.15218608E+03 -2.66485099E+01
$T \leq 1000$K	3.34476784E+00 2.31869650E-02 3.28261040E-05 -5.96398514E-08 2.58980820E-11 6.66201200E+03 9.68860372E+00
C_4H_9t	
$T > 1000$K	6.72557390E+00 2.53649194E-02 -9.05306262E-06 1.45474620E-09 -8.67934112E-14 2.57430692E+03 -8.89920414E+00
$T \leq 1000$K	6.45910754E+00 -1.02015930E-02 1.06310577E-04 -1.25717030E-07 4.75543216E-11 4.43420391E+03 1.30648608E+00
C_4H_9n	
$T > 1000$K	8.97401527E+00 2.39704154E-02 -8.48703645E-06 1.35644127E-09 -8.06234913E-14 5.19161526E+03 -2.31075609E+01
$T \leq 1000$K	4.73737837E+00 9.69051565E-03 6.63846383E-05 -9.24799302E-08 3.74006099E-11 7.57382332E+03 4.91063455E+00
C_4H_9s	
$T > 1000$K	7.72287211E+00 2.43427284E-02 -8.65476475E-06 1.38712529E-09 -8.26084187E-14 4.15004489E+03 -1.43949625E+01
$T \leq 1000$K	5.42089393E+00 -9.12146870E-04 8.84998581E-05 -1.12115531E-07 4.38222782E-11 6.28927311E+03 5.04210029E+00
$C_4H_{10}n$	
$T > 1000$K	8.92213454E+00 2.62597428E-02 -9.42142441E-06 1.51500444E-09 -9.03538061E-14 -1.98790900E+04 -2.23198916E+01
$T \leq 1000$K	6.84977207E+00 -1.75116891E-03 9.48605428E-05 -1.19284063E-07 4.65100207E-11 -1.76822354E+04 -3.51832851E+00
$C_4H_{10}i$	
$T > 1000$K	9.76991697E+00 2.54997141E-02 -9.14142587E-06 1.47328201E-09 -8.80799697E-14 -2.14052667E+04 -3.00329670E+01
$T \leq 1000$K	4.45479140E+00 8.26058864E-03 8.29886433E-05 -1.14647616E-07 4.64569994E-11 -1.84593929E+04 4.92740653E+00

C_4H_2O						
$T > 1000$K	9.40908701E+00	8.64021882E-03	-3.12908612E-06	5.07868742E-10	-3.05160749E-14	2.24615264E+04 -2.18745001E+01
$T \leq 1000$K	2.15973548E+00	3.72020987E-02	-5.14278090E-05	4.03137307E-08	-1.28501835E-11	2.41419803E+04 1.37260239E+01
C_4H_4O						
$T > 1000$K	9.61322922E+00	1.39225141E-02	-5.05874715E-06	8.23043284E-10	-4.95420588E-14	5.87078239E+02 -2.66451271E+01
$T \leq 1000$K	1.78782779E+00	1.73722022E-02	3.80649464E-05	-6.80589897E-08	3.00845106E-11	3.50676877E+03 1.78264604E+01
C_4H_5Ox						
$T > 1000$K	1.00109193E+01	1.56609245E-02	-5.64859331E-06	9.14217653E-10	-5.48218361E-14	3.70525874E+03 -2.37578616E+01
$T \leq 1000$K	5.01239905E+00	1.50193265E-02	2.82372524E-05	-4.74581120E-08	2.00717803E-11	5.79705805E+03 5.56182744E+00
C_4H_5Oy						
$T > 1000$K	1.05082001E+01	1.56939134E-02	-5.67000455E-06	9.18897935E-10	-5.51590124E-14	-5.18511078E+02 -2.90238850E+01
$T \leq 1000$K	3.28894051E+00	1.95544826E-02	2.97994330E-05	-5.57675403E-08	2.45205321E-11	2.20378942E+03 1.20012623E+01
C_4H_6Ob						
$T > 1000$K	1.04017539E+01	1.91801473E-02	-7.15850045E-06	1.17439803E-09	-7.08810109E-14	-1.75011636E+04 -3.00059373E+01
$T \leq 1000$K	3.94073764E+00	2.32480563E-02	1.80932390E-05	-3.81207793E-08	1.63656642E-11	-1.49548630E+04 6.92065946E+00
C_4H_6Oa						
$T > 1000$K	1.06955708E+01	1.76034072E-02	-6.31551730E-06	1.01520407E-09	-6.05533529E-14	-3.74306952E+03 -3.07187354E+01
$T \leq 1000$K	2.43462425E+00	2.77197540E-02	1.56055031E-05	-4.30249223E-08	2.02031524E-11	-8.90012699E+02 1.48831206E+01
C_4H_7Ox						
$T > 1000$K	1.03519991E+01	2.03385849E-02	-7.35907392E-06	1.18946887E-09	-7.11844228E-14	1.75561028E+03 -2.59117862E+01
$T \leq 1000$K	4.80290347E+00	1.26829060E-02	5.37008113E-05	-7.94047836E-08	3.26679573E-11	4.37998505E+03 8.22571029E+00

C_4H_7Om	
$T > 1000$K	9.95812346E+00 2.00549144E-02 -7.19396488E-06 1.15740437E-09 -6.91060030E-14 -1.17601480E+04 -2.24695101E+01
$T \leq 1000$K	4.68146299E+00 1.86787473E-02 2.95246310E-05 -4.97395546E-08 2.07620847E-11 -9.47693435E+03 8.75509363E+00
C_4H_8Ox	
$T > 1000$K	1.01453808E+01 2.30313259E-02 -8.27843616E-06 1.33674487E-09 -8.00286667E-14 -2.18459352E+04 -2.86842582E+01
$T \leq 1000$K	4.91524246E+00 1.07110614E-02 6.48871041E-05 -9.10021090E-08 3.66436878E-11 -1.91042078E+04 4.78044074E+00
C_4H_8Om	
$T > 1000$K	9.74197781E+00 2.30221779E-02 -8.28513329E-06 1.33580581E-09 -7.98631500E-14 -3.08246201E+04 -2.35538706E+01
$T \leq 1000$K	6.85713509E+00 1.73287406E-03 7.75498242E-05 -9.87341435E-08 3.83292752E-11 -2.85711183E+04 -1.49989282E+00
C_4H_8OHi	
$T > 1000$K	1.20408349E+01 2.27109222E-02 -8.09318390E-06 1.29534127E-09 -7.69845061E-14 -1.47279195E+04 -3.27518521E+01
$T \leq 1000$K	3.50432963E+00 4.36215967E-02 -2.32342059E-05 1.29922560E-09 2.68598392E-12 -1.21533089E+04 1.21840368E+01
$O_2C_4H_9O$	
$T > 1000$K	1.58754061E+01 2.45143718E-02 -9.02792662E-06 1.47136702E-09 -8.84192089E-14 -3.37499714E+04 -4.87350426E+01
$T \leq 1000$K	1.20350104E+01 4.07786695E-03 8.13917304E-05 -1.06870642E-07 4.21108331E-11 -3.11855572E+04 -2.14156628E+01

Appendix E

Knudsen efficiency factors

The following Table includes the average Knudsen efficiency factors for the temperature range of $450 \leq \mathrm{T[K]} \leq 800$, at different Pt loadings [2]. The mean values originate from the corresponding values of $\bar{D}_i^{eff}/D_i^{eff}$ ratios of the selected species, shown in Table 2.1.

Table E.1: Variation of the average Knudsen efficiency factor values with the temperature, for different Pt loadings. The values indicated in a bold font are applied in Chapter 4, apart from Section 4.3.4 which illustrates the effect of the different Pt loadings.

T [K]	$\bar{\eta}_e$ [–] (0.5 wt%)	$\bar{\eta}_e$ [–] (1 wt%)	$\bar{\eta}_e$ [–] (3 wt%)
450	$3.19 \cdot 10^{-2}$	$\mathbf{3.00 \cdot 10^{-2}}$	$3.36 \cdot 10^{-2}$
460	$3.22 \cdot 10^{-2}$	$\mathbf{3.03 \cdot 10^{-2}}$	$3.39 \cdot 10^{-2}$
470	$3.26 \cdot 10^{-2}$	$\mathbf{3.06 \cdot 10^{-2}}$	$3.43 \cdot 10^{-2}$
480	$3.29 \cdot 10^{-2}$	$\mathbf{3.09 \cdot 10^{-2}}$	$3.46 \cdot 10^{-2}$
490	$3.32 \cdot 10^{-2}$	$\mathbf{3.12 \cdot 10^{-2}}$	$3.50 \cdot 10^{-2}$
500	$3.36 \cdot 10^{-2}$	$\mathbf{3.15 \cdot 10^{-2}}$	$3.53 \cdot 10^{-2}$
510	$3.39 \cdot 10^{-2}$	$\mathbf{3.18 \cdot 10^{-2}}$	$3.57 \cdot 10^{-2}$
520	$3.42 \cdot 10^{-2}$	$\mathbf{3.21 \cdot 10^{-2}}$	$3.60 \cdot 10^{-2}$
530	$3.45 \cdot 10^{-2}$	$\mathbf{3.24 \cdot 10^{-2}}$	$3.63 \cdot 10^{-2}$
540	$3.48 \cdot 10^{-2}$	$\mathbf{3.27 \cdot 10^{-2}}$	$3.67 \cdot 10^{-2}$
550	$3.51 \cdot 10^{-2}$	$\mathbf{3.30 \cdot 10^{-2}}$	$3.70 \cdot 10^{-2}$
560	$3.55 \cdot 10^{-2}$	$\mathbf{3.33 \cdot 10^{-2}}$	$3.73 \cdot 10^{-2}$

T [K]	$\bar{\eta}_e$ [–] (0.5 wt%)	$\bar{\eta}_e$ [–] (1 wt%)	$\bar{\eta}_e$ [–] (3 wt%)
570	$3.58 \cdot 10^{-2}$	$\mathbf{3.36 \cdot 10^{-2}}$	$3.76 \cdot 10^{-2}$
580	$3.61 \cdot 10^{-2}$	$\mathbf{3.39 \cdot 10^{-2}}$	$3.79 \cdot 10^{-2}$
590	$3.64 \cdot 10^{-2}$	$\mathbf{3.42 \cdot 10^{-2}}$	$3.83 \cdot 10^{-2}$
600	$3.66 \cdot 10^{-2}$	$\mathbf{3.44 \cdot 10^{-2}}$	$3.86 \cdot 10^{-2}$
610	$3.69 \cdot 10^{-2}$	$\mathbf{3.47 \cdot 10^{-2}}$	$3.89 \cdot 10^{-2}$
620	$3.72 \cdot 10^{-2}$	$\mathbf{3.50 \cdot 10^{-2}}$	$3.92 \cdot 10^{-2}$
630	$3.75 \cdot 10^{-2}$	$\mathbf{3.53 \cdot 10^{-2}}$	$3.95 \cdot 10^{-2}$
640	$3.78 \cdot 10^{-2}$	$\mathbf{3.55 \cdot 10^{-2}}$	$3.98 \cdot 10^{-2}$
650	$3.81 \cdot 10^{-2}$	$\mathbf{3.58 \cdot 10^{-2}}$	$4.01 \cdot 10^{-2}$
660	$3.84 \cdot 10^{-2}$	$\mathbf{3.61 \cdot 10^{-2}}$	$4.04 \cdot 10^{-2}$
670	$3.86 \cdot 10^{-2}$	$\mathbf{3.63 \cdot 10^{-2}}$	$4.07 \cdot 10^{-2}$
680	$3.89 \cdot 10^{-2}$	$\mathbf{3.66 \cdot 10^{-2}}$	$4.10 \cdot 10^{-2}$
690	$3.92 \cdot 10^{-2}$	$\mathbf{3.68 \cdot 10^{-2}}$	$4.12 \cdot 10^{-2}$
700	$3.95 \cdot 10^{-2}$	$\mathbf{3.71 \cdot 10^{-2}}$	$4.15 \cdot 10^{-2}$
710	$3.97 \cdot 10^{-2}$	$\mathbf{3.74 \cdot 10^{-2}}$	$4.18 \cdot 10^{-2}$
720	$4.00 \cdot 10^{-2}$	$\mathbf{3.76 \cdot 10^{-2}}$	$4.21 \cdot 10^{-2}$
730	$4.03 \cdot 10^{-2}$	$\mathbf{3.79 \cdot 10^{-2}}$	$4.24 \cdot 10^{-2}$
740	$4.05 \cdot 10^{-2}$	$\mathbf{3.81 \cdot 10^{-2}}$	$4.26 \cdot 10^{-2}$
750	$4.08 \cdot 10^{-2}$	$\mathbf{3.84 \cdot 10^{-2}}$	$4.29 \cdot 10^{-2}$
760	$4.11 \cdot 10^{-2}$	$\mathbf{3.86 \cdot 10^{-2}}$	$4.32 \cdot 10^{-2}$
770	$4.13 \cdot 10^{-2}$	$\mathbf{3.88 \cdot 10^{-2}}$	$4.35 \cdot 10^{-2}$
780	$4.16 \cdot 10^{-2}$	$\mathbf{3.91 \cdot 10^{-2}}$	$4.37 \cdot 10^{-2}$
790	$4.18 \cdot 10^{-2}$	$\mathbf{3.93 \cdot 10^{-2}}$	$4.40 \cdot 10^{-2}$
800	$4.21 \cdot 10^{-2}$	$\mathbf{3.96 \cdot 10^{-2}}$	$4.43 \cdot 10^{-2}$